Department of Signal Processing and Acoustics

Design and Analysis of Duplexing Modes and Forwarding Protocols for OFDM(A) Relay Links

Taneli Riihonen

A!

DOCTORAL DISSERTATIONS

Aalto University publication series
DOCTORAL DISSERTATIONS 81/2014

Design and Analysis of Duplexing Modes and Forwarding Protocols for OFDM(A) Relay Links

Taneli Riihonen

A doctoral dissertation completed for the degree of Doctor of Science in Technology to be defended, with the permission of Aalto University School of Electrical Engineering, at a public examination held at the lecture hall S1 of the school on 4 July 2014 at 12 o'clock noon.

Aalto University
School of Electrical Engineering
Department of Signal Processing and Acoustics

Supervising professor
Prof. Risto Wichman

Thesis advisor
Dr. Stefan Werner

Preliminary examiners
Dr. Golnaz Farhadi, Fujitsu Laboratories of America, CA, USA
Dr. Himal A. Suraweera, University of Peradeniya, Sri Lanka

Opponent
Prof. Robert Schober, University of Erlangen-Nuremberg, Germany

Aalto University publication series
DOCTORAL DISSERTATIONS 81/2014

ISBN 978-952-60-5714-9
ISBN 978-952-60-5715-6 (pdf)
ISSN-L 1799-4934
ISSN 1799-4934 (printed)
ISSN 1799-4942 (pdf)
http://urn.fi/URN:ISBN:978-952-60-5715-6

Unigrafia Oy
Helsinki 2014

Finland

Publication orders (printed book):
taneli.riihonen@iki.fi
http://www.iki.fi/taneli.riihonen

Aalto University

Abstract

Aalto University, P.O. Box 11000, FI-00076 Aalto www.aalto.fi

Author
Taneli Riihonen

Name of the doctoral dissertation
Design and Analysis of Duplexing Modes and Forwarding Protocols for OFDM(A) Relay Links

Publisher School of Electrical Engineering

Unit Department of Signal Processing and Acoustics

Series Aalto University publication series DOCTORAL DISSERTATIONS 81/2014

Field of research Signal Processing for Communications

Manuscript submitted 20 January 2014 **Date of the defence** 4 July 2014

Permission to publish granted (date) 28 March 2014 **Language** English

☒ **Monograph** ☐ **Article dissertation (summary + original articles)**

Abstract

Relaying, i.e., multihop communication via so-called relay nodes, has emerged as an advanced technology for economically realizing long transmission ranges and high data rates in wireless systems. The focus of this thesis is on multihop multiuser systems where signals are modulated with orthogonal frequency-division multiplexing or multiple access, i.e., OFDM(A), and relays are infrastructure-based network nodes. In general, the thesis contributes by investigating how to operate relay links optimally under spectrum, transmit power and processing capability limitations, as well as how to improve signal processing in relays by exploiting other advanced concepts such as multiantenna techniques, spectrum reuse, transmit power adaptation, and new options for multicarrier protocol design.

The first theme is the design and analysis of duplexing modes which define how a relay link reuses allocated frequency bands in each hop. Especially, the full-duplex relaying mode is promoted as a feasible, advantageous alternative to conventional half-duplex operation while its inherent loopback self-interference is recognized and dealt with: New techniques are developed and evaluated for the mitigation of self-interference while transmit power control is proposed as a countermeasure against residual distortion. Finally, the fundamental criteria to prefer one mode over the other are determined which not only serves as a comparison between the modes but allows for opportunistic mode switching during operation.

The second theme is the design and analysis of forwarding protocols which specify signal processing done between reception and retransmission in a relay. The study identifies a comprehensive set of design options for OFDM(A) relaying protocols and evaluates their combinations. Similar analysis is conducted for evaluating the duplexing modes and multiuser scheduling. Furthermore, a new analytical framework is developed for studying the channel delay spread characteristics of non-regenerative multihop OFDM links in conjunction with inter-carrier and inter-symbol interference as well as time synchronization error.

Throughout the thesis, the design of relaying modes and protocols is conducted together with statistical performance analysis which facilitates discerning comparisons between existing and proposed concepts. Especially, all the contributions are established by means of closed-form expressions derived for the considered systems. The results cover all essential system variations, including amplify-and-forward and decode-and-forward protocols as well as downlink and uplink relaying reflecting their differences in infrastructure-based relaying.

Keywords OFDM, OFDMA, wireless communication, relays

ISBN (printed) 978-952-60-5714-9 **ISBN (pdf)** 978-952-60-5715-6

ISSN-L 1799-4934 **ISSN (printed)** 1799-4934 **ISSN (pdf)** 1799-4942

Location of publisher Helsinki **Location of printing** Helsinki **Year** 2014

Pages 300 **urn** http://urn.fi/URN:ISBN:978-952-60-5715-6

A? Aalto-yliopisto

Tiivistelmä

Aalto-yliopisto, PL 11000, 00076 Aalto www.aalto.fi

Tekijä
Taneli Riihonen

Väitöskirjan nimi
Monihyppyisten OFDM(A)-linkkien dupleksitilojen ja välitysprotokollien kehitys ja analyysi

Julkaisija Sähkötekniikan korkeakoulu

Yksikkö Signaalinkäsittelyn ja akustiikan laitos

Sarja Aalto University publication series DOCTORAL DISSERTATIONS 81/2014

Tutkimusala Tietoliikenteen signaalinkäsittely

Käsikirjoituksen pvm 20.01.2014 **Väitöspäivä** 04.07.2014

Julkaisuluvan myöntämispäivä 28.03.2014 **Kieli** Englanti

☒ **Monografia** ☐ **Yhdistelmäväitöskirja (yhteenveto-osa + erillisartikkelit)**

Tiivistelmä

Monihyppyinen tiedonsiirto niin kutsuttujen välittimien kautta on muodostunut kehittyneeksi teknologiaksi, jolla voi toteuttaa langattomissa järjestelmissä tehokkaasti pitkiä yhteysvälejä ja suuria datanopeuksia. Tämä tutkielma keskittyy monihyppyisiin monen käyttäjän järjestelmiin, joissa signaalit käyttävät OFDM(A)-modulaatiota ("orthogonal frequency-division multiplexing" tai "- multiple access") ja välittimet ovat osa verkko-infrastruktuuria. Yleisesti ottaen tämä tutkielma selvittää kuinka välittimiä voi käyttää optimaalisesti spektri-, lähetysteho- ja prosessointirajoitusten vallitessa sekä kuinka välittimien suorittamaa signaalinkäsittelyä voi parantaa käyttämällä muita edistyneitä konsepteja kuten moniantennitekniikoita, taajuuksien uudelleenkäyttöä, tehon säätöä ja uusia vaihtoehtoja monikantoaaltoprotokollien suunnittelussa.

Ensimmäinen pääaihe käsittelee dupleksitilojen kehitystä ja analyysiä; ne määrittävät, miten välitinlinkki uudelleenkäyttää taajuuskaistoja jokaisessa hypyssään. Erityisesti "full-duplex"-tila nostetaan esiin toteuttamiskelpoisena ja edistyneenä vaihtoehtona perinteiselle "half-duplex"-tilalle vaikka sen luontainen itse-interferenssi otetaankin huomioon. Uusia tekniikoita kehitetään ja arvioidaan itse-interferenssin poistoa varten ja lähetystehon säätö esitetään vastakeinona jäännöshäiriölle. Lopulta määritetään pohjimmaiset kriteerit, joiden perusteella dupleksitilat voi asettaa paremmuusjärjestykseen, joka toimii näiden vertailuna mutta myös mahdollistaa opportunistisen tilanvalinnan lähetyksen aikana.

Toinen pääaihe käsittelee välitysprotokollien kehitystä ja analyysiä; ne määrittelevät signaalinkäsittelyn, joka tehdään välittimissä vastaanoton ja uudelleenlähetyksen välissä. Tämä tutkielma tunnistaa kattavan joukon vaihtoehtoja OFDM(A)-välitysprotokollien suunnittelulle ja arvioi niiden yhdistelmien toimintaa. Samankaltainen analyysi suoritetaan myös dupleksitiloille ja monen käyttäjän vuoronjaolle. Lisäksi kehitetään uusi analyyttinen kehys, jolla tutkitaan kanavien viivehajontaa pelkkään vahvistukseen perustuvissa monihyppyisissä OFDM-linkeissä kun otetaan huomioon kantoaaltojen ja symbolien väliset häiriöt sekä aikasynkronisointivirheet.

Läpi koko tutkielman dupleksitilojen ja välitysprotokollien kehitys tehdään yhdessä tilastollisen tehokkuusanalyysin kanssa, joka mahdollistaa täsmälliset vertailut aikaisempien ja ehdotettujen konseptien välillä. Erityisesti kaikki tulokset muodostetaan suljetun muodon kaavojen avulla. Esitetty analyysi kattaa kaikki olennaiset systeemivariaatiot mukaan lukien tyypilliset protokollat sekä ala- ja ylälinkin tiedonsiirron havainnollistaen näiden eroja.

Avainsanat OFDM, OFDMA, langaton tiedonsiirto, välittimet

ISBN (painettu) 978-952-60-5714-9	**ISBN (pdf)** 978-952-60-5715-6	
ISSN-L 1799-4934	**ISSN (painettu)** 1799-4934	**ISSN (pdf)** 1799-4942
Julkaisupaikka Helsinki	**Painopaikka** Helsinki	**Vuosi** 2014
Sivumäärä 300	**urn** http://urn.fi/URN:ISBN:978-952-60-5715-6	

To the women in my life

Preface

The research work for this doctoral thesis was carried out in the Department of Signal Processing and Acoustics at Aalto University School of Electrical Engineering (formerly known as the Signal Processing Laboratory at Helsinki University of Technology), Helsinki, Finland, around the years 2008–2011 under the supervision of Professor Risto Wichman whose group was part of the Smart Radios and Wireless Research (SMARAD) Center of Excellence, nominated by the Academy of Finland for the periods 2002–2007 and 2008–2013. My doctoral studies, and especially all the coursework, were also greatly facilitated by a position in the nationwide postgraduate program of the Graduate School in Electronics, Telecommunications and Automation (GETA) from May 2006 to April 2010.

A part of these results were also reported to industry research projects funded by Nokia Siemens Networks (now Nokia Solutions and Networks) from October 2006 to December 2010 and Renesas Mobile Europe (now Broadcom) from April to September in 2012. The wrap-up phase in 2013 was mainly funded by SMARAD allowing me finally to concentrate almost completely on manuscript preparation. Recently I have been working on projects "In-band Full-Duplex MIMO Transmission: A Breakthrough to High-Speed Low-Latency Mobile Networks," funded since September 2012 by the Academy of Finland, and "Full-Duplex Cognitive Radio: Technology and Application to Cognitive M2M Communications," funded since January 2013 by the Finnish Funding Agency for Innovation (Tekes).

My postgraduate research was also supported by personal grants from the Emil Aaltonen Foundation, the Finnish Science Foundation for Economics and Technology (KAUTE), the Foundation of the Finnish Society of Electronics Engineers (EIS), HPY Research Foundation, the Jenny and Antti Wihuri Foundation, and the Nokia Foundation; I greatly appreciate their generosity and belief in my eventual success.

First of all, I am grateful to my supervisor Prof. Risto Wichman for his unceasing support that has allowed me to concentrate on science and for trusting me to choose and develop research topics by myself. My advisor Dr. Stefan Werner fulfilled his duty perfectly by asking the right technical questions (but letting me to find the answers!) as well as by mentoring me to understand that academic work involves much more than writing. Perhaps I could have written all the papers alone but certainly they would not have been accepted for publication without his guidance and spurring. He taught me to stand up and fight when we defeated Prof. Lizard together and comforted me when recovering from my encounter with Dr. Dementor.

The preliminary examiners of this dissertation, Dr. Golnaz Farhadi and Dr. Himal A. Suraweera, are greatly acknowledged for their glowing review statements and discerning comments which, I believe, significantly improved the clarity of presentation. With this evidence, it is no wonder at all why Dr. Suraweera has been recognized as an Exemplary Reviewer multiple times in the best journals of the field. I must also express special gratitude to Dr. Farhadi for accepting the invitation to serve as an examiner on such extremely short notice. Furthermore, I would like to thank in advance Prof. Robert Schober for finding time to serve as an opponent at the public examination. It is a privilege to get grilled, hopefully in a friendly manner though, by such a renowned world-class scientist, and I am already looking forward to interesting technical discussions.

It has been a really great pleasure to co-author papers with so many talented researchers: Thank you all and especially Prof. Katsuyuki Haneda, Dr. Fernando Gregorio, Prof. Juan Cousseau, Viet-Anh Le, Dr. Renaud-Alexandre Pitaval, Prof. Jyri Hämäläinen, and Dr. Timo Roman! In addition to the work reported herein, I have recently very much enjoyed collaborating with Pramod Mathecken, Emilio Antonio-Rodríguez, Dr. Mikko Vehkaperä, Dani Korpi, Dr. Ville Syrjälä, Dr. Lauri Anttila, Prof. Mikko Valkama, Umut Ugurlu, and Dr. Prathapasinghe Dharmawansa.

I am thankful for all the opportunities to gain experience and contacts as well as to disseminate my thoughts beyond the academic world. My work for the industry was supervised by Drs. Klaus Doppler, Ari Hottinen, Pirjo Pasanen, and Kari Kalliojärvi at Nokia Research Center; Bernhard Raaf and Dr. Simone Redana at Nokia Siemens Networks; and Juho Pirskanen and Dr. Yrjö Kaipainen at Renesas Mobile Europe. In general, Profs. Wichman, Hämäläinen and Olav Tirkkonen are recognized for setting up cooperation between the companies and the university.

Special thanks go to two scientists whom I regard as idols that initiated my research career: Prof. Patric Östergård, who gave me a chance to do science after my freshman year which eventually led to my first journal publication; and Dr. Ari Hottinen, whose talent as a genuine innovator I admire — we actually discussed full-duplex MIMO relaying already as early as June 2005 (although calling it something else back then).

I also acknowledge GETA directors Prof. Iiro Hartimo and Prof. Ari Sihvola for supervising my studies; the department head Prof. Jorma Skyttä for patience with me despite my being "an HR-problem"; Prof. Visa Koivunen for so generously lending his contacts for postdoc position chasing; secretaries Mirja Lemetyinen and Heidi Koponen as well as GETA coordinator Marja Leppäharju for always handling all practical matters smoothly; and network admin Tarmo Simonen for solving my IT-problems.

The folks of the Signal Processing Lab have always been excellent company at work, at lunch, at courses, while traveling etc. I am only too pleased to be acquainted with Dr. Traian Abrudan, Tuomas Aittomäki, Dr. Sachin Chaudhari, Dr. Mei Yen Cheong, Michal Čierny, Dr. Mário Costa, Dr. Jan Eriksson, Juha Forsten, Dr. Pekka Jänis, Dr. Kimmo Järvinen, Neelabh Kashyap, Dr. Jarmo Lundén, Dr. Alexandra Oborina, Sampo Ojala, Jaakko Ojaniemi, Jan Oksanen, Keijo Pölönen, Jayaprakash Rajasekharan, Victor del Razo, Dr. Jussi Salmi, Karol Schober, Prof. Sergiy Vorobyov, and Dr. Eduardo Zacarías, to name but a few alphabetically.

Last but foremost, I would like to thank heartily my dear family. Although having no direct effect on scientific matters, they are the tower of strength to me: my father Pekka, grandfather Ahti, and grandmothers Aune and Laila; my brother Teemu (who will, surely, soon qualify as an English teacher but at my own risk I didn't let him proof-read this book!); and my sisters Mariia and Terttu as well as brothers-in-law (or candidates thereof). I regret that working on this thesis has taken so much time which I could have spend with you instead. My ultimately warmest thanks go to you Jutta-Noora, the muse to my research work, for all love and happiness you have brought me over the last ten years.

Otaniemi, May 26, 2014,

Taneli Riihonen

Contents

List of Abbreviations

2D	two-dimensional
AD	analog-to-digital
AF	amplify-and-forward
AP	adaptive pairing
APS	average power scaling
AS	antenna selection
AWGN	additive white Gaussian noise
BER	bit-error rate
BS	base station
CDF	cumulative distribution function
CDMA	code-division multiple access
CP	cyclic prefix
CSI	channel state information
D	destination
DA	digital-to-analog
DAS	distributed antenna system
DF	decode-and-forward
DFT	discrete Fourier transform
DL	downlink
DT	direct transmission

DVB	digital video broadcasting
DVB-H	digital video broadcasting for handheld terminals
DVB-T	digital video broadcasting for terrestrial terminals
ES	eigenbeam selection
EVM	error-vector magnitude
FCF	frequency-correlation function
FD	full-duplex
FDD	frequency-division duplexing
FFT	fast Fourier transform
FG	fixed gain
FP	fixed pairing
GETA	Graduate School in Electronics, Telecommunications and Automation
HD	half-duplex
ICI	inter-carrier interference
IEEE	Institute of Electrical and Electronics Engineers
IPS	instantaneous power scaling
I/Q	in-phase/quadrature
ISI	inter-symbol interference
LOS	line-of-sight
LTE	Long-Term Evolution
MIMO	multiple-input multiple-output
MISO	multiple-input single-output
MMSE	minimum mean square error
MPC	multipath component
MRC	maximum ratio combining
MSE	mean square error

NB no buffering

NLOS non-line-of-sight

NSP null-space projection

OCR on-channel repeater

OFDM orthogonal frequency-division multiplexing

OFDMA orthogonal frequency-division multiple access

OR optimal resources

PA power amplifier

PDF probability density function

PDP power–delay profile

PRB physical resource block

R relay or repeater

RB resource block

RD relay-to-destination

RFID radio-frequency identification

RMS root mean square

RN relay node

RP random pairing

RR relay-to-relay

RW resource block-wise

S source

SC-FDMA single-carrier frequency-division multiple access

SD source-to-destination

SFN single-frequency network

SIMO single-input multiple-output

SINR signal-to-interference and noise ratio

SISO single-input single-output

SMARAD Smart Radios and Wireless Research

SNR signal-to-noise ratio

SR source-to-relay

SVD singular value decomposition

SW symbol-wise

TDC time-domain cancellation

TDD time-division duplexing

TOR time of reference

UE user equipment

UL uplink

UR uniform resources

VG variable gain

WB with buffering

WINNER Wireless World Initiative New Radio

WLAN wireless local area network

WSSUS wide-sense stationary uncorrelated scattering

List of Symbols

$\mathbf{0}$	zero matrix with compatible dimensions
$\mathbf{C}$	filtering matrix for cancellation
$\mathcal{C}$	link capacity
$\bar{\mathcal{C}}$	average link capacity
$\mathcal{C}_{\mathrm{DT}}$	capacity of direct transmission
$\mathcal{C}_{\mathrm{FD}}$	capacity of full-duplex relaying
$\bar{\mathcal{C}}_{\mathrm{FD}}$	average capacity of full-duplex relaying
$\mathcal{C}_{\mathrm{HD}}$	capacity of half-duplex relaying
$\bar{\mathcal{C}}_{\mathrm{HD}}$	average capacity of half-duplex relaying
$\mathcal{C}_{\mathrm{hybrid}}$	capacity of hybrid full/half-duplex relaying
$\bar{\mathcal{C}}_{\mathrm{hybrid}}$	average capacity of hybrid full/half-duplex relaying
$\mathcal{C}_{\mathrm{out}}$	outage capacity
$\mathcal{C}_{\mathrm{RD}}$	service link capacity
$\bar{\mathcal{C}}_{\mathrm{RD}}$	average service link capacity
$\mathcal{C}_{\mathrm{SR}}$	backhaul link capacity
$\bar{\mathcal{C}}_{\mathrm{SR}}$	average backhaul link capacity
d_{RR}	distance between antenna arrays
$\mathcal{E}\{\cdot\}$	expectation operation
$E_k(z)$	exponential integral function
$F_{\Delta I}(\cdot)$	cumulative distribution function of additional isolation

$F_{I_{\text{physical}}}(\cdot)$	cumulative distribution function of physical isolation
$\mathbf{G}_{\text{rx}}$	filtering matrix for receive-side spatial suppression
$\mathbf{G}_{\text{tx}}$	filtering matrix for transmit-side spatial suppression
$\mathbf{H}_{\text{RD}}$	relay-to-destination channel matrix
$\mathbf{H}_{\text{RR}}$	relay-to-relay loopback channel matrix
$\tilde{\mathbf{H}}_{\text{RR}}$	estimated relay-to-relay loopback channel matrix
$\boldsymbol{\Delta}\tilde{\mathbf{H}}_{\text{RR}}$	additive error in $\tilde{\mathbf{H}}_{\text{RR}}$
$\mathbf{H}_{\text{SD}}$	source-to-destination channel matrix
$\mathbf{H}_{\text{SR}}$	source-to-relay channel matrix
$\tilde{\mathbf{H}}_{\text{SR}}$	estimated source-to-relay channel matrix
$\boldsymbol{\Delta}\tilde{\mathbf{H}}_{\text{SR}}$	additive error in $\tilde{\mathbf{H}}_{\text{SR}}$
h_{RD}	relay-to-destination channel coefficient
h_{RR}	relay-to-relay loopback channel coefficient
h_{SD}	source-to-destination channel coefficient
h_{SR}	source-to-relay channel coefficient
$\mathbf{I}$	identity matrix
I_{physical}	physical isolation
M	number of hops
$\mathbf{n}$	generic noise vector
N_{CP}	number of samples in cyclic prefix
N_{D}	number of receive antennas in destination(s)
N_{FFT}	number of subcarriers
$\hat{N}_{\text{max}}$	maximum of $\hat{N}_{\text{rx}}$ and $\hat{N}_{\text{tx}}$
$\hat{N}_{\text{min}}$	minimum of $\hat{N}_{\text{rx}}$ and $\hat{N}_{\text{tx}}$
N_{RB}	number of resource blocks
N_{rx}	number of receive antennas in relay

$\hat{N}_{\mathrm{rx}}$	number of receive streams in relay
N_{S}	number of transmit antennas in source(s)
N_{tx}	number of transmit antennas in relay
$\hat{N}_{\mathrm{tx}}$	number of transmit streams in relay
$P(t)$	power–delay profile (PDP)
P_{D}	total received power at destination
P_{I}	interference power
P_{ICI}	inter-carrier interference power
P_{ISI}	inter-symbol interference power
$P_M(t)$	hypoexponential PDP
P_{N}	noise power
$\mathcal{P}_{\mathrm{out}}$	outage probability
P_{R}	transmit power of relay
p_{R}	normalized transmit power of relay
$\bar{p}_{\mathrm{R}}$	normalized long-term transmit power of relay
$P_{\mathrm{RD}}(t)$	PDP of relay-to-destination channel
$P_{\mathrm{RR}}(t)$	PDP of relay-to-relay loopback channel
P_{S}	transmit power of source
p_{S}	normalized transmit power of source
$P_{\mathrm{SD}}(t)$	PDP of source-to-destination channel
$P_{\mathrm{SR}}(t)$	PDP of source-to-relay channel
P_{U}	useful signal power
$\mathbf{R}_{\mathbf{x}}$, $\mathbf{R}_{\mathbf{n}}$	covariance matrices of random vectors $\mathbf{x}$ and $\mathbf{n}$
$\mathbf{S}_{\mathrm{rx}}$	receive-side antenna or eigenbeam selection matrix
$\mathbf{S}_{\mathrm{tx}}$	transmit-side antenna or eigenbeam selection matrix
T_{CP}	duration of cyclic prefix

T_{FFT}	duration of symbol payload
t_{RD}	time share of service link
t_{SR}	time share of backhaul link
$\tilde{\mathbf{U}}_{\mathrm{RR}}$	matrix containing left singular vectors of $\tilde{\mathbf{H}}_{\mathrm{RR}}$
$\tilde{\mathbf{V}}_{\mathrm{RR}}$	matrix containing right singular vectors of $\tilde{\mathbf{H}}_{\mathrm{RR}}$
$w(t)$	weighting function
$\mathbf{x}$, $\mathbf{y}$	generic signal vectors
$\|\mathbf{x}\|_2$	Euclidean norm of $\mathbf{x}$
$\mathbf{X}$	generic matrix
$\mathbf{X}^H$	conjugate transpose of $\mathbf{X}$
$\|\mathbf{X}\|_F$	Frobenius norm of $\mathbf{X}$
$\mathbf{X}^{-1}$	inverse of $\mathbf{X}$
$\mathbf{X}^+$	pseudoinverse of $\mathbf{X}$
$\mathrm{rk}\{\mathbf{X}\}$	rank of $\mathbf{X}$
$\mathrm{tr}\{\mathbf{X}\}$	trace of $\mathbf{X}$
$\mathbf{X}^T$	transpose of $\mathbf{X}$
β	amplification factor
γ	SNR or SINR
$\bar{\gamma}$	average SNR or SINR
$\hat{\gamma}$	target SINR
γ_{D}	SINR at destination input
γ_{DT}	SNR of direct transmission
γ_{FD}	SINR of full-duplex relaying
γ_{HD}	SNR of half-duplex relaying
γ_{R}	SINR at relay input
γ_{RD}	SNR of relay-to-destination channel

$\bar{\gamma}_{\mathrm{RD}}$	average SNR of relay-to-destination channel
Γ_{RR}	break-even level for γ_{RR}
γ_{RR}	SNR of relay-to-relay loopback channel
$\bar{\gamma}_{\mathrm{RR}}$	average SNR of relay-to-relay loopback channel
Γ_{SD}	break-even level for γ_{SD}
γ_{SD}	SNR of source-to-destination channel
$\bar{\gamma}_{\mathrm{SD}}$	average SNR of source-to-destination channel
γ_{SR}	SNR of source-to-relay channel
$\bar{\gamma}_{\mathrm{SR}}$	average SNR of source-to-relay channel
γ_{th}	target threshold for S(I)NR
Δ_{GM}	gain margin
ΔI	additional isolation
$\epsilon_{\mathbf{H}}$	level of channel estimation error
$\epsilon_{\mathbf{x}}$	error-vector magnitude (EVM)
η	modulation efficiency
λ	system load
σ^2_{D}	noise power at destination
σ^2_{R}	noise power at relay
$\tilde{\mathbf{\Sigma}}_{\mathrm{RR}}$	diagonal matrix containing singular values of $\tilde{\mathbf{H}}_{\mathrm{RR}}$
$\tilde{\Sigma}_{\mathrm{RR}}[n]$	singular value of $\tilde{\mathbf{H}}_{\mathrm{RR}}$
$\bar{\tau}$	mean delay
τ_{1st}	delay of first multipath component
τ_{max}	delay of strongest multipath component
τ_{R}	processing delay in relay
τ_{TOR}	time of reference
$\chi^{\mathrm{DL}}_{\mathrm{hybrid}}$	switching boundary in downlink
$\chi^{\mathrm{UL}}_{\mathrm{hybrid}}$	switching boundary in uplink

1. Introduction

Wireless communication, which is the general context of this thesis, means the transfer of information or data between remote locations without physical contact, e.g., cables, or delivering material messages. Conversation already represents basic wireless information exchange, but only technical appliances facilitate instant information propagation beyond earshot or even to anywhere in the world. No doubt such technology is vital for modern civilizations serving as a catalyst for many cultural and social activities. In what follows, common *electromagnetic fields* oscillating at *radio* frequencies, i.e., "microwaves", are adopted as the sole medium for wireless communication while leaving aside ancient techniques, e.g., semaphore telegraphs, heliographs, and fire/smoke/drum/bugle signaling.

The general scope of this thesis is to study *multihop relaying* within wireless communication systems. Thus, all focal concepts considered in this study involve, in some form, indirect data transmission through two or more successive radio links which are connected in series by so-called *relays*. As an example, one may keep in mind a repeater device deployed in a cellular mobile communication system for extending coverage.

This thesis contributes within the field of *signal processing in wireless communications* which deals with operations done by *transceivers*, i.e., transmitter–receiver pairs, in between electronics and higher abstraction layers that merge separate links into networks. Given its scope, the study thus concerns the design and analysis of *relaying protocols* and *modes* in relation to relays' processing tasks between reception and retransmission.

The remainder of this chapter is organized as follows for introducing the foundations and outcomes of this dissertation. First, Sections 1.1 and 1.2 specify the motivation and scope of the study. Second, Sections 1.3 and 1.4 summarize scientific contributions reported herein and the author's share in related publications. Finally, Section 1.5 describes the structure of the following chapters while distinguishing the prior art from novel results.

1.1 Motivation for the Thesis

The general objective of this study is to improve the performance of wireless communication systems. In a broad sense, this requires achieving enhanced signal quality at receiver terminals together with economical usage of natural resources, e.g., radio spectrum and transmitted energy, while still aiming at reasonable processing complexity. Furthermore, the performance of the considered systems needs to be measured analytically on the side for demonstrating true improvements. The motivation for this thesis is discussed also in Section 2.4 by contrasting it with related works that are summarized in a literature survey.

There are many emerging concepts that could efficiently render high performance in the next generation of wireless systems; relaying in itself is already one of them. This study begins from the presumption that relays are employed in systems at hand after which open research questions arise in investigating how to design and operate relay links optimally when they exploit other advanced concepts. This gives motivation for developing relaying technology in conjunction with multiple-input multiple-output (MIMO) techniques, spectrum reuse, transmit power adaptation, and various signal-processing options for multicarrier protocol design.

The study is motivated also by the general interest to provide new theoretical insight into different relaying concepts. Especially, it is important to conduct the design of relaying modes and protocols all the time in parallel with their performance analysis which also facilitates discerning comparisons between existing and proposed schemes.

1.2 Scope of the Thesis

The general scope of this study is on the signal-processing aspects of multihop relaying. Thus, its contributions are inherently inclined toward the design and analysis of physical-layer protocols and link-level operation modes. The focus is on systems where signals are modulated with orthogonal frequency-division multiplexing (OFDM) and relays are infrastructure-based network elements rather than mobile terminals. The scope is discussed also in Section 2.4 by contrasting it with related works.

The scope on infrastructure-based relaying further implies that the main usage scenario for relays is to extend the coverage of a primary transceiver, e.g., a cellular base station, when the corresponding direct signals are

heavily attenuated. Both downlink and uplink cases are studied, and systems may involve multihop backhauls with more than one relay in series.

The study focuses on relaying systems that employ OFDM and its multiuser variant, orthogonal frequency-division multiple access (OFDMA); they are collectively referred to as OFDM(A). Thus, the analysis is not limited to concern single-subcarrier models but the true multicarrier nature of OFDM(A) relaying protocols is reflected in their design, e.g., by taking into account frequency-domain processing options, inter-carrier interference (ICI), and inter-symbol interference (ISI) as well as multipath fading. Yet main narrowband concepts, i.e., so-called amplify-and-forward (AF) and decode-and-forward (DF) protocols, are also covered.

Throughout the thesis, its contributions are established by presenting rigorous statistical analysis by means of closed-form performance expressions rather than plain computer simulations.

1.3 Contributions of the Thesis

In general, this thesis contributes by developing new advanced relaying techniques and analyzing extensively the performance of multihop links including comparisons and combinations of earlier and proposed concepts. These aspects are classified into two main themes: *modes* and *protocols*. The following discussion is an overview of the main contributions while specific results are detailed in the beginning of each technical chapter.

The relaying mode in use is a central factor for link-level performance. Several full-duplex (FD) relaying concepts are developed herein to facilitate spectrum reuse and offer a feasible alternative to conventional half-duplex (HD) operation. Especially, the study recognizes the loopback self-interference of FD relays and formulates a fundamental rate–interference trade-off specifying the choice between the FD mode and the HD mode when the former is subject to self-interference and the latter needs more spectrum resources. Firstly, new schemes are developed for the mitigation of self-interference, e.g., by exploiting advanced MIMO techniques, and evaluated extensively based on simulations, analysis, and experiments. This characterizes the main factors which render residual distortion and leave an opportunity for consequently developing transmit power adaptation to alleviate its effect. Finally, the criteria to prefer one mode over the other are determined which not only serves as a comparison between the modes but allows for opportunistic mode switching during operation.

Relaying protocols specify signal processing tasks done between reception and retransmission in a relay node. Thus, their design directly defines and offers means of improving the performance of multihop links. This study identifies a comprehensive set of design options for OFDM(A) relaying protocols and evaluates their combinations by deriving closed-form capacity expressions. Similar analysis is conducted for evaluating the relaying modes as a baseline for opportunistic mode switching. Different variations of AF and DF protocols are analyzed in the case of multiuser multihop relaying in terms of a large set of performance metrics; the results characterize the benefit of multiuser scheduling and the cost of having a wireless backhaul while being valid for any duplexing scheme. In order to characterize the relations between the number of hops, time synchronization and OFDM symbol parameters, a new framework is developed for studying the delay-spread properties of non-regenerative multihop OFDM links in conjunction with ICI and ISI.

1.4 Summary of Author's Contributions and Publications

Although this dissertation is composed in the form of a monograph, all the essential parts of its results are presented also in twenty-nine original scientific contributions **[208–236]**[1] published in open literature with proper referee practice. This implies that the presented material has already undergone rigorous peer-review in addition to the actual preliminary examination of this manuscript by eminent scholars.

The main scientific works comprise eight journal-level articles **[214,217, 220,221,223,232,234,236]**, eighteen papers in the proceedings of international conferences **[208–213,215,218,219,222,224,225,227,229–231,233, 235]**, and three domestic workshop presentations **[216, 226, 228]**. Especially, five of the journal articles are full-length regular papers and all the foregoing conferences are regarded as highly respectable scientific events in the field. Furthermore, the author of this thesis has himself attended most of the conferences and the workshops and presented the papers.

In addition, the author of this thesis has contributed to several related publications, including five journal articles **[82, 113, 146, 172, 174]**, fourteen conference papers **[26, 81, 83, 97, 98, 145, 147, 148, 158, 173, 201, 205, 296, 309]**, and two patent applications **[53, 54]**. With the primary pub-

[1] References to articles in which the author of this thesis is one of the (co-)authors, i.e., self-citations, are typeset in a boldfaced font throughout the monograph.

lications **[208–236]**, this totals round fifty independent scientific works during the progress of the postgraduate research. It can be especially highlighted that six of the articles are full-length regular papers in the most prestigious TRANSACTIONS of the Institute of Electrical and Electronics Engineers (IEEE), and that the author has presented his work in the flagship events such as IEEE Global Communications Conference.

The contributions of the author are laid out herein with a unified presentation while **[208–236]** are independent publications varying in focus and notation.[2] For this monograph, the scope of the work is crystallized and the vast research material is distilled by extracting, in the author's opinion, the best and most significant results. Yet, the contribution of this thesis is not a subset or a superset of that of **[208–236]**, but they are complementary to each other: The material left out from this thesis offers alternative perspectives for applying the results in a broader scope, and the thesis contains new consolidating material that is not available in the papers. Results from the supplementary publications are referenced in appropriate locations to explain how this thesis fits in the general scope of the author's wide-ranging research interests.

The author confirms that the work presented in this monograph is completely his own and that appropriate credit is given whenever reference is made to the work of others. The supervisor and the instructor of this thesis have only aided the manuscript drafting by giving proof-reading comments to improve its presentation.

In related publications **[208–236]**, the author of this thesis is the first author and has had the sole responsibility in everything during the research cycle: the overall planning of research work, formulating the research problems, developing the original ideas, performing the analysis as well as the simulations, and writing the papers. The co-authors have only supervised the first author by giving feedback to guide the research process and provided proof-reading comments on the paper drafts with the following three exceptions: For conference paper **[208]**, the second author processed the channel measurement data (courtesy of the third and fourth authors) following detailed instructions given by the author of this thesis; for conference paper **[224]**, the fourth author sketched out the integrals presented in its Appendix; and for conference paper **[235]**, the second author wrote a couple of sentences in its Section II-B.

[2] All raw material adapted from the original IEEE copyrighted papers is reproduced with permission.

1.5 Structure of the Thesis

The main body of this dissertation is organized as summarized below. This outline specifies also the major correspondences and differences between the material presented herein and in the original publications.

- The prologue part forms a baseline for developing new contributions.

  Chapter 2 presents an overview of multihop OFDM(A) relaying technologies and a survey on reference literature about their analysis. In addition to the background material, optimal symbol dimensions are solved for a new two-dimensional OFDM modulation format; this takes place in Section 2.1.2 which is partly based on **[228,234]**.

  After this point, the focus shifts from summarizing textbook knowledge and the recent results of other researchers to presenting mainly the author's own scientific contributions. The following parts will be thus referred to as "technical chapters".

- The first part of the technical content focuses on *relaying modes*.

  Chapter 3 studies the mitigation of loopback self-interference occurring when relays operate in the full-duplex mode. The main novel contribution lies in developing and evaluating MIMO techniques for spatial-domain suppression; scarce parallel work is reviewed in Section 3.2. The results are not restricted to any specific protocol.

  This chapter is partly based on **[208, 215, 219, 221]**. However, the chapter contains also a significant amount of consolidating material for binding together simulation, analytical and experimental results originally presented in separate publications.

  Chapter 4 studies transmit power control in full-duplex relaying for alleviating the effect of residual distortion remaining after mitigation. The proposed schemes are analyzed in terms of closed-form outage probability expressions in both downlink and uplink transmission through an infrastructure-based relay.

  This chapter is partly based on **[214, 220, 224, 225]**. However, the original article **[214]** considers only amplify-and-forward relaying while the chapter considerably extends the study to cover also the important decode-and-forward counterpart. Thus, roughly half of the contributions can be regarded as previously unpublished.

Chapter 5 studies the rate–interference trade-off between half-duplex and full-duplex relaying in the presence of residual self-interference. This not only involves comparison between the modes but also leads to the development of opportunistic mode switching. The study covers both amplify-and-forward and decode-and-forward relaying.

This chapter is partly based on **[213, 218, 220, 225]**.

The results of the foregoing chapters are summarized also in **[207]**.

- The second part of the technical content focuses on *relaying protocols*.

Chapter 6 studies non-regenerative OFDM relaying over cascaded multipath channels. Assuming time-domain amplification, the study is formulated in terms of the resulting multihop power–delay profiles. Gain control in full-duplex repeaters is revisited in Section 6.4.1.

This chapter is partly based on **[210, 216, 217]** but the notation is revised completely in order to achieve unified presentation.

Chapter 7 studies multiuser scheduling in multihop relay links by deriving closed-form expressions for a comprehensive set of performance measures. Both downlink and uplink relaying are covered.

This chapter is partly based on **[158,232]**. However, the original article **[232]** considers only amplify-and-forward protocols while the chapter considerably extends the study to cover also decode-and-forward relaying. Furthermore, the statistical analysis is generalized to the case of non-identical fading distributions. Almost all of this material can be thus regarded as previously unpublished.

Chapter 8 studies the performance of infrastructure-based multiuser multihop OFDM(A) relay links in downlink transmission. The analysis characterizes a comprehensive set of feasible relaying protocols and derives closed-form capacity expressions for all of them.

This chapter is partly based on **[233, 235, 236]**.

As indicated above, only the scope of Chapter 6 is limited to a specific variation of amplify-and-forward relaying because the adopted analytical methodology would be irrelevant for other protocols. However, even these results are briefly contrasted with the decode-and-forward case.

- The epilogue part presents the conclusion of this dissertation.

Chapter 9 summarizes the contributions of the technical chapters. Future research directions are also envisioned.

2. Overview of Baseline Concepts and Research Literature

Multihop relaying and OFDM(A), i.e., orthogonal frequency-division multiplexing or multiple access, are common baseline techniques for all the contents of this dissertation. Presenting a tutorial on them is unnecessary herein but some central physical- and link-layer details still deserve an overview to form solid background for the technical chapters and to define nomenclature thereof. Likewise, a survey on recent literature and landmark publications is worthwhile for situating novel contributions in a proper context. The remainder of this chapter is organized as follows.

Section 2.1 deals with the physical-layer aspects of OFDM transceivers specifying parameters related to the modulation format, transmitter imperfections and receiver time synchronization. Other key attributes are linked to narrowband single-subcarrier and wideband multicarrier signal and channel models under multipath propagation. A new symbol structure is also introduced and optimized for the use of full-duplex relaying.

Section 2.2 summarizes the essential physical- and link-layer aspects of different relaying scenarios, half- and full-duplex operation modes and forwarding protocols. A brief survey on relaying concepts at large helps to outline the scope of this study and differentiate it from earlier works. In particular, open research topics are found regarding loopback self-interference in full-duplex relays and a trade-off between duplexing modes.

Section 2.3 presents a survey on related analytical studies of relay protocols and links emphasizing the signal processing aspects of multiantenna, multihop and OFDM(A) relaying techniques that are relevant in the scope of this study. Nevertheless, the reviewed material indicates that earlier works typically focus on two-hop single-subcarrier transmission and mobile half-duplex relays in contrast to the scope adopted herein.

Finally, Section 2.4 sums up the background material surveyed for this study and draws generalized conclusions as a basis for the research problems that are formulated and solved in the following technical chapters.

2.1 Orthogonal Frequency-Division Multiplexing (OFDM)

All the technical chapters of this study are formulated in the popular context (or, occasionally, subtext) of OFDM modulation. The history of OFDM is comprehensively related already in [301]: After early origins in wireline data transmission, it was introduced to mobile radio communications in [44] and then gradually adopted for almost all modern wideband wireless systems. The physical- and link-layer principles of OFDM modulation can be also read in a textbook of choice. Thereby, only some essential properties need to be highlighted in the following by recapitulating details on symbol structures, signal and channel models, transmitter distortion effects as well as imperfections in receiver time synchronization.

2.1.1 OFDM(A) Transmission and Reception

Modulation and Demodulation

In an OFDM transmitter, frequency-domain data samples are modulated to subcarriers by calculating inverse fast Fourier transform (FFT) after which the time-domain block is extended by copying a cyclic prefix (CP). The operations are parametrized by N_{FFT} and N_{CP} denoting the respective block sizes; their integer values can be translated to T_{FFT} and T_{CP} measured in time units when subcarrier spacing or signal bandwidth is set. Conversely, demodulation employs FFT which requires a time of reference (TOR) to locate the beginning of the data block after skipping the CP. Synchronization can be parametrized by τ_{TOR} measured in time units.

With respect to physical-layer processing, orthogonal frequency-division multiple access (OFDMA) is the same as OFDM except for the conceptual difference that OFDMA subcarriers may be modulated with data that are designated for *different* receivers. In the opposite direction, multiple synchronized terminals would transmit simultaneously on different subcarriers but the sibling of OFDMA, i.e., single-carrier frequency-division multiple access (SC-FDMA), is often used instead in such scenarios.

Multicarrier Signal Models

When $x(t)$ represents the time-domain output signal of an OFDM transmitter, the corresponding input signal of a receiver can be expressed as

$$y(t) = h(t) * x(t) + \text{noise}, \tag{2.1}$$

where $h(t)$ denotes a multipath radio channel between modulation and reception shaping the signal spectrum through convolution operation ($*$).

In practice, the orthogonality of subcarriers is always slightly broken when $y(t)$ is demodulated because the length of the CP window may be insufficient and $h(t)$ may remain imperfectly stationary over the FFT window. This causes inter-carrier interference (ICI) and inter-symbol interference (ISI) which are often modeled by simply increasing receiver noise levels. However, their effects as such become a relevant research topic whenever the delay spread of $h(t)$ is pronounced. The accurate signal-to-interference and noise ratio (SINR) of OFDM reception, which is denoted by γ, can be calculated based on the results of [263]: In Chapter 6, their methodology is transformed to the case of continuous multipath profiles and then applied for the study of multihop relay links.

The physical-layer efficiency of OFDM modulation can be defined as

$$\eta \triangleq \frac{T_{\mathrm{FFT}}}{T_{\mathrm{FFT}} + T_{\mathrm{CP}}} = \frac{N_{\mathrm{FFT}}}{N_{\mathrm{FFT}} + N_{\mathrm{CP}}}, \tag{2.2}$$

which measures the overhead incurred by the CP. Consequently, the existence of ICI and ISI imposes a trade-off between η and γ: Higher modulation efficiency comes at the cost of reduced SINR due to interference.

Single-Subcarrier Signal Models

Assuming ICI and ISI are insignificant, it is common to formulate system models based on the narrowband frequency-domain equivalent of (2.1):

$$y[n] = h[n]\, x[n] + \text{noise (and interference)}, \tag{2.3}$$

which implicitly represents the signal of the nth OFDM subcarrier. In fact, this OFDM subtext is often left unmentioned in related literature. However, the subcarriers may be also grouped into resource blocks (RBs), each of which is modeled by (2.3); herein their number is denoted by N_{RB} and variable $\gamma[n]$ represents the signal-to-noise ratio (SNR) of the nth RB.

In principle, multiple-input multiple-output (MIMO), i.e., multiantenna, techniques can be used together with OFDM by simply connecting a parallel transceiver to each antenna element. Thereby, the single-input single-output (SISO) model of (2.3) is usually directly extended to a vector form:

$$\mathbf{y}[n] = \mathbf{H}[n]\, \mathbf{x}[n] + \text{noise (and interference)}. \tag{2.4}$$

This highlights the synergy of MIMO–OFDM where spatial filtering, e.g., beamforming, is not complicated by the frequency selectivity of channels.

One may note that, despite of a risk of minor confusion, subcarrier indices ($[n]$) shall be omitted and replaced by time indices ($[i]$) whenever focus is on single-subcarrier transmission in an implicit OFDM context. Such models thus represent an arbitrary subcarrier in the ith symbol.

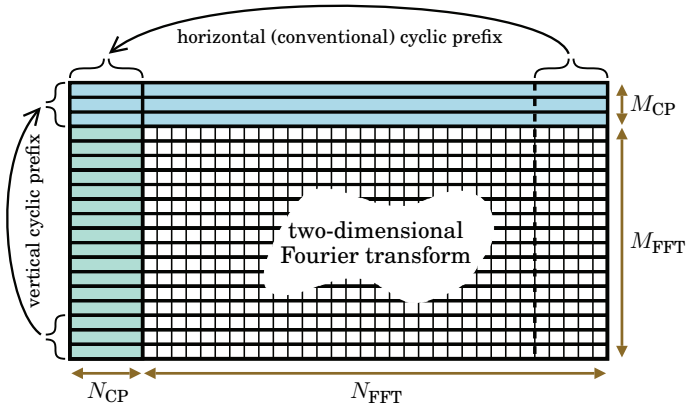

Figure 2.1. Two-dimensional (2D) OFDM symbol structure which is transmitted row-by-row starting from the upper-left corner. The conventional (one-dimensional) OFDM symbol structure is obtained as a special case by setting $M_{\mathrm{FFT}} = 1$ and $M_{\mathrm{CP}} = 0$, i.e., the vertical Fourier transform and cyclic prefix are omitted.

2.1.2 Two-Dimensional (2D) OFDM

Standard OFDM signaling has a disadvantage in relay applications: long processing delay. In particular, each FFT block must be fully received before demodulation and frequency-domain processing, due to which relayed signal components do not remain inside of the CP window together with direct components bypassing relays. This ISI problem can be avoided by splitting each symbol into multiple short FFT blocks and adding another CP to accommodate multipath spread due to relay processing delay [194]. The concept can be referred to as two-dimensional (2D) OFDM **[234]**.

The remainder of this section[1] is organized as follows. After defining the 2D symbol structure, its dimensions are optimized to maximize modulation efficiency (or to minimize the overhead of the CPs). Finally, numerical results exemplify the benefit of 2D OFDM modulation in relaying.

Symbol Structure

The 2D OFDM symbol structure is shown in Fig. 2.1. It contains M_{FFT} stacked conventional ("horizontal") OFDM symbols of length $N_{\mathrm{FFT}} + N_{\mathrm{CP}}$ and an extra "vertical" CP added after calculating FFT between the horizontal symbols. Effectively, 2D FFT is calculated for the data matrix. In demodulation, the horizontal CP with N_{CP} samples removes ICI due to normal multipath delay spread and the vertical CP with M_{CP} subsymbols removes ISI due to delay from frequency-domain processing in relays. One may refer to [194] for the exact definition of the transmitted signal.

[1] This section is partially based on the material presented in **[228, 234]**.

The physical-layer efficiency of 2D OFDM modulation becomes

$$\eta_{\text{2D}} \triangleq \frac{M_{\text{FFT}}\, N_{\text{FFT}}}{(M_{\text{FFT}} + M_{\text{CP}})(N_{\text{FFT}} + N_{\text{CP}})} = \frac{M_{\text{FFT}}}{M_{\text{FFT}} + M_{\text{CP}}} \cdot \eta \tag{2.5}$$

for which (2.2) is a special case with $M_{\text{FFT}} = 1$ and $M_{\text{CP}} = 0$. If $M_{\text{CP}} \geq 1$, $\eta_{\text{2D}} < \eta$ since $\frac{M_{\text{FFT}}}{M_{\text{FFT}}+M_{\text{CP}}} < 1$, i.e., the vertical CP causes extra overhead.

Optimal Symbol Dimensions

The modulation efficiency of 2D OFDM given in (2.5) depends on multiple parameters which can be optimized to minimize the overhead of the vertical CP. The characteristics of radio channels set some constraints though. To avoid significant ICI and ISI, the horizontal cyclic prefix needs to be longer than multipath delay spread limiting N_{CP} and channels should remain approximately static during the transmission of each symbol such that N_{tot} samples can be transmitted within expected coherence time.

The relaying scenario defines a constant value for M_{CP} while, to begin with, respective N_{CP} and N_{tot} can be set to the smallest and largest constants allowed by the radio environment. Especially, the total number of samples transmitted per each 2D OFDM symbol must be limited as

$$(M_{\text{FFT}} + M_{\text{CP}})(N_{\text{FFT}} + N_{\text{CP}}) \leq N_{\text{tot}} \tag{2.6}$$

and correspondingly $N_{\text{FFT}} + N_{\text{CP}} \leq N_{\text{tot}}$ for standard OFDM. By requiring $M_{\text{FFT}} \geq 1$ as well as $N_{\text{FFT}} \geq 1$ and setting (2.6) to hold with an equality, inherent upper bounds are imposed on the symbol dimensions:

$$M_{\text{FFT}} \leq \frac{N_{\text{tot}}}{N_{\text{CP}} + 1} - M_{\text{CP}} \quad \text{and} \quad N_{\text{FFT}} \leq \frac{N_{\text{tot}}}{M_{\text{CP}} + 1} - N_{\text{CP}}. \tag{2.7}$$

In spite of fixing M_{CP}, N_{CP}, and N_{tot}, modulation efficiency still depends on the symbol dimensions $(M_{\text{FFT}}, N_{\text{FFT}})$ which can be freely optimized.

The optimization task boils down to maximizing $M_{\text{FFT}} \cdot N_{\text{FFT}}$ under the constraints given in (2.7) where N_{FFT} is a function of M_{FFT} when (2.6) is satisfied with an equality. The optimal vertical dimension is solved as

$$M^*_{\text{FFT}} \triangleq \arg\max_{M_{\text{FFT}}} \eta_{\text{2D}} = \sqrt{\frac{M_{\text{CP}}}{N_{\text{CP}}} N_{\text{tot}}} - M_{\text{CP}} \tag{2.8a}$$

and the optimal horizontal dimension then follows directly from (2.6) as

$$N^*_{\text{FFT}} = \frac{N_{\text{tot}}}{M^*_{\text{FFT}} + M_{\text{CP}}} - N_{\text{CP}} = \sqrt{\frac{N_{\text{CP}}}{M_{\text{CP}}} N_{\text{tot}}} - N_{\text{CP}}. \tag{2.8b}$$

Finally, substitution in (2.5) yields the maximal modulation efficiency as

$$\eta^*_{\text{2D}} = \left(1 - \sqrt{\frac{M_{\text{CP}} N_{\text{CP}}}{N_{\text{tot}}}}\right)^2 \tag{2.9}$$

but, in practice, the dimensions must be integers or, even, powers of two (for faster FFT) which slightly lowers efficiency as observed shortly.

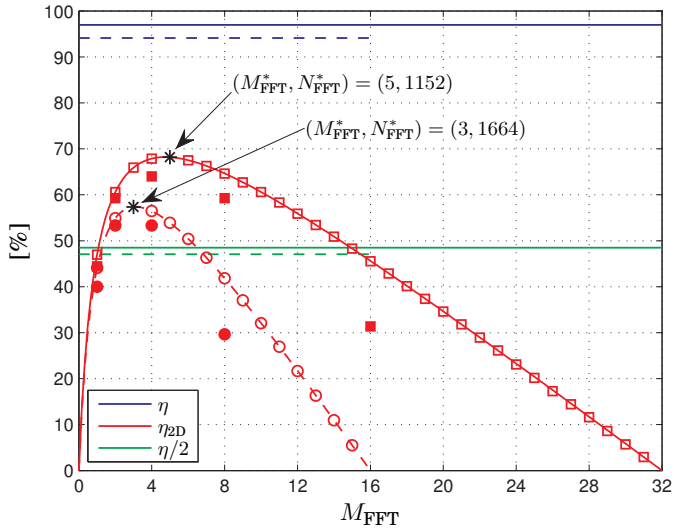

Figure 2.2. Modulation efficiency versus the vertical symbol dimension in 2D OFDM when $M_{\mathrm{CP}} = 1$. The solid curves are for a short CP ($N_{\mathrm{tot}} = 8448$, $N_{\mathrm{CP}} = 256$) and the dashed curves correspond to a long CP ($N_{\mathrm{tot}} = 8704$, $N_{\mathrm{CP}} = 512$). The open (resp. filled) markers indicate feasible symbol dimensions that are rounded to integers (resp. powers of two).

Discussion

Figure 2.2 illustrates two examples on the optimization of the symbol dimensions. The parameter values are adapted from DVB-T/H systems [72] assuming 8 MHz bandwidth and choosing the "8K mode" ($N_{\mathrm{FFT}} = 8192$) for standard OFDM. As a reference case for 2D OFDM, the ISI problem is avoided also with standard OFDM by allocating different time slots for direct and relayed signals which halves efficiency. For the shortest CP, the optimal symbol dimensions are $(M^*_{\mathrm{FFT}}, N^*_{\mathrm{FFT}}) \approx (4.74, 1214.61)$ or $(M^*_{\mathrm{FFT}}, N^*_{\mathrm{FFT}}) = (5, 1152)$ with rounding which causes minimal loss unlike making them powers of two. Especially, the usage of 2D OFDM can improve modulation efficiency by 40.6% in comparison with its alternative. Usually $M^*_{\mathrm{FFT}} \ll N^*_{\mathrm{FFT}}$ because $M_{\mathrm{CP}} \ll N_{\mathrm{CP}}$ and setting $M_{\mathrm{FFT}} = N_{\mathrm{FFT}}$, although it might be intuitive, leads to extremely large CP overhead. Furthermore, the upper bound in (2.7) may exclude symmetric dimensions.

The 2D OFDM modulation facilitates frequency-domain relay protocols at the cost of extra overhead from the vertical CP. In particular, it can be preferred over standard OFDM when $\eta^*_{\mathrm{2D}} > \eta/2$ with the substitution of (2.2) and (2.9). When $M_{\mathrm{CP}} = 1$, a baseline condition is thus established as follows for determining whether modulation efficiency can be improved:

$$N_{\mathrm{CP}} < \frac{1}{9} N_{\mathrm{tot}}. \tag{2.10}$$

This is satisfied, e.g., with the two shortest CPs of DVB-T/H (cf. Fig. 2.2).

2.1.3 Transceiver Imperfections

Practical OFDM transceivers are subject to various imperfections [73] underneath theoretical frequency-domain signal models, e.g., (2.3) and (2.4). Two of them are essential for this study: distortion noise induced at the transmit side and non-ideal time synchronization at the receive side.

Nonlinear Distortion in OFDM Transmitters

Nonlinear distortion occurs when digital signals are converted to high-energy electromagnetic fields radiated from antennas; for instance, power amplifiers (PAs) are major contributors. It especially impedes interference mitigation in full-duplex relays in Chapter 3. Nonlinear effects can be included in single-subcarrier signal models as Gaussian "transmitter noise" [46, 280] since (in essence) an OFDM signal envelope is closely Gaussian [300]. The relative noise variance is denoted by $\epsilon_{\mathbf{x}}^2$ which can be translated to error-vector magnitude (EVM) as $\epsilon_{\mathbf{x}} \cdot 100\%$. For example, $\epsilon_{\mathbf{x}}^2 = 0.001 = -30$ dB corresponds to a slightly optimistic 3.2% EVM value.

Time Synchronization in OFDM Receivers

Time synchronization is needed in order to use correct signal samples for symbol demodulation [186]. In general, OFDM is robust to time-domain non-idealities due to the long symbol duration and the usage of the CP, but severe multipath fading makes it more complicated to sample the FFT window optimally. This issue is emphasized in transmission over relay links where the effective delay spread is accumulated in each hop.

Receiver models often consider a two-step synchronization procedure. The first step results in initial coarse synchronization by aligning the receiver with the symbol rate. Assuming that the initial step is successful, the second step is modeled herein by the strategy used for choosing τ_{TOR}, i.e., how the CP window is positioned versus the multipath profile of the channel between modulation and demodulation. In particular, Chapter 6 analyzes the following four synchronization strategies adopted from [30]. The first strategy models the reference case of ideal synchronization:

Maximization of the SINR ("*Max-SINR*"): In principle, demodulation always aims at minimizing ICI and ISI, which at best results in

$$\tau_{\mathrm{TOR}}^{*} \triangleq \arg\max_{\tau_{\mathrm{TOR}}} \gamma. \tag{2.11}$$

In the analysis, the optimal TOR value can be evaluated only numerically although the SINR itself, γ, is expressed in a closed form.

The other three strategies model non-ideal synchronization:

Around the mean delay ("*Mean delay*"): The mean delay of a channel (denoted with $\bar{\tau}$) represents the middle point with multipath components (MPCs) on both sides. By choosing $\tau_{\mathrm{TOR}} = \bar{\tau} - T_{\mathrm{CP}}/2$, the CP window becomes centered around the multipath delay spread collecting useful signal power approximately from every MPC.

Around the strongest multipath component ("*Strongest MPC*"): Signal energy is usually concentrated close to the strongest MPC whose delay is denoted with τ_{max}. Thereby, the receiver can roughly maximize the useful signal power by centering the CP window around the peak of the channel profile with the choice $\tau_{\mathrm{TOR}} = \tau_{\mathrm{max}} - T_{\mathrm{CP}}/2$.

After the first multipath component ("*First MPC*"): In the FFT window, signal samples collected prior to the arrival of the first MPC with lag τ_{1st} will only cause ISI. Hence, a conservative synchronization strategy selects $\tau_{\mathrm{TOR}} = \tau_{\mathrm{1st}}$, i.e., collects the useful signal power from the beginning of the profile. This strategy results in perfect synchronization if the multipath channel is shorter than the CP.

It should be noted that these strategies implicitly model different implementations while $\bar{\tau}$, τ_{max} and τ_{1st} may not be explicitly used in practice.

2.1.4 Models for Wireless Channels

Between aerials, electromagnetic signals go through frequency-selective and time-varying multipath propagation which is modeled by choosing fittingly the statistics of $h(t)$, $h[n]$, and $\mathbf{H}[n]$ for (2.1), (2.3), and (2.4). One may note that channels can be estimated only at receivers but channel state information (CSI) is needed also for transmission. Thus, the considered systems contain also feedback channels or rely on channel reciprocity although such implementation details are not specified explicitly.

Static Frequency-Selective Channels

The considered OFDM(A) relay systems feature wireless channels whose both ends are stationary, e.g., part of network infrastructure, such as those from base stations to relay nodes. These channels vary only due to moving scatterers [283] while all strong MPCs are assumed to reflect via static objects. Thereby, the SNR of the nth RB can be modeled as $\gamma[n] = \bar{\gamma}[n] \triangleq \mathcal{E}\{\gamma[n]\}$. The channels may be still frequency selective if line-of-sight (LOS) is not achieved, i.e., typically $\gamma[n_1] \neq \gamma[n_2]$ for $n_1 \neq n_2$.

Fast-fading Statistics for Subchannels

Rayleigh-fading [257,258] is the most common model for non-line-of-sight (NLOS) channels where one end, e.g., user equipment, is mobile. In particular, as a sum of multiple incoherent reflections, $h[n]$ becomes a Gaussian random variable with zero mean and, thus, the signal amplitude $|h[n]|$ follows the Rayleigh distribution (hence the name). Most importantly, the probability density function (PDF) and cumulative distribution function (CDF) of $\gamma[n]$ become those of an exponential random variable:

$$f_{\gamma[n]}(x) = \frac{1}{\bar{\gamma}[n]} \exp\left(-\frac{x}{\bar{\gamma}[n]}\right) \quad \text{and} \quad F_{\gamma[n]}(x) = 1 - \exp\left(-\frac{x}{\bar{\gamma}[n]}\right) \tag{2.12}$$

for $x \geq 0$, respectively.

Other typical channel models are Nakagami fading [189] (where $\gamma[n]$ is gamma distributed) and Rice fading (which extends $h[n]$ to have non-zero mean). Also slow shadow-fading models may be used in the analysis of relay links although they often yield intractable performance expressions.

It is important to note that $\gamma[n_1]$ and $\gamma[n_2]$ are strongly correlated in *OFDM* and it would not be justified to approximate otherwise unless the corresponding RBs are allocated widely apart from each other, i.e., $|n_1 - n_2|$ is large. However, these subchannels can be regarded accurately independent with any n_1 and n_2 if the RBs are received by different terminals in an *OFDMA* context. This fact is crucial for the usage of order statistics in Chapters 7 and 8. Likewise, the OFDMA context likely renders also $\bar{\gamma}[n_1] \neq \bar{\gamma}[n_2]$ due to differences in path-loss and shadowing states.

Multipath Propagation

When using explicit wideband signal models, e.g., (2.1), the delay-spread properties of the channel impulse response $h(t)$ become as essential as fading statistics. They can be modeled with a power–delay profile (PDP):

$$P(t) \triangleq \mathcal{E}\{|h(t)|^2\}. \tag{2.13}$$

Especially, demodulation generates ICI and ISI whenever multipath delay spread is longer than the CP in use which facilitates the analysis of relay links by characterizing their effective end-to-end PDPs in Chapter 6.

The most common model, the classic exponential PDP [243], decays as

$$\frac{P_1(t)}{P_1(\tau_{1\text{st}})} = \exp\left(-\frac{t - \tau_{1\text{st}}}{s_1}\right) \tag{2.14}$$

with a rate specified by the root mean square (RMS) delay spread s_1 after sharp onset at $t = \tau_{1\text{st}}$. Another popular model is the so-called typical urban six-path ("TU6" [57]) profile whose original impulse version can be extended to represent six exponentially decaying multipath clusters.

2.2 Summary of Multihop Relaying Technologies

This section presents an overview of multihop technologies to form a solid background for the main technical chapters. In principle, relaying simply means just indirect data transmission from a source node to a destination node via intermediate relay nodes, e.g., not so unlike repeaters, gap-fillers, or signal boosters do in conventional systems. However, modern relay systems are much more advanced as shown by the following introduction to essential relaying scenarios, modes, concepts, and protocols.

2.2.1 Communication Scenarios

The relaying systems studied in this dissertation are shown in Fig. 2.3; they employ the combination of OFDM and OFDMA, which is referred to as OFDM(A), or represent single-subcarrier transmission in an implicit multicarrier framework. There are multiple destination nodes which requires scheduling or multiplexing using OFDMA. The main focus is on infrastructure relaying although the considered systems have their counterparts with cable-connected distributed antennas and mobile relays.

Infrastructure-Based Relays
As emphasized in Fig. 2.3, the considered relays are fixed nodes and belong to infrastructure deployed by a network operator. This scope choice is similar to, e.g., that of [76, 134, 165, 295], but one may note that it is rather uncommon in related mainstream literature which is inclined toward ad hoc mobile relaying by user terminals. When discussing cellular systems, the link elements may be referred to as base stations (BSs), relay nodes (RNs), and user equipments (UEs); BSs and RNs form a “backhaul link” while UEs are always connected to a “service link”. There is typically only one relay per each group of destinations (except for special handover situations) while backhaul links may involve multihop relaying.

Distributed Antennas
An evident reference case for relays is given by distributed antennas, an age-old concept [242]. Each relay link in Fig. 2.3 can be understood as a distributed antenna system (DAS) by imagining a cable connection that replaces the wireless backhaul channels from the source to the last relay (which transmits on the wireless service channel to the ultimate destinations). In comparison with wireless channels, the cable connection has superior quality and, thus, it can be considered ideal in the analysis.

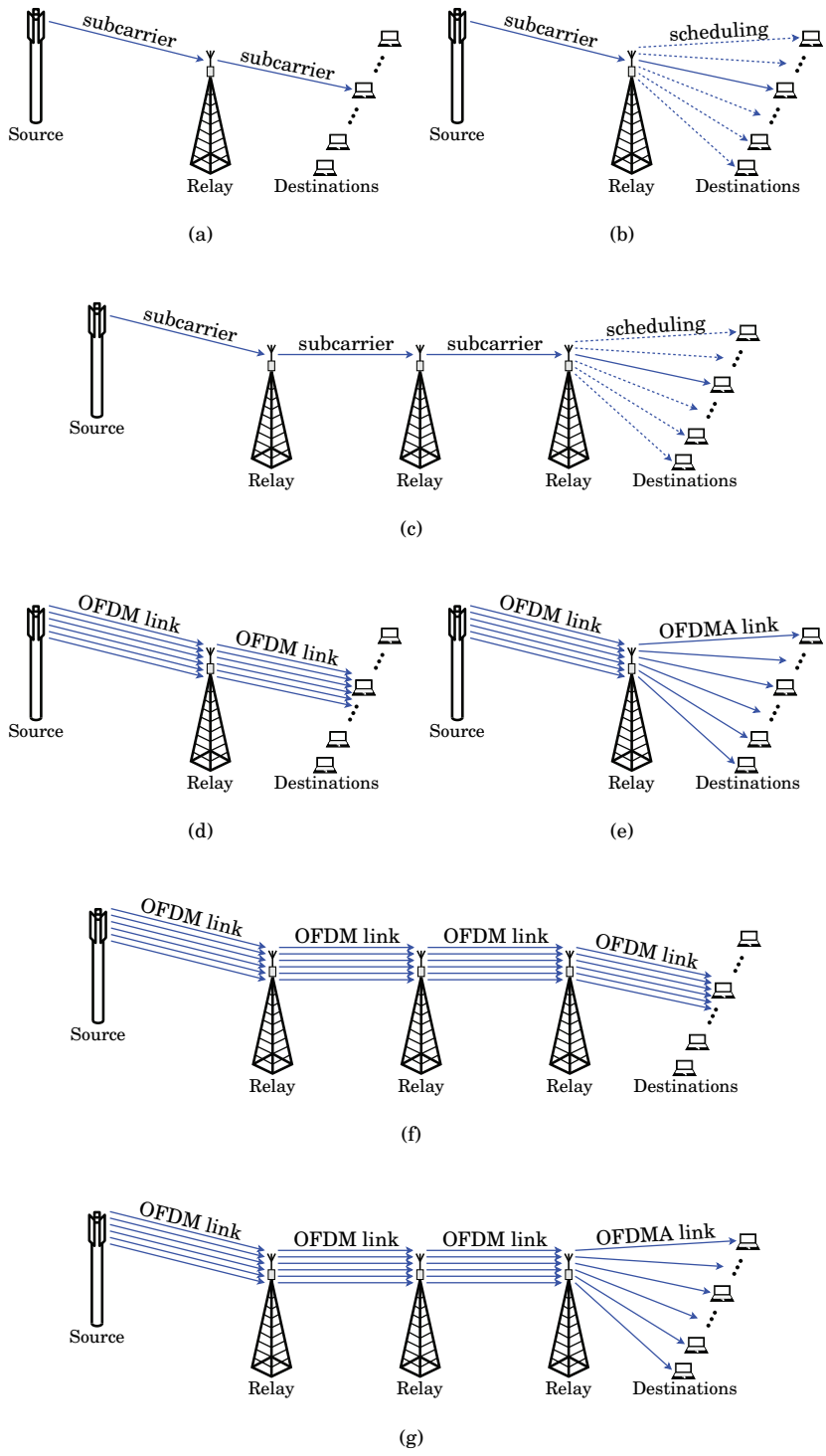

Figure 2.3. Common OFDM(A) relaying scenarios which are in the main focus of this study. Only downlink (DL) transmission is illustrated above although the corresponding reversed uplink (UL) scenarios are studied as well.

Mobile Terminals as Relays

In the spirit of seminal works on user cooperation, e.g., [121, 142, 143, 188, 249, 250], recent literature often concentrates on systems with mobile relays. Sometimes this scope choice is implied only by fading models adopted for considered system setups since it would not be reasonable to assume severe fading for the backhaul channels of infrastructure-based links. The systems of Fig. 2.3 represent some mobile relaying scenarios if the relay towers are imaginarily replaced with portable user terminals (cf. the destinations); also scenarios with fixed relays but mobile sources and destinations are regarded in the category of mobile relaying due to the similarity of feasible fading models. However, cooperative connectivity models are even more diverse [28], e.g., it is common to study systems with multiple parallel relays. As opposed to infrastructure-based relaying, making distinction between downlink (DL) and uplink (UL) transmission directions is not usually relevant when studying mobile relaying.

2.2.2 Duplexing Modes for Relays

Full-Duplex Mode vs. Half-Duplex Mode

Operation modes are key factors in the spectral efficiency of relay links and the contributions of this work. They are defined as follows (cf. Fig. 2.4).

Full duplex (FD) designates or pertains to a mode of operation by which information is transmitted to and from a relay in two directions simultaneously on the same physical channel.

Half duplex (HD) designates or pertains to a mode of operation by which information is transmitted to and from a relay in two directions, but not simultaneously on the same physical channel.

In particular, HD operation needs orthogonal channels before and after each relay while FD relaying exploits channel reuse. However, FD operation induces processing delay such that relayed signals are subject to an offset that is pronounced in OFDM with frequency-domain processing.

Direct Transmission Mode

Eventually, relaying should be contrasted with the conventional scenario of not using relays at all but directly transmitting from sources to destinations. The reference case is referred to as a direct transmission (DT) mode when considering degenerate full-duplex relaying where relays are switched off and destinations receive only direct signals from sources.

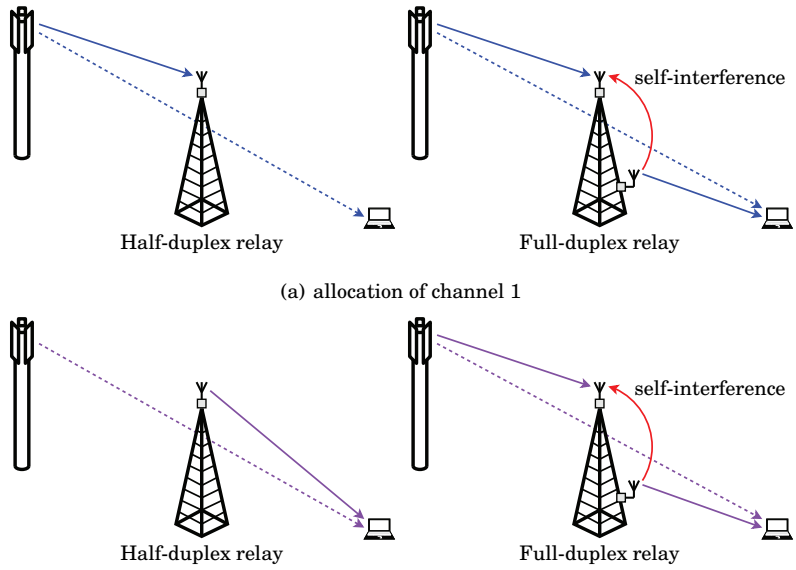

Figure 2.4. Comparison of half-duplex and full-duplex relays when two orthogonal (in time or frequency) channels are allocated for two-hop communication.

Loopback Self-interference in Full-Duplex Relaying

Full-duplex relaying achieves twice the end-to-end symbol rate of half-duplex relaying per allocated channel resources. This causes inevitably a feedback loop (cf. Fig. 2.4) where signals transmitted by relays leak back to their receive side. The phenomenon can be referred to, in short, as self-, loop(back) or echo interference, and it calls for gain control to avoid saturation or oscillation in conventional repeater systems.

A full-duplex relay needs separate antennas for reception and transmission in contrast to half-duplex relays (cf. Fig. 2.4). This provides passive physical isolation which facilitates active signal processing for additional mitigation. However, mobile terminals are almost invariably assumed to act as relays in the half-duplex mode due to their small size.

After recognizing the existence of self-interference, its mitigation and efficient operation under residual distortion are formulated as the main novel theme for Chapters 3–5; gain control is revisited also in Chapter 6. Limited parallel work on MIMO mitigation concepts is reviewed in Section 3.2. Moreover, the prior art tends to choose one mode over the other at an early design stage whereas this study proposes to design relays that can operate in both modes and, hence, opportunistically switch between them for maximizing performance. Eventually, choosing a proper mode involves the fundamental trade-off between symbol rate and SINR.

2.2.3 Relaying Concepts at Large

Historically, the analytical study of relay links originates from the information theory of three-node communication systems [293] while the practical relaying techniques have evolved from repeaters [251] used in various systems. Eventually, the research topic boomed in the form of user cooperation. Essential relaying concepts are summarized below including techniques to cope with direct source-to-destination transmission, schemes to combat rate loss due to half-duplex operation, and discussion on how multiantenna protocols and OFDM(A) fit into the big picture.

Origins in Information / Communication Theory and Practical Systems
In information theory, full-duplex relays provide an idealistic benchmark when deriving capacity results for generic relay channels [45, 107, 136, 293, 298]. Studies in this context assume that self-interference can be eliminated perfectly and, consequently, the potential existence of residual distortion is neglected. Yet half-duplex relaying has received more attention since the theory of cooperative communications was developed in the pioneering works, e.g., [27, 112, 121, 142, 143, 188, 249, 250, 264, 316].

Practical systems have exploited the simplest form of full-duplex relays, i.e., analog repeaters, since the early days of wireless communications. For instance, repeaters are successfully employed in digital television broadcasting [244, 253] and cellular systems [119]. In this more down-to-earth context, the existence of self-interference is widely acknowledged and many techniques are available for its mitigation [89, 190]. However, these studies typically adhere to the full-duplex mode from the start without rationalizing whether it is the proper choice.

Relaying for Diversity Gain vs. Coverage Extension
As indicated also by Fig. 2.4, the direct source-to-destination link bypassing a relay opens up some design options. The related HD time-slot allocations are classified in [188]: The direct link can be neglected by not receiving the transmission at all but the source may transmit again also simultaneously with the relay. In cooperative communications, it is typical to use the direct signal as another diversity branch which can be implemented with, e.g., selection or maximum ratio combining (MRC) [29]. On the other hand, coverage extension is more relevant for infrastructure relays implying that direct transmission, which is weak by default, can be left as co-channel interference in FD operation or neglected altogether. Especially, 2D OFDM facilitates transparent equalization in this case.

Operation under Half-Duplex Constraint

Early communication-theoretical results consider mostly applications, e.g., user cooperation, in which the self-interference problem can be reasonably considered to be insurmountable. Thus, research focus is often on finding detours to overcome the limitations of the half-duplex mode.

A recent overview article [52] summarizes comprehensively key techniques for "combating the half-duplex constraint", not so unlike the introduction of **[220]**. In particular, it is straightforward to achieve diversity gain with the half-duplex mode but the allocation of two orthogonal time slots imposes severe degradation in the multiplexing gain [142]. They are classified in the context of infrastructure-based relaying as follows.

Non-orthogonal relaying refers to systems where the BS may transmit new data during RN transmission and the UE applies extra techniques for decoding the superimposed transmissions [10, 188]. Related ideas are presented also in [5, 71, 267]. Non-orthogonal relaying can be also used to gain an additional diversity path without essentially reducing the effect of half-duplex constraint [143].

Successive relaying systems are based on the idea that two alternating half-duplex RNs can mimic the full-duplex mode [61, 204]. This requires the cancellation of inter-relay interference instead of self-interference in full-duplex relaying. The former signal is unknown unlike the latter which makes the task more challenging.

Two-way half-duplex relaying schemes [193,202,292] relax the orthogonality of DL and UL after proper signal design and receiver structures facilitate interference mitigation. In this case, self-interference echoes from a source BS or UE back to itself via the RN.

Cognitive radio-based relaying systems allow a half-duplex relay link reuse licensed spectrum as a secondary user whenever interference to primary users is guaranteed to be weak enough [320].

Other related concepts are discussed in [116, 180].

In summary, common for these schemes is to relax the orthogonality of half-duplex transmissions by providing means of suppressing the resulting interference or tolerating its presence. This is both in contrast with and, also, similar to full-duplex relaying where self-interference emerges inherently without any special design that renders spectrum reuse.

Relay Selection vs. User Scheduling

Systems with multiple potential relays, i.e., other users, are typical for cooperative communications: Single-antenna nodes can collaboratively implement distributed multiantenna diversity which is efficiently realized by relay selection (cf. Section 2.3). In infrastructure-based systems, relay selection equates to relay-to-relay handover procedures [76], and multiuser systems translate inherently to scenarios with multiple source or destination nodes whose multiple access is implemented in the form of scheduling [133,157,295]. Controlling relay selection and user scheduling is handled by radio resource management [95,245] above the link layer.

Loopback Self-interference in MIMO Relaying

Related literature on MIMO relaying techniques can be classified into three groups based on how the potential self-interference problem is dealt with. The landmark references are collected in Table 2.1. Most of these papers study the classical two-hop three-node relay link (a source, a relay and a destination) which is assumed also below although the study on self-interference mitigation is applicable for any generic network topology.

The largest class of earlier papers, e.g., Group 1 in Table 2.1, considers half-duplex relaying in which *the loopback self-interference is inherently avoided*. Over half of the papers, i.e., Group 1(a) in Table 2.1, develop half-duplex protocols for the case in which *the direct source-to-destination link is blocked*. The current results (cf. Chapter 3) are directly applicable for the full-duplex counterparts of these systems and enable more spectrally-efficient implementation once the loop interference is appropriately mitigated. The other papers, i.e., Group 1(b) in Table 2.1, *exploit the direct link* as an extra diversity branch. The direct link is orthogonal by design in the half-duplex mode whereas the destination receives a superposition of the direct and relayed transmissions in the full-duplex mode. Also for these systems, the full-duplex counterparts are feasible by implementing signal separation in the destination receiver.

Another large class of earlier papers, e.g., Group 2 in Table 2.1, studies various full-duplex relaying schemes *without considering the deleterious effect of the self-interference* albeit otherwise presenting many seminal contributions. In particular, these papers tend to provide minimal (if any at all) explanations and references for interference mitigation and operation under residual distortion. The current results will support this body of literature by providing validation and a retroactive reference for this central baseline assumption which is not verified in detail before.

Table 2.1. Classification for landmark references on half-duplex MIMO, full-duplex SISO and full-duplex MIMO relaying.

Group 1(a), half-duplex relaying without direct link:	Group 1(b), half-duplex relaying with direct link:	Group 2, full-duplex relaying (no self-interference):
MIMO [13, 25, 32, 34, 51, 59, 79, 84, 85, 92, 111, 123, 149, 150, 159, 166, 168, 183, 195, 238, 239, 252, 297, 310, 311]	MIMO [4, 24, 33, 35, 132, 134, 184, 187, 199, 237, 255, 256, 261, 281, 287, 288, 306, 308]	SISO [45, 107, 136, 249, 250, 293, 319]; MIMO [31, 60, 127, 160, 163, 255, 265, 286, 298, 308, 315]

Two-Array Relays

The study on full-duplex relaying considers a two-array setup which allows separate antennas for transmission and reception while the number of receiver–transmitter pairs is conserved. Using two arrays in the relay is useful not only for the full-duplex mode due to interference mitigation but the half-duplex mode benefits from it as well because antenna configurations, e.g., location and beam pattern, can be optimized separately in two directions, while the placement of a single array is a compromise over the quality of the two hops. For example, both FD and HD can avoid building wall penetration loss which is inherent for the DT mode, and the self-interference is also suppressed by the very same effect in the FD mode. At the same time, beamforming using both arrays in half-duplex relaying is difficult because the branches are highly imbalanced.

Two-array deployment is advantageous in scenarios, where the coverage of a macro BS is extended to inside a building, to a metro tunnel, or to a shadowed area between buildings. Typically [119], highly directive backhaul antennas can be placed on the roof of a building and pointed toward the BS possibly with a line-of-sight connection, and service antennas are placed on the street-level or indoors with wider beam pattern toward the covered area. The physical isolation can ideally be large enough to allow neglecting the self-interference in measurements [119]. Another typical scenario is RN deployment on a (lamp) pole. Sufficient isolation is then ensured by vertical distance or an isolating plate between the arrays and by exploiting antenna directivity. Measurements have demonstrated that inter-antenna path loss varies from -50 dB to even -100 dB, which can be further improved with cancellation [89, 104, 190].

2.2.4 Single-Subcarrier Forwarding Protocols

The elementary relaying protocols specify frequency-domain processing between demodulation and retransmission in a relay node. It is difficult to attribute these common concepts to their original inventors. Instead, references are given to some landmark articles which popularized them.

Amplify-and-Forward Relaying

The linear family of relay processing concepts is referred to as amplify-and-forward (AF) protocols [142]. They are based on simple scaling such that any AF relay only filters its input signal before retransmission due to which also noise is forwarded. The corresponding amplification factor and relay gain coefficient are denoted by β and β^2, respectively.

Amplify-and-forward protocols are usually categorized as follows according to the way how the relay gain is chosen.

Variable gain (VG) operation [99, 101] adapts β to instantaneous channel fluctuations. In literature, other common names for this protocol are CSI-based gain and instantaneous power scaling (IPS) relaying.

Most commonly variable gain is needed for normalizing the relay transmit power to a constant level which requires that the relay estimates the instantaneous source-to-relay channel gain and its input noise power. The other variants are "unlimited gain" and "clipped gain" relaying **[230]** while the most advanced schemes implement gain adaptation in the form of "waterfilling" over time [75, 241].

Fixed gain (FG) operation [103, 270] sets a constant value for β. It is called also average power scaling (APS) protocol in literature.

In principle, FG protocols are somewhat simpler than their VG counterparts, because the relay exploits only statistical channel state information or alternatively it can just adaptively adjust its average transmit power to the desired level. Instead of controlling average transmit power as usual, some studies assume that the gain itself is set to match the average gain of VG amplification [103].

All the essential AF protocols can be collectively analyzed using a generic end-to-end SNR expression [248] although they are usually studied separately. Performance differences emerge between the variations when the relay input channel is fading as with mobile or uplink infrastructure-based relays and they are intensified by the full-duplex self-interference.

Decode-and-Forward Relaying

The regenerative family of relay processing concepts is referred to as decode-and-forward (DF) protocols [136, 142]. They can be implemented in many different abstract ways but the common task for any DF relay is to decode its input data and re-encode it in some form for retransmission. Thereby, the relay forwards a "clean" signal in contrast to AF protocols while input noise only reduces the quality of incoming signals. Although reference link-level studies usually assume that DF protocols operate in a symbol-by-symbol manner, buffering is also possible [303].

Other Protocol Concepts

Literature considers also other protocols such as compress-and-forward, quantize-and-forward, and estimate-and-forward [78, 136] (different authors use their own favorite names for similar processing), which can be mainly understood as information-theoretical concepts and are not so well translated to practical systems unlike AF and DF. In particular, these protocols represent something which is in between AF and DF processing: A relay forwards quantized or compressed "soft" information instead of linear amplification or generating "hard" information by decoding. Actually, hybrid AF/DF relaying itself has also been proposed [307].

Extension to MIMO Systems

Studies on multiantenna relays are usually limited to single-subcarrier system setups, and MIMO relaying protocols can be classified in the same general way as the SISO protocols above. However, having multiple antennas necessitates to incorporate spatial processing into the protocols. In this study, the mitigation of self-interference is decoupled from the design of inner MIMO protocols. Consequently, considered relay concepts may adopt directly (or after minor modifications) any of the protocols designed for cases without loopback self-interference such as those discussed by the references collected in Table 2.1.

Surveying extensively MIMO protocol concepts is unnecessary herein. It can be still noted that the design of MIMO gain matrices for AF protocols seems to be an especially popular topic in recent literature. Typically the related studies formulate and solve complicated optimization problems while the performance of the proposed protocols over fading channels is evaluated with simulations. A specific original concept worth to highlight is channel rank improvement [286] where MIMO repeaters facilitate spatial multiplexing despite of line-of-sight (LOS) conditions.

Extension to Broadband Systems

Two generalizations are available for extrapolating narrowband single-subcarrier system models for practical broadband transmission. Physical channels with a dominant multipath component can be approximated with frequency-flat fading also in broadband systems. A FD relay then becomes an analog AF repeater which amplifies the time-domain waveform like those studied in [119, 244, 253]; however, the relay processing delay should be longer than the OFDM cyclic prefix or the code-division multiple access (CDMA) equalization window to conform with models in which loopback and direct link signals are interference. Alternatively, the models can be interpreted to correspond to a single subcarrier in OFDM, if the relay demodulates the frequency-division multiplexed signal and processes all subcarriers in parallel in the frequency domain. Thereby, the relayed signal is delayed by at least one OFDM symbol with respect to the direct signal, because OFDM symbols cannot be demodulated before they are completely received. In this case, 2D OFDM is useful. This approach, valid for both AF and DF, is similar to that of [104].

2.2.5 Multicarrier OFDM(A) Forwarding Protocols

Proceeding from single-subcarrier systems to the case of infrastructure-based OFDM(A) relaying, the purpose of relaying protocols becomes to provide an advanced interface between an OFDM backhaul link and an OFDMA service link. Their design is not a straightforward task due to a multitude of techniques available for optimizing system performance.

The set of protocols considered in this study arise from the following design choices which are also enumerated in Table 8.1 (at Page 212) where the rows represent the design choices and the columns show their feasible combinations, i.e., the protocols. As elaborated in the following subsections, the design choices form a hierarchical structure illustrated in Fig. 2.5 such that some choices must be made before others, and one choice may eliminate another.

The implementation complexity of the design choices and their combinations varies significantly but their joint effect on the system performance is not known so far. In Chapter 8, this gives motivation for evaluating the link capacity achieved by all these variations in a unified analytical framework which further facilitates rational comparison between OFDM(A) relaying protocols.

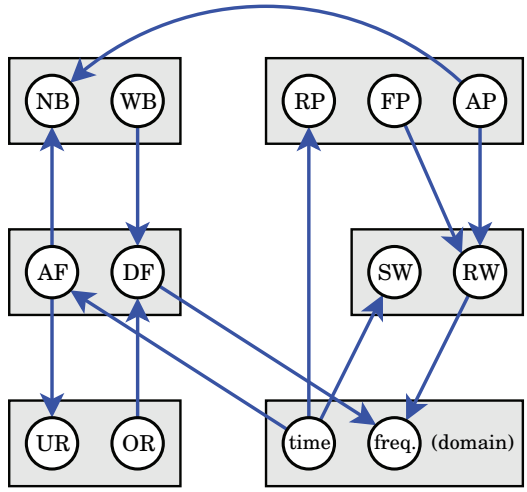

Figure 2.5. The hierarchy of the design choices which are represented by circles. The rectangles indicate mutually exclusive choices, and the arrows show how certain choices imply inevitably some others. For example, time-domain processing implies the usage of an amplify-and-forward (AF) protocol which further implies the allocation of uniform resources (UR). The abbreviations are defined again in Table 8.1 at Page 212 for concise reference.

Time-Domain vs. Frequency-Domain Processing

Protocol design needs to first account for the dual nature of OFDM(A): The physical signal is transferred in the time domain, while the actual data is modulated on frequency-domain subcarriers. Relaying protocols may operate in either domain although time-domain processing is limited to simple signal waveform amplification. With frequency-domain processing, the RN first demodulates its input OFDM symbols using the FFT which facilitates the direct processing of actual RBs. Finally, the RN converts the processed data back to the time domain using the inverse FFT and adds the cyclic prefix.

Resource Block-wise vs. Symbol-wise Processing

With multicarrier transmission, it is necessary to discriminate between resource block-wise (RW) and symbol-wise (SW) protocols, i.e., whether the RN processes received RBs independently or jointly. With RW processing, the BS forms a virtual circuit-switched connection to each UE via the RNs such that data from each backhaul RB are processed separately and routed to a single service RB. This requires inevitably frequency-domain implementation. With SW protocols, the RN processes its input OFDM symbols in one piece to generate the output OFDM(A) symbols.

Amplify-and-Forward vs. Decode-and-Forward Processing

The common classification between amplify-and-forward (AF) and decode-and-forward (DF) protocols is relevant also in OFDM(A) relaying. Both time- and frequency-domain operation are viable for AF protocols: SW processing in the time domain means OFDM symbol amplification with scalar gain, while RW processing in the frequency domain facilitates independent RB amplification and frequency-selective gain. The different variations of choosing the relay amplification factor can be also employed. Symbol-wise amplification in the frequency domain would be possible, but it is discouraged as it needs two unnecessary FFT operations. All DF protocols require inherently frequency-domain operation: With RW processing, the RN decodes and re-encodes each backhaul RB separately, while SW processing facilitates coding across the whole OFDM bandwidth such that the RN decodes jointly the information of all backhaul RBs and redistributes it for the service RBs.

Subcarrier Pairing

Subcarrier pairing refers to the opportunistic reordering of RBs during processing. Its idea was first introduced in [108] and, almost at the same time, the concept was independently discussed also in [90, 91] while [105] proposed a RB-based pairing strategy that creates significantly less overhead when signaling subcarrier pair mapping to a single destination. In [105], the optimality of the pairing strategy was proven in a special case assuming that the received signal in the relay is noise-free. A full optimality proof for general AF relaying was first presented in [109]; another related study worth to mention is [162]. In [106], a new pilot design was introduced for facilitating the estimation and feedback of CSI by mitigating the effect of destroyed correlation between reordered RBs.

The distribution of service RBs among the active UEs is not fixed or predefined when it is based on scheduling. Therefore, basic RW processing, e.g., by routing RBs sequentially, results in random pairing (RP) of the backhaul and service RBs. The total system capacity can be improved by reordering RBs to form backhaul–service RB pairs in the order of SNR: The backhaul RB with the best SNR is routed to the UE with the best SNR, that with the second best SNR to that with the second-best SNR, and so forth. This kind of opportunistic reordering can optimize either fixed pairing (FP) based on average SNRs or adaptive pairing (AP) based on instantaneous SNRs. Symbol-wise processing inherently results in RP for AF and makes the RB reordering irrelevant for DF.

Transmit Power Allocation

Subcarrier pairing has been considered along with transmit power allocation for amplify-and-forward OFDM [91] and MIMO–OFDM [90,92] relaying. Especially, article [313] applies the idea of time and power allocation for ideal (interference-free) *multihop* OFDM relay links to minimize the outage probability. Other noteworthy works are reported in [86, 192, 312]. While a generic solution for pairing alone is given by the Hungarian algorithm [140] and it can be simplified to ordered pairing, joint power and subcarrier allocation needs to be formulated as optimization problems which usually admit only numerical (iterative) solutions.

Optimization of Time Sharing

Basic protocol design assigns equal time shares for the backhaul and service links, i.e., assumes the allocation of uniform resources (UR). In fact, all AF protocols require UR allocation because they cannot change the modulation and coding scheme. On the contrary, if backhaul and service link RBs are allowed to use different transmission rates, the performance of DF protocols can be boosted by adjusting the time shares based on average channel SNRs. This leads to the allocation of optimal resources (OR) guaranteeing that the per-link throughputs are balanced. In particular, when the system load is low, UR allocation leads to significant overcapacity in the backhaul link. The optimization of time slots can be seen also as another countermeasure for the half-duplex constraint: It minimizes the overhead although does not avoid the loss completely, and moreover, it works well only if the channels are imbalanced.

Buffering over Fading States

All basic protocols store and process only the data of the latest BS time slot, i.e., no buffering (NB) is exploited. To improve the system performance, DF protocols can be implemented also with buffering (WB). This compensates for the effect of fading on the service link if data is stored over different channel states: The buffer is filled when the throughput of the service link is the bottleneck of the system which allows more data (taken from the buffer) to be transmitted when the backhaul link is in turn the bottleneck. Statistical analysis may assume that the buffers are infinite (or very long) which means that they cannot overflow or underflow. Such a simplification is justified because the narrowband simulations of [303] show that the system capacity with a quite small finite buffer is already very close to that with an infinite buffer.

2.3 Survey on Design and Analysis of Relay Links

This section presents an overview of the statistical performance analysis of relaying over fading channels. The body of relevant research literature is enormous: Even if covering it thoroughly herein was possible, it would not be meaningful. Hence, the focus is limited to aspects and references that are the most significant in the scope of the following technical chapters. The first three subsections adopt the subtext of narrowband single-subcarrier signal models assuming frequency-flat block-fading channels (in the spirit of the majority of related papers) while the fourth subsection discusses works that concern relaying in the explicit context of wideband multicarrier signal models and frequency-selective multipath channels.

2.3.1 Multiantenna Relaying

Most of the references collected in Table 2.1 study MIMO relaying concepts in the case of instantaneous snapshot channels while performance over fading channels is evaluated using only Monte Carlo simulations. As briefly summarized below, some works contribute also statistical analysis although the main focus is usually on the design of relaying protocols.

Analytical outage probability results have been presented for various multiantenna relaying concepts and spatial-processing protocols: zero-forcing filtering [168], systems with a direct link [33,35] and single-stream transmission with beamforming [305]. The cumulative distribution function (CDF) results of [149] are analogous to the outage probability while related bit-error rate (BER) results are also available, e.g., in [4, 150]; article [4] evaluates also forwarding probabilities which quantify outage events at a source–relay link. These results are often limited to two-hop scenarios but multihop relaying has also been evaluated [152].

The ergodic capacity analysis of MIMO relaying is available for dual-hop [124] and multihop [265] scenarios; especially, the keyhole effect due to a low-rank relay–destination channel is studied in terms of capacity in [74]. The asymptotic analyses of [25, 153, 297] concern cases where the number of antennas or relays grows large, while the degrees of freedom characterize high-SNR situations, e.g., as in [31] for full-duplex relaying.

The diversity–multiplexing trade-off has been evaluated for full-duplex (and half-duplex) MIMO relaying in [60,160,308] without self-interference and for non-orthogonal relaying using multiple parallel half-duplex relays in [306]. Some works concentrate on diversity-order analysis [199, 261].

2.3.2 Two-Hop Relaying

The analysis of relay links concentrates often on *strictly two*-hop scenarios which yield the most tractable expressions and realize well the benefits of cooperative communication while adding more hops may actually induce losses due to a need for extra spectrum resources. The works referenced below concern mobile half-duplex relays unless otherwise specified.

Three-Node Relay Links

Many pioneering works, e.g., [99, 101, 103, 196, 206], and their successors limit the scope of statistical analysis to basic three-node systems where a single relay assists two-hop transmission from a source to a destination. They can be classified based on their stance toward a potential direct link.

On the one hand, a significant portion of literature assumes that the direct link is blocked or the destination just neglects it. These studies, e.g., [18, 270, 271, 289], are usually differentiated by the considered protocol variations and fading models. Especially, mixed Rayleigh and Rice fading [272] is related to models in infrastructure-based relaying, and systems with co-channel interference [269, 275] have similarities with full-duplex relaying under self-interference. Some studies consider single-antenna relays but employ multiple antennas at the source or destination [167, 182, 279]. The countermeasures for combating the half-duplex rate loss have also been studied analytically: In two-slot two-way relaying [94, 161, 200], the reception of direct-link transmission is impossible by design.

On the other hand, the direct link can be exploited using variations of the fixed, selective, or incremental combining schemes of [142]. The analytical results cover well all essential fading models and selection schemes [176, 273, 291], non-orthogonal relaying [135] as well as scheduling users between relaying or receiving [137, 138]. The source or destination may apply also multiantenna techniques for combining direct and relayed signals [175, 254, 277]. Despite of neglecting self-interference, the analysis of [319] is a good reference for the present study on full-duplex relays.

In the spirit of the pioneering works, outage probability is by far the most common performance measure in related literature. There are also many studies on ergodic capacity as surveyed shortly. Other relevant measures include the moments of the end-to-end SNR (especially the average value) [154, 289] and error rates. Some distinctive measures such as the probability of SNR gain [151], the frequency of outages [196] and average outage duration [196] provide an extension for outage analysis.

Two-Hop Links with Multiple Relays

Typical mobile relaying scenarios involve multiple potential relays for two-hop transmission. The reference studies can be classified based on whether a system setup employs all of them all the time or activates each time only "the best" one; some papers, e.g., [317], cover both variations.

On the one hand, all available nodes may participate in relaying [143] which usually requires the allocation of an orthogonal channel for each relays' transmission to allow for diversity combining in the destination while the scheme of [21] renders incoherent signal superposition. Related statistical analysis is reported in [8, 12, 69, 70, 93, 114, 117, 156, 181, 247, 276, 290], to name but a few key references: These works cover jointly all the essential protocol variations, fading models and performance metrics.

On the other hand, spectrum efficiency can be improved by letting just a single relay perform forwarding, which requires only a single channel use and still realizes the cooperative diversity gains. It is impossible to attribute this idea to the very first inventor but it appeared simultaneously in multiple publications, e.g., [20, 22, 177–179, 282], in 2007–2008. Other analytical works worth mentioning are [16, 17, 139, 262, 274, 278, 294]. Studies in this area concern the design and analysis of relay selection with different variations of performance criteria and background constraints.

The multi-relay scenarios discussed above can be contrasted with typical multi-user scenarios in infrastructure-based relaying: Instead of relay selection, downlink/uplink systems apply destination/source selection, i.e., scheduling. This aspect has been studied also with mobile relays [133].

Ergodic Capacity of Relay Links

Notable studies related to the capacity analyses presented herein are reported in [15, 58, 62, 118, 154, 299, 302, 318]; they concern only half-duplex relaying. With differences mainly in the adopted fading models, the capacity of classic three-node relay links with fixed gain (FG) forwarding is evaluated in [299, 302, 318]. The other works study more complex systems with multiple parallel relays [62] and relay selection [15, 58, 118, 154]. Furthermore, [191, 284, 285] analyze the capacity of two-hop multi-relay AF links when their source nodes apply rate and transmit power adaptation schemes developed in [77]: The work of [191] presumes that all relays participate in cooperation while [284, 285] study the impact of outdated CSI in relay selection. Earlier, the capacity of a distributed antenna system (DAS) is evaluated in [40], providing a baseline for relaying at large.

2.3.3 Multihop Relaying

The survey progresses now from abundant two-hop studies to related analytical works which consider systems with *strictly multiple* hops; this means that there are more than one relay in series between a source and a destination. All the works discussed below concentrate on mobile relaying while analytical (cf. simulation-based) studies on multihop infrastructure relay links are rather uncommon, e.g., [134] is an exemplary exception.

Articles [64, 88, 100, 102, 129, 130, 304, 314] can be identified as the key references for the analytical multihop results presented herein. Outage probability analysis is performed for AF relaying over Nakagami channels in [100] and over multiantenna Rayleigh channels in [152]. Similar type of performance analysis for both AF and DF relaying in [102] shows that optimal transmit power allocation is needed if the number of hops is large or the links are highly unbalanced. Transmit power adaptation schemes are discussed also in [314], where the emphasis is on the consequences of exploiting practical, limited, feedback. The work in [129, 130] studies the general statistics of the end-to-end SNR and derives bounds for the outage probability and the average bit-error probability in AF relaying with a comprehensive set of fading models such as Rician, Hoyt and Nakagami channels. In [64], an in-depth study on ergodic capacity is presented for both AF and DF relay links over Rayleigh channels. Furthermore, the second-order statistics (e.g., average fade duration and level crossing rate) are studied for the DF protocol over Rayleigh, Nakagami and Rician channels in [304], and for the AF protocol over Rayleigh channels in [88].

Other notable related works are reported in [7, 11, 63, 65–68]; except for [67], they concern only AF relaying. Article [65] presents outage analysis when power adaptation is used in all relays while article [66] analyzes capacity with adaptive transmission as per [77] at a source only. Symbol-error rates are evaluated in [7,68]; a new end-to-end SNR bound is also developed in [7]. In contrast to usual scope limitation on a single relay chain, some studies adopt networks with multiple multihop branches [7, 63, 206] and connections to also other relays than the nearest neighbor [67].

Studies on the design and analysis of multihop MIMO relay links can be found in [152, 160, 238, 265, 308] as summarized in an earlier subsection; their count is relatively low w.r.t. common two-hop studies (cf. Table 2.1). Likewise, multihop techniques have also been investigated in conjuction with OFDM [313] and, even, multicarrier MIMO [239] transmission.

2.3.4 OFDM(A) Relaying

Finally, this subsection presents an introduction to the statistical analysis of relay links in the context of multicarrier transmission. The massive body of related simulation-based studies cannot be covered herein while the design of OFDM(A) relaying protocols is discussed in Section 2.2.5.

All the studies referenced in the previous subsections can be interpreted to concern an isolated subcarrier within OFDM; this is explained well by [268] where the OFDM context is specified explicitly in contrast to almost all other works. However, single-subcarrier systems do not convey the true multicarrier nature of OFDM(A) or permit the analysis of advanced relaying protocols that exploit frequency-domain processing, e.g., subcarrier pairing. The extension from narrowband systems, e.g., Fig. 2.3(a), to *OFDM* systems, e.g., Figs. 2.3(d) and 2.3(f), is straightforward when analysis needs only marginal fading distributions but usually the usage of joint distributions makes expressions intractable unless "the correlation of the adjacent subcarriers is ignored for simplicity" [38]. In Chapters 7 and 8, such approximations are avoided due to the *OFDMA* context, i.e., as shown by Figs. 2.3(b), 2.3(c), 2.3(e), and 2.3(g), the subcarriers are received by different destinations through independent channels.

Some especially noteworthy works on the statistical analysis of OFDM relay links are reported in [38, 126, 203, 268], all concerning AF relays: Their main results include the evaluation of bit-error rate with variable- and fixed-gain amplification [268], symbol-error rate with subcarrier pairing [38], and outage probability with relay selection [126]; article [203] studies ICI due to oscillator phase noise which is pronounced with OFDM.

2.4 Conclusions

This chapter presented an overview of background concepts related to OFDM relay links, which should be kept in mind when reading through the following technical chapters, and surveyed recent research works that are relevant in the scope of the present study. The discussions allow one to identify scope limitations and differences in earlier studies, thus establishing a niche for the research results reported herein. The observations summarized next should be understood as generalized conclusions drawn from the whole body of literature which the author has studied as a baseline for this dissertation. Thereby, specific citations to individual works

are suppressed below like in the following chapters where these general observations are harnessed to motivate the considered research topics.

The mainstream literature on physical- and link-layer relaying techniques generally overlooks the potential of full-duplex operation: The necessity of the half-duplex constraint due to self-interference is taken for granted and, thus, the main research problem is often to develop advanced concepts to combat the inherent rate loss. But then many theoretical works overlook also the existence of loopback signals analyzing idealized full-duplex relaying without providing good references for their mitigation. With this background, Chapter 3 takes a fresh look at the self-interference issue developing, inter alia, multiantenna techniques for suppressing residual distortion to a tolerable level.

Transmit power allocation in half-duplex relaying is a well-investigated subject but transition to full-duplex context opens up plenty of room for new research, especially when taking residual loopback self-interference into consideration. In addition to end-to-end link optimization, transmit power control is then required by default to avoid relay oscillation due to the feedback loop after passive physical isolation and it can be regarded as a countermeasure for residual interference as discussed in Chapter 4.

Related to the above aspects, earlier literature reflects a rather conservative, polarized view on full-duplex and half-duplex relaying: One mode is usually selected, often without explanations, over the other at an early stage when formulating system models. Adopting a more progressive premise, Chapter 5 poses the trade-off between the modes under residual self-interference by itself as the central research subject.

The analysis of relaying protocols typically assumes single-subcarrier system models which can be implicitly extrapolated to some multicarrier OFDM scenarios. However, such studies do not reveal the effect of intercarrier interference or cover the entire family of feasible OFDM(A) protocols which gives motivation for Chapters 6 and 8, respectively.

Probably due to the huge popularity of cooperative communications, the major part of related studies, which present analytical performance results, focus on multihop transmission through transceivers that are deemed strictly *mobile relays* in the context this study; this point can be inferred from channel fading models in use but it is seldom specified explicitly. In contrast, the present study is formulated consistently to focus on *infrastructure-based relaying* although some concepts would be universally applicable to other kinds of scenarios. This choice of a scope makes it

also necessary to differentiate between downlink and uplink relaying and shifts focus from relay selection to multiuser scheduling in Chapter 7.

Furthermore, one may make the quantitative observation that literature on *two-hop relaying* is significantly more extensive than that on links with three or more hops. Moreover, a typical two-hop study permits of no straightforward extension to the multihop case. In the present study, the first half of the results concerns two-hop transmission through a generic relay node which could be a part of a larger network of nodes comprising *any number of hops*. The latter half concerns explicitly *multihop relaying* or, otherwise, system specifications are accompanied by explanations how the two-hop results can be *extended to the multihop case*.

Many research articles limit their scope to a particular protocol (usually choosing between AF and DF processing) or even to a specific variation (e.g., choosing between FG and VG amplification). Herein all the essential protocols are covered side-by-side in a unified framework whenever feasible. Since the OFDM(A) context adds a multitude of potential options to the design of relaying protocols, such an approach is especially relevant for facilitating general yet discerning comparison. In contrast, earlier studies too often compare system performance after implementing some new protocol concept only to the obvious reference case without it.

Finally, it can be also noted that there are numerous *simulation-based* studies proposing new concepts for the design of OFDM relaying protocols. Such orientation is justified since simulation experiments serve well their purpose of providing a proof of concept and some schemes, e.g., power allocation, often render the analysis of signal-to-noise ratios intractable. However, this dissertation purposefully establishes its contributions by means of rigorous *analytical results* throughout its technical chapters.

3. Mitigation of Self-interference in Full-Duplex Relaying

A substantial, yet unheeded, technical problem in full-duplex relaying is *how to mitigate the effect of unavoidable loopback interference.* For investigating and comparing several solutions, research is motivated by the potential of improving the spectral efficiency of relay systems by avoiding the need of two channel uses for one end-to-end transmission that is inherent for half-duplex relaying. Consequently, it is imperative to show that relays' self-interference can be mitigated sufficiently and that the full-duplex mode is a truly feasible alternative to the half-duplex mode.

This chapter analyzes a broad range of MIMO mitigation schemes from passive isolation to active time-domain cancellation and spatial-domain suppression. Cancellation subtracts a replica of interference from the relay input while suppression reserves spatial dimensions for receive and transmit filtering; the latter can implement antenna subset selection, null-space projection, i.e., reception and transmission in orthogonal directions, or joint transmit and receive eigenbeam selection to support more spatial streams by choosing the weakest eigenmodes for overlapping subspaces. Furthermore, minimum mean squared error filtering can be employed to maintain the desired signal quality, which is inherent for cancellation, and combined time–space processing may be better than either alone. Targeting at minimal interference power, optimal filters are solved for each scheme in the cases of joint, separate and independent design.

The remainder of this chapter[1] is organized as follows. Sections 3.1–3.3 briefly introduce the scope of the study, survey recent related works, and specify a system setup with imperfect side information. The main contributions are presented in Sections 3.4 and 3.5 where mitigation schemes are introduced and evaluated with simulation, experimental and analytical results. Finally, Section 3.6 presents general summary for the chapter.

[1]This chapter is partially based on the material presented in **[208,215,219,221]**.

3.1 Introduction

Spectrum reuse with full-duplex operation would be especially advantageous for relaying. Basically, the same amount of data is transmitted to and from each relay; effective capacity could thus double if two signals allocated only one time/frequency resource. The reality strikes back with loopback self-interference which must be mitigated before the potential gains are realized or full-duplex relaying can be declared viable at all.

All *mitigation* schemes can be categorized into three general subtypes as follows. The same structure is adopted later for the subparts of the technical section where they are elaborated further.

1) Passive physical *isolation* manipulates the electromagnetic properties of relay antennas and loopback channels such that physical signal leakage becomes low. This can be facilitated with antenna partitioning by placing transmit and receive antennas at separate arrays.

2) Time-domain *cancellation* applies the principle of subtraction by creating an artificial feedback circuit which reversely matches and thereby compensates for the physical loopback channel. This can be implemented in the analog or digital domain.

3) Spatial-domain *suppression* exploits multiantenna techniques, e.g., beamforming, by filtering transmitted and received signals such that propagation through strong reflections is avoided or, even, the signals appear orthogonal. This necessitates antenna partitioning.

The latter two involve *active* mitigation by means of signal processing.

Shaking up the status quo, this chapter reports seminal results on the full-duplex loopback problem which is highlighted by the fact that parallel work on self-interference mitigation in full-duplex MIMO relays is scarce as summarized shortly. In particular, earlier literature pessimistically sees loopback interference as an insurmountable issue and resorts to the half-duplex mode by allocating separate time slots or frequency bands for relay reception and transmission. This is a primitive way to avoid relays' feedback loops by splurging spectrum although imperative for cooperative communications. On the other hand, information theory-oriented articles typically study full-duplex relaying without considering the deleterious effect of loopback signals albeit presenting otherwise rigorous results; they actually tend to provide minimal (if any at all) explanations and references for the mitigation of loopback self-interference.

This chapter contributes to the study of full-duplex MIMO relays as follows. The first half concerns the development of mitigation schemes.

- Section 3.3 sets up a generic system model that explicitly accounts for the loopback self-interference and the relay processing delay. As a novel factor, the study recognizes and characterizes the imperfections of the side information which is needed for interference mitigation.
- Section 3.4.1 summarizes thoroughly the means of providing physical isolation. Since the earlier time-domain cancellation techniques almost exclusively deal with the case of analog SISO repeaters, Section 3.4.2 generalizes these concepts to the case of digital MIMO relays.
- The increased degrees of freedom offered by the deployment of multiple antennas in relays opens up a range of new options for suppressing self-interference in the spatial domain. Section 3.4.3 proposes novel spatial suppression schemes based on antenna selection, eigenbeam selection, null-space projection, and minimum mean squared error filters. The combination of subtractive cancellation and spatial suppression is also proposed for reducing the effect of imperfect side information.

The second half concerns the evaluation of the mitigation schemes.

- The simulation results of Section 3.5.1 compare extensively the proposed mitigation schemes in terms of achieved additional isolation using a unified framework. The results verify that the effect of self-interference can be indeed mitigated significantly or even eliminated completely in the ideal case but, in practice, there will be at least weak residual distortion due to imperfect side information used for signal processing.
- The analytical results of Section 3.5.2 present closed-form expressions of additional isolation for schemes that ideally eliminate loopback signals. This characterizes residual distortion occurring in practice due to the joint effect of channel estimation errors and transceiver imperfections.
- The experimental results of Section 3.5.3 evaluate physical isolation arising from array positioning and orientation in the case of antenna partitioning and additional isolation given by spatial suppression using real channel measurement data on propagation environments.

In summary, the study covers loopback self-interference mitigation all the way from problem formulation to solution development and assessment.

3.2 Overview of Parallel Work

This section presents a brief literature survey on studies that consider full-duplex MIMO relays in the presence of loopback self-interference and, thus, forms a solid background for developing new mitigation schemes. The references are chosen to accurately represent the state-of-the-art concepts at the time when the results of this chapter were originally developed and reported in **[208, 215, 219, 221]**; the baseline literature was rather scarce back then before the subject gained popularity. Actually, only [23, 104] can be considered to strictly pre-date the present study, and also the parallel works are published mostly in conference papers due to the newness of the research area. On the other hand, there is a rather large body of literature on conventional SISO repeaters which is not reviewed herein for brevity since the focus is on modern MIMO setups. However, MIMO relaying concepts that do not explicitly recognize the existence of self-interference are already surveyed in Section 2.2.3.

Regarding full-duplex MIMO relays with loop interference, the literature search elicited preliminary ideas [23,104] and recent studies [41,125, 128, 144, 169, 246] conducted in parallel with the present work reported initially in **[208,215,219]**, in a fully-developed form in **[221]**, and now yet again in this chapter. These papers tackle the problem of loop interference mitigation only in a limited scope as discussed next. Especially, the relay processing delay is neglected in [128, 144, 246], which may render the relay practically impossible to implement or make the loop interference not harmful. With focus deviating from the present analysis, [169] considers channel estimation whereas the present study begins from the presumption that such side information is already made available with *any* scheme (including those of [169]). Some contributions of **[215]** and [23,41,125] are summarized in an overview tutorial presentation [110].

Mitigation schemes considered in related literature range from time-domain cancellation [128, 169, 246] (cf. **[215, 219]**) to different variations of spatial-domain suppression such as minimum mean squared error filtering [164] (cf. **[215]**), null-space projection [23,41,42] (cf. **[215,219]**), antenna selection [104], eigenbeam selection [144], and the usage of receive and transmit antennas with orthogonal polarizations [259, 260]. Thus, the diversity of research ideas is wide. However, examples are presented later to elaborate that the techniques of [41, 104, 125, 144] are simplified or suboptimal special cases for some of the schemes developed herein.

The common limitation of some studies, e.g., [128, 144, 164, 246], is to neglect the relay processing delay. In an OFDM context, their system concepts require that the relay demodulates its input symbols and processes them within the cyclic prefix window which is obviously impossible because each symbol needs to be received completely before demodulation. To emphasize the novelty of this work that explicitly accounts for the delay, the behavior of some example protocols is summarized in the converse case. Even if placing causality problems aside, it is observed that the delay-free case makes self-interference a useful signal and, thus, its mitigation would not anymore be any relevant research problem.

The design of MIMO relaying protocols can be separated from that of interference mitigation [164] as assumed also in this study. In particular, after solving a generalized eigenvalue problem for spatial suppression, [164] formulates the design of an optimal relay amplification matrix. More specific results are obtained for joint protocol and mitigation design in [246] while general rate analysis does not need to specify explicitly the processing steps [128]. When limiting the scope to single-stream transmission, the null-space projection concepts developed herein can be used together with beamforming in the relay protocol [39, 43].

The effect of limited transceiver dynamic range in decode-and-forward MIMO relay links is studied in [49]; herein the transmitter-induced nonlinearities are modeled as distortion noise in the same way. Their system setup employs straightforward time-domain cancellation for interference mitigation. However, the rate analysis incorporates also implicit spatial-domain suppression because the proposed relaying protocol optimizes the covariance matrices of transmitted signals.

Seminal channel measurement results on full-duplex MIMO relaying can be found in [96, 198]. The study reported in [198] compares channel gain with and without repeaters in coverage-extension and outdoor-to-indoor forwarding scenarios. The self-interference phenomenon is not observed in [198] though, probably because their measurement scenarios guarantee large passive physical isolation and repeater gain is set to a low level. On the other hand, the study reported in [96] builds the (perhaps) first-ever prototypes of antenna arrays to be used as a full-duplex MIMO relay and concentrates explicitly on measuring loopback channels and physical isolation achieved with the prototypes. By courtesy of the authors of [96], the measurement data is reused in this chapter (and in **[208]**) for the evaluation of spatial-domain suppression.

3.3 System Model

Figure 3.1 shows the considered system setup in a pared-down form with only the most essential components. The system implements two-hop communication via a full-duplex relay (R) node from a source (S) node to a destination (D) node. Adopting the full-duplex (FD) operation mode, the relay receives and transmits simultaneously on a single frequency band which necessitates to efficiently mitigate self-interference coupling back to the relay from a loopback channel. This study is valid as well for generic multihop networks (cf. Fig. 1 of **[221]**) with multiple sources or destinations and mesh-type interconnections between nodes, e.g., direct source-to-destination links. Such systems may also include mixed half- and full-duplex operation and they are not restricted to any specific routing or multiple access strategy for enabling concurrent transmissions.

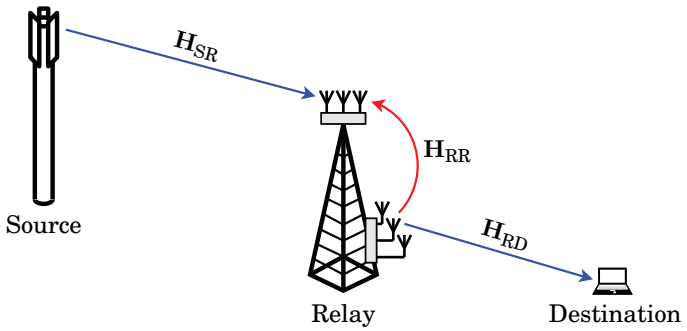

Figure 3.1. Full-duplex multiantenna relay link in the presence of self-interference where $\mathbf{H}_{\mathrm{SR}}$, $\mathbf{H}_{\mathrm{RR}}$, and $\mathbf{H}_{\mathrm{RD}}$ denote the wireless MIMO channels.

Next, signal models are specified in detail including examples on relay protocols and the significance of processing delay, and the introduction of imperfect side information explains why mitigation is a non-trivial task.

3.3.1 MIMO Signal Model

The source(s) and destination(s) have altogether N_{S} transmit and N_{D} receive antennas, respectively, and the relay is equipped with N_{rx} receive and N_{tx} transmit antennas. In practice, FD transceivers are likely implemented with spatially separated receive and transmit arrays which yields physical isolation (cf. Section 3.4.1). However, the following results are also applicable for full-duplex relaying with a single array which is optimistically considered in [125, 259, 260]; this special case is covered by setting $N_{\mathrm{rx}} = N_{\mathrm{tx}}$ and assuming high gain for the loopback channel.

The theoretical signal model is built upon frequency-flat block-fading channels, following the common practice seen in related open literature, e.g., [25, 107, 136, 195, 298, 315]. Given the general context of this thesis, the model is perceived as a representation of a single narrowband subcarrier within practical broadband OFDM transmission throughout the chapter. However, other implementations could be feasible as well.

Matrices $\mathbf{H}_{\mathrm{SR}}[i] \in \mathbb{C}^{N_{\mathrm{rx}} \times N_{\mathrm{S}}}$, $\mathbf{H}_{\mathrm{SD}}[i] \in \mathbb{C}^{N_{\mathrm{D}} \times N_{\mathrm{S}}}$, and $\mathbf{H}_{\mathrm{RD}}[i] \in \mathbb{C}^{N_{\mathrm{D}} \times N_{\mathrm{tx}}}$ shall represent respective combined MIMO channels from all sources to the relay, from all sources to all destinations, and from the relay to all destinations; they may vary between transmitted symbols. At time instant i, the source(s) transmit combined signal vector $\mathbf{x}_{\mathrm{S}}[i] \in \mathbb{C}^{N_{\mathrm{S}}}$, and the relay transmits signal vector $\mathbf{x}_{\mathrm{R}}[i] \in \mathbb{C}^{N_{\mathrm{tx}}}$ while it simultaneously receives signal vector $\mathbf{y}_{\mathrm{R}}[i] \in \mathbb{C}^{N_{\mathrm{rx}}}$. This creates an unavoidable feedback loop from the relay output to the relay input through channel $\mathbf{H}_{\mathrm{RR}}[i] \in \mathbb{C}^{N_{\mathrm{rx}} \times N_{\mathrm{tx}}}$.

Finally, the respective received signals in the relay and in a collective destination node can be expressed as

$$\mathbf{y}_{\mathrm{R}}[i] = \mathbf{H}_{\mathrm{SR}}[i]\,\mathbf{x}_{\mathrm{S}}[i] + \mathbf{H}_{\mathrm{RR}}[i]\,\mathbf{x}_{\mathrm{R}}[i] + \mathbf{n}_{\mathrm{R}}[i], \tag{3.1a}$$

$$\mathbf{y}_{\mathrm{D}}[i] = \mathbf{H}_{\mathrm{SD}}[i]\,\mathbf{x}_{\mathrm{S}}[i] + \mathbf{H}_{\mathrm{RD}}[i]\,\mathbf{x}_{\mathrm{R}}[i] + \mathbf{n}_{\mathrm{D}}[i], \tag{3.1b}$$

where $\mathbf{n}_{\mathrm{R}}[i] \in \mathbb{C}^{N_{\mathrm{rx}}}$ and $\mathbf{n}_{\mathrm{D}}[i] \in \mathbb{C}^{N_{\mathrm{D}}}$ are additive noise vectors in the relay and in the destination, respectively. All these signal and noise vectors are assumed to have zero mean throughout the study and the corresponding covariance matrices are denoted with $\mathbf{R}_{\mathbf{x}_{\mathrm{S}}} \triangleq \mathcal{E}\{\mathbf{x}_{\mathrm{S}}[i]\mathbf{x}_{\mathrm{S}}^{H}[i]\}$, $\mathbf{R}_{\mathbf{x}_{\mathrm{R}}} \triangleq \mathcal{E}\{\mathbf{x}_{\mathrm{R}}[i]\mathbf{x}_{\mathrm{R}}^{H}[i]\}$, and $\mathbf{R}_{\mathbf{n}_{\mathrm{R}}} \triangleq \mathcal{E}\{\mathbf{n}_{\mathrm{R}}[i]\mathbf{n}_{\mathrm{R}}^{H}[i]\}$, from which related transmit powers are defined as $P_{\mathrm{S}} \triangleq \mathrm{tr}\{\mathbf{R}_{\mathbf{x}_{\mathrm{S}}}\}$ and $P_{\mathrm{R}} \triangleq \mathrm{tr}\{\mathbf{R}_{\mathbf{x}_{\mathrm{R}}}\}$.

Relaying Protocols

The concepts developed in this chapter focus on the mitigation of loopback interference and, thereby, the analysis is kept at a general level such that the proposed schemes are versatile and applicable with most of the readily available relaying protocols. In particular, relay processing is denoted universally with a generic function $f(\cdot)$ which generates an output sample based on a sequence of input samples causing integer processing delay τ_{R}. Thus, the input–output relation of the relay is given by

$$\mathbf{x}_{\mathrm{R}}[i] \triangleq f(\mathbf{y}_{\mathrm{R}}[i - \tau_{\mathrm{R}}], \mathbf{y}_{\mathrm{R}}[i - (\tau_{\mathrm{R}} + 1)], \mathbf{y}_{\mathrm{R}}[i - (\tau_{\mathrm{R}} + 2)], \ldots), \tag{3.2}$$

including both the mitigation of self-interference and the processing of data-bearing signals at the moment. For improving clarity without any loss of generality, time indices shall be gradually omitted in the following.

The following two example protocols can be recalled for the purpose of illustration although this study is not by any means limited to them.

Decode-and-forward (DF) relaying is exemplified by a protocol which uses the same codebook in both hops while proper rate adaptation guarantees that the relay can decode its input signal without errors. Thus, $f(\mathbf{y}_\mathrm{R}[i-\tau_\mathrm{R}], \mathbf{y}_\mathrm{R}[i-(\tau_\mathrm{R}+1)], \mathbf{y}_\mathrm{R}[i-(\tau_\mathrm{R}+2)], \ldots) = \mathbf{B}\,\mathbf{x}_\mathrm{S}[i-\tau_\mathrm{R}]$ with some filter $\mathbf{B} \in \mathbb{C}^{N_\mathrm{tx} \times N_\mathrm{S}}$, and the complete signal model becomes

$$\mathbf{y}_\mathrm{R}[i] = \mathbf{H}_\mathrm{SR}\,\mathbf{x}_\mathrm{S}[i] + \mathbf{H}_\mathrm{RR}\mathbf{B}\,\mathbf{x}_\mathrm{S}[i-\tau_\mathrm{R}] + \mathbf{n}_\mathrm{R}[i], \tag{3.3a}$$

$$\mathbf{y}_\mathrm{D}[i] = \mathbf{H}_\mathrm{SD}\,\mathbf{x}_\mathrm{S}[i] + \mathbf{H}_\mathrm{RD}\mathbf{B}\,\mathbf{x}_\mathrm{S}[i-\tau_\mathrm{R}] + \mathbf{n}_\mathrm{D}[i]. \tag{3.3b}$$

In spite of the assumption of error-free decoding in the relay, the loopback signal should be considered harmful because residual self-interference reduces the maximum achievable rate in the first hop.

Amplify-and-forward (AF) relaying is exemplified by a protocol where the relay filters its input signal with some matrix $\mathbf{B} \in \mathbb{C}^{N_\mathrm{tx} \times N_\mathrm{rx}}$. Now $f(\mathbf{y}_\mathrm{R}[i-\tau_\mathrm{R}]) = \mathbf{B}\,\mathbf{y}_\mathrm{R}[i-\tau_\mathrm{R}]$, and the complete signal model becomes

$$\mathbf{y}_\mathrm{R}[i] = \sum_{j=0}^{\infty} (\mathbf{H}_\mathrm{RR}\mathbf{B})^j \left(\mathbf{H}_\mathrm{SR}\,\mathbf{x}_\mathrm{S}[i-j\,\tau_\mathrm{R}] + \mathbf{n}_\mathrm{R}[i-j\,\tau_\mathrm{R}]\right), \tag{3.4a}$$

$$\begin{aligned}\mathbf{y}_\mathrm{D}[i] = {} & \mathbf{H}_\mathrm{SD}\,\mathbf{x}_\mathrm{S}[i] + \mathbf{H}_\mathrm{RD}\mathbf{B} \sum_{j=1}^{\infty} (\mathbf{H}_\mathrm{RR}\mathbf{B})^{j-1} \mathbf{H}_\mathrm{SR}\,\mathbf{x}_\mathrm{S}[i-j\,\tau_\mathrm{R}] \\ & + \mathbf{H}_\mathrm{RD}\mathbf{B} \sum_{j=1}^{\infty} (\mathbf{H}_\mathrm{RR}\mathbf{B})^{j-1}\,\mathbf{n}_\mathrm{R}[i-j\,\tau_\mathrm{R}] + \mathbf{n}_\mathrm{D}[i].\end{aligned} \tag{3.4b}$$

The end-to-end transmission is degraded because the feedback loop channel causes both noise amplification and infinitely repeating echo signal components. Especially, proper gain control is thus needed, such that $\mathbf{H}_\mathrm{RR}\mathbf{B}$ is guaranteed to be a convergent matrix, in order to prevent relay oscillation and to bound transmit power.

As can be noted from above, both example protocols are "repetition-based", i.e., they try to match $\mathbf{x}_\mathrm{R}$ with $\mathbf{x}_\mathrm{S}$ under different processing constraints.

Processing Delay

The processing delay τ_R is regarded as strictly positive in contrast to studies in [128, 144, 246] for two reasons. Firstly, the loopback signal may not otherwise be interference or harmful at all as also noted in [128]. Secondly, there are severe causality problems in the implementation of relaying protocols that could avoid all delay. The behavior of the example protocols without the processing delay is briefly discussed next to emphasize the novelty of the present work that explicitly accounts for this factor.

With the example DF protocol, the complete signal model is reduced after setting $\tau_\mathrm{R} = 0$ in (3.3) to

$$\mathbf{y}_\mathrm{R} = (\mathbf{H}_\mathrm{SR} + \mathbf{H}_\mathrm{RR}\mathbf{B})\mathbf{x}_\mathrm{S} + \mathbf{n}_\mathrm{R}, \tag{3.5a}$$

$$\mathbf{y}_\mathrm{D} = (\mathbf{H}_\mathrm{SD} + \mathbf{H}_\mathrm{RD}\mathbf{B})\mathbf{x}_\mathrm{S} + \mathbf{n}_\mathrm{D}. \tag{3.5b}$$

Hence, the feedback loop does not cause any interference but instead the desired signal components are actually just amplified. Moreover, causality would be violated when translating this theoretical system into practice because it is impossible to sequentially decode, process, re-encode, and retransmit a symbol before it has been completely received, i.e., the minimum viable delay is one sample.

With the example AF protocol, the received signal at the relay is simplified after setting $\tau_\mathrm{R} = 0$ from (3.4a) to

$$\mathbf{y}_\mathrm{R} = (\mathbf{I} - \mathbf{H}_\mathrm{RR}\mathbf{B})^{-1}(\mathbf{H}_\mathrm{SR}\,\mathbf{x}_\mathrm{S} + \mathbf{n}_\mathrm{R}). \tag{3.6a}$$

To allow the inverse to exist, none of the eigenvalues of $\mathbf{H}_\mathrm{RR}\mathbf{B}$ can be equal to one; the condition is needed for avoiding transmitting a signal that cancels the useful signal in the relay input in some dimension. In fact, this anomaly appears only due to the neglected processing delay. The system becomes equivalent to an interference-free AF relay link with a conventional end-to-end signal model

$$\mathbf{y}_\mathrm{D} = (\mathbf{H}_\mathrm{SD} + \mathbf{H}_\mathrm{RD}\hat{\mathbf{B}}\mathbf{H}_\mathrm{SR})\mathbf{x}_\mathrm{S} + \mathbf{H}_\mathrm{RD}\hat{\mathbf{B}}\,\mathbf{n}_\mathrm{R} + \mathbf{n}_\mathrm{D}, \tag{3.6b}$$

in which the effective amplification factor of the relay is given by $\hat{\mathbf{B}} = \mathbf{B}(\mathbf{I} - \mathbf{H}_\mathrm{RR}\mathbf{B})^{-1}$. Earlier literature has already studied such systems extensively and there are many solutions for designing $\hat{\mathbf{B}}$. Assuming that $\mathbf{H}_\mathrm{RR}$ is sufficiently well known, almost any desired effective amplification $\hat{\mathbf{B}}$ can then be implemented simply by selecting $\mathbf{B} = \hat{\mathbf{B}}(\mathbf{I} + \mathbf{H}_\mathrm{RR}\hat{\mathbf{B}})^{-1}$ as pointed out in [128]. Thereby, loopback interference cannot be considered harmful in the delay-free case.

In summary, there would be no need for the mitigation of loopback signals if it was feasible to implement relay processing without any delay.

When $\tau_\mathrm{R} = 0$, these narrowband signal models with frequency-flat channels are also incompatible with any wideband implementation. The narrowband context is valid for each OFDM subcarrier but then $\tau_\mathrm{R} > 0$ since a complete symbol needs to be received and demodulated before subcarriers can be processed in the frequency domain. As discussed in Chapter 8, time-domain processing limits the design options of OFDM(A) protocols to simplistic waveform repetition.

3.3.2 Side Information for Mitigation

The considered mitigation techniques are tailored to allow transparent implementation, i.e., they only require information which the relay should know by design or is able to measure by itself. In other words, mitigation may exploit knowledge of only $\mathbf{x}_\mathrm{R}$, $\mathbf{H}_\mathrm{RR}$, and $\mathbf{H}_\mathrm{SR}$. However, the available side information is still degraded due to the following non-idealities, which makes it impossible to eliminate loopback self-interference completely and, consequently, the minimization of residual interference power becomes a challenging research problem.

Channel Estimation Error

The relay may exploit any off-the-shelf technique or some scheme developed specifically for full-duplex relays [169, 190] to obtain respective estimates $\tilde{\mathbf{H}}_\mathrm{RR}$ and $\tilde{\mathbf{H}}_\mathrm{SR}$ of $\mathbf{H}_\mathrm{RR}$ and $\mathbf{H}_\mathrm{SR}$. Such processes are non-ideal in practice, which is modeled herein with additive error coefficients $\boldsymbol{\Delta}\tilde{\mathbf{H}}_\mathrm{RR}$ and $\boldsymbol{\Delta}\tilde{\mathbf{H}}_\mathrm{SR}$ so that estimates differ from physical channels as

$$\mathbf{H}_\mathrm{RR} = \tilde{\mathbf{H}}_\mathrm{RR} + \boldsymbol{\Delta}\tilde{\mathbf{H}}_\mathrm{RR}, \tag{3.7a}$$

$$\mathbf{H}_\mathrm{SR} = \tilde{\mathbf{H}}_\mathrm{SR} + \boldsymbol{\Delta}\tilde{\mathbf{H}}_\mathrm{SR}, \tag{3.7b}$$

while all elements of $\boldsymbol{\Delta}\tilde{\mathbf{H}}_\mathrm{RR}$ and $\boldsymbol{\Delta}\tilde{\mathbf{H}}_\mathrm{SR}$ are assumed to be independent (both mutually and from the corresponding channels) circularly symmetric complex Gaussian random variables [266]. The variance of the estimation error components is defined with relative error level $\epsilon_\mathbf{H}$ such that

$$\mathcal{E}\{|\{\boldsymbol{\Delta}\tilde{\mathbf{H}}_\mathrm{RR}\}_{i,j}|^2\} = \epsilon_\mathbf{H}^2 \mathcal{E}\{|\{\mathbf{H}_\mathrm{RR}\}_{i,j}|^2\} \tag{3.8a}$$

for all $i = 1, 2, \ldots, N_\mathrm{rx}$ and $j = 1, 2, \ldots, N_\mathrm{tx}$. Thus, $\|\boldsymbol{\Delta}\tilde{\mathbf{H}}_\mathrm{RR}\|_F^2 \sim \mathcal{G}(k, \theta)$ which means that the Frobenius norm of the error matrix becomes a gamma random variable with shape $k = N_\mathrm{rx}N_\mathrm{tx}$ and scale $\theta = \epsilon_\mathbf{H}^2 \frac{\mathcal{E}\{\|\mathbf{H}_\mathrm{RR}\|_F^2\}}{N_\mathrm{rx}N_\mathrm{tx}}$. Analogous relations hold also between $\tilde{\mathbf{H}}_\mathrm{SR}$ and $\mathbf{H}_\mathrm{SR}$, i.e.,

$$\mathcal{E}\{|\{\boldsymbol{\Delta}\tilde{\mathbf{H}}_\mathrm{SR}\}_{i,j}|^2\} = \epsilon_\mathbf{H}^2 \mathcal{E}\{|\{\mathbf{H}_\mathrm{SR}\}_{i,j}|^2\} \tag{3.8b}$$

for all $i = 1, 2, \ldots, N_\mathrm{rx}$ and $j = 1, 2, \ldots, N_\mathrm{S}$.

Transmit Signal Noise

The relay obviously knows the digital baseband signal $\tilde{\mathbf{x}}_\mathrm{R}$ it generates itself, but the corresponding transmitted analog signal $\mathbf{x}_\mathrm{R}$ cannot be *perfectly* identified. This is because any practical implementation of signal conversion between baseband and radio frequencies is prone to various

distortion effects such as carrier frequency offset, oscillator phase noise, digital-to-analog conversion imperfections, I/Q imbalance, and high-power amplifier nonlinearity among others [73, 280].

The joint effect of all such imperfections is modeled herein by introducing additive transmit distortion noise vector $\mathbf{\Delta}\tilde{\mathbf{x}}_{\mathrm{R}}$ based on which

$$\mathbf{x}_{\mathrm{R}} = \tilde{\mathbf{x}}_{\mathrm{R}} + \mathbf{\Delta}\tilde{\mathbf{x}}_{\mathrm{R}}. \tag{3.9}$$

The elements of $\mathbf{\Delta}\tilde{\mathbf{x}}_{\mathrm{R}}$ are modeled as independent identically-distributed circularly symmetric complex Gaussian random variables, and their variance is defined with relative distortion level $\epsilon_{\mathbf{x}}$. Consequently, the covariance matrix of transmit signal noise is chosen as

$$\mathbf{R}_{\mathbf{\Delta}\tilde{\mathbf{x}}_{\mathrm{R}}} \triangleq \mathcal{E}\{\mathbf{\Delta}\tilde{\mathbf{x}}_{\mathrm{R}}\mathbf{\Delta}\tilde{\mathbf{x}}_{\mathrm{R}}^{H}\} = \epsilon_{\mathbf{x}}^{2}\frac{\mathrm{tr}\{\mathbf{R}_{\tilde{\mathbf{x}}_{\mathrm{R}}}\}}{N_{\mathrm{tx}}}\mathbf{I} \tag{3.10}$$

in which $\mathbf{R}_{\tilde{\mathbf{x}}_{\mathrm{R}}} \triangleq \mathcal{E}\{\tilde{\mathbf{x}}_{\mathrm{R}}\tilde{\mathbf{x}}_{\mathrm{R}}^{H}\}$. In addition, $\tilde{\mathbf{x}}_{\mathrm{R}}$ and $\mathbf{\Delta}\tilde{\mathbf{x}}_{\mathrm{R}}$ are assumed to be uncorrelated which implies that $\mathbf{R}_{\mathbf{x}_{\mathrm{R}}} = \mathbf{R}_{\tilde{\mathbf{x}}_{\mathrm{R}}} + \mathbf{R}_{\mathbf{\Delta}\tilde{\mathbf{x}}_{\mathrm{R}}}$. The level of transmit distortion is typically well below the actual data signal, i.e., $\epsilon_{\mathbf{x}} \ll 1$, although it has fundamental effect on full-duplex transceivers. Thus, the relay transmit power can be re-defined as $P_{\mathrm{R}} \triangleq \mathrm{tr}\{\mathbf{R}_{\tilde{\mathbf{x}}_{\mathrm{R}}}\} \approx \mathrm{tr}\{\mathbf{R}_{\mathbf{x}_{\mathrm{R}}}\}$ and it is reasonable to use both definitions interchangeably.

Similar models have been adopted recently in [19, 48, 49]. Furthermore, it should be noted that analogous distortion effects occur also at receiver side when transforming radio-frequency signal $\tilde{\mathbf{y}}_{\mathrm{R}}$ into digital baseband signal $\mathbf{y}_{\mathrm{R}}$ which is used as an input for the relay protocol $f(\cdot)$. This fact is not neglected in this study but, as per common practice, the joint effect of all receiver imperfections is implicitly included within the conventional thermal noise vector $\mathbf{n}_{\mathrm{R}}$. Thus, one may effectively denote $\mathbf{y}_{\mathrm{R}} = \tilde{\mathbf{y}}_{\mathrm{R}}$.

3.4 Self-interference Mitigation Techniques

This section proceeds to the first part of the main technical contribution of this chapter by proposing solutions for self-interference mitigation.

In what follows, the mitigation of loopback self-interference is decoupled from the design of relaying protocols in order to develop "transparent" solutions that transform the physical $N_{\mathrm{rx}} \times N_{\mathrm{tx}}$ relay to an equivalent "interference-free" $\hat{N}_{\mathrm{rx}} \times \hat{N}_{\mathrm{tx}}$ relay. Here $\hat{N}_{\mathrm{rx}}$ and $\hat{N}_{\mathrm{tx}}$ represent the input and output dimensions, i.e., the number of spatial streams, reserved for the actual relaying protocol $\hat{f}(\cdot)$. Without loss of generality, the concepts presume that $\hat{N}_{\mathrm{rx}} \leq N_{\mathrm{rx}}$ and $\hat{N}_{\mathrm{tx}} \leq N_{\mathrm{tx}}$ because the end-to-end system cannot benefit from extra artificial dimensions inside of the relay.

The target is to make residual loopback self-interference so infinitesimal that it can be regarded simply as additional relay input noise. Omitting the direct source–destination link for compactness, the signal model should be effectively transformed from (3.1) to

$$\hat{\mathbf{y}}_{\mathrm{R}} = \hat{\mathbf{H}}_{\mathrm{SR}}\,\mathbf{x}_{\mathrm{S}} + \hat{\mathbf{n}}_{\mathrm{R}}, \tag{3.11a}$$

$$\mathbf{y}_{\mathrm{D}} = \hat{\mathbf{H}}_{\mathrm{RD}}\,\hat{\mathbf{x}}_{\mathrm{R}} + \mathbf{n}_{\mathrm{D}}. \tag{3.11b}$$

Above $\hat{\mathbf{y}}_{\mathrm{R}} \in \mathbb{C}^{\hat{N}_{\mathrm{rx}}}$ and $\hat{\mathbf{x}}_{\mathrm{R}} \in \mathbb{C}^{\hat{N}_{\mathrm{tx}}}$ are the respective receive and transmit signal vectors of the equivalent interference-free relay, $\hat{\mathbf{H}}_{\mathrm{SR}} \in \mathbb{C}^{\hat{N}_{\mathrm{rx}} \times N_{\mathrm{S}}}$ and $\hat{\mathbf{H}}_{\mathrm{RD}} \in \mathbb{C}^{N_{\mathrm{D}} \times \hat{N}_{\mathrm{tx}}}$ represent respective equivalent MIMO channels from sources to the interference-free relay and from the interference-free relay to destinations, and $\hat{\mathbf{n}}_{\mathrm{R}} \in \mathbb{C}^{\hat{N}_{\mathrm{rx}}}$ is an equivalent noise vector including all residual self-interference after mitigation, receiver distortion and usual thermal noise. The covariance matrix of $\hat{\mathbf{x}}_{\mathrm{R}}$ is defined as $\mathbf{R}_{\hat{\mathbf{x}}_{\mathrm{R}}} \triangleq \mathcal{E}\{\hat{\mathbf{x}}_{\mathrm{R}}\hat{\mathbf{x}}_{\mathrm{R}}^{H}\}$.

The equivalent "interference-free" relay applies generic relaying protocol $\hat{f}(\cdot)$ to obtain $\hat{\mathbf{x}}_{\mathrm{R}}$ from $\hat{\mathbf{y}}_{\mathrm{R}}$ in the spirit of (3.2). By decoupling mitigation from protocol design, the relay may adopt, directly or after minor modifications, any of the protocols designed for cases without loop interference in earlier literature. However, the system setup or the relaying protocol can still affect the choices of $\hat{N}_{\mathrm{rx}}$ and $\hat{N}_{\mathrm{tx}}$ that need to be supported.

3.4.1 Passive Physical Isolation

Relay installation must guarantee some *physical isolation*, which is directly represented by channel matrix $\mathbf{H}_{\mathrm{RR}}$, to facilitate the usage of active signal processing techniques which provide additional *man-made* isolation. This is because, in practice, the dynamic range of any front-end circuitry is finite and, thus, large difference in power levels may saturate the receiver rendering any attempt to recover the desired signal futile.

The development of physical isolation schemes is of experimental nature, i.e., such research requires prototype manufacturing and measurements, whereas this thesis lies essentially in the context of digital signal processing. For completeness, physical isolation is briefly surveyed below.

Antenna Partitioning, Antenna Directivity, and Blocked Line-of-Sight
By partitioning transmit and receive antennas into separate arrays, physical isolation arises already from the sheer *physical distance of the arrays* due to propagation loss. This is studied in Section 3.5.3 and in **[208]** based on the measurement data of [96]. Furthermore, antenna partition-

ing facilitates benefits from the physical properties of the relay installation and its arrays. However, physical isolation remains rather low when implementing *compact* full-duplex transceivers, such as the SISO prototype of [55], and the design challenges become even more pronounced in MIMO cases [96] with coupling between multiple antennas.

Especially, *antenna elements can be directional* and pointed at different angles (which is inherent for relaying) with antenna partitioning. This option is studied in MIMO relaying scenarios in Section 3.5.3, **[208]**, and [96] as well as with SISO antenna deployment in [56]. When the system geometry permits, rational relay deployment should also guarantee obstacles in between the arrays to block their line-of-sight which obviously gives significant additional physical isolation. For this purpose, the installation may exploit surrounding structures or add, e.g., a shielding plate but already a thick window glass can be rather useful even though the optical path is not blocked, as noted in Section 3.5.3.

If the same antenna array is used for both receiving and transmitting, as assumed in [125], all physical isolation comes solely from a *duplex circuit* connecting input and output feeds to each physical antenna element. Such duplexers are used in continuous-wave radars and radio-frequency identification (RFID) readers but isolation offered by the most high-end devices may not be sufficient for modern high-rate communication.

Different Polarizations for Receive and Transmit Antennas

The polarization of electromagnetic waves can be also exploited for improving the physical isolation. It is well known how to design and manufacture antenna elements that radiate or absorb linearly polarized waves; a simple dipole is a textbook example of such antennas. Typically, systems will use either vertical, horizontal or slant 45-degree polarization (w.r.t. the Earth's surface). The self-interference signal is attenuated significantly if the transmit and receive antenna arrays have different polarizations and the loopback channel does not distort the polarization too much. Antenna polarization is an essential aspect in the systems considered in [96, 259, 260] and it is also mentioned in **[208, 219, 221]**.

In theory, the self-interference signal could be blocked completely when all the elements of the receive antenna array have the same polarization which is orthogonal to the polarization of the transmit antenna elements. Such an idealistic setup is considered in [259, 260], where the authors study the performance of two-hop full-duplex communication using

a SISO amplify-and-forward relay. Although the self-interference problem of full-duplex relays is not mentioned at all in these papers, the authors assume implicitly that it can be solved perfectly by using one dual-polarized antenna element for full-duplex operation such that the vertically (resp. horizontally) polarized feed is reserved for reception (resp. transmission). Consequently, their signal model does not incorporate any residual self-interference that could arise due to non-idealities.

In practice, the usage of different polarizations should be regarded only as one of many techniques to improve the physical isolation, instead of proclaiming it to be the ultimate solution for the self-interference problem. This is because real-world antenna elements are not perfectly polarized and the polarization is preserved only in ideal line-of-sight channels without reflections. The usage of different polarizations to yield higher isolation is demonstrated in [96] by building experimental antenna arrays for a MIMO full-duplex relay. In particular, the transmit antenna elements are slanted 45 degrees w.r.t. the receive antenna elements. The authors also test similar arrays with orthogonal polarizations and observe minimal isolation improvement; this can be attributed to the depolarization effect of multipath scattering in the self-interference channel.

Residual Self-interference Level

Without active mitigation, the mean square error (MSE) matrix of the relay input signal is derived from the original signal model (3.1a) as

$$\begin{aligned}\mathbf{M} &\triangleq \mathcal{E}\{[(\mathbf{H}_{\mathrm{SR}}\,\mathbf{x}_{\mathrm{S}}+\mathbf{n}_{\mathrm{R}})-\mathbf{y}_{\mathrm{R}}][(\mathbf{H}_{\mathrm{SR}}\,\mathbf{x}_{\mathrm{S}}+\mathbf{n}_{\mathrm{R}})-\mathbf{y}_{\mathrm{R}}]^{H}\}\\ &= \mathcal{E}\{\mathbf{H}_{\mathrm{RR}}\,\mathbf{x}_{\mathrm{R}}\mathbf{x}_{\mathrm{R}}^{H}\,\mathbf{H}_{\mathrm{RR}}^{H}\}\\ &= \mathbf{H}_{\mathrm{RR}}\mathbf{R}_{\mathbf{x}_{\mathrm{R}}}\mathbf{H}_{\mathrm{RR}}^{H},\end{aligned} \tag{3.12}$$

which yields the residual loopback self-interference power as

$$P_{\mathrm{I}} \triangleq \mathrm{tr}\{\mathbf{M}\} = \mathcal{E}\{\mathrm{tr}\{\mathbf{H}_{\mathrm{RR}}\,\mathbf{x}_{\mathrm{R}}\mathbf{x}_{\mathrm{R}}^{H}\,\mathbf{H}_{\mathrm{RR}}^{H}\}\} = \mathcal{E}\{\|\mathbf{H}_{\mathrm{RR}}\,\mathbf{x}_{\mathrm{R}}\|_2^2\}. \tag{3.13}$$

In the following, it is presumed that all means of improving physical isolation have been exploited and the study concentrates on signal processing techniques to mitigate residual interference, i.e., the effect of $\mathbf{H}_{\mathrm{RR}} \neq \mathbf{0}$.

Especially, measurements [96] indicate that physical isolation is not usually sufficient alone. Thereby, this study pays less attention to rather exceptional setups in which passive isolation is large already before active mitigation. As a trivial example of such setups, one could imagine a relay with its receive antenna array placed outdoors and its transmit antenna array providing coverage in an underground metro tunnel.

3.4.2 Time-Domain Cancellation

Subtractive interference elimination is perhaps the first form of active mitigation that occurs to anyone educated in radio engineering. In principle, time-domain cancellation is based on the reasonable presumption that the relay always knows its own transmitted signals at least approximately; if the relay can also emulate the loopback channel, interfering signals may be replicated and subtracted from received signals.

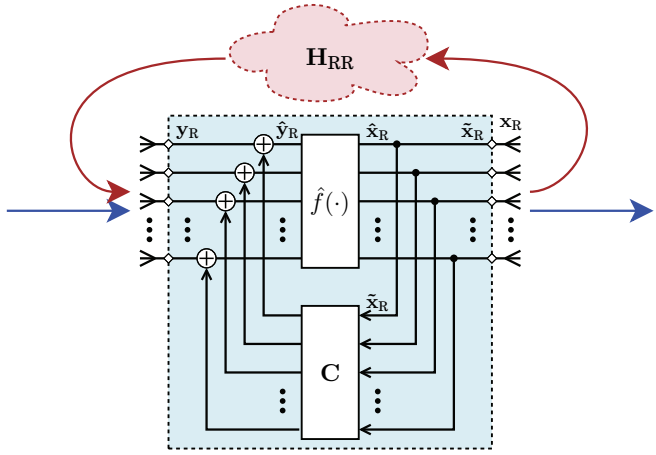

Figure 3.2. Time-domain self-interference cancellation in a full-duplex MIMO relay by subtracting replicated loopback signals from input signals.

Analog Cancellation

The relay may apply conventional *analog pre-cancellation* [37] to improve the feasibility of digital mitigation techniques for lower dynamic range. Unfortunately, the implementation of electronics becomes expensive and difficult if the respective circuit is more sophisticated than a phase shifter that removes one (ideally the strongest) multipath component. Thereby, all mitigation techniques exploit digital baseband signal processing in the rest of the chapter. However, if analog cancellation is used, matrix $\mathbf{H}_{\mathrm{RR}}$ will represent the corresponding residual channel.

Digital Cancellation

The proposed time-domain cancellation (TDC) scheme can be seen as the MIMO version of earlier digital baseband SISO concepts [89,190]; it is implemented as shown in Fig. 3.2 where signals correspond to those used in (3.1a), (3.9), and (3.11a). Especially, the relay contains a digital baseband feedback loop with MIMO cancellation filter $\mathbf{C} \in \mathbb{C}^{N_{\mathrm{rx}} \times N_{\mathrm{tx}}}$.

As the block diagram of Fig. 3.2 indicates, signal models (3.1a), (3.9), and (3.11a) are linked together in the case of cancellation according to

$$\hat{\mathbf{y}}_\mathrm{R} = \mathbf{y}_\mathrm{R} + \mathbf{C}\,\tilde{\mathbf{x}}_\mathrm{R}, \tag{3.14a}$$

$$\tilde{\mathbf{x}}_\mathrm{R} = \hat{\mathbf{x}}_\mathrm{R}. \tag{3.14b}$$

The latter equation implies $\mathbf{R}_{\tilde{\mathbf{x}}_\mathrm{R}} = \mathbf{R}_{\hat{\mathbf{x}}_\mathrm{R}}$ for the covariance matrices. Since there is no filtering in the feedforward path, $\hat{\mathbf{H}}_\mathrm{SR} = \mathbf{H}_\mathrm{SR}$ and $\hat{\mathbf{H}}_\mathrm{RD} = \mathbf{H}_\mathrm{RD}$.

To be used in (3.11a), the equivalent receiver noise vector of the intended "interference-free" relay becomes

$$\hat{\mathbf{n}}_\mathrm{R} = \hat{\mathbf{H}}_\mathrm{RR}\,\hat{\mathbf{x}}_\mathrm{R} + \mathbf{H}_\mathrm{RR}\,\boldsymbol{\Delta}\tilde{\mathbf{x}}_\mathrm{R} + \mathbf{n}_\mathrm{R}, \tag{3.15}$$

in which the residual loopback channel is given by

$$\hat{\mathbf{H}}_\mathrm{RR} = \mathbf{H}_\mathrm{RR} + \mathbf{C} = \tilde{\mathbf{H}}_\mathrm{RR} + \mathbf{C} + \boldsymbol{\Delta}\tilde{\mathbf{H}}_\mathrm{RR}. \tag{3.16}$$

Thus, the MSE matrix of the relay input signal becomes

$$\begin{aligned}\mathbf{M} &\triangleq \mathcal{E}\{[(\mathbf{H}_\mathrm{SR}\,\mathbf{x}_\mathrm{S} + \mathbf{n}_\mathrm{R}) - \hat{\mathbf{y}}_\mathrm{R}][(\mathbf{H}_\mathrm{SR}\,\mathbf{x}_\mathrm{S} + \mathbf{n}_\mathrm{R}) - \hat{\mathbf{y}}_\mathrm{R}]^H\} \\ &= (\mathbf{H}_\mathrm{RR} + \mathbf{C})\mathbf{R}_{\tilde{\mathbf{x}}_\mathrm{R}}(\mathbf{H}_\mathrm{RR} + \mathbf{C})^H + \mathbf{H}_\mathrm{RR}\mathbf{R}_{\boldsymbol{\Delta}\tilde{\mathbf{x}}_\mathrm{R}}\mathbf{H}_\mathrm{RR}^H. \end{aligned} \tag{3.17}$$

If cancellation is not used, i.e., $\mathbf{C} = \mathbf{0}$, (3.17) is reduced to (3.12).

The first term of the MSE matrix includes the channel estimation error and the second term arises due to the transmit signal noise. Cancellation can only eliminate the known part of the first term by choosing $\mathbf{C} = -\tilde{\mathbf{H}}_\mathrm{RR}$ which results in $\hat{\mathbf{H}}_\mathrm{RR} = \boldsymbol{\Delta}\tilde{\mathbf{H}}_\mathrm{RR}$. Thereby, (3.17) yields the residual self-interference power as

$$\begin{aligned}P_\mathrm{I} &\triangleq \mathrm{tr}\{\mathbf{M}\} \\ &= \mathrm{tr}\{\boldsymbol{\Delta}\tilde{\mathbf{H}}_\mathrm{RR}\mathbf{R}_{\tilde{\mathbf{x}}_\mathrm{R}}\boldsymbol{\Delta}\tilde{\mathbf{H}}_\mathrm{RR}^H\} + \mathrm{tr}\{\mathbf{H}_\mathrm{RR}\mathbf{R}_{\boldsymbol{\Delta}\tilde{\mathbf{x}}_\mathrm{R}}\mathbf{H}_\mathrm{RR}^H\} \\ &= \mathcal{E}\{\|\boldsymbol{\Delta}\tilde{\mathbf{H}}_\mathrm{RR}\,\hat{\mathbf{x}}_\mathrm{R} + \mathbf{H}_\mathrm{RR}\,\boldsymbol{\Delta}\tilde{\mathbf{x}}_\mathrm{R}\|_2^2\}. \end{aligned} \tag{3.18}$$

As can be directly seen from above, the main drawback of time-domain cancellation is its blindness to the spatial domain, e.g., low rank of $\mathbf{H}_\mathrm{RR}$ is not expected to yield better isolation. Additionally, the scheme is sensitive to both channel estimation error $\boldsymbol{\Delta}\tilde{\mathbf{H}}_\mathrm{RR}$ and transmit signal noise $\boldsymbol{\Delta}\tilde{\mathbf{x}}_\mathrm{R}$ as shown by (3.18). In fact, a new signal is added in the relay input which may actually even lead to degraded isolation compared to pure physical passive isolation with high level of channel estimation error.

The advantage of cancellation is that it does not distort the signals of interest which is illustrated by the fact that $\hat{\mathbf{H}}_\mathrm{SR} = \mathbf{H}_\mathrm{SR}$ and $\hat{\mathbf{H}}_\mathrm{RD} = \mathbf{H}_\mathrm{RD}$. Especially, cancellation reserves all input and output dimensions of the relay for the protocol, i.e., $\hat{f}(\cdot) = f(\cdot)$, $\hat{N}_\mathrm{rx} = N_\mathrm{rx}$ and $\hat{N}_\mathrm{tx} = N_\mathrm{tx}$, as opposed to spatial-domain suppression schemes discussed shortly.

Hybrid Digital/Analog Cancellation

In summary, it is beneficial to do cancellation before analog-to-digital converters to avoid their saturation due to self-interference while signal filtering to match the loopback channel output is much easier in the digital domain. These good sides can be combined in hybrid digital/analog cancellation [55] where a digitally filtered signal is fed through digital-to-analog converters to eliminate interference in the analog domain; the most this costs is an extra transmitter chain per each receive antenna. In the context of this thesis, hybrid cancellation is analytically equivalent to pure digital cancellation and, thus, it is not considered separately.

3.4.3 Spatial-Domain Suppression

While only cancellation is possible in SISO relays, a new dimension opens up for mitigation when considering modern MIMO relays. Especially, suppression exploits feedforward filtering so that, although signals overlap in the time domain, their interference is weak in the spatial domain.

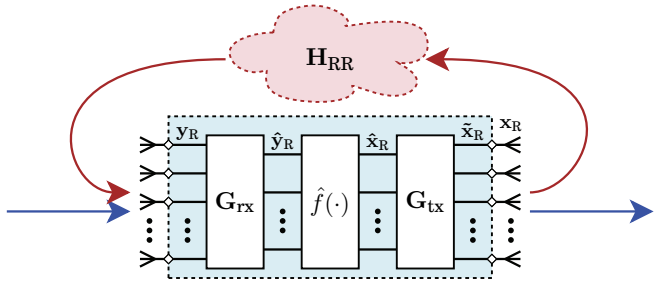

Figure 3.3. Spatial-domain self-interference suppression in a full-duplex MIMO relay by using linear receive and transmit filters in the feedforward path.

The relay applies MIMO receive filter $\mathbf{G}_{\mathrm{rx}} \in \mathbb{C}^{\hat{N}_{\mathrm{rx}} \times N_{\mathrm{rx}}}$ and MIMO transmit filter $\mathbf{G}_{\mathrm{tx}} \in \mathbb{C}^{N_{\mathrm{tx}} \times \hat{N}_{\mathrm{tx}}}$ for suppression as illustrated in Fig. 3.3. Their gain is normalized such that $\|\mathbf{G}_{\mathrm{rx}}\|_F^2 = N_{\mathrm{rx}}$ and $\|\mathbf{G}_{\mathrm{tx}}\|_F^2 = \hat{N}_{\mathrm{tx}}$ with all schemes throughout this chapter. Especially, this will allow one to conveniently re-define (yet again) the relay transmit power as $P_{\mathrm{R}} \triangleq \mathrm{tr}\{\mathbf{R}_{\hat{\mathbf{x}}_{\mathrm{R}}}\}$.

Like the block diagram of Fig. 3.3 indicates, signal models (3.1a), (3.9), and (3.11a) are linked together in the case of suppression according to

$$\hat{\mathbf{y}}_{\mathrm{R}} = \mathbf{G}_{\mathrm{rx}}\, \mathbf{y}_{\mathrm{R}}, \tag{3.19a}$$

$$\tilde{\mathbf{x}}_{\mathrm{R}} = \mathbf{G}_{\mathrm{tx}}\, \hat{\mathbf{x}}_{\mathrm{R}}. \tag{3.19b}$$

Equivalent filtered channels used in (3.11) become $\hat{\mathbf{H}}_{\mathrm{SR}} = \mathbf{G}_{\mathrm{rx}}\mathbf{H}_{\mathrm{SR}}$ and $\hat{\mathbf{H}}_{\mathrm{RD}} = \mathbf{H}_{\mathrm{RD}}\mathbf{G}_{\mathrm{tx}}$ while the latter equation implies $\mathbf{R}_{\tilde{\mathbf{x}}_{\mathrm{R}}} = \mathbf{G}_{\mathrm{tx}}\mathbf{R}_{\hat{\mathbf{x}}_{\mathrm{R}}}\mathbf{G}_{\mathrm{tx}}^H$.

To be used in (3.11a), the equivalent receiver noise vector of the intended "interference-free" relay becomes

$$\hat{\mathbf{n}}_{\mathrm{R}} = \hat{\mathbf{H}}_{\mathrm{RR}}\,\hat{\mathbf{x}}_{\mathrm{R}} + \mathbf{G}_{\mathrm{rx}}\mathbf{H}_{\mathrm{RR}}\,\boldsymbol{\Delta}\tilde{\mathbf{x}}_{\mathrm{R}} + \mathbf{G}_{\mathrm{rx}}\,\mathbf{n}_{\mathrm{R}}, \tag{3.20}$$

in which the residual loopback channel is given by

$$\hat{\mathbf{H}}_{\mathrm{RR}} = \mathbf{G}_{\mathrm{rx}}\mathbf{H}_{\mathrm{RR}}\mathbf{G}_{\mathrm{tx}} = \mathbf{G}_{\mathrm{rx}}\tilde{\mathbf{H}}_{\mathrm{RR}}\mathbf{G}_{\mathrm{tx}} + \mathbf{G}_{\mathrm{rx}}\boldsymbol{\Delta}\tilde{\mathbf{H}}_{\mathrm{RR}}\mathbf{G}_{\mathrm{tx}}. \tag{3.21}$$

Consequently, the residual self-interference power can be expressed as

$$\begin{aligned} P_{\mathrm{I}} &= \mathcal{E}\{\|\hat{\mathbf{H}}_{\mathrm{RR}}\,\hat{\mathbf{x}}_{\mathrm{R}} + \mathbf{G}_{\mathrm{rx}}\mathbf{H}_{\mathrm{RR}}\,\boldsymbol{\Delta}\tilde{\mathbf{x}}_{\mathrm{R}}\|_2^2\} \\ &= \mathrm{tr}\{\hat{\mathbf{H}}_{\mathrm{RR}}\mathbf{R}_{\hat{\mathbf{x}}_{\mathrm{R}}}\hat{\mathbf{H}}_{\mathrm{RR}}^H\} + \mathrm{tr}\left\{\mathbf{G}_{\mathrm{rx}}\mathbf{H}_{\mathrm{RR}}\mathbf{R}_{\boldsymbol{\Delta}\tilde{\mathbf{x}}_{\mathrm{R}}}\mathbf{H}_{\mathrm{RR}}^H\mathbf{G}_{\mathrm{rx}}^H\right\}. \end{aligned} \tag{3.22}$$

On the other hand, (3.22) is reduced to its counterpart given in (3.13) for mere physical isolation when $\mathbf{G}_{\mathrm{rx}} = \mathbf{I}$ and $\mathbf{G}_{\mathrm{tx}} = \mathbf{I}$ without suppression.

In principle, self-interference will be now suppressed by appropriately designing $\mathbf{G}_{\mathrm{rx}}$ and $\mathbf{G}_{\mathrm{tx}}$ to minimize the first term of P_{I} and/or by designing only $\mathbf{G}_{\mathrm{rx}}$ to minimize the second term that is due to transmit signal noise. The implementation depends largely upon the adopted procedure:

Independent design refers to the case where one filter is designed without knowledge of the other filter. Effectively, the unknown filter can be provisionally replaced by an identity like without suppression.

Separate design refers to the case where one filter is designed given the other. The value of the fixed filter is explicitly used in each step but one may continue iteratively after swapping the design order.

Joint design refers to the best case where the filters can be designed together. The procedure is completed in a single step without need to choose any initial value for either filter.

These procedures are developed next for all main variations of suppression, namely antenna selection (AS), general eigenbeam selection (ES), null-space projection (NSP), and minimum mean squared error filtering.

It can be noted that spatial-domain suppression comes at the cost of a reduction in the input or output dimensions given for the relaying protocol $\hat{f}(\cdot)$, when compared to time-domain cancellation. In general, the relay needs to be thus equipped with more antennas for the same number of spatial streams. However, (3.20) reveals readily one significant advantage over cancellation: the receive filter $\mathbf{G}_{\mathrm{rx}}$ can be designed to suppress the portion of self-interference that is due to the transmit signal noise term. In fact, information on the physical signal $\mathbf{x}_{\mathrm{R}}$ is not needed at all because both $\boldsymbol{\Delta}\tilde{\mathbf{x}}_{\mathrm{R}}$ and the signal $\tilde{\mathbf{x}}_{\mathrm{R}}$ propagate through the same channel $\mathbf{H}_{\mathrm{RR}}$.

Antenna Selection

The simplified receive antenna selection (AS) scheme studied early in [104] gives inspiration to formulate and analyze self-interference suppression based on generalized antenna subset selection as follows.

Antenna selection is studied herein within the same general framework as all the other suppression schemes. To that end, the respective receive and transmit filters are constructed from row and column subset selection matrices with scaling for gain normalization:

$$\mathbf{G}_{\mathrm{rx}} = \sqrt{\frac{N_{\mathrm{rx}}}{\hat{N}_{\mathrm{rx}}}}\mathbf{S}_{\mathrm{rx}}^T, \tag{3.23a}$$

$$\mathbf{G}_{\mathrm{tx}} = \mathbf{S}_{\mathrm{tx}}. \tag{3.23b}$$

Throughout the chapter, $\mathbf{S}_{\mathrm{rx}} \in \{0,1\}^{N_{\mathrm{rx}} \times \hat{N}_{\mathrm{rx}}}$ and $\mathbf{S}_{\mathrm{tx}} \in \{0,1\}^{N_{\mathrm{tx}} \times \hat{N}_{\mathrm{tx}}}$ denote binary matrices for which $\sum_i \{\mathbf{S}_{\mathrm{rx}}\}_{i,j} = 1$ and $\sum_i \{\mathbf{S}_{\mathrm{tx}}\}_{i,j} = 1$ with all j as well as $\sum_j \{\mathbf{S}_{\mathrm{rx}}\}_{i,j} \leq 1$ and $\sum_j \{\mathbf{S}_{\mathrm{tx}}\}_{i,j} \leq 1$ with all i.

To reduce the gain of the residual loopback channel given in (3.21), the general objective for spatial-domain suppression is defined as

$$\mathcal{J} \triangleq \min \|\mathbf{G}_{\mathrm{rx}}\tilde{\mathbf{H}}_{\mathrm{RR}}\mathbf{G}_{\mathrm{tx}}\|_F^2 \tag{3.24}$$

for decreasing the known part of $\|\hat{\mathbf{H}}_{\mathrm{RR}}\|_F^2$. With (3.23), this becomes

$$\mathcal{J}_{\mathrm{AS}} \triangleq \frac{N_{\mathrm{rx}}}{\hat{N}_{\mathrm{rx}}} \cdot \min \|\mathbf{S}_{\mathrm{rx}}^T\tilde{\mathbf{H}}_{\mathrm{RR}}\mathbf{S}_{\mathrm{tx}}\|_F^2 \tag{3.25}$$

specifically for antenna selection.

Optimal joint filter design can be solved by calculating the Frobenius norm for all $\binom{N_{\mathrm{rx}}}{\hat{N}_{\mathrm{rx}}}\binom{N_{\mathrm{tx}}}{\hat{N}_{\mathrm{tx}}}$ combinations and choosing the lowest. Although one may easily devise suboptimal methods of lower complexity, only global search gives the exact optimum in the general case. However, this is feasible because the number of antennas is in practice reasonably small.

The design of $\mathbf{S}_{\mathrm{rx}}^T$ can be considered to illustrate the case of separate filter design while the procedure is symmetric for designing $\mathbf{S}_{\mathrm{tx}}$. Now $\mathbf{G}_{\mathrm{tx}}$ needs to be first fixed based on any spatial suppression scheme and the unique solution for $\min \|\mathbf{S}_{\mathrm{rx}}^T\tilde{\mathbf{H}}_{\mathrm{RR}}\mathbf{G}_{\mathrm{tx}}\|_F^2$ is simply one of the $\binom{N_{\mathrm{rx}}}{\hat{N}_{\mathrm{rx}}}$ possible combinations. If the transmit filter is not known (as in independent filter design) or not yet selected, one should substitute $\mathbf{G}_{\mathrm{tx}} = \mathbf{I}$, reducing the objective from (3.25) to $\mathcal{J}_{\mathrm{AS}} = \frac{N_{\mathrm{rx}}}{\hat{N}_{\mathrm{rx}}} \cdot \min \|\mathbf{S}_{\mathrm{rx}}^T\tilde{\mathbf{H}}_{\mathrm{RR}}\|_F^2$.

Example: The scheme proposed in [104] is a special case of general antenna selection where $N_{\mathrm{rx}} = 2$ and $\hat{N}_{\mathrm{rx}} = N_{\mathrm{tx}} = \hat{N}_{\mathrm{tx}} = 1$, i.e., $\mathbf{G}_{\mathrm{tx}} = 1$. When setting $\tilde{\mathbf{H}}_{\mathrm{RR}} = [\tilde{h}_1\ \tilde{h}_2]^T$, residual channel gain $2\|\mathbf{S}_{\mathrm{rx}}^T\tilde{\mathbf{H}}_{\mathrm{RR}}\|_F^2$ is minimized by choosing $\mathbf{S}_{\mathrm{rx}}^T = [1\ 0]$ if $|\tilde{h}_1|^2 < |\tilde{h}_2|^2$ and $\mathbf{S}_{\mathrm{rx}}^T = [0\ 1]$ otherwise.

Eigenbeam Selection

Signals sent from each antenna propagate to all receive antennas. Thus, eigenbeam selection (ES) makes MIMO subchannels effectively orthogonal allowing subset selection over virtual antennas with less coupling.

Eigenbeamforming is based on the singular value decomposition (SVD):

$$\tilde{\mathbf{H}}_{\mathrm{RR}} \triangleq \tilde{\mathbf{U}}_{\mathrm{RR}}\tilde{\mathbf{\Sigma}}_{\mathrm{RR}}\tilde{\mathbf{V}}_{\mathrm{RR}}^{H} = \begin{bmatrix}\tilde{\mathbf{U}}_{\mathrm{RR}}^{(1)} & \tilde{\mathbf{U}}_{\mathrm{RR}}^{(0)}\end{bmatrix} \tilde{\mathbf{\Sigma}}_{\mathrm{RR}} \begin{bmatrix}\tilde{\mathbf{V}}_{\mathrm{RR}}^{(1)} & \tilde{\mathbf{V}}_{\mathrm{RR}}^{(0)}\end{bmatrix}^{H}, \tag{3.26}$$

in which $\tilde{\mathbf{U}}_{\mathrm{RR}} \in \mathbb{C}^{N_{\mathrm{rx}}\times N_{\mathrm{rx}}}$ and $\tilde{\mathbf{V}}_{\mathrm{RR}} \in \mathbb{C}^{N_{\mathrm{tx}}\times N_{\mathrm{tx}}}$ are unitary matrices from singular vectors while diagonal matrix $\tilde{\mathbf{\Sigma}}_{\mathrm{RR}} \in \mathbb{R}^{N_{\mathrm{rx}}\times N_{\mathrm{tx}}}$ comprises singular values $\tilde{\Sigma}_{\mathrm{RR}}[n] \triangleq \{\tilde{\mathbf{\Sigma}}_{\mathrm{RR}}\}_{n,n}$, $n = 1, 2, \ldots, \min\{N_{\mathrm{rx}}, N_{\mathrm{tx}}\}$, in descending order. In the last form, submatrices $\tilde{\mathbf{U}}_{\mathrm{RR}}^{(0)}$ and $\tilde{\mathbf{V}}_{\mathrm{RR}}^{(0)}$ collect basis vectors associated with the null-space of the matrix, i.e., zero singular values.

After realizing that the singular vectors represent the set of available eigenbeams, the spatial filters can be constructed by combining selection and beamforming matrices with scaling for gain normalization as follows:

$$\mathbf{G}_{\mathrm{rx}} = \sqrt{\frac{N_{\mathrm{rx}}}{\hat{N}_{\mathrm{rx}}}}\mathbf{S}_{\mathrm{rx}}^{T}\tilde{\mathbf{U}}_{\mathrm{RR}}^{H}, \tag{3.27a}$$

$$\mathbf{G}_{\mathrm{tx}} = \tilde{\mathbf{V}}_{\mathrm{RR}}\mathbf{S}_{\mathrm{tx}}. \tag{3.27b}$$

This transforms the general objective from (3.24) to

$$\mathcal{J}_{\mathrm{ES}} \triangleq \frac{N_{\mathrm{rx}}}{\hat{N}_{\mathrm{rx}}} \cdot \min \|\mathbf{S}_{\mathrm{rx}}^{T}\tilde{\mathbf{\Sigma}}_{\mathrm{RR}}\mathbf{S}_{\mathrm{tx}}\|_{F}^{2}, \tag{3.28}$$

as $\tilde{\mathbf{U}}_{\mathrm{RR}}^{H}\tilde{\mathbf{U}}_{\mathrm{RR}} = \mathbf{I}$ and $\tilde{\mathbf{V}}_{\mathrm{RR}}^{H}\tilde{\mathbf{V}}_{\mathrm{RR}} = \mathbf{I}$ by definition. Thus, filter design remains conceptually similar to antenna selection but row and column subset selection is now based on the effective diagonal channel $\tilde{\mathbf{\Sigma}}_{\mathrm{RR}}$ instead of $\tilde{\mathbf{H}}_{\mathrm{RR}}$.

In fact, objective $\mathcal{J}_{\mathrm{ES}}$ readily indicates that eigenbeam selection is superior to antenna selection: In (3.28) most row and column combinations pick off-diagonal elements of $\tilde{\mathbf{\Sigma}}_{\mathrm{RR}}$, which are zero by definition, leading to $\mathcal{J}_{\mathrm{ES}} = 0$ for many subsolutions whereas in (3.25) the elements of $\tilde{\mathbf{H}}_{\mathrm{RR}}$ are likely non-zero implying that virtually $\mathcal{J}_{\mathrm{AS}} \gg 0$ for any subsolution.

Intuitively, (3.28) could be solved by testing all $\binom{N_{\mathrm{rx}}}{\hat{N}_{\mathrm{rx}}}\binom{N_{\mathrm{tx}}}{\hat{N}_{\mathrm{tx}}}$ combinations as with antenna selection. However, the diagonalized structure of the residual loopback channel facilitates direct offline selection based on the values of N_{rx}, N_{tx}, $\hat{N}_{\mathrm{rx}}$, and $\hat{N}_{\mathrm{tx}}$ while only a part of singular vectors need to be estimated online. In particular, optimal joint selection is achieved with the algorithm given in Table 3.1. If $\hat{N}_{\mathrm{rx}} + \hat{N}_{\mathrm{tx}} \leq \max\{N_{\mathrm{rx}}, N_{\mathrm{tx}}\}$, *Step 2* is omitted and the solution is reduced to null-space projection (NSP) as discussed in the next subsection. On the other hand, separate or independent filter design applies only *Step 2* for all $\hat{N}_{\mathrm{rx}} + \hat{N}_{\mathrm{tx}}$ rows and columns.

Table 3.1. Algorithm for achieving optimal joint eigenbeam selection (ES).

Design $\mathbf{S}_{\text{rx}}^T$ and $\mathbf{S}_{\text{tx}}$ to select $\hat{N}_{\text{rx}}$ rows and $\hat{N}_{\text{tx}}$ columns of $\tilde{\mathbf{\Sigma}}_{\text{RR}}$ as follows.
Step 1: Select in total $\min\{\hat{N}_{\text{rx}}+\hat{N}_{\text{tx}}, \max\{N_{\text{rx}}, N_{\text{tx}}\}\}$ rows and columns such that all combinations pick only off-diagonal elements, which are zero, from $\tilde{\mathbf{\Sigma}}_{\text{RR}}$. For this NSP subsolution $\mathcal{J}_{\text{ES}} = 0$.
Step 2: To satisfy minimization objective $\mathcal{J}_{\text{ES}}$, select the rest of the rows and columns such that the final selection matrices pick only the $\hat{N}_{\text{rx}}+\hat{N}_{\text{tx}}-\max\{N_{\text{rx}}, N_{\text{tx}}\}$ smallest singular values of $\tilde{\mathbf{H}}_{\text{RR}}$.

Assuming that $\hat{N}_{\text{rx}}+\hat{N}_{\text{tx}} > \max\{N_{\text{rx}}, N_{\text{tx}}\}$ in the following, one straightforward illustrative example solution can be obtained using the optimal joint eigenbeam selection algorithm as follows:

$$\mathbf{S}_{\text{rx}}^T\tilde{\mathbf{\Sigma}}_{\text{RR}}\mathbf{S}_{\text{tx}} = \begin{bmatrix} \mathbf{I}_{\text{rx1}} & \mathbf{0} & \mathbf{0} \\ \mathbf{0} & \mathbf{0} & \mathbf{I}_{\text{rx2}} \end{bmatrix} \tilde{\mathbf{\Sigma}}_{\text{RR}} \begin{bmatrix} \mathbf{0} \\ \mathbf{I}_{\text{tx}} \end{bmatrix}, \tag{3.29}$$

in which $\mathbf{I}_{\text{rx1}}$, $\mathbf{I}_{\text{rx2}}$, and $\mathbf{I}_{\text{tx}}$ denote identity matrices with respective dimensions $(N_{\text{tx}}-\hat{N}_{\text{tx}})$, $(\hat{N}_{\text{rx}}+\hat{N}_{\text{tx}}-N_{\text{tx}})$, and $\hat{N}_{\text{tx}}$. Although the above solution itself is not unique, all optimal solutions render the same value of $\mathcal{J}_{\text{ES}}$. Thus, a substitution shows that optimal joint design translates (3.28) to

$$\mathcal{J}_{\text{ES}} = \frac{N_{\text{rx}}}{\hat{N}_{\text{rx}}} \sum_{n=N_{\text{rx}}-\hat{N}_{\text{rx}}+N_{\text{tx}}-\hat{N}_{\text{tx}}+1}^{\min\{N_{\text{rx}},N_{\text{tx}}\}} \tilde{\Sigma}_{\text{RR}}^2[n]. \tag{3.30}$$

This should be contrasted with the prior art as discussed below.

Example: The suboptimal scheme proposed in [144] for the special case of $N_{\text{rx}} = N_{\text{tx}}$ and $\hat{N}_{\text{rx}} = \hat{N}_{\text{tx}}$ is a consequence of independent filter design. The scheme selects eigenbeams using $\mathbf{S}_{\text{rx}} = \mathbf{S}_{\text{tx}} = [\mathbf{0}\ \mathbf{I}]^T$ where $\mathbf{0}$ is an $\hat{N}_{\text{rx}} \times (N_{\text{rx}}-\hat{N}_{\text{rx}})$ zero matrix and $\mathbf{I}$ is an $\hat{N}_{\text{rx}} \times \hat{N}_{\text{rx}}$ identity matrix. This picks the $\hat{N}_{\text{rx}}$ smallest singular values of $\tilde{\mathbf{H}}_{\text{RR}}$ transforming (3.28) to

$$\mathcal{J}_{\text{ES, [144]}} = \frac{N_{\text{rx}}}{\hat{N}_{\text{rx}}} \sum_{n=N_{\text{rx}}-\hat{N}_{\text{rx}}+1}^{N_{\text{rx}}} \tilde{\Sigma}_{\text{RR}}^2[n] \ > \ \mathcal{J}_{\text{ES}}. \tag{3.31}$$

The result is worse than (3.30) obtained in the optimal case because the scheme does not exploit the possibility to suppress interference by picking the off-diagonal elements of $\tilde{\mathbf{\Sigma}}_{\text{RR}}$ in *Step 1*.

In summary, the above discussions reveal that general eigenbeamforming may leave residual self-interference even if perfect side information is available. This gives motivation to consider next special cases where all interference would ideally be eliminated. Incidentally, then $\hat{N}_{\text{rx}}+\hat{N}_{\text{tx}} \leq \max\{N_{\text{rx}}, N_{\text{tx}}\}$ as opposed to what is momentarily assumed above.

Null-Space Projection

This subsection develops spatial-domain suppression schemes that, like time-domain cancellation, block completely loopback signals if given ideal side information. That could be desirable when self-interference is dominant but general eigenbeamforming does not offer sufficient attenuation.

In null-space projection (NSP), the spatial filters $\mathbf{G}_{\text{rx}}$ and $\mathbf{G}_{\text{tx}}$ are selected such that the relay receives and transmits in different subspaces, i.e., transmit beams are projected to the null-space of the loopback channel combined with the receive filter and vice versa. Such a condition can be formalized for joint or separate filter design as

$$\mathbf{G}_{\text{rx}}\tilde{\mathbf{H}}_{\text{RR}}\mathbf{G}_{\text{tx}} = \mathbf{0} \tag{3.32}$$

to eliminate the known part of the first term in (3.22). Similarly, for suppressing the transmit signal noise, the condition becomes $\mathbf{G}_{\text{rx}}\tilde{\mathbf{H}}_{\text{RR}} = \mathbf{0}$ to partly eliminate the second term in (3.22).

One solution for joint null-space projection can be obtained with the optimal joint eigenbeam selection (ES) algorithm given in Table 3.1 if $\hat{N}_{\text{rx}}$, $\hat{N}_{\text{tx}}$ and the rank of the loopback channel ($\text{rk}\{\tilde{\mathbf{H}}_{\text{RR}}\}$) are low enough w.r.t. N_{rx} and N_{tx}. Firstly, a total of $\max\{N_{\text{rx}}, N_{\text{tx}}\}$ beams are selected in *Step 1* corresponding to different singular values. Secondly, the last terms in (3.30) are zero if $\text{rk}\{\tilde{\mathbf{H}}_{\text{RR}}\} < \min\{N_{\text{rx}}, N_{\text{tx}}\}$. Thus, $\min\{N_{\text{rx}}, N_{\text{tx}}\} - \text{rk}\{\tilde{\mathbf{H}}_{\text{RR}}\}$ input and output beams may correspond to the same singular values after *Step 2* and still $\mathcal{J}_{\text{ES}} = 0$, i.e., $\mathbf{S}_{\text{rx}}^T\tilde{\mathbf{\Sigma}}_{\text{RR}}\mathbf{S}_{\text{tx}} = \mathbf{0}$ which is equivalent to (3.32).

In particular, the ES algorithm yields null-space projection whenever

$$\hat{N}_{\text{rx}} + \hat{N}_{\text{tx}} + \text{rk}\{\tilde{\mathbf{H}}_{\text{RR}}\} \leq N_{\text{rx}} + N_{\text{tx}}. \tag{3.33}$$

This condition defines also the general existence of joint null-space projection, if $\mathbf{G}_{\text{rx}}$ and $\mathbf{G}_{\text{tx}}$ are additionally constrained to have full rank.

Even if $\mathbf{H}_{\text{RR}}$ may be rank-deficient, $\tilde{\mathbf{H}}_{\text{RR}}$ is of full rank in practice due to estimation errors which also cause residual self-interference. Thereby, the condition in (3.33) can be alternatively evaluated using the anticipated value of $\text{rk}\{\mathbf{H}_{\text{RR}}\}$ based on prior information or by defining $\text{rk}\{\tilde{\mathbf{H}}_{\text{RR}}\}$ with a threshold below which singular values are rounded to zero.

In the case of $\hat{N}_{\text{rx}} = \hat{N}_{\text{tx}}$, the total number of antennas ($N_{\text{rx}} + N_{\text{tx}}$) is minimized for null-space projection by choosing $N_{\text{rx}} = 2\hat{N}_{\text{rx}} = 2N_{\text{tx}} = 2\hat{N}_{\text{tx}}$ or $N_{\text{tx}} = 2\hat{N}_{\text{tx}} = 2N_{\text{rx}} = 2\hat{N}_{\text{rx}}$ when $\text{rk}\{\tilde{\mathbf{H}}_{\text{RR}}\} = \min\{N_{\text{rx}}, N_{\text{tx}}\}$ (full rank), or by choosing $N_{\text{rx}} = \hat{N}_{\text{rx}} + 1 = N_{\text{tx}} + 1 = \hat{N}_{\text{tx}} + 1$ or $N_{\text{tx}} = \hat{N}_{\text{tx}} + 1 = N_{\text{rx}} + 1 = \hat{N}_{\text{rx}} + 1$ when $\text{rk}\{\tilde{\mathbf{H}}_{\text{RR}}\} = 1$ (minimum rank). Selecting $N_{\text{rx}} > N_{\text{tx}}$ may be preferable due to transmit signal noise as discussed later.

For separate filter design, one should recall that the Moore–Penrose pseudoinverse $\mathbf{X}^+$ is unique, always exists and satisfies $\mathbf{X}\mathbf{X}^+\mathbf{X} = \mathbf{X}$ by definition [197]. For designing $\mathbf{G}_{\text{rx}}$ separately given $\mathbf{G}_{\text{tx}}$, null-space projection can, thereby, be implemented by applying projection matrix

$$\mathbf{G}_{\text{rx}} = \sqrt{\frac{N_{\text{rx}}}{N_{\text{rx}} - \mathrm{rk}\{\tilde{\mathbf{H}}_{\text{RR}}\mathbf{G}_{\text{tx}}\}}}\,(\mathbf{I} - \tilde{\mathbf{H}}_{\text{RR}}\mathbf{G}_{\text{tx}}[\tilde{\mathbf{H}}_{\text{RR}}\mathbf{G}_{\text{tx}}]^+), \tag{3.34}$$

if $\mathrm{rk}\{\tilde{\mathbf{H}}_{\text{RR}}\mathbf{G}_{\text{tx}}\} < N_{\text{rx}}$. Separate design for $\mathbf{G}_{\text{tx}}$ is given by a similar projection matrix which is obtained by replacing $\tilde{\mathbf{H}}_{\text{RR}}\mathbf{G}_{\text{tx}}$ above with $\mathbf{G}_{\text{rx}}\tilde{\mathbf{H}}_{\text{RR}}$. Unfortunately, the case of having full rank for $\tilde{\mathbf{H}}_{\text{RR}}\mathbf{G}_{\text{tx}}$ or $\mathbf{G}_{\text{rx}}\tilde{\mathbf{H}}_{\text{RR}}$ in above leads evidently to $\mathbf{G}_{\text{rx}} = \mathbf{0}$ or $\mathbf{G}_{\text{tx}} = \mathbf{0}$, respectively.

Example: The scheme proposed in [41] is a special case of independent transmit-side null-space projection applicable to a minimal system with $N_{\text{rx}} = \hat{N}_{\text{rx}} = \hat{N}_{\text{tx}} = 1$ and $N_{\text{tx}} = 2$. When denoting $\tilde{\mathbf{H}}_{\text{RR}} = [\tilde{h}_1 \;\; \tilde{h}_2]$, condition $\tilde{\mathbf{H}}_{\text{RR}}\mathbf{G}_{\text{tx}} = 0$ can be guaranteed by selecting

$$\mathbf{G}_{\text{tx}} = \frac{1}{\sqrt{|\tilde{h}_1|^2 + |\tilde{h}_2|^2}} \cdot [\pm\tilde{h}_2 \;\; \mp\tilde{h}_1]^T, \tag{3.35}$$

which includes scaling for gain normalization as $\|\mathbf{G}_{\text{tx}}\|_F^2 = \hat{N}_{\text{tx}} = 1$.

For designing either filter independently, the above schemes may be exploited by setting the other filter to identity. However, simpler design (at least with regard to how the expressions look) is obtained by choosing

$$\mathbf{G}_{\text{rx}} = \sqrt{\frac{N_{\text{rx}}}{N_{\text{rx}} - \mathrm{rk}\{\tilde{\mathbf{H}}_{\text{RR}}\}}}\,\left[\tilde{\mathbf{U}}_{\text{RR}}^{(0)}\right]^H \tag{3.36a}$$

with appropriate gain normalization, because the row space of $\mathbf{G}_{\text{rx}}$ should be in the left null space of $\tilde{\mathbf{H}}_{\text{RR}}$ or by choosing

$$\mathbf{G}_{\text{tx}} = \tilde{\mathbf{V}}_{\text{RR}}^{(0)} \tag{3.36b}$$

because the column space of $\mathbf{G}_{\text{tx}}$ should be in the null space of $\tilde{\mathbf{H}}_{\text{RR}}$.

It should be noted that joint design solutions satisfying the null-space projection (NSP) condition (3.32) are not unique in most cases. Especially, *Step 1* in the optimal joint eigenbeam selection (ES) algorithm allows to choose rows and columns in different ways. Furthermore, general ES inherits the same property except for the subsolution picking the non-zero diagonal values of $\tilde{\mathbf{\Sigma}}_{\text{RR}}$ is unique in *Step 2*. Choice between solutions of the same cost can be made based on any other performance criterion as illustrated by the next example. In this case, compared to the previous example, the extra receive antenna facilitates additional selection diversity available for improving the quality of the useful signal as in [125] or for reducing the effect of transmit signal noise as in following simulations.

Example: The scheme proposed in [125] for a system where $N_{\text{rx}} = N_{\text{tx}} = 2$ and $\hat{N}_{\text{rx}} = \hat{N}_{\text{tx}} = 1$ is a special case of null-space projection. When denoting the SVD of the loopback channel as $\tilde{\mathbf{H}}_{\text{RR}} = [\tilde{\mathbf{u}}_1\ \tilde{\mathbf{u}}_2]\tilde{\mathbf{\Sigma}}_{\text{RR}}[\tilde{\mathbf{v}}_1\ \tilde{\mathbf{v}}_2]^H$, condition $\mathbf{G}_{\text{rx}}\tilde{\mathbf{H}}_{\text{RR}}\mathbf{G}_{\text{tx}} = 0$ can be guaranteed by choosing either of the following filter pairs:

$$\mathbf{G}_{\text{rx}} = \sqrt{2}\,\tilde{\mathbf{u}}_1^H \quad \text{and} \quad \mathbf{G}_{\text{tx}} = \tilde{\mathbf{v}}_2, \tag{3.37a}$$

$$\mathbf{G}_{\text{rx}} = \sqrt{2}\,\tilde{\mathbf{u}}_2^H \quad \text{and} \quad \mathbf{G}_{\text{tx}} = \tilde{\mathbf{v}}_1. \tag{3.37b}$$

Although not recognized in [125], also the filter pair

$$\mathbf{G}_{\text{rx}} = \sqrt{2}\,\tilde{\mathbf{u}}_2^H \quad \text{and} \quad \mathbf{G}_{\text{tx}} = \tilde{\mathbf{v}}_2 \tag{3.37c}$$

can be used if $\text{rk}\{\tilde{\mathbf{H}}_{\text{RR}}\} = 1$, i.e., the loopback channel is rank-deficient.

Minimum Mean Squared Error Filtering

All the above spatial-domain suppression schemes aim at minimizing the effect of loopback self-interference with the side cost of spatially shaping the useful signals which does not happen with time-domain cancellation. In order to reduce the effect of this drawback, a minimum mean square error (MMSE) scheme is developed next to both minimize the distortion and attenuate self-interference.

Now $\hat{N}_{\text{rx}} = N_{\text{rx}}$ and $\hat{N}_{\text{tx}} = N_{\text{tx}}$ as with cancellation. Thus, the mean square error (MSE) matrix of the relay input signal is given by

$$\begin{aligned}\mathbf{M} &\triangleq \mathcal{E}\{(\mathbf{H}_{\text{SR}}\,\mathbf{x}_{\text{S}} - \hat{\mathbf{y}}_{\text{R}})(\mathbf{H}_{\text{SR}}\,\mathbf{x}_{\text{S}} - \hat{\mathbf{y}}_{\text{R}})^H\} \\ &= (\mathbf{I} - \mathbf{G}_{\text{rx}})\mathbf{H}_{\text{SR}}\mathbf{R}_{\mathbf{x}_{\text{S}}}\mathbf{H}_{\text{SR}}^H(\mathbf{I} - \mathbf{G}_{\text{rx}}^H) + \mathbf{R}_{\hat{\mathbf{n}}_{\text{R}}}\end{aligned} \tag{3.38}$$

in which $\mathbf{R}_{\hat{\mathbf{n}}_{\text{R}}} \triangleq \mathcal{E}\{\hat{\mathbf{n}}_{\text{R}}\hat{\mathbf{n}}_{\text{R}}^H\} = \mathbf{G}_{\text{rx}}(\mathbf{H}_{\text{RR}}\mathbf{R}_{\mathbf{x}_{\text{R}}}\mathbf{H}_{\text{RR}}^H + \mathbf{R}_{\mathbf{n}_{\text{R}}})\mathbf{G}_{\text{rx}}^H$.

On the one hand, for separate filter design given $\mathbf{G}_{\text{tx}}$, the minimum MSE receive filter is derived from the condition $\frac{\partial}{\partial \mathbf{G}_{\text{rx}}}\text{tr}\{\mathbf{M}\} = \mathbf{0}$ yielding

$$\mathbf{G}_{\text{rx}} = \tilde{\mathbf{H}}_{\text{SR}}\mathbf{R}_{\mathbf{x}_{\text{S}}}\tilde{\mathbf{H}}_{\text{SR}}^H(\tilde{\mathbf{H}}_{\text{SR}}\mathbf{R}_{\mathbf{x}_{\text{S}}}\tilde{\mathbf{H}}_{\text{SR}}^H + \tilde{\mathbf{H}}_{\text{RR}}\mathbf{R}_{\mathbf{x}_{\text{R}}}\tilde{\mathbf{H}}_{\text{RR}}^H + \mathbf{R}_{\mathbf{n}_{\text{R}}})^{-1}, \tag{3.39}$$

which needs to be additionally scaled to satisfy $\|\mathbf{G}_{\text{rx}}\|_F^2 = N_{\text{rx}}$. One can note that MMSE filtering requires knowledge of $\mathbf{H}_{\text{SR}}$ and signal covariance matrices as opposed to the other mitigation schemes.

On the other hand, the converse condition

$$\frac{\partial}{\partial \mathbf{G}_{\text{tx}}}\text{tr}\{\mathbf{M}\} = \mathbf{0} \tag{3.40}$$

to minimize MSE at the transmit side can be reduced to the condition of null-space projection given in (3.32). Therefore, the evident order for joint filter design is to firstly minimize interference at the transmit side using any scheme, and then secondly design the receive filter using (3.39).

Hybrid Combination of Cancellation and Suppression

Time-domain cancellation suffers from residual interference that is mainly due to the transmit signal noise while spatial-domain schemes may need many extra antennas for effective mitigation. However, these two approaches are not mutually exclusive but a smart hybrid combination may harness the advantages of both schemes for achieving enhanced isolation.

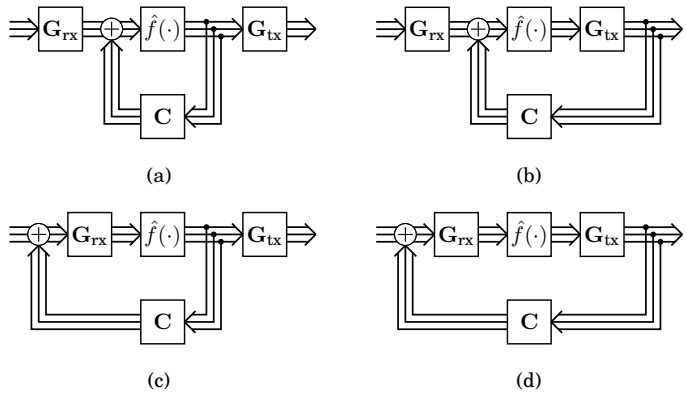

Figure 3.4. Different variations for combining subtractive cancellation with suppression.

Four variations are identified for the combination as shown in Fig. 3.4. With independent or separate filter design, the design (and performance) of the variations differs according to the residual loop interference channels (cf. (3.16) without suppression or (3.21) without cancellation):

$$\hat{\mathbf{H}}_{\text{RR}} = \begin{cases} \mathbf{G}_{\text{rx}}\mathbf{H}_{\text{RR}}\mathbf{G}_{\text{tx}} + \mathbf{C}, & \text{with Variation (a)}, \\ (\mathbf{G}_{\text{rx}}\mathbf{H}_{\text{RR}} + \mathbf{C})\mathbf{G}_{\text{tx}}, & \text{with Variation (b)}, \\ \mathbf{G}_{\text{rx}}(\mathbf{H}_{\text{RR}}\mathbf{G}_{\text{tx}} + \mathbf{C}), & \text{with Variation (c)}, \\ \mathbf{G}_{\text{rx}}(\mathbf{H}_{\text{RR}} + \mathbf{C})\mathbf{G}_{\text{tx}}, & \text{with Variation (d)}. \end{cases} \tag{3.41}$$

However, these become equivalent if all three filters are designed jointly.

Variations (a) and (d) allow the most straightforward implementation since the two layers of mitigation can be decoupled and joint design is still feasible for $\mathbf{G}_{\text{rx}}$ and $\mathbf{G}_{\text{tx}}$: in Variation (a), spatial suppression is first applied, and the residual interference is mitigated with cancellation while Variation (d) is the converse case. In Variations (b) and (c), all three filters must be implemented sequentially leading to suboptimal separate design. Moreover, Variations (b) and (d) cannot exploit the potential of the spatial transmit filter because cancellation has already eliminated the known part of interference. Thus, Variation (a) turns out to be the best choice: As cancellation is blind to the spatial domain, it is better to first design jointly $\mathbf{G}_{\text{rx}}$ and $\mathbf{G}_{\text{tx}}$ for exploiting all possible degrees of freedom.

3.5 Performance Evaluation

This section analyzes all the foregoing mitigation schemes in three ways adopting a broad scope for general assessment while providing also a detailed view on their most central attributes. Firstly, simulation results provide coherent comparison between the schemes for identifying the key parameters related to their performance. Secondly, analytical results are presented for evaluating the effect of imperfect side information on mitigation in terms of closed-form expressions. Thirdly, experimental results characterize, based on real-world channel measurement data, how and when isolation is inherently limited, even with perfect side information, due to the schemes themselves and the scattering environment.

The main objective is to study how much isolation is improved with mitigation and why it is typically limited leading to significant residual self-interference. To that end, specific factors to be explored are the antenna configuration, the rank of the self-interference channel, the distance and orientation of antenna arrays when there is (or is not) line-of-sight present, and the quality of side information. However, physical isolation realized with prototype arrays is also analyzed based on measurements for understanding the baseline case before active mitigation.

3.5.1 Simulation Results

In this subsection, the performance of the mitigation schemes is evaluated and compared in a unified simulation framework which gives enough flexibility to allow covering all the key factors mentioned above. Thereby, these results also lay foundations for the later subsections where a closer look is taken at some specific schemes and their particular properties.

The following discussion begins with the specification of a system setup assumed for the simulations. Then, as a starting point, bit-error rate (BER) results justify the usage of the main performance metric, namely *additional isolation*, after which the main focus remains on analyzing the benefit of spatial-domain suppression although time-domain cancellation is also covered as the quintessential reference scheme. The study flows from considering perfect side information and imperfections in the side information via analyzing the effect of the channel rank to evaluating minimum mean square error (MMSE) filtering and the combination of time-domain cancellation and spatial-domain suppression. Finally, the subsection concludes with discussion and overview on the main findings.

Simulation Setup

In the following simulation results, channels are modeled with Rayleigh fading such that the elements of $\mathbf{H}_{\text{SR}} \in \mathbb{C}^{N_{\text{rx}} \times N_{\text{S}}}$ and $\mathbf{H}_{\text{RR}} \in \mathbb{C}^{N_{\text{rx}} \times N_{\text{tx}}}$ are identically distributed, but not necessarily independent, circularly-symmetric complex Gaussian random variables. And all experiments are iterated in a Monte Carlo manner over $K = 10^7$ independent trials.

While $\mathbf{H}_{\text{SR}}$ will always have full rank, many of the results illustrate cases where $\mathbf{H}_{\text{RR}}$ is rank-deficient, i.e., $\text{rk}\{\mathbf{H}_{\text{RR}}\} < N_{\min} \triangleq \min\{N_{\text{rx}}, N_{\text{tx}}\}$. In order to both control the rank and yield identically distributed elements with proper correlation, channel matrices are generated as follows:

$$\mathbf{H}_{\text{RR}} = \sqrt{\frac{N_{\min}}{\text{rk}\{\mathbf{H}_{\text{RR}}\}}} \cdot \begin{cases} [\mathbf{W}\ \mathbf{0}]\mathbf{Q}, & \text{if } N_{\text{rx}} \geq N_{\text{tx}}, \\ ([\mathbf{W}\ \mathbf{0}]\mathbf{Q})^H, & \text{if } N_{\text{rx}} < N_{\text{tx}}, \end{cases} \tag{3.42}$$

where, using shorthand notation $N_{\max} \triangleq \max\{N_{\text{rx}}, N_{\text{tx}}\}$,

- $\mathbf{W}$ is an $N_{\max} \times \text{rk}\{\mathbf{H}_{\text{RR}}\}$ complex Gaussian random matrix where all elements are independent and identically distributed,
- $\mathbf{0}$ is an $N_{\max} \times (N_{\min} - \text{rk}\{\mathbf{H}_{\text{RR}}\})$ constant all-zero matrix, and
- $\mathbf{Q}$ is an $N_{\min} \times N_{\min}$ random unitary matrix, independent from $\mathbf{W}$, and uniformly distributed according to the Haar measure.

When $\text{rk}\{\mathbf{H}_{\text{RR}}\} = N_{\min}$ in the full-rank case, matrix $\mathbf{0}$ disappears and $\mathbf{H}_{\text{RR}} = \mathbf{WQ}$ (resp. $\mathbf{H}_{\text{RR}} = \mathbf{Q}^H\mathbf{W}^H$), if $N_{\text{rx}} \geq N_{\text{tx}}$ (resp. $N_{\text{rx}} < N_{\text{tx}}$), which is statistically equivalent to $\mathbf{H}_{\text{RR}} = \mathbf{W}$ (resp. $\mathbf{H}_{\text{RR}} = \mathbf{W}^H$) omitting the unitary rotation. Thus, full-rank channel matrices can be generated by simply picking all elements independently from identical distributions.

The transmitted signals are assumed to be spatially white with equal power per transmitted stream, thus

$$\mathbf{R}_{\mathbf{x}_{\text{S}}} = \frac{P_{\text{S}}}{N_{\text{S}}}\mathbf{I} \quad \text{and} \quad \mathbf{R}_{\hat{\mathbf{x}}_{\text{R}}} = \frac{P_{\text{R}}}{\hat{N}_{\text{tx}}}\mathbf{I}, \tag{3.43}$$

where P_{S} and P_{R} denote the total transmit power in the source and in the relay, respectively. The thermal receiver noise is white and Gaussian with $\mathbf{R}_{\mathbf{n}_{\text{R}}} = \sigma_{\text{R}}^2\mathbf{I}$, where σ_{R}^2 denotes noise power per antenna. Consequently, the quality of the channels is parametrized with

$$\gamma_{\text{SR}} \triangleq \frac{P_{\text{S}}}{\sigma_{\text{R}}^2} \cdot \frac{\|\mathbf{H}_{\text{SR}}\|_F^2}{N_{\text{S}} N_{\text{rx}}}, \tag{3.44a}$$

$$\gamma_{\text{RR}} \triangleq \frac{P_{\text{R}}}{\sigma_{\text{R}}^2} \cdot \frac{\|\mathbf{H}_{\text{RR}}\|_F^2}{N_{\text{rx}} N_{\text{tx}}}, \tag{3.44b}$$

which can be referred to as the channel signal-to-noise ratios (SNRs).

The imperfect side information available for mitigation is generated as explained in Section 3.3.2. In particular, it should be recalled that the associated key parameters $\epsilon_{\mathbf{H}}$ and $\epsilon_{\mathbf{x}}$ are given by

$$\epsilon_{\mathbf{H}}^2 \triangleq \frac{\mathcal{E}\{\|\boldsymbol{\Delta}\tilde{\mathbf{H}}_{\mathrm{RR}}\|_F^2\}}{\mathcal{E}\{\|\mathbf{H}_{\mathrm{RR}}\|_F^2\}}, \tag{3.45}$$

$$\epsilon_{\mathbf{x}}^2 \triangleq \frac{\mathcal{E}\{\|\boldsymbol{\Delta}\tilde{\mathbf{x}}_{\mathrm{R}}\|_2^2\}}{\mathcal{E}\{\|\tilde{\mathbf{x}}_{\mathrm{R}}\|_2^2\}}, \tag{3.46}$$

controlling the relative level of additive error included in the respective channel and signal estimates. The case of perfect side information, considered in some of the first results, can be obtained by setting $\epsilon_{\mathbf{H}} = \epsilon_{\mathbf{x}} = 0$.

Additional Isolation from Mitigation

Figure 3.5 shows simulated bit-error rate (BER) for a specific setup with a decode-and-forward relay that uses linear zero-forcing detector for independent spatial streams. The purpose of this initial result is to serve as an illustrative example for the general principles. Thus, the exact parameter values are not important although they are still enumerated in the figure caption. Related BER simulations are reported also in **[215]**.

With proper self-interference mitigation or large physical isolation, a full-duplex relay achieves the same BER as its half-duplex counterpart, but offers significantly higher spectral efficiency by forwarding two symbols from the source to the destination within a time interval during which a half-duplex link forwards only one. This sets the target for interference mitigation: The full-duplex mode is definitely superior to the half-duplex mode whenever *residual* interference is weak enough such that its effect is not more significant than the effect of usual thermal noise.

In principle, interference mitigation manifests itself as a shift in BER (or similar measures) which is herein referred to as the *additional isolation* obtained with signal processing w.r.t. physical isolation. The observed shift is unique for each mitigation scheme, but similar for all relaying protocols, system setups and performance metrics. Thus, the performance of the mitigation schemes can be compared by studying directly the statistics of additional isolation which is a versatile metric and even the intuitive choice since the schemes are formulated to minimize self-interference power at the first place. Given any level of physical isolation, the statistics of additional isolation show comprehensively how different schemes are affected by errors in side information (parametrized with $\epsilon_{\mathbf{H}}$ and $\epsilon_{\mathbf{x}}$), configurations for antennas ($N_{\mathrm{rx}} \times N_{\mathrm{tx}}$) or streams ($\hat{N}_{\mathrm{rx}} \times \hat{N}_{\mathrm{tx}}$) and the loop channel rank ($\mathrm{rk}\{\mathbf{H}_{\mathrm{RR}}\}$), to name but a few key factors.

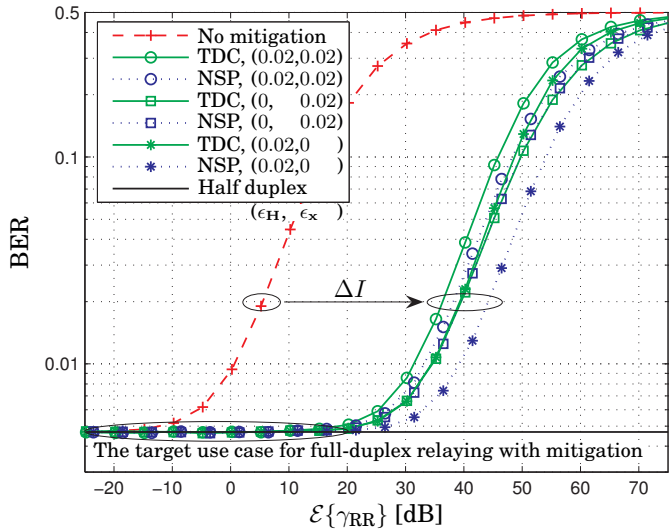

Figure 3.5. Bit-error rate (BER) of quadrature phase-shift keying at a decode-and-forward relay with zero-forcing detection when $N_{\mathrm{S}} = N_{\mathrm{rx}} = \hat{N}_{\mathrm{rx}} = \hat{N}_{\mathrm{tx}} = 3$, $\mathrm{rk}\{\mathbf{H}_{\mathrm{RR}}\} = 1$, and $\mathcal{E}\{\gamma_{\mathrm{SR}}\} = 25$ dB. The number of transmit antennas is chosen as $N_{\mathrm{tx}} = 3$ for physical isolation and time-domain cancellation (TDC) and $N_{\mathrm{tx}} = 4$ for eigenbeam selection that is reduced to null-space projection (NSP) in this scenario. A shift by ΔI denotes additional isolation from mitigation.

With the above motivation, the rest of the analysis is conducted in terms of *additional isolation*, ΔI, obtained by implementing active mitigation after passive physical isolation:

$$\Delta I \triangleq \frac{P_{\mathrm{I}} \text{ with mere physical isolation}}{P_{\mathrm{I}} \text{ after cancellation or suppression}} \tag{3.47}$$

for which the numerator is given by (3.13) and the denominator is given by (3.18) or (3.22) with time-domain cancellation or spatial-domain suppression, respectively. It should be noted that average channel gains and total transmit powers do not actually affect (3.47) because such parameters scale equivalently both the numerator and the denominator.

As ΔI is a random variable, the performance of the mitigation schemes can be comprehensively quantified by the cumulative distribution function (CDF), $F_{\Delta I}(\cdot)$, and the average additional isolation, $\mathcal{E}\{\Delta I\}$. In the following, these metrics refer to their values estimated from a sample of simulated values $\{\Delta I[k]\}_{k=1}^{K}$, with each $\Delta I[k]$ given by (3.47), as

$$F_{\Delta I}(x) \triangleq \frac{1}{K}\sum_{k=1}^{K} \mathrm{U}(x - \Delta I[k]), \tag{3.48}$$

$$\mathcal{E}\{\Delta I\} \triangleq \frac{1}{K}\sum_{k=1}^{K} \Delta I[k], \tag{3.49}$$

where the unit step function $\mathrm{U}(x) = 1$ when $x \geq 0$ and otherwise $\mathrm{U}(x) = 0$.

The sample size is chosen as $K = 10^7$ which is more than sufficient to guarantee that the estimated CDFs are accurate for $F_{\Delta I}(\cdot) \geq 0.01$ and the estimated average values are accurate, at least, down to two digits below the decimal point. Comparable statistics are also evaluated analytically in terms of closed-form expressions and empirically based on channel measurement data later in Sections 3.5.2 and 3.5.3, respectively.

In the following, the content of simulation results on the statistics of additional isolation is first described in detail, before proceeding to more in-depth discussions on observations and comparisons between schemes.

Performance with Perfect Side Information

The focus shall be first on schemes that are subject to residual loop interference even if the relay has perfect side information for mitigation, i.e., when $\epsilon_{\mathbf{H}} = \epsilon_{\mathbf{x}} = 0$. These schemes are namely antenna selection (AS) and general eigenbeam selection (ES). On the contrary, all interference is now eliminated by time-domain cancellation with any $\hat{N}_{\text{rx}} = N_{\text{rx}}$ and $\hat{N}_{\text{tx}} = N_{\text{tx}}$ as well as by eigenbeam selection whenever (3.33) is satisfied, i.e., null-space projection (NSP) is applicable.

Figures 3.6(a) and 3.6(b) illustrate the additional isolation brought by antenna and eigenbeam selection, respectively, when the loop channel is of full rank. The plots show the cumulative distribution functions for different configurations of input and output streams which are denoted by $\hat{N}_{\text{rx}} \times \hat{N}_{\text{tx}}$. The legend also tabulates the average additional isolation. With the parameters chosen for the illustration, eigenbeam selection is reduced to null-space projection and all self-interference is suppressed, rendering theoretically $\Delta I \to \infty$, whenever $\hat{N}_{\text{rx}} + \hat{N}_{\text{tx}} \leq 4$. These results are related to those presented based on measurement data in Section 3.5.3.

Similarly, Fig. 3.7 illustrates how a low rank of the loopback interference channel (shown in parentheses in the legend) facilitates the selection schemes with different receive and transmit antenna configurations which are denoted by $N_{\text{rx}} \times N_{\text{tx}}$. The plots show the cumulative distribution functions and average additional isolation is again tabulated in the legend. With the chosen parameters, eigenbeam selection is now reduced to null-space projection, i.e., $\Delta I \to \infty$, whenever $N_{\text{rx}} + N_{\text{tx}} \geq 6 + \mathbf{rk}\{\mathbf{H}_{\text{RR}}\}$.

At this point, it becomes evident that antenna selection (AS) offers very low additional isolation w.r.t. the other schemes while still consuming many spatial degrees of freedom that could be used in actual data transmission instead. Hence, it is fairly justified to omit AS in later results.

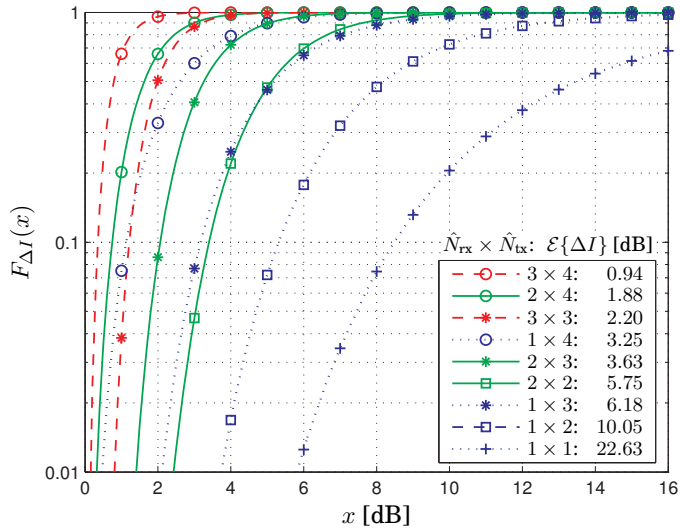

(a) antenna selection (AS)

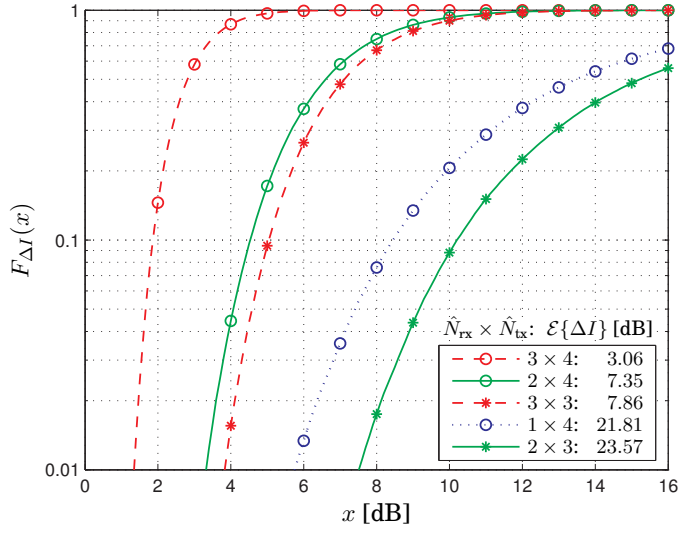

(b) eigenbeam selection (ES)

Figure 3.6. The performance of the spatial selection schemes when $N_{\mathrm{rx}} = N_{\mathrm{tx}} = 4$, the side information is perfect ($\epsilon_{\mathbf{H}} = \epsilon_{\mathbf{x}} = 0$), and $\mathbf{H}_{\mathrm{RR}}$ is of full rank.

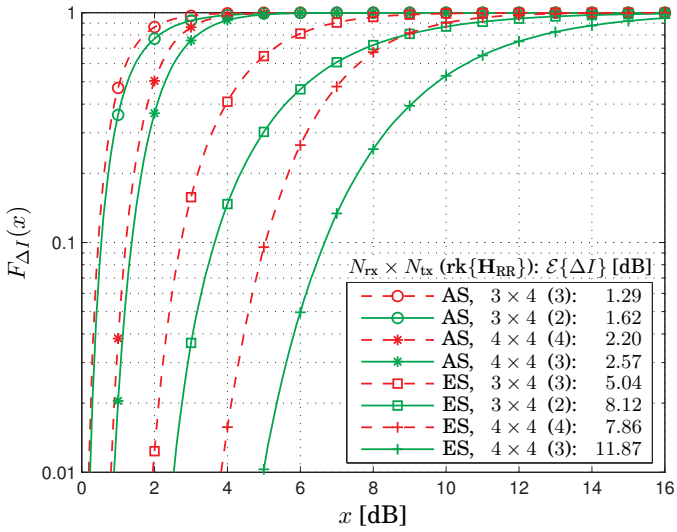

Figure 3.7. The effect of loop channel rank on antenna and eigenbeam selection (AS and ES) when $\hat{N}_{\mathrm{rx}} = \hat{N}_{\mathrm{tx}} = 3$ and the side information is perfect ($\epsilon_{\mathbf{H}} = \epsilon_{\mathbf{x}} = 0$).

Performance with Imperfect Side Information

Continuing to the practical case of having imperfect side information, Fig. 3.8 illustrates how channel estimation error, which is parametrized by $\epsilon_{\mathbf{H}}$, degrades the average additional isolation. The side information on the transmitted signal is ideal in this plot which implies $\Delta I \to \infty$ with time-domain cancellation and null-space projection when $\epsilon_{\mathbf{H}} \to 0$.

All illustrated schemes are sensitive to channel estimation error. At low error levels, the average additional isolation of time-domain cancellation (TDC) and null-space projection (NSP) is linearly proportional to the relative estimation error on a log-log scale with some constant gain which depends on the number of antennas, the rank of the loop channel, and the number of input and output streams. With perfect side information, the mitigation schemes always improve isolation as expected. However, TDC may actually degrade isolation at high estimation error levels because it adds a new signal in the relay input contrary to spatial suppression schemes, e.g., NSP, that only filter the existing ones.

Figure 3.9 illustrates how transmit signal noise, which is parametrized by $\epsilon_{\mathbf{x}}$, degrades the average additional isolation. The figure also reveals the joint effect of the two side-information imperfections. The selection diversity within the set of equivalent eigenbeam selection (ES) and NSP solutions is exploited by choosing the solution that reduces the effect of transmit signal noise the most. Consequently, the spatial suppression

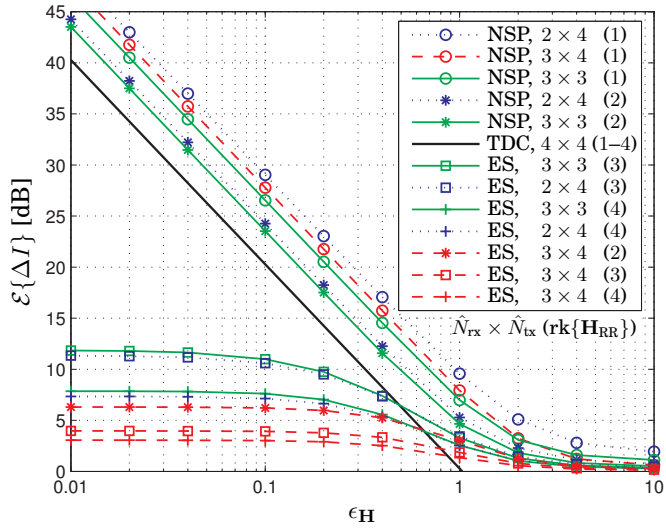

Figure 3.8. The effect of channel estimation error when $N_{\text{rx}} = N_{\text{tx}} = 4$ and $\epsilon_{\mathbf{x}} = 0$. Eigenbeam selection (ES) is reduced to null-space projection (NSP) whenever $\hat{N}_{\text{rx}} + \hat{N}_{\text{tx}} + \mathbf{rk}\{\mathbf{H}_{\text{RR}}\} \leq 8$.

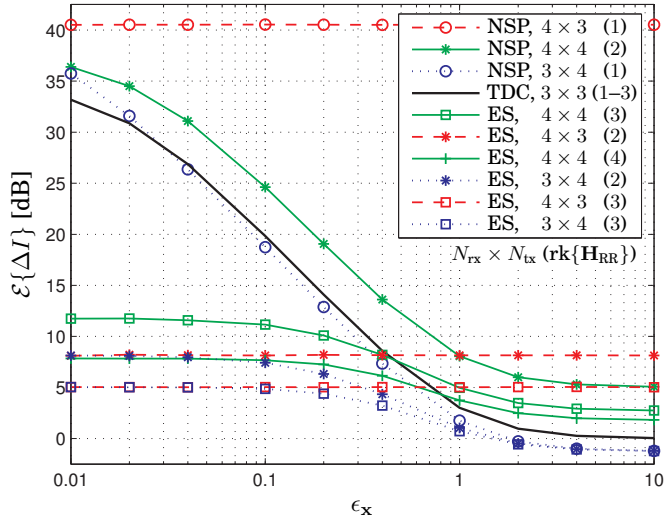

Figure 3.9. The effect of transmit signal noise when $\hat{N}_{\text{rx}} = \hat{N}_{\text{tx}} = 3$ and $\epsilon_{\mathbf{H}} = 0.02$. Eigenbeam selection (ES) is reduced to null-space projection (NSP) whenever $N_{\text{rx}} + N_{\text{tx}} - \mathbf{rk}\{\mathbf{H}_{\text{RR}}\} \geq 6$.

schemes become immune to its effect whenever the degrees of freedom are sufficiently high at the relay receiver side. In contrast, subtractive cancellation cannot mitigate the effect of transmit signal noise at all.

MMSE Filtering

Figure 3.10 compares minimum mean square error (MMSE) suppression with the other schemes in terms of both the cumulative distribution function and the average of additional isolation; the latter is again enumerated in the legend. In this setup, MMSE filtering and time-domain cancellation (TDC) have the same number of antennas which is sufficient for avoiding the distortion of the useful signal. On the other hand, eigenbeam selection (ES) and null-space projection (NSP) are implemented by adding an extra antenna at the receiver side since this is required in order to achieve any interference suppression at all.

In general, the rank of the loop channel defines which scheme is preferable and the variance of the additional isolation is considerably higher with spatial suppression than with TDC. In particular, it can be noted that the average additional isolation of NSP and MMSE filtering is approximately the same with rank-one loop channel, but MMSE filtering yields much larger variance. At first sight, equal average value may seem impossible given the CDF plots, but such deceptive illusion is created only due to the combination of the log-log scale used in the figure and the heavy tail of the probability distribution observed with MMSE filtering.

Combination of Cancellation and Suppression

Finally, Fig. 3.11 illustrates the benefit of combining time-domain cancellation (TDC) and spatial suppression assuming joint design or separate design with Variation (a). The performance of the other variations with separate and independent filter design was also evaluated but, in this setup, the differences are minimal because N_{rx} and N_{tx} are small w.r.t. $\hat{N}_{\mathrm{rx}}$ and $\hat{N}_{\mathrm{tx}}$. Thus, the results represent all variations accurately enough.

The combination of TDC and spatial suppression can indeed offer better performance than either alone. However, when the rank-deficient loop channel enables the usage of null-space projection (NSP), adding TDC on top of suppression may actually reduce the overall performance due to transmit signal noise. This is because NSP can be made immune to transmit signal noise such that it becomes eliminated together with the actual interference signal while TDC effectively acts as an extra interference signal due to channel estimation error.

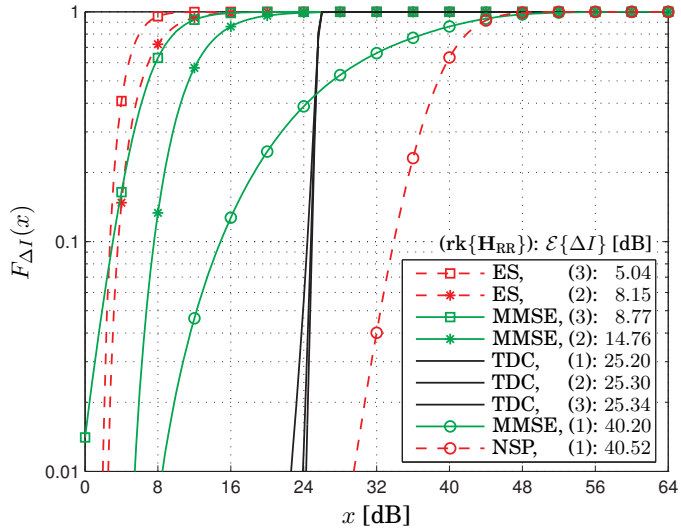

Figure 3.10. Comparison of minimum mean square error (MMSE) suppression and the other mitigation schemes when $N_{\mathrm{S}} = \hat{N}_{\mathrm{rx}} = N_{\mathrm{tx}} = \hat{N}_{\mathrm{tx}} = 3$, $\epsilon_{\mathbf{H}} = 0.02$, and $\epsilon_{\mathbf{x}} = 0.05$. The number of receive antennas is chosen as $N_{\mathrm{rx}} = 3$ for MMSE suppression and time-domain cancellation (TDC) while as $N_{\mathrm{rx}} = 4$ for eigenbeam selection (ES) and null-space projection (NSP).

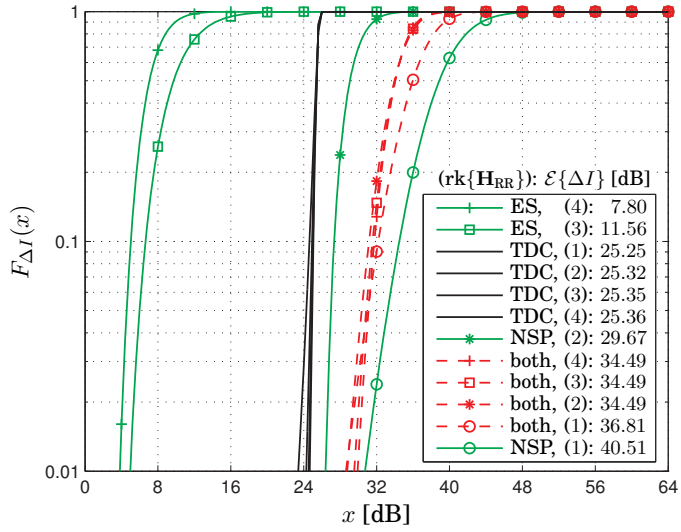

Figure 3.11. The joint performance of the combination of time-domain cancellation (TDC) and spatial suppression in comparison to their separate performance when $\hat{N}_{\mathrm{rx}} = \hat{N}_{\mathrm{tx}} = 3$, $N_{\mathrm{rx}} = N_{\mathrm{tx}} = 4$, $\epsilon_{\mathbf{H}} = 0.02$, and $\epsilon_{\mathbf{x}} = 0.05$.

Discussion on Simulation Results

In general, the simulation results show that spatial-domain suppression is better than time-domain cancellation (TDC) whenever there is a sufficient number of antennas compared to the number of spatial streams. In other words, time-domain processing is preferred if the spatial domain is congested. However, the level of isolation is more stable in TDC than in suppression which can be seen from the figures, e.g., by comparing the first percentile of additional isolation to its average. When it is beneficial to limit the distortion of the useful signal, TDC and MMSE filtering can be preferred, while the combination of TDC and spatial suppression is especially advantageous if the level of transmit signal noise is high.

The performance of spatial-domain suppression depends highly on the rank of the loop channel which is related to the channel condition number that can be high, especially if there is line-of-sight between the antenna arrays. The interplay involves also the spatial degrees of freedom, i.e., channel dimensions and the number of streams. It can be postulated as a rule of thumb that suppression is superior to cancellation whenever null-space projection is applicable. On the contrary, the rank has minimal effect on the performance of TDC, e.g., additional isolation is roughly the same with any rank in Figs. 3.8 and 3.9. Actually, low rank leads to slightly worse isolation due to transmit noise in Figs. 3.10 and 3.11.

Without transmit signal noise, all mitigation schemes reflect symmetric behavior w.r.t. the number of antennas and streams. Thus, isolation stays the same if N_{rx} and $\hat{N}_{\mathrm{rx}}$ are swapped respectively with N_{tx} and $\hat{N}_{\mathrm{tx}}$ in Figs. 3.6–3.8. The presence of transmit signal noise breaks the symmetry and so $N_{\mathrm{rx}} > N_{\mathrm{tx}}$ renders generally better isolation than $N_{\mathrm{rx}} < N_{\mathrm{tx}}$. Likewise, antenna or eigenbeam selection with $\hat{N}_{\mathrm{rx}} \times \hat{N}_{\mathrm{tx}}$ is worse than with $(\hat{N}_{\mathrm{rx}} + 1) \times (\hat{N}_{\mathrm{tx}} - 1)$, promoting for asymmetric stream configurations.

Antenna selection (AS) improves isolation modestly and its performance is not comparable to the other schemes. In the example case of Fig. 3.6(a), only one transmit and receive antenna can be selected from the total of eight antennas for notable additional isolation. However, AS is a low-complexity solution that may be still adopted if it is sufficient to suppress self-interference without complete elimination, e.g., if physical isolation is large and there are a few extra antennas to spare. Especially, AS can be implemented using fewer transceiver radio-frequency front-ends than antennas contrary the other mitigation schemes and, thus, it can be used also during relay mounting for actively enhancing physical isolation.

3.5.2 Analytical Results

In this subsection, time-domain cancellation (TDC) and null-space projection (NSP) are analyzed by deriving closed-form expressions for additional isolation. These two schemes ideally eliminate the feedback loop but residual interference occurs in practice due to the joint effect of channel estimation error and transmit signal noise, which yields motivation for the analysis. The key parameters are imperfection levels ($\epsilon_{\mathbf{H}}$ and $\epsilon_{\mathbf{x}}$) together with antenna and stream configurations ($N_{\text{rx}} \times N_{\text{tx}}$ and $\hat{N}_{\text{rx}} \times \hat{N}_{\text{tx}}$).

System Setup

The system setup considered in these analytical results is the same as what is described in Section 3.3. Two specific extra details are adopted for mathematical convenience though: Firstly, the gain of the physical feedback loop is normalized by setting $\|\mathbf{H}_{\text{RR}}\|_F^2 \triangleq \text{tr}\{\mathbf{H}_{\text{RR}}\mathbf{H}_{\text{RR}}^H\} = N_{\text{rx}}N_{\text{tx}}$ without loss of generality; And secondly, the $\hat{N}_{\text{tx}}$ spatial streams transmitted by the relay are assumed to be independent with equal power, i.e., $\mathbf{R}_{\hat{\mathbf{x}}_{\text{R}}} \triangleq \mathcal{E}\{\hat{\mathbf{x}}_{\text{R}}\hat{\mathbf{x}}_{\text{R}}^H\} = \frac{P_{\text{R}}}{\hat{N}_{\text{tx}}}\mathbf{I}$, rendering a worst-case scenario. This implies $\mathbf{R}_{\boldsymbol{\Delta}\tilde{\mathbf{x}}_{\text{R}}} \triangleq \mathcal{E}\{\boldsymbol{\Delta}\tilde{\mathbf{x}}_{\text{R}}\boldsymbol{\Delta}\tilde{\mathbf{x}}_{\text{R}}^H\} = \epsilon_{\mathbf{x}}^2\frac{P_{\text{R}}}{\hat{N}_{\text{tx}}}\mathbf{I}$ for transmit signal noise as per (3.10).

Generic Statistics for Additional Isolation

The reference case of passive physical isolation arising readily by deploying separated receive and transmit antenna arrays is equivalent to setting the mitigation filters as $\mathbf{G}_{\text{rx}} = \mathbf{I}$, $\mathbf{G}_{\text{tx}} = \mathbf{I}$, and $\mathbf{C} = \mathbf{0}$. Given the above system setup, the power of self-interference included in (3.1a) becomes

$$P_{\text{I}} \triangleq \mathcal{E}\{\|\mathbf{H}_{\text{RR}}\,\mathbf{x}_{\text{R}}\|_2^2\} = \text{tr}\{\mathbf{H}_{\text{RR}}\mathbf{R}_{\mathbf{x}_{\text{R}}}\mathbf{H}_{\text{RR}}^H\} = N_{\text{rx}}(1+\epsilon_{\mathbf{x}}^2)P_{\text{R}} \tag{3.50}$$

after noting that $\mathbf{R}_{\mathbf{x}_{\text{R}}} \triangleq \mathcal{E}\{\mathbf{x}_{\text{R}}\mathbf{x}_{\text{R}}^H\} = \mathbf{R}_{\hat{\mathbf{x}}_{\text{R}}} + \mathbf{R}_{\boldsymbol{\Delta}\tilde{\mathbf{x}}_{\text{R}}} = (1+\epsilon_{\mathbf{x}}^2)\frac{P_{\text{R}}}{\hat{N}_{\text{tx}}}\mathbf{I}$.

Reinforcing the simulation results of the previous subsection, the analysis continues evaluating the statistics of *additional isolation* to measure the gain of active mitigation schemes over passive physical isolation. The substitution of P_{I} before active mitigation from (3.50) into (3.47) yields

$$\Delta I = \frac{N_{\text{rx}}(1+\epsilon_{\mathbf{x}}^2)P_{\text{R}}}{P_{\text{I}}\text{ after active mitigation}} \simeq \frac{a}{X+b} \leq \frac{a}{b} \triangleq \Delta I_{\max}, \tag{3.51}$$

where $\{a, b\}$ is a pair of real non-negative constants and X is a gamma random variable with shape k and scale θ, i.e., $X \sim \mathcal{G}(k, \theta)$, as seen later.

Transformed random variables of form $\frac{a}{X+b}$ turn out to be handy for the analysis. In particular, the statistics of additional isolation can be characterized with the following general expressions once the parameter pairs $\{k, \theta\}$ and $\{a, b\}$ are determined specifically for each mitigation scheme.

Channel estimation error makes P_{I} after mitigation and ΔI random variables; with TDC or NSP, the latter is a transformed gamma variable, generic form of which is characterized in Appendix A.1. Especially, the cumulative distribution function (CDF) of additional isolation is given by

$$F_{\Delta I}(x) \simeq 1 - \sum_{l=0}^{k-1} \frac{1}{l!} \left(\frac{a - b\,x}{\theta\,x} \right)^{l} \exp\left(\frac{b\,x - a}{\theta\,x} \right) \tag{3.52}$$

for $x \leq \Delta I_{\max}$ while $F_{\Delta I}(x) = 1$ for $x > \Delta I_{\max}$, reflecting the inherent limitation $\Delta I \leq \Delta I_{\max}$. Likewise, average additional isolation is given by

$$\mathcal{E}\{\Delta I\} \simeq \frac{a}{\theta} \exp\left(\frac{b}{\theta} \right) E_k\left(\frac{b}{\theta} \right), \tag{3.53}$$

in which $E_k(\cdot)$ denotes the generalized exponential integral [3, Eq. 5.1.4].

Additional Isolation from Time-Domain Cancellation

Time-domain cancellation (TDC) subtracts an approximated interference signal from the relay input without spatial filtering, i.e., $\mathbf{C} = -\tilde{\mathbf{H}}_{\mathrm{RR}}$ while $\mathbf{G}_{\mathrm{rx}} = \mathbf{I}$ and $\mathbf{G}_{\mathrm{tx}} = \mathbf{I}$. Hence, any practical implementation is imperfect for two reasons: channel estimation errors render $\tilde{\mathbf{H}}_{\mathrm{RR}} \neq \mathbf{H}_{\mathrm{RR}}$ and the unknown (random) transmit signal noise term $\boldsymbol{\Delta}\tilde{\mathbf{x}}_{\mathrm{R}}$ cannot be eliminated.

With TDC, the power of residual interference in (3.15) becomes then

$$P_{\mathrm{I}} \triangleq \mathcal{E}\{\|\boldsymbol{\Delta}\tilde{\mathbf{H}}_{\mathrm{RR}}\,\hat{\mathbf{x}}_{\mathrm{R}} + \mathbf{H}_{\mathrm{RR}}\,\boldsymbol{\Delta}\tilde{\mathbf{x}}_{\mathrm{R}}\|_2^2\} = N_{\mathrm{rx}} \left(\frac{\|\boldsymbol{\Delta}\tilde{\mathbf{H}}_{\mathrm{RR}}\|_F^2}{N_{\mathrm{rx}} N_{\mathrm{tx}}} + \epsilon_{\mathbf{x}}^2 \right) P_{\mathrm{R}}, \tag{3.54}$$

where $\|\boldsymbol{\Delta}\tilde{\mathbf{H}}_{\mathrm{RR}}\|_F^2 \sim \mathcal{G}(N_{\mathrm{rx}} N_{\mathrm{tx}}, \epsilon_{\mathbf{H}}^2)$ by definition. In the context of (3.51), ΔI and $\frac{\|\boldsymbol{\Delta}\tilde{\mathbf{H}}_{\mathrm{RR}}\|_F^2}{N_{\mathrm{rx}} N_{\mathrm{tx}}}$ are matched to $\frac{a}{X+b}$ and $X \sim \mathcal{G}(k, \theta)$, respectively, when

$$\begin{cases} \{k,\ \theta\} = \{N_{\mathrm{rx}} N_{\mathrm{tx}},\ \epsilon_{\mathbf{H}}^2/(N_{\mathrm{rx}} N_{\mathrm{tx}})\}, \\ \{a,\ b\} = \{1 + \epsilon_{\mathbf{x}}^2,\ \epsilon_{\mathbf{x}}^2\}. \end{cases} \tag{3.55}$$

Thus, the statistics of additional isolation from TDC are characterized by generic expressions (3.52) and (3.53) with the above parameter settings.

Additional Isolation from Null-Space Projection

Null-space projection (NSP) directs relay receive and transmit beams to orthogonal subspaces, i.e., $\mathbf{G}_{\mathrm{rx}}\tilde{\mathbf{H}}_{\mathrm{RR}}\mathbf{G}_{\mathrm{tx}} = \mathbf{0}$, rendering cancellation redundant and thus $\mathbf{C} = \mathbf{0}$. As $\tilde{\mathbf{H}}_{\mathrm{RR}}$ has full rank due to estimation errors (even if the actual channel $\mathbf{H}_{\mathrm{RR}}$ may be rank-deficient), the number of supported streams is limited by $\hat{N}_{\mathrm{rx}} + \hat{N}_{\mathrm{tx}} \leq \max\{N_{\mathrm{rx}}, N_{\mathrm{tx}}\}$. However, the choice of the beamforming filters is not usually unique, but one may still adopt a solution that additionally minimizes $\mathbf{G}_{\mathrm{rx}}\tilde{\mathbf{H}}_{\mathrm{RR}}$, i.e., the effect of transmit signal noise. For example, setting $\mathbf{S}_{\mathrm{rx}}^T = [\mathbf{0}\ \mathbf{I}]$ and $\mathbf{S}_{\mathrm{tx}} = [\mathbf{I}\ \mathbf{0}]^T$ in the context of general eigenbeam selection is recommended when $N_{\mathrm{rx}} \geq N_{\mathrm{tx}}$.

By designing eigenbeamforming filters to obtain NSP as described in Section 3.4.3, the power of residual interference in (3.20) becomes

$$\begin{aligned} P_{\mathrm{I}} &\triangleq \mathcal{E}\{\|\mathbf{G}_{\mathrm{rx}}\boldsymbol{\Delta}\tilde{\mathbf{H}}_{\mathrm{RR}}\mathbf{G}_{\mathrm{tx}}\,\hat{\mathbf{x}}_{\mathrm{R}} + \mathbf{G}_{\mathrm{rx}}\mathbf{H}_{\mathrm{RR}}\,\boldsymbol{\Delta}\tilde{\mathbf{x}}_{\mathrm{R}}\|_2^2\} \\ &= N_{\mathrm{rx}}\left(\frac{\|\mathbf{S}_{\mathrm{rx}}^T\tilde{\mathbf{U}}_{\mathrm{RR}}^H\boldsymbol{\Delta}\tilde{\mathbf{H}}_{\mathrm{RR}}\tilde{\mathbf{V}}_{\mathrm{RR}}\mathbf{S}_{\mathrm{tx}}\|_F^2}{\hat{N}_{\mathrm{rx}}\hat{N}_{\mathrm{tx}}} + \epsilon_{\mathbf{x}}^2\frac{\|\mathbf{S}_{\mathrm{rx}}^T\tilde{\mathbf{U}}_{\mathrm{RR}}^H\mathbf{H}_{\mathrm{RR}}\|_F^2}{\hat{N}_{\mathrm{rx}}N_{\mathrm{tx}}}\right)P_{\mathrm{R}}, \end{aligned} \tag{3.56}$$

from which one may note that $\|\mathbf{S}_{\mathrm{rx}}^T\tilde{\mathbf{U}}_{\mathrm{RR}}^H\boldsymbol{\Delta}\tilde{\mathbf{H}}_{\mathrm{RR}}\tilde{\mathbf{V}}_{\mathrm{RR}}\mathbf{S}_{\mathrm{tx}}\|_F^2 \sim \mathcal{G}(\hat{N}_{\mathrm{rx}}\hat{N}_{\mathrm{tx}}, \epsilon_{\mathbf{H}}^2)$ and $\|\mathbf{S}_{\mathrm{rx}}^T\tilde{\mathbf{U}}_{\mathrm{RR}}^H\mathbf{H}_{\mathrm{RR}}\|_F^2 \approx \|\mathbf{S}_{\mathrm{rx}}^T\mathbf{U}_{\mathrm{RR}}^H\mathbf{H}_{\mathrm{RR}}\|_F^2$ representing a constant derived from the singular-value decomposition $\mathbf{H}_{\mathrm{RR}} = \mathbf{U}_{\mathrm{RR}}\boldsymbol{\Sigma}_{\mathrm{RR}}\mathbf{V}_{\mathrm{RR}}^H$. In the context of (3.51), ΔI and $\frac{\|\mathbf{S}_{\mathrm{rx}}^T\tilde{\mathbf{U}}_{\mathrm{RR}}^H\boldsymbol{\Delta}\tilde{\mathbf{H}}_{\mathrm{RR}}\tilde{\mathbf{V}}_{\mathrm{RR}}\mathbf{S}_{\mathrm{tx}}\|_F^2}{\hat{N}_{\mathrm{rx}}\hat{N}_{\mathrm{tx}}}$ are then approximately matched to $\frac{a}{X+b}$ and $X \sim \mathcal{G}(k,\theta)$, respectively, by choosing

$$\begin{cases} \{k,\ \theta\} = \{\hat{N}_{\mathrm{rx}}\hat{N}_{\mathrm{tx}},\ \epsilon_{\mathbf{H}}^2/(\hat{N}_{\mathrm{rx}}\hat{N}_{\mathrm{tx}})\}, \\ \{a,\ b\} = \{1+\epsilon_{\mathbf{x}}^2,\ \epsilon_{\mathbf{x}}^2\|\mathbf{S}_{\mathrm{rx}}^T\mathbf{U}_{\mathrm{RR}}^H\mathbf{H}_{\mathrm{RR}}\|_F^2/(\hat{N}_{\mathrm{rx}}N_{\mathrm{tx}})\}. \end{cases} \tag{3.57}$$

Comparison with simulation results proves that replacing the random variable $\frac{\|\mathbf{S}_{\mathrm{rx}}^T\tilde{\mathbf{U}}_{\mathrm{RR}}^H\mathbf{H}_{\mathrm{RR}}\|_F^2}{\hat{N}_{\mathrm{rx}}N_{\mathrm{tx}}}$ by a constant $b/\epsilon_{\mathbf{x}}^2$ causes a minor error. Thus, the statistics of additional isolation from NSP are accurately characterized by generic expressions (3.52) and (3.53) with the above parameter settings.

Suppression of Transmit Signal Noise

Null-space projection can also partly suppress $\boldsymbol{\Delta}\tilde{\mathbf{x}}_{\mathrm{R}}$ from (3.20) by setting $\mathbf{G}_{\mathrm{rx}}\tilde{\mathbf{H}}_{\mathrm{RR}} = \mathbf{0}$ (which obviously implies $\mathbf{G}_{\mathrm{rx}}\tilde{\mathbf{H}}_{\mathrm{RR}}\mathbf{G}_{\mathrm{tx}} = \mathbf{0}$ also). However, the transmit filter becomes useless in this perspective (thus, $\mathbf{G}_{\mathrm{tx}} = \mathbf{I}$) because it cannot affect unknown noise that is generated just after it. As already noted, $\tilde{\mathbf{H}}_{\mathrm{RR}}$ is in practice of full rank. Thus, the unique solution for the selection matrix, i.e., $\mathbf{S}_{\mathrm{rx}}^T = [\mathbf{0}\ \mathbf{I}]$, is available only if $N_{\mathrm{rx}} > N_{\mathrm{tx}}$, and the maximum number of supported input streams becomes $\hat{N}_{\mathrm{rx}} = N_{\mathrm{rx}} - N_{\mathrm{tx}}$.

By designing the receive filter for eliminating transmit signal noise in the context of general eigenbeam selection as discussed in Section 3.4.3, the power of residual interference in (3.20) becomes

$$P_{\mathrm{I}} = \mathcal{E}\{\|\mathbf{G}_{\mathrm{rx}}\boldsymbol{\Delta}\tilde{\mathbf{H}}_{\mathrm{RR}}\,\mathbf{x}_{\mathrm{R}}\|_2^2\} = N_{\mathrm{rx}}(1+\epsilon_{\mathbf{x}}^2)\frac{\|\mathbf{S}_{\mathrm{rx}}^T\tilde{\mathbf{U}}_{\mathrm{RR}}^H\boldsymbol{\Delta}\tilde{\mathbf{H}}_{\mathrm{RR}}\|_F^2}{\hat{N}_{\mathrm{rx}}N_{\mathrm{tx}}}P_{\mathrm{R}}, \tag{3.58}$$

where $\|\mathbf{S}_{\mathrm{rx}}^T\tilde{\mathbf{U}}_{\mathrm{RR}}^H\boldsymbol{\Delta}\tilde{\mathbf{H}}_{\mathrm{RR}}\|_F^2 \sim \mathcal{G}(\hat{N}_{\mathrm{rx}}N_{\mathrm{tx}}, \epsilon_{\mathbf{H}}^2)$. In the context of (3.51), ΔI and $\frac{\|\mathbf{S}_{\mathrm{rx}}^T\tilde{\mathbf{U}}_{\mathrm{RR}}^H\boldsymbol{\Delta}\tilde{\mathbf{H}}_{\mathrm{RR}}\|_F^2}{\hat{N}_{\mathrm{rx}}N_{\mathrm{tx}}}$ are matched to $\frac{a}{X+b}$ and $X \sim \mathcal{G}(k,\theta)$, respectively, when

$$\begin{cases} \{k,\ \theta\} = \{\hat{N}_{\mathrm{rx}}N_{\mathrm{tx}},\ \epsilon_{\mathbf{H}}^2/(\hat{N}_{\mathrm{rx}}N_{\mathrm{tx}})\}, \\ \{a,\ b\} = \{1,\ 0\}. \end{cases} \tag{3.59}$$

Thus, the statistics of additional isolation after suppressing transmit signal noise with NSP are characterized (exactly without approximations) by generic expressions (3.52) and (3.53) adopting above parameter settings.

Numerical Results

In the following, analytical expressions (3.52) and (3.53) are implemented with the substitution of the specific values of k, θ, a, and b determined above for each mitigation scheme. The purpose of hereby obtained numerical results is to study the effect of noisy side information on additional isolation from active mitigation while the physical self-interference channels $\mathbf{H}_{\mathrm{RR}}$ are chosen simply as representative samples from the family of MIMO Rayleigh channels which is generated in the same way as with simulation results in Section 3.5.1. In the plots, markers represent numerical values provided by the closed-form expressions while solid lines correspond to reference simulation results; their close match proves that the approximation assumed with NSP incurs rather insignificant error.

First of all, Fig. 3.12 illustrates the fluctuation of additional isolation based on (3.52) in the case of 4×4 antenna configuration. The result indicates that TDC supports more streams and offers more stable isolation than NSP but such CDF plots are still restricted to illustrate only a single parameter set. The remaining performance plots shall thus focus on average additional isolation to facilitate comparison between the schemes. It should be also noted that, irrespective of $\boldsymbol{\Delta}\tilde{\mathbf{H}}_{\mathrm{RR}}$, ΔI remains below

$$\Delta I_{\max} = \frac{1+\epsilon_{\mathbf{x}}^2}{\epsilon_{\mathbf{x}}^2} \quad \text{with TDC}, \tag{3.60a}$$

$$\Delta I_{\max} = \frac{\hat{N}_{\mathrm{rx}} N_{\mathrm{tx}}}{\|\mathbf{S}_{\mathbf{rx}}^T \mathbf{U}_{\mathrm{RR}}^H \mathbf{H}_{\mathrm{RR}}\|_F^2} \cdot \frac{1+\epsilon_{\mathbf{x}}^2}{\epsilon_{\mathbf{x}}^2} \quad \text{with NSP}, \tag{3.60b}$$

although $\Delta I_{\max} \to \infty$ if NSP is capable of eliminating completely transmit signal noise. For example when $\epsilon_{\mathbf{x}} = 0.05$ as in Fig. 3.12, $\Delta I_{\max} = 26.0$ dB and $\Delta I_{\max} \in \{29.0, 41.1\}$ dB with TDC and NSP, respectively.

At the cost of reserving some spatial dimensions for interference suppression, NSP achieves usually higher isolation than TDC. This is shown especially by Fig. 3.13, which illustrates the analytical expression given in (3.53). Without transmit signal noise, the average additional isolation is approximately linearly proportional to the channel estimation error level. Otherwise it converges to a maximum value determined by the level of transmit signal noise, when the channel estimation error is small. In particular, transmit signal noise is seen to affect more TDC than NSP, e.g., in the same context, Fig. 3.14 shows contours for 30 dB additional isolation for revealing the joint effect of channel estimation error and transmit signal noise. Thus, the analysis is useful also for characterizing the maximum allowed error in side information given the difference of target isolation and physical isolation, which would be difficult to simulate.

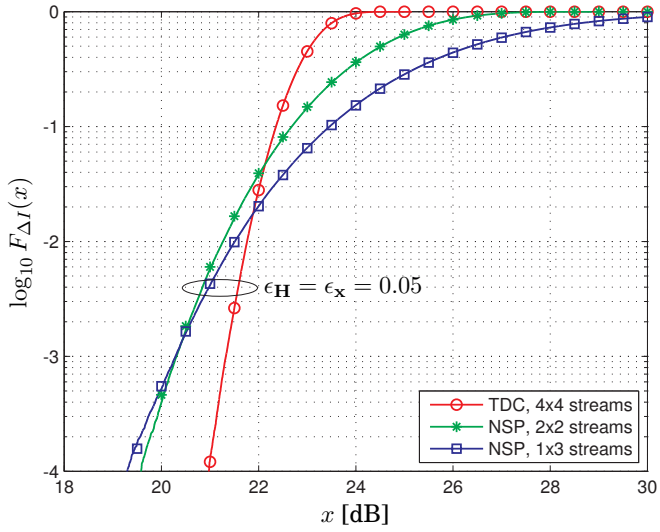

Figure 3.12. Cumulative distribution function of additional isolation from time-domain cancellation (TDC) and null-space projection (NSP) when the relay supports varying number of streams ($\hat{N}_{\text{rx}} \times \hat{N}_{\text{tx}}$) using $N_{\text{rx}} \times N_{\text{tx}} = 4 \times 4$ antennas.

Representing essential counterparts for the foregoing numerical results, the next experiments vary antenna configuration while the number of streams is fixed (namely, $\hat{N}_{\text{rx}} = \hat{N}_{\text{tx}} = 2$). Figure 3.15 shows the effect of transmit signal noise on the average additional isolation based on (3.53). As already formulated in (3.33), NSP needs more antennas than TDC to support the same number of streams with equal additional isolation but, as corroborated by these results, it has a significant advantage: spatial-domain suppression can be made immune to transmit signal noise. This is also verified in Fig. 3.16, which shows the 30 dB contours of average additional isolation. Without channel estimation error, achieved isolation decreases linearly in terms of transmit signal noise level (cf. Fig. 3.15).

Conclusions on Analytical Results

This section evaluated the performance of time-domain cancellation and null-space projection which is a particular variation of general spatial-domain suppression. As both of these schemes can ideally eliminate all interference, the study focused on explaining the significance of interference remaining in practice when side information used in mitigation is imperfect. In particular, the statistics of additional isolation given by the mitigation schemes were evaluated in a closed form in terms of the noise levels of the side information and then used for the comparison of the schemes based on numerical results.

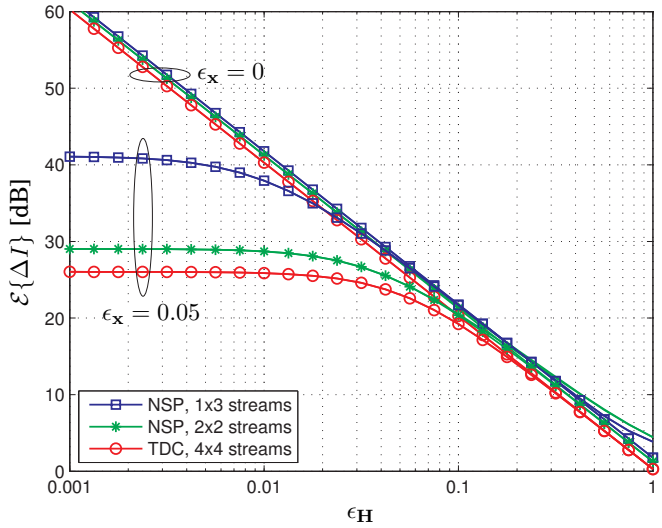

Figure 3.13. Average additional isolation versus channel estimation error level when the relay supports varying number of streams ($\hat{N}_{\text{rx}} \times \hat{N}_{\text{tx}}$) using $N_{\text{rx}} \times N_{\text{tx}} = 4 \times 4$ antennas. In the same setup, the joint effect of channel estimation error and transmit signal noise is illustrated below as a contour plot.

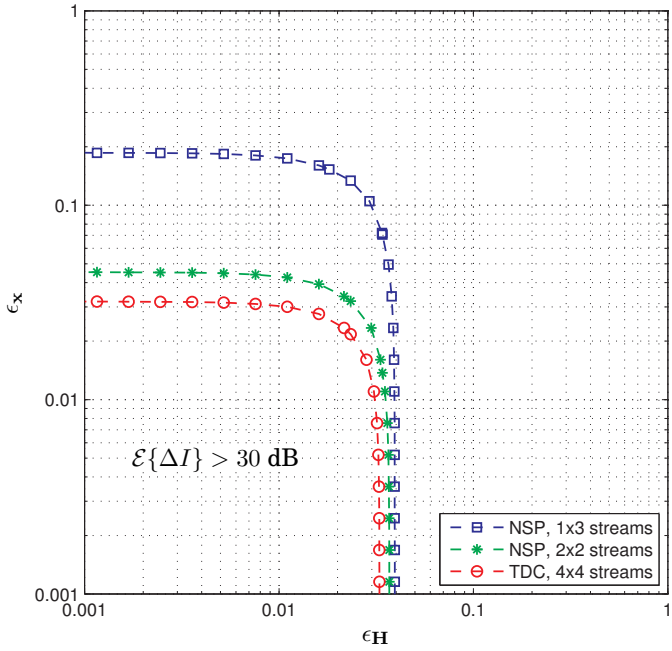

Figure 3.14. The robustness of mitigation against noisy side information when the relay supports varying number of streams ($\hat{N}_{\text{rx}} \times \hat{N}_{\text{tx}}$) using $N_{\text{rx}} \times N_{\text{tx}} = 4 \times 4$ antennas. Isolation is improved at least by 30 dB in the enclosed region where channel estimation error and transmit signal noise are low enough.

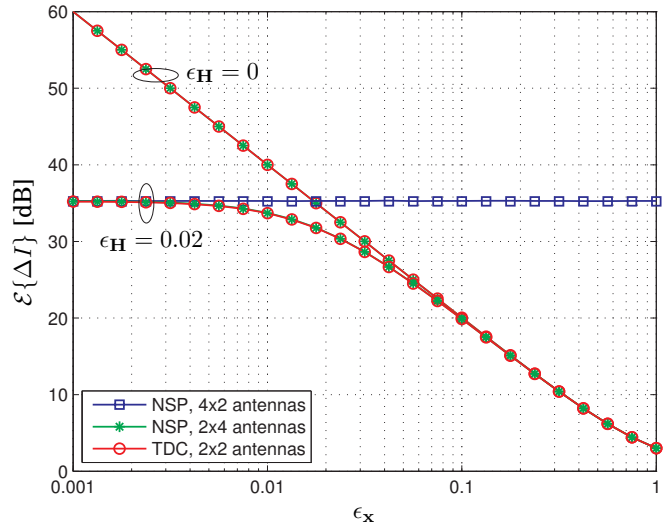

Figure 3.15. Average additional isolation versus transmit signal noise level when the relay supports $\hat{N}_{\text{rx}} \times \hat{N}_{\text{tx}} = 2 \times 2$ streams using different antenna configurations ($N_{\text{rx}} \times N_{\text{tx}}$). In the same setup, the joint effect of channel estimation error and transmit signal noise is illustrated below as a contour plot.

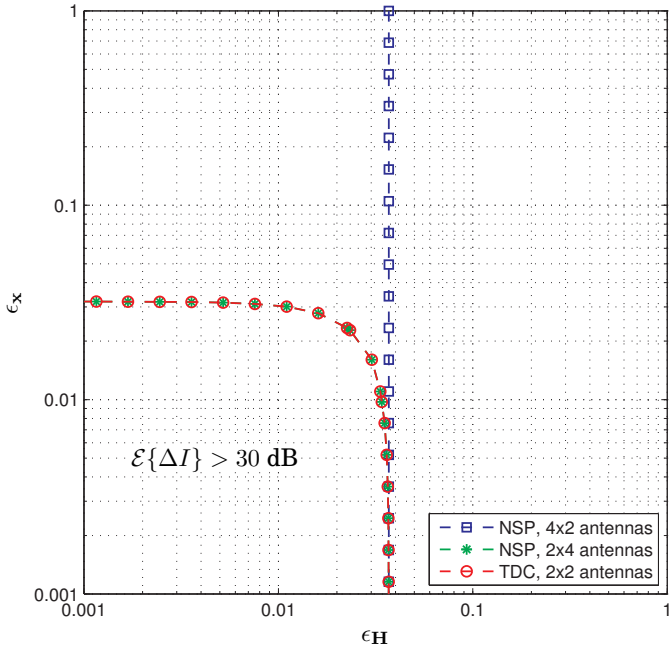

Figure 3.16. The robustness of mitigation against noisy side information when the relay supports $\hat{N}_{\text{rx}} \times \hat{N}_{\text{tx}} = 2 \times 2$ streams using different antenna configurations ($N_{\text{rx}} \times N_{\text{tx}}$). Isolation is improved at least by 30 dB in the enclosed region where channel estimation error and transmit signal noise are low enough.

3.5.3 Experimental Results

Probably the first-ever experimental results on full-duplex MIMO relays are reported in [96,198]. Herein, the performance of self-interference mitigation is evaluated using real-world channel measurement data provided by the authors of [96]. The focus is on schemes that are subject to residual self-interference even with perfect side information. In particular, this subsection studies the physical isolation arising from the directivity and spatial separation of the antenna elements, as explained in Section 3.4.1, and evaluates the additional isolation given by the optimal eigenbeam selection (ES) scheme introduced in Section 3.4.3. Perfect side information, i.e., $\epsilon_{\mathbf{H}} = \epsilon_{\mathbf{x}} = 0$, is assumed throughout the subsection in order to separate the effect of the inherent residual interference of mitigation schemes from the effects of imperfections in side information, which are analyzed instead in Section 3.5.2.

The following discussion begins by summarizing the origins of the channel measurement data while the detailed specifications of the experimental full-duplex antenna arrays and the measurement campaign are available in [96]. The practical physical isolation is then studied by evaluating its variation over different relay locations as well as array orientations and in terms of the distance between the antenna arrays. As a brief side note, the empirical channel condition number illustrates the general motivation—the non-uniformity of channel gain over eigendirections—for using spatial-domain suppression schemes. Finally, the additional isolation given by eigenbeam selection is studied by evaluating its empirical distributions and average values when supporting different stream configurations in the equivalent "interference-free" full-duplex relay.

Measurement Data on MIMO Loopback Channels

The experimental antenna arrays built in [96] are targeted for full-duplex outdoor-to-indoor relaying at 2.6 GHz band. Their main design criteria were to implement a real MIMO relay with multiple mutually uncoupled receive and transmit feeds, to support at least 100 MHz bandwidth, and to achieve compact size but as high isolation as possible. The array prototypes were manufactured according to the final design obtained after revisions based on extensive electromagnetic simulations. As a validity check, the performance of the prototype antenna arrays was then measured in an anechoic chamber which proved that the manufactured relay prototype indeed performs well as indicated by the simulations.

Both antenna arrays comprise two dual-polarized square (5×5 cm) patch antennas placed over a rectangular (15×18 cm) ground plate. The arrays are identical except that transmit polarizations are slanted 45 degrees w.r.t. receive polarizations to improve physical isolation slightly.[2] Thus, there are four antenna feeds in each array. The mutual coupling between the feeds is low enough to allow forming four orthogonal spatial beams at both receive and transmit side as concluded in [96]. With this background in experiments, the case

$$N_{\mathbf{rx}} = N_{\mathbf{tx}} = 4$$

is assumed in all numerical results of this subsection, i.e., $\mathbf{H}_{\mathrm{RR}} \in \mathbb{C}^{4\times4}$.

The experimental data covers measurements for two antenna array configurations from [96] and a set of simulated channel samples as follows.

Compact array configuration refers to the case where the arrays are attached side by side (while facing opposite directions) using plastic spacers. The distance between the arrays is only $d_{\mathrm{RR}} = 2$ cm. By placing the transceiver electronics between the arrays, the complete relay device could be integrated into a small box that is about the same size as typical wireless local area network (WLAN) routers.

The samples of the channel $\mathbf{H}_{\mathrm{RR}}$ are measured by deploying the relay at several locations in a meeting room such that the receive array points outdoors (toward an imaginary base station) through windows and the transmit array provides indoor coverage. The detailed floor plan of the measurements can be found in [96, Fig. 4(a)].

Separate array configuration refers to the case where the receive array is deployed on the outer surface of a meeting room window, such that it points outwards to an imaginary outdoor base station, and the transmit array is deployed indoors. The distance between the arrays, d_{RR}, varies roughly from 20 centimeters to 12 meters.

The samples of the channel $\mathbf{H}_{\mathrm{RR}}$ are measured by deploying the transmit array at various locations in the same meeting room and in the adjacent corridor rendering line-of-sight (LOS) and non-line-of-sight (NLOS) channels, respectively. Furthermore, the measurements include four horizontal array orientations as illustrated in Fig. 3.17: Orientations 1 and 2 represent the case where the transmit array is perpendicular to the receive array; Orientation 3 points

[2]The blueprint and photo of the antenna arrays can be found in [96, Figs. 1,2].

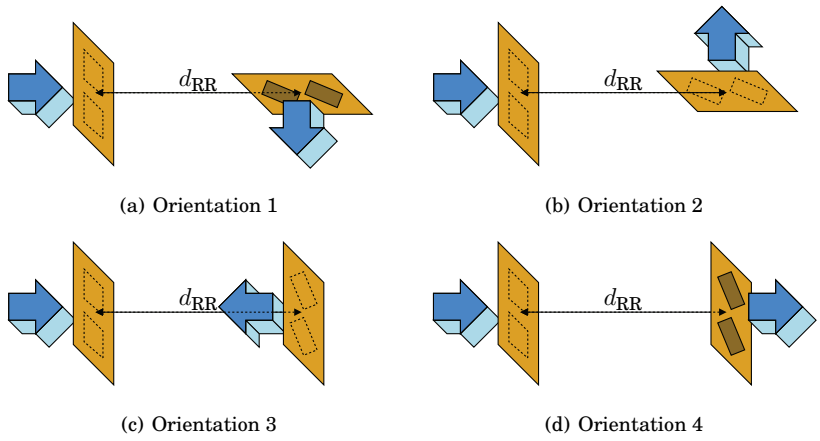

(a) Orientation 1 (b) Orientation 2

(c) Orientation 3 (d) Orientation 4

Figure 3.17. Four horizontal orientations (as seen from above) for the relay transmit antenna array (on the right) w.r.t. the relay receive antenna array (on the left) in measurements with the separate array configuration. The arrows indicate the main beam directions of the antenna elements. The distance between the arrays is denoted by d_{RR}. The compact array configuration results by design in Orientation 4 and $d_{\mathrm{RR}} = 2$ cm.

the main beams of the transmit antenna elements toward the receive array; and Orientation 4 points the two arrays in opposite directions. The detailed floor plan of the measurements can be found in [96, Fig. 4(b)].

Simulated Rayleigh channel is used as an additional performance reference. In particular, a set of random MIMO channel samples is generated assuming independent and identically distributed complex Gaussian elements. Thereby, these reference results are consistent with those presented in Section 3.5.1 for the case of $N_{\mathrm{rx}} = N_{\mathrm{tx}} = 4$ with full channel rank, i.e., $\mathrm{rk}\{\mathbf{H}_{\mathrm{RR}}\} = 4$.

The collected data sets are of the form $\{\mathbf{H}_{\mathrm{RR}}[k]\}_{k=1}^{K}$ where K denotes the number of channel samples. For each array location and orientation, $\mathbf{H}_{\mathrm{RR}}$ is measured at $K = 401$ (with compact array configuration) or $K = 385$ (with separate array configuration) equally-spaced frequency bins, each spanning roughly 500 kHz, over the 2.5–2.7 GHz band which forms the baseline data sets. The full data set is obtained for each array configuration by combining the baseline data sets from all array locations and orientations. In total, the data set includes $K = 88220$ channel samples for the compact array configuration. The combined data set for the separate array configuration includes $K = 43120$ channel samples. This can be further divided into four data sets covering Orientations 1, 2, 3, and 4 with $K = 19250$, $K = 4620$, $K = 5390$, and $K = 13860$ channel samples,

respectively, or into two data sets covering LOS and NLOS channels with $K = 13475$ and $K = 29645$ samples, respectively. With $K = 88220$, the set of simulated Rayleigh channels has about the same size as the others.

Physical Isolation

Given the covariance matrix of the relay transmit signal $\mathbf{R}_{\mathbf{x}_\mathrm{R}}$ and the relay transmit power $P_\mathrm{R} = \mathrm{tr}\{\mathbf{R}_{\mathbf{x}_\mathrm{R}}\}$, the power of the self-interference term $\mathbf{H}_{\mathrm{RR}}\mathbf{x}_\mathrm{R}$ in (3.1a) becomes

$$P_\mathrm{I} \triangleq \mathcal{E}\{\|\mathbf{H}_{\mathrm{RR}}\,\mathbf{x}_\mathrm{R}\|_2^2\} = \mathrm{tr}\{\mathbf{H}_{\mathrm{RR}}\mathbf{R}_{\mathbf{x}_\mathrm{R}}\mathbf{H}_{\mathrm{RR}}^H\} = \frac{P_\mathrm{R}}{N_\mathrm{tx}}\|\mathbf{H}_{\mathrm{RR}}\|_F^2. \tag{3.61}$$

In the last step, the transmitted test signal is considered to be spatially white, i.e., $\mathbf{R}_{\mathbf{x}_\mathrm{R}} = \frac{P_\mathrm{R}}{N_\mathrm{tx}}\mathbf{I}$. However, if necessary, the following results can be repeated with any $\mathbf{R}_{\mathbf{x}_\mathrm{R}}$ experienced in a particular relaying scenario.

Consequently, the physical isolation, arising readily by deploying spatially separated receive and transmit arrays, is given by the ratio of the transmitted power to the received interference power per antenna:

$$\begin{aligned} I_\mathrm{physical} \triangleq \frac{P_\mathrm{R}}{P_\mathrm{I}/N_\mathrm{rx}} &= \frac{N_\mathrm{rx}N_\mathrm{tx}}{\|\mathbf{H}_{\mathrm{RR}}\|_F^2} \\ &= \left(\frac{1}{N_\mathrm{rx}N_\mathrm{tx}}\sum_{i=1}^{N_\mathrm{rx}}\sum_{j=1}^{N_\mathrm{tx}}|\{\mathbf{H}_{\mathrm{RR}}\}_{i,j}|^2\right)^{-1}. \end{aligned} \tag{3.62}$$

This is the key quantity in the following empirical results.

Channel fluctuation over frequency bins and different relay positions makes I_physical a random variable. Thus, the isolation can be characterized and analyzed well in terms of its cumulative distribution function $F_{I_\mathrm{physical}}(\cdot)$ and average $\mathcal{E}\{I_\mathrm{physical}\}$. It should be noted that, in the following, these metrics refer to their empirical values estimated from a sample of measured channels $\{\mathbf{H}_{\mathrm{RR}}[k]\}_{k=1}^K$:

$$F_{I_\mathrm{physical}}(x) \triangleq \frac{1}{K}\sum_{k=1}^{K}\mathrm{U}(x - I_\mathrm{physical}[k]), \tag{3.63}$$

$$\mathcal{E}\{I_\mathrm{physical}\} \triangleq \frac{1}{K}\sum_{k=1}^{K} I_\mathrm{physical}[k], \tag{3.64}$$

where $\mathrm{U}(\cdot)$ is the unit step function, for which $\mathrm{U}(x) = 1$ if $x \geq 0$ and otherwise $\mathrm{U}(x) = 0$, and the values of $I_\mathrm{physical}[k]$, $k = 1, 2, \ldots, K$, are calculated by substituting $\mathbf{H}_{\mathrm{RR}} = \mathbf{H}_{\mathrm{RR}}[k]$ in (3.62).

Some numerical reference results on the empirical statistics of physical isolation are presented also in [96] based on the same measurement data. However, they assume a different definition for the physical isolation, which fundamentally changes the statistics although only small

effect is visible in the average values. In particular, [96, Figs. 5,6] apply

$$I_{\text{physical, [96]}} = \frac{1}{N_{\text{rx}} N_{\text{tx}}} \sum_{i=1}^{N_{\text{rx}}} \sum_{j=1}^{N_{\text{tx}}} \frac{1}{|\{\mathbf{H}_{\text{RR}}\}_{i,j}|^2} \tag{3.65}$$

in contrast to (3.62) used herein. This isolation value is effectively observed in the case of a SISO relay that employs randomly one antenna at each side. To avoid limiting the current study to such a marginal scenario from the start, it is necessary to first extend the earlier results to the real MIMO case, after which all following results are completely new.

Figure 3.18 shows the cumulative distribution function of physical isolation which is normalized by the average value at each array location. Thus, the random variation of physical isolation is separated from the effect of propagation loss that depends mainly on the distance between the arrays. In general, the results show that about 90% of channel samples yield a level of physical isolation which is within ± 3 dB from the average value. This observation can be used as a safety margin when estimating achievable isolation levels using only path loss information.

In particular, the fluctuation of physical isolation reveals the following.

Spatial correlation between MIMO subchannels makes physical isolation vary more in the case of measured channels than in the case of Rayleigh-fading channel samples which are generated assuming independent subchannels. Furthermore, subchannel correlation and, consequently, the variation of physical isolation are larger with the compact array configuration than with the separate array configuration because strong direct coupling between the closely attached arrays does not vary much over different relay positions. On the contrary, both direct coupling and multipath propagation are variable when the arrays are separated.

Multipath richness explains intuitively why physical isolation fluctuates more with NLOS channels than with LOS channels. Although the difference is small, NLOS channels include only scattered components which are subject to higher variance than LOS components. As the propagation environment is heterogeneous, also the transmit array orientation affects the variance of isolation by changing the direction from which multipath components are reflected or scattered to the receive array. However, this observation is also linked to the above NLOS/LOS difference because Orientation 2 (resp. Orientation 3) is measured only in a LOS (resp. NLOS) scenario.

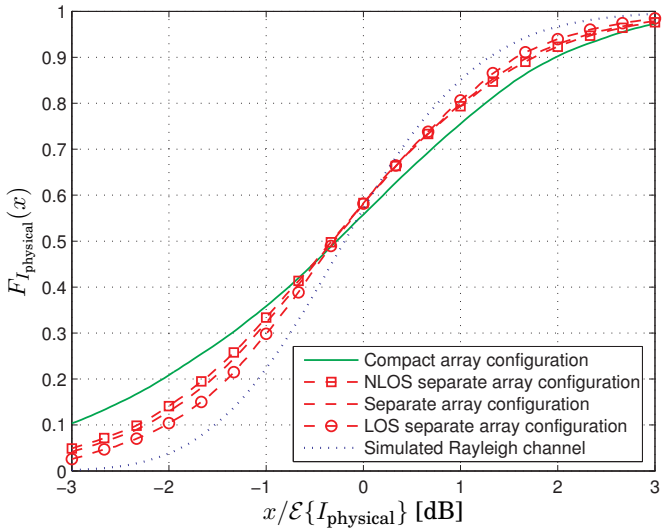

(a) comparison of array configurations

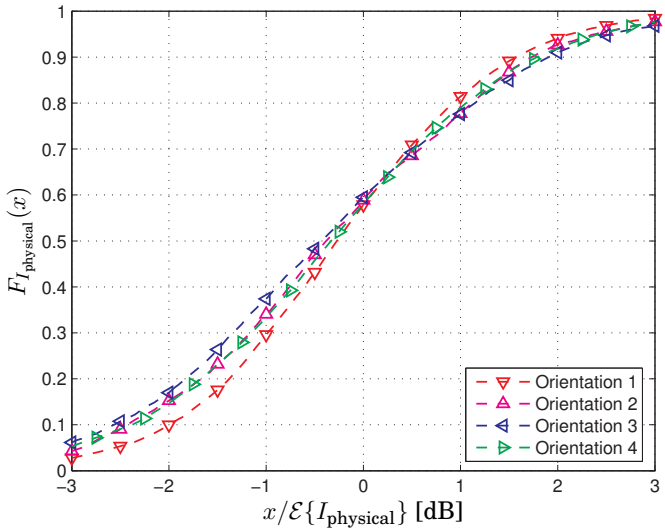

(b) comparison of orientations for separate array configuration

Figure 3.18. The variation of physical isolation with the different array configurations. For the compact array configuration $\mathcal{E}\{I_{\text{physical}}\} = 48.3$ dB, while for the separate array configuration the average physical isolation depends on the distance d_{RR} between the relay antenna arrays as illustrated in Fig. 3.19.

The compact array configuration, in which the distance between the arrays is fixed to two centimeters, achieves 48.3 dB physical isolation on average. For comparison, Fig. 3.19 illustrates the average physical isolation as a function of the distance between the arrays in the separate array configuration. Thus, these results reveal the additional propagation loss that can be achieved by moving arrays further away from each other. In fact, the average isolation closely follows a linear trend (in decibel scale) in terms of the distance between the arrays: with all orientations, the average isolation is improved roughly 2–3 dB per meter.

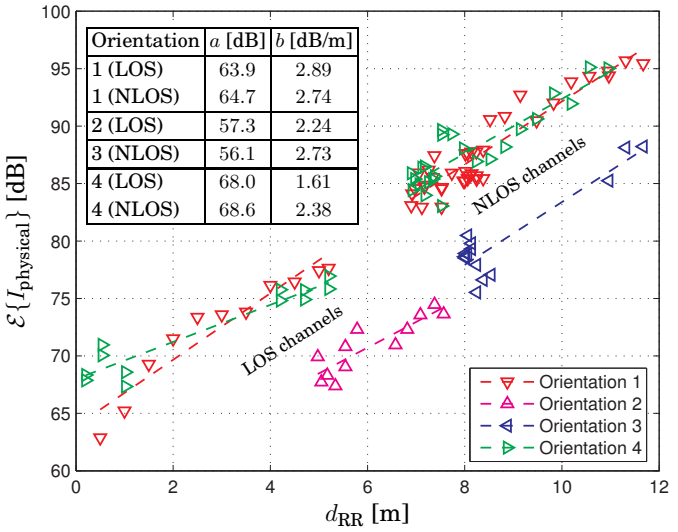

Figure 3.19. Average physical isolation in terms of the distance from the transmit antenna array to the receive antenna array in the separate array configuration. The embedded table shows the parameters (intercept a and slope b) of the linear least-squares fit $\mathcal{E}\{I_{\text{physical}}\} \approx a + b \cdot d_{\text{RR}}$ [dB].

Although the isolation of NLOS channels fluctuates slightly more than that of LOS channels, as seen from Fig. 3.18(a), there is no statistical difference in the average isolation shown in Fig. 3.19. On the other hand, the transmit antenna orientation affects significantly the average physical isolation: Orientations 2 and 3 result in around 10 dB lower isolation than Orientations 1 and 4 with the same distance between the arrays. This is expectable since the antenna elements are not omnidirectional.

By extrapolating the average physical isolation of Orientation 4 with LOS channels down to 2 cm antenna separation, roughly 68 dB isolation is observed with the separate array configuration when it is made equivalent to the compact array configuration that achieves only 48 dB isolation. Obviously, this additional 20 dB isolation originates partly from the

coated glass windowpanes which attenuate the propagation path between the outdoor receive array and indoor transmit array. However, the two array configurations are measured in different buildings which implies that the differences of multipath richness in the propagation environment may be another significant reason for the higher isolation.

In conclusion, the empirical results suggest that mere physical isolation may be insufficient for high-rate full-duplex transmission with high power and long range (especially with compact arrays), even if it is a necessary prerequisite to avoid receiver saturation. This gives general motivation to develop and evaluate signal processing schemes for additional isolation.

Channel Condition Number

The feasibility of applying spatial-domain suppression can be explained by studying the characteristics of the channel condition number $\kappa\{\mathbf{H}_{\mathrm{RR}}\}$. It can be defined in terms of the spectral norm as

$$\kappa\{\mathbf{H}_{\mathrm{RR}}\} \triangleq \|\mathbf{H}_{\mathrm{RR}}\|_2 \cdot \|\mathbf{H}_{\mathrm{RR}}^{-1}\|_2 = \frac{\Sigma_{\mathrm{RR}}[1]}{\Sigma_{\mathrm{RR}}[\min\{N_{\mathsf{rx}}, N_{\mathsf{tx}}\}]}, \tag{3.66}$$

where the first form is applicable only for square channel matrices, i.e., when $N_{\mathsf{rx}} = N_{\mathsf{tx}}$, like with the measurement data at hand. In particular, the case of $\kappa\{\mathbf{H}_{\mathrm{RR}}\} \gg 1$, seen in the following empirical results, indicates that the gain of the self-interference channel is highly non-uniform over its eigendirections, i.e., singular values admit $\Sigma_{\mathrm{RR}}[n_1] \gg \Sigma_{\mathrm{RR}}[n_2]$ when $n_1 > n_2$, which can be exploited by directing the self-interference power to the least harmful dimensions using spatial filters.

Channel fluctuation over frequency bins and different relay positions makes also $\kappa\{\mathbf{H}_{\mathrm{RR}}\}$ a random variable. Figure 3.20 shows the empirical cumulative distribution function of the channel condition number estimated from a sample of measured channels $\{\mathbf{H}_{\mathrm{RR}}[k]\}_{k=1}^{K}$:

$$F_{\kappa\{\mathbf{H}_{\mathrm{RR}}\}}(x) \triangleq \frac{1}{K}\sum_{k=1}^{K} \mathrm{U}(x - \kappa\{\mathbf{H}_{\mathrm{RR}}[k]\}), \tag{3.67}$$

in which the values of $\kappa\{\mathbf{H}_{\mathrm{RR}}[k]\}$, $k = 1, 2, \ldots, K$, are calculated according to (3.66). Similarly, the average condition number can be determined from

$$\mathcal{E}\{\kappa\{\mathbf{H}_{\mathrm{RR}}\}\} \triangleq \frac{1}{K}\sum_{k=1}^{K} \kappa\{\mathbf{H}_{\mathrm{RR}}[k]\}, \tag{3.68}$$

which yields 9.2, 11.9, and 10.9 for the compact array configuration, separate array configuration and simulated Rayleigh channel, respectively.

The empirical results indicate that practical self-interference channels are indeed subject to non-uniform scattering environment. With the current relay prototype, the amplitude of an interference signal propagated

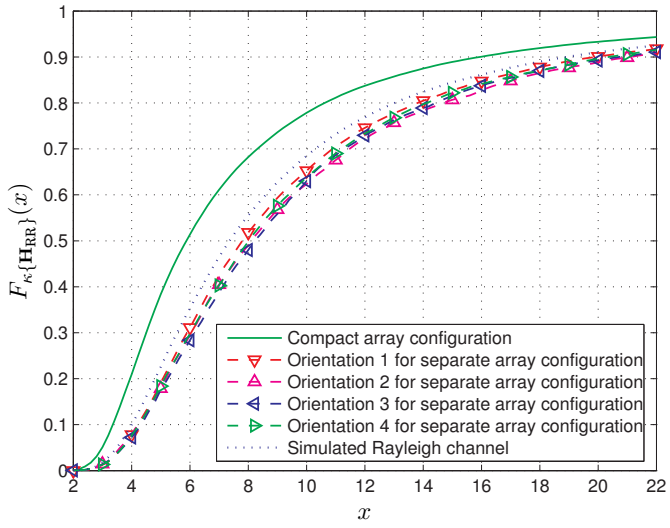

Figure 3.20. The variation of the condition number of the self-interference channel matrix with the different array configurations.

through the strongest spatial eigendirection is on average about ten times higher than that of a signal received from the weakest one. However, the compact array configuration yields typically smaller condition number than the separate array configuration. Thus, it can be expected that spatial suppression gives more additional isolation when the arrays are separated and direct coupling between them is reduced with proper installation. On the other hand, differences between the orientations and LOS versus NLOS channels (not shown herein) are minor.

Furthermore, the case of $\mathrm{rk}\{\mathbf{H}_{\mathrm{RR}}\} = 4$, i.e., $\Sigma_{\mathrm{RR}}[4] > 0$, is observed with all measured and simulated channel samples which implies that the channel condition number is always finite in practice although its distribution has a rather heavy tail as shown by Fig. 3.20. Thus, the self-interference channel should be considered to be of full rank in practice, i.e.,

$$\mathrm{rk}\{\mathbf{H}_{\mathrm{RR}}\} = N_{\mathrm{min}} \triangleq \min\{N_{\mathrm{rx}}, N_{\mathrm{tx}}\}.$$

This may be against intuition by which LOS channels, at least, are typically of low rank due to the weakness of multipath scattering. However, it should be noted that the arrays are too near each other to allow resorting to such presumption that holds only in the far field. Finally, by noting that $N_{\mathrm{rx}} + N_{\mathrm{tx}} - N_{\mathrm{min}} = \max\{N_{\mathrm{rx}}, N_{\mathrm{tx}}\}$, the general condition given in (3.33) for the applicability of null-space projection (NSP) can be restated as

$$\hat{N}_{\mathrm{rx}} + \hat{N}_{\mathrm{tx}} \leq N_{\mathrm{max}} \triangleq \max\{N_{\mathrm{rx}}, N_{\mathrm{tx}}\} \tag{3.69}$$

in a more restricted form under the assumption of full channel rank.

Additional Isolation from Eigenbeam Selection

When applying any spatial suppression scheme proposed in Section 3.4.3, the power of the residual self-interference term in (3.20) becomes

$$P_{\mathrm{I}} \triangleq \mathcal{E}\{\|\hat{\mathbf{H}}_{\mathrm{RR}}\,\hat{\mathbf{x}}_{\mathrm{R}}\|_2^2\} = \mathrm{tr}\{\hat{\mathbf{H}}_{\mathrm{RR}}\mathbf{R}_{\hat{\mathbf{x}}_{\mathrm{R}}}\hat{\mathbf{H}}_{\mathrm{RR}}^H\} = \frac{P_{\mathrm{R}}}{\hat{N}_{\mathrm{tx}}}\|\hat{\mathbf{H}}_{\mathrm{RR}}\|_F^2, \tag{3.70}$$

where $\hat{\mathbf{H}}_{\mathrm{RR}} = \mathbf{G}_{\mathrm{rx}}\mathbf{H}_{\mathrm{RR}}\mathbf{G}_{\mathrm{tx}}$ and the transmitted test signal is again considered to be spatially white with total power P_{R}, i.e., $\mathbf{R}_{\hat{\mathbf{x}}_{\mathrm{R}}} = \frac{P_{\mathrm{R}}}{\hat{N}_{\mathrm{tx}}}\mathbf{I}$ and $P_{\mathrm{R}} \triangleq \mathrm{tr}\{\mathbf{R}_{\hat{\mathbf{x}}_{\mathrm{R}}}\} = \mathrm{tr}\{\mathbf{R}_{\mathbf{x}_{\mathrm{R}}}\}$, in order to have fair comparison with the case of mere physical isolation. More specifically, the substitution of spatial filtering matrices from (3.27a) and (3.27b) yields

$$\hat{\mathbf{H}}_{\mathrm{RR}} = \sqrt{\frac{N_{\mathrm{rx}}}{\hat{N}_{\mathrm{rx}}}}\mathbf{S}_{\mathrm{rx}}^T\mathbf{\Sigma}_{\mathrm{RR}}\mathbf{S}_{\mathrm{tx}} \tag{3.71}$$

with eigenbeam selection (ES) that is in the focus of the following study.

Consequently, isolation with eigenbeam selection is given by the ratio of the transmitted power to the received interference power per antenna:

$$I_{\mathrm{ES}} \triangleq \frac{P_{\mathrm{R}}}{P_{\mathrm{I}}/N_{\mathrm{rx}}} = \frac{\hat{N}_{\mathrm{rx}}\hat{N}_{\mathrm{tx}}}{\|\mathbf{S}_{\mathrm{rx}}^T\mathbf{\Sigma}_{\mathrm{RR}}\mathbf{S}_{\mathrm{tx}}\|_F^2}. \tag{3.72}$$

The following experimental results measure the performance of interference suppression in terms of the additional isolation ΔI_{ES} given by the optimal ES scheme with different stream configurations. It is defined as the ratio of isolation with suppression to physical isolation:

$$\Delta I_{\mathrm{ES}} \triangleq \frac{I_{\mathrm{ES}}}{I_{\mathrm{physical}}} = \frac{\hat{N}_{\mathrm{rx}}\hat{N}_{\mathrm{tx}}}{N_{\mathrm{rx}}N_{\mathrm{tx}}} \cdot \frac{\|\mathbf{H}_{\mathrm{RR}}\|_F^2}{\|\mathbf{S}_{\mathrm{rx}}^T\mathbf{\Sigma}_{\mathrm{RR}}\mathbf{S}_{\mathrm{tx}}\|_F^2}, \tag{3.73}$$

where, according to the basic property of the Frobenius norm,

$$\|\mathbf{H}_{\mathrm{RR}}\|_F^2 = \frac{N_{\mathrm{rx}}N_{\mathrm{tx}}}{I_{\mathrm{physical}}} = \sum_{n=1}^{\min\{N_{\mathrm{rx}},N_{\mathrm{tx}}\}} \Sigma_{\mathrm{RR}}^2[n] \tag{3.74}$$

and, by assuming the usage of optimal selection matrices,

$$\|\mathbf{S}_{\mathrm{rx}}^T\mathbf{\Sigma}_{\mathrm{RR}}\mathbf{S}_{\mathrm{tx}}\|_F^2 = \frac{\hat{N}_{\mathrm{rx}}\hat{N}_{\mathrm{tx}}}{I_{\mathrm{ES}}} = \sum_{n=N_{\mathrm{rx}}-\hat{N}_{\mathrm{rx}}+N_{\mathrm{tx}}-\hat{N}_{\mathrm{tx}}+1}^{\min\{N_{\mathrm{rx}},N_{\mathrm{tx}}\}} \Sigma_{\mathrm{RR}}^2[n] \tag{3.75}$$

as shown in (3.30). However, it should be noted that the above definition is relevant only when the condition of (3.69) is not satisfied. On the contrary, if (3.69) holds then trivially $P_{\mathrm{I}} = 0$ and $\Delta I_{\mathrm{ES}} \to \infty$ because the side information used in mitigation is assumed to be perfect in this subsection.

Similar to the above metrics, channel variation over array locations and frequency bins makes ΔI_{ES} a random variable. Hence, the analysis is conducted in terms of its empirical cumulative distribution function and

average which are denoted by $\mathcal{E}\{\Delta I_{\mathrm{ES}}\}$ and $F_{\Delta I_{\mathrm{ES}}}(\cdot)$, respectively. They are estimated from a sample of measured channels $\{\mathbf{H}_{\mathrm{RR}}[k]\}_{k=1}^{K}$ as follows:

$$F_{\Delta I_{\mathrm{ES}}}(x) \triangleq \frac{1}{K}\sum_{k=1}^{K} \mathrm{U}(x - \Delta I_{\mathrm{ES}}[k]), \tag{3.76}$$

$$\mathcal{E}\{\Delta I_{\mathrm{ES}}\} \triangleq \frac{1}{K}\sum_{k=1}^{K} \Delta I_{\mathrm{ES}}[k], \tag{3.77}$$

where the values of $\Delta I_{\mathrm{ES}}[k]$, $k = 1, 2, \ldots, K$, are calculated according to (3.73)–(3.75) by substituting $\mathbf{H}_{\mathrm{RR}} = \mathbf{H}_{\mathrm{RR}}[k]$.

Before discussing the numerical results, it is worth recalling that the lack of transmit signal noise brings inherent symmetry to the system as discussed in Section 3.5.1. In particular, the performance of any stream combination $\hat{N}_{\mathrm{rx}} \times \hat{N}_{\mathrm{tx}}$ (input streams times output streams) is exactly the same as that of the swapped stream combination $\hat{N}_{\mathrm{tx}} \times \hat{N}_{\mathrm{rx}}$ in the following. Thus, both cases can be analyzed with a single set of results by denoting $\hat{N}_{\mathrm{min}} \triangleq \min\{\hat{N}_{\mathrm{rx}}, \hat{N}_{\mathrm{tx}}\}$ and $\hat{N}_{\mathrm{max}} \triangleq \max\{\hat{N}_{\mathrm{rx}}, \hat{N}_{\mathrm{tx}}\}$.

Figure 3.21 shows the cumulative distribution function of additional isolation given by optimal eigenbeam selection with the two array configurations. For reference, Fig. 3.6(b) presented in Section 3.5.1 shows the related results in the case of the simulated Rayleigh channel. Similar comparison can be found in Fig. 7(b) of **[208]** also for the orientations of the separate array configuration, but this result is omitted herein because there is no visible difference between them. In fact, results for the orientations differ less than what is seen in terms of the condition number in Fig. 3.20. The values of average additional isolation are listed in Table 3.2.

Table 3.2. The average additional isolation $\mathcal{E}\{\Delta I_{\mathrm{ES}}\}$ given by the optimal eigenbeamforming scheme with the different array configurations.

(a) compact array configuration

	$\hat{N}_{\mathrm{max}} = 3$	$\hat{N}_{\mathrm{max}} = 4$
$\hat{N}_{\mathrm{min}} = 1$	∞	18.7 dB
$\hat{N}_{\mathrm{min}} = 2$	20.5 dB	7.2 dB
$\hat{N}_{\mathrm{min}} = 3$	7.7 dB	3.5 dB

(b) separate array configuration

	$\hat{N}_{\mathrm{max}} = 3$	$\hat{N}_{\mathrm{max}} = 4$
$\hat{N}_{\mathrm{min}} = 1$	∞	20.5 dB
$\hat{N}_{\mathrm{min}} = 2$	22.2 dB	7.9 dB
$\hat{N}_{\mathrm{min}} = 3$	8.4 dB	3.4 dB

(c) simulated Rayleigh channel

	$\hat{N}_{\mathrm{max}} = 3$	$\hat{N}_{\mathrm{max}} = 4$
$\hat{N}_{\mathrm{min}} = 1$	∞	20.1 dB
$\hat{N}_{\mathrm{min}} = 2$	21.9 dB	7.3 dB
$\hat{N}_{\mathrm{min}} = 3$	7.9 dB	3.1 dB

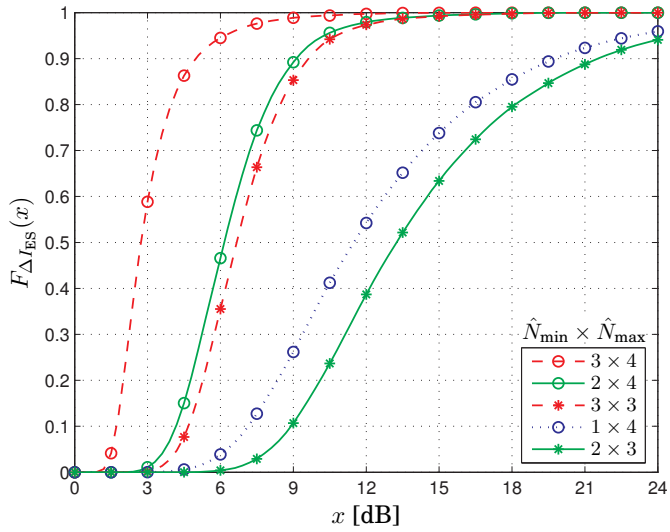

(a) compact array configuration

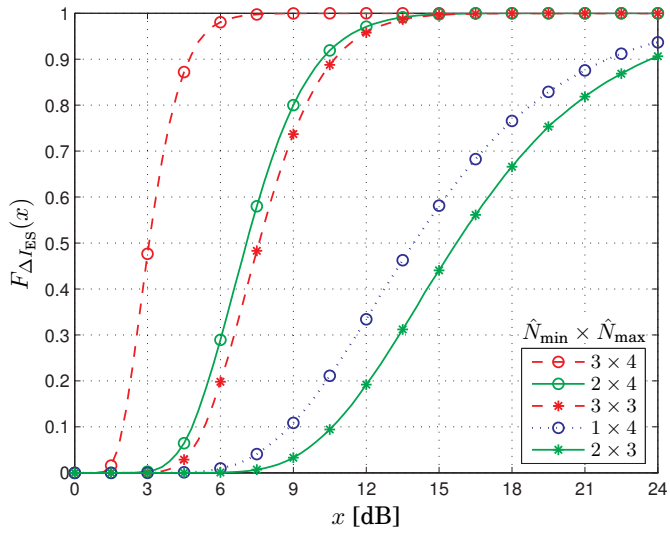

(b) separate array configuration

Figure 3.21. The variation of the additional isolation given by optimal eigenbeam selection with different number of input and output streams. Figure 3.6 shows reference results in the case of the simulated Rayleigh channel. See Table 3.2 for the corresponding average values of additional isolation.

Specific observations can be classified according to the total number of streams ($\hat{N}_{\min} + \hat{N}_{\max}$) supported in the relay as follows.

Null-space projection (NSP) takes place when the total number of supported streams is four or less ($\hat{N}_{\min} + \hat{N}_{\max} \leq 4$). Theoretically, the self-interference is suppressed completely and the measure of additional isolation tends to infinity. However, isolation is in practice limited also by imperfections in the side information needed for suppression as discussed in previous subsections and in **[215, 219]**.

Eigenbeam selection (ES) yields on average around 19–22 dB, 7–8 dB or 3–4 dB additional isolation, depending on the array configuration, when supporting in total five, six or seven input and output streams ($5 \leq \hat{N}_{\min} + \hat{N}_{\max} \leq 7$), respectively. In general, the separate array configuration benefits slightly more from eigenbeam selection than the compact array configuration. Unfortunately, the variation of additional isolation is also increased with its average, and the distributions have rather heavy tails with five streams. Furthermore, it can be noted that the stream combination $\hat{N}_{\min} \times \hat{N}_{\max}$ yields always more additional isolation than the stream combination $(\hat{N}_{\min} - 1) \times (\hat{N}_{\max} + 1)$, i.e., a symmetric setup is preferable.

The additional isolation is almost exactly the same with all orientations of the transmit antenna array as shown in Fig. 7(b) of **[208]**, and the difference of LOS and NLOS channels is even smaller than that of the orientations. This is in contrast with the physical isolation for which the orientations behave rather differently. Thus, initial array deployment, i.e., orientation and position, can be planned effectively based on the physical isolation only since one can expect that the statistics of additional isolation are not affected much.

Physical isolation is all that can be achieved when the total number of supported streams is set to its maximum, eight ($\hat{N}_{\min} = \hat{N}_{\max} = 4$). The additional isolation is even theoretically 0 dB which highlights the fact that at least one dimension needs to be reserved for spatial-domain suppression in order to reduce the self-interference at all. On the other hand, time-domain cancellation is still applicable in this case rendering additional isolation which depends mainly on the quality of side information.

The raw channel measurement data contain a few, but not too many, optimistic outliers for which the additional isolation is extremely high

(above 50 dB to be exact). Thus, in order to improve the reliability of the numerical results, the outliers are excluded from the data set when using (3.77). For consistency, the same clipping is introduced for the simulated Rayleigh channels which, in fact, allows to quantify the effect of the exclusion by comparing the values tabulated in the legend of Fig. 3.6(b) without clipping to those given in Table 3.2(c). In particular, by excluding all values that are above 50 dB, the average additional isolation is decreased by 1.7 dB when supporting in total five streams. With six or seven streams, clipping has no visible effect on the average value.

Although the exact performance achieved with simulated Rayleigh channels differs considerably from the case of measured channels, the general observations are coherent and the Rayleigh channel represents something that is in between the two array configurations of different type. Thus, the Rayleigh model can be reasonably used for generic theoretical studies if measurement data is not available or one wants to avoid constraining the analysis to a specific example setup.

Conclusions on Experimental Results

This section evaluated the performance of self-interference mitigation using, primarily, real-world channel measurement data and, secondarily, simulated reference channels. The results concern compact 4×4 prototype arrays designed for wideband outdoor-to-indoor relaying at 2.6 GHz center frequency. Their focus is on eigenbeam selection (ES) that is subject to residual self-interference even with perfect side information like antenna selection which can be omitted herein due to inferior performance. Thereby, the inherent joint properties of the prototype and propagation environment were analyzed separately from the effects of imperfect side information which are covered for their part in the previous sections.

Firstly, the analysis studied the practical physical isolation arising from the directivity and spatial separation of the prototype antenna arrays by evaluating its variation over different relay locations as well as array orientations and in terms of inter-array distance in line-of-sight and non-line-of-sight scenarios. Secondly, the evaluation of empirical condition number revealed that self-interference channels are typically of full rank and feature non-uniform scattering establishing foundations for spatial-domain suppression. Finally, and most saliently, the additional isolation given by the proposed ES scheme was characterized by evaluating its empirical statistics and demonstrating average levels of up to 20 dB.

3.6 Conclusions

This chapter studied the performance of MIMO relaying making innovative leap into advanced full-duplex operation in contrast to many studies which adopt the conventional half-duplex mode. In particular, the full-duplex mode has huge potential for significantly improving spectral efficiency by reusing a single band for simultaneous transmission to and from a relay. The related technical challenge, loopback self-interference in the relay, can be first eased by deploying spatially separated receive and transmit arrays, which provides passive isolation, after which active signal processing should improve isolation further. This represents another significant novel factor hereof since there is a large body of prior research literature on idealistic full-duplex relays without self-interference (or even a mention of it!). Thus, the study may serve as validation and a retroactive reference for this central, often implicit, baseline assumption which has not been recognized well and verified in detail before.

The first part of the chapter presented the whole variety of interference mitigation schemes ranging from physical isolation and subtractive cancellation to spatial-domain suppression. In the corresponding section, the former two were mainly surveyed for completeness, since their principles are straightforward from a signal processing perspective, while interference suppression by transmit and receive filtering formed the core of the novel contribution. In particular, spatial-domain suppression can be implemented in various ways for which optimization problems were specified and solved by proposing techniques for designing the spatial filtering matrices. It should be noted that the mitigation schemes can be used directly also in other types of MIMO full-duplex transceivers although only relaying is considered explicitly herein due to the scope of this thesis.

The second part of the chapter conducted a diverse performance evaluation of the mitigation schemes including extensive simulation results for their general comparison, analytical results for investigating the effect of imperfect side information, and experimental results based on measurement data. In general, mitigation was demonstrated to yield large additional isolation, level of which is essentially characterized by the quality of side information, the rank of the loopback channel as well as supported antenna and stream configurations. All discussions on specific observations and conclusions drawn from these subparts are presented in the ends of the corresponding subsections.

As an ultimate general conclusion for this chapter, the results indicated that, in practice, there will most likely be significant residual self-interference, even with smart design for passive isolation and advanced active mitigation schemes. Thereby, the following chapters develop techniques for tolerating such distortion and for successfully operating in its presence. Yet, one still needs to choose eventually whether the full-duplex mode would really be preferred after all whenever self-interference cannot be mitigated extremely well. Especially, when expecting different residual self-interference levels and fading channel states, one cannot choose the best mode during an early design stage before actual operation but this calls for opportunistic switching.

4. Transmit Power Control in Full-Duplex Relaying

The self-interference situation of full-duplex relays is extremely challenging. Since mitigation cannot be perfect in practice, the relays are likely subject to significant residual distortion, effect of which may be tolerable but should not be neglected. In particular, a relay's input channel may remain the bottleneck of the system which can still be compensated by decreasing transmit power at the cost of degrading the output channel.

This chapter develops transmit power control schemes for full-duplex relay links taking into account the effect of residual loopback interference that remains after imperfect mitigation. Throughout the analysis, the amplify-and-forward (AF) and decode-and-forward (DF) protocols are analyzed side-by-side in the same framework; the latter avoids an infinite feedback loop through the relay that is inherent for the former. With the proposed schemes, the end-to-end signal-to-interference and noise ratio (SINR) can be maximized while, at the same time, transmit power is decreased. Related target-SINR approach allows to relieve the need for the feedback of channel state information on the hop after the relay. In addition to SINR illustrations, the system performance is evaluated by deriving closed-form outage probability expressions for all the transmit power control schemes which covers both downlink and uplink relaying.

The remainder of this chapter[1] is organized as follows. First, Section 4.1 presents a brief introduction to the purpose of power control, conventional methods, and the contributions of this study. The considered system and signal models are specified in Section 4.2; they are adopted in the next chapter as well. Sections 4.3 and 4.4 feature the main results of this study, namely the design and analysis of transmit power control schemes for full-duplex relays, while associated numerical results explain their principles and performance. Finally, Section 4.5 summarizes the discussion.

[1]This chapter is partially based on the material presented in **[214,220,224,225]**.

4.1 Introduction

Presumably most full-duplex relays will need to tolerate residual self-interference adapting to its presence as best they can. To that end, inherent imbalance in full-duplex relay links offers an opportunity to minimize the effect of residual distortion. In particular, loopback interference distorts the channel before a relay, but not the one after it, and the trade-off between their qualities can be controlled with relay transmit power.

Assuming antenna partitioning which divides transmit and receive elements into separate arrays, three basic types of countermeasures against loopback interference are broadly classified in [89] as follows:

1) the features of propagation paths between the antennas;

2) the directivity characteristics of the antennas; and

3) signal processing techniques for interference mitigation.

The original list is rephrased above to clarify that these concepts are already dealt with in the previous chapter. Namely, Countermeasures 1) and 2) represent together *passive physical isolation* while original Countermeasure 3) is now extended to cover both *time-domain cancellation* and *spatial-domain suppression* since the scope of [89] is limited to basic repeaters without the capability of applying multiantenna techniques.

This chapter shows that the list can be complemented with another countermeasure working against residual distortion after the other three:

4) the optimization of relay gain.

The completed list of Countermeasures 1)–4) was first compiled in **[210]**. In particular, Countermeasure 4) is motivated by observing that useful signal power at a destination receiver is linearly proportional to relay gain while residual self-interference level at the relay itself may not be. Gain setting that is considerably below its maximum allowed value may thus render improved effective signal-to-interference and noise ratio (SINR) for the end-to-end link although, obviously, backing off too much will not come out well either. This poses a challenge to choose optimal relay gain, or equivalently transmit power, and maximize the end-to-end performance by balancing the wireless links before and after the relay.

Instead of end-to-end performance optimization, relay gain control is conventionally applied only to satisfy certain constraints pertaining to transceiver electronics and relay installation. In particular, variable gain

adaptation may be necessary for maintaining relay transmit power at a constant level below limitations set by regulations or the capability of high-power amplifiers. Likewise, the gain of the feedback loop sets a maximum level for the gain of an amplify-and-forward relay to guarantee that loopback echoes fade away in a reasonable time or, otherwise, the signal of interest will be distorted due to the oscillation or saturation of transceivers. A conventional approach may thus adopt constant amplification, but variable transmit power, by setting relay gain to leave a fixed safety margin w.r.t. an estimate of the maximum possible level.

The contributions of this chapter are summarized as follows.

- The gain control challenge is formalized as optimization problems to maximize the effective end-to-end SINRs. The system framework and analysis accommodate both common relaying protocols: amplify-and-forward (AF) as well as decode-and-forward (DF).

- As solutions to the optimization problems, explicit expressions are provided for the optimal relay amplification factors which can be translated to optimal transmit power levels. These are contrasted with conventional methods to prove that transmit power constraints are still satisfied and relay oscillation is avoided by design.

- The optimal solutions are modified to target-SINR approaches which reduces the need for channel state information (CSI) feedback at the cost of rendering suboptimal, but still improved, performance.

- Finally, the principles of gain control are illustrated with numerical SINR results, and unified outage probability analysis is conducted for the considered gain control schemes by deriving closed-form performance expressions in both downlink (DL) and uplink (UL) relaying.

This also lays foundations for the next chapter which compares half- and full-duplex relaying, with and without power control, in the same setup.

In an OFDM context, the study concerns a single-subcarrier relaying model with frequency-domain processing due to which loopback interference manifests itself as residual distortion after mitigation; the effect of inter-carrier interference (ICI) due to excessive multipath delay spread from full-duplex operation is analyzed in Chapter 6 in the case of an explicit wideband OFDM model. The results can be also interpreted to concern an end-to-end orthogonal spatial stream in a MIMO context, while an extension with power allocation between streams can be found in **[222]**.

4.2 System Model

This section specifies a signal model for a two-hop single-frequency OFDM link and derives expressions for the effective signal-to-interference and noise ratio (SINR) achieved by end-to-end transmission via a relay. Both amplify-and-forward (AF) and decode-and-forward (DF) protocols are considered like everywhere in this thesis but the scope of the current chapter is limited to the full-duplex (FD) mode. The half-duplex counterparts are added in by the next chapter which works on the same setup to analyze trade-offs between relaying modes with or without power control.

The overall system setup is illustrated in Fig. 4.1; it comprises four slowly time-varying multipath channels which model the source-to-relay (SR), loopback relay-to-relay (RR), relay-to-destination (RD) and source-to-destination (SD) links. The channels are assumed to remain approximately stationary during a relatively long observation period and their multipath delay spread is assumed to be shorter than the cyclic prefix of OFDM symbols. By assuming also decent frequency and time synchronization, all subcarriers become orthogonal and subject to flat fading although frequency selectivity still causes different channel coefficients for each subcarrier since wideband transmission is assumed implicitly. In summary, there is no significant inter-carrier interference at all and no other inter-symbol interference than that due to full-duplex operation.

4.2.1 Two-Hop Single-Subcarrier Transmission

Given the foregoing assumptions, the following signal models correspond to a single arbitrary OFDM subcarrier in frequency domain. Yet subcarrier indices are omitted and the system is studied at generic time instant i, i.e., when the ith OFDM symbol is being forwarded by the relay.

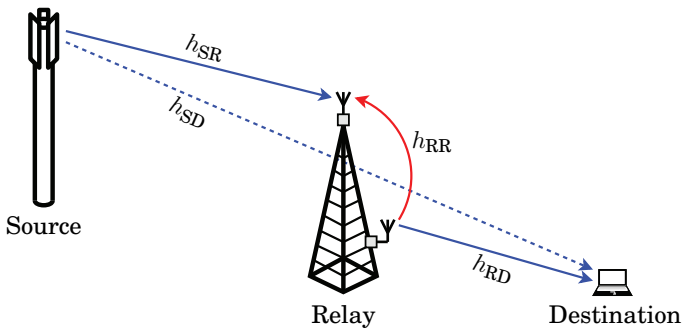

Figure 4.1. Full-duplex relay link in the presence of self-interference where narrowband wireless channels are denoted by h_{SR}, h_{SD}, h_{RR}, and h_{RD}.

The source (S) transmits signal $x_{\mathrm{S}}[i]$ to the relay (R) with constant normalized transmit power $p_{\mathrm{S}} \triangleq \mathcal{E}\{|x_{\mathrm{S}}[i]|^2\} = 1$ which is also overheard by the destination (D). The link operates in a single-frequency full-duplex mode, i.e., the relay concurrently receives signal $y_{\mathrm{R}}[i]$ and transmits signal $x_{\mathrm{R}}[i]$ for which $p_{\mathrm{R}} \triangleq \mathcal{E}\{|x_{\mathrm{R}}[i]|^2\} \leq 1$. Thus, the relay input signal is a combination of the desired source signal, self-interference and noise:

$$y_{\mathrm{R}}[i] = h_{\mathrm{SR}} x_{\mathrm{S}}[i] + h_{\mathrm{RR}} x_{\mathrm{R}}[i] + n_{\mathrm{R}}[i], \tag{4.1}$$

where h_{SR} is the flat-fading source-to-relay channel, h_{RR} is the loopback channel between the transmit antenna and the receive antenna of the relay, and the power of the thermal noise term is $\mathcal{E}\{|n_{\mathrm{R}}[i]|^2\} \triangleq \sigma_{\mathrm{R}}^2$.

The desired signal component in (4.1) is $h_{\mathrm{SR}} x_{\mathrm{S}}[i]$ and the relay may apply mitigation (cf. the previous chapter) to partly eliminate the adverse component $h_{\mathrm{RR}} x_{\mathrm{R}}[i]$. However, in practice, total interference elimination cannot be achieved due to non-ideal side information and signal processing, e.g., the dynamic range of the receiver front-end may be insufficient for both the useful and the interference signal causing quantization noise.

After mitigation, the residual self-interference distortion and noise can be denoted with an aggregate term $\hat{n}_{\mathrm{R}}[i]$ translating effectively (4.1) to

$$\hat{y}_{\mathrm{R}}[i] = h_{\mathrm{SR}} x_{\mathrm{S}}[i] + \hat{n}_{\mathrm{R}}[i], \tag{4.2}$$

where $\mathcal{E}\{|\hat{n}_{\mathrm{R}}[i]|^2\} \triangleq (p_{\mathrm{R}} \gamma_{\mathrm{RR}} + 1)\sigma_{\mathrm{R}}^2$ and γ_{RR} represents the normalized gain of residual interference due to imperfect mitigation. As each combination of mitigation schemes is characterized by different, implementation-specific residual self-interference level, parametrization by γ_{RR} makes the analysis more generic. In fact, the model covers also the extreme case where the relay uses a single antenna for both transmission and reception which yields a large value for γ_{RR}. Likewise, $\gamma_{\mathrm{RR}} \triangleq |h_{\mathrm{RR}}|^2/\sigma_{\mathrm{R}}^2$ when only passive physical antenna isolation is used without active mitigation.

As described shortly, $\hat{y}_{\mathrm{R}}[i]$ is translated to $x_{\mathrm{R}}[i]$ in an AF or DF manner:

$$x_{\mathrm{R}}[i] \triangleq \hat{f}(\hat{y}_{\mathrm{R}}[i - \tau_{\mathrm{R}}], \hat{y}_{\mathrm{R}}[i - (\tau_{\mathrm{R}} + 1)], \hat{y}_{\mathrm{R}}[i - (\tau_{\mathrm{R}} + 2)], \ldots), \tag{4.3}$$

in which delay $\tau_{\mathrm{R}} \geq 1$ is required to allow frequency-domain subcarrier-wise processing. Especially, each OFDM symbol must be received in its entirety before demodulation using the discrete Fourier transform.

Finally, the received signal in the destination is given by

$$y_{\mathrm{D}}[i] = h_{\mathrm{RD}} x_{\mathrm{R}}[i] + h_{\mathrm{SD}} x_{\mathrm{S}}[i] + n_{\mathrm{D}}[i], \tag{4.4}$$

where respective h_{RD} and h_{SD} denote flat-fading relay- and source-to-destination channels and $n_{\mathrm{D}}[i]$ is thermal noise with $\mathcal{E}\{|n_{\mathrm{D}}[i]|^2\} \triangleq \sigma_{\mathrm{D}}^2$.

Amplify-and-Forward Relaying

When adopting the linear amplify-and-forward (AF) protocol, the relay simply increases (by factor $\beta > 0$) the amplitude of the post-processing input signal obtained after self-interference mitigation. This aims at boosting the power of the desired signal sufficiently high to facilitate decoding in the destination even after the attenuation of the second-hop channel. Unfortunately, also the residual self-interference and noise components are amplified and forwarded to the destination at the same time.

The output signal of the AF relay can be expressed as

$$x_{\mathrm{R}}[i] = \beta\, \hat{y}_{\mathrm{R}}[i-\tau_{\mathrm{R}}] = \beta\, h_{\mathrm{SR}} x_{\mathrm{S}}[i-\tau_{\mathrm{R}}] + \beta\, \hat{n}_{\mathrm{R}}[i-\tau_{\mathrm{R}}], \tag{4.5}$$

where the last form is obtained by substituting (4.2). In particular, the amplification factor β (or equivalently the relay gain β^2) shall be the key parameter for all the concepts discussed in this chapter. In (4.5), the amplitude of the desired signal is linearly proportional to β while residual self-interference is not only amplified by β but also its input level, namely $p_{\mathrm{R}}(\beta)\, \gamma_{\mathrm{RR}}\, \sigma_{\mathrm{R}}^2$, already increases monotonically as a function of β.

The case of using only passive antenna isolation lends itself to illustrating the problem of signal circulation through the relay and the feedback loop. Then $\hat{n}_{\mathrm{R}}[i] = h_{\mathrm{RR}} x_{\mathrm{R}}[i] + n_{\mathrm{R}}[i]$ in (4.2) and recursive substitution with (4.5) reveals that the relay transmits an infinite sum of echoes:

$$x_{\mathrm{R}}[i] = \beta \sum_{j=1}^{\infty} (h_{\mathrm{RR}}\beta)^{j-1} \left(h_{\mathrm{SR}} x_{\mathrm{S}}[i-j\tau_{\mathrm{R}}] + n_{\mathrm{R}}[i-j\tau_{\mathrm{R}}]\right). \tag{4.6}$$

The expected value of $|x_{\mathrm{R}}[i]|^2$ may diverge, i.e., the system is unstable, unless $|h_{\mathrm{RR}}\beta| < 1$. With active mitigation, $\hat{n}_{\mathrm{R}}[i]$ is caused by $h_{\mathrm{RR}} x_{\mathrm{R}}[i]$ through a complex, possibly unknown nonlinear process but, in principle, residual self-interference power is subject to an analogous feedback loop.

As an alternative for parametrization with the amplification factor β, one may normalize protocols to guarantee constant transmit power p_{R} for the relay. Firstly, the relay input power can be calculated from (4.2) as

$$\mathcal{E}\{|\hat{y}_{\mathrm{R}}[i]|^2\} = |h_{\mathrm{SR}}|^2 + (p_{\mathrm{R}}\gamma_{\mathrm{RR}} + 1)\sigma_{\mathrm{R}}^2 \tag{4.7}$$

assuming that $x_{\mathrm{S}}[i]$ and $\hat{n}_{\mathrm{R}}[i]$ (or equivalently $x_{\mathrm{S}}[i-\tau_{\mathrm{R}}]$) are uncorrelated. With any given value of p_{R}, (4.5) and the definition of p_{R} then imply $\mathcal{E}\{|x_{\mathrm{R}}[i]|^2\} = \beta^2 \mathcal{E}\{|\hat{y}_{\mathrm{R}}[i-\tau_{\mathrm{R}}]|^2\} = p_{\mathrm{R}}$ and the amplification factor becomes

$$\beta(p_{\mathrm{R}}) = \sqrt{\frac{p_{\mathrm{R}}}{|h_{\mathrm{SR}}|^2 + (p_{\mathrm{R}}\gamma_{\mathrm{RR}} + 1)\sigma_{\mathrm{R}}^2}}. \tag{4.8}$$

The resulting gain level is always bounded, e.g., $\beta^2 < 1/(\gamma_{\mathrm{RR}}\sigma_{\mathrm{R}}^2)$, which guarantees the stability of the relay and prevents oscillation.

Decode-and-Forward Relaying

When adopting the nonlinear decode-and-forward (DF) protocol, the relay regenerates the original signal transmitted by the source. Assuming proper rate adaptation, modulation and coding schemes are selected for the end-to-end link according to the weakest hop to guarantee reliable decoding and re-encoding process $\hat{f}(\cdot)$ from $\hat{y}_{\mathrm{R}}[i]$ to $x_{\mathrm{R}}[i]$. Thus, the destination receives a *clean* amplified signal from the relay unlike with AF relaying. However, residual interference lowers the achievable transmission rate in the first hop which indirectly affects the second hop as well.

Throughout the chapter, transmit power control is formulated in terms of the amplification factor β which is inherent in the context of the AF protocol. The same framework can be utilized also with the DF protocol by recognizing that $h_{\mathrm{SR}}x_{\mathrm{S}}[i]$ in (4.2) represents the clean signal before amplification in the relay. Incorporating the processing delay $\tau_{\mathrm{R}} > 0$, the effective output signal of the DF relay can be thus expressed as

$$x_{\mathrm{R}}[i] = \beta\, h_{\mathrm{SR}}x_{\mathrm{S}}[i-\tau_{\mathrm{R}}]. \tag{4.9}$$

The amplification factor can be determined by setting relay transmit power to p_{R} since (4.9) yields $\mathcal{E}\{|x_{\mathrm{R}}[i]|^2\} = \beta^2|h_{\mathrm{SR}}|^2 = p_{\mathrm{R}}$ and, consequently,

$$\beta(p_{\mathrm{R}}) = \sqrt{\frac{p_{\mathrm{R}}}{|h_{\mathrm{SR}}|^2}}. \tag{4.10}$$

This can be contrasted with (4.8) which is lower due to noise amplification.

4.2.2 Signal-to-Interference and Noise Ratios

The end-to-end signal-to-interference and noise ratios (SINRs) are used for measuring and optimizing the performance observed by the destination. At time instant i, the receiver aims at decoding $y_{\mathrm{D}}[i]$ given in (4.4); with both protocols, the desired signal is $x_{\mathrm{S}}[i-\tau_{\mathrm{R}}]$ included within $x_{\mathrm{R}}[i]$ and the other components act as interference and noise. Useful auxiliary variables to be kept in mind are the channel signal-to-noise ratios (SNRs) which are given by $\gamma_{\mathrm{SR}} \triangleq |h_{\mathrm{SR}}|^2/\sigma_{\mathrm{R}}^2$, $\gamma_{\mathrm{RD}} \triangleq |h_{\mathrm{RD}}|^2/\sigma_{\mathrm{D}}^2$, and $\gamma_{\mathrm{SD}} \triangleq |h_{\mathrm{SD}}|^2/\sigma_{\mathrm{D}}^2$.

The weak direct-link signal $h_{\mathrm{SD}}x_{\mathrm{S}}[i]$ in (4.4) is treated as co-channel interference embedded in the destination receiver noise which is justified when the relay is employed for coverage extension. In hotspot scenarios, where the direct and relayed transmissions are both strong, equalization or multiantenna techniques could facilitate signal separation and two-branch diversity combining although the next chapter shows that simple switching between direct transmission and relaying is already sufficient.

Amplify-and-Forward Relaying

The end-to-end SINR of the AF protocol is derived below with two intermediate steps expressing relay output power and destination input power.

By assuming that all successive signal and noise samples are mutually independent and that the channels vary slowly, the transmit power of the AF relay can be calculated from (4.5)–(4.7) as

$$\mathcal{E}\{|x_{\mathrm{R}}[i]|^2\} = \beta^2 \sum_{j=1}^{\infty} \left(|h_{\mathrm{RR}}|^2\beta^2\right)^{j-1} \left(|h_{\mathrm{SR}}|^2 + \sigma_{\mathrm{R}}^2\right) = \frac{\beta^2(|h_{\mathrm{SR}}|^2 + \sigma_{\mathrm{R}}^2)}{1 - \sigma_{\mathrm{R}}^2\beta^2\,\gamma_{\mathrm{RR}}} \quad (4.11)$$

for the respective cases of passive physical isolation and active mitigation. Especially, this shows that the relay gain must be limited according to

$$|h_{\mathrm{RR}}|^2\beta^2 < 1 \quad \text{or, with active mitigation,} \quad \sigma_{\mathrm{R}}^2\beta^2 < \frac{1}{\gamma_{\mathrm{RR}}} \quad (4.12)$$

to prevent oscillation and guarantee finite relay transmit power. All the gain control methods considered herein ensure this condition by design.

Again by requiring signal and noise independence, the received signal power in the destination is calculated from (4.4) as

$$\mathcal{E}\{|y_{\mathrm{D}}[i]|^2\} = |h_{\mathrm{RD}}|^2\mathcal{E}\{|x_{\mathrm{R}}[i]|^2\} + |h_{\mathrm{SD}}|^2 + \sigma_{\mathrm{D}}^2. \quad (4.13)$$

This expression with the substitution of (4.11) can be further reorganized as a sum of desired signal power, residual loopback interference power, source-to-destination interference power, and noise power, respectively:

$$\begin{aligned}\mathcal{E}\{|y_{\mathrm{D}}[i]|^2\} = {} & |h_{\mathrm{SR}}|^2\beta^2|h_{\mathrm{RD}}|^2 \\ & + \left(|h_{\mathrm{SR}}|^2 + \sigma_{\mathrm{R}}^2\right)\beta^2|h_{\mathrm{RD}}|^2\frac{\sigma_{\mathrm{R}}^2\beta^2\,\gamma_{\mathrm{RR}}}{1 - \sigma_{\mathrm{R}}^2\beta^2\,\gamma_{\mathrm{RR}}} \\ & + |h_{\mathrm{SD}}|^2 + \beta^2|h_{\mathrm{RD}}|^2\sigma_{\mathrm{R}}^2 + \sigma_{\mathrm{D}}^2.\end{aligned} \quad (4.14)$$

Finally, the SINR of AF relaying can be stated based on (4.14) as

$$\gamma = \frac{\sigma_{\mathrm{R}}^2\beta^2\,\gamma_{\mathrm{SR}}\gamma_{\mathrm{RD}}}{\left(\gamma_{\mathrm{SR}} + 1\right)\sigma_{\mathrm{R}}^2\beta^2\,\gamma_{\mathrm{RD}}\frac{\sigma_{\mathrm{R}}^2\beta^2\,\gamma_{\mathrm{RR}}}{1-\sigma_{\mathrm{R}}^2\beta^2\,\gamma_{\mathrm{RR}}} + \sigma_{\mathrm{R}}^2\beta^2\,\gamma_{\mathrm{RD}} + \gamma_{\mathrm{SD}} + 1}. \quad (4.15)$$

Decode-and-Forward Relaying

The end-to-end SINR of the DF protocol is an "equivalent" variable which corresponds to the SINR of the AF protocol resulting in the same transmission rate, i.e., $\log_2(1+\gamma) \triangleq \min\{\log_2(1+\gamma_{\mathrm{R}}), \log_2(1+\gamma_{\mathrm{D}})\}$ for which

$$\gamma_{\mathrm{R}} \triangleq \frac{\gamma_{\mathrm{SR}}}{\sigma_{\mathrm{R}}^2\beta^2\,\gamma_{\mathrm{SR}}\gamma_{\mathrm{RR}} + 1} \quad \text{and} \quad \gamma_{\mathrm{D}} \triangleq \frac{\sigma_{\mathrm{R}}^2\beta^2\,\gamma_{\mathrm{SR}}\gamma_{\mathrm{RD}}}{\gamma_{\mathrm{SD}} + 1} \quad (4.16)$$

are given by (4.7) and (4.13). Especially, it is not a measurable quantity but adopted for handling both protocols in the same framework. Finally,

$$\gamma = \min\{\gamma_{\mathrm{R}}, \gamma_{\mathrm{D}}\} = \min\left\{\frac{\gamma_{\mathrm{SR}}}{\sigma_{\mathrm{R}}^2\beta^2\,\gamma_{\mathrm{SR}}\gamma_{\mathrm{RR}} + 1}, \frac{\sigma_{\mathrm{R}}^2\beta^2\,\gamma_{\mathrm{SR}}\gamma_{\mathrm{RD}}}{\gamma_{\mathrm{SD}} + 1}\right\}. \quad (4.17)$$

4.3 Transmit Power Optimization

This section develops new methods for choosing the amplification factor β. To that end, SINR maximization is formalized as an optimization task:

$$\beta^* = \arg\max_{\beta} \gamma, \tag{4.18}$$

for which γ is given by (4.15) and (4.17) with AF and DF relaying, respectively. Ideal channel state information (CSI) is required for this purpose but the assumption can be relaxed with suboptimal target-SINR schemes.

The analysis is formulated in terms of β which can be translated to

$$p_{\mathrm{R}}(\beta^2) = \begin{cases} \frac{\sigma_{\mathrm{R}}^2 \beta^2 (\gamma_{\mathrm{SR}}+1)}{1-\sigma_{\mathrm{R}}^2 \beta^2 \gamma_{\mathrm{RR}}}, & \text{with AF,} \\ \sigma_{\mathrm{R}}^2 \beta^2 \gamma_{\mathrm{SR}}, & \text{with DF.} \end{cases} \tag{4.19}$$

Especially, the values of β^* solved shortly yield (5.11) in the next chapter.

4.3.1 Amplify-and-Forward Relaying

As summarized to begin with, conventional methods render suboptimal SINR and transmit power limits may be exceeded due to fading channels.

The gain of AF repeaters is often set, after measuring the loopback gain $|h_{\mathrm{RR}}|^2$, by choosing constant amplification which satisfies the stability condition (4.12) with a *fixed* gain margin $\Delta_{\mathrm{GM}} > 1$. This yields

$$\beta = \frac{1}{\sqrt{\Delta_{\mathrm{GM}}}|h_{\mathrm{RR}}|} \quad \text{or, with active mitigation,} \quad \beta = \frac{1}{\sigma_{\mathrm{R}}} \cdot \frac{1}{\sqrt{\Delta_{\mathrm{GM}}\gamma_{\mathrm{RR}}}}. \tag{4.20}$$

However, condition $p_{\mathrm{R}} \leq 1$ for (4.19) may be violated, e.g., if γ_{SR} fluctuates.

Another typical method lets the relay gain vary in such a way that maximum transmit power is used constantly. In particular, the substitution of $p_{\mathrm{R}} \triangleq \mathcal{E}\{|x_{\mathrm{R}}[i]|^2\} = 1$ in (4.8) yields the maximum amplification factor as

$$\beta = \frac{1}{\sigma_{\mathrm{R}}} \cdot \frac{1}{\sqrt{\gamma_{\mathrm{SR}} + \gamma_{\mathrm{RR}} + 1}}, \tag{4.21}$$

which also guarantees that (4.12) holds. Thus, this method can be considered to exploit the other conventional method with an *adaptive* gain margin $\Delta_{\mathrm{GM}} = 1 + (\gamma_{\mathrm{SR}} + 1)/\gamma_{\mathrm{RR}}$. By substituting (4.21) into (4.15), the end-to-end SINR with maximum transmit power usage becomes

$$\gamma = \frac{\gamma_{\mathrm{SR}}\gamma_{\mathrm{RD}}}{\gamma_{\mathrm{SR}}(\gamma_{\mathrm{SD}}+1) + \gamma_{\mathrm{RD}}(\gamma_{\mathrm{RR}}+1) + (\gamma_{\mathrm{SD}}+1)(\gamma_{\mathrm{RR}}+1)}. \tag{4.22}$$

It should be noted that implementation is actually simpler than it looks, since the relay can just adaptively drive its transmit power to a constant level without using explicit CSI, and this method also maximizes the end-to-end SINR if there is zero or only negligible residual self-interference.

Neither simple gain control method offers optimal end-to-end performance in the presence of significant residual self-interference though. In particular, (4.14) shows that the desired signal power is linear as a function of the relay gain β^2 but the interference power is highly nonlinear. Increasing gain can thus raise the self-interference level faster than the desired signal level leading eventually to reduced effective SINR.

It turns out that (4.15) has a single maximum point at $0 \leq \beta^2 < \frac{1}{\sigma_{\mathrm{R}}^2 \gamma_{\mathrm{RR}}}$. By finding the correct root of the derivative of γ in terms of β^2, the optimal amplification factor can be consequently solved for (4.18) as

$$\beta^* = \frac{1}{\sigma_{\mathrm{R}}} \cdot \sqrt{\frac{\gamma_{\mathrm{SD}} + 1}{\gamma_{\mathrm{RR}}(\gamma_{\mathrm{SD}} + 1) + \sqrt{(\gamma_{\mathrm{SR}} + 1)\,\gamma_{\mathrm{RD}}\gamma_{\mathrm{RR}}(\gamma_{\mathrm{SD}} + 1)}}}, \tag{4.23}$$

which obviously satisfies (4.12). Actually, this represents an enhanced version of the conventional method with an *optimal adaptive* gain margin

$$\Delta_{\mathrm{GM}}^* = 1 + \sqrt{\frac{(\gamma_{\mathrm{SR}} + 1)\gamma_{\mathrm{RD}}}{\gamma_{\mathrm{RR}}(\gamma_{\mathrm{SD}} + 1)}}. \tag{4.24}$$

By substituting (4.23) into (4.15), the maximum end-to-end SINR becomes

$$\gamma^* = \frac{\gamma_{\mathrm{SR}}\gamma_{\mathrm{RD}}}{\gamma_{\mathrm{RD}} + \gamma_{\mathrm{RR}}(\gamma_{\mathrm{SD}} + 1) + 2\sqrt{(\gamma_{\mathrm{SR}} + 1)\,\gamma_{\mathrm{RD}}\gamma_{\mathrm{RR}}(\gamma_{\mathrm{SD}} + 1)}}. \tag{4.25}$$

In practice, $\beta = \min\{\beta^*, \frac{1}{\sigma_{\mathrm{R}}} \cdot \frac{1}{\sqrt{\gamma_{\mathrm{SR}} + \gamma_{\mathrm{RR}} + 1}}\}$ is employed to satisfy also a transmit power constraint $p_{\mathrm{R}} \leq 1$. By solving $(\sigma_{\mathrm{R}}\beta^*)^2 \geq (\gamma_{\mathrm{SR}} + \gamma_{\mathrm{RR}} + 1)^{-1}$, the essential condition for residual loopback interference is shown to be

$$\gamma_{\mathrm{RR}} \leq \frac{(\gamma_{\mathrm{SR}} + 1)(\gamma_{\mathrm{SD}} + 1)}{\gamma_{\mathrm{RD}}} \tag{4.26}$$

for determining whether the transmit power limitation restricts the relay to use maximum gain instead of the optimal amplification factor.

An inevitable drawback of the above method is that it exploits the knowledge of γ_{RD} and γ_{SD} which can be estimated only at the destination; a feedback channel is thus required for conveying CSI to the relay. Instead, one may consider restricted gain control that results in consuming a constant fraction ($p_{\mathrm{R}} \leq 1$) of the maximum allowed power although, e.g., γ_{RD} varies in downlink relaying. Expressions for β and the end-to-end SINR γ are given by (4.8) and (4.15) with (4.8), respectively. To avoid using CSI from the destination, target end-to-end SINR $\hat{\gamma} < \gamma_{\mathrm{SR}}$ can then be chosen aiming at designing β to result in optimal performance only when $\gamma \approx \hat{\gamma}$.

With the target-SINR scheme, p_{R} is selected in such a way that the end-to-end SINR is maximized whenever it coincides with $\hat{\gamma}$ because γ_{RD} and γ_{SD} meet their respective target values. Thus, by eliminating $\frac{\gamma_{\mathrm{RD}}}{\gamma_{\mathrm{SD}}+1}$ from

the equation pair $\{\hat{\gamma} = \gamma,\ \hat{\gamma} = \gamma^*\}$, the desired normalized transmit power can be shown to admit the form

$$p_{\mathrm{R}} = \frac{\sqrt{\gamma_{\mathrm{SR}}(\gamma_{\mathrm{SR}}+1)\hat{\gamma}(\hat{\gamma}+1)}}{\hat{\gamma}\,\gamma_{\mathrm{RR}}} - \frac{\gamma_{\mathrm{SR}}+1}{\gamma_{\mathrm{RR}}} \tag{4.27}$$

when the target SINR satisfies

$$\hat{\gamma} > \frac{\gamma_{\mathrm{SR}}(\gamma_{\mathrm{SR}}+1)}{\gamma_{\mathrm{SR}} + 2\gamma_{\mathrm{SR}}\gamma_{\mathrm{RR}} + (\gamma_{\mathrm{RR}}+1)^2} \tag{4.28}$$

and otherwise $p_{\mathrm{R}} = 1$ due to the transmit power constraint.

4.3.2 Decode-and-Forward Relaying

With the DF protocol, the nonlinear de/encoding process effectively cuts the feedback loop through the relay. Thus, self-interference echoes do not remain circulating endlessly as with AF relaying, and the gain-margin method is irrelevant because relay stability is guaranteed by default.

The gain of DF relays is conventionally set to yield maximum transmit power usage constantly. In such cases, the substitution of $p_{\mathrm{R}} = 1$ in (4.10) yields the maximum amplification factor and the corresponding SINR as

$$\beta = \frac{1}{\sigma_{\mathrm{R}}} \cdot \frac{1}{\sqrt{\gamma_{\mathrm{SR}}}} \quad \text{and} \quad \gamma = \min\left\{\frac{\gamma_{\mathrm{SR}}}{\gamma_{\mathrm{RR}}+1}, \frac{\gamma_{\mathrm{RD}}}{\gamma_{\mathrm{SD}}+1}\right\}, \tag{4.29}$$

respectively, which is actually equivalent to using (4.20) with $\Delta_{\mathrm{GM}} = 1$.

Transmit power optimization is now motivated by the fact that, in (4.17), γ_{R} decreases and γ_{D} increases in terms of β^2. Thus, their minimum is maximized when $\gamma_{\mathrm{R}} = \gamma_{\mathrm{D}}$ which renders the solution for (4.18) as

$$\beta^* = \frac{1}{\sigma_{\mathrm{R}}} \cdot \sqrt{\frac{\sqrt{\gamma_{\mathrm{RD}}^2 + 4\gamma_{\mathrm{SR}}\gamma_{\mathrm{RD}}\gamma_{\mathrm{RR}}(\gamma_{\mathrm{SD}}+1)} - \gamma_{\mathrm{RD}}}{2\gamma_{\mathrm{SR}}\gamma_{\mathrm{RD}}\gamma_{\mathrm{RR}}}}, \tag{4.30}$$

and substitution in (4.17) yields the maximum end-to-end SINR as

$$\gamma^* = \frac{\gamma_{\mathrm{RD}}}{\gamma_{\mathrm{RR}}(\gamma_{\mathrm{SD}}+1)}\left(\sqrt{\frac{\gamma_{\mathrm{SR}}\gamma_{\mathrm{RR}}(\gamma_{\mathrm{SD}}+1)}{\gamma_{\mathrm{RD}}} + \frac{1}{4}} - \frac{1}{2}\right). \tag{4.31}$$

However, the transmit power constraint $p_{\mathrm{R}} \leq 1$ clips them at (4.29) if

$$\gamma_{\mathrm{RR}} \leq \frac{\gamma_{\mathrm{SR}}(\gamma_{\mathrm{SD}}+1)}{\gamma_{\mathrm{RD}}} - 1, \tag{4.32}$$

which is solved from $(\sigma_{\mathrm{R}}\beta^*)^2 \geq \gamma_{\mathrm{SR}}^{-1}$ (cf. $\beta = \min\{\beta^*, \frac{1}{\sigma_{\mathrm{R}}} \cdot \frac{1}{\sqrt{\gamma_{\mathrm{SR}}}}\}$ in practice).

Expressions for β and γ are given by (4.10) and (4.17) with (4.10), respectively, when a constant fraction ($p_{\mathrm{R}} \leq 1$) of the maximum allowed power is used. Especially, optimal SINR can be approached without using CSI from the destination in the vicinity of a target value $\hat{\gamma}$ by choosing

$$p_{\mathrm{R}} = \frac{\gamma_{\mathrm{SR}} - \hat{\gamma}}{\hat{\gamma}\,\gamma_{\mathrm{RR}}} \quad \text{when} \quad \hat{\gamma} > \frac{\gamma_{\mathrm{SR}}}{\gamma_{\mathrm{RR}}+1} \tag{4.33}$$

and otherwise $p_{\mathrm{R}} = 1$ due to the transmit power constraint; this result is solved from the equation pair $\{\hat{\gamma} = \gamma,\ \hat{\gamma} = \gamma^*\}$ as with AF relaying.

4.4 Performance Analysis

The performance of full-duplex relaying and the transmit power control schemes is analyzed next with both short-term and long-term perspective. Firstly, instantaneous end-to-end SINR lends itself to illustrating the principles of transmit power control. Secondly, outage probability statistics characterize relaying over fading channels. While the short-term analysis is not specific to any system scenario, the long-term analysis concentrates on cellular relaying where downlink (DL) and uplink (UL) directions turn out to be rather different in nature. Further outage analysis and more numerical results can be found in **[214]** and **[224]**.

Signal-to-Interference and Noise Ratio

The analytical SINR expressions are illustrated in Fig. 4.2 for a fixed example scenario where $\gamma_{\mathrm{SR}} = 15$ dB and $\frac{\gamma_{\mathrm{RD}}}{\gamma_{\mathrm{SD}}+1} = 20$ dB. Only the achievable SINR area bounded by the cases of no/low residual self-interference and maximum power usage is shown. In particular, the figures display the performance of the different gain control methods in terms of both the residual self-interference level γ_{RR} and the relay gain β^2. The DF protocol reflects similar general behavior as the AF protocol but there is much sharper transition from the second hop being the bottleneck (low β^2) to the case where self-interference limits the overall performance (high β^2).

For each fixed value of γ_{RR}, the end-to-end SINR has a distinct global maximum (in terms of the relay gain β^2) which is reached with optimal gain control. For reasonably large γ_{RR}, the optimal β^* provides both significant SINR improvement and transmit power reduction compared to maximum power usage with $p_{\mathrm{R}} = 1$ in β. Inequalities (4.26) and (4.32) show that maximum transmit power is optimal due to the transmit power constraint when $\gamma_{\mathrm{RR}} < -4.9$ dB with the AF protocol while the DF protocol benefits from transmit power reduction with any γ_{RR} since $\gamma_{\mathrm{SR}} < \frac{\gamma_{\mathrm{RD}}}{\gamma_{\mathrm{SD}}+1}$.

The SINR loss of using the target-SINR approach instead of the optimal gain can be also inferred from Fig. 4.2. The free design parameter $\hat{\gamma}$ defines the SINR operation area, where the performance of the target-SINR approach is nearly optimal, and the loss is rather small in a large gain range around it, but the DF protocol is more sensitive. In particular, the target-SINR approach with $\hat{\gamma} = 12$ is optimal only when $\gamma_{\mathrm{RR}} \approx 3.0$ dB (resp. $\gamma_{\mathrm{RR}} \approx 11.3$ dB), but performance is always improved over setting $p_{\mathrm{R}} = 1$ in β except when $\gamma_{\mathrm{RR}} \leq 0.9$ dB (resp. $\gamma_{\mathrm{RR}} \leq 2.1$ dB) with the AF (resp. DF) protocol and the transmit power constraints become activated.

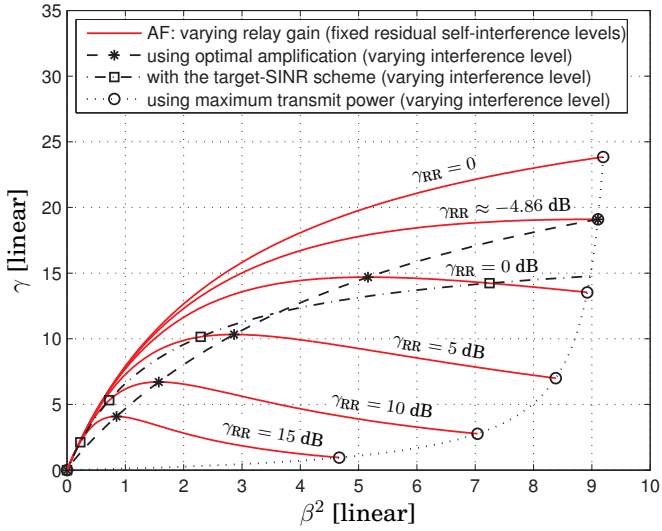

(a) amplify-and-forward (AF) relaying

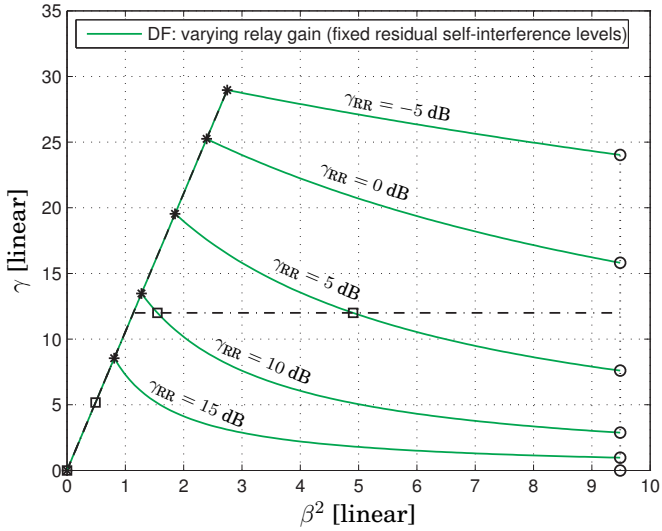

(b) decode-and-forward (DF) relaying

Figure 4.2. Effective end-to-end SINR with the different transmit power control methods when channel SNRs are given by $\gamma_{SR} = 15$ dB, $\gamma_{RD} = 23$ dB, and $\gamma_{SD} = 0$ dB. The target SINR is set at $\hat{\gamma} = 12$, and an unimportant constant value, i.e., $\sigma_R^2 = \frac{1}{300}$ to be specific, is chosen for the thermal noise level in order to scale the relay gain level within the single-digit range for illustration purposes.

Outage Probability

The following analysis concentrates on the long-term performance of a cellular relay node (RN) deployed for extending base station (BS) coverage area; this is especially reflected in the choice of fading distributions for the wireless channels. In particular, the performance of the different gain control schemes is evaluated in terms of outage probability $\mathcal{P}_{\text{out}}(\gamma_{\text{th}})$ which is directly given by the cumulative distribution function (CDF) of SINR:

$$\mathcal{P}_{\text{out}}(\gamma_{\text{th}}) \triangleq F_{\gamma}(\gamma_{\text{th}}) \triangleq \text{Prob}(\gamma < \gamma_{\text{th}}). \tag{4.34}$$

In other words, the analysis quantifies the probability, $\text{Prob}(\cdot)$, that the end-to-end SINR falls below a target threshold γ_{th} due to fading and self-interference. Since this characterizes any arbitrary subcarrier, joint performance over the whole OFDM bandwidth is also explained implicitly.

The RN is likely a fixed transceiver, like the BS of the cellular system, in order to facilitate full-duplex operation. Thus, it is reasonable to assume that the backhaul (BS–RN or RN–BS) channel is static, which is the closest approximation for Rice-fading with a strong line-of-sight (LOS) component that could be expected in practice. The destination is assumed to be a mobile user equipment (UE) without LOS to the RN. Thus, the service (RN–UE or UE–RN) channel admits Rayleigh-fading statistics; when denoting the average service-link SNRs by $\bar{\gamma}_{\text{RD}} \triangleq \mathcal{E}\{\gamma_{\text{RD}}\}$ and $\bar{\gamma}_{\text{SR}} \triangleq \mathcal{E}\{\gamma_{\text{SR}}\}$, the respective downlink and uplink CDFs are given by

$$F_{\gamma_{\text{RD}}}(x) = 1 - \exp\left(-\frac{x}{\bar{\gamma}_{\text{RD}}}\right) \quad \text{and} \quad F_{\gamma_{\text{SR}}}(x) = 1 - \exp\left(-\frac{x}{\bar{\gamma}_{\text{SR}}}\right) \tag{4.35}$$

for $x > 0$. Finally, focus on coverage extension implies $\gamma_{\text{SD}} \ll 0$ dB and $\sigma_{\text{D}}^2 \approx (\gamma_{\text{SD}} + 1)\sigma_{\text{D}}^2$. However, the case of a strong direct link can be still approximately covered by setting $\gamma_{\text{SD}} = 0$ and replacing γ_{RD} with $\frac{\gamma_{\text{RD}}}{\mathcal{E}\{\gamma_{\text{SD}}\}+1}$ while **[224]** provides exact complementary analysis where γ_{SD} is fading.

With each power control scheme, the end-to-end SINR is a specific function of the fading channel's SNR, i.e., $\gamma = \gamma_{\text{DL}}(\gamma_{\text{RD}})$ or $\gamma = \gamma_{\text{UL}}(\gamma_{\text{SR}})$, as shown in the previous sections. After determining the respective inverse functions, namely $\gamma_{\text{RD}} = \gamma_{\text{DL}}^{-1}(\gamma)$ and $\gamma_{\text{SR}} = \gamma_{\text{UL}}^{-1}(\gamma)$, for $0 \leq \gamma < \gamma_{\max}$, the result outage probabilities are given by the transform of random variables:

$$\mathcal{P}_{\text{out}}^{\text{DL}}(\gamma_{\text{th}}) = F_{\gamma_{\text{RD}}}\left(\gamma_{\text{DL}}^{-1}(\gamma_{\text{th}})\right) = 1 - \exp\left(-\frac{\gamma_{\text{DL}}^{-1}(\gamma_{\text{th}})}{\bar{\gamma}_{\text{RD}}}\right), \tag{4.36a}$$

$$\mathcal{P}_{\text{out}}^{\text{UL}}(\gamma_{\text{th}}) = F_{\gamma_{\text{SR}}}\left(\gamma_{\text{UL}}^{-1}(\gamma_{\text{th}})\right) = 1 - \exp\left(-\frac{\gamma_{\text{UL}}^{-1}(\gamma_{\text{th}})}{\bar{\gamma}_{\text{SR}}}\right) \tag{4.36b}$$

for $\gamma_{\text{th}} < \gamma_{\max}$ and $\mathcal{P}_{\text{out}}(\gamma_{\text{th}}) = 1$ otherwise. Here the boundary value $\gamma_{\max}$ denotes the SINR limit that is approached when $\gamma_{\text{RD}} \to \infty$ or $\gamma_{\text{SR}} \to \infty$.

The inverse functions are obtained for the different transmit power control methods and system variations (DL vs. UL and AF vs. DF) as follows.

In downlink AF relaying, the inverse of (4.15) including (4.8) becomes

$$\gamma_{\mathrm{DL}}^{-1}(x) = \frac{\gamma_{\mathrm{SR}} + p_{\mathrm{R}}\gamma_{\mathrm{RR}} + 1}{\gamma_{\mathrm{SR}} - (p_{\mathrm{R}}\gamma_{\mathrm{RR}} + 1)x} \cdot \frac{x}{p_{\mathrm{R}}} \tag{4.37a}$$

with $\gamma_{\max} = \gamma_{\mathrm{SR}}/(p_{\mathrm{R}}\gamma_{\mathrm{RR}} + 1)$ while the inverse of (4.25) is given by

$$\gamma_{\mathrm{DL}}^{-1}(x) = \frac{\left(\sqrt{(\gamma_{\mathrm{SR}} + 1)\gamma_{\mathrm{RR}}}\, x + \sqrt{\gamma_{\mathrm{SR}}\gamma_{\mathrm{RR}} x(x+1)}\right)^2}{(\gamma_{\mathrm{SR}} - x)^2} \tag{4.37b}$$

with $\gamma_{\max} = \gamma_{\mathrm{SR}}$.

In downlink DF relaying, the inverse of (4.17) including (4.10) becomes

$$\gamma_{\mathrm{DL}}^{-1}(x) = \frac{x}{p_{\mathrm{R}}} \tag{4.38a}$$

with $\gamma_{\max} = \gamma_{\mathrm{SR}}/(p_{\mathrm{R}}\gamma_{\mathrm{RR}} + 1)$ while the inverse of (4.31) is given by

$$\gamma_{\mathrm{DL}}^{-1}(x) = \frac{\gamma_{\mathrm{RR}}\, x^2}{\gamma_{\mathrm{SR}} - x} \tag{4.38b}$$

with $\gamma_{\max} = \gamma_{\mathrm{SR}}$.

In uplink AF relaying, the inverse of (4.15) including (4.8) becomes

$$\gamma_{\mathrm{UL}}^{-1}(x) = \frac{p_{\mathrm{R}}\gamma_{\mathrm{RD}} + 1}{p_{\mathrm{R}}\gamma_{\mathrm{RD}} - x} \cdot (p_{\mathrm{R}}\gamma_{\mathrm{RR}} + 1)x \tag{4.39a}$$

with $\gamma_{\max} = p_{\mathrm{R}}\gamma_{\mathrm{RD}}$ while the inverse of (4.25) is given by

$$\gamma_{\mathrm{UL}}^{-1}(x) = \frac{\left(\sqrt{\gamma_{\mathrm{RR}}}\, x + \sqrt{(\gamma_{\mathrm{RD}} + \gamma_{\mathrm{RR}} x)(x+1)}\right)^2}{\gamma_{\mathrm{RD}}} - 1 \tag{4.39b}$$

with $\gamma_{\max} \to \infty$.

In uplink DF relaying, the inverse of (4.17) including (4.10) becomes

$$\gamma_{\mathrm{UL}}^{-1}(x) = (p_{\mathrm{R}}\gamma_{\mathrm{RR}} + 1)x \tag{4.40a}$$

with $\gamma_{\max} = p_{\mathrm{R}}\gamma_{\mathrm{RD}}$ while the inverse of (4.31) is given by

$$\gamma_{\mathrm{UL}}^{-1}(x) = \frac{(\gamma_{\mathrm{RD}} + \gamma_{\mathrm{RR}} x)x}{\gamma_{\mathrm{RD}}} \tag{4.40b}$$

with $\gamma_{\max} \to \infty$.

In addition, power constraints may be invoked such that a)-expressions replace b)-expressions if the inequality (4.26), or (4.32), is true when setting $\gamma_{\mathrm{RD}} = \gamma_{\mathrm{DL}}^{-1}(x)$ (resp. $\gamma_{\mathrm{SR}} = \gamma_{\mathrm{UL}}^{-1}(x)$) in the DL (resp. UL) direction.

One may also note from the above that the analysis of the target-SINR approach is omitted in the UL direction. This is reasonable because the cost of acquiring CSI for the static backhaul channel is relatively low.

The outage probability expressions are illustrated by Fig. 4.3 in an example setup where the static backhaul SNR is 20 dB and the average SNR of the fading service link is 25 dB. In general, it is noted that the bottleneck of the end-to-end link is the first hop due to residual self-interference and the relay should often back off from its maximum transmit power.

The downlink relaying direction is shown in Fig. 4.3(a). With both protocols, the maximum achievable SINR is only 4.9 dB (resp. 13.8 dB) when $\gamma_{\mathrm{RR}} = 15$ dB (resp. $\gamma_{\mathrm{RR}} = 5$ dB) while optimal transmit power control minimizes the effect of residual self-interference and, in theory, the maximum SINR increases to 20 dB irrespective of γ_{RR}. Furthermore, at the median level (γ_{th} with $\mathcal{P}_{\mathrm{out}}(\gamma_{\mathrm{th}}) = 0.5$), the gain of transmit power optimization over maximum power usage is approximately 5.8 dB (resp. 1.3 dB) when $\gamma_{\mathrm{RR}} = 15$ dB (resp. $\gamma_{\mathrm{RR}} = 5$ dB) with amplify-and-forward (AF) relaying and the decode-and-forward (DF) protocol gains roughly 3 dB more.

The target-SINR approach is nearly optimal when the threshold SINR is close to its target as intended. When $\gamma_{\mathrm{RR}} = 15$ dB (resp. $\gamma_{\mathrm{RR}} = 5$ dB), $\hat{\gamma}$ is set to 10 dB (resp. 15 dB) resulting in the transmit power fraction $p_{\mathrm{R}} = 0.14$ (resp. $p_{\mathrm{R}} = 0.34$) in AF relaying, i.e., power savings are also significant although the outage probability remains often slightly suboptimal. The corresponding power fraction is 0.28 (resp. 0.68) in DF relaying where higher, roughly doubled, transmit power can be used since the nonlinear de/encoding process prevents infinite interference circulation through the relay. However, the target-SINR approach saturates the outage probability of the DF protocol for $\gamma_{\mathrm{th}} > \hat{\gamma}$ by rendering too high transmit power when the second hop observes a better-than-expected SNR level.

The uplink relaying direction is shown in Fig. 4.3(b); general observations from therein are in line with the downlink case. Yet the two directions are rather different because self-interference distorts a fading channel in the uplink case. In particular, fading amplifies the effect of self-interference and transmit power optimization such that both ends of the SINR range are achieved with higher probability than in downlink relaying. The theoretical maximum of SINR is 20 dB even without transmit power optimization although it is rarely met in practice due to self-interference. As indicated by (4.26) and (4.32), the maximum transmit power is optimal, i.e., the optimal gain factor is clipped due to power constraints, when γ_{SR} and the end-to-end SINR fluctuate to a large level and, consequently, the uplink outage probabilities coincide for large γ_{th}; the converse case holds true in the downlink case where γ_{RD} is fading.

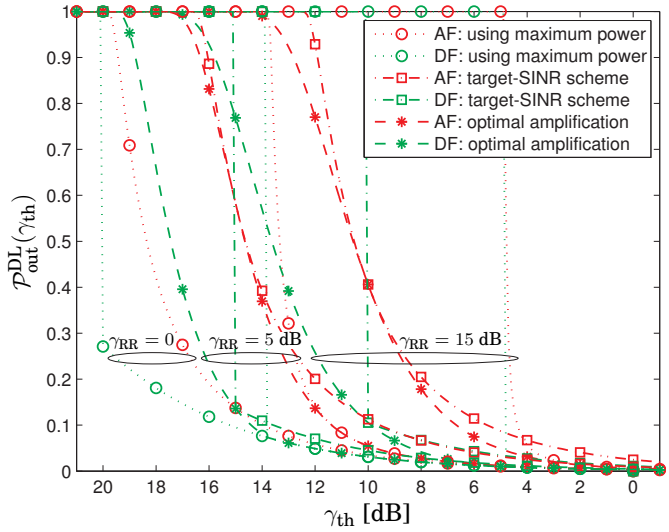

(a) downlink (DL) relaying when $\gamma_{\text{SR}} = 20$ dB and $\bar{\gamma}_{\text{RD}} = 25$ dB

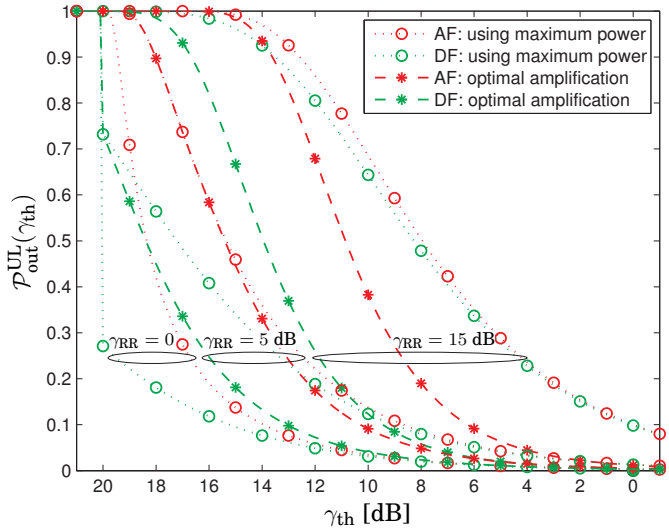

(b) uplink (UL) relaying when $\bar{\gamma}_{\text{SR}} = 25$ dB and $\gamma_{\text{RD}} = 20$ dB

Figure 4.3. Effective end-to-end outage probability in terms of the threshold SNR with the different transmit power control methods when the transmission directions have the same (average) backhaul- and service-link SNRs and $\gamma_{\text{SD}} \approx 0$. In the downlink direction, the target SINR is set at $\hat{\gamma} = 10$ dB (resp. $\hat{\gamma} = 15$ dB) when $\gamma_{\text{RR}} = 15$ dB (resp. $\gamma_{\text{RR}} = 5$ dB).

4.5 Conclusions

This chapter studied the effect of residual loopback self-interference in single-frequency full-duplex relay links. Both amplify-and-forward as well as decode-and-forward relaying were considered within a unified analytical framework. The study was motivated by the previous chapter which concluded that, even with efficient self-interference mitigation, performance loss due to residual distortion cannot be completely avoided. Transmit power adaptation proposed herein offers a win-win solution for still alleviating further the remaining problem: With smart relay gain selection, less transmit power is consumed while the end-to-end link quality is also improved. Especially, the chapter presented two reference gain control schemes and proposed two enhanced ones that improve effective signal-to-interference and noise ratios. Finally, the performance of the schemes was evaluated also in terms of outage probability.

5. Half- vs. Full-Duplex Relaying with Self-interference

Successful design of full-duplex (FD) relaying should be always contrasted with the choice to revert back to conventional half-duplex (HD) relaying or even to plain direct transmission (DT). This requires analytical comparison between the choices and poses a fundamental rate–interference trade-off: The HD mode avoids inherently self-interference at the cost of halving end-to-end symbol rate while the FD mode offers full symbol rate but, in practice, suffers from self-interference even after mitigation.

This chapter introduces the concept of hybrid relaying to switch opportunistically between FD relaying, HD relaying, and the DT mode, which serves also as a thorough comparison between the modes. In particular, the combination of opportunistic mode selection and transmit power adaptation is developed for maximizing instantaneous and average link capacity after noting that the trade-off favors alternately the modes during operation. The analysis covers both amplify-and-forward (AF) and decode-and-forward (DF) relaying as well as reflects the difference of downlink (DL) and uplink (UL) systems. In summary, the results show that the proposed schemes offer significant capacity gain over system design that is confined to any mode without rationalization.

The remainder of this chapter[1] is organized as follows. First, Sections 5.1 and 5.2 explain the scope of the study and specify the considered system setup which amends the classic three-node relay links by explicitly modeling inherent co-channel interference. The main analytical results are two-fold: Section 5.3 focuses on short-term capacity analysis assuming static channels and instantaneous channel state information (CSI) while Section 5.4 proceeds to the case of fading channels and long-term capacity optimization using statistical CSI in infrastructure-based relaying. Finally, Section 5.5 concludes with a summary of observations.

[1]This chapter is partially based on the material presented in **[213,218,220,225]**.

5.1 Introduction

The presence of (residual) self-interference is undisputed with full-duplex operation. Scanning through the related literature, the prior art turns out to be polarized such that its effect is considered either ultimately destructive or virtually negligible. In practice, the truth may lie in between the two extremes, especially with infrastructure relay nodes (RNs) and efficient mitigation solutions. For example, practical systems have employed the simplest form of FD relays, i.e., analog repeaters, since the early days of wireless communications and, in this down-to-earth context, the existence of self-interference is recognized. However, such activity typically adheres upfront to the FD mode, like cooperative communications resorts to the HD mode, without rationalizing which one is the proper choice.

The present work, as the first of its kind, charts what happens between the extremes when making a calculated choice between the modes. In terms of both instantaneous and average link capacity, this study provides explicit conditions under which one relaying mode can be preferred over the other and evaluates the benefit of opportunistic switching between modes which is referred to as "hybrid FD/HD relaying". All essential aspects of hybrid FD/HD relaying are elaborated within a unified framework, and the treatment is not limited to a specific example setup but covers all typical scenarios encountered in infrastructure relaying: The study illustrates the differences of using instantaneous or statistical CSI, employing AF or DF protocol, communicating in DL or UL direction as well as variations of transmit power normalization and adaptation.

More specifically, this chapter contributes to the design and analysis of advanced relaying technologies as follows.

- The study rationalizes the trade-off between FD and HD modes by explicitly modeling the residual self-interference remaining in practice after mitigation. Still the FD mode is shown to be a feasible choice for infrastructure-based relay links in contrast to cooperative communication systems, and it can also achieve higher capacity than the HD mode.

- The analysis indicates that in many cases neither mode is the obvious choice and premature mode selection in early design stage leads to inefficient spectrum utilization. Thus, new hybrid FD/HD relaying schemes are introduced to facilitate switching optimally between the modes based on either instantaneous or statistical CSI.

- Optimal short-term and long-term transmit power control is adopted to minimize the effect of residual self-interference. Opportunistic mode switching is optimized also when combined with these techniques. It is observed that the employment of transmit power adaptation changes drastically the trade-off between the FD mode and the HD mode, making the choice of the former even more attractive.

- Throughout the chapter, the performance of the system with opportunistic mode switching and transmit power adaptation is evaluated by deriving new closed-form expressions for the instantaneous and average link capacity. Consequently, the study demonstrates that FD and hybrid FD/HD modes offer great potential for increasing spectral efficiency w.r.t. the conventional HD mode and plain direct transmission (DT).

The presented results are useful in two ways. Firstly, they show how to improve the efficiency of spectrum utilization during relay operation by introducing new opportunistic protocols. Secondly, they apply as system design guidelines by determining the suitable use cases for the DT, FD, HD and hybrid FD/HD modes, and by setting targets for the performance of interference mitigation when the FD mode is pre-selected.

While the short-term performance is not tied to fading statistics, the analysis of average link capacity concerns an infrastructure relay node (RN) deployed for extending the coverage area of a cellular base station (BS). Thus, the backhaul link is fixed while the service link to/from a user equipment (UE) is subject to fast fading. Instead of capacity, the results can be reproduced also using outage probability (cf. [141] and **[224]**).

When it comes to the rest of the chapter, system models are first formulated based on the signal models of the previous chapter for two-hop relay links that, as a novel factor, account for the residual self-interference remaining after any combination of mitigation schemes, e.g., as discussed in Chapter 3. Section 5.3 is devoted to hybrid FD/HD and transmit power adaptation schemes which optimize the instantaneous link capacity based on instantaneous CSI. The focus of Section 5.4 is in average link capacity when exploiting statistical CSI. In particular, the comparison of the proposed schemes explains the differences of DT, FD, HD and hybrid FD/HD, AF and DF, DL and UL directions as well as short- and long-term performance optimization. Finally, Section 5.5 summarizes the observations: Hybrid FD/HD relaying is an attractive concept for infrastructure relays whenever the self-interference can be first sufficiently mitigated.

5.2 System Model

The study of this chapter considers generic two-hop systems in which a source (S) communicates to a destination (D) via a relay (R) in the spirit of Fig. 2.3(a) while focusing on coverage extension scenarios in which direct source-to-destination (SD) connection is weak and relays are deployed to help other nodes without having own data to transmit. Thus, the system comprises four wireless links; namely source-to-relay (SR), residual loopback relay-to-relay (RR), relay-to-destination (RD), and direct link channels whose SNRs are denoted by γ_{SR}, γ_{RR}, γ_{RD}, and γ_{SD}, respectively. These channels are modeled to be frequency-flat and quasi-static, i.e., they may represent equivalent subchannels when the signals are transmitted on narrowband subcarriers in a full OFDM framework.

The novelty of this study lies in *taking explicitly account of residual self-interference* that is inevitable in practical full-duplex (FD) relays (cf. Chapter 3). As shown in Fig. 5.1, the system thus chooses upfront or switches opportunistically between FD relaying, with or without power control, under co-channel interference and half-duplex (HD) relaying, with or without diversity combining, under reduced spectral efficiency.

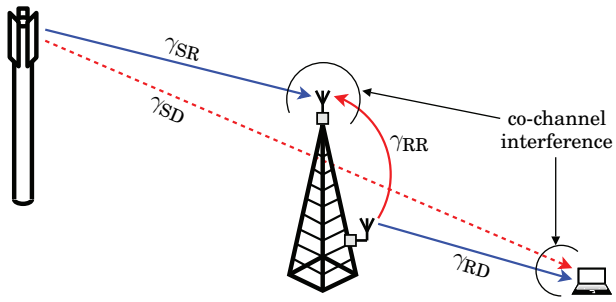

(a) full-duplex (FD) mode

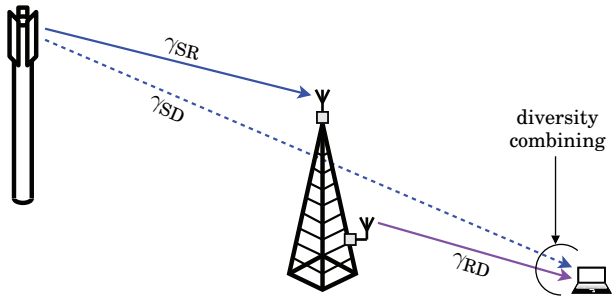

(b) half-duplex (HD) mode

Figure 5.1. Two operation modes of a two-hop relay link in which γ_{SR}, γ_{SD}, γ_{RR}, and γ_{RD} denote the instantaneous signal-to-noise ratios of the narrowband channels.

The system is parametrized with channel SNRs, i.e., $\gamma_{\mathrm{SR}} \triangleq |h_{\mathrm{SR}}|^2/\sigma_{\mathrm{R}}^2$, $\gamma_{\mathrm{RD}} \triangleq |h_{\mathrm{RD}}|^2/\sigma_{\mathrm{D}}^2$, and $\gamma_{\mathrm{SD}} \triangleq |h_{\mathrm{SD}}|^2/\sigma_{\mathrm{D}}^2$, as in the previous chapter. These variables represent SNR levels that single-hop transmission could achieve over each channel with maximum power usage. Likewise, γ_{RR} represents the level of residual distortion due to loopback interference. The underlying signal models are summarized below for complementing Section 4.2.1.

5.2.1 Full-Duplex Relaying and Direct Transmission

Whenever the full-duplex (FD) mode is used, the end-to-end signal model is exactly the same as what is described in Section 4.2.1 and, thus, it is not repeated herein. Yet one should keep in mind that parameter γ_{RR} measures *residual* self-interference remaining after all means of mitigation.

As a degenerate case of the FD mode, the system may shut down the relay and revert to a direct transmission (DT) mode, in which the source transmits $x_{\mathrm{S}}[i]$ over channel h_{SD} and the destination decodes noisy signal

$$y_{\mathrm{D}}[i] = h_{\mathrm{SD}} x_{\mathrm{S}}[i] + n_{\mathrm{D}}[i]. \tag{5.1}$$

Thus, the link avoids both the co-channel interference of the FD mode and the extra resource usage of the HD mode. In "selective"/"incremental" relaying [142], the DT mode is used with relatively strong direct connection.

5.2.2 Half-Duplex Relaying with Diversity Combining

The end-to-end transmission of one symbol can be spread over two orthogonal time slots to eliminate self-interference. This is common in earlier literature, e.g., with "fixed" relaying [142]. Analytically, such separation could as well be achieved in frequency domain but practical implementation may impose other constraints for time and frequency duplexing.

In the half-duplex (HD) mode, the source transmits $x_{\mathrm{S}}[2i]$ only during the even time slots while the relay receives $y_{\mathrm{R}}[2i]$ during the even time slots and transmits $x_{\mathrm{R}}[2i+1]$ during the uneven time slots. Thereby, the noisy received signals in the relay and in the destination are expressed as

$$y_{\mathrm{R}}[2i] = h_{\mathrm{SR}} x_{\mathrm{S}}[2i] + n_{\mathrm{R}}[2i], \tag{5.2a}$$

$$y_{\mathrm{D}}[2i] = h_{\mathrm{SD}} x_{\mathrm{S}}[2i] + n_{\mathrm{D}}[2i], \tag{5.2b}$$

$$y_{\mathrm{D}}[2i+1] = h_{\mathrm{RD}} x_{\mathrm{R}}[2i+1] + n_{\mathrm{D}}[2i+1]. \tag{5.2c}$$

As for relaying protocols, processing steps to obtain x_{R} from y_{R} are equivalent to those described in Section 4.2.1 for the FD mode except processing delay τ_{R} is always uneven and self-interference is inherently avoided.

5.3 Analysis of Short-Term Performance

This section studies link capacity with hybrid FD/HD relaying and transmit power adaptation in the case of static channels and, thus, exploiting instantaneous channel state information (CSI). Alternatively, the study can be interpreted to explain instantaneous snapshot performance within channel coherence time in a slow-fading environment. This is referred to as short-term link performance analysis where γ_{SR}, γ_{RR}, γ_{RD}, and γ_{SD} are regarded as constants representing the instantaneous channel states. The key optimization parameters are transmit powers in the source and in the relay, i.e., $p_{\mathrm{S}} \triangleq \mathcal{E}\{|x_{\mathrm{S}}[i]|^2\}$ and $p_{\mathrm{R}} \triangleq \mathcal{E}\{|x_{\mathrm{R}}[i]|^2\}$, respectively.

To begin with, Section 5.3.1 presents the instantaneous link capacities of the three conventional fixed modes: direct transmission (DT), full-duplex (FD) and half-duplex (HD). The system is directly characterized by their performance when any mode is chosen upfront during design stage. The new concept of hybrid switching between the modes is developed later in Section 5.3.2 by formulating corresponding cross-over boundaries.

5.3.1 Instantaneous Link Capacity

The instantaneous link capacities achieved with the different conventional fixed operation modes can be expressed as

$$\mathcal{C}_{\mathrm{FD}} = \log_2(1+\gamma_{\mathrm{FD}}), \tag{5.3a}$$

$$\mathcal{C}_{\mathrm{HD+MRC}} = \log_2(1+\hat{\gamma}_{\mathrm{HD+MRC}}) \triangleq \frac{1}{2}\log_2(1+\gamma_{\mathrm{HD+MRC}}), \tag{5.3b}$$

$$\mathcal{C}_{\mathrm{DT}} = \log_2(1+\gamma_{\mathrm{SD}}), \tag{5.3c}$$

for which the end-to-end signal-to-interference and noise ratios (SINRs), namely γ_{FD}, $\gamma_{\mathrm{HD+MRC}}$, and γ_{SD}, are specified shortly; without maximum ratio combining (MRC), the link capacity of HD relaying is denoted by $\mathcal{C}_{\mathrm{HD}} = \log_2(1+\hat{\gamma}_{\mathrm{HD}}) \triangleq \frac{1}{2}\log_2(1+\gamma_{\mathrm{HD}})$. Capacities are illustrated in Fig. 5.2.

It is worth emphasizing that middle equation (5.3b) exploits definition

$$\hat{\gamma}_{\mathrm{HD+MRC}} \triangleq \sqrt{1+\gamma_{\mathrm{HD+MRC}}} - 1, \tag{5.4}$$

which represents an equivalent SNR level after compensating for the pre-log factor $1/2$ of the capacity expression. This notation is adopted to allow capacity comparison indirectly in terms of only end-to-end SINRs by making the pre-log factors the same in all modes. Likewise, the S(I)NR of the DF protocol is not a real measurable quantity, but a "capacity-equalizing" variable adopted for handling both protocols in parallel as before.

SINR in Full-Duplex Relaying

In the FD mode, respective received signal powers in the relay and in the destination are given by $\mathcal{E}\{|\hat{y}_{\mathrm{R}}[i]|^2\}$, as shown in (4.7), and

$$\mathcal{E}\{|y_{\mathrm{D}}[i]|^2\} = p_{\mathrm{R}}|h_{\mathrm{RD}}|^2 + p_{\mathrm{S}}|h_{\mathrm{SD}}|^2 + \sigma_{\mathrm{D}}^2, \tag{5.5}$$

where terms $p_{\mathrm{S}}|h_{\mathrm{SR}}|^2$ and $p_{\mathrm{R}}|h_{\mathrm{RD}}|^2$ are useful signal power and co-channel interference produces $p_{\mathrm{R}}\gamma_{\mathrm{RR}}\sigma_{\mathrm{R}}^2$ and $p_{\mathrm{S}}|h_{\mathrm{SD}}|^2$. The signal-to-interference and noise ratios (SINRs) of the two hops can be thus compactly defined as

$$\gamma_{\mathrm{R}} \triangleq \frac{p_{\mathrm{S}}\gamma_{\mathrm{SR}}}{p_{\mathrm{R}}\gamma_{\mathrm{RR}}+1} \quad \text{and} \quad \gamma_{\mathrm{D}} \triangleq \frac{p_{\mathrm{R}}\gamma_{\mathrm{RD}}}{p_{\mathrm{S}}\gamma_{\mathrm{SD}}+1}. \tag{5.6}$$

Finally, following the derivations of Section 4.2.2, the above parameters allow to state the instantaneous end-to-end SINR of the FD mode as

$$\gamma_{\mathrm{FD}} = \begin{cases} \frac{\gamma_{\mathrm{R}}\gamma_{\mathrm{D}}}{\gamma_{\mathrm{R}}+\gamma_{\mathrm{D}}+1}, & \text{with AF,} \\ \min\{\gamma_{\mathrm{R}}, \gamma_{\mathrm{D}}\}, & \text{with DF.} \end{cases} \tag{5.7}$$

These expressions update the earlier models presented for the HD mode, e.g., in [142], by explicitly including the effects of the residual loopback self-interference and overheard direct link transmission.

SNR in Half-Duplex Relaying

In the HD mode, the destination receives two independent copies of each transmitted symbol due to the adopted repetition-based protocols. The de facto standard way to benefit from such diversity is to apply maximum ratio combining (MRC). Following the derivations of [142], the end-to-end SNR of the HD mode with MRC can be expressed as

$$\gamma_{\mathrm{HD+MRC}} = \begin{cases} p_{\mathrm{S}}\gamma_{\mathrm{SD}} + \frac{p_{\mathrm{S}}\gamma_{\mathrm{SR}}p_{\mathrm{R}}\gamma_{\mathrm{RD}}}{p_{\mathrm{S}}\gamma_{\mathrm{SR}}+p_{\mathrm{R}}\gamma_{\mathrm{RD}}+1}, & \text{with AF,} \\ \min\{p_{\mathrm{S}}\gamma_{\mathrm{SR}}, p_{\mathrm{S}}\gamma_{\mathrm{SD}} + p_{\mathrm{R}}\gamma_{\mathrm{RD}}\}, & \text{with DF.} \end{cases} \tag{5.8}$$

Without MRC, the end-to-end SNR is γ_{HD} obtained from above expressions simply by setting $\gamma_{\mathrm{SD}} = 0$ and, consequently, $\hat{\gamma}_{\mathrm{HD}} \triangleq \sqrt{1+\gamma_{\mathrm{HD}}} - 1$.

SNR in Direct Transmission

If the direct link is strong in FD relaying, the destination may conversely regard respective $p_{\mathrm{S}}|h_{\mathrm{SD}}|^2$ and $p_{\mathrm{R}}|h_{\mathrm{RD}}|^2$ as useful and interference power, i.e., $\gamma_{\mathrm{D}} \triangleq \frac{p_{\mathrm{S}}\gamma_{\mathrm{SD}}}{p_{\mathrm{R}}\gamma_{\mathrm{RD}}+1}$ in contrast to (5.6). Obviously, the system should shut down the relay completely in this case. In the DT mode, the end-to-end SNR is thus simply given by the source-to-destination link SNR:

$$\gamma_{\mathrm{DT}} = p_{\mathrm{S}}\gamma_{\mathrm{SD}}. \tag{5.9}$$

Effectively $p_{\mathrm{R}} = 0$ and $\gamma_{\mathrm{FD}} = \gamma_{\mathrm{D}} = p_{\mathrm{S}}\gamma_{\mathrm{SD}}$ replaces (5.6) and (5.7) when the DT mode is understood as a degenerate case of the FD mode.

Transmit Power Adaptation for Full-Duplex Relaying

Transmit power adaptation is proposed in the previous chapter as a technique to mitigate the effect of residual self-interference and now it shall be integrated with the concept of hybrid mode switching.

Transmission power levels are subject to individual constraints throughout the chapter: $p_{\mathrm{S}} \leq 1$ and $p_{\mathrm{R}} \leq 1$. This is practical for infrastructure-based deployments where the total energy consumption of a system is less critical than each transmitter's power limitations set by regulations and the physical capabilities of radio circuitry. In this thesis, the performance of infrastructure relay links will not be optimized under a joint sum power constraint ($p_{\mathrm{S}} + p_{\mathrm{R}} \leq 2$), which may be relevant for cooperative communications instead, but this complementary analysis can be found in **[225]**.

Without transmit power optimization in the FD mode, the relay simply uses the maximum allowed power, i.e., $p_{\mathrm{R}} = 1$. The remaining chapter concentrates on power adaptation in the relay implying that the source uses always the maximum transmit power, i.e., $p_{\mathrm{S}} = 1$. This is justified in coverage extension scenarios: $\gamma_{\mathrm{R}} \triangleq \frac{p_{\mathrm{S}}\gamma_{\mathrm{SR}}}{p_{\mathrm{R}}\gamma_{\mathrm{RR}}+1}$ is then maximized and, because typically $\gamma_{\mathrm{SD}} \ll \gamma_{\mathrm{RR}}$, the effect on $\gamma_{\mathrm{D}} \triangleq \frac{p_{\mathrm{R}}\gamma_{\mathrm{RD}}}{p_{\mathrm{S}}\gamma_{\mathrm{SD}}+1}$ is insignificant; the best performance under constraint $p_{\mathrm{S}} \leq 1$ is thus achieved when $p_{\mathrm{S}} \approx 1$.

Transmit power adaptation in FD relaying is motivated by the observation that the end-to-end performance is limited by the weakest hop: If the limiting factor is the first hop due to excessive self-interference, the link capacity can be, in fact, *improved* by *decreasing* the relay transmit power. This reasoning can be formulated as an optimization problem

$$p_{\mathrm{R}}^{*} = \arg\max_{p_{\mathrm{R}}} \mathcal{C}_{\mathrm{FD}} \text{ subject to } p_{\mathrm{R}} \leq 1, \tag{5.10}$$

for which $\mathcal{C}_{\mathrm{FD}}$ is given by (5.3a) with (5.6) and (5.7).

The power control problem is already solved in the previous chapter for both protocols: The optimal gain factors β^{*} obtained therein imply that

$$p_{\mathrm{R}}^{*} = \begin{cases} \min\left\{1, \frac{1}{\gamma_{\mathrm{RR}}}\sqrt{\frac{(\gamma_{\mathrm{SR}}+1)\gamma_{\mathrm{RR}}(\gamma_{\mathrm{SD}}+1)}{\gamma_{\mathrm{RD}}}}\right\}, & \text{with AF,} \\ \min\left\{1, \frac{1}{\gamma_{\mathrm{RR}}}\left(\sqrt{\frac{\gamma_{\mathrm{SR}}\gamma_{\mathrm{RR}}(\gamma_{\mathrm{SD}}+1)}{\gamma_{\mathrm{RD}}} + \frac{1}{4}} - \frac{1}{2}\right)\right\}, & \text{with DF,} \end{cases} \tag{5.11}$$

and reveal that the transmit power constraint is invoked ($p_{\mathrm{R}}^{*} = 1$) when

$$\gamma_{\mathrm{RR}} \leq \begin{cases} \frac{(\gamma_{\mathrm{SR}}+1)(\gamma_{\mathrm{SD}}+1)}{\gamma_{\mathrm{RD}}}, & \text{with AF,} \\ \frac{\gamma_{\mathrm{SR}}(\gamma_{\mathrm{SD}}+1)}{\gamma_{\mathrm{RD}}} - 1, & \text{with DF.} \end{cases} \tag{5.12}$$

In particular, these inequalities show that the maximum transmit power is optimal only in the case of weak interference while otherwise link performance can be improved by backing off from the maximum. Furthermore, the limitation appears to be the most critical for the AF protocol.

The substitution of (5.6) and (5.11) in (5.7) yields end-to-end SINRs with optimal transmit power adaptation as

$$\gamma_{\mathrm{FD}}^{*} = \begin{cases} \frac{\gamma_{\mathrm{SR}}\gamma_{\mathrm{RD}}}{\gamma_{\mathrm{RD}}+\gamma_{\mathrm{RR}}(\gamma_{\mathrm{SD}}+1)+2\sqrt{(\gamma_{\mathrm{SR}}+1)\gamma_{\mathrm{RD}}\gamma_{\mathrm{RR}}(\gamma_{\mathrm{SD}}+1)}}, & \text{with AF,} \\ \frac{\gamma_{\mathrm{RD}}}{\gamma_{\mathrm{RR}}(\gamma_{\mathrm{SD}}+1)}\left(\sqrt{\frac{\gamma_{\mathrm{SR}}\gamma_{\mathrm{RR}}(\gamma_{\mathrm{SD}}+1)}{\gamma_{\mathrm{RD}}}+\frac{1}{4}}-\frac{1}{2}\right), & \text{with DF.} \end{cases} \tag{5.13}$$

This expression disregards (for clarity and compactness) the saturation of transmit power such that $p_{\mathrm{R}}^{*} \leq 1$. Yet the following analysis still considers constrained power adaptation for which the SINRs coincide with those of the unconstrained case given above whenever the conditions in (5.12) are *not* satisfied; the maximum transmit power is used otherwise and the SINRs are given by (5.7) with the substitution of (5.6) where $p_{\mathrm{S}} = p_{\mathrm{R}} = 1$.

Transmit Power in Direct Transmission and Half-Duplex Relaying

Under independent power constraints, the performance of the HD mode is optimized simply by using maximum power in both transmitters. Likewise, the DT mode simply adopts maximum transmit power for obtaining the highest capacity. Thus, the analysis shall focus on power adaptation only in the FD mode while $p_{\mathrm{S}} = p_{\mathrm{R}} \in \{1, 2\}$ is set for the other modes.

The comparison of the FD and DT modes to the HD mode is not totally straightforward because there are two different ways to normalize transmit power in the HD mode; both of them are common in related literature.

Energy normalization: Since the source and the relay transmit only half of the time when compared to the FD mode, the HD mode should use double power ($p_{\mathrm{S}} = p_{\mathrm{R}} = 2$) to equalize the total average transmitted energy in all modes. Further analysis for this normalization is available in **[218]** but it is used as a reference case herein too.

Power normalization: The present study mainly adopts the other normalization scheme, i.e., the same constraints $p_{\mathrm{S}} \leq 1$ and $p_{\mathrm{R}} \leq 1$ are set for all modes. This is because hybrid FD/HD relaying uses the same radio equipment for both modes while doubled instantaneous power in the HD mode would imply that the emission regulations or the radio front-ends were different. Furthermore, total energy consumption is a less critical factor for cellular relays connected to a power grid than for battery-operated relays in user cooperation.

The *energy normalization* scheme is relevant in conjunction with the joint transmit power constraint, i.e., $p_{\mathrm{S}} + p_{\mathrm{R}} \leq 4$, since both concepts share energy budget between two *separate* nodes. However, $p_{\mathrm{S}} = p_{\mathrm{R}} = 2$ becomes suboptimal then and also the HD mode needs transmit power adaptation.

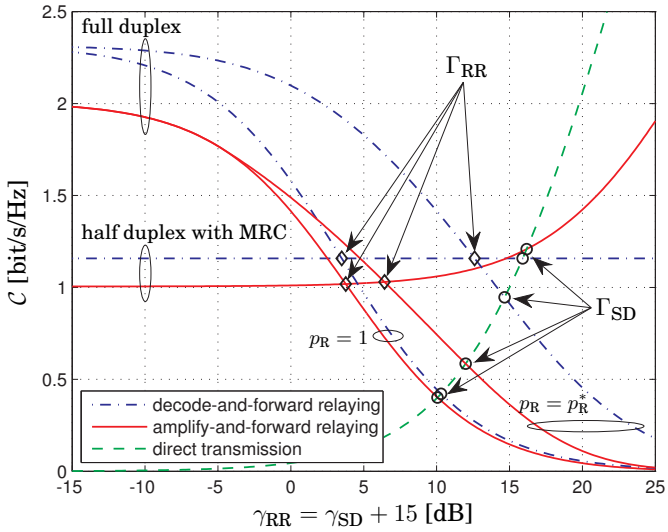

Figure 5.2. Instantaneous link capacities when $\gamma_{\mathrm{SR}} = 6$ dB and $\gamma_{\mathrm{RD}} = 12$ dB. The full-duplex mode is preferred over the half-duplex mode if $\gamma_{\mathrm{RR}} < \Gamma_{\mathrm{RR}}$, and direct transmission is preferred over relaying when $\gamma_{\mathrm{SD}} > \Gamma_{\mathrm{SD}}$. Transmit power adaptation ($p_{\mathrm{R}} = p_{\mathrm{R}}^*$) improves capacity w.r.t. maximum power usage ($p_{\mathrm{R}} = 1$).

5.3.2 Hybrid Relaying Modes

The need for proper mode selection is motivated by Fig. 5.2 which shows the instantaneous link capacities given by (5.3a)–(5.3c) in terms of γ_{RR} and γ_{SD}. Especially, this reveals two relevant break-even levels for the SNRs. Sufficient and necessary condition for the FD mode to outperform the HD mode is that the residual self-interference gain γ_{RR} is below a break-even self-interference level Γ_{RR}. Similarly, if the direct link SNR γ_{SD} is above a break-even level Γ_{SD}, the DT mode is superior to either relaying mode. These break-even levels can be formally defined such that

$$\mathcal{C}_{\mathrm{FD}} \geq \mathcal{C}_{\mathrm{HD}} \text{ if and only if } \gamma_{\mathrm{RR}} \leq \Gamma_{\mathrm{RR}}, \tag{5.14a}$$

$$\mathcal{C}_{\mathrm{HD+MRC}} \geq \mathcal{C}_{\mathrm{DT}} \text{ or } \mathcal{C}_{\mathrm{FD}} \geq \mathcal{C}_{\mathrm{DT}} \text{ if and only if } \gamma_{\mathrm{SD}} \leq \Gamma_{\mathrm{SD}}. \tag{5.14b}$$

For end-to-end performance optimization, opportunistic hybrid relaying switches to the best mode based on instantaneous CSI, i.e., the values of γ_{SR}, γ_{RD}, γ_{RR}, and γ_{SD}. The resulting instantaneous link capacity becomes

$$\mathcal{C}_{\mathrm{hybrid}} \triangleq \max\left\{\mathcal{C}_{\mathrm{FD}}, \mathcal{C}_{\mathrm{HD+MRC}}, \mathcal{C}_{\mathrm{DT}}\right\}, \tag{5.15}$$

while link capacity is fixed to either $\mathcal{C}_{\mathrm{FD}}$, $\mathcal{C}_{\mathrm{HD+MRC}}$, or $\mathcal{C}_{\mathrm{DT}}$ in conventional reference cases. With (5.15), Fig. 5.2 shows readily the advantage of hybrid relaying w.r.t. conventional modes: Each mode achieves in turn much higher link capacity than the others in different channel states.

In what follows, the explicit implementation of the hybrid relaying mode is formulated by deriving the switching boundaries between the modes. In particular, expressions are given for break-even levels Γ_{SD} and Γ_{RR}.

Switching Between Direct Transmission and Relaying

The direct link SNR γ_{SD} is the key parameter for switching between DT and relaying modes. Its effect can be quantified with closed-form expressions for $\Gamma_{\mathrm{SD}}(\gamma_{\mathrm{SR}}, \gamma_{\mathrm{RD}}, \gamma_{\mathrm{RR}})$ as summarized in the following property.

- The DT mode is preferred over FD relaying if

$$\gamma_{\mathrm{SD}} \geq \Gamma_{\mathrm{SD}} = \begin{cases} \frac{\gamma_{\mathrm{R}}+\gamma_{\mathrm{RD}}+1}{\gamma_{\mathrm{R}}+1} \left(\sqrt{\frac{\gamma_{\mathrm{R}}(\gamma_{\mathrm{R}}+1)\gamma_{\mathrm{RD}}}{(\gamma_{\mathrm{R}}+\gamma_{\mathrm{RD}}+1)^2} + \frac{1}{4}} - \frac{1}{2} \right), & \text{with AF,} \\ \min\left\{ \gamma_{\mathrm{R}}, \sqrt{\gamma_{\mathrm{RD}} + \frac{1}{4}} - \frac{1}{2} \right\}, & \text{with DF,} \end{cases} \tag{5.16a}$$

  and the DT mode is preferred over HD relaying (which uses MRC) if

$$\gamma_{\mathrm{SD}} \geq \Gamma_{\mathrm{SD}} = \begin{cases} \sqrt{\frac{\gamma_{\mathrm{SR}}\gamma_{\mathrm{RD}}}{\gamma_{\mathrm{SR}}+\gamma_{\mathrm{RD}}+1} + \frac{1}{4}} - \frac{1}{2}, & \text{with AF,} \\ \min\left\{ \sqrt{\gamma_{\mathrm{SR}}+1} - 1, \sqrt{\gamma_{\mathrm{RD}} + \frac{1}{4}} - \frac{1}{2} \right\}, & \text{with DF,} \end{cases} \tag{5.16b}$$

  without transmit power adaptation. As before, $\gamma_{\mathrm{R}} \triangleq \gamma_{\mathrm{SR}}/(\gamma_{\mathrm{RR}}+1)$.

The break-even levels of (5.16a) and (5.16b) are obtained by solving γ_{SD} in terms of the other parameters of (5.6)–(5.9) from the respective inequalities $\mathcal{C}_{\mathrm{DT}} \geq \mathcal{C}_{\mathrm{FD}}$ and $\mathcal{C}_{\mathrm{DT}} \geq \mathcal{C}_{\mathrm{HD+MRC}}$ for which $\mathcal{C}_{\mathrm{FD}}$, $\mathcal{C}_{\mathrm{HD+MRC}}$ and $\mathcal{C}_{\mathrm{DT}}$ are given in (5.3a)–(5.3c) and $p_{\mathrm{S}} = p_{\mathrm{R}} = 1$ in the absence of power adaptation.

With optimal transmit power adaptation, similar break-even level Γ_{SD} for both AF and DF can be (in theory) solved explicitly from $\gamma_{\mathrm{SD}} \geq \gamma_{\mathrm{FD}}^{*}$ with the substitution of (5.13). However, the expressions are in practice too tedious to be presented here because they correspond to the roots of fourth-order polynomials. A lookup table of numerical values can be used for mode switching in this case. Moreover, power adaptation reduces only slightly the range of direct-link SNRs that guarantee the superiority of the DT mode over the FD mode. Thus, nothing essential is left unseen.

The switching boundaries as per (5.16a) and (5.16b) are illustrated in Fig. 5.3 for the case in which the residual self-interference is negligible to emphasize the effect of the direct link. Thereby, the FD mode dominates the choice between relaying and mere direct transmission. In fact, adding loopback interference into consideration just further extends the range of γ_{SR} and γ_{RD} for which the DT mode is preferred. Furthermore, MRC does not offer significant gain for the HD mode which is also demonstrated by Fig. 5.2 in which the link capacity of the AF protocol increases only slightly before the DT mode becomes preferable. In fact, MRC is not beneficial at all for the DF protocol in Fig. 5.2 because $\gamma_{\mathrm{SR}} < \gamma_{\mathrm{RD}}$.

It should be especially noted that neither relaying mode is preferred in a large range of practical source–relay and relay–destination channel states with a relatively weak direct link, e.g., even $\gamma_{\mathrm{SD}} < 3$ dB. Thus, it is beneficial to retain the possibility to revert to a plain DT mode instantaneously because it is probable that the direct link is momentarily usable although it remains blocked on average in coverage extension scenarios.

Switching Between Full-Duplex and Half-Duplex Relaying

As demonstrated in Fig. 5.2, the residual loopback channel gain γ_{RR} is the key parameter for switching between relaying modes. Explicit closed-form expressions are derived for break-even levels $\Gamma_{\mathrm{RR}}(\gamma_{\mathrm{SR}}, \gamma_{\mathrm{RD}}, \gamma_{\mathrm{SD}})$ and the switching conditions are summarized in the following properties.

- The HD mode is preferred over the FD mode without transmit power adaptation if $\gamma_{\mathrm{D}} < \hat{\gamma}_{\mathrm{HD+MRC}} \triangleq \sqrt{1+\gamma_{\mathrm{HD+MRC}}} - 1$ for which $\gamma_{\mathrm{HD+MRC}}$ is given in (5.8); otherwise, the FD mode is preferred over the HD mode if

$$\gamma_{\mathrm{RR}} < \Gamma_{\mathrm{RR}} = \begin{cases} \frac{\gamma_{\mathrm{SR}}(\gamma_{\mathrm{D}} - \hat{\gamma}_{\mathrm{HD+MRC}})}{\hat{\gamma}_{\mathrm{HD+MRC}}(\gamma_{\mathrm{D}}+1)} - 1, & \text{with AF,} \\ \frac{\gamma_{\mathrm{SR}}}{\hat{\gamma}_{\mathrm{HD+MRC}}} - 1, & \text{with DF.} \end{cases} \tag{5.17}$$

  As before, $\gamma_{\mathrm{D}} \triangleq \gamma_{\mathrm{RD}}/(\gamma_{\mathrm{SD}}+1)$.

After setting $p_{\mathrm{R}} = 1$ for the FD mode as power adaptation is not used, the break-even levels in (5.17) are obtained by solving γ_{RR} in terms of the other parameters of (5.6) and (5.7) from the inequality $\mathcal{C}_{\mathrm{FD}} \geq \mathcal{C}_{\mathrm{HD+MRC}}$ for which $\mathcal{C}_{\mathrm{FD}}$ and $\mathcal{C}_{\mathrm{HD+MRC}}$ are given in (5.3a) and (5.3b), respectively.

Transmit power adaptation is beneficial for the FD mode in the presence of strong self-interference as discussed in Chapter 4. Consequently, lowering transmit power from its maximum guarantees the superiority of the FD mode in an extended region of channel states as observed next.

- With optimal *unconstrained* transmit power adaptation, the FD mode is preferred over the HD mode if

$$\gamma_{\mathrm{RR}} < \Gamma_{\mathrm{RR}} = \begin{cases} \frac{\gamma_{\mathrm{RD}}}{\hat{\gamma}_{\mathrm{HD+MRC}}(\gamma_{\mathrm{SD}}+1)} \Big[\gamma_{\mathrm{SR}} + (2\gamma_{\mathrm{SR}}+1)\hat{\gamma}_{\mathrm{HD+MRC}} \\ \quad -2\sqrt{\gamma_{\mathrm{SR}}(\gamma_{\mathrm{SR}}+1)\hat{\gamma}_{\mathrm{HD+MRC}}(\hat{\gamma}_{\mathrm{HD+MRC}}+1)}\Big], & \text{with AF,} \\ \frac{\gamma_{\mathrm{RD}}}{\hat{\gamma}_{\mathrm{HD+MRC}}(\gamma_{\mathrm{SD}}+1)} \left(\frac{\gamma_{\mathrm{SR}}}{\hat{\gamma}_{\mathrm{HD+MRC}}} - 1\right), & \text{with DF,} \end{cases} \tag{5.18}$$

  for which $\hat{\gamma}_{\mathrm{HD+MRC}} \triangleq \sqrt{1+\gamma_{\mathrm{HD+MRC}}} - 1$ and $\gamma_{\mathrm{HD+MRC}}$ is given in (5.8).

The conditions in (5.12) are not invoked with unconstrained power adaptation and, thus, γ_{FD} is given by (5.13). The break-even levels in (5.18) are then obtained by solving γ_{RR} from the inequality $\mathcal{C}_{\mathrm{FD}} \geq \mathcal{C}_{\mathrm{HD+MRC}}$ for which $\mathcal{C}_{\mathrm{FD}}$ and $\mathcal{C}_{\mathrm{HD+MRC}}$ are given in (5.3a) and (5.3b), respectively.

Naturally, one will always in practice apply *constrained* power adaptation for which the foregoing unconstrained case represents a subsolution. However, it is remarkable that the activation of transmit power limitations does not affect at all the break-even self-interference level Γ_{RR} given in (5.18) for the DF protocol. On the contrary in the case of AF relaying, the break-even self-interference level Γ_{RR} is given by (5.18) only if

$$\sqrt{\frac{(\gamma_{\mathrm{SR}}+1)[(\gamma_{\mathrm{SR}}+1)(\gamma_{\mathrm{SD}}+1)+\gamma_{\mathrm{RD}}]}{\gamma_{\mathrm{RD}}+\gamma_{\mathrm{SD}}+1}} \geq \frac{(\gamma_{\mathrm{SR}}+1)(\gamma_{\mathrm{SD}}+1)}{\gamma_{\mathrm{RD}}} \tag{5.19}$$

while otherwise it is as with maximum power usage ($p_{\mathrm{R}}^{*}=1$) shown in (5.17). Unfortunately, this inequality does not admit a compact solution in terms of any variable which hides explicit limiting conditions.

The switching boundaries of (5.17) are illustrated in Fig. 5.4. Without transmit power adaptation, the choice between FD and HD relaying is mostly defined by the first-hop SNR such that the HD mode is preferred for small γ_{SR}. Figure 5.5 illustrates the boundaries for optimal transmit power adaptation according to (5.18); now the FD mode is preferred in an extended region of channel states and, in particular, with small γ_{SR} and large γ_{RD}. The right hand side of the condition in (5.19) corresponds to the power limitation given in (5.12) indicating that the limitation is effective only with small γ_{RD} as also demonstrated in Fig. 5.5. Both with and without power adaptation, one should notice that the FD mode is preferable with all γ_{RD} if γ_{SR} is large enough. According to (5.19), the power constraint limits Γ_{RR} with AF relaying below the dashed curve.

For comparison with Figs. 5.4 and 5.5, Fig. 5.6 illustrates the switching boundaries when using *energy normalization* instead of *power normalization* assumed above. This clearly favors the HD mode but the FD mode is still useful in a large region of practical channel states and the gain of transmit power adaptation is consistent for both normalization schemes.

One should also recall that the foregoing analysis assumes that the relay is implemented with a single transmitter–receiver pair per two antenna elements. An extra transceiver would allow the HD mode to exploit receive and transmit beamforming and achieve higher γ_{SR} and γ_{RD} than the FD mode. Figure 5.6 illustrates also this case as two-antenna beamforming brings ideally (with balanced branches) up to 3 dB SNR gain for both hops which is equivalent to doubled transmit powers assumed with energy normalization. However, in practice, the potential beamforming gain becomes insignificant and, thus, not worth the cost of another transceiver, because the branches are highly imbalanced in typical target scenarios.

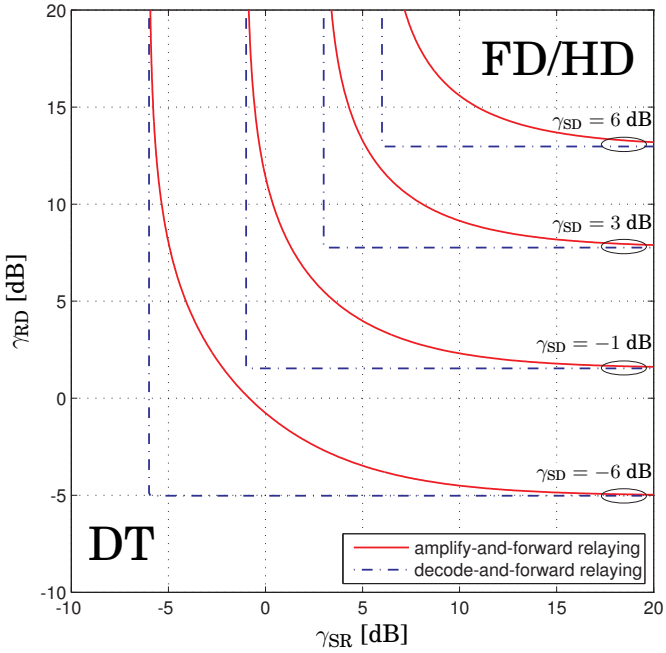

Figure 5.3. Switching boundaries Γ_{SD} between direct transmission (DT) and either of the relaying modes when $\gamma_{RR} = 0$. Full-duplex (FD) or half-duplex (HD) relaying is preferred over DT inside the boundaries.

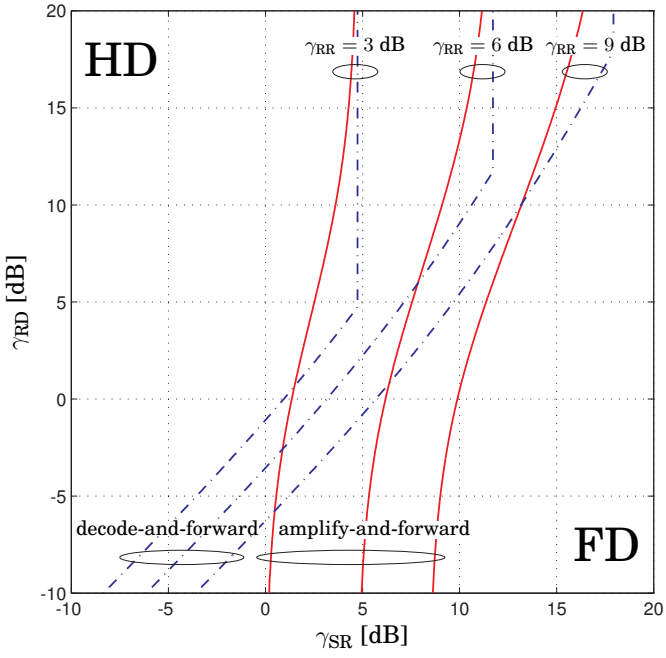

Figure 5.4. Switching boundaries Γ_{RR} between the two relaying modes when $\gamma_{SD} = 0$ and maximum transmit power is used ($p_R = 1$). The full-duplex (FD) mode is preferred over the half-duplex (HD) mode on the right hand side of the boundaries, and vice versa on the left hand side.

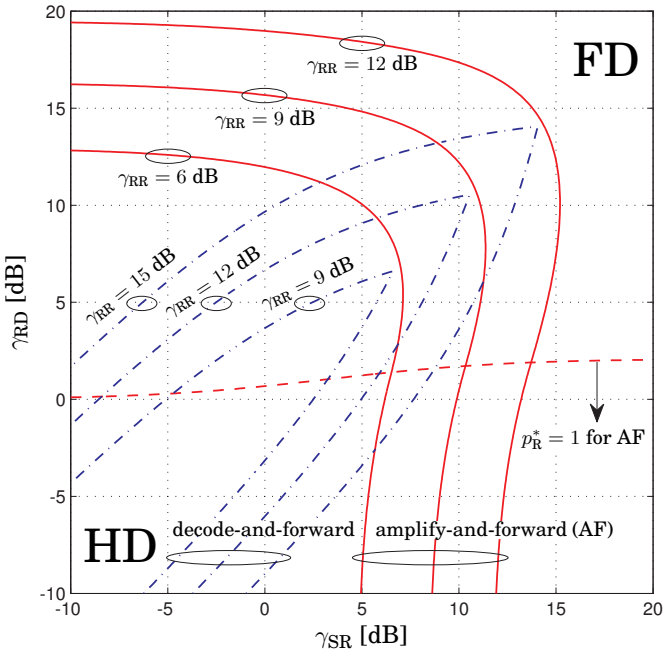

Figure 5.5. Switching boundaries Γ_{RR} between the two relaying modes when $\gamma_{SD} = 0$ and the relay transmit power is optimized ($p_R = p_R^*$). The full-duplex (FD) mode is preferred over the half-duplex (HD) mode outside the boundaries.

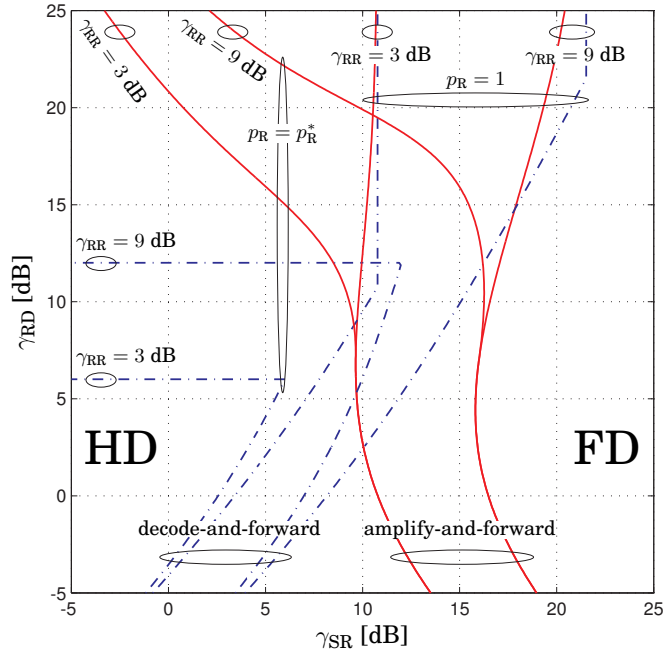

Figure 5.6. Switching boundaries between the two relaying modes when $\gamma_{SD} = 0$ and energy normalization ($p_S = p_R = 2$) is assumed for the half-duplex (HD) mode. The full-duplex (FD) mode is preferred over the HD mode outside and on the right hand side of the boundaries, and vice versa on the left hand side.

5.4 Analysis of Long-Term Performance

Proceeding to relaying over fading channels, objective shifts to optimizing long-term link capacity using statistical channel state information (CSI); downlink (DL) and uplink (UL) directions are now studied separately as they are of different nature due to asymmetry caused by setting scope on fixed relays. The key system parameters are now *average* channel SNRs: $\bar{\gamma}_{\mathrm{SR}} \triangleq \mathcal{E}\{\gamma_{\mathrm{SR}}\}$, $\bar{\gamma}_{\mathrm{RR}} \triangleq \mathcal{E}\{\gamma_{\mathrm{RR}}\}$, $\bar{\gamma}_{\mathrm{RD}} \triangleq \mathcal{E}\{\gamma_{\mathrm{RD}}\}$, and $\bar{\gamma}_{\mathrm{SD}} \triangleq \mathcal{E}\{\gamma_{\mathrm{SD}}\}$.

The base station (BS) and the relay node (RN) are assumed to be part of fixed infrastructure, and line-of-sight connection is often achieved by planning RN antenna locations properly. Thereby, it is reasonable to model the backhaul channels and the residual self-interference gain as static, i.e., $\gamma_{\mathrm{SR}} = \bar{\gamma}_{\mathrm{SR}}$ (in DL), $\gamma_{\mathrm{RD}} = \bar{\gamma}_{\mathrm{RD}}$ (in UL), and $\gamma_{\mathrm{RR}} = \bar{\gamma}_{\mathrm{RR}}$. The user equipment (UE) is assumed to be a mobile terminal without line-of-sight to the RN which justifies to conventionally model the service channels by Rayleigh fading, i.e., γ_{RD} (in DL) and γ_{SR} (in UL) become exponential random variables with probability density functions $f_{\gamma_{\mathrm{RD}}}(x) = \frac{1}{\bar{\gamma}_{\mathrm{RD}}} \exp\left(-\frac{x}{\bar{\gamma}_{\mathrm{RD}}}\right)$ and $f_{\gamma_{\mathrm{SR}}}(x) = \frac{1}{\bar{\gamma}_{\mathrm{SR}}} \exp\left(-\frac{x}{\bar{\gamma}_{\mathrm{SR}}}\right)$. Finally, scope on coverage extension implies $\bar{\gamma}_{\mathrm{SD}} \ll \bar{\gamma}_{\mathrm{RD}}$ rendering the contribution of BS–UE and UE–BS channels insignificant for average link capacity although they are intermittently useful for diversity. Thus, the following long-term performance analysis sets $\gamma_{\mathrm{SD}} \approx 0$, i.e., interference from the direct link is effectively embedded in thermal noise in FD relaying and MRC can be omitted in HD relaying.

5.4.1 Average Link Capacity

Average link capacity shall be denoted by $\bar{\mathcal{C}}_{\mathrm{FD}}$ (resp. $\bar{\mathcal{C}}_{\mathrm{HD}}$) if the fixed FD (resp. HD) mode is preselected during system design. Additional superscripts help to distinguish between different variations, e.g., $\bar{\mathcal{C}}_{\mathrm{FD}}^{\text{DL-AF}}$ means naturally the average downlink capacity of full-duplex AF relaying.

Omitting subscripts FD and HD as well as superscripts AF and DF since the following expressions look identical for these variations, downlink and uplink capacities are calculated by averaging over fading distributions as

$$\bar{\mathcal{C}}^{\mathrm{DL}} \triangleq \mathcal{E}\{\mathcal{C}(\bar{\gamma}_{\mathrm{SR}}, \gamma_{\mathrm{RD}})\} = \int_0^\infty \mathcal{C}(\bar{\gamma}_{\mathrm{SR}}, x) f_{\gamma_{\mathrm{RD}}}(x)\,\mathrm{d}x, \tag{5.20a}$$

$$\bar{\mathcal{C}}^{\mathrm{UL}} \triangleq \mathcal{E}\{\mathcal{C}(\gamma_{\mathrm{SR}}, \bar{\gamma}_{\mathrm{RD}})\} = \int_0^\infty \mathcal{C}(x, \bar{\gamma}_{\mathrm{RD}}) f_{\gamma_{\mathrm{SR}}}(x)\,\mathrm{d}x, \tag{5.20b}$$

respectively. Above $\mathcal{C}(\gamma_{\mathrm{SR}}, \gamma_{\mathrm{RD}})$ is substituted by $\mathcal{C}_{\mathrm{FD}}(\gamma_{\mathrm{SR}}, \gamma_{\mathrm{RD}})$ from (5.3a) with the FD mode and by $\mathcal{C}_{\mathrm{HD}}(\gamma_{\mathrm{SR}}, \gamma_{\mathrm{RD}})$ from (5.3b) with the HD mode; the instantaneous link SNRs are defined in (5.6)–(5.8) for AF and DF relaying.

With both relaying protocols, the average link capacity admits closed-form expressions which can be neatly presented in terms of auxiliary integrals $\mathcal{I}_{\text{AF}}$ and $\mathcal{I}_{\text{DF}}$ (or their variations) derived below; all of them are based on the exponential integral $E_1(z) = \int_z^\infty \frac{\exp(-t)}{t}\,\mathrm{d}t$ [3, Eq. 5.1.1]. The final capacity expressions are collected in Table 5.1 for concise reference.

Generic Capacity Integrals

The integral needed for the amplify-and-forward protocol is calculated with integration by parts as follows:

$$\begin{aligned}\mathcal{I}_{\text{AF}}^{\text{tail}}(a,b,c) &\triangleq \int_c^\infty \log_2\left(1+\frac{a\,x}{a+1+x}\right)\frac{\exp\left(-\frac{x}{b}\right)}{b}\,\mathrm{d}x \qquad (5.21a)\\ &= e^{\frac{1}{b}}\frac{E_1\left(\frac{c+1}{b}\right)-e^{\frac{a}{b}}E_1\left(\frac{a+c+1}{b}\right)}{\log_e(2)}-e^{-\frac{c}{b}}\log_2\left(\frac{a+c+1}{(a+1)(c+1)}\right),\end{aligned}$$

in which constants a, b, and c are real-valued and non-negative. Based on the above expression, the other two integrals are given by

$$\mathcal{I}_{\text{AF}}(a,b) = \lim_{c\to 0}\mathcal{I}_{\text{AF}}^{\text{tail}}(a,b,c) = e^{\frac{1}{b}}\frac{E_1\left(\frac{1}{b}\right)-e^{\frac{a}{b}}E_1\left(\frac{a+1}{b}\right)}{\log_e(2)}, \qquad (5.21b)$$

$$\mathcal{I}_{\text{AF}}^{\text{head}}(a,b,c) = \mathcal{I}_{\text{AF}}(a,b)-\mathcal{I}_{\text{AF}}^{\text{tail}}(a,b,c). \qquad (5.21c)$$

Similarly, integration by parts yields the integral needed for the decode-and-forward protocol as follows:

$$\begin{aligned}\mathcal{I}_{\text{DF}}^{\text{head}}(a,b,c) &\triangleq \int_0^c \log_2\left(1+\min\{a,x\}\right)\frac{\exp\left(-\frac{x}{b}\right)}{b}\,\mathrm{d}x \qquad (5.22a)\\ &= \begin{cases} e^{\frac{1}{b}}\frac{E_1\left(\frac{1}{b}\right)-E_1\left(\frac{c+1}{b}\right)}{\log_e(2)}-e^{-\frac{c}{b}}\log_2(c+1), & c\le a,\\ e^{\frac{1}{b}}\frac{E_1\left(\frac{1}{b}\right)-E_1\left(\frac{a+1}{b}\right)}{\log_e(2)}-e^{-\frac{c}{b}}\log_2(a+1), & c>a.\end{cases}\end{aligned}$$

And the other integrals are given by

$$\mathcal{I}_{\text{DF}}(a,b) = \lim_{c\to\infty}\mathcal{I}_{\text{DF}}^{\text{head}}(a,b,c) = e^{\frac{1}{b}}\frac{E_1\left(\frac{1}{b}\right)-E_1\left(\frac{a+1}{b}\right)}{\log_e(2)}, \qquad (5.22b)$$

$$\mathcal{I}_{\text{DF}}^{\text{tail}}(a,b,c) = \mathcal{I}_{\text{DF}}(a,b)-\mathcal{I}_{\text{DF}}^{\text{head}}(a,b,c). \qquad (5.22c)$$

Transmit Power Adaptation

When using statistical CSI, the relay can adapt only its long-term transmit power, i.e., $p_{\text{R}} = \bar{p}_{\text{R}}$. To obtain average link capacity without transmit power adaptation, $\bar{p}_{\text{R}} = 1$ is substituted in the expressions of Table 5.1. On the other hand, long-term power optimization is formulated as

$$\bar{p}_{\text{R}}^{*} \triangleq \arg\max_{\bar{p}_{\text{R}}} \bar{C}_{\text{FD}} \text{ subject to } \bar{p}_{\text{R}} \le 1. \qquad (5.23)$$

The concave objective function clearly has a global maximum, but it can be determined only numerically. In particular, the derivative $\frac{\mathrm{d}\bar{C}_{\text{FD}}}{\mathrm{d}\bar{p}_{\text{R}}}$ admits a closed-form expression and has exactly one root for $\bar{p}_{\text{R}} \ge 0$ which can be computed with standard numerical tools to obtain $\bar{p}_{\text{R}}^{*}$.

5.4.2 Hybrid Relaying Modes

With hybrid FD/HD relaying based on *statistical CSI*, the average link capacity becomes similar to its instantaneous counterpart from (5.15):

$$\bar{\mathcal{C}}_{\text{hybrid}} = \max\left\{\bar{\mathcal{C}}_{\text{FD}}, \bar{\mathcal{C}}_{\text{HD}}\right\} \tag{5.24}$$

for which $\bar{\mathcal{C}}_{\text{FD}}$ and $\bar{\mathcal{C}}_{\text{HD}}$ are the average link capacities derived on the previous pages and expressed in Table 5.1. The corresponding break-even residual self-interference level $\bar{\Gamma}_{\text{RR}}$ can be formally defined such that

$$\bar{\mathcal{C}}_{\text{FD}} \geq \bar{\mathcal{C}}_{\text{HD}} \text{ if and only if } \bar{\gamma}_{\text{RR}} \leq \bar{\Gamma}_{\text{RR}}. \tag{5.25}$$

Unlike hybrid FD/HD relaying based on instantaneous CSI, which is considered shortly, the present case does not admit closed-form expressions for switching conditions. Instead, a numerically-evaluated lookup table should be precalculated offline after which mode switching becomes a straightforward task based on the average channel SNRs.

To calculate the average link capacity for the reference case of hybrid FD/HD relaying based on *instantaneous CSI* by averaging $\mathcal{C}_{\text{hybrid}}$ over the fading distributions, one should first recall how the relaying mode is chosen for each channel state as explained in Section 5.3.2. In DL relaying, the determining factor is γ_{RD} such that the FD mode is used whenever $\gamma_{\text{RD}} < \chi^{\text{DL}}_{\text{hybrid}}$; the switching boundary $\chi^{\text{DL}}_{\text{hybrid}}$ is solved from (5.17) as given in Table 5.1 for both protocols ($\chi^{\text{DL-AF}}_{\text{hybrid}}$ vs. $\chi^{\text{DL-DF}}_{\text{hybrid}}$). Consequently, the average downlink capacity can be divided into two integrals as follows:

$$\begin{aligned}\bar{\mathcal{C}}^{\text{DL}}_{\text{hybrid}} &\triangleq \mathcal{E}\{\max\{\mathcal{C}_{\text{FD}}(\bar{\gamma}_{\text{SR}}, \gamma_{\text{RD}}), \mathcal{C}_{\text{HD}}(\bar{\gamma}_{\text{SR}}, \gamma_{\text{RD}})\}\} \\ &= \int_0^{\chi^{\text{DL}}_{\text{hybrid}}} \mathcal{C}_{\text{FD}}(\bar{\gamma}_{\text{SR}}, x) f_{\gamma_{\text{RD}}}(x)\,\mathrm{d}x + \int_{\chi^{\text{DL}}_{\text{hybrid}}}^{\infty} \mathcal{C}_{\text{HD}}(\bar{\gamma}_{\text{SR}}, x) f_{\gamma_{\text{RD}}}(x)\,\mathrm{d}x.\end{aligned} \tag{5.26}$$

On the contrary, γ_{SR} is the determining factor in UL relaying such that the FD mode is used if $\gamma_{\text{SR}} > \chi^{\text{UL}}_{\text{hybrid}}$ for which the switching boundary $\chi^{\text{UL}}_{\text{hybrid}}$ is solved from (5.17) as shown in Table 5.1 for both protocols ($\chi^{\text{UL-AF}}_{\text{hybrid}}$ vs. $\chi^{\text{UL-DF}}_{\text{hybrid}}$). The average uplink capacity $\bar{\mathcal{C}}^{\text{UL}}_{\text{hybrid}}$ is also calculated similarly to (5.26) by integrating over density function $f_{\gamma_{\text{SR}}}(x)$ and switching mode at $x = \chi^{\text{UL}}_{\text{hybrid}}$. As with (5.20), the capacity expressions can be compactly solved in terms of the auxiliary integrals derived on the previous page. The first (resp. second) integral in (5.26) is translated to $\mathcal{I}^{\text{head}}_{\text{AF}}$ or $\mathcal{I}^{\text{head}}_{\text{DF}}$ (resp. $\mathcal{I}^{\text{tail}}_{\text{AF}}$ or $\mathcal{I}^{\text{tail}}_{\text{DF}}$) depending on the considered protocol (AF or DF).

The final expressions of the above calculations are again collected in Table 5.1 and illustrated with numerical results in Figs. 5.7, 5.8(a), and 5.8(b). The switching boundaries χ are also reflected in what follows.

Table 5.1. Closed-form expressions for average downlink (DL) and uplink (UL) capacity with amplify-and-forward (AF) and decode-and-forward (DF) relaying. With different sub/superscripts, constants χ represent the switching points between the full-duplex (FD) and half-duplex (HD) modes and integrals $\mathcal{I}$ are given by (5.21) and (5.22).

<table>
<tr><td colspan="4">static mode selection</td></tr>
<tr><td>$\bar{\mathcal{C}}_{\text{FD}}^{\text{DL-AF}} = \mathcal{I}_{\text{AF}}\left(\frac{\bar{\gamma}_{\text{SR}}}{\bar{p}_{\text{R}}\bar{\gamma}_{\text{RR}}+1}, \bar{p}_{\text{R}}\bar{\gamma}_{\text{RD}}\right)$</td><td>$\bar{\mathcal{C}}_{\text{HD}}^{\text{DL-AF}} = \frac{1}{2}\mathcal{I}_{\text{AF}}\left(\bar{\gamma}_{\text{SR}}, \bar{\gamma}_{\text{RD}}\right)$</td><td>$\bar{\mathcal{C}}_{\text{FD}}^{\text{UL-AF}} = \mathcal{I}_{\text{AF}}\left(\bar{p}_{\text{R}}\bar{\gamma}_{\text{RD}}, \frac{\bar{\gamma}_{\text{SR}}}{\bar{p}_{\text{R}}\bar{\gamma}_{\text{RR}}+1}\right)$</td><td>$\bar{\mathcal{C}}_{\text{HD}}^{\text{UL-AF}} = \frac{1}{2}\mathcal{I}_{\text{AF}}\left(\bar{\gamma}_{\text{RD}}, \bar{\gamma}_{\text{SR}}\right)$</td></tr>
<tr><td>$\bar{\mathcal{C}}_{\text{FD}}^{\text{DL-DF}} = \mathcal{I}_{\text{DF}}\left(\frac{\bar{\gamma}_{\text{SR}}}{\bar{p}_{\text{R}}\bar{\gamma}_{\text{RR}}+1}, \bar{p}_{\text{R}}\bar{\gamma}_{\text{RD}}\right)$</td><td>$\bar{\mathcal{C}}_{\text{HD}}^{\text{DL-DF}} = \frac{1}{2}\mathcal{I}_{\text{DF}}\left(\bar{\gamma}_{\text{SR}}, \bar{\gamma}_{\text{RD}}\right)$</td><td>$\bar{\mathcal{C}}_{\text{FD}}^{\text{UL-DF}} = \mathcal{I}_{\text{DF}}\left(\bar{p}_{\text{R}}\bar{\gamma}_{\text{RD}}, \frac{\bar{\gamma}_{\text{SR}}}{\bar{p}_{\text{R}}\bar{\gamma}_{\text{RR}}+1}\right)$</td><td>$\bar{\mathcal{C}}_{\text{HD}}^{\text{UL-DF}} = \frac{1}{2}\mathcal{I}_{\text{DF}}\left(\bar{\gamma}_{\text{RD}}, \bar{\gamma}_{\text{SR}}\right)$</td></tr>
<tr><td colspan="4">hybrid FD/HD relaying</td></tr>
<tr><td colspan="2">FD if $\gamma_{\text{RD}} < \chi_{\text{hybrid}}^{\text{DL-AF}} \triangleq \frac{(\bar{\gamma}_{\text{SR}}+1)^2-\bar{\gamma}_{\text{RR}}^2}{\bar{\gamma}_{\text{RR}}^2-(\bar{\gamma}_{\text{SR}}+1)}$</td><td colspan="2">FD if $\gamma_{\text{SR}} > \chi_{\text{hybrid}}^{\text{UL-AF}} \triangleq \sqrt{\bar{\gamma}_{\text{RR}}^2(\bar{\gamma}_{\text{RD}}+1)+\frac{1}{4}\bar{\gamma}_{\text{RD}}^2} - \frac{1}{2}\bar{\gamma}_{\text{RD}} - 1$</td></tr>
<tr><td colspan="2">$\bar{\mathcal{C}}_{\text{hybrid}}^{\text{DL-AF}} = \begin{cases} \bar{\mathcal{C}}_{\text{HD}}^{\text{DL-AF}}, & \bar{\gamma}_{\text{SR}} < \bar{\gamma}_{\text{RR}} - 1 \\ \bar{\mathcal{C}}_{\text{FD}}^{\text{DL-AF}}, & \bar{\gamma}_{\text{SR}} > \bar{\gamma}_{\text{RR}}^2 - 1 \\ \mathcal{I}_{\text{AF}}^{\text{head}}\left(\frac{\bar{\gamma}_{\text{SR}}}{\bar{\gamma}_{\text{RR}}+1}, \bar{\gamma}_{\text{RD}}, \chi_{\text{hybrid}}^{\text{DL-AF}}\right) & \\ \quad + \frac{1}{2}\mathcal{I}_{\text{AF}}^{\text{tail}}\left(\bar{\gamma}_{\text{SR}}, \bar{\gamma}_{\text{RD}}, \chi_{\text{hybrid}}^{\text{DL-AF}}\right), & \text{otherwise} \end{cases}$</td><td colspan="2">$\bar{\mathcal{C}}_{\text{hybrid}}^{\text{UL-AF}} = \frac{1}{2}\mathcal{I}_{\text{AF}}^{\text{head}}\left(\bar{\gamma}_{\text{RD}}, \bar{\gamma}_{\text{SR}}, \chi_{\text{hybrid}}^{\text{UL-AF}}\right) + \mathcal{I}_{\text{AF}}^{\text{tail}}\left(\bar{\gamma}_{\text{RD}}, \frac{\bar{\gamma}_{\text{SR}}}{\bar{\gamma}_{\text{RR}}+1}, \chi_{\text{hybrid}}^{\text{UL-AF}}\right)$</td></tr>
<tr><td colspan="2">FD if $\gamma_{\text{RD}} < \chi_{\text{hybrid}}^{\text{DL-DF}} \triangleq \frac{2\bar{\gamma}_{\text{SR}}(\bar{\gamma}_{\text{RR}}+1)+\bar{\gamma}_{\text{SR}}^2}{(\bar{\gamma}_{\text{RR}}+1)^2}$</td><td colspan="2">FD if $\gamma_{\text{SR}} > \chi_{\text{hybrid}}^{\text{UL-DF}} \triangleq \begin{cases} \bar{\gamma}_{\text{RR}}^2 - 1, & \bar{\gamma}_{\text{RD}} > \bar{\gamma}_{\text{RR}}^2 - 1 \\ (\bar{\gamma}_{\text{RR}}+1)(\sqrt{\bar{\gamma}_{\text{RD}}+1}-1), & \text{otherwise} \end{cases}$</td></tr>
<tr><td colspan="2">$\bar{\mathcal{C}}_{\text{hybrid}}^{\text{DL-DF}} = \begin{cases} \bar{\mathcal{C}}_{\text{FD}}^{\text{DL-DF}}, & \bar{\gamma}_{\text{SR}} > \bar{\gamma}_{\text{RR}}^2 - 1 \\ \mathcal{I}_{\text{DF}}^{\text{head}}\left(\frac{\bar{\gamma}_{\text{SR}}}{\bar{\gamma}_{\text{RR}}+1}, \bar{\gamma}_{\text{RD}}, \chi_{\text{hybrid}}^{\text{DL-DF}}\right) & \\ \quad + \frac{1}{2}\mathcal{I}_{\text{DF}}^{\text{tail}}\left(\bar{\gamma}_{\text{SR}}, \bar{\gamma}_{\text{RD}}, \chi_{\text{hybrid}}^{\text{DL-DF}}\right), & \text{otherwise} \end{cases}$</td><td colspan="2">$\bar{\mathcal{C}}_{\text{hybrid}}^{\text{UL-DF}} = \frac{1}{2}\mathcal{I}_{\text{DF}}^{\text{head}}\left(\bar{\gamma}_{\text{RD}}, \bar{\gamma}_{\text{SR}}, \chi_{\text{hybrid}}^{\text{UL-DF}}\right) + \mathcal{I}_{\text{DF}}^{\text{tail}}\left(\bar{\gamma}_{\text{RD}}, \frac{\bar{\gamma}_{\text{SR}}}{\bar{\gamma}_{\text{RR}}+1}, \chi_{\text{hybrid}}^{\text{UL-DF}}\right)$</td></tr>
</table>

In uplink direction, the RN switches frequently between the modes with all $\bar{\gamma}_{\mathrm{SR}}$ and $\bar{\gamma}_{\mathrm{RD}}$ while downlink relaying is rather different in this perspective. The following properties show that the RN uses constantly (for all γ_{RD} and $\bar{\gamma}_{\mathrm{RD}}$) the HD mode if $\bar{\gamma}_{\mathrm{SR}}$ is below a certain level with the AF protocol and the FD mode if $\bar{\gamma}_{\mathrm{SR}}$ is above a certain level with both protocols. This is also visualized by Fig. 5.4 as a corroboration for the proofs.

Low BS–RN backhaul SNR gives an advantage for the HD mode:

- If $\gamma_{\mathrm{SR}} < \gamma_{\mathrm{RR}} - 1$ then $\mathcal{C}_{\mathrm{FD}}^{\mathrm{AF}} < \mathcal{C}_{\mathrm{HD}}^{\mathrm{AF}}$ for all γ_{RD} and $\mathcal{C}_{\mathrm{FD}}^{\mathrm{DF}} < \mathcal{C}_{\mathrm{HD}}^{\mathrm{DF}}$ whenever $\gamma_{\mathrm{RD}} > \chi_{\mathrm{hybrid}}^{\text{DL-DF}}$. Consequently, $\bar{\mathcal{C}}_{\mathrm{FD}}^{\text{DL-AF}} < \bar{\mathcal{C}}_{\mathrm{HD}}^{\text{DL-AF}}$ for all $\bar{\gamma}_{\mathrm{RD}}$ if $\bar{\gamma}_{\mathrm{SR}} < \bar{\gamma}_{\mathrm{RR}} - 1$.

The above property can be proven by substituting (5.6)–(5.8) in (5.3a) and (5.3b) with $p_{\mathrm{S}} = p_{\mathrm{R}} = 1$ and $\gamma_{\mathrm{SD}} = 0$, after which $\mathcal{C}_{\mathrm{FD}}^{\mathrm{AF}}/\mathcal{C}_{\mathrm{HD}}^{\mathrm{AF}}$ is formulated and discovered to be a monotonically decreasing function in terms of γ_{RD}. Then $\mathcal{C}_{\mathrm{FD}}^{\mathrm{AF}}/\mathcal{C}_{\mathrm{HD}}^{\mathrm{AF}} \leq \lim_{\gamma_{\mathrm{RD}} \to 0} \mathcal{C}_{\mathrm{FD}}^{\mathrm{AF}}/\mathcal{C}_{\mathrm{HD}}^{\mathrm{AF}} = 2(\gamma_{\mathrm{SR}} + 1)/(\gamma_{\mathrm{SR}} + \gamma_{\mathrm{RR}} + 1) < 1$ as a limiting case; this condition can be transformed to $\gamma_{\mathrm{SR}} < \gamma_{\mathrm{RR}} - 1$ concluding the proof for the instantaneous case. The average case follows from the fact that the instantaneous case holds for all γ_{RD}, i.e., for all fading states of the RN–UE service channel in downlink direction.

High BS–RN backhaul SNR gives an advantage for the FD mode:

- If $\gamma_{\mathrm{SR}} > \gamma_{\mathrm{RR}}^2 - 1$ then $\mathcal{C}_{\mathrm{FD}}^{\mathrm{AF}} > \mathcal{C}_{\mathrm{HD}}^{\mathrm{AF}}$ and $\mathcal{C}_{\mathrm{FD}}^{\mathrm{DF}} > \mathcal{C}_{\mathrm{HD}}^{\mathrm{DF}}$ for all γ_{RD}. Consequently, $\bar{\mathcal{C}}_{\mathrm{FD}}^{\text{DL-AF}} > \bar{\mathcal{C}}_{\mathrm{HD}}^{\text{DL-AF}}$ and $\bar{\mathcal{C}}_{\mathrm{FD}}^{\text{DL-DF}} > \bar{\mathcal{C}}_{\mathrm{HD}}^{\text{DL-DF}}$ for all $\bar{\gamma}_{\mathrm{RD}}$ if $\bar{\gamma}_{\mathrm{SR}} > \bar{\gamma}_{\mathrm{RR}}^2 - 1$.

With (5.3)–(5.8), $p_{\mathrm{S}} = p_{\mathrm{R}} = 1$ and $\gamma_{\mathrm{SD}} = 0$, one can show that $\mathcal{C}_{\mathrm{FD}}^{\mathrm{DF}}/\mathcal{C}_{\mathrm{HD}}^{\mathrm{DF}}$ is a monotonically decreasing function in terms of γ_{RD} in addition to $\mathcal{C}_{\mathrm{FD}}^{\mathrm{AF}}/\mathcal{C}_{\mathrm{HD}}^{\mathrm{AF}}$ (which is already dealt with above). With both protocols, the condition from a limiting case, namely $\mathcal{C}_{\mathrm{FD}}/\mathcal{C}_{\mathrm{HD}} \geq \lim_{\gamma_{\mathrm{RD}} \to \infty} \mathcal{C}_{\mathrm{FD}}/\mathcal{C}_{\mathrm{HD}} > 1$ with $\lim_{\gamma_{\mathrm{RD}} \to \infty} \mathcal{C}_{\mathrm{FD}} = \log_2(1 + \gamma_{\mathrm{SR}}/(\gamma_{\mathrm{RR}} + 1))$ and $\lim_{\gamma_{\mathrm{RD}} \to \infty} \mathcal{C}_{\mathrm{HD}} = \frac{1}{2}\log_2(1 + \gamma_{\mathrm{SR}})$, can be transformed to $\gamma_{\mathrm{SR}} > \gamma_{\mathrm{RR}}^2 - 1$. The instantaneous case holds for any γ_{RD} which proves the average case by rendering fading in the downlink RN–UE service channel ineffective whenever $\bar{\gamma}_{\mathrm{SR}} > \bar{\gamma}_{\mathrm{RR}}^2 - 1$.

Furthermore, the fact that always $\gamma_{\mathrm{SR}} \geq 0$ by definition (since it is a power ratio) proves the following consequence of the latter property which holds true in both downlink and uplink relaying:

- If $\gamma_{\mathrm{RR}} < 1$ then $\mathcal{C}_{\mathrm{FD}}^{\mathrm{AF}} > \mathcal{C}_{\mathrm{HD}}^{\mathrm{AF}}$ and $\mathcal{C}_{\mathrm{FD}}^{\mathrm{DF}} > \mathcal{C}_{\mathrm{HD}}^{\mathrm{DF}}$ for all γ_{SR} and γ_{RD}. Consequently, $\bar{\mathcal{C}}_{\mathrm{FD}}^{\mathrm{AF}} > \bar{\mathcal{C}}_{\mathrm{HD}}^{\mathrm{AF}}$ and $\bar{\mathcal{C}}_{\mathrm{FD}}^{\mathrm{DF}} > \bar{\mathcal{C}}_{\mathrm{HD}}^{\mathrm{DF}}$ for all $\bar{\gamma}_{\mathrm{SR}}$ and $\bar{\gamma}_{\mathrm{RD}}$ if $\bar{\gamma}_{\mathrm{RR}} < 1$.

In plain words, the FD mode is always superior to the HD mode if the power of the residual interference can be suppressed below the noise level ($\bar{\gamma}_{\mathrm{RR}} < 0$ dB). This condition could be adopted as an ultimate target for self-interference mitigation although it is difficult to achieve in reality.

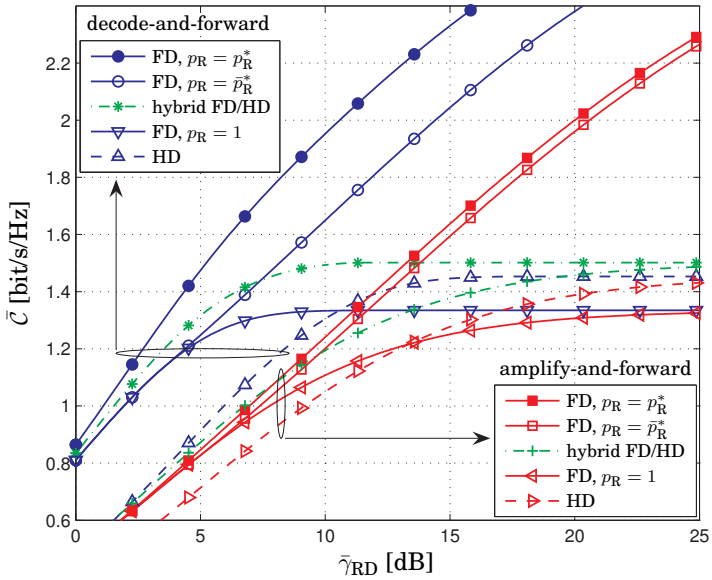

Figure 5.7. Average uplink capacities with and without transmit power optimization when $\bar{\gamma}_{SR} = 10$ dB and $\bar{\gamma}_{RR} = 6$ dB. The curves labeled as "hybrid FD/HD" represent instantaneous mode switching under maximum transmit power usage ($p_R = 1$) while the respective curves with transmit power optimization ($p_R = p_R^*$) overlap with the topmost curves labeled as "FD, $p_R = p_R^*$".

Average uplink capacity is illustrated in Fig. 5.7 after implementing the analytical expressions derived in (5.20) for conventional relaying modes and in (5.26) for hybrid FD/HD relaying as they are summarized in Table 5.1. This again verifies that hybrid mode switching gives significant performance improvement w.r.t. adhering to either conventional mode especially when transmit power adaptation is not used. With hybrid FD/HD relaying, exploiting instantaneous CSI gives the largest performance improvement w.r.t. exploiting only statistical CSI when the UE–RN service channel is approximately balanced with the RN–BS backhaul channel.

Combining hybrid FD/HD mode switching with either instantaneous or long-term transmit power adaptation gives the largest performance improvement when the backhaul channel is relatively of better quality. This is because the RN may then set transmit power lower to significantly reduce self-interference which makes full duplex the most frequently chosen mode. In this scenario, instantaneous transmit power adaptation actually renders approximately equal performance for hybrid FD/HD mode switching and static FD relaying due to the very same reason. Furthermore, the DF protocol benefits more from instantaneous transmit power adaptation than the AF protocol. Similar observations can be made also in downlink relaying although absolute performance is different in that case.

Finally, Fig. 5.8(a) illustrates the benefit of hybrid FD/HD relaying with statistical CSI w.r.t. conventional FD and HD relaying while similar comparison is shown in Fig. 5.8(b) for the case of optimal long-term power adaptation; these numerical results are again computed using the expressions of Table 5.1. In particular, switching to proper relaying mode brings up to 50% improvement in link capacity depending on the average channel SNRs. The switching boundaries are smoothed in comparison to those shown in Figs. 5.4 and 5.5 for the respective instantaneous case.

The benefit of long-term transmit power adaptation can be seen by comparing Fig. 5.8(a) to Fig. 5.8(b) in which the relay transmit power is chosen according to (5.23). Under transmit power adaptation, it is reasonable to choose the HD mode only when both the backhaul and service channels have very low SNR and otherwise switching to the FD mode improves significantly link capacity. These result plots also reflect the differences of AF and DF protocols as well as DL and UL transmission directions.

5.5 Conclusions

This chapter studied the fundamental rate–interference trade-off arising from the choice of using either a full-duplex mode or a half-duplex mode in a relay link. For this purpose, it is essential to model explicitly the effect of residual self-interference which remains inevitably in the full-duplex mode after mitigation and transmit power control. The analysis covered both common relaying protocols, namely amplify-and-forward and decode-and-forward processing, in both downlink and uplink direction.

Contrary to earlier literature which typically adheres to either mode at an early design stage, the study suggested opportunistic switching between full-duplex and half-duplex modes as a new scheme to optimize relay links' short-term and long-term capacity. The performance was further improved by transmit power adaptation in the spirit of the previous chapter; especially, its implementation was also reflected in the design of opportunistic mode switching. The analysis was conducted by deriving closed-form expressions for link capacity as well as for break-even interference levels and switching boundaries which determine the choice of one mode over the other based on channel state information. The respective numerical results illustrated that full-duplex and hybrid full-duplex/half-duplex relaying are indeed attractive techniques for infrastructure-based relay links in which the self-interference can be mitigated efficiently.

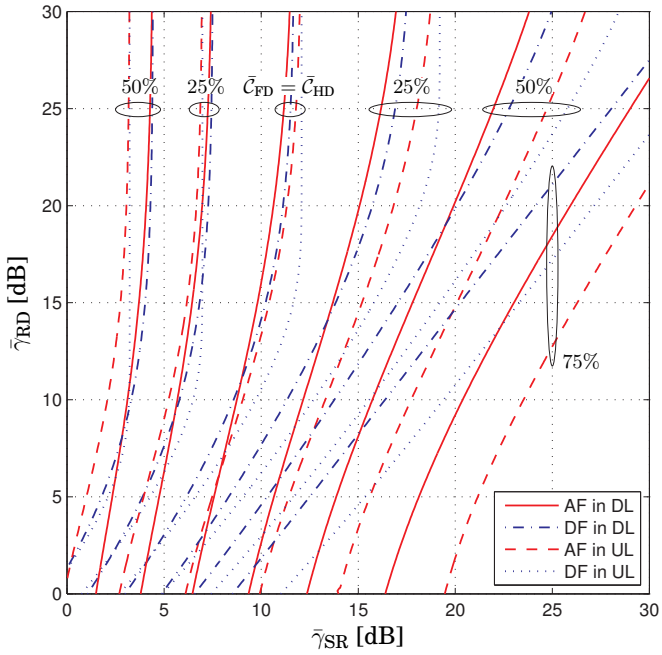

(a) when using maximum transmit power in the relay ($\bar{p}_{\mathrm{R}} = 1$)

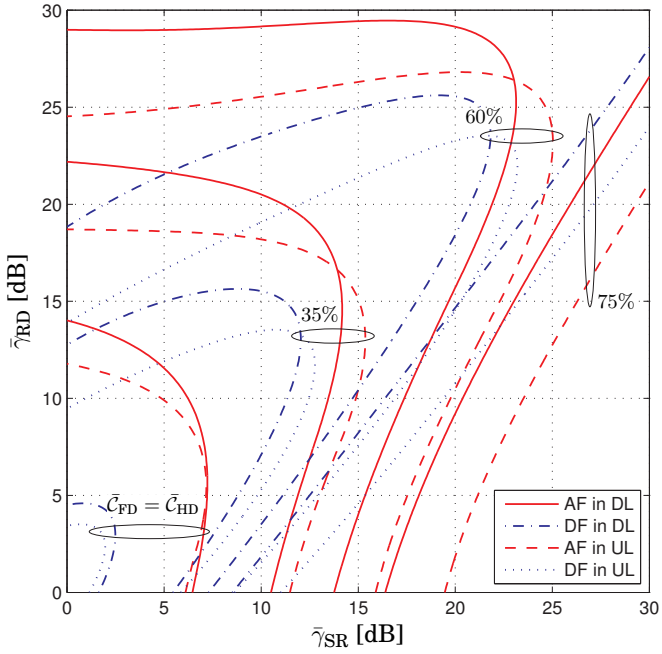

(b) when using optimized transmit power in the relay ($\bar{p}_{\mathrm{R}} = \bar{p}_{\mathrm{R}}^{*}$)

Figure 5.8. Contour plots for $(\max\{\bar{C}_{\mathrm{FD}}, \bar{C}_{\mathrm{HD}}\} / \min\{\bar{C}_{\mathrm{FD}}, \bar{C}_{\mathrm{HD}}\} - 1) \cdot 100\%$ when $\bar{\gamma}_{\mathrm{RR}} = 6$ dB. The full-duplex mode is preferred over the half-duplex mode outside and on the right hand side of the switching boundaries labeled as "$\bar{C}_{\mathrm{FD}} = \bar{C}_{\mathrm{HD}}$".

6. SINR Analysis of Multihop OFDM Repeater Links

Robustness against multipath fading is one of the main advantages of OFDM modulation, also when used in conjunction with relaying. Yet there have not been many explicit studies on the effects of multihop multipath propagation on the end-to-end system performance. In particular, a comprehensive analysis should reveal the relations between the number of hops, OFDM design parameters such as symbol and cyclic prefix duration, synchronization, time dispersion, frequency selectivity as well as inter-carrier interference (ICI) and inter-symbol interference (ISI).

The analysis of this chapter focuses on a practical time-domain amplify-and-forward (AF) protocol used for repeating OFDM signals over two or more hops. The novelty of the system setup is in assuming multipath channels for all hops. In particular, the study formulates a new analytical approach in which they are specified with clustered exponentially decaying power–delay profiles (PDPs). Consequently, the distinctive form of the effective end-to-end PDP leads to the introduction and characterization of a new "hypoexponential PDP". This allows to study delay spread and frequency correlation in the effective multihop channel and facilitates the development of a new analytical framework for evaluating the end-to-end signal-to-interference and noise ratio (SINR) of OFDM relaying.

The remainder of this chapter[1] is organized as follows. First, Section 6.1 briefly outlines the scope of the study. The main analytical results are presented in Sections 6.2 and 6.3, where the new hypoexponential power–delay profile is introduced, characterized and used for evaluating SINR in OFDM transmission. This analytical framework is then applied for the numerical performance evaluation of full-duplex repeater links with self-interference and multihop AF relaying in Sections 6.4.1 and 6.4.2, respectively. Finally, Section 6.5 summarizes the discussion.

[1]This chapter is partially based on the material presented in **[210, 216, 217]**.

6.1 Introduction

In general, OFDM transmission requires that multipath delay spread is short enough and time synchronization is realized well enough such that the channel between OFDM modulation and demodulation fits inside the guard interval. There are two particular effects which increase considerably the delay spread and frequency selectivity of the effective end-to-end channel in amplify-and-forward (AF) relaying: Firstly, a full-duplex relay link is inherently subject to recurrent echoes due to a feedback loop between relay antennas; and, secondly, each additional hop amplifies the intensity of scattering. Consequently, the increased delay spread imposes significant effect on the design of receiver time synchronization and pilot structures, and on the choice of OFDM physical-layer parameters.

Reading through the key references related to the following results as summarized in Chapter 2, it is reasonable to conclude that most physical layer aspects of multihop relay links have been studied thoroughly but only in the case of narrowband channels. In particular, the common limitation of earlier research is the assumption on flat fading, although wideband channels are in practice subject to multipath propagation. In the context of OFDM systems such as those considered herein, the earlier studies are restricted to represent a single subcarrier assuming ideal time synchronization, a long cyclic prefix, and that there is no inter-carrier interference (ICI) or inter-symbol interference (ISI). As a consequence, the earlier work is only applicable to idealistic setups.

A direct extension of previous works to cope with multipath propagation will be intractable and one would need to resort to simulations. Instead, a different approach is introduced herein by modeling the channels with power–delay profiles (PDPs) without constraining fast-fading statistics. In particular, each hop of the AF relay link is specified in terms of any clustered exponentially-decaying PDP, readily available in channel modeling literature. The cascaded end-to-end PDPs then characterize how the number of hops and loopback echoes are linked to the typical time-domain issues of OFDM transmission such as excessive delay spread, non-ideal time synchronization, and interference due to insufficient cyclic prefix duration. In a different context, the results support also the empirical model of [131, 185] proposed for certain single-hop channels with rich scattering in industrial and office environments. The approach also incorporates the effects of ICI and ISI into the analysis of OFDM transmission.

The contributions of this chapter are summarized as follows.

- The first contribution is to introduce the so-called hypoexponential PDP by generalizing the classic single-exponential PDP to the case of cascaded channels. Especially, the hypoexponential PDP is shown to be effectively a superposition of constructively and destructively combined single-exponential PDPs. From the PDP models, analytical expressions are derived for mean delay, delay spread, the lag of the strongest multipath component, frequency correlation function, and coherence bandwidth, which measure time dispersion and frequency selectivity.

- The second contribution is to derive closed-form expressions for the signal-to-interference and noise ratio (SINR) in an OFDM receiver by modifying the methodology of [263] to the case of continuous PDPs. This allows for incorporating the effects of non-ideal time synchronization in the presence of excessive delay spread which causes ICI and ISI.

- Finally, the framework is exploited in the form of numerical results for studying how to tune the gain of a cellular full-duplex gap-filler with loopback interference and for evaluating the performance of the most common synchronization strategies in a multihop relay link. This serves as a guideline for choosing the OFDM design parameters, e.g., the number of subcarriers, subcarrier spacing, and cyclic prefix duration.

In summary, these results offer a new perspective to multihop relaying which should be addressed in system design and network deployment when upgrading an existing system with multihop capabilities.

The study reveals that relay links with two or more hops and feedback echoes are of different nature than single-hop transmission due to differences in their effective end-to-end PDPs. Increased hop count drastically changes the shape of the PDP as shown by the mean delay, the delay spread, and the lag of the strongest multipath component. This affects frequency selectivity, defined by the frequency correlation function and the coherence bandwidth and, consequently, the design of wideband channel estimators and equalizers. Especially with full-duplex operation, multihop OFDM relay links have to adapt to more frequency-selective channels and they are more prone to ICI and ISI due to non-ideal time synchronization and insufficient cyclic prefix duration. These effects can be compensated by adjusting OFDM physical layer parameters and, due to decreased frequency correlation, adopting a more dense pilot structure.

6.2 Hypoexponential Power–Delay Profile

The analysis of this chapter is built on a new kind of wideband framework where non-regenerative relaying systems are characterized based on the power–delay profiles (PDPs) of their effective end-to-end multipath channels. In the following, the main building block of the framework is derived from the cascade of multiple generic wideband multipath channels, leading to the introduction of the so-called hypoexponential PDP when each of the component channels is modeled with conventional exponential decay. Finally, the new hypoexponential PDP is also analyzed by evaluating its delay-spread and frequency-correlation characteristics.

6.2.1 Amplify-and-Forward Relaying

When adopting time-domain processing (as specified in Section 2.2.5) for multihop systems such as those depicted in Figs. 2.3(f) and 2.3(g), OFDM or OFDMA relaying is implemented by an end-to-end protocol where the source node's signal is amplified and forwarded through M multipath channels between OFDM modulation and demodulation. In the following, $h_{[m]}(t)$ denotes the impulse response of the mth component channel.

The time-domain signal model between the output of OFDM modulation $x_{\mathrm{S}}(t)$ in the source node and the input of OFDM demodulation $y_{\mathrm{D}}(t)$ in the destination node can be expressed using the convolution operation ($*$) as

$$y_{\mathrm{D}}(t) = \beta\, h(t) * x_{\mathrm{S}}(t) + n(t), \tag{6.1}$$

where the impulse response of the effective end-to-end channel is

$$h(t) = h_{[1]}(t) * h_{[2]}(t) * \ldots * h_{[M]}(t) \tag{6.2}$$

and $n(t)$ denotes an aggregate thermal noise term including all noise propagated from, and amplified at, all the relays as well as that taking place in the destination receiver. Likewise, total signal amplification in all the relays can be collectively represented as a scalar factor β.

It should be noted that the concise model specified by (6.1) and (6.2) is just a building block for the generic analytical framework. It allows to characterize also complex systems, e.g., those with multiple multipath clusters or parallel relays and feedback loops due to full-duplex operation.

This chapter formulates a new framework for performance analysis in which component multipath channels, i.e., $\{h_{[m]}(t)\}_{m=1}^{M}$, are specified in terms of their power–delay profiles (PDPs), facilitating the characterization of the PDP corresponding to the effective end-to-end channel $h(t)$.

Denoting the expectation over the distribution of channel fading by $\mathcal{E}\{\cdot\}$, the PDP of channel $h_{[m]}(t)$ is defined as $P_{[m]}(t) \triangleq \mathcal{E}\{|h_{[m]}(t)|^2\}$. In particular, it can be noted that the analysis does not require one to set the complete statistics of $|h_{[m]}(t)|^2$, but the following results are valid for any type of fading, e.g., with Rayleigh, Nakagami or Rician multipath components, as long as they have zero mean and their variance is specified.

The component channels are regarded as quasi-static, i.e., they remain stationary during the transmission of each OFDM symbol. This is reasonable for real-world applications because, following good system design practices, the symbol duration is selected to be shorter than channel coherence time with expected maximum mobility level. Furthermore, all multipath components are assumed to be mutually independent, i.e., $\mathcal{E}\{h_{[m_1]}(t)\, h^*_{[m_2]}(t+\Delta t)\} = P_{[m_1]}(t)\, \delta(\Delta t)\, \delta(m_1 - m_2)$, where $\delta(\cdot)$ denotes the Dirac delta function. This conforms with Bello's wide-sense stationary uncorrelated scattering (WSSUS) model [14] which is valid for most real radio channels. Thus, the effective end-to-end PDP can be calculated as

$$P(t) \triangleq \mathcal{E}\{|h(t)|^2\} = P_{[1]}(t) * P_{[2]}(t) * \ldots * P_{[M]}(t), \tag{6.3}$$

replacing the convolution of channels in (6.2) by the convolution of PDPs.

6.2.2 Cascaded Exponential Power–Delay Profiles

The classic single-exponential PDP is defined as

$$P_1(t) \triangleq P_1(t, g_1, \tau_1, s_1) \triangleq \frac{g_1}{s_1} \exp\left(-\frac{t-\tau_1}{s_1}\right) \mathrm{U}(t-\tau_1), \tag{6.4}$$

where the unit step function $\mathrm{U}(\cdot)$ renders $P_1(t) = 0$ if $t < \tau_1$ and $P_1(t) > 0$ with $\mathrm{U}(t-\tau_1) = 1$ if $t \geq \tau_1$. The key parameters of the model are the gain $g_1 = \int_{-\infty}^{\infty} P_1(t)\,\mathrm{d}t$, the lag τ_1, mean delay $\bar{\tau}_1 = \frac{1}{g_1}\int_{-\infty}^{\infty} t\, P_1(t)\,\mathrm{d}t = s_1 + \tau_1$, and the mean square delay spread $s_1^2 = \frac{1}{g_1}\int_{-\infty}^{\infty}(t-\bar{\tau}_1)^2 P_1(t)\,\mathrm{d}t$. The frequency-correlation function (FCF) is given by the Fourier transform of the PDP as $r_1(f) \triangleq \int_{-\infty}^{\infty} P_1(t)\exp(-j2\pi f t)\,\mathrm{d}t = g_1 \exp(-j2\pi f \tau_1)/(1 + j2\pi f s_1)$.

By assuming that each component channel in (6.2) and (6.3) follows conventional (single-)exponential decay, i.e., $P_{[m]}(t) = P_1(t, g[m], \tau[m], s[m])$, and denoting the respective gain, lag and root mean square (RMS) delay spread of the mth channel by $g[m]$, $\tau[m]$ and $s[m]$, the hypoexponential power–delay profile can be finally expressed as

$$P_M(t) \triangleq P_1\left(t, g[1], \tau[1], s[1]\right) * \ldots * P_1\left(t, g[M], \tau[M], s[M]\right). \tag{6.5}$$

As a minor terminology detail, the "order" of hypoexponential decay is specified by $M \geq 1$ which corresponds to the number of hops in relaying.

For obvious analytical purposes, it is worth to seek ways to express the inconvenient multiple convolutions of (6.5) in a compact closed form as

$$P_M(t) \triangleq P_M(t, g_M, \tau_M, \{s[m]\}_{m=1}^{M}) \tag{6.6}$$

in which the total gain and the combined lag are given by

$$g_M \triangleq \int_{-\infty}^{\infty} P_M(t)\,\mathrm{d}t = \prod_{m=1}^{M} g[m] \quad \text{and} \quad \tau_M = \sum_{m=1}^{M} \tau[m], \tag{6.7}$$

respectively. Such forms also facilitate the performance analysis of OFDM transmission in the next section. The following discussion is divided into separate cases where $s[m_1] \neq s[m_2]$ or $s[m_1] = s[m_2]$ for all $m_1 \neq m_2$.

Asymmetric Delay Spread

The general case of unequal delay-spread parameters arises at practical scenarios because separate channels will never have *exactly* the same decay rate. As derived in Appendix A.2.1, if $s[m_1] \neq s[m_2]$ for all $m_1 \neq m_2$, the hypoexponential PDP can be expressed as

$$P_M(t, g_M, \tau_M, \{s[m]\}_{m=1}^{M}) = \sum_{l=1}^{M} \left(\prod_{\substack{m=1 \\ m \neq l}}^{M} \frac{s[l]}{s[l] - s[m]} \right) P_1(t, g_M, \tau_M, s[l]) \tag{6.8}$$

to get rid of the multiple convolutions in (6.5).

The hypoexponential PDP becomes effectively a weighted sum of single-exponential PDPs that interfere both constructively and destructively as noted in **[216]**. Furthermore, the form of the PDP resembles the probability density function of hypoexponential, i.e., generalized Erlang, random variables [240], hence the name. In the special case of $M = 2$, the double-exponential decay model postulated in [131, Eq. 9] and [185, Eq. 18] can be transformed into the form of (6.8) by appropriate parameter choice.

Symmetric Delay Spread

The special case of equal delay-spread parameters is useful for analytical comparisons and illustrations due to the smaller number of involved parameters. This case also facilitates analytical evaluations using readily available channel models before initiating costly and time-consuming measurement campaigns. For more compact calculations, the PDP is now reformulated to resemble the probability density function of Erlang and gamma distributed random variables [240]. If $s[m_1] = s[m_2] = s_1$ for all m_1 and m_2, the hypoexponential PDP is reduced from (6.5) to

$$P_M(t, g_M, \tau_M, \{s_1\}_{m=1}^{M}) = \frac{(t - \tau_M)^{M-1}}{s_1^{M-1}(M-1)!}\, P_1(t, g_M, \tau_M, s_1), \tag{6.9}$$

for which the details of the derivation are provided in Appendix A.2.2.

6.2.3 Delay Spread and Frequency Selectivity

In the following, a closer look shall be taken at the main characteristics of the proposed hypoexponential power–delay profile versus its order M and delay-spread parameters $\{s[m]\}_{m=1}^{M}$, including some numerical examples.

Based on (6.8), the mean delay and the root mean square (RMS) delay spread of the hypoexponential PDP can be calculated as

$$\begin{aligned}\bar{\tau}_M &= \frac{1}{g_M}\int_{-\infty}^{\infty} tP_M(t)\,\mathrm{d}t \\ &= \tau_M + \sum_{m=1}^{M} s[m], \end{aligned} \tag{6.10}$$

$$\begin{aligned}s_M &= \sqrt{\frac{1}{g_M}\int_{-\infty}^{\infty}(t-\bar{\tau}_M)^2 P_M(t)\,\mathrm{d}t} \\ &= \sqrt{2\sum_{l=1}^{M}\sum_{m=1}^{l} s[l]s[m] - \left(\sum_{l=1}^{M} s[l]\right)^2} = \sqrt{\sum_{m=1}^{M}(s[m])^2}, \end{aligned} \tag{6.11}$$

respectively. By calculating the Fourier transform of (6.8), the frequency-correlation function (FCF) of the hypoexponential PDP becomes

$$r_M(f) \triangleq \int_{-\infty}^{\infty} P_M(t)\exp(-j2\pi ft)\,\mathrm{d}t = \frac{g_M\exp(-j2\pi f\tau_M)}{\prod_{m=1}^{M}(1+j2\pi fs[m])}. \tag{6.12}$$

It should be noted that the above general expressions (6.10)–(6.12) are valid also when $s[m_1] = s[m_2]$ for some $m_1 \neq m_2$ despite the fact that such cases are excluded from the derivation of the actual PDP stated in (6.8).

Although absolute delay spread always grows with M, normalized excess delay spread is smaller with hypoexponential PDPs than with the single-exponential PDP, i.e.,

$$\frac{1}{\sqrt{M}} \leq \frac{s_M}{\bar{\tau}_M - \tau_M} = \sqrt{\frac{\sum_{m=1}^{M}(s[m])^2}{(\sum_{m=1}^{M} s[m])^2}} < \frac{s_1}{\bar{\tau}_1 - \tau_1} = 1 \tag{6.13}$$

for $M > 1$. This explains why it is appropriate to use prefix "hypo-" originating from Ancient Greek where it refers to "under" or "below". Thus, the proposed PDP could be also said to represent "sub-exponential" decay.

Figure 6.1 illustrates hypoexponential PDPs of various orders from (6.9). With symmetric delay spread, the mean delay and the RMS delay spread of the hypoexponential PDP can be simplified from (6.10) and (6.11) to

$$\bar{\tau}_M = \tau_M + M\,s_1, \tag{6.14}$$

$$s_M = \sqrt{M}\,s_1, \tag{6.15}$$

respectively, while normalized excess delay spread reaches its minimum $s_M/(\bar{\tau}_M - \tau_M) = 1/\sqrt{M}$. These relations are clearly visible also in Fig. 6.1, where the PDP is shifted to the right and stretched when M is increased.

For receiver time synchronization, it may be useful to know the lag of the strongest multipath component which is denoted by $\tau_{\max}$. Unfortunately, it can be determined in general cases only numerically from (6.5) or (6.8) but, with equal delay-spread parameters, i.e., if $s[m] = s_1$ for all m, the maximization of (6.9) admits the closed-form solution

$$\tau_{\max} \triangleq \arg\max_t P_M(t) = \tau_M + (M-1)s_1 = \bar{\tau}_M - s_1. \tag{6.16}$$

As also shown in Fig. 6.1, the first arriving multipath component with lag $\tau_{1\text{st}} = \tau_M$ is the strongest one in the case of the single-exponential PDP ($M = 1$) while, if $M \geq 2$, $P_M(\tau_{1\text{st}}) = 0$ by definition and the hypoexponential PDP contains a soft onset when $t \in [\tau_{1\text{st}}, \tau_{\max}]$. This is a significant novel property considering existing decay models at large.

After the soft onset and the arrival of the strongest multipath component, the hypoexponential PDP with $M \geq 2$ starts to decay similarly as the single-exponential PDP and $P_M(t) \to 0$ when $t \to \infty$. Analytically,

$$10\log_{10}\left(\frac{P_M(t)}{P_1(t)}\right) = 10\log_{10}\left(\frac{(g_M/g_1)\,t^{M-1}}{s_1^{M-1}(M-1)!}\right) \approx A + B\,t \ \text{[dB]} \tag{6.17}$$

when omitting excess delay by assuming $\tau[m] = 0$ for all m. Thus, decay is slower ($A > 0$ and $B > 0$) but still approximately exponential for $t > \tau_{\max}$.

In the case of symmetric delay spread, the FCF of the hypoexponential PDP reduces from (6.12) to

$$r_M(f) = \frac{g_M \exp(-j2\pi f \tau_M)}{(1 + j2\pi f s_1)^M}, \tag{6.18}$$

which is illustrated in Fig. 6.2. Based on the FCF, one can determine the 3-decibel coherence bandwidth $f_{\text{coherence}}$ which is a useful measure in OFDM system design, e.g., for choosing subcarrier spacing and frequency-domain pilot structures. It is defined in an implicit form as a solution for $|r_M(f_{\text{coherence}})| = \frac{1}{2}|r_M(0)|$, which can be calculated only numerically with the general PDP given in (6.5) or (6.8). However, with symmetric delay spread, a closed-form expression can be solved using (6.18) as

$$f_{\text{coherence}} = \frac{\sqrt{2^{2/M} - 1}}{2\pi s_1}. \tag{6.19}$$

For example in the context of Fig. 6.2, two OFDM subcarriers are subject to coherent, or approximately the same, narrowband channels if they are separated by less than 276 kHz (resp. 1.38 MHz) when the delay-spread parameter is $s_1 = 1.0$ μs (resp. 0.2 μs) for $M = 1$. The coherence bandwidth with the hypoexponential PDP of order 2, 3, 4, 5, or 6 is 58%, 44%, 37%, 33%, or 29% of that with the single-exponential PDP, respectively. Thus, frequency selectivity is seen to increase significantly.

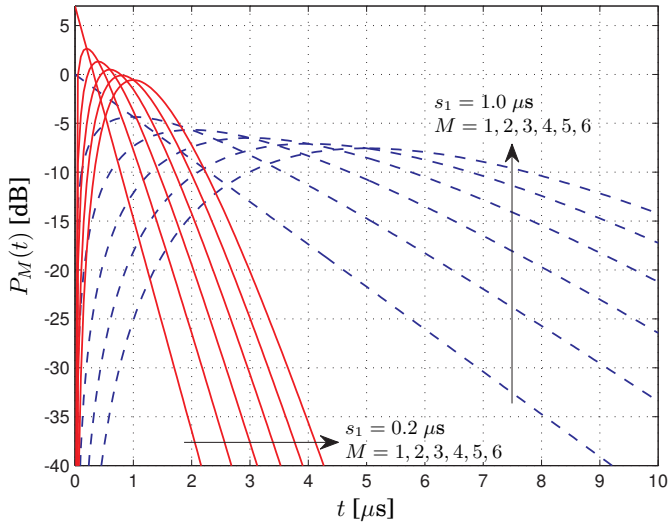

Figure 6.1. Hypoexponential power–delay profiles versus order M when $g_M = 1$, $\tau_M = 0$, and $s[m] = s_1 \in \{0.2, 1.0\}$ μs for all M and m. The corresponding frequency-correlation functions are shown below.

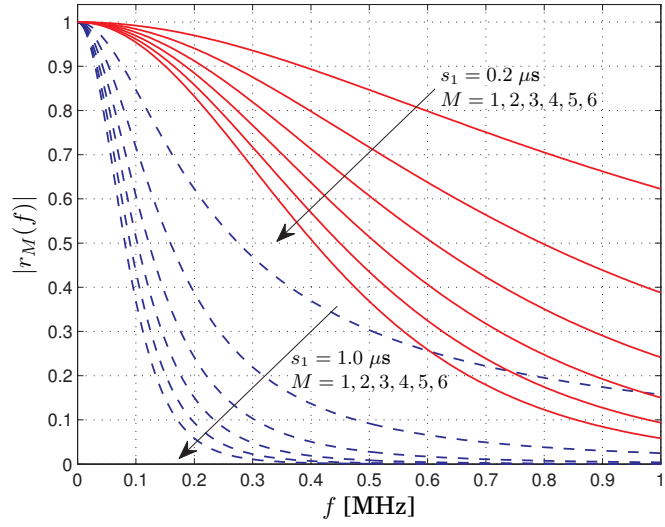

Figure 6.2. Magnitude of the frequency-correlation functions corresponding to the hypo-exponential power–delay profiles shown above with symmetric delay spread.

6.3 SINR Analysis for OFDM Transmission

As an integral application for the analytical framework where a relay link is characterized by its effective end-to-end decay profile, this section proceeds to evaluate useful signal power and interference power as well as signal-to-interference and noise ratio (SINR) when a standard OFDM signal is transmitted over a channel specified by the hypoexponential PDP. This result already corresponds as such to a basic multihop relay link where each hop comprises a single multipath cluster or to a single-hop system with rich scattering studied in [131, 185], and related numerical results are available in Fig. 5 of **[217]**. However, the following expressions are developed herein, to start with, mainly as a tool for the evaluation of generic relaying systems while the next section specializes on two key applications for this framework: a full-duplex repeater link with a feedback loop and a multihop link with clustered scattering at each hop.

In what follows, the main focus is on the effects of multipath delay spread and imperfect time synchronization, both of which are linked to the effective end-to-end PDP and can be quantified in terms of inter-carrier interference (ICI) and inter-symbol interference (ISI). Hence, other non-idealities typically associated with OFDM are beyond the scope of this chapter, e.g., interference and distortion are also caused by carrier frequency offset, in-phase/quadrature (I/Q) imbalance, oscillator phase noise, channel estimation error, analog-to-digital/digital-to-analog (AD/DA) conversion imperfections, and power amplifier (PA) nonlinearity; the author of this thesis has contributed to their study elsewhere **[81, 174, 212]**.

The SINR of the generic OFDM link formulated in (6.1) is defined as

$$\gamma \triangleq \frac{P_{\mathrm{U}}}{P_{\mathrm{ICI}} + P_{\mathrm{ISI}} + P_{\mathrm{N}}} = \frac{P_{\mathrm{U}}}{P_{\mathrm{I}} + P_{\mathrm{N}}}, \tag{6.20}$$

in which P_{U}, $P_{\mathrm{I}} \triangleq P_{\mathrm{ICI}} + P_{\mathrm{ISI}}$, and $P_{\mathrm{N}} \triangleq \mathcal{E}\{|n(t)|^2\}$ represent the useful signal power, the interference (both ICI and ISI) power, and the total noise power, respectively. Denoting the transmitted power by $P_{\mathrm{S}} \triangleq \mathcal{E}\{|x_{\mathrm{S}}(t)|^2\}$, the total received power at the destination can be calculated from (6.1) as

$$P_{\mathrm{D}} \triangleq \mathcal{E}\{|y_{\mathrm{D}}(t)|^2\} = \beta^2 P_{\mathrm{S}} \int_{-\infty}^{\infty} P(t)\,\mathrm{d}t + P_{\mathrm{N}}. \tag{6.21}$$

For SINR evaluation, this aggregate term needs to be split into parts as

$$P_{\mathrm{D}} = P_{\mathrm{U}} + P_{\mathrm{ICI}} + P_{\mathrm{ISI}} + P_{\mathrm{N}}, \tag{6.22}$$

or simply as $P_{\mathrm{D}} - P_{\mathrm{N}} = P_{\mathrm{U}} + P_{\mathrm{I}}$ if the different sources of interference do not need to be identified separately for any other analytical reason.

The methodology for determining P_{U}, P_{ICI}, and P_{ISI} from $P(t)$ in the case of OFDM transmission can be adopted from the single-hop studies of [263]. A variation of the same approach is used also in [30]. In this analytical framework, the power of all multipath components is divided into useful and interference portions based on their delays according to a weighting function which is denoted by $w(\cdot)$ in the following. The most central OFDM physical-layer parameters in this context are T_{FFT} and T_{CP} denoting the length of the fast Fourier transform (FFT) and the length of the cyclic prefix (CP), respectively. Thus, the total duration of each OFDM symbol becomes $T_{\mathrm{CP}} + T_{\mathrm{FFT}}$. As pertinently, time synchronization in the destination is parametrized by the time of reference (TOR), τ_{TOR}, marking the relative time instant for the start of symbol demodulation.

The weighting function, originally formulated in [263, Eq. A2] using a set of if-clauses, can be expressed in a compact form as

$$w(t) = \max\left\{0, \min\left\{1, \frac{t-\tau_{\mathrm{a}}}{T_{\mathrm{FFT}}}, \frac{\tau_{\mathrm{d}}-t}{T_{\mathrm{FFT}}}\right\}\right\}, \tag{6.23}$$

which is also illustrated in Fig. 6.3. In particular, the four breakpoints of this five-part piecewise linear function are defined as

$$\tau_{\mathrm{a}} \triangleq \tau_{\mathrm{TOR}} - T_{\mathrm{FFT}}, \tag{6.24a}$$

$$\tau_{\mathrm{b}} \triangleq \tau_{\mathrm{TOR}}, \tag{6.24b}$$

$$\tau_{\mathrm{c}} \triangleq \tau_{\mathrm{TOR}} + T_{\mathrm{CP}}, \tag{6.24c}$$

$$\tau_{\mathrm{d}} \triangleq \tau_{\mathrm{TOR}} + T_{\mathrm{CP}} + T_{\mathrm{FFT}}. \tag{6.24d}$$

For understanding the effect of time synchronization below, it is useful to especially note at this point that changing τ_{TOR} only shifts the weighting function while its shape remains intact.

In general terms, the weighting approach quantifies how the useful contribution of a multipath component, arriving at time instant t with average gain $P(t)$, decreases gradually due to loss of orthogonality between

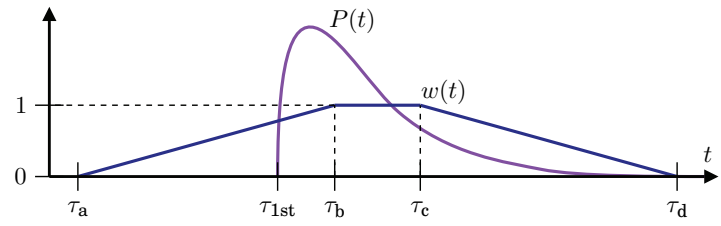

Figure 6.3. The time-domain weighting function with an example PDP. The breakpoints τ_{a}, τ_{b}, τ_{c}, and τ_{d} are determined by the time of reference τ_{TOR} and the OFDM physical-layer parameters T_{FFT} and T_{CP} according to (6.24a)–(6.24d).

subcarriers and between consecutive OFDM symbols when it is received too early ($t < \tau_\mathrm{b}$) or too late ($t > \tau_\mathrm{c}$) w.r.t. the CP interval. For instance, the FFT is calculated for the window $[\tau_\mathrm{TOR} + T_\mathrm{CP}, \tau_\mathrm{TOR} + T_\mathrm{CP} + T_\mathrm{FFT}]$ and all multipath components that have delays in the window $[\tau_\mathrm{TOR}, \tau_\mathrm{TOR} + T_\mathrm{CP}]$, i.e., within the CP, contribute to useful power without ICI or ISI because the corresponding signal echoes remain ideal sinusoids over the whole FFT duration. Thus, $w(t) = 1$ for $t \in [\tau_\mathrm{b}, \tau_\mathrm{c}]$.

As emphasized in Fig. 6.3, the delay spread of effective multipath channels under consideration is, however, typically longer than the duration of the CP. Thus, time synchronization has an important role in balancing the effects of the onset and tail of the channel, both of which cause ICI and ISI, by controlling the TOR which defines the position of the weighting window relatively to the PDP model.

In mathematical terms, the useful received signal power in OFDM transmission can be determined as

$$P_\mathrm{U} = \beta^2 P_\mathrm{S} \int_{-\infty}^{\infty} [w(t)]^2 P(t)\,\mathrm{d}t, \tag{6.25}$$

and the interference component powers are given by

$$\begin{aligned} P_\mathrm{ICI} &= \beta^2 P_\mathrm{S} \int_{-\infty}^{\infty} w(t)[1 - w(t)]P(t)\,\mathrm{d}t \\ &= \beta^2 P_\mathrm{S} \int_{-\infty}^{\infty} w(t)P(t)\,\mathrm{d}t - P_\mathrm{U}, \end{aligned} \tag{6.26a}$$

$$P_\mathrm{ISI} = \beta^2 P_\mathrm{S} \int_{-\infty}^{\infty} [1 - w(t)]P(t)\,\mathrm{d}t. \tag{6.26b}$$

By combining (6.26a) and (6.26b) when ICI and ISI do not need to be separated, the total received interference power follows as

$$P_\mathrm{I} = \beta^2 P_\mathrm{S} \int_{-\infty}^{\infty} (1 - [w(t)]^2)P(t)\,\mathrm{d}t = (P_\mathrm{D} - P_\mathrm{N}) - P_\mathrm{U}. \tag{6.27}$$

The above expressions are obtained by extending the discrete-case derivation of [263, Eqs. 10–12] to the case of continuous PDPs. In particular, the summations of [263] can be transformed to integrals by interpreting them in the context of Riemann integration, which is well justified and yields accurate results since the number of OFDM subcarriers is typically large.

In the following, P_U is computed from (6.25) assuming transmission over the hypoexponential PDP. Thus, $\int_{-\infty}^{\infty} P(t)\,\mathrm{d}t = g_M$ by definition and

$$P_\mathrm{D} - P_\mathrm{N} = \beta^2 g_M P_\mathrm{S}. \tag{6.28}$$

Finally, SINR can be evaluated without (6.26a), (6.26b) or (6.27) as

$$\gamma = \frac{P_\mathrm{U}}{\beta^2 g_M P_\mathrm{S} - P_\mathrm{U} + P_\mathrm{N}}, \tag{6.29}$$

although P_ICI, P_ISI and P_I would admit closed-form expressions like P_U.

The analysis begins from the special case of equal delay-spread parameters and then generalizes the result for the case of unequal delay-spread parameters, which actually simplifies the expressions.

Symmetric Delay Spread

The integral (6.25) is first solved assuming $P(t) = P_M(t, g_M, \tau_M, \{s_1\}_{m=1}^{M})$ as per (6.9). If $s[m_1] = s[m_2] = s_1$ for all m_1 and m_2, the useful signal power in OFDM transmission over the hypoexponential PDP is given by

$$P_{\mathrm{U}} = \beta^2 P_{\mathrm{S}}\, \mathcal{I}_{\mathrm{SINR}}(M, g_M, \tau_M, s_1), \tag{6.30}$$

where $\mathcal{I}_{\mathrm{SINR}}$ is an SINR integral obtained by substituting (6.4) and (6.9) into (6.25). Changing the integration variable to $x = \frac{t-\tau_M}{s_1}$ yields

$$\mathcal{I}_{\mathrm{SINR}}(M, g, \tau, s) \triangleq \frac{g}{(M-1)!} \int_0^{\infty} [w(s\,x + \tau)]^2 x^{M-1} \exp(-x)\,\mathrm{d}x, \tag{6.31}$$

where the integration interval begins from zero since $P_M(t) = 0$ for $t < \tau_M$.

After denoting $\tilde{\tau}_{\mathtt{a}} = \frac{\tau_{\mathtt{a}}-\tau}{s}$, $\tilde{\tau}_{\mathtt{b}} = \frac{\tau_{\mathtt{b}}-\tau}{s}$, $\tilde{\tau}_{\mathtt{c}} = \frac{\tau_{\mathtt{c}}-\tau}{s}$, and $\tilde{\tau}_{\mathtt{d}} = \frac{\tau_{\mathtt{d}}-\tau}{s}$ for compressing notation, the above expression can be separated into three sub-integrals according to the different parts of the piecewise linear weighting function $w(\cdot)$, given in (6.23), as follows:

$$\begin{aligned}
&\mathcal{I}_{\mathrm{SINR}}(M, g, \tau, s) \\
&= \frac{g\,s^2}{(M-1)!\,T_{\mathtt{FFT}}^2} \int_{\max\{0,\tilde{\tau}_{\mathtt{a}}\}}^{\tilde{\tau}_{\mathtt{b}}} (x - \tilde{\tau}_{\mathtt{a}})^2 x^{M-1} \exp(-x)\,\mathrm{d}x\, \mathrm{U}(\tilde{\tau}_{\mathtt{b}}) \\
&\quad + \frac{g}{(M-1)!} \int_{\max\{0,\tilde{\tau}_{\mathtt{b}}\}}^{\tilde{\tau}_{\mathtt{c}}} x^{M-1} \exp(-x)\,\mathrm{d}x\, \mathrm{U}(\tilde{\tau}_{\mathtt{c}}) \\
&\quad + \frac{g\,s^2}{(M-1)!\,T_{\mathtt{FFT}}^2} \int_{\max\{0,\tilde{\tau}_{\mathtt{c}}\}}^{\tilde{\tau}_{\mathtt{d}}} (x - \tilde{\tau}_{\mathtt{d}})^2 x^{M-1} \exp(-x)\,\mathrm{d}x\, \mathrm{U}(\tilde{\tau}_{\mathtt{d}}).
\end{aligned} \tag{6.32}$$

Firstly, the middle integral can be directly expressed with the upper incomplete gamma function [3, Eq. 6.5.3] which is defined as

$$\Gamma(M, b) \triangleq \int_b^{\infty} x^{M-1} \exp(-x)\,\mathrm{d}x. \tag{6.33}$$

Secondly, the other two integrals are of equivalent form, and they are expressed using an auxiliary function Ψ which can be written by expanding the second-order polynomial as

$$\begin{aligned}
\Psi(M, a, b) &\triangleq \int_b^{\infty} (x-a)^2 x^{M-1} \exp(-x)\,\mathrm{d}x \\
&= \int_b^{\infty} \left(x^{M+1} - 2a\,x^M + a^2\,x^{M-1}\right) \exp(-x)\,\mathrm{d}x \\
&= \Gamma(M+2, b) - 2a\,\Gamma(M+1, b) + a^2\,\Gamma(M, b),
\end{aligned} \tag{6.34}$$

where the last form exploits again the upper incomplete gamma function.

Consequently, the definite integrals are solved based on the elementary rule $\int_b^c f(x)\,\mathrm{d}x = \int_b^\infty f(x)\,\mathrm{d}x - \int_c^\infty f(x)\,\mathrm{d}x$. It can be also noted that

$$\Psi\left(M-2,0,b\right) = \Gamma(M,b), \tag{6.35}$$

which allows for aesthetically representing the middle integral using the same auxiliary function although $\Gamma(M,b)$ is of course simpler than (6.34).

The SINR integral can be now stated in a compact closed form as

$$\begin{aligned}
&\mathcal{I}_{\text{SINR}}(M,g,\tau,s)\\
&= \frac{g\,s^2}{(M-1)!\,T_{\text{FFT}}^2}\left[\Psi\left(M,\tilde{\tau}_{\mathtt{a}},\max\{0,\tilde{\tau}_{\mathtt{a}}\}\right) - \Psi\left(M,\tilde{\tau}_{\mathtt{a}},\tilde{\tau}_{\mathtt{b}}\right)\right]\mathrm{U}(\tilde{\tau}_{\mathtt{b}})\\
&\quad + \frac{g}{(M-1)!}\left[\Psi\left(M-2,0,\max\{0,\tilde{\tau}_{\mathtt{b}}\}\right) - \Psi\left(M-2,0,\tilde{\tau}_{\mathtt{c}}\right)\right]\mathrm{U}(\tilde{\tau}_{\mathtt{c}})\\
&\quad + \frac{g\,s^2}{(M-1)!\,T_{\text{FFT}}^2}\left[\Psi\left(M,\tilde{\tau}_{\mathtt{d}},\max\{0,\tilde{\tau}_{\mathtt{c}}\}\right) - \Psi\left(M,\tilde{\tau}_{\mathtt{d}},\tilde{\tau}_{\mathtt{d}}\right)\right]\mathrm{U}(\tilde{\tau}_{\mathtt{d}}),
\end{aligned} \tag{6.36}$$

in which $\tilde{\tau}_{\mathtt{a}} = \frac{\tau_{\mathtt{a}}-\tau}{s}$, $\tilde{\tau}_{\mathtt{b}} = \frac{\tau_{\mathtt{b}}-\tau}{s}$, $\tilde{\tau}_{\mathtt{c}} = \frac{\tau_{\mathtt{c}}-\tau}{s}$, and $\tilde{\tau}_{\mathtt{d}} = \frac{\tau_{\mathtt{d}}-\tau}{s}$.

Finally, the useful signal power P_{U} is given by (6.30) with the substitution of (6.33)–(6.36) and SINR can be evaluated using (6.29).

Asymmetric Delay Spread

In the general case of unequal delay spread parameters, (6.25) needs to be solved with the substitution of $P(t) = P_M(t, g_M, \tau_M, \{s[m]\}_{m=1}^M)$ as per (6.8). If $s[m_1] \neq s[m_2]$ for all $m_1 \neq m_2$, the useful signal power in OFDM transmission over the hypoexponential PDP becomes

$$P_{\mathrm{U}} = \beta^2 P_{\mathrm{S}} \sum_{l=1}^{M}\left(\prod_{\substack{m=1\\m\neq l}}^{M}\frac{s[l]}{s[l]-s[m]}\right)\mathcal{I}_{\text{SINR}}(1,g_M,\tau_M,s[l]), \tag{6.37}$$

for which the SINR integral $\mathcal{I}_{\text{SINR}}$ is given by (6.36) with the substitution of (6.33)–(6.35). However, a simplified form of $\mathcal{I}_{\text{SINR}}$ without the incomplete gamma function is available when $M = 1$ in (6.34) as shown below.

In particular, $\Psi(M,a,b)$ appearing in $\mathcal{I}_{\text{SINR}}(M,g,\tau,s)$ can be simplified considerably when $M = 1$. Firstly, the identity [80, Eq. 8.352.4] shows that $\Gamma(M,b) = (M-1)!\exp(-b)\sum_{m=0}^{M-1}\frac{b^m}{m!}$ for all integers $M \geq 1$, yielding

$$\begin{aligned}
&\Psi\left(M,a,b\right) \qquad\qquad (6.38)\\
&= \left[(M+1)!\sum_{m=0}^{M+1}\frac{b^m}{m!} - 2aM!\sum_{m=0}^{M}\frac{b^m}{m!} + a^2(M-1)!\sum_{m=0}^{M-1}\frac{b^m}{m!}\right]\exp(-b).
\end{aligned}$$

This could be useful in the above special case of symmetric delay spread as well. However, when setting $M = 1$, (6.34) used in (6.36) becomes

$$\Psi\left(1,a,b\right) = \left[1+(1-a+b)^2\right]\exp(-b), \tag{6.39}$$

and $\Psi\left(-1,0,b\right) = \Gamma(1,b) = \exp(-b)$ replacing (6.33) and (6.35).

6.4 Performance Evaluation

In this section, the analytical PDP and SINR framework is applied for case studies on two key amplify-and-forward systems where the delay spread of effective end-to-end channels is pronounced: The first subsection considers full-duplex repeater links with self-interference and the second subsection focuses on multihop scenarios with increasing number of relays in series. In both case studies, the analytical results of the previous sections are first translated into the scope of the respective example systems after which discussions are illustrated with numerical results.

6.4.1 Full-Duplex OFDM Repeater Links

The effective end-to-end multipath channels of full-duplex repeater links are spread intensively due to feedback loops which cause an infinite sequence of echoing multipath clusters. After introducing the system model considered in this case study and deriving corresponding closed-form PDP and SINR expressions, the following analysis explains the relations between repeater gain control, loopback channel isolation, multipath delay spread, and resulting end-to-end performance after OFDM demodulation.

System Setup

The two-hop OFDM system consists of a source (S) node, a repeater (R) node with separate receive and transmit antennas, and a destination (D) node as shown by Fig. 6.4. The repeater amplifies-and-forwards its input time-domain signal waveform such that the same frequency band is used for both receiving and transmitting. This full-duplex operation causes a feedback loop from the output of the repeater to its input limiting the maximum usable amplification factor. However, in contrast with earlier

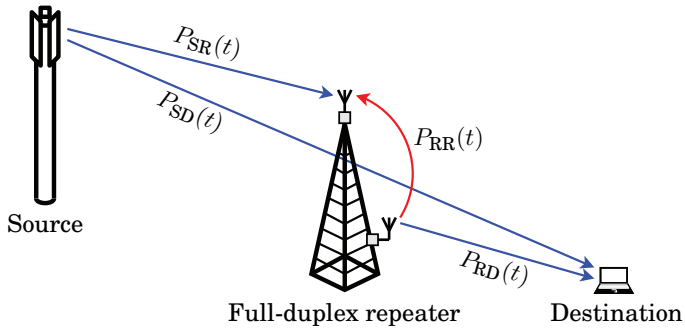

Figure 6.4. Full-duplex repeater link with a feedback loop where $P_{\mathrm{SR}}(t)$, $P_{\mathrm{RD}}(t)$, $P_{\mathrm{RR}}(t)$, and $P_{\mathrm{SD}}(t)$ denote the power–delay profiles (PDPs) of the multipath channels.

chapters, the feedback signal is not pure self-interference, but its effect is manifested indirectly due to finite cyclic prefix (CP) duration.

The study considers communication using a standard OFDM signal, which is parametrized with the length of the fast Fourier transform (FFT) represented by T_{FFT} and the length of the cyclic prefix represented by T_{CP}. Thus, the total duration of each OFDM symbol is $T_{\mathrm{CP}} + T_{\mathrm{FFT}}$. Specifying the absolute signal bandwidth or the number of subcarriers is not needed or relevant for the following analysis, but both of them are assumed to be large which is typical for wideband systems.

The main focus is on studying the effect of multipath delay spread due to the repeater feedback loop. Thus, frequency synchronization and channel estimation are assumed to be accurate. Furthermore, the channel coherence times are reasonably longer than the symbol duration, due to which the channels can be regarded as static. Thereby, the multipath components that are spread outside the CP are the only significant source of inter-carrier and inter-symbol interference (ICI and ISI).

The concurrent end-to-end full-duplex operation takes place as follows.

The source starts transmitting each OFDM symbol at normalized time instant $t = 0$, broadcasting it using power P_{S} to both the repeater and the destination. After corresponding wireless channels, the powers of thermal noise components induced into the received signals are denoted by σ^2_{R} and σ^2_{D}, respectively.

The repeater amplifies-and-forwards the simultaneously received input signal sample-by-sample with factor β causing processing delay τ_{R}; fixing β^2 sets the repeater transmit power P_{R} and vice versa. The repeater gain response can be equivalently expressed as $\beta^2\delta(t - \tau_{\mathrm{R}})$.

The destination demodulates the superposition of signals received from both the source and the repeater. Synchronization is parametrized by the time of reference (TOR) represented by τ_{TOR}, which marks the start OFDM symbol demodulation. Thus, the received signal is discarded during the CP interval $[\tau_{\mathrm{TOR}}, \tau_{\mathrm{TOR}} + T_{\mathrm{CP}}]$ and the FFT is calculated for the interval $[\tau_{\mathrm{TOR}} + T_{\mathrm{CP}}, \tau_{\mathrm{TOR}} + T_{\mathrm{CP}} + T_{\mathrm{FFT}}]$.

In summary, the system consists of four wireless channels: source-to-relay (SR), relay-to-destination (RD), and source-to-destination (SD) feed-forward channels plus a relay-to-relay (RR) feedback channel. The respective total channel gains, which include all individual multipath components, are denoted by G_{SR}, G_{RD}, G_{SD}, and G_{RR}.

End-to-End Power–Delay Profile

In the spirit of the new analytical framework developed in this chapter, every multipath channel of the system is characterized by specifying its power–delay profile (PDP). In particular, the individual channels are modeled as clustered single-exponential PDPs for feedforward propagation and an impulse PDP for approximating direct line-of-sight (LOS) feedback coupling, which makes the effective end-to-end PDP a "super-clustered" hypoexponential PDP comprising uncountably many clusters of multipath clusters. The end-to-end PDP, denoted by $P(t)$, is shortly derived from the individual PDPs, namely $P_{\mathrm{SR}}(t)$, $P_{\mathrm{RD}}(t)$, $P_{\mathrm{SD}}(t)$, and $P_{\mathrm{RR}}(t)$ shown in Fig. 6.4, which are specified below to start with.

With obvious subscripts, the PDPs of the feedforward channels are assumed to have K_{SR}, K_{RD}, and K_{SD} single-exponential multipath clusters:

$$P_{\mathrm{SR}}(t) = \sum_{i=1}^{K_{\mathrm{SR}}} P_1\left(t, g_{\mathrm{SR}}[i], \tau_{\mathrm{SR}}[i], s_{\mathrm{SR}}[i]\right), \tag{6.40a}$$

$$P_{\mathrm{RD}}(t) = \sum_{j=1}^{K_{\mathrm{RD}}} P_1\left(t, g_{\mathrm{RD}}[j], \tau_{\mathrm{RD}}[j], s_{\mathrm{RD}}[j]\right), \tag{6.40b}$$

$$P_{\mathrm{SD}}(t) = \sum_{k=1}^{K_{\mathrm{SD}}} P_1\left(t, g_{\mathrm{SD}}[k], \tau_{\mathrm{SD}}[k], s_{\mathrm{SD}}[k]\right), \tag{6.40c}$$

for which $P_1(t, g, \tau, s)$ is given by (6.4). Parameters $\{g_{\mathrm{SR}}[i]\}_{i=1}^{K_{\mathrm{SR}}}$, $\{g_{\mathrm{RD}}[j]\}_{j=1}^{K_{\mathrm{RD}}}$, and $\{g_{\mathrm{SD}}[k]\}_{k=1}^{K_{\mathrm{SD}}}$ denote the gains of the individual clusters and, thereby, the total gains of the respective channels become

$$G_{\mathrm{SR}} = \sum_{i=1}^{K_{\mathrm{SR}}} g_{\mathrm{SR}}[i], \quad G_{\mathrm{RD}} = \sum_{j=1}^{K_{\mathrm{RD}}} g_{\mathrm{RD}}[j], \quad \text{and} \quad G_{\mathrm{SD}} = \sum_{k=1}^{K_{\mathrm{SD}}} g_{\mathrm{SD}}[k]. \tag{6.41}$$

The lag parameters $\{\tau_{\mathrm{SR}}[i]\}_{i=1}^{K_{\mathrm{SR}}}$, $\{\tau_{\mathrm{RD}}[j]\}_{j=1}^{K_{\mathrm{RD}}}$, and $\{\tau_{\mathrm{SD}}[k]\}_{k=1}^{K_{\mathrm{SD}}}$ incorporate the total over-the-air propagation times as well as the delay spread between the clusters. Last but not least, parameters $\{s_{\mathrm{SR}}[i]\}_{i=1}^{K_{\mathrm{SR}}}$, $\{s_{\mathrm{RD}}[j]\}_{j=1}^{K_{\mathrm{RD}}}$, and $\{s_{\mathrm{SD}}[k]\}_{k=1}^{K_{\mathrm{SD}}}$ define the root mean square delay spread of each individual single-exponential multipath cluster.

The PDP of the feedback channel from the repeater output to the repeater input is approximated to be impulse-like. In particular, the residual loop interference channel after imperfect cancellation is modeled as a single channel tap with gain G_{RR} and delay τ_{RR}:

$$P_{\mathrm{RR}}(t) = G_{\mathrm{RR}}\, \delta(t - \tau_{\mathrm{RR}}), \tag{6.42}$$

where $\delta(\cdot)$ denotes the unit impulse function. This model is reasonably practical, because the main source of self-interference is the direct coupling between the directive transmit and receive antennas.

The effective end-to-end PDP of the complete system can be divided as

$$P(t) = P_{\mathrm{SD}}(t) + P_{\mathrm{SRD}}(t), \tag{6.43}$$

for which the PDP of the direct link, $P_{\mathrm{SD}}(t)$, is given by (6.40c) and the PDP of the two-hop repeater link, $P_{\mathrm{SRD}}(t)$, can be derived as follows.

By combining the channel PDPs, i.e., $P_{\mathrm{SR}}(t)$, $P_{\mathrm{RD}}(t)$, and $P_{\mathrm{RR}}(t)$, with the effective repeater response, i.e., $\beta^2\delta(t-\tau_{\mathrm{R}})$, one may deduce that

$$P_{\mathrm{SRD}}(t) = \beta^2 P_{\mathrm{SR}}(t) * \delta(t-\tau_{\mathrm{R}}) * P_{\mathrm{RR}}^{(\infty)}(t) * P_{\mathrm{RD}}(t), \tag{6.44}$$

where $P_{\mathrm{RR}}^{(\infty)}(t) \triangleq \lim_{n\to\infty} P_{\mathrm{RR}}^{(n)}(t)$ stressing the fact that the number of echoes becomes infinite due to the repeater-to-repeater feedback loop. In particular, $P_{\mathrm{RR}}^{(n)}(t)$ denotes the PDP of a subsystem, where a signal circulates n times through $P_{\mathrm{RR}}(t)$, and it can be defined recursively as

$$\begin{aligned} P_{\mathrm{RR}}^{(0)}(t) &= \delta(t), \\ P_{\mathrm{RR}}^{(n)}(t) &= \delta(t) + \beta^2 P_{\mathrm{RR}}(t) * \delta(t-\tau_{\mathrm{R}}) * P_{\mathrm{RR}}^{(n-1)}(t). \end{aligned} \tag{6.45}$$

The calculation of the convolutions with (6.40a), (6.40b), and (6.42) yields

$$P_{\mathrm{SRD}}(t) = \sum_{n=0}^{\infty} \sum_{i=1}^{K_{\mathrm{SR}}} \sum_{j=1}^{K_{\mathrm{RD}}} P_2(t, g_2^{(n)}[i,j], \tau_2^{(n)}[i,j], \{s_{\mathrm{SR}}[i], s_{\mathrm{RD}}[j]\}), \tag{6.46}$$

where the gain and lag of an end-to-end multipath component become

$$g_2^{(n)}[i,j] = g_{\mathrm{SR}}[i]\,\beta^2\left(\beta^2 G_{\mathrm{RR}}\right)^n g_{\mathrm{RD}}[j], \tag{6.47}$$

$$\tau_2^{(n)}[i,j] = \tau_{\mathrm{SR}}[i] + \tau_{\mathrm{R}} + (\tau_{\mathrm{R}} + \tau_{\mathrm{RR}})\, n + \tau_{\mathrm{RD}}[j], \tag{6.48}$$

respectively, when it circulates n times through the feedback channel.

The remainder of this section assumes $s_{\mathrm{SR}}[i] \neq s_{\mathrm{RD}}[j]$ for all i and j corresponding to the case of asymmetric delay spread. The theoretical case where $s_{\mathrm{SR}} = s_{\mathrm{RD}}$ is omitted in order to avoid verbosity because two practical channels never encounter *exactly* the same value, but the analysis can be easily extended to cover also this special case by determining the limits $s_{\mathrm{RD}} \to s_{\mathrm{SR}}$ for the expressions. Alternatively, the analysis can be directly exploited with diminishing loss of accuracy, if either parameter is perturbed with an infinitesimal constant by substituting $s_{\mathrm{RD}} = s_{\mathrm{SR}} \pm \epsilon$.

Since the delay spread is asymmetric in the repeater link, the double-exponential PDPs appearing in (6.46) can be rewritten using (6.8) as

$$P_2(t, g_2, \tau_2, \{s_{\mathrm{SR}}, s_{\mathrm{RD}}\}) = \frac{P_1(t, g_2, \tau_2, s_{\mathrm{SR}})}{1 - s_{\mathrm{RD}}/s_{\mathrm{SR}}} + \frac{P_1(t, g_2, \tau_2, s_{\mathrm{RD}})}{1 - s_{\mathrm{SR}}/s_{\mathrm{RD}}}. \tag{6.49}$$

As a useful consequence, $P_{\mathrm{SRD}}(t)$ and $P(t)$ become analogous with (6.8) by being weighted summations of single-exponential power–delay profiles.

The total repeater receive power becomes $P_{\mathrm{S}}G_{\mathrm{SR}} + P_{\mathrm{R}}G_{\mathrm{RR}} + \sigma_{\mathrm{R}}^2$ by summing up the signal power propagated from the source and the repeater itself with the thermal noise power σ_{R}^2. Recalling that the repeater gain is denoted by β^2, the transmit power can be first stated recursively as

$$P_{\mathrm{R}} = \beta^2 \left(P_{\mathrm{S}}G_{\mathrm{SR}} + P_{\mathrm{R}}G_{\mathrm{RR}} + \sigma_{\mathrm{R}}^2 \right) \tag{6.50}$$

which, provided that $\beta^2 G_{\mathrm{RR}} < 1$, has a finite and positive root:

$$P_{\mathrm{R}} = \beta^2 \frac{P_{\mathrm{S}}G_{\mathrm{SR}} + \sigma_{\mathrm{R}}^2}{1 - \beta^2 G_{\mathrm{RR}}} = \beta^2 \frac{P_{\mathrm{S}}G_{\mathrm{SR}}}{1 - \beta^2 G_{\mathrm{RR}}} + \beta^2 \frac{\sigma_{\mathrm{R}}^2}{1 - \beta^2 G_{\mathrm{RR}}}. \tag{6.51}$$

Above the first and second term correspond to the transmitted signal and noise power, respectively. It should be especially noted that they are in a nonlinear relationship with the repeater gain due to the feedback loop.

The repeater gain β^2 and the feedback channel gain G_{RR} are the main factors for determining the stability of the repeater. In particular,

$$\beta^2 < \frac{1}{G_{\mathrm{RR}}} \tag{6.52}$$

must be guaranteed in order to avoid oscillation or saturation. Otherwise, the repeater becomes useless or even harmful for the system at large by transmitting mainly noise and distortion. In fact, only $\beta^2 G_{\mathrm{RR}} \ll 1$ will render reasonable SINR. Stability is concretely shown by (6.47) where $\lim_{n\to\infty} g_2^{(n)}[i,j] = 0$ when (6.52) is satisfied while $\lim_{n\to\infty} g_2^{(n)}[i,j] = \infty$ otherwise. Thereby, the infinite sum of (6.46) can be truncated in practice.

Finally, it can be noted that the presented system model and the following performance analysis could be easily extended to cover also generic single-frequency networks (SFNs) with multiple main transmitters and full-duplex repeaters. In such systems, the destination may receive a superposition of signals from N_{S} sources and N_{R} parallel repeaters for which the respective PDPs can be obtained as $\{P_{\mathrm{SD}[n]}(t)\}_{n=1}^{N_{\mathrm{S}}}$ using (6.40c) and $\{P_{\mathrm{SRD}[n]}(t)\}_{n=1}^{N_{\mathrm{R}}}$ using (6.46). Thus, (6.43) just needs to be replaced by

$$P(t) = \sum_{n=1}^{N_{\mathrm{S}}} P_{\mathrm{SD}[n]}(t) + \sum_{n=1}^{N_{\mathrm{R}}} P_{\mathrm{SRD}[n]}(t), \tag{6.53}$$

which is still a mix of single- and double-exponential PDPs that can be again recasted into a weighted summation of single-exponential PDPs only. With slightly more involved notation, multihop scenarios (with two or more repeaters in series) can be covered by characterizing each end-to-end relay link as explained later in Section 6.4.2: Assuming M hops for the nth link, $P_{\mathrm{SRD}[n]}(t)$ becomes a weighted summation of Mth-order hypoexponential PDPs. In summary, the following SINR results are thus useful after minor changes for many kind of SFN systems as well.

Effective Signal-to-Interference and Noise Ratio

In this section, the end-to-end power–delay profile model of the repeater link is used for deriving the closed-form expressions of useful signal power and interference power in the case of OFDM transmission. Together with an expression for the total noise power, these results then allow one to quantify analytically the end-to-end SINR of the system. In particular, by splitting the total signal power into useful power P_{U} and interference power P_{I} (that includes both ICI and ISI) as $P_{\mathrm{D}}-P_{\mathrm{N}} = P_{\mathrm{U}}+P_{\mathrm{I}}$, the effective SINR at the output of an OFDM demodulator can be evaluated as

$$\gamma \triangleq \frac{P_{\mathrm{U}}}{P_{\mathrm{I}}+P_{\mathrm{N}}} = \frac{P_{\mathrm{U}}}{P_{\mathrm{D}}-P_{\mathrm{U}}}, \tag{6.54}$$

in which P_{N} denotes the total thermal noise power included in P_{D}. The expressions of P_{D}, P_{N}, P_{U}, and P_{I} required for (6.54) are derived below.

Firstly, the total received power in the destination can be summed up as

$$P_{\mathrm{D}} = P_{\mathrm{S}}G_{\mathrm{SD}} + P_{\mathrm{R}}G_{\mathrm{RD}} + \sigma_{\mathrm{D}}^2 = P_{\mathrm{S}}G_{\mathrm{SD}} + \beta^2\frac{P_{\mathrm{S}}G_{\mathrm{SR}}G_{\mathrm{RD}}}{1-\beta^2 G_{\mathrm{RR}}} + P_{\mathrm{N}}, \tag{6.55}$$

where the latter step extracts the power of thermal noise forwarded by the repeater from P_{R} given in (6.51) and combines it with the thermal noise power σ_{D}^2 of the destination. Consequently, the total noise power becomes

$$P_{\mathrm{N}} = \beta^2\frac{\sigma_{\mathrm{R}}^2 G_{\mathrm{RD}}}{1-\beta^2 G_{\mathrm{RR}}} + \sigma_{\mathrm{D}}^2. \tag{6.56}$$

Secondly, the useful signal power P_{U} is derived by calculating the integral $\int_{-\infty}^{\infty}[w(t)]^2 P(t)\,\mathrm{d}t$ defined in (6.25) for the specific power–delay profile given by (6.43) with (6.40c) and (6.46). By using (6.49) in (6.46), $P(t)$ becomes a weighted sum of single-exponential PDPs like (6.8) and, consequently, the counterpart of (6.37) can be almost directly expressed as

$$\begin{aligned} P_{\mathrm{U}} = {} & P_{\mathrm{S}}\sum_{i=1}^{K_{\mathrm{SD}}}\mathcal{I}_{\mathrm{SINR}}\left(g_{\mathrm{SD}}[i],\tau_{\mathrm{SD}}[i],s_{\mathrm{SD}}[i]\right) \\ & + \beta^2 P_{\mathrm{S}}\sum_{n=0}^{\infty}\sum_{i=1}^{K_{\mathrm{SR}}}\sum_{j=1}^{K_{\mathrm{RD}}}\left(\frac{\mathcal{I}_{\mathrm{SINR}}(1,g_2^{(n)}[i,j],\tau_2^{(n)}[i,j],s_{\mathrm{SR}}[i])}{1-s_{\mathrm{RD}}[j]/s_{\mathrm{SR}}[i]}\right. \\ & \left. + \frac{\mathcal{I}_{\mathrm{SINR}}(1,g_2^{(n)}[i,j],\tau_2^{(n)}[i,j],s_{\mathrm{RD}}[j])}{1-s_{\mathrm{SR}}[i]/s_{\mathrm{RD}}[j]}\right), \end{aligned} \tag{6.57}$$

for which the integral $\mathcal{I}_{\mathrm{SINR}}$ is given by (6.36) with (6.39). It should be noted that the infinite sum can be always reduced to a few terms without loss of accuracy since $\mathcal{I}_{\mathrm{SINR}}(M,g,\tau,s) = 0$ when $\tau > \tau_{\mathrm{d}} \triangleq \tau_{\mathrm{TOR}}+T_{\mathrm{CP}}+T_{\mathrm{FFT}}$.

Finally, the interference power can be calculated according to (6.27) as

$$P_{\mathrm{I}} \triangleq P_{\mathrm{ICI}} + P_{\mathrm{ISI}} = (P_{\mathrm{D}}-P_{\mathrm{N}}) - P_{\mathrm{U}} = P_{\mathrm{S}}G_{\mathrm{SD}} + \beta^2\frac{P_{\mathrm{S}}G_{\mathrm{SR}}G_{\mathrm{RD}}}{1-\beta^2 G_{\mathrm{RR}}} - P_{\mathrm{U}} \tag{6.58}$$

by substituting P_{U} from (6.57), whenever it is analyzed separately.

Discussion

The analytical SINR framework is applied next for studying the effect of loopback signals in OFDM repeaters, especially to illustrate how repeater gain control improves performance in the presence of excess multipath delay spread due to feedback echoes. Adopted example parameter values are specified below before proceeding to numerical results and discussions.

The OFDM signal is characterized by choosing $T_{\mathrm{FFT}} = 64$ μs and testing $T_{\mathrm{CP}} \in \{4, 12\}$ μs which can be regarded as practical values. The repeater processing delay is $\tau_{\mathrm{R}} = 4$ μs and, for simplicity, the time of reference is set to $\tau_{\mathrm{TOR}} = \tau_{\mathrm{R}}$ which is now equivalent to synchronization according to the first arrival, i.e., $\tau_{1\mathrm{st}} = \tau_{\mathrm{R}}$. Example channels are chosen as follows.

The source–repeater channel comprises $K_{\mathrm{SR}} = 6$ multipath clusters for which $\{g_{\mathrm{SR}}[i]\}_{i=1}^{6} = \{-90, -91, -92, -93, -94, -95\}$ dB rendering $G_{\mathrm{SR}} = \sum_{i=1}^{6} g_{\mathrm{SR}}[i] = -84.39$ dB, $\{\tau_{\mathrm{SR}}[i]\}_{i=1}^{6} = \{0, 1, 2, 3, 4, 5\}$ μs, and $s_{\mathrm{SR}}[i] = 2$ μs for all i;

The repeater–destination channel comprises also $K_{\mathrm{RD}} = 6$ clusters for which $\{g_{\mathrm{RD}}[j]\}_{j=1}^{6} = \{-40, -41, -42, -43, -44, -45\}$ dB rendering $G_{\mathrm{RD}} = \sum_{j=1}^{6} g_{\mathrm{RD}}[j] = -34.39$ dB, $\{\tau_{\mathrm{RD}}[j]\}_{j=1}^{6} = \{0, 1, 2, 3, 4, 5\}$ μs, and $s_{\mathrm{RD}}[j] = 1$ μs for all j;

The loopback channel gain is varied as $G_{\mathrm{RR}} \in [-70, -30]$ dB using $G_{\mathrm{RR}} = -50$ dB as a particular example and the propagation delay in the feedback channel is $\tau_{\mathrm{RR}} = 30$ ns, which corresponds to roughly 10-meter effective propagation distance implying that antenna separation d_{RR} is 5 meters or less due to cabling and other factors;

The source–destination channel is assumed to be blocked by setting $G_{\mathrm{SD}} = 0$ because the focus is put on the effect of the feedback channel in the repeater link and the direct link would just increase the achieved SINR levels without essentially changing any observation.

Consequently, lag values can be normalized, i.e., $\tau_{\mathrm{SR}}[1] = \tau_{\mathrm{RD}}[1] = 0$ μs with any $\{g_{\mathrm{SD}}[k]\}_{k=1}^{K_{\mathrm{SD}}}$, because measuring absolute delays is not needed.

It should be noted that the above describes just a representative setup for illustrating the general trends while similar observations could be made also in other practical cases. Noise power is now normalized to $\sigma_{\mathrm{R}}^2 = \sigma_{\mathrm{D}}^2 = 1$, and source transmit power is $P_{\mathrm{S}} = 100$ dB above noise level before propagation loss. To aid comparison with other results, this implies $\bar{\gamma}_{\mathrm{SR}} = 15.6$ dB and, when $P_{\mathrm{R}} = 60$ dB, $\bar{\gamma}_{\mathrm{RD}} = 25.6$ dB. However, the absolute values of P_{S}, P_{R}, σ_{R}^2, σ_{D}^2, G_{SR}, G_{RR}, and G_{RD} are not so important.

As per (6.51) and (6.55)–(6.58), Fig. 6.5 illustrates the powers of all essential signal, interference, and noise components in the system with increasing repeater gain β^2 when the isolation of the loopback channel is fixed to $G_{\mathrm{RR}} = -50$ dB. With large gain, the effective end-to-end PDP with an infinite feedback loop decays slowly and many multipath echoes are transferred outside the cyclic prefix. Consequently, the interference power increases faster than the useful signal power. Also the noise power shoots up when the repeater gain approaches its maximum level.

Figure 6.6 shows the end-to-end SINR using (6.54) with (6.55)–(6.57). For reference, an upper bound can be obtained by assuming an infinite cyclic prefix ($T_{\mathrm{CP}} \to \infty$), which eliminates all ICI and ISI such that $P_{\mathrm{I}} = 0$, and a lower bound can be obtained by assuming that all loopback signal is pure interference, which corresponds to a case of long processing delay ($\tau_{\mathrm{R}} \gg T_{\mathrm{CP}}$). In particular, this explains why an extended cyclic prefix is necessary for repeater links since the OFDM demodulator at the destination can partly exploit residual feedback echoes as useful components.

It can be shown analytically with straightforward, but tedious, calculations that the SINR admits a global maximum in terms of the repeater gain while degrading close to zero at both extremes, as also shown by Fig. 6.6. This gives motivation for determining the optimal gain as

$$\beta^2 = \arg\max_{\beta^2} \gamma, \tag{6.59}$$

which can be solved by numerically maximizing the closed-form SINR expression (6.54). For instance, when $G_{\mathrm{RR}} = -50$ dB and $T_{\mathrm{CP}} = 12$ μs as in Fig. 6.6, optimal gain control sets $\beta^2 = 41.1$ dB and yields $\gamma = 13.9$ dB.

Alternatively, one may consider also two simplified gain control methods originating from the requirement that (6.52) should be satisfied to avoid repeater saturation. In the *gain margin* approach, the gain of the residual loopback channel is first estimated and the repeater gain is then set below the isolation reserving a fixed pre-defined margin, i.e., with $\Delta_{\mathrm{GM}} > 1$,

$$\beta^2 = \frac{1}{\Delta_{\mathrm{GM}} G_{\mathrm{RR}}} < \frac{1}{G_{\mathrm{RR}}}. \tag{6.60}$$

Suitable values for Δ_{GM} are around 10–15 decibels. The *power normalization* approach sets the repeater transmit power P_{R} to a given fixed level and the resulting gain can then be solved in terms of P_{R} from (6.51) as

$$\beta^2 = \frac{P_{\mathrm{R}}}{P_{\mathrm{S}} G_{\mathrm{SR}} + P_{\mathrm{R}} G_{\mathrm{RR}} + \sigma_{\mathrm{R}}^2} < \frac{1}{G_{\mathrm{RR}}}, \tag{6.61}$$

i.e., repeater stability is again guaranteed. The latter, unlike the former, scheme can be implemented by adaptively controlling the output power.

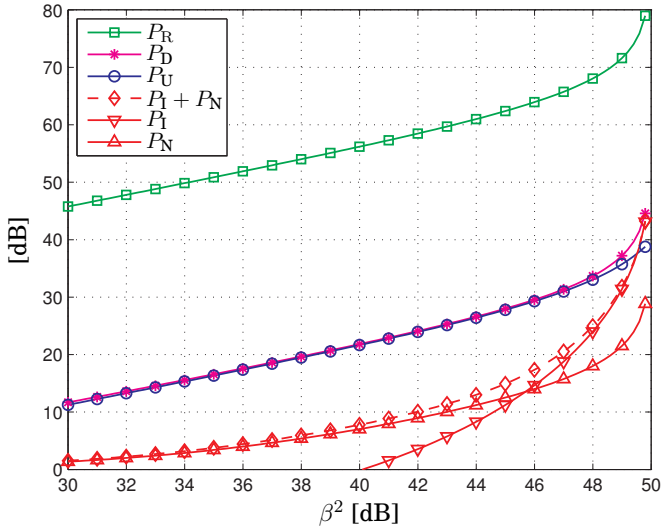

Figure 6.5. Power levels of different signal and noise components in the full-duplex repeater link versus the repeater gain when $G_{RR} = -50$ dB. The length of the cyclic prefix is selected as $T_{CP} = 12$ μs.

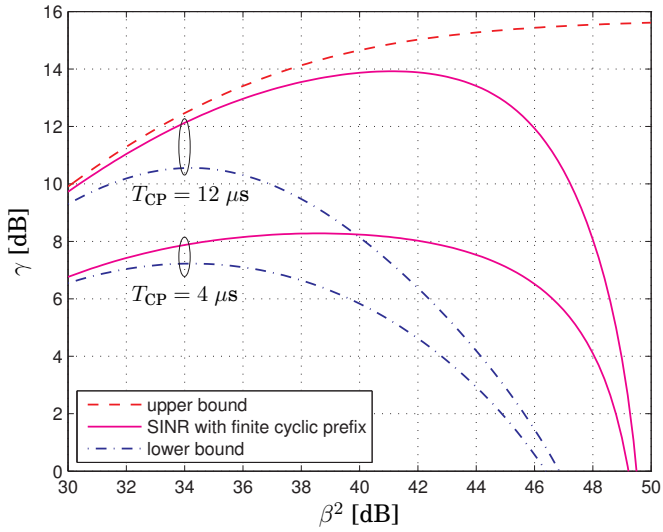

Figure 6.6. Signal-to-interference and noise ratio (SINR) and its bounds in the full-duplex repeater link versus the repeater gain when $G_{RR} = -50$ dB. The corresponding signal, interference and noise levels constituting the SINR curve are shown above for the case of $T_{CP} = 12$ μs.

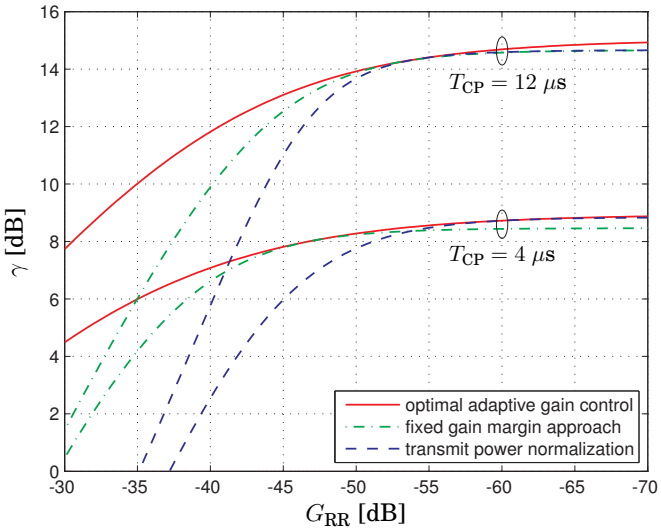

Figure 6.7. Signal-to-interference and noise ratio in the full-duplex repeater link versus loopback channel isolation with different gain control methods. In particular, reasonable example values $\Delta_{\mathrm{GM}} = 10$ dB and $P_{\mathrm{R}} = 60$ dB are assumed for the gain margin and transmit power normalization schemes, respectively.

Finally, Fig. 6.7 illustrates SINR with the different methods for tuning the repeater gain when residual feedback gain is varied. The conventional methods yield roughly optimal performance when $G_{\mathrm{RR}} \approx -55$ dB. They tend to use too high transmit power in the case of low isolation causing excessive loopback echoes; yet, this is the likely operation regime as indicated by measurement results presented in Section 3.5.3 for average physical isolation $\mathcal{E}\{I_{\mathrm{physical}}\}$ which is related to G_{RR}. Conversely, the conventional methods set the gain too low when loopback isolation is good although the performance loss is small in this example. In summary, the optimization of the repeater gain is shown to balance the power of multipath components that fall inside and outside of the OFDM cyclic prefix.

Conclusions

This section derived novel closed-form expressions for evaluating SINR in full-duplex OFDM repeater links with loop interference. Especially, the discussion showed why the repeater gain should be properly controlled for mitigating the effect of residual loop interference in addition to guaranteeing large spatial separation between directive repeater antennas and implementing efficient cancellation. The presented analysis can be used also for studying the effects of synchronization errors, symbol and cyclic prefix duration, delay difference between relayed and direct transmissions as well as relay processing delay on the end-to-end performance.

6.4.2 Multihop Amplify-and-Forward Relaying

This section applies the hypoexponential PDP and the SINR analysis for multihop relaying in order to discuss the effect of end-to-end delay spread and receiver time synchronization. On the side, the study also investigates how the performance of relay links is affected by the choice of the OFDM physical-layer parameters. The number of hops, i.e., the order of the hypoexponential PDP, is the main factor for intensifying multipath spread in this case study, which is formulated to illustrate the analysis of Sections 6.2 and 6.3 with numerical results. However, the system framework is also generalized by introducing clustered multipath propagation.

System Setup

The considered system setup, illustrated in Fig. 6.8, is similar to those of [64, 88, 100, 102, 129, 130, 152, 304, 314] except that multipath propagation is introduced for the model and wideband transmission is considered instead of assuming frequency-flat narrowband channels. In this M-hop communication system, a standard OFDM signal with a cyclic prefix is routed from a source node to a destination node via $M-1$ intermediate relay nodes. As in the works mentioned above, all nodes are connected in series such that communication is performed (or possible) only between two adjacent nodes. To avoid inter-hop interference, channel separation and reuse should be implemented in time, frequency or spatial domain.

All hops are assumed to be subject to independent, but not necessarily identical, multipath statistics specified with their PDPs. The received signals in the mth relay and in the destination are degraded due to white additive noise, power of which is given by $\sigma_{\mathrm{R}}^2[m]$ and σ_{D}^2, respectively.

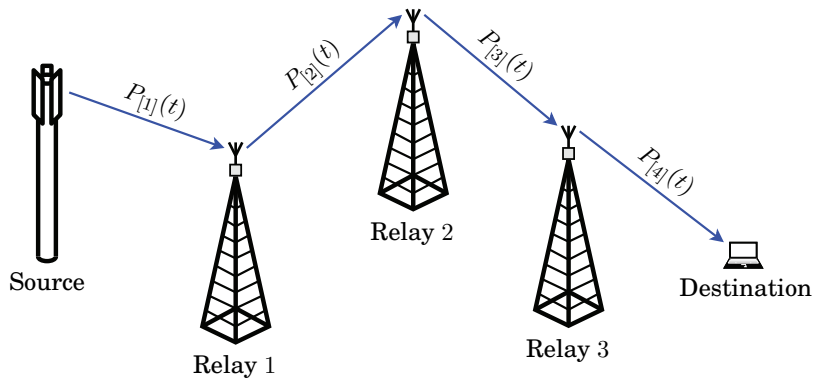

Figure 6.8. Multihop relay link with $M = 4$ hops where $P_{[m]}(t)$, $m = 1, 2, 3, 4$, denote the power–delay profiles (PDPs) of the multipath channels at each hop.

The effective end-to-end channel is given by (6.2), for which the multipath channel $h_{[m]}(t)$ of the mth hop is modeled with a *clustered* single-exponential PDP. In particular, there are $K[m]$ independent exponentially decaying multipath clusters such that the gain, lag, and root mean square delay spread of the kth cluster are denoted by $g[m,k]$, $\tau[m,k]$, and $s[m,k]$, respectively; the total gain of the mth hop becomes $G[m] = \sum_{k=1}^{K[m]} g[m,k]$. In summary, the profile of the mth hop can be thus expressed as

$$P_{[m]}(t) \triangleq \mathcal{E}\{|h_{[m]}(t)|^2\} = \sum_{k=1}^{K[m]} P_1\left(t, g[m,k], \tau[m,k], s[m,k]\right), \tag{6.62}$$

for which $P_1(t,g,\tau,s)$ is given by (6.4), and the end-to-end profile $P(t)$ is still derived from $\{P_{[m]}(t)\}_{m=1}^{M}$ using (6.3). Without loss of generality, the lag parameters of each hop are sorted in ascending order, i.e., $\tau[m,k_1] \leq \tau[m,k_2]$ for all $k_1 \leq k_2$. Furthermore, they can be normalized in such a way that $\tau[m,1] = 0$ for all m, because the absolute propagation delays are not relevant for the analysis, as opposed to relative delay spread.

The signal model (6.1) is valid also for the generalized setup after characterizing the aggregate noise term $n(t)$; its power can be summed up as

$$P_{\mathrm{N}} \triangleq \mathcal{E}\{|n(t)|^2\} = \sum_{m=1}^{M-1} \sigma_{\mathrm{R}}^2[m] \prod_{n=m}^{M-1} \beta^2[n] G[n+1] + \sigma_{\mathrm{D}}^2 \tag{6.63}$$

when $\beta^2[m]$ denotes the gain of the mth relay. The total received power at the destination then becomes analogous with (6.21), i.e.,

$$P_{\mathrm{D}} \triangleq \mathcal{E}\{|y_{\mathrm{D}}(t)|^2\} = \beta^2 G P_{\mathrm{S}} + P_{\mathrm{N}}, \tag{6.64}$$

where $P_{\mathrm{S}} \triangleq \mathcal{E}\{|x_{\mathrm{S}}(t)|^2\}$ denoting the total transmitted power at the source,

$$G \triangleq \int_{-\infty}^{\infty} P(t)\,\mathrm{d}t = \prod_{m=1}^{M} G[m], \quad \text{and} \quad \beta \triangleq \prod_{m=1}^{M-1} \beta[m]. \tag{6.65}$$

For the purpose of illustration, the following numerical results assume a symmetric relay link, e.g., deployed for economical coverage extension with equal link span for all hops, where all component channels are statistically identical. The so-called typical urban six-cluster ("TU6" [57]) channel profile is selected with the same delay spread at every hop and cluster, i.e., $s[m,k] = s_1 = 0.2\ \mu$s for all m and k. Thus, $K[m] = 6$ and

$$\{g[m,k] - G[m] + 4.219\}_{k=1}^{6} = \{-3, 0, -2, -6, -8, -10\}\ \text{dB},$$
$$\{\tau[m,k]\}_{k=1}^{6} = \{0.0, 0.2, 0.5, 1.6, 2.3, 5.0\}\ \mu\text{s}$$

for all m. This allows to vary the number of hops within the same framework while the following analysis is still valid for a general setup.

Without loss of generality, the numerical results also normalize transmission power in the source and all relays as well as receiver noise power in all relays and the destination to unity. Thus, $P_{\mathrm{S}} = 1$, $\sigma^2_{\mathrm{R}}[m] = \sigma^2_{\mathrm{D}} = 1$ for all m, and the gain of the mth relay is set to $\beta^2[m] = 1/(G[m]+1)$ since its total input power is $G[m]+1$, while (6.63) and (6.64) are simplified to

$$P_{\mathrm{N}} = \sum_{m=1}^{M-1} \prod_{n=m}^{M-1} \frac{G[n+1]}{G[n]+1} + 1 \quad \text{and} \quad P_{\mathrm{D}} = G[1] \prod_{m=1}^{M-1} \frac{G[m+1]}{G[m]+1} + P_{\mathrm{N}}, \quad (6.66)$$

respectively. The quality of the individual hops is consequently defined by the channel gains $\{G[m]\}_{m=1}^{M}$ alone. Furthermore, all hops are set to have equal gain and the end-to-end performance is normalized such that $\gamma_{\max} \triangleq (P_{\mathrm{D}} - P_{\mathrm{N}})/P_{\mathrm{N}}$ remains the same with any number of hops M to facilitate fair comparison. This yields $G = (G[m])^M$ with

$$G[m] = \left[\left(1 + \frac{1}{\gamma_{\max}} \right)^{1/M} - 1 \right]^{-1} \quad (6.67)$$

for any m. Example value $\gamma_{\max} = 15$ dB is chosen for the illustrations.

End-to-End Power–Delay Profile

The effective source–destination PDP is derived by substituting the PDPs of the component channels, i.e., $\{P_{[m]}(t)\}_{m=1}^{M}$ defined in (6.62), into (6.3):

$$P(t) = \sum_{k_1=1}^{K[1]} \cdots \sum_{k_M=1}^{K[M]} P_M(t, \textstyle\prod_{m=1}^{M} g[m,k_m], \sum_{m=1}^{M} \tau[m,k_m], \{s[m,k_m]\}_{m=1}^{M}) \quad (6.68)$$

comprising $\prod_{m=1}^{M} K[m]$ independent clusters, each of which is given by

$$\begin{aligned} &P_M(t, \textstyle\prod_{m=1}^{M} g[m,k_m], \sum_{m=1}^{M} \tau[m,k_m], \{s[m,k_m]\}_{m=1}^{M}) \quad (6.69) \\ &= P_1(t, g[1,k_1], \tau[1,k_1], s[1,k_1]) * \ldots * P_1(t, g[M,k_M], \tau[M,k_M], s[M,k_M]). \end{aligned}$$

These clusters are M-fold cascades of single-exponential PDPs, i.e., hypoexponential PDPs, which can be further reformulated using (6.8) or (6.9). Thus, $P(t)$ accommodates also parallel multihop paths with different M.

The source–destination PDP as per the above expressions is illustrated in Fig. 6.9. Going from a single-hop system to a multihop system causes a soft onset in the PDP and increases both the overall delay and the delay spread. The intuitive conclusion is that the receiver synchronization will be influenced by the modified shape of the PDP. Since delay spread should be considerably smaller than the cyclic prefix duration in order to avoid ICI and ISI, a relay link typically needs to use a longer cyclic prefix than conventional single-hop transmission. These impacts are expected to be more severe when the number of hops is increased. Likewise, the frequency selectivity will increase as a consequence of the delay spread.

Frequency Selectivity and Delay Spread

Like (6.68) generalizes (6.5), the frequency-correlation function (FCF) of the end-to-end PDP is obtained by generalizing (6.12) to include multipath clusters at each hop according to (6.62):

$$r(f) = \sum_{k_1=1}^{K[1]} \cdots \sum_{k_M=1}^{K[M]} \left(\prod_{m=1}^{M} g[m,k_m] \right) \frac{\exp(-j2\pi f \sum_{m=1}^{M} \tau[m,k_m])}{\prod_{m=1}^{M}(1+j2\pi f s[m,k_m])}. \quad (6.70)$$

The corresponding 3-decibel coherence bandwidth $f_{\text{coherence}}$ can be determined only numerically from the lowest positive root of $|r(f)| = \frac{1}{2}|r(0)|$.

The FCF of the example relay link is illustrated in Fig. 6.10 accompanied by a table showing respective 3-decibel coherence bandwidth values. Especially, the frequency correlation of relay links ($M \geq 2$) is seen to differ considerably from what is observed in a single-hop system ($M = 1$). This will be of importance for channel estimation and frequency-domain equalization in OFDM systems. In particular, the correlation of adjacent frequency-domain pilot subcarriers should be high in order to facilitate accurate interpolation of channel state information for the data subcarriers. Hence, if the system is originally designed for single-hop transmission and the relays are added later, the pilot structure and subcarrier spacing may need to be revised due to the increased frequency selectivity.

The above observations on the characteristics of the end-to-end PDP and the corresponding FCF are inherently connected with the mean delay τ, the RMS delay spread s, and the lag of the strongest multipath component τ_{max}. These can be calculated as described next while numerical values are listed for the example scenario in the embedded table of Fig. 6.9.

The average end-to-end delay is calculated by combining the sum over all clusters from (6.68) with the average delay of a single cluster in (6.10):

$$\bar{\tau} = \sum_{k_1=1}^{K[1]} \cdots \sum_{k_M=1}^{K[M]} \left(\prod_{m=1}^{M} \frac{g[m,k_m]}{G[m]} \right) \sum_{m=1}^{M} \left(\tau[m,k_m] + s[m,k_m] \right). \quad (6.71)$$

Similarly, by combining (6.11), (6.68) and (6.71), the end-to-end mean square delay spread becomes

$$s^2 = \sum_{k_1=1}^{K[1]} \cdots \sum_{k_M=1}^{K[M]} \left(\prod_{m=1}^{M} \frac{g[m,k_m]}{G[m]} \right) \quad (6.72)$$
$$\times \sum_{l=1}^{M} \left(2s[l,k_l] \sum_{m=1}^{l} s[m,k_m] + \tau[l,k_l] \sum_{m=1}^{M} \left(\tau[m,k_m] + 2s[m,k_m] \right) \right) - \bar{\tau}^2.$$

It should be especially noted that the relay gains $\{\beta[m]\}_{m=1}^{M-1}$ do not affect expressions (6.70)–(6.72), which are thus not limited to the example setup. However, they can be simplified slightly when $s[m,k] = s_1$ for all m and k.

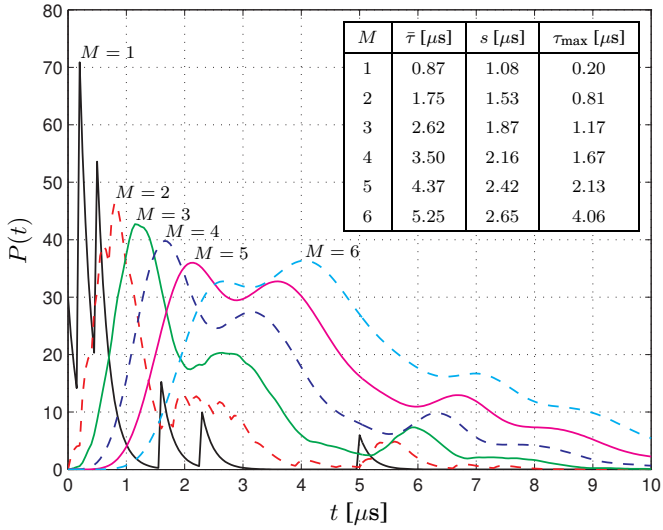

M	$\bar{\tau}$ [μs]	s [μs]	$\tau_{\max}$ [μs]
1	0.87	1.08	0.20
2	1.75	1.53	0.81
3	2.62	1.87	1.17
4	3.50	2.16	1.67
5	4.37	2.42	2.13
6	5.25	2.65	4.06

Figure 6.9. End-to-end source–destination power–delay profiles (PDPs) in the example M-hop relay links. The embedded table lists the mean delay $\bar{\tau}$, the root mean square delay spread s and the lag of the strongest multipath component $\tau_{\max}$ versus the number of hops M.

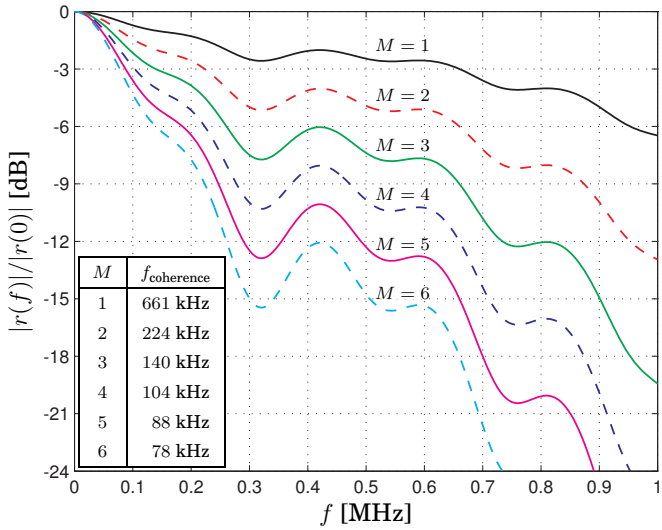

M	$f_{\text{coherence}}$
1	661 kHz
2	224 kHz
3	140 kHz
4	104 kHz
5	88 kHz
6	78 kHz

Figure 6.10. Normalized magnitude of the frequency-correlation functions corresponding to the PDPs shown above for the example relaying scenario. The embedded table lists the respective 3-decibel coherence bandwidth values $f_{\text{coherence}}$ versus the number of hops M.

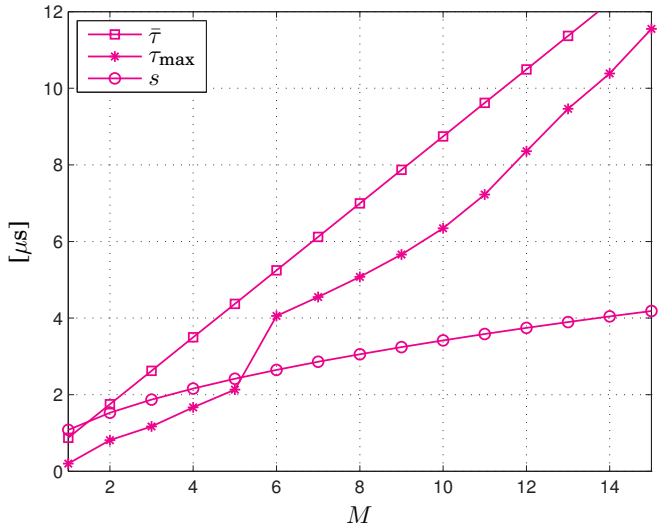

Figure 6.11. The mean delay $\bar{\tau}$, the root mean square delay spread s and the lag of the strongest multipath component $\tau_{\max}$ when the number of hops M grows large in the example relaying scenario.

The lag of the strongest multipath component is given by

$$\tau_{\max} \triangleq \arg\max_t P(t) \tag{6.73}$$

with the substitution of the closed-form PDP defined in (6.68) and its value can be computed only numerically. However, when M grows large,

$$\tau_{\max} \approx \bar{\tau} - \Delta\tau \tag{6.74}$$

where $\Delta\tau$ is a constant bias originating from the skewness of the PDP.

The asymptotic delay spread characteristics, i.e., the values of $\bar{\tau}$, s and $\tau_{\max}$ when the number of hops becomes large, are illustrated in Fig. 6.11. The respective average delay and RMS delay spread are seen to increase proportionally to M and $\sqrt{M}$ which is analytically shown by (6.14) and (6.15) for the single-cluster case. Similarly, the lag of the strongest multipath component follows approximately linear trend except for the jump from $M = 5$ to $M = 6$ which is corroborated also by Fig. 6.9: The PDPs contain two major lobes and their order of magnitude is inverted when going from $M = 5$ to $M = 6$, but further jumps do not occur for any $M > 6$ because the PDP converges to a bell-shaped curve with a single maximum. In summary, respective τ_{TOR} and T_{CP} need to be increased proportionally to M and $\sqrt{M}$ when M is large. All the above trends continue also beyond the values of M illustrated in Fig. 6.11, i.e., when $M > 15$.

Effective Signal-to-Interference and Noise Ratio

In the case of flat-fading channels (or, equivalently, zero delay spread), the signal-to-noise ratio (SNR) in the destination is calculated simply as

$$\gamma_{\max} \triangleq \frac{P_{\mathrm{D}} - P_{\mathrm{N}}}{P_{\mathrm{N}}} = \frac{\beta^2 G P_{\mathrm{S}}}{P_{\mathrm{N}}} \tag{6.75}$$

using (6.63)–(6.65), which appears earlier in [100, Eq. 12], [129, Eq. 1], [130, Eq. 8], and [152, Eq. 2] to name but a few references. However, with multipath fading and OFDM transmission, one needs to consider instead the signal-to-interference and noise ratio (SINR), because the large delay spread of the end-to-end channel and non-ideal time synchronization may cause inter-carrier and inter-symbol interference due to multipath components that are transferred outside of the cyclic prefix. With non-zero delay spread, SINR is bounded from above by $\gamma_{\max}$ which is achieved only when the length of the OFDM cyclic prefix approaches infinity.

Similar to (6.20), the effective end-to-end SINR after OFDM demodulation in the destination of the general multihop relay link is given by

$$\gamma = \frac{P_{\mathrm{U}}}{P_{\mathrm{D}} - P_{\mathrm{U}}} = \frac{P_{\mathrm{U}}}{\beta^2 G P_{\mathrm{S}} - P_{\mathrm{U}} + P_{\mathrm{N}}} \leq \gamma_{\max}. \tag{6.76}$$

By combining the summation over all clusters from (6.68) with (6.30) or (6.37), the useful end-to-end signal power is now determined as

$$P_{\mathrm{U}} = \beta^2 P_{\mathrm{S}} \sum_{k_1=1}^{K[1]} \cdots \sum_{k_M=1}^{K[M]} \mathcal{I}_{\mathrm{SINR}}\left(M, \textstyle\prod_{m=1}^{M} g[m,k_m], \sum_{m=1}^{M} \tau[m,k_m], s_1\right) \tag{6.77}$$

when all delay spreads are equal to s_1, and

$$\begin{aligned} P_{\mathrm{U}} = \beta^2 P_{\mathrm{S}} \sum_{k_1=1}^{K[1]} \cdots \sum_{k_M=1}^{K[M]} \sum_{l=1}^{M} \left(\prod_{\substack{m=1 \\ m\neq l}}^{M} \frac{s[l,k_l]}{s[l,k_l] - s[m,k_m]} \right) \\ \times \mathcal{I}_{\mathrm{SINR}}\left(1, \textstyle\prod_{m=1}^{M} g[m,k_m], \sum_{m=1}^{M} \tau[m,k_m], s[l,k_l]\right) \end{aligned} \tag{6.78}$$

for unequal delay spreads, respectively.

Above expressions (6.77) and (6.78) consist of sums over $\prod_{m=1}^{M} K[m]$ and $M\prod_{m=1}^{M} K[m]$ terms, respectively, e.g., rendering 6^M terms for the example relay link. Consequently, the direct evaluation of P_{U} may become impractical with a large number of hops or multipath clusters because the complexity is directly proportional to the number of terms. Fortunately, a part of the sum terms may be pruned, because the cluster lags are sorted in ascending order and $\mathcal{I}_{\mathrm{SINR}}(M,g,\tau,s) = 0$ if $\tau \geq \tau_{\mathrm{d}}$. Thereby, the summation needs to be calculated only over the set of lower indices for which $\sum_{m=1}^{M} \tau[m,k_m] < \tau_{\mathrm{d}}$, while the other terms are zero by definition.

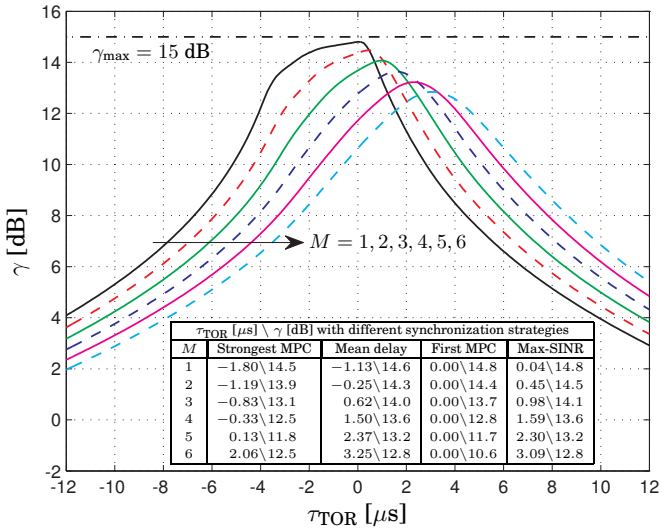

τ_{TOR} [μs] \ γ [dB] with different synchronization strategies

M	Strongest MPC	Mean delay	First MPC	Max-SINR
1	$-1.80\backslash 14.5$	$-1.13\backslash 14.6$	$0.00\backslash 14.8$	$0.04\backslash 14.8$
2	$-1.19\backslash 13.9$	$-0.25\backslash 14.3$	$0.00\backslash 14.4$	$0.45\backslash 14.5$
3	$-0.83\backslash 13.1$	$0.62\backslash 14.0$	$0.00\backslash 13.7$	$0.98\backslash 14.1$
4	$-0.33\backslash 12.5$	$1.50\backslash 13.6$	$0.00\backslash 12.8$	$1.59\backslash 13.6$
5	$0.13\backslash 11.8$	$2.37\backslash 13.2$	$0.00\backslash 11.7$	$2.30\backslash 13.2$
6	$2.06\backslash 12.5$	$3.25\backslash 12.8$	$0.00\backslash 10.6$	$3.09\backslash 12.8$

Figure 6.12. End-to-end SINR of the example M-hop OFDM relay links in terms of the time of reference (TOR) when the OFDM physical-layer parameters are selected as $T_{\mathrm{FFT}} = 64$ μs and $T_{\mathrm{CP}} = 4$ μs. The embedded table shows the chosen TOR and the resulting SINR for the key synchronization strategies.

In the following, the OFDM physical-layer parameters are selected as $T_{\mathrm{FFT}} = 64$ μs and $T_{\mathrm{CP}} = 4$ μs. Using (6.76) and (6.77), Fig. 6.12 then illustrates the SINR of the example relay link emphasizing the effect of non-ideal time synchronization. The embedded table of Fig. 6.12 also lists the time of reference (TOR) values and SINRs achieved with different time-synchronization strategies. These key synchronization models, namely "*Strongest MPC*", "*Mean delay*", "*First MPC*" and "*Max-SINR*", are specified with more details in Section 2.1.3, but it is worth to quickly recall that they basically define how the cyclic prefix (CP) window is aligned with the multipath components (MPCs) of the channel response.

A single-hop system is seemingly more robust to time synchronization errors than amplify-and-forward relay links because, with $M = 1$, all strategies result in similar, nearly-optimal, performance. This is mainly because the PDP of the single-hop system is only slightly longer than the CP. The single-hop case ($M = 1$) in Fig. 6.12 reflects also the performance of decode-and-forward relay links with any number of hops because they are essentially limited by the weakest of the hops (which are symmetric in the example scenario). Due to intermediate signal regeneration, decode-and-forward links avoid the cascaded structure and consequent spreading of the end-to-end multipath channel which become significant issues in amplify-and-forward links as discussed next.

When the number of hops is increased, the end-to-end SINR is degraded even with the ideal *Max-SINR*-strategy, because the end-to-end PDP is spread (cf. Fig. 6.9) and more MPCs are left outside of the CP. The *First MPC*-strategy is nearly optimal for single-hop systems, but too conservative for multihop relaying in which most of the signal energy is received after the soft onset of the PDP. The *Mean delay*-strategy offers rather good performance with any number of hops. With $M \leq 4$ and $M \leq 2$, the respective *Strongest MPC*- and *Mean delay*-strategies result in negative TOR which leads to unnecessary performance degradation because the ideal TOR is always non-negative in this example setup. These observations are only valid for the relatively short CP employed in this example.

Consequently, Fig. 6.13 illustrates how the TOR setting varies in terms of the physical-layer parameters. It can be seen that the length of the CP also affects the design of receiver time synchronization while the different synchronization strategies result in relatively similar performance irrespective of the FFT duration. Likewise, the TOR with the non-ideal synchronization strategies depends, by definition, only on T_{CP}, but not on T_{FFT}. The value of T_{FFT} neither affects the TOR with ideal synchronization, i.e., the *Max-SINR* strategy as demonstrated by the minor difference between TORs determined for two different FFT durations.

In the multihop case, the SINR degradation due to larger delay spread can be compensated by appropriately tuning the OFDM physical-layer parameters T_{CP} and T_{FFT} as illustrated in Fig. 6.14. The usage of longer FFT and/or longer CP improves SINR, and with a very long FFT, reasonable SINR can be achieved even without adding the CP at all. However, the channel coherence time still sets a limit for the maximum feasible FFT size. Thus, fixing the modulation efficiency, i.e., $\eta \triangleq T_{\mathrm{FFT}}/(T_{\mathrm{FFT}} + T_{\mathrm{CP}})$, imposes a trade-off for the choice of the OFDM parameters.

In Fig. 6.14, a short CP yields similar low SINR with all synchronization strategies because the PDP does not fit inside the CP even if the TOR is chosen optimally. With a long CP, TOR with the *Max-SINR* strategy converges close to zero, which implies that the *First MPC* strategy is also nearly optimal. Actually, it is a reasonably good strategy with any T_{CP} as indicated by the shape of the PDP in Fig. 6.9 where a large part of the signal energy is received in the early interval for which $t \in [0.2, 1.5]$ μs. However, the tail of the PDP is long which causes the poor performance of the *Mean delay* and *Strongest MPC* strategies. Yet, the *Mean delay* strategy is favorable with a short CP as already noticed above.

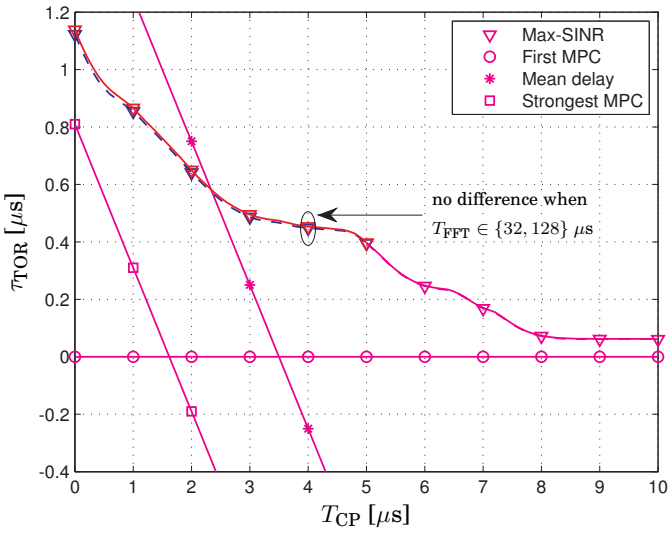

Figure 6.13. The time of reference chosen for the example dual-hop OFDM relay link ($M = 2$) with the key synchronization strategies in terms of the physical-layer OFDM parameters. The resulting SINR levels are shown below.

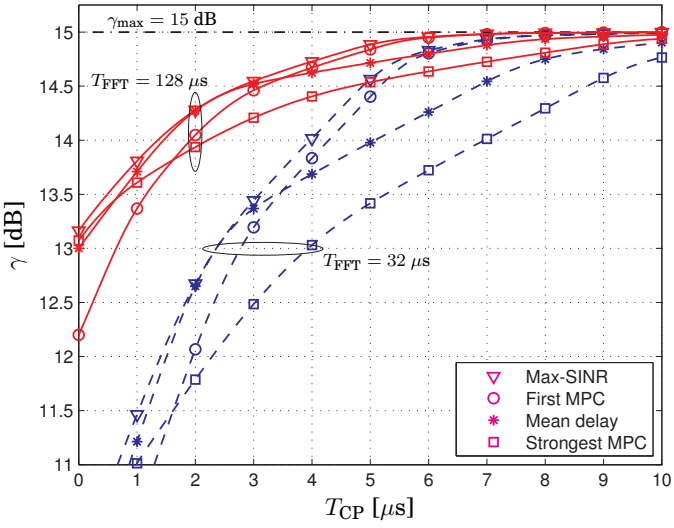

Figure 6.14. End-to-end SINR of the example dual-hop OFDM relay link ($M = 2$) in terms of the physical-layer OFDM parameters with the key synchronization strategies. The corresponding TOR values are chosen as shown above.

6.5 Conclusions

This chapter presented an analysis of wideband multihop OFDM links under the realistic assumption of multipath propagation, as opposed to typical prior works which are limited to frequency-flat channels and narrowband single-subcarrier transmission. The focus was on non-regenerative relay links where the relaying protocol applies time-domain amplification. The developed new analytical framework models all channels in terms of power–delay profiles (PDPs) while the actual fading statistics can be arbitrary. Consequently, the effective end-to-end source–destination PDP may be expressed in terms of a new hypoexponential PDP obtained by cascading classic single-exponential PDPs. Actually, the proposed PDP model is not even limited to relay links, but it is also applicable for modeling certain single-hop radio channels with multiple scattering.

The results showed how the properties of the end-to-end multihop multipath channel and the physical layer OFDM parameters are involved in a trade-off between the mean delay and delay spread, the onset and decay of the PDP, frequency selectivity, and signal-to-interference and noise ratio which is evaluated in a closed form. Furthermore, the approach facilitated the comparison of different receiver time synchronization strategies in the presence of inter-carrier and inter-symbol interference.

Finally, numerical results for OFDM relay links in two example scenarios showed that relaying not only increases delay spread, but it also significantly alters the profile of the end-to-end channel which causes interference and increases the frequency selectivity. In the case of full-duplex repeaters, the feedback loop causes further spread for the effective end-to-end multipath channel due to echoes circulating through the repeater. Thus, gain control is a useful technique for keeping the total delay spread tolerable. In summary, the choice of physical layer OFDM parameters, e.g., the length of the cyclic prefix, the receiver time synchronization strategy, and the frequency-domain pilot structures may need to be changed when a conventional single-hop system is upgraded to a multihop amplify-and-forward relay link.

7. Analysis of Multiuser Scheduling in Multihop Relaying

Multiuser scheduling is an integral part of OFDMA-based wireless systems where users need to be assigned to subcarriers, and vice versa, before actual data transmission. Since fading channels are typically highly frequency-selective, significant gains can be achieved with opportunistic scheduling decisions. Intuitively, the same should hold also when a base station serves indirectly mobile users via a multihop backhaul link but its effect with different relaying protocols deserves closer investigation.

This chapter analyzes the performance of a multiuser multihop system by deriving closed-form expressions for outage probability, outage capacity, ergodic capacity, average end-to-end signal-to-noise ratio (SNR), and the amount of fading. These performance measures reveal that multiuser scheduling offers significant diversity, rate and SNR gain over single-user transmission and round-robin scheduling, also in relaying systems. Furthermore, they facilitate comparison between amplify-and-forward (AF) and decode-and-forward (DF) protocols performing resource block-wise processing. Finally, the performance of the relay link is also contrasted with that of a distributed antenna system, which shows that a non-ideal wireless backhaul link induces tolerable performance deterioration compared to deploying a cable-connected distributed antenna.

The remainder of this chapter[1] is organized as follows. After a brief introduction given in the next section to the scope of the study, Section 7.2 specifies the adopted system model of the infrastructure-based multihop relay system with multiuser scheduling. The main analytical results of this chapter are presented in Section 7.3, where closed-form expressions are derived for the aforementioned performance measures. Then in Section 7.4, the analytical measures are translated to asymptotic and numerical performance results. Finally, Section 7.5 summarizes the discussion.

[1]This chapter is partially based on the material presented in **[158, 232]**.

7.1 Introduction

As the number of users and demand for higher data rates increases, desired quality of service on the borders of micro and macro cells cannot be guaranteed by simply increasing transmit powers. Instead, the density of network infrastructure has to be increased. In addition to small-cell technology such as nano, pico or even femto base stations (BSs), relay nodes (RNs) and distributed antennas can bring the network infrastructure closer to the user equipments (UEs) and thereby extend the service area into BS coverage gaps, or enhance hotspot capacity. A wireless multihop backhaul link can be especially employed for this purpose.

In general, OFDMA is inherently suitable for cellular multiuser systems that require two kinds of scheduling: choosing a resource block (RB) out of many for each UE and choosing a UE out of many for each RB. The latter task fits well in the framework of RB-wise relaying protocols adopted herein, while the former is analyzed in **[158]**. Since service links are subject to fading, large gain is achieved with opportunistic multiuser diversity; this is exemplified herein by maximum signal-to-noise ratio (SNR) scheduling to allow tractable closed-form performance analysis.

In particular, this chapter focuses on fixed relay nodes that are part of the network infrastructure assuming a multihop system where, in the downlink (DL) direction, a signal is transmitted from the BS and then processed and forwarded by RNs toward the UEs. The backhaul link may comprise any mix of amplify-and-forward (AF) and decode-and-forward (DF) relays, and the corresponding uplink (UL) transmission is also considered. The fixed nature of the BS and the RNs leads to a system where the BS–RN and RN–RN links are stationary while the RN-UE links are subject to Rayleigh fading due to UE movement and multipath propagation. In contrast, many earlier analytical examinations, e.g., those surveyed in Chapter 2, have assumed mobile relaying scenarios with all links admitting Rayleigh fading while research on fixed infrastructure relaying systems has been rather limited, except for simulation-based studies.

As also summarized in Chapter 2, earlier literature has considered a wide variety of different scheduling and selection diversity schemes for relaying, also in the context of cellular systems, but their analysis is usually based on simulations. Multiuser scheduling and antenna selection diversity with mobile relays have also been studied. Nevertheless, the contributions of this chapter are novel by default, because the relay nodes are

fixed and part of the cellular infrastructure. Furthermore, some earlier results are generalized without assuming noise-free backhaul channels. In fact, the results are not specific for any scheme to separate backhaul links. The separation can be implemented by any means, even with full-duplex relaying. Instead of physical isolation, the separation between relay's transmit and receive signals can be done also in frequency and/or in time, which corresponds to half-duplex relaying. If frequency separation is used, then additional frequency bands are needed for UEs that are connected to a BS via RNs. Irrespective of the applied receive and transmit signal separation approach the baseline assumption is that direct signals between the BS and the UEs are not usually visible.

The contributions of this chapter are summarized as follows.

- The first contribution is to derive exact closed-form expressions for an assorted set of performance measures being outage probability, outage capacity, average end-to-end SNR, the amount of fading and ergodic capacity. Earlier analytical works on this area concern mobile relaying and relay selection in contrast to scheduling in an infrastructure setup. Additional results for bit-error probability with fixed uncoded modulation are available in **[212]** although the current scope is on modern communication systems which employ adaptive modulation and coding.

- The second contribution is to evaluate the performance improvement due to maximum-SNR scheduling in downlink and uplink relaying, and to compare DF relaying to two different methods for normalizing relay transmit power in AF relaying, namely the "variable" and "fixed gain" protocols. The analysis includes also asymptotic high-SNR results.

- Finally, the third contribution is to perform comparison to a reference system with a distributed antenna by means of asymptotic analysis. In practice, the distributed antenna system (DAS) is seldom attractive because of the high costs of wired backhaul connection to the BS.

Throughout the discussions, the main theme is to investigate the joint effect of the wireless backhaul link and service link with multiuser scheduling. Since both the DAS and relay link use the same scheduling algorithm, any difference in performance follows from the amplification of input noise or decoding errors in the RNs. Especially, a closer look is taken at the different relaying protocols that apply resource block-wise processing to characterize their performance in a multiuser setting.

7.2 System Model

This chapter analyzes a bidirectional multihop cellular relay link that consists of a base station (BS), M fixed infrastructure relay nodes (RNs) connected in series, and N_{D} mobile user equipments (UEs) as illustrated in Fig. 2.3(c) at Page 19 for the downlink (DL) direction while its uplink (UL) counterpart is also covered. In the following, the considered system setup is described incrementally in two parts: Analytical models are formulated first for a generic two-hop link with different relaying protocols, and then they are extended by adopting multihop relaying in the backhaul link and opportunistic multiuser scheduling in the service link.

7.2.1 Two-Hop Single-Subcarrier Transmission

In essence, two-hop relaying models are the same for any three consecutive nodes in the multihop system. Thus, this subsection describes two-hop transmission from an arbitrary source (S) node via a relay (R) node to an arbitrary destination (D) node as exemplified in Fig. 7.1. In the DL direction, the source (resp. destination) may be either the BS (resp. a scheduled UE) or a RN and vice versa in the UL direction. The system needs two orthogonal channels, and the destination is assumed to listen only to the second-hop channel since, due to the minimization of the total hop count, the direct source–destination link is weak.

Throughout the analysis, the instantaneous signal-to-noise ratio (SNR) of the source–relay (SR) link is denoted by γ_{SR} and the instantaneous SNR of the relay–destination (RD) link is denoted by γ_{RD}. Each of these parameters corresponds to a single subcarrier or resource block (RB) in OFDM which is transmitted over a narrowband frequency-flat channel. The re-

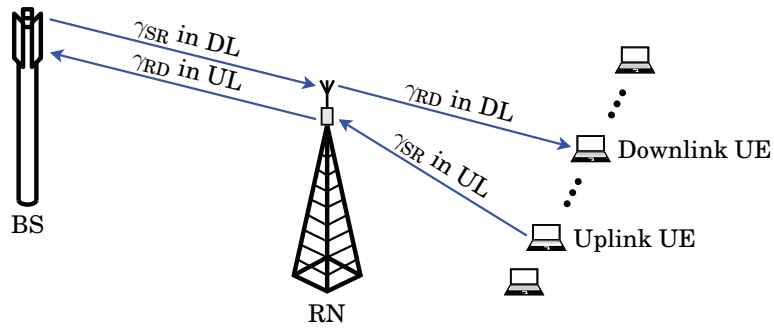

Figure 7.1. Two-hop infrastructure relay link in which γ_{SR} and γ_{RD} denote the instantaneous signal-to-noise ratios of the narrowband OFDM subcarriers or resource blocks in the respective source–relay and relay–destination links.

ceivers in the relay and destination are subject to additive white Gaussian noise (AWGN), power of which is denoted by σ_{R}^2 and σ_{D}^2, respectively.

The performance analysis of this chapter focuses on protocols that apply RB-wise (RW) processing which means the source forms a "virtual one-hop connection" via the relay to the destination over RBs allocated within OFDM(A) symbols. In particular, both essential variations of RW processing, amplify-and-forward (AF) as well as decode-and-forward (DF), are covered: The source node first transmits a RB to the relay node over the first-hop channel, the relay then amplifies or regenerates the RB and finally retransmits it over the second-hop channel to the destination node. All the relaying protocols are discussed in more detail in Section 2.2.4.

Amplify-and-Forward Relaying

An AF relay node simply scales its input RB by a real-valued amplification factor β. Hence, the instantaneous SNR at the destination can be derived by dividing the received signal power with the total noise power as

$$\gamma = \frac{\gamma_{\mathrm{SR}}\gamma_{\mathrm{RD}}}{\gamma_{\mathrm{RD}} + \frac{1}{\sigma_{\mathrm{R}}^2\beta^2}}, \tag{7.1}$$

and the corresponding instantaneous transmission rate becomes

$$\mathcal{C} = \log_2(1+\gamma). \tag{7.2}$$

There are two well-established practices in literature for choosing the amplification factor β, namely variable-gain and fixed-gain relaying protocols, which normalize the instantaneous relay transmit power differently while guaranteeing the same average transmit power.

Variable-gain amplification [142] adjusts the instantaneous relay transmit power to a constant level which is achieved by choosing

$$\beta = \frac{1}{\sigma_{\mathrm{R}}} \cdot \frac{1}{\sqrt{\gamma_{\mathrm{SR}}+1}}. \tag{7.3}$$

Such AF operation is referred to as the variable gain (VG) protocol because varying β^2 is adapted according to source–relay channel fluctuations caused by fast fading. Thereby, the usage of the VG protocol requires that the relay node estimates the instantaneous source–relay channel gain and its input noise power σ_{R}^2.

Finally, by substituting (7.3) into (7.1), the instantaneous end-to-end SNR of the two-hop variable-gain AF relay link becomes

$$\gamma = \frac{\gamma_{\mathrm{SR}}\gamma_{\mathrm{RD}}}{\gamma_{\mathrm{SR}} + \gamma_{\mathrm{RD}} + 1} \tag{7.4}$$

in terms of the instantaneous link SNRs.

Fixed-gain amplification [188], while allowing variable instantaneous transmit power, adjusts the average relay transmit power to a constant level which is achieved by choosing

$$\beta = \frac{1}{\sigma_{\mathrm{R}}} \cdot \frac{1}{\sqrt{\mathcal{E}\{\gamma_{\mathrm{SR}}\}+1}}. \tag{7.5}$$

Due to this constant amplification factor, the scheme is usually referred to as the fixed gain (FG) protocol in literature. This protocol is somewhat simpler than its VG counterpart because the relay node exploits only long-term channel state information for determining the gain factor or, alternatively, it can simply adaptively drive the average transmit power to the desired level.

Finally, by substituting (7.5) into (7.1), the instantaneous end-to-end SNR of the two-hop fixed-gain AF relay link becomes

$$\gamma = \frac{\gamma_{\mathrm{SR}}\gamma_{\mathrm{RD}}}{\mathcal{E}\{\gamma_{\mathrm{SR}}\}+\gamma_{\mathrm{RD}}+1} \tag{7.6}$$

in terms of the instantaneous and average link SNRs.

The above variations of the AF protocol become equivalent in the DL direction of the considered infrastructure-based multihop system although they perform rather differently in the opposite UL direction.

Decode-and-Forward Relaying

A DF relay node decodes its input RB and re-encodes it as an output RB. The possibility of buffering is put aside herein to allow fair comparison with AF relaying (where it is impractical). Hence, the original transmission rate at the source node needs to be lower than the achievable transmission rates of the individual hops, i.e., $\log_2(1+\gamma_{\mathrm{SR}})$ and $\log_2(1+\gamma_{\mathrm{RD}})$, to avoid data overflow and underflow in the relay node. Then, by choosing modulation and coding schemes properly, error-free decoding can be guaranteed both in the relay and destination. The maximum instantaneous end-to-end transmission rate of the two-hop DF relay link becomes

$$\mathcal{C} = \min\{\log_2(1+\gamma_{\mathrm{SR}}), \log_2(1+\gamma_{\mathrm{RD}})\} \tag{7.7}$$

in terms of the instantaneous link SNRs.

Furthermore, by equating $\mathcal{C} = \log_2(1+\gamma)$, the "effective" instantaneous end-to-end SNR of the two-hop DF relay link can be expressed as

$$\gamma = \min\{\gamma_{\mathrm{SR}}, \gamma_{\mathrm{RD}}\} \tag{7.8}$$

which, however, is not a real measurable quantity but only an auxiliary variable for the performance analysis. Thus, it is not meaningful to show explicit performance results for the moments of γ in the case of DF relays.

7.2.2 Multiuser Scheduling in Multihop Relay Links

The complete system setup, sketched in Fig. 2.3(c) at Page 19, is specified next by extending the generic two-hop protocols with multihop relaying in the backhaul link and multiuser scheduling in the service link. The UEs are assumed to communicate with the closest RN which is reasonable when aiming at cell coverage extension, because deploying an extra relay is costly if fewer hops already provide the required quality of service.

In the considered system, N_{D} UEs share one service-link subchannel while the BS and the M RNs need different subchannels for each hop in the backhaul link, in addition to the separation of DL and UL transmissions. Thus, the system allocates in total $2\,(M+1)$ independent time, frequency or physically-isolated RBs within OFDMA symbols. However, RB assignment is an implementation detail which does not need to be specified for the analysis, e.g., in practice, each physical RB may be reused spatially after few hops and some relays may adopt the full-duplex mode if their self-interference is mitigated sufficiently well.

Multihop Backhaul Link

The backhaul relay link consists of M hops between the BS and the RN connected to the UEs; the instantaneous SNR of the mth hop is denoted by $\gamma_{\mathrm{SR}[m]}$ (resp. $\gamma_{\mathrm{RD}[m]}$) in the DL (resp. UL) direction. To simplify notation in the analysis, the backhaul link is compressed into a virtual single-hop link as illustrated in Fig. 7.2. Thus, provided that all the RNs are connected in series, the complete multihop backhaul link is characterized by a single SNR parameter, namely γ_{SR} (resp. γ_{RD}) in the DL (resp. UL) case.

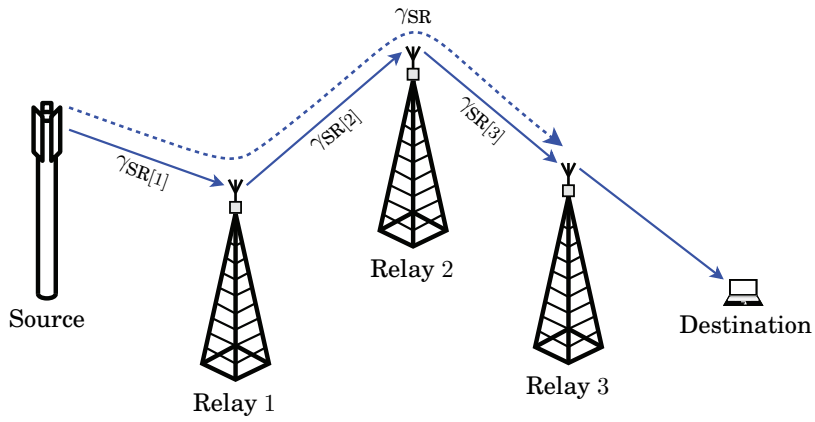

Figure 7.2. Multihop infrastructure backhaul link with $M = 3$ relay nodes where $\gamma_{\mathrm{SR}[m]}$, $m = 1, 2, 3$, denote the signal-to-noise ratios (SNRs) of the individual hops which can be compressed into a single parameter, γ_{SR}.

More specifically, the multihop backhaul link can be transformed by means of expressions to a virtual single-hop link as shown below.

With amplify-and-forward relaying, the SNR of the virtual single-hop link corresponds to the end-to-end SNR of a generic M-hop relay link. Thus, it is possible to exploit well-known expressions from the earlier literature, e.g., Eq. 17 from [100], by directly defining

$$\gamma_{\mathrm{SR}} \triangleq \left[\prod_{m=1}^{M}\left(1+\frac{1}{\gamma_{\mathrm{SR}[m]}}\right)-1\right]^{-1}, \tag{7.9a}$$

$$\gamma_{\mathrm{RD}} \triangleq \left[\prod_{m=1}^{M}\left(1+\frac{1}{\gamma_{\mathrm{RD}[m]}}\right)-1\right]^{-1}, \tag{7.9b}$$

in the downlink and uplink directions, respectively.

With decode-and-forward relaying, the end-to-end transmission rate should be low enough to guarantee error-free decoding after each hop by choosing proper modulation and coding schemes. Thereby, the end-to-end rate of the virtual single-hop link is defined as

$$\log_2(1+\gamma_{\mathrm{SR}}) \triangleq \min_{m=1,2,\ldots,M} \log_2(1+\gamma_{\mathrm{SR}[m]}), \tag{7.10a}$$

$$\log_2(1+\gamma_{\mathrm{RD}}) \triangleq \min_{m=1,2,\ldots,M} \log_2(1+\gamma_{\mathrm{RD}[m]}), \tag{7.10b}$$

in the downlink and uplink directions, respectively. Consequently, the "effective" SNR of the virtual single-hop link can be solved as

$$\gamma_{\mathrm{SR}} \triangleq \min_{m=1,2,\ldots,M} \gamma_{\mathrm{SR}[m]} \quad \text{and} \quad \gamma_{\mathrm{RD}} \triangleq \min_{m=1,2,\ldots,M} \gamma_{\mathrm{RD}[m]} \tag{7.11}$$

in the downlink and uplink directions, respectively.

Throughout the rest of this chapter, parameters γ_{SR} and γ_{RD} are referred to as the backhaul link SNRs and they are exploited as if there was only one hop in the backhaul link to simplify notations. However, the analysis is still valid for any $M \geq 1$ and, actually, the backhaul link could as well comprise any mix of AF and DF relays for which the backhaul link SNRs become combinations of (7.9) and (7.11).

The BS and RNs are assumed to be fixed infrastructure-based nodes. Thus, the wireless channels of the backhaul relay link vary only due to changes in propagation environment which can be regarded as slow and negligible, at least when compared to any link with a mobile end point. It is reasonable to model BS–RN, RN–RN, and RN–BS links as static AWGN channels which implies that $\gamma_{\mathrm{SR}} = \bar{\gamma}_{\mathrm{SR}} \triangleq \mathcal{E}\{\gamma_{\mathrm{SR}}\}$ in the DL direction and $\gamma_{\mathrm{RD}} = \bar{\gamma}_{\mathrm{RD}} \triangleq \mathcal{E}\{\gamma_{\mathrm{RD}}\}$ in the UL direction. Consequently, VG and FG amplification become equivalent in the DL direction which can be verified by comparing (7.6) with (7.4) when $\mathcal{E}\{\gamma_{\mathrm{SR}}\} = \gamma_{\mathrm{SR}}$.

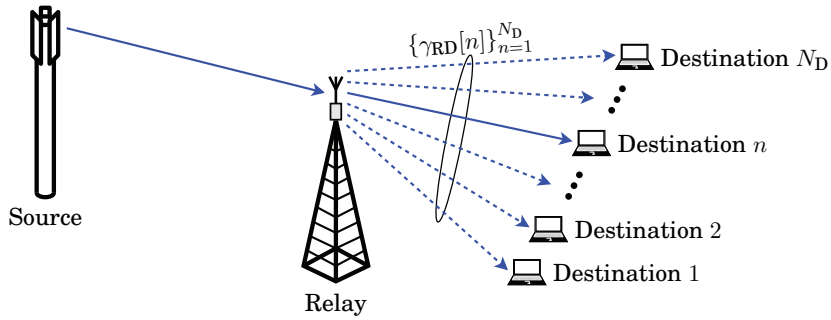

Figure 7.3. Infrastructure relay link with multiuser scheduling in its service link where $\gamma_{\mathrm{RD}}[n]$ denotes the instantaneous signal-to-noise ratio of the fading channel between the relay and the nth destination.

Service Link with Multiuser Scheduling

The service link is shared by N_{D} UEs as illustrated in Fig. 7.3; the instantaneous SNR of the nth UE is denoted by $\gamma_{\mathrm{RD}}[n]$ (resp. $\gamma_{\mathrm{SR}}[n]$) in the DL (resp. UL) direction, and the corresponding average SNRs are marked with overbars, i.e., $\bar{\gamma}_{\mathrm{RD}}[n] \triangleq \mathcal{E}\{\gamma_{\mathrm{RD}}[n]\}$ and $\bar{\gamma}_{\mathrm{SR}}[n] \triangleq \mathcal{E}\{\gamma_{\mathrm{SR}}[n]\}$. The UEs are considered to be moving in a rich scattering environment and, thus, their channels are modeled with non-line-of-sight Rayleigh fading. Consequently, the service link SNRs become independent exponential random variables which, however, are not (necessarily) identically distributed.

The BS schedules each UE in turn as the activated service-link user, whose SNR is denoted by γ_{RD} (resp. γ_{SR}) in the DL (resp. UL) direction. Herein, the maximum-SNR principle is adopted as the scheduling algorithm, which facilitates performance analysis in terms of closed-form expressions using the order statistics of random variables. In particular, the BS chooses always the UE that has momentarily the largest service-link SNR to receive (or to transmit in the UL direction). Since all UEs share the same backhaul link, scheduling can be equivalently done based on the end-to-end SNRs without explicitly knowing the link SNRs of all hops.

Obviously, scheduling decisions require channel state information (CSI) like many other transmission concepts. In the DL direction, it can be obtained by transmitting common pilot subcarriers from which UEs estimate the SNRs and report them via UL feedback channels to the BS. Likewise, uplink UEs can transmit dedicated pilot subcarriers in a time-division manner with the scheduled UE's data, and the BS can then estimate the SNRs by exploiting the knowledge of transmission powers.

In summary, the statistics of the service link with multiuser scheduling based on the maximum-SNR principle can be expressed as follows.

In downlink relaying, the destination node is the scheduled UE for which the instantaneous service-link SNR is given by

$$\gamma_{\mathrm{RD}} = \gamma_{\mathrm{RD}}[w^*[1]] \triangleq \max_{n=1,\ldots,N_{\mathrm{D}}} \gamma_{\mathrm{RD}}[n], \tag{7.12}$$

where $w^*[1]$ denotes the index of the largest variable in $\{\gamma_{\mathrm{RD}}[n]\}_{n=1}^{N_{\mathrm{D}}}$. Recalling the adopted fading models, this calls for the order statistics of exponential random variables which are characterized in Appendix A.3. Especially, the probability density function (PDF) and cumulative distribution function (CDF) of γ_{RD} are obtained as

$$f_{\gamma_{\mathrm{RD}}}(x) = \sum_{m=1}^{M[1,N_{\mathrm{D}}]} a[m,1,N_{\mathrm{D}}] \cdot \frac{1}{b[m,1,N_{\mathrm{D}}]} \exp\left(-\frac{x}{b[m,1,N_{\mathrm{D}}]}\right), \tag{7.13}$$

$$F_{\gamma_{\mathrm{RD}}}(x) = 1 - \sum_{m=1}^{M[1,N_{\mathrm{D}}]} a[m,1,N_{\mathrm{D}}] \cdot \exp\left(-\frac{x}{b[m,1,N_{\mathrm{D}}]}\right), \tag{7.14}$$

for which the coefficients $\{a[m,1,N_{\mathrm{D}}]\}_{m=1}^{M[1,N_{\mathrm{D}}]}$ and $\{b[m,1,N_{\mathrm{D}}]\}_{m=1}^{M[1,N_{\mathrm{D}}]}$ are tabulated based on $\{\bar{\gamma}_{\mathrm{RD}}[n]\}_{n=1}^{N_{\mathrm{D}}}$. When $\bar{\gamma}_{\mathrm{RD}}[n] = \bar{\gamma}_{\mathrm{RD}}$ for all n in a special case, (7.14) admits a simplified form without summation as

$$F_{\gamma_{\mathrm{RD}}}(x) = \left[F_{\gamma_{\mathrm{RD}}[n]}(x)\right]^{N_{\mathrm{D}}} = \left[1 - \exp\left(-\frac{x}{\bar{\gamma}_{\mathrm{RD}}}\right)\right]^{N_{\mathrm{D}}}. \tag{7.15}$$

In uplink relaying, the source node is the scheduled UE for which the instantaneous service-link SNR is given by

$$\gamma_{\mathrm{SR}} = \gamma_{\mathrm{SR}}[w^*[1]] \triangleq \max_{n=1,\ldots,N_{\mathrm{D}}} \gamma_{\mathrm{SR}}[n], \tag{7.16}$$

where $w^*[1]$ denotes the index of the largest variable in $\{\gamma_{\mathrm{SR}}[n]\}_{n=1}^{N_{\mathrm{D}}}$. The PDF and CDF expressions, $f_{\gamma_{\mathrm{SR}}}(x)$ and $F_{\gamma_{\mathrm{SR}}}(x)$, are identical to (7.13) and (7.14) derived for DL relaying although $\{a[m,1,N_{\mathrm{D}}]\}_{m=1}^{M[1,N_{\mathrm{D}}]}$ and $\{b[m,1,N_{\mathrm{D}}]\}_{m=1}^{M[1,N_{\mathrm{D}}]}$ are now tabulated based on $\{\bar{\gamma}_{\mathrm{SR}}[n]\}_{n=1}^{N_{\mathrm{D}}}$.

The fixed-gain protocol becomes different from its variable-gain counterpart because $\mathcal{E}\{\gamma_{\mathrm{SR}}\} \neq \gamma_{\mathrm{SR}}$ in (7.6) when $N_{\mathrm{D}} \geq 2$. Instead

$$\mathcal{E}\{\gamma_{\mathrm{SR}}\} = \int_0^\infty x\, f_{\gamma_{\mathrm{SR}}}(x)\,\mathrm{d}x = \sum_{m=1}^{M[1,N_{\mathrm{D}}]} a[m,1,N_{\mathrm{D}}] \cdot b[m,1,N_{\mathrm{D}}]. \tag{7.17}$$

Thus, when $\bar{\gamma}_{\mathrm{SR}}[n] = \bar{\gamma}_{\mathrm{SR}}$ for all n, the substitution of specific values $M[1,N_{\mathrm{D}}] = N_{\mathrm{D}}$, $a[m,1,N_{\mathrm{D}}] = (-1)^{m-1}\binom{N_{\mathrm{D}}}{m}$, and $b[m,1,N_{\mathrm{D}}] = \frac{\bar{\gamma}_{\mathrm{RD}}}{m}$ from Appendix A.3 yields

$$\mathcal{E}\{\gamma_{\mathrm{SR}}\} = \sum_{m=1}^{N_{\mathrm{D}}} (-1)^{m-1}\binom{N_{\mathrm{D}}}{m}\frac{\bar{\gamma}_{\mathrm{SR}}}{m} = H_{N_{\mathrm{D}}}^{(1)}\,\bar{\gamma}_{\mathrm{SR}}, \tag{7.18}$$

where $H_N^{(r)} \triangleq \sum_{m=1}^{N} \frac{1}{m^r}$ is the Nth harmonic number of order r.

It can be noted that the statistics of DL and UL directions are generally equivalent, but not in the specific case of the fixed-gain AF protocol.

7.3 Performance Analysis

This section proceeds to the main analytical contribution of the chapter by presenting closed-form expressions for the key performance measures used for evaluating wireless systems at large, namely outage probability, outage capacity, average end-to-end SNR, amount of fading, and ergodic capacity. These results hold for any configuration of the multihop relay link with maximum-SNR scheduling specified in the previous section. The analysis is organized to consider separately downlink (DL) and uplink (UL) relaying where the statistics of fixed-gain amplify-and-forward relaying are different while the other protocols are characterized by one set of expressions in both directions with a simple parameter swap.

7.3.1 Downlink Relaying

As formulated in Section 7.2.2 for DL relaying, $\gamma_{\mathrm{SR}} = \bar{\gamma}_{\mathrm{SR}}$ in the backhaul link while γ_{RD} is a random variable given by (7.12) in the service link. Thus, the end-to-end SNR of the scheduled downlink UE becomes

$$\gamma = \frac{\bar{\gamma}_{\mathrm{SR}}\gamma_{\mathrm{RD}}}{\bar{\gamma}_{\mathrm{SR}} + \gamma_{\mathrm{RD}} + 1} \tag{7.19}$$

from (7.4) or (7.6) with both variable- and fixed-gain AF relaying, because $\gamma_{\mathrm{SR}} = \bar{\gamma}_{\mathrm{SR}}$ implies $\mathcal{E}\{\gamma_{\mathrm{SR}}\} = \bar{\gamma}_{\mathrm{SR}}$. With DF relaying, substitution in (7.7) yields the end-to-end transmission rate of the scheduled downlink UE as

$$\mathcal{C} = \min\left\{\log_2(1+\bar{\gamma}_{\mathrm{SR}}), \log_2\left(1+\gamma_{\mathrm{RD}}\right)\right\} \tag{7.20}$$

and, effectively, $\gamma = \min\{\bar{\gamma}_{\mathrm{SR}}, \gamma_{\mathrm{RD}}\}$. In the following, the system performance measures are derived from the statistics of these random variables.

Outage-Based Performance Measures

The first two performance measures deal with the frequency of outages.

Outage probability $\mathcal{P}_{\mathrm{out}}(\gamma_{\mathrm{th}})$ quantifies events where end-to-end SNR, or transmission rate, falls below a target threshold: $\gamma < \gamma_{\mathrm{th}}$, or $\mathcal{C} < \mathcal{C}_{\mathrm{th}}$. In performance analysis, it serves as an approximation and a lower bound for frame-error rate and it is useful in measuring diversity gain. By defining $\mathcal{C}_{\mathrm{th}} \triangleq \log_2(1+\gamma_{\mathrm{th}})$ to equalize rates with AF and DF relaying, outage probability is given by the CDF of γ as $\mathcal{P}_{\mathrm{out}}(\gamma_{\mathrm{th}}) \triangleq F_{\gamma}(\gamma_{\mathrm{th}})$ for which a straightforward transform of random variables yields

$$F_{\gamma}(x) = F_{\gamma_{\mathrm{RD}}}\left(\frac{(\bar{\gamma}_{\mathrm{SR}}+1)x}{\bar{\gamma}_{\mathrm{SR}}-x}\right) \quad \text{for } x \leq \bar{\gamma}_{\mathrm{SR}} \tag{7.21}$$

with AF relaying, while $F_{\gamma}(x) = F_{\gamma_{\mathrm{RD}}}(x)$ for $x \leq \bar{\gamma}_{\mathrm{SR}}$ with DF relaying.

Then, by substituting (7.14) into (7.21), the downlink outage probability of both amplify-and-forward protocols becomes

$$\mathcal{P}_{\text{out}}(\gamma_{\text{th}}) = 1 - \sum_{m=1}^{M[1,N_{\text{D}}]} a[m,1,N_{\text{D}}] \cdot \exp\left(-\frac{\bar{\gamma}_{\text{SR}}+1}{\bar{\gamma}_{\text{SR}}-\gamma_{\text{th}}} \cdot \frac{\gamma_{\text{th}}}{b[m,1,N_{\text{D}}]}\right) \quad (7.22)$$

for $\gamma_{\text{th}} \leq \bar{\gamma}_{\text{SR}}$ while $\mathcal{P}_{\text{out}}(\gamma_{\text{th}}) = 1$ for $\gamma_{\text{th}} > \bar{\gamma}_{\text{SR}}$. Alternatively, by assuming $\bar{\gamma}_{\text{RD}}[n] = \bar{\gamma}_{\text{RD}}$ for all n, (7.15) can be used instead of (7.14) which yields

$$\mathcal{P}_{\text{out}}(\gamma_{\text{th}}) = \left[1 - \exp\left(-\frac{\bar{\gamma}_{\text{SR}}+1}{\bar{\gamma}_{\text{SR}}-\gamma_{\text{th}}} \cdot \frac{\gamma_{\text{th}}}{\bar{\gamma}_{\text{RD}}}\right)\right]^{N_{\text{D}}} \quad (7.23)$$

for $\gamma_{\text{th}} \leq \bar{\gamma}_{\text{SR}}$ while $\mathcal{P}_{\text{out}}(\gamma_{\text{th}}) = 1$ for $\gamma_{\text{th}} > \bar{\gamma}_{\text{SR}}$. Likewise, the downlink outage probability of the DF protocol is $\mathcal{P}_{\text{out}}(\gamma_{\text{th}}) = 1$ for $\gamma_{\text{th}} > \bar{\gamma}_{\text{SR}}$ while

$$\mathcal{P}_{\text{out}}(\gamma_{\text{th}}) = F_{\gamma_{\text{RD}}}(\gamma_{\text{th}}) \quad (7.24)$$

for $\gamma_{\text{th}} \leq \bar{\gamma}_{\text{SR}}$ with the substitution of (7.14) or (7.15).

In the following, it is reasonable to presume $\gamma_{\text{th}} \leq \bar{\gamma}_{\text{SR}}$, because the system is limited by its weakest hop and, if the fixed backhaul link alone does not exceed the desired performance level, relaying in general is useless as shown by the fact that $\mathcal{P}_{\text{out}}(\gamma_{\text{th}}) = 1$ for $\gamma_{\text{th}} > \bar{\gamma}_{\text{SR}}$ with all protocols.

Outage capacity $\mathcal{C}_{\text{out}}(\delta)$ [bit/s/Hz] measures the maximum transmission rate supported with limited outage probability: $\mathcal{P}_{\text{out}}(\gamma_{\text{th}}) \leq \delta$. It is useful for measuring achievable rates in delay-constrained communication and with slow fading, i.e., in cases where coding over multiple channel instances is not practical. Analytically, the maximum threshold SNR satisfying $\mathcal{P}_{\text{out}}(\gamma_{\text{th}}) = F_{\gamma}(\gamma_{\text{th}}) \leq \delta$ is solved as $\gamma_{\text{th}}(\delta) = F_{\gamma}^{-1}(\delta)$ in terms of the inverse CDF of the end-to-end SNR which yields $\mathcal{C}_{\text{out}}(\delta) = \log_2(1+\gamma_{\text{th}}(\delta))$.

Using (7.21), the downlink outage capacity of both AF protocols becomes

$$\mathcal{C}_{\text{out}}(\delta) = \log_2(1+F_{\gamma}^{-1}(\delta)) = \log_2\left(1 + \frac{\bar{\gamma}_{\text{SR}}\, F_{\gamma_{\text{RD}}}^{-1}(\delta)}{\bar{\gamma}_{\text{SR}} + F_{\gamma_{\text{RD}}}^{-1}(\delta) + 1}\right), \quad (7.25)$$

for which the quantile function, i.e., the inverse of (7.14), cannot be expressed in an explicit form necessitating numerical evaluation in general cases. However, when $\bar{\gamma}_{\text{RD}}[n] = \bar{\gamma}_{\text{RD}}$ for all n, (7.15) can be inverted as

$$F_{\gamma_{\text{RD}}}^{-1}(\delta) = -\bar{\gamma}_{\text{RD}} \log_e\left(1-\delta^{1/N_{\text{D}}}\right), \quad (7.26)$$

which yields the outage capacity in a closed form as

$$\mathcal{C}_{\text{out}}(\delta) = \log_2\left(1 + \frac{\bar{\gamma}_{\text{SR}}\bar{\gamma}_{\text{RD}} \log_e\left(1-\delta^{1/N_{\text{D}}}\right)}{\bar{\gamma}_{\text{RD}} \log_e\left(1-\delta^{1/N_{\text{D}}}\right) - (\bar{\gamma}_{\text{SR}}+1)}\right). \quad (7.27)$$

Likewise, the downlink outage capacity of the DF protocol becomes

$$\mathcal{C}_{\text{out}}(\delta) = \min\left\{\log_2(1+\bar{\gamma}_{\text{SR}}), \log_2\left(1+F_{\gamma_{\text{RD}}}^{-1}(\delta)\right)\right\} \quad (7.28)$$

for which, in an implicit form, $F_{\gamma_{\text{RD}}}(F_{\gamma_{\text{RD}}}^{-1}(\delta)) = \delta$ with (7.14) admitting an explicit closed-form expression given in (7.26) when $\bar{\gamma}_{\text{RD}}[n] = \bar{\gamma}_{\text{RD}}$ for all n.

Moment-Based Performance Measures

The second two performance measures exploit the raw moments of the end-to-end SNR, which can be calculated directly from an expectation integral involving (7.13) and (7.19), after binomial expansion, as

$$\begin{aligned}\mathcal{E}\{\gamma^K\} &= \int_0^\infty \left(\frac{\bar{\gamma}_{\mathrm{SR}}\, x}{\bar{\gamma}_{\mathrm{SR}}+1+x}\right)^K f_{\gamma_{\mathrm{RD}}}(x)\,\mathrm{d}x \\ &= \bar{\gamma}_{\mathrm{SR}}^K \sum_{m=1}^{M[1,N_{\mathrm{D}}]} a[m,1,N_{\mathrm{D}}] \cdot \sum_{k=0}^{K} (-1)^k \binom{K}{k} \\ &\quad \times \frac{\bar{\gamma}_{\mathrm{SR}}+1}{b[m,1,N_{\mathrm{D}}]} \exp\left(\frac{\bar{\gamma}_{\mathrm{SR}}+1}{b[m,1,N_{\mathrm{D}}]}\right) E_k\left(\frac{\bar{\gamma}_{\mathrm{SR}}+1}{b[m,1,N_{\mathrm{D}}]}\right),\end{aligned} \tag{7.29}$$

where $E_k(z)$ is the exponential integral [3, Eq. 5.1.4] defined by

$$E_k(z) \triangleq \int_1^\infty \frac{\exp(-zt)}{t^k}\,\mathrm{d}t. \tag{7.30}$$

Thus, the following analysis is relevant only for AF relaying while the effective end-to-end SNR of DF relaying is merely an auxiliary variable.

Average end-to-end SNR $\bar{\gamma} \triangleq \mathcal{E}\{\gamma\}$ can be exploited in link-budget calculations and optimization when designing cellular networks, and it is also basis for slow power control in many systems. Thus, it is an essential measure for theoretical performance analysis as well. In particular with amplify-and-forward relaying, the average end-to-end SNR gives insight into the impact of relay input noise to the long-term performance.

The average downlink end-to-end SNR is obtained by using (7.29) to calculate the first raw moment ($K=1$) as

$$\bar{\gamma} = \bar{\gamma}_{\mathrm{SR}} \sum_{m=1}^{M[1,N_{\mathrm{D}}]} a[m,1,N_{\mathrm{D}}] \cdot \exp\left(\frac{\bar{\gamma}_{\mathrm{SR}}+1}{b[m,1,N_{\mathrm{D}}]}\right) E_2\left(\frac{\bar{\gamma}_{\mathrm{SR}}+1}{b[m,1,N_{\mathrm{D}}]}\right), \tag{7.31}$$

which is simplified by exploiting [3, Eq. 5.1.14] and [3, Eq. 5.1.24].

It is relevant also to study the amount of fading $\mathcal{F}\{\gamma\}$ that has been introduced in [36] as a measure for the severity of fading, before the diversity order was established for the same purpose. With this measure, fading intensity in AF relaying can be compared to that in single-hop transmission, e.g., over Rayleigh ($\mathcal{F}=1$), Nakagami-m ($\mathcal{F}=\frac{1}{m}$) and static AWGN ($\mathcal{F}=0$) channels. In particular, the amount of fading is defined as

$$\mathcal{F}\{\gamma\} \triangleq \frac{\mathrm{Var}\{\gamma\}}{(\mathcal{E}\{\gamma\})^2} = \frac{\mathcal{E}\{\gamma^2\}}{\bar{\gamma}^2} - 1, \tag{7.32}$$

where $\mathrm{Var}\{\gamma\} = \mathcal{E}\{\gamma^2\} - (\mathcal{E}\{\gamma\})^2$ is the variance of the end-to-end SNR.

Finally, the amount of fading in downlink relaying is calculated by substituting (7.29) with $K=2$ and (7.31) into (7.32). It can be noted that resulting $\mathcal{F}\{\gamma\}$ does not directly depend on the link SNRs but mainly on their ratios, e.g., since $\frac{\bar{\gamma}_{\mathrm{SR}}+1}{b[m,1,N_{\mathrm{D}}]} = \frac{\bar{\gamma}_{\mathrm{SR}}+1}{\bar{\gamma}_{\mathrm{RD}}} m$ when $\bar{\gamma}_{\mathrm{RD}}[n] = \bar{\gamma}_{\mathrm{RD}}$ for all n.

Ergodic Capacity

The last performance measure, ergodic capacity $\bar{\mathcal{C}}$ [bit/s/Hz], is obtained by averaging the instantaneous end-to-end transmission rate over fading distributions: $\bar{\mathcal{C}} \triangleq \mathcal{E}\{\mathcal{C}\}$. For achieving transmission rate that closely attains the ergodic capacity, the system should encode transmitted data over reasonably many channel instances while the fading distributions remain constant, i.e., ergodicity assumption is satisfied. Thus, the ergodic capacity is practical for analyzing available transmission rates in communication over fast-fading channels and with loose delay constraints.

Using (7.2), (7.13), and (7.19), the downlink ergodic capacity of both AF protocols is calculated in terms of the exponential integral as

$$\begin{aligned}\bar{\mathcal{C}} &= \mathcal{E}\{\log_2(1+\gamma)\} \qquad (7.33)\\ &= \int_0^{\infty} \log_2\left(1+\frac{\bar{\gamma}_{\mathrm{SR}}\, x}{\bar{\gamma}_{\mathrm{SR}}+1+x}\right) f_{\gamma_{\mathrm{RD}}}(x)\,\mathrm{d}x\\ &= \sum_{m=1}^{M[1,N_{\mathrm{D}}]} \frac{a[m,1,N_{\mathrm{D}}]}{\log_e(2)} \cdot \left[\exp\left(\frac{1}{b[m,1,N_{\mathrm{D}}]}\right) E_1\left(\frac{1}{b[m,1,N_{\mathrm{D}}]}\right)\right.\\ &\qquad \left. - \exp\left(\frac{\bar{\gamma}_{\mathrm{SR}}+1}{b[m,1,N_{\mathrm{D}}]}\right) E_1\left(\frac{\bar{\gamma}_{\mathrm{SR}}+1}{b[m,1,N_{\mathrm{D}}]}\right)\right]\end{aligned}$$

by separating the logarithm of a fraction into a sum of two logarithms and applying integration by parts. Similarly, the downlink ergodic capacity of the DF protocol can be derived from (7.13) and (7.20), by partitioning the integral into two integrals over intervals $[0, \bar{\gamma}_{\mathrm{SR}}]$ and $[\bar{\gamma}_{\mathrm{SR}}, \infty)$, as

$$\begin{aligned}\bar{\mathcal{C}} &= \mathcal{E}\{\min\{\log_2(1+\bar{\gamma}_{\mathrm{SR}}), \log_2(1+\gamma_{\mathrm{RD}})\}\} \qquad (7.34)\\ &= \int_0^{\infty} \log_2\left(1+\min\{\bar{\gamma}_{\mathrm{SR}}, x\}\right) f_{\gamma_{\mathrm{RD}}}(x)\,\mathrm{d}x\\ &= \sum_{m=1}^{M[1,N_{\mathrm{D}}]} \frac{a[m,1,N_{\mathrm{D}}]}{\log_e(2)} \cdot \left[\exp\left(\frac{1}{b[m,1,N_{\mathrm{D}}]}\right) E_1\left(\frac{1}{b[m,1,N_{\mathrm{D}}]}\right)\right.\\ &\qquad \left. - \exp\left(\frac{1}{b[m,1,N_{\mathrm{D}}]}\right) E_1\left(\frac{\bar{\gamma}_{\mathrm{SR}}+1}{b[m,1,N_{\mathrm{D}}]}\right)\right].\end{aligned}$$

The minor, but essential, difference between the AF and DF protocols can be observed from the comparison of (7.33) and (7.34) in which the negative terms, that degrade capacity from the single-hop case, are increased with AF relaying by a factor of $\exp(\bar{\gamma}_{\mathrm{SR}}/b[m,1,N_{\mathrm{D}}])$ due to relay input noise.

As a significant numerical issue reported first in **[223]**, it should be noted that the above expressions contain $\exp(x)\,E_1(y)$ in which $\exp(x)$ may overflow and $E_1(y)$ may underflow rather easily. Thus, special care needs to be taken when evaluating ergodic capacity values for the following numerical results as discussed in Appendix A.4. Fortunately, the

exactly same issue does not concern the average SNR, which contains $\exp(x)\,E_2(x)$, because for $k>1$, $E_k(0)=\frac{1}{k-1}$ [3, Eq. 5.1.23] which is finite.

7.3.2 Uplink Relaying

As formulated in Section 7.2.2 for UL relaying, γ_{SR} is a random variable given by (7.16) in the service link while $\gamma_{\mathrm{RD}}=\bar{\gamma}_{\mathrm{RD}}$ in the backhaul link. Thus, the variable-gain AF and DF uplink relaying protocols are statistically equivalent to their downlink counterparts due to obvious symmetry in (7.19) and (7.20). Analytically, this implies that all the performance measures can be directly obtained for these protocols from those presented in the previous subsection by simply swapping $\bar{\gamma}_{\mathrm{SR}}$ and $\{\bar{\gamma}_{\mathrm{RD}}[n]\}_{n=1}^{N_{\mathrm{D}}}$ with $\bar{\gamma}_{\mathrm{RD}}$ and $\{\bar{\gamma}_{\mathrm{SR}}[n]\}_{n=1}^{N_{\mathrm{D}}}$, respectively. In contrast, the fixed-gain AF relaying protocol is not subject to similar symmetry and it must, therefore, be analyzed separately in the uplink direction as follows.

In FG relaying, the substitution of $\gamma_{\mathrm{RD}}=\bar{\gamma}_{\mathrm{RD}}$ into (7.6) yields the end-to-end SNR of the scheduled uplink UE as

$$\gamma=\frac{\gamma_{\mathrm{SR}}\bar{\gamma}_{\mathrm{RD}}}{\mathcal{E}\{\gamma_{\mathrm{SR}}\}+\bar{\gamma}_{\mathrm{RD}}+1}, \tag{7.35}$$

for which $\mathcal{E}\{\gamma_{\mathrm{SR}}\}$ is given by (7.17) or (7.18), i.e., $\mathcal{E}\{\gamma_{\mathrm{SR}}\}\neq\bar{\gamma}_{\mathrm{SR}}$ causing asymmetry in the general case due to multiuser scheduling. Consequently, the CDF of γ is obtained as

$$F_{\gamma}(x)=F_{\gamma_{\mathrm{SR}}}\left(\frac{\mathcal{E}\{\gamma_{\mathrm{SR}}\}+\bar{\gamma}_{\mathrm{RD}}+1}{\bar{\gamma}_{\mathrm{RD}}}x\right) \tag{7.36}$$

with a straightforward transform of random variables.

Recalling $\mathcal{P}_{\mathrm{out}}(\gamma_{\mathrm{th}})\triangleq F_{\gamma}(\gamma_{\mathrm{th}})$ and by substituting $F_{\gamma_{\mathrm{SR}}}(x)$, which admits the same expression as shown in (7.14) for $F_{\gamma_{\mathrm{RD}}}(x)$ in downlink relaying, into (7.36), the uplink outage probability of the FG protocol becomes

$$\mathcal{P}_{\mathrm{out}}(\gamma_{\mathrm{th}})=1-\sum_{m=1}^{M[1,N_{\mathrm{D}}]}a[m,1,N_{\mathrm{D}}]\cdot\exp\left(-\frac{\mathcal{E}\{\gamma_{\mathrm{SR}}\}+\bar{\gamma}_{\mathrm{RD}}+1}{b[m,1,N_{\mathrm{D}}]\,\bar{\gamma}_{\mathrm{RD}}}\,\gamma_{\mathrm{th}}\right) \tag{7.37}$$

for which $\{a[m,1,N_{\mathrm{D}}]\}_{m=1}^{M[1,N_{\mathrm{D}}]}$ and $\{b[m,1,N_{\mathrm{D}}]\}_{m=1}^{M[1,N_{\mathrm{D}}]}$ are tabulated based on $\{\bar{\gamma}_{\mathrm{SR}}[n]\}_{n=1}^{N_{\mathrm{D}}}$ as explained in Appendix A.3. When $\bar{\gamma}_{\mathrm{SR}}[n]=\bar{\gamma}_{\mathrm{SR}}$ for all n, $\mathcal{E}\{\gamma_{\mathrm{SR}}\}=H_{N_{\mathrm{D}}}^{(1)}\bar{\gamma}_{\mathrm{SR}}$ as derived in (7.18) and the outage probability expression can be simplified to

$$\mathcal{P}_{\mathrm{out}}(\gamma_{\mathrm{th}})=\left[1-\exp\left(-\frac{H_{N_{\mathrm{D}}}^{(1)}\bar{\gamma}_{\mathrm{SR}}+\bar{\gamma}_{\mathrm{RD}}+1}{\bar{\gamma}_{\mathrm{SR}}\bar{\gamma}_{\mathrm{RD}}}\,\gamma_{\mathrm{th}}\right)\right]^{N_{\mathrm{D}}} \tag{7.38}$$

using an alternative form of $F_{\gamma_{\mathrm{SR}}}(x)$ which is obtained from (7.15) by replacing $\bar{\gamma}_{\mathrm{RD}}$ with $\bar{\gamma}_{\mathrm{SR}}$ in order to translate it to the uplink context.

After solving $\gamma_{\text{th}}(\delta) = F_{\gamma}^{-1}(\delta)$ from (7.36), the uplink outage capacity of the FG protocol becomes

$$\mathcal{C}_{\text{out}}(\delta) = \log_2\left(1+\gamma_{\text{th}}(\delta)\right) = \log_2\left(1+\frac{F_{\gamma_{\text{SR}}}^{-1}(\delta)\,\bar{\gamma}_{\text{RD}}}{\mathcal{E}\{\gamma_{\text{SR}}\}+\bar{\gamma}_{\text{RD}}+1}\right) \tag{7.39}$$

for which the quantile function $F_{\gamma_{\text{SR}}}^{-1}(\delta)$ is generally available only in an implicit form as $F_{\gamma_{\text{SR}}}(F_{\gamma_{\text{SR}}}^{-1}(\delta)) = \delta$. However, when $\bar{\gamma}_{\text{SR}}[n] = \bar{\gamma}_{\text{SR}}$ for all n,

$$F_{\gamma_{\text{SR}}}^{-1}(\delta) = -\bar{\gamma}_{\text{SR}}\log_e\left(1-\delta^{1/N_{\text{D}}}\right) \tag{7.40}$$

which together with $\mathcal{E}\{\gamma_{\text{SR}}\}$ from (7.18) yields the outage capacity in an explicit closed form as

$$\mathcal{C}_{\text{out}}(\delta) = \log_2\left(1-\frac{\bar{\gamma}_{\text{SR}}\bar{\gamma}_{\text{RD}}\log_e\left(1-\delta^{1/N_{\text{D}}}\right)}{H_{N_{\text{D}}}^{(1)}\bar{\gamma}_{\text{SR}}+\bar{\gamma}_{\text{RD}}+1}\right). \tag{7.41}$$

The average uplink end-to-end SNR can be stated rather directly, since only the numerator of (7.35) contains a random variable, as

$$\bar{\gamma} \triangleq \mathcal{E}\{\gamma\} = \frac{\mathcal{E}\{\gamma_{\text{SR}}\}\bar{\gamma}_{\text{RD}}}{\mathcal{E}\{\gamma_{\text{SR}}\}+\bar{\gamma}_{\text{RD}}+1} \tag{7.42}$$

for which $\mathcal{E}\{\gamma_{\text{SR}}\}$ is given by (7.17) or (7.18). Recalling that $f_{\gamma_{\text{SR}}}(x)$ admits the same expression as $f_{\gamma_{\text{RD}}}(x)$ given in (7.13), except for the coefficients $\{a[m,1,N_{\text{D}}]\}_{m=1}^{M[1,N_{\text{D}}]}$ and $\{b[m,1,N_{\text{D}}]\}_{m=1}^{M[1,N_{\text{D}}]}$ which are tabulated based on $\{\bar{\gamma}_{\text{SR}}[n]\}_{n=1}^{N_{\text{D}}}$, the raw moments of the end-to-end SNR can be expressed as a weighted sum of the moments of exponential random variables as

$$\begin{aligned}\mathcal{E}\{\gamma^K\} &= \int_0^{\infty}\left(\frac{x\,\bar{\gamma}_{\text{RD}}}{\mathcal{E}\{\gamma_{\text{SR}}\}+\bar{\gamma}_{\text{RD}}+1}\right)^K f_{\gamma_{\text{SR}}}(x)\,\mathrm{d}x \\ &= K!\sum_{m=1}^{M[1,N_{\text{D}}]} a[m,1,N_{\text{D}}]\cdot\left(\frac{b[m,1,N_{\text{D}}]\,\bar{\gamma}_{\text{RD}}}{\mathcal{E}\{\gamma_{\text{SR}}\}+\bar{\gamma}_{\text{RD}}+1}\right)^K.\end{aligned} \tag{7.43}$$

This yields the amount of fading $\mathcal{F}\{\gamma\}$ in uplink FG relaying as expressed in (7.32) with the substitution of $\mathcal{E}\{\gamma\}$ and $\mathcal{E}\{\gamma^2\}$. In a special case, the average end-to-end SNR and the amount of fading can be simplified to

$$\bar{\gamma} = \frac{H_{N_{\text{D}}}^{(1)}\bar{\gamma}_{\text{SR}}\bar{\gamma}_{\text{RD}}}{H_{N_{\text{D}}}^{(1)}\bar{\gamma}_{\text{SR}}+\bar{\gamma}_{\text{RD}}+1} \quad \text{and} \quad \mathcal{F}\{\gamma\} = \frac{H_{N_{\text{D}}}^{(2)}}{\left(H_{N_{\text{D}}}^{(1)}\right)^2}, \tag{7.44}$$

respectively, when $\bar{\gamma}_{\text{SR}}[n] = \bar{\gamma}_{\text{SR}}$ for all n.

Finally, using (7.2) with (7.35) and the PDF of γ_{SR}, the uplink ergodic capacity of the FG protocol can be calculated as

$$\begin{aligned}\bar{\mathcal{C}} &= \mathcal{E}\{\log_2(1+\gamma)\} \\ &= \int_0^{\infty}\log_2\left(1+\frac{x\,\bar{\gamma}_{\text{RD}}}{\mathcal{E}\{\gamma_{\text{SR}}\}+\bar{\gamma}_{\text{RD}}+1}\right) f_{\gamma_{\text{SR}}}(x)\,\mathrm{d}x \\ &= \sum_{m=1}^{M[1,N_{\text{D}}]}\frac{a[m,1,N_{\text{D}}]}{\log_e(2)}\cdot\exp\left(\frac{\mathcal{E}\{\gamma_{\text{SR}}\}+\bar{\gamma}_{\text{RD}}+1}{b[m,1,N_{\text{D}}]\,\bar{\gamma}_{\text{RD}}}\right)E_1\left(\frac{\mathcal{E}\{\gamma_{\text{SR}}\}+\bar{\gamma}_{\text{RD}}+1}{b[m,1,N_{\text{D}}]\,\bar{\gamma}_{\text{RD}}}\right)\end{aligned} \tag{7.45}$$

by applying integration by parts.

7.4 Performance Evaluation

This section illustrates the analytical measures derived in the previous section for evaluating the performance gains given by multiuser scheduling in multihop relaying, for comparing the relaying protocols, and for measuring the performance losses due to using a non-ideal wireless backhaul link instead of a wired connection. These generic numerical results are valid for any number of hops, because the M-hop backhaul link can be compressed into a virtual single-hop link as explained in Section 7.2.2.

For illustration purposes, the average service link SNRs of all UEs are set equal, i.e., for all n, $\bar{\gamma}_{\mathrm{RD}}[n] = \bar{\gamma}_{\mathrm{RD}}$ in the downlink (DL) direction and $\bar{\gamma}_{\mathrm{SR}}[n] = \bar{\gamma}_{\mathrm{SR}}$ in the uplink (UL) direction. This is approximately valid in practical scenarios as well, if slow power control is employed to balance the average link SNRs or the results concern performance within a resource pool shared by a group of UEs that have similar average SNRs. With balanced channels, maximum-SNR scheduling becomes also fair, since all UEs are guaranteed to be scheduled with equal probability.

7.4.1 Gains from Multiuser Scheduling

In the following, the performance of multiuser scheduling among N_{D} UEs is compared to that of single-user transmission and round-robin (or random) scheduling; with any N_{D}, these reference cases are covered by substituting $N_{\mathrm{D}} = 1$ into performance expressions. As noted in the previous sections, VG and FG amplify-and-forward protocols are equivalent in the DL direction, and it will be seen that the low-SNR performance of all the protocols is also almost the same. Thus, the discussion concentrates mostly on the mid-SNR and asymptotic high-SNR scenarios. In particular, performance is analyzed in terms of the average service link SNRs, i.e., varying $\bar{\gamma}_{\mathrm{RD}}$ (resp. $\bar{\gamma}_{\mathrm{SR}}$), while the backhaul link SNR is fixed to a constant value $\bar{\gamma}_{\mathrm{SR}} = 20$ dB (resp. $\bar{\gamma}_{\mathrm{RD}} = 20$ dB) in the DL (resp. UL) direction.

Figure 7.4 illustrates the outage probability for a target threshold of $\gamma_{\mathrm{th}} = 10$ dB, i.e., $\mathcal{C}_{\mathrm{th}} = 3.46$ bit/s/Hz, using (7.23), (7.24), and (7.38). In the UL direction, the outage probability of the fixed-gain AF protocol is always worse than that of the other protocols and converges to a floor level:

$$\mathcal{P}_{\mathrm{out}}(\gamma_{\mathrm{th}}) \geq \left[1 - \exp\left(-\frac{\gamma_{\mathrm{th}}}{H_{N_{\mathrm{D}}}^{(1)}\bar{\gamma}_{\mathrm{RD}}}\right)\right]^{N_{\mathrm{D}}}, \tag{7.46}$$

which is tight in the high-SNR regime where $\bar{\gamma}_{\mathrm{SR}} \to \infty$. The outage proba-

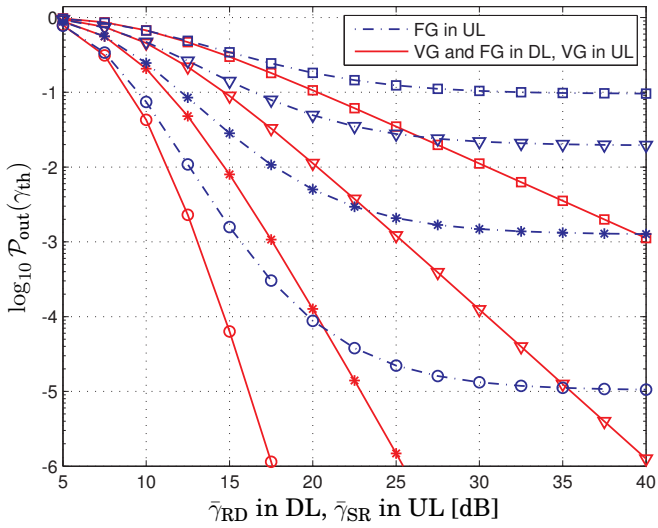

(a) amplify-and-forward (AF) relaying

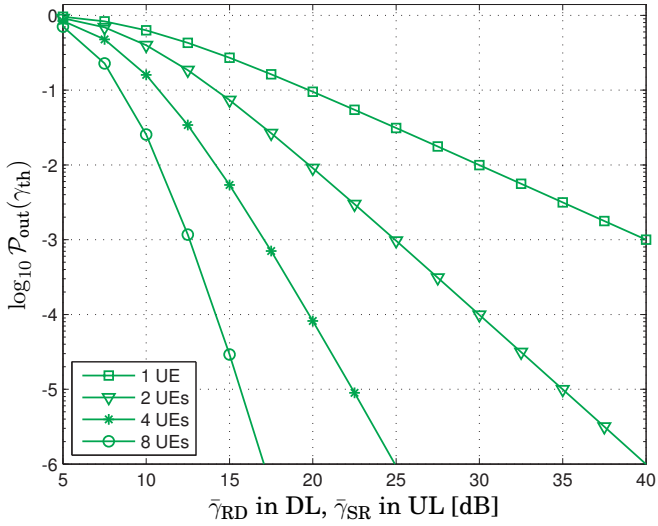

(b) decode-and-forward (DF) relaying

Figure 7.4. Outage probability for threshold SNR $\gamma_{\text{th}} = 10$ dB in terms of the service link SNRs when the backhaul link SNRs are fixed to 20 dB. The curves for maximum-SNR scheduling among $N_{\text{D}} = 1, 2, 4, 8$ users are denoted with markers ($\square$), ($\triangledown$), ($*$), ($\circ$), respectively, and located top-down in the figures.

bility expressions of the other AF protocols can be asymptotically approximated by the first-order term in Taylor's series expansion as

$$\mathcal{P}_{\text{out}}(\gamma_{\text{th}}) \approx \left(\frac{(\bar{\gamma}_{\text{SR}}+1)\gamma_{\text{th}}}{\bar{\gamma}_{\text{SR}}-\gamma_{\text{th}}} \right)^{N_{\text{D}}} (\bar{\gamma}_{\text{RD}})^{-N_{\text{D}}}, \tag{7.47a}$$

$$\mathcal{P}_{\text{out}}(\gamma_{\text{th}}) \approx \left(\frac{(\bar{\gamma}_{\text{RD}}+1)\gamma_{\text{th}}}{\bar{\gamma}_{\text{RD}}-\gamma_{\text{th}}} \right)^{N_{\text{D}}} (\bar{\gamma}_{\text{SR}})^{-N_{\text{D}}} \tag{7.47b}$$

for large $\bar{\gamma}_{\text{RD}}$ (in the DL direction) or large $\bar{\gamma}_{\text{SR}}$ (in the UL direction), respectively. Similarly, the respective DL and UL outage probability expressions of the DF protocol can be approximated as

$$\mathcal{P}_{\text{out}}(\gamma_{\text{th}}) \approx (\gamma_{\text{th}})^{N_{\text{D}}} (\bar{\gamma}_{\text{RD}})^{-N_{\text{D}}} \quad \text{and} \quad \mathcal{P}_{\text{out}}(\gamma_{\text{th}}) \approx (\gamma_{\text{th}})^{N_{\text{D}}} (\bar{\gamma}_{\text{SR}})^{-N_{\text{D}}}. \tag{7.48}$$

Except for uplink VG relaying, all the protocols thus achieve diversity order of N_{D}, which is seen from the exponents of the asymptotic outage probabilities, i.e., the magnitude of the high-SNR slope on a log-log scale.

Continuing with outage-based measures, Fig. 7.5 shows the 1%-outage capacity by using (7.27), (7.28), and (7.41). With all protocols, transmission rates are limited by the AWGN channels of the backhaul link, i.e.,

$$\mathcal{C}_{\text{out}}(\delta) \leq \log_2(1+\bar{\gamma}_{\text{SR}}) \quad \text{and} \quad \mathcal{C}_{\text{out}}(\delta) \leq \log_2(1+\bar{\gamma}_{\text{RD}}), \tag{7.49}$$

in DL and UL relaying, respectively, and these limits are approached with large $\bar{\gamma}_{\text{RD}}$ and large $\bar{\gamma}_{\text{SR}}$, respectively. The AF protocols are in general worse than the DF protocol which is also indicated by the lower SNR gain of asymptotic outage probability in (7.47) versus (7.48). Furthermore, the uplink outage capacity of the FG protocol is significantly lower than that of the other protocols, and (7.41) converges to a tight upper bound

$$\mathcal{C}_{\text{out}}(\delta) \leq \log_2 \left(1 - \frac{\bar{\gamma}_{\text{RD}}}{H_{N_{\text{D}}}^{(1)}} \log_e \left(1-\delta^{1/N_{\text{D}}} \right) \right) \tag{7.50}$$

in the high-SNR regime where $\bar{\gamma}_{\text{SR}} \to \infty$.

As can be deduced from the outage capacity expressions given in (7.27) and (7.28), maximum-SNR scheduling among N_{D} UEs offers SNR gain of

$$\Delta\bar{\gamma}_{\text{RD}} = \Delta\bar{\gamma}_{\text{SR}} = 10\log_{10} \left(\frac{\log_e\left(1-\delta^{1/N_{\text{D}}}\right)}{\log_e(1-\delta)} \right) \text{ [dB]}, \tag{7.51}$$

which does not depend on the link SNRs, over round-robin scheduling with all protocols other than uplink FG relaying. For example, by choosing $\delta = 0.01$ as in the figures, the SNR gain manifests itself as a shift which is significantly 10.2 dB, 15.8 dB, 19.1 dB and 21.4 dB when scheduling among 2, 4, 8, and 16 UEs, respectively. In uplink FG relaying, the SNR gain is actually larger, converging to (7.51) in the low-SNR regime.

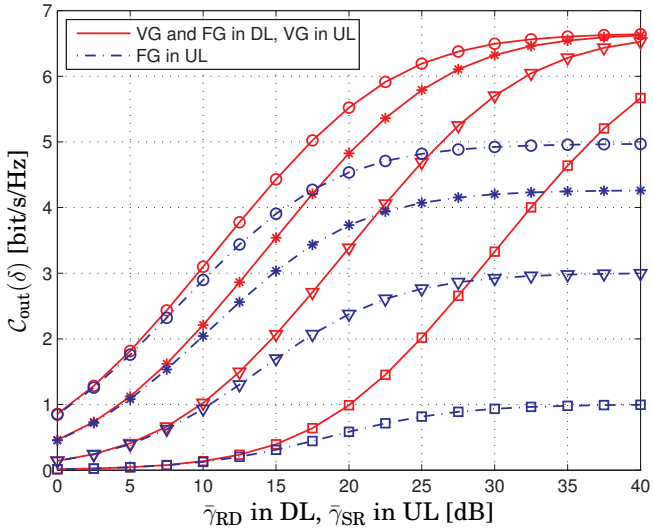

(a) amplify-and-forward (AF) relaying

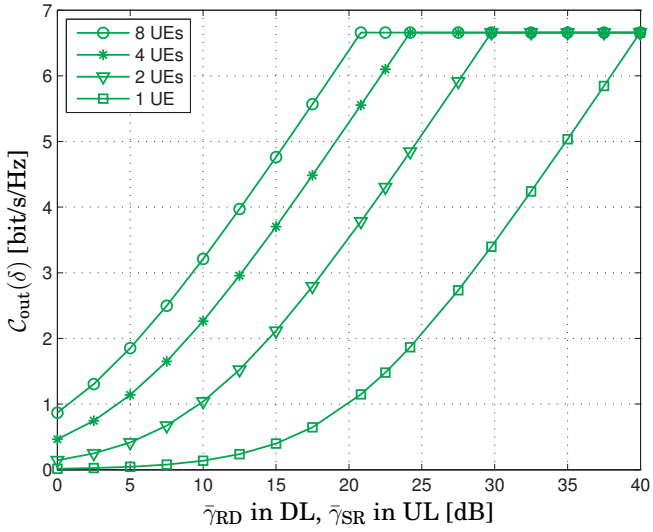

(b) decode-and-forward (DF) relaying

Figure 7.5. Outage capacity with limit $\delta = 0.01$ for outage probability in terms of the service link SNRs when the backhaul link SNRs are fixed to 20 dB. The curves for maximum-SNR scheduling among $N_{\mathrm{D}} = 1, 2, 4, 8$ users are denoted with markers (□), (▽), (∗), (○), respectively, and located bottom-up in the figures.

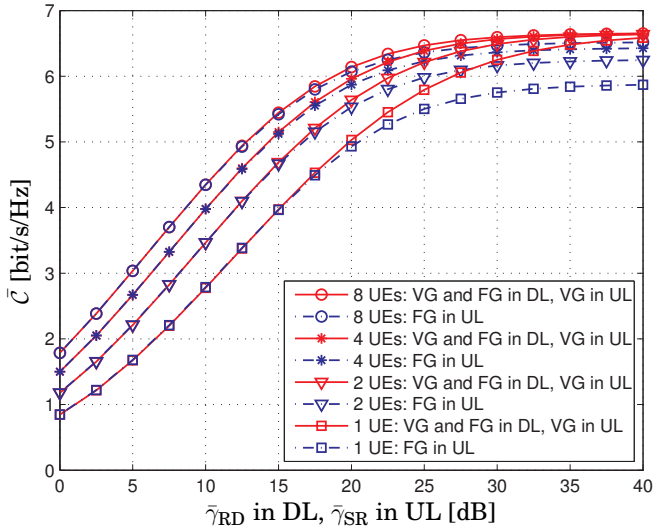

(a) amplify-and-forward (AF) relaying

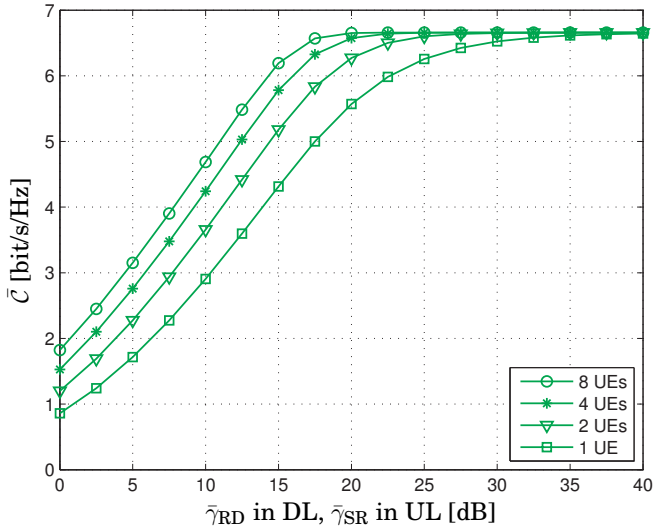

(b) decode-and-forward (DF) relaying

Figure 7.6. Ergodic capacity in terms of the service link SNRs when the backhaul link SNRs are fixed to 20 dB. The curves for maximum-SNR scheduling among $N_{\mathrm{D}} = 1, 2, 4, 8$ users are denoted with markers (□), (▽), (∗), (○), respectively, and located bottom-up in the figures.

Ergodic capacity is illustrated in Fig. 7.6 using (7.33), (7.34), and (7.45). It is naturally limited by the AWGN channel capacity of the backhaul link, i.e., the bounds shown in (7.49) apply also for the ergodic capacity. Especially, the uplink ergodic capacity of the FG protocol is worse than that of the VG protocol, and it converges to a lower upper bound

$$\bar{\mathcal{C}} \leq \frac{1}{\log_e(2)} \sum_{m=1}^{N_{\mathrm{D}}} (-1)^{m-1} \binom{N_{\mathrm{D}}}{m} \exp\left(\frac{H_{N_{\mathrm{D}}}^{(1)}}{\bar{\gamma}_{\mathrm{RD}}} m\right) E_1\left(\frac{H_{N_{\mathrm{D}}}^{(1)}}{\bar{\gamma}_{\mathrm{RD}}} m\right) \tag{7.52}$$

in the high-SNR regime where $\bar{\gamma}_{\mathrm{SR}} \to \infty$.

Average end-to-end SNR is shown in Fig. 7.7 for the AF protocols based on (7.31) and (7.42). In terms of this particular performance measure, the FG protocol is better than the VG protocol in the uplink direction. This rather unexpected observation can be verified by applying Jensen's inequality [122] to the expectation of the concave end-to-end SNR function of γ_{SR} as also shown in [50, Proposition 1]. In particular, starting from the average SNR of the VG protocol, Jensen's inequality yields

$$\mathcal{E}\left\{\frac{\gamma_{\mathrm{SR}}\bar{\gamma}_{\mathrm{RD}}}{\gamma_{\mathrm{SR}} + \bar{\gamma}_{\mathrm{RD}} + 1}\right\} \leq \frac{\mathcal{E}\left\{\gamma_{\mathrm{SR}}\right\}\bar{\gamma}_{\mathrm{RD}}}{\mathcal{E}\{\gamma_{\mathrm{SR}}\} + \bar{\gamma}_{\mathrm{RD}} + 1} = \mathcal{E}\left\{\frac{\gamma_{\mathrm{SR}}\bar{\gamma}_{\mathrm{RD}}}{\mathcal{E}\{\gamma_{\mathrm{SR}}\} + \bar{\gamma}_{\mathrm{RD}} + 1}\right\}, \tag{7.53}$$

resulting in the expectation of (7.35), i.e., average SNR in FG relaying.

In the low-SNR regime, the VG and FG protocols achieve asymptotically the same average SNR in both DL and UL relaying, and maximum-SNR scheduling among N_{D} UEs offers $10\log_{10}\left(H_K^{(1)}\right)$ [dB] increase over round-robin scheduling or single-user transmission, which corresponds to selection diversity between N_{D} Rayleigh channels. For example, the SNR increase is 1.76 dB, 3.19 dB, 4.34 dB, and 5.29 dB when scheduling among 2, 4, 8, and 16 UEs, respectively. In the high-SNR regime where $\bar{\gamma}_{\mathrm{RD}}[n] \to \infty$ (resp. $\bar{\gamma}_{\mathrm{SR}}[n] \to \infty$) in the DL (resp. UL) direction for all n, average end-to-end SNR converges to the limit set by the fixed backhaul link SNR, thus approaching the upper bound $\bar{\gamma} \leq \bar{\gamma}_{\mathrm{SR}}$ (resp. $\bar{\gamma} \leq \bar{\gamma}_{\mathrm{RD}}$).

Finally, Fig. 7.8 illustrates the amount of fading using (7.32) and (7.44). In fixed-gain UL relaying, this measure is independent of the link SNRs unlike in DL and variable-gain UL relaying. In the UL direction, VG relaying is subject to weaker fading than FG relaying, but if $\bar{\gamma}_{\mathrm{RD}}[n] \ll \bar{\gamma}_{\mathrm{SR}}$ (resp. $\bar{\gamma}_{\mathrm{SR}}[n] \ll \bar{\gamma}_{\mathrm{RD}}$) for all n in the DL (resp. UL) direction, the protocols are approximately equivalent; with scheduling among 1, 2, 4 and 8 UEs, $\mathcal{F}\{\gamma\}$ corresponds to classic Nakagami-m channels with $m = 1$ (Rayleigh fading), $m = 1.8$, $m = 3.05$, and $m = 4.84$, respectively. In contrast, when $\bar{\gamma}_{\mathrm{RD}}[n] \gg \bar{\gamma}_{\mathrm{SR}}$ in DL relaying or $\bar{\gamma}_{\mathrm{SR}}[n] \gg \bar{\gamma}_{\mathrm{RD}}$ in UL relaying for all n, $\mathcal{F}\{\gamma\} \approx 0$ which implies that the end-to-end link is virtually static.

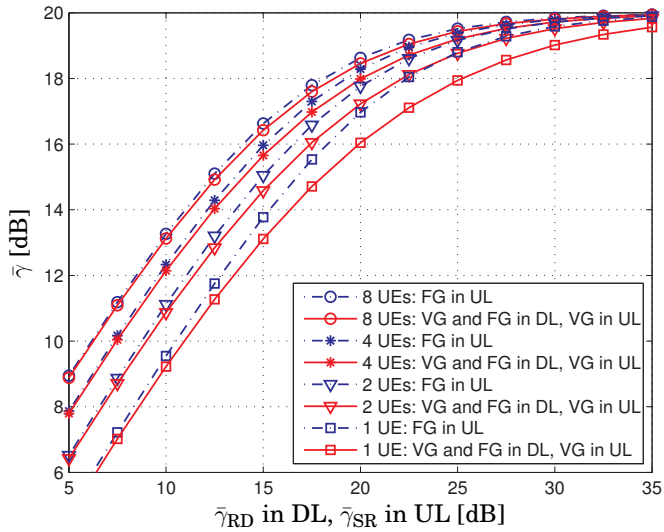

Figure 7.7. Average end-to-end SNR in amplify-and-forward relaying in terms of the service link SNRs when the backhaul link SNRs are fixed to 20 dB. The curves for maximum-SNR scheduling among $N_{\mathrm{D}} = 1, 2, 4, 8$ users are denoted with markers (□), (▽), (∗), (○), respectively, and located bottom-up in the figures.

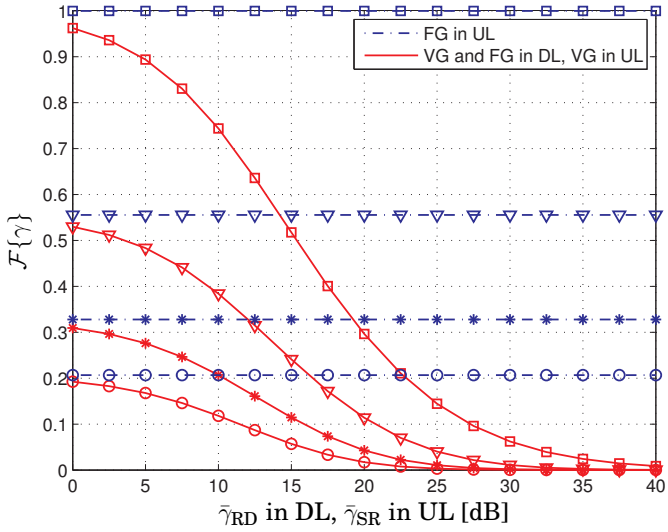

Figure 7.8. The amount of fading in amplify-and-forward relaying in terms of the service link SNRs when the backhaul link SNRs are fixed to 20 dB. The curves for maximum-SNR scheduling among $N_{\mathrm{D}} = 1, 2, 4, 8$ users are denoted with markers (□), (▽), (∗), (○), respectively, and located top-down in the figures.

7.4.2 Losses from Wireless Backhaul

Another kind of relevant analysis can be realized by contrasting relaying with its asymptotic case, where the multihop backhaul link is noise-free in addition to being static, i.e., $\bar{\gamma}_{\mathrm{SR}} \to \infty$ in the downlink direction and $\bar{\gamma}_{\mathrm{RD}} \to \infty$ in the uplink direction. The reference case corresponds effectively to a distributed antenna system (DAS), where the last RN in the end of the multihop backhaul link is actually a remote BS antenna with a cable connection or dedicated microwave links to and from the BS. By comparing the non-ideal multihop relay link to the ideal DAS, this subsection thus evaluates the performance loss due to input noise amplification in AF relaying. Related comparison results are available also in Chapter 8 with all kind of OFDM(A) relaying protocols.

Throughout this subsection, all comparisons are conducted by varying the backhaul link SNR, i.e., $\bar{\gamma}_{\mathrm{SR}}$ in DL relaying and $\bar{\gamma}_{\mathrm{RD}}$ in UL relaying, while the average service link SNRs are now fixed to a constant value, which is $\bar{\gamma}_{\mathrm{RD}} = 20$ dB (resp. $\bar{\gamma}_{\mathrm{SR}} = 20$ dB) in the DL (resp. UL) direction. In many cases, DF relaying achieves the same performance as the DAS because its backhaul link SNR becomes sufficiently high such that the service link is the main bottleneck of the system. Thus, comparison between AF and DF relaying protocols is presented as a by-product due to the fact that regenerative DF processing eliminates input noise amplification.

With a noise-free backhaul channel, the VG and FG protocols are equivalent in both communication directions. Thus, the DL and UL performance of the DAS can be related to each other with a parameter swap. By taking the limits $\bar{\gamma}_{\mathrm{SR}} \to \infty$ and $\bar{\gamma}_{\mathrm{RD}} \to \infty$ of (7.23), (7.24) and (7.38), the downlink and uplink outage probability of the DAS become

$$\mathcal{P}_{\mathrm{out}}(\gamma_{\mathrm{th}}) = \left[1 - \exp\left(-\frac{\gamma_{\mathrm{th}}}{\bar{\gamma}_{\mathrm{RD}}}\right)\right]^{N_{\mathrm{D}}}, \tag{7.54a}$$

$$\mathcal{P}_{\mathrm{out}}(\gamma_{\mathrm{th}}) = \left[1 - \exp\left(-\frac{\gamma_{\mathrm{th}}}{\bar{\gamma}_{\mathrm{SR}}}\right)\right]^{N_{\mathrm{D}}}, \tag{7.54b}$$

respectively. Asymptotically (for large $\bar{\gamma}_{\mathrm{RD}}$ in the DL direction and for large $\bar{\gamma}_{\mathrm{SR}}$ in the UL direction), the above expressions converge to

$$\mathcal{P}_{\mathrm{out}}(\gamma_{\mathrm{th}}) \approx (\gamma_{\mathrm{th}})^{N_{\mathrm{D}}} (\bar{\gamma}_{\mathrm{RD}})^{-N_{\mathrm{D}}} \quad \text{and} \quad \mathcal{P}_{\mathrm{out}}(\gamma_{\mathrm{th}}) \approx (\gamma_{\mathrm{th}})^{N_{\mathrm{D}}} (\bar{\gamma}_{\mathrm{SR}})^{-N_{\mathrm{D}}} \tag{7.55}$$

which are exactly the same as what is given for DF relaying in (7.48) provided that $\gamma_{\mathrm{th}} \leq \bar{\gamma}_{\mathrm{SR}}$ and $\gamma_{\mathrm{th}} \leq \bar{\gamma}_{\mathrm{RD}}$, respectively. In conclusion, the DAS is seen to offer exactly the same, not any better, diversity order of N_{D} as all the protocols other than the FG protocol in UL relaying.

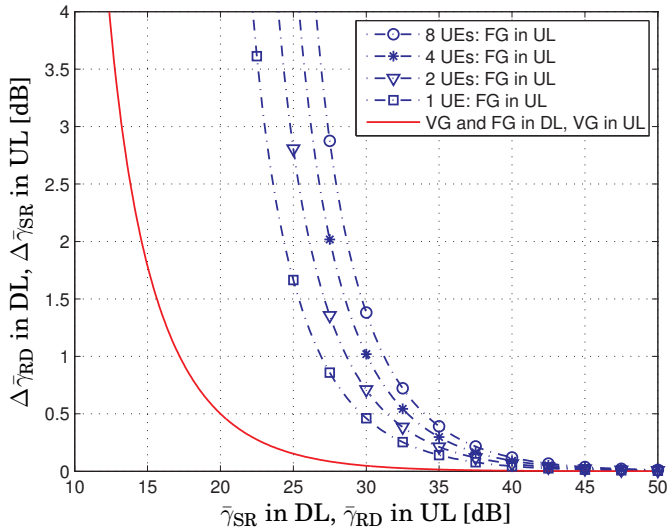

Figure 7.9. SNR loss due to the non-ideal wireless backhaul link in amplify-and-forward relaying in terms of the backhaul link SNRs when the service link SNRs are fixed to 20 dB in the distributed antenna system. This measures the transmit power increase required for achieving the same outage probability as a distributed antenna system when the threshold SNR is $\gamma_{\mathrm{th}} = 10$ dB.

The respective instantaneous SNRs of the DL and UL distributed antenna systems are simply $\gamma = \gamma_{\mathrm{RD}}$ and $\gamma = \gamma_{\mathrm{SR}}$, and their average values can be computed as

$$\bar{\gamma} = \mathcal{E}\{\gamma_{\mathrm{RD}}\} = H_{N_{\mathrm{D}}}^{(1)}\,\bar{\gamma}_{\mathrm{RD}} \quad \text{and} \quad \bar{\gamma} = \mathcal{E}\{\gamma_{\mathrm{SR}}\} = H_{N_{\mathrm{D}}}^{(1)}\,\bar{\gamma}_{\mathrm{SR}}. \tag{7.56}$$

More interesting analysis arises by measuring the SNR loss in terms of the increase in transmit power(s) which is needed in the case of relaying for compensating input noise amplification to achieve the same outage probability as the DAS. By equating (7.23) with (7.54a), it can be seen that variable-gain AF relaying suffers from SNR losses of

$$\Delta\bar{\gamma}_{\mathrm{RD}} = \frac{\bar{\gamma}_{\mathrm{SR}} + 1}{\bar{\gamma}_{\mathrm{SR}} - \gamma_{\mathrm{th}}} \quad \text{and} \quad \Delta\bar{\gamma}_{\mathrm{SR}} = \frac{\bar{\gamma}_{\mathrm{RD}} + 1}{\bar{\gamma}_{\mathrm{RD}} - \gamma_{\mathrm{th}}} \tag{7.57}$$

compared to the DAS due to noise amplification in the DL and UL direction, respectively. Similarly in fixed-gain uplink relaying, the SNR loss is obtained by equating (7.38) with (7.54b) which yields

$$\Delta\bar{\gamma}_{\mathrm{SR}} = \frac{\bar{\gamma}_{\mathrm{RD}} + 1}{\bar{\gamma}_{\mathrm{RD}} - H_{N_{\mathrm{D}}}^{(1)}\,\bar{\gamma}_{\mathrm{SR}}} \tag{7.58}$$

while the SNR loss is given by (7.57) in the downlink direction.

Figure 7.9 visualizes (7.57) and (7.58). In the context of this particular illustration, DF relaying does not incur any SNR loss because the target

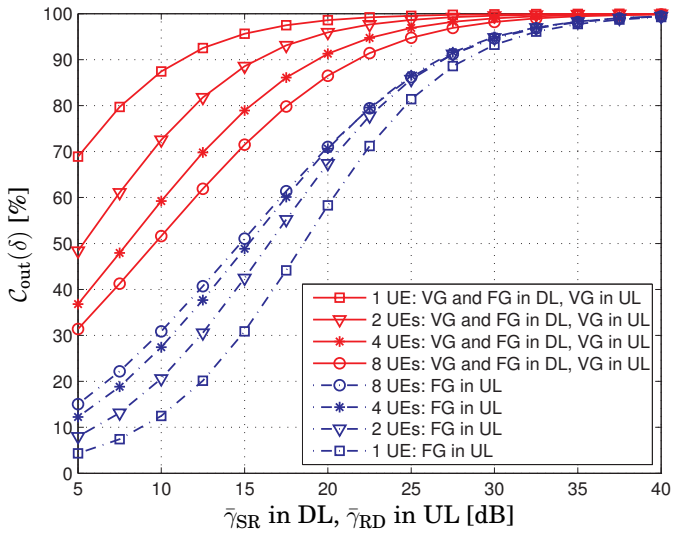

(a) amplify-and-forward (AF) relaying

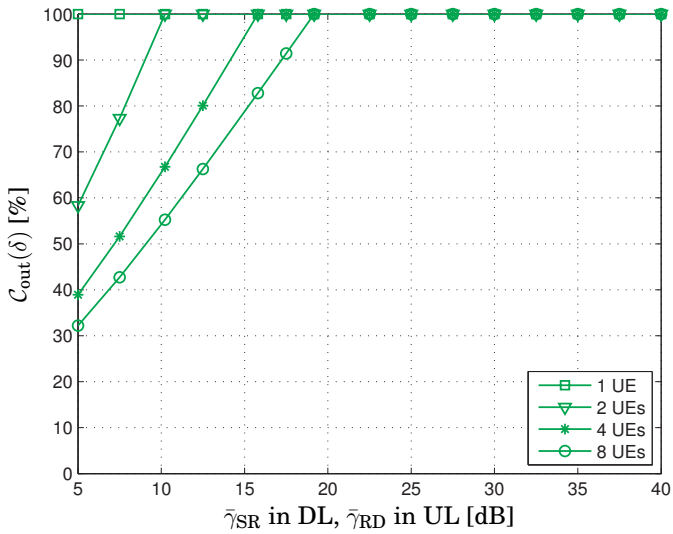

(b) decode-and-forward (DF) relaying

Figure 7.10. Relative outage capacity of multihop relaying versus a distributed antenna system with limit $\delta = 0.01$ for outage probability in terms of the backhaul link SNRs when the service link SNRs are fixed to 20 dB.

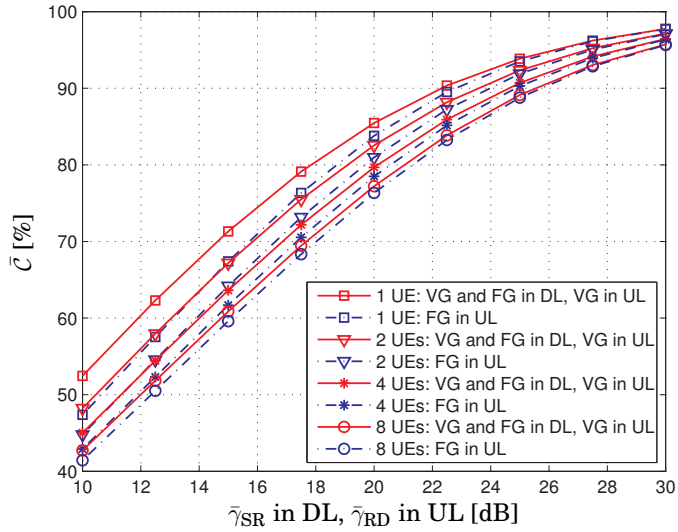

(a) amplify-and-forward (AF) relaying

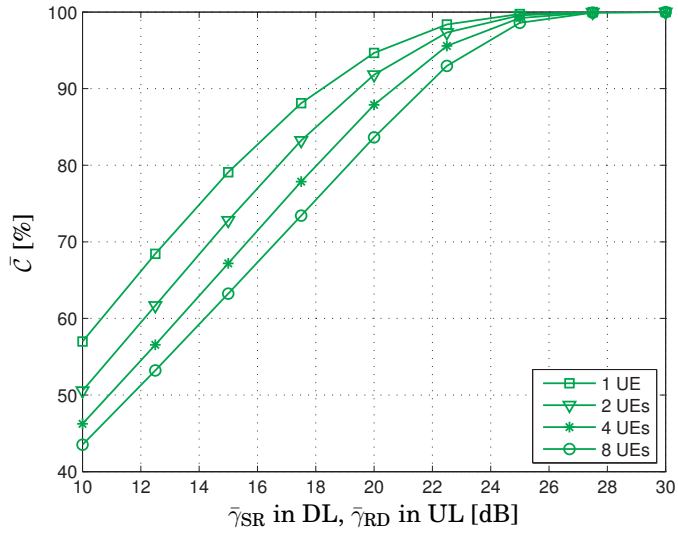

(b) decode-and-forward (DF) relaying

Figure 7.11. Relative ergodic capacity of multihop relaying versus a distributed antenna system in terms of the backhaul link SNRs when the service link SNRs are fixed to 20 dB.

threshold SNR is always less than the backhaul link SNR. The required compensation at transmit power decreases radically when the backhaul link SNR is improved. In DL and variable-gain UL relaying, the required compensation is small if the backhaul link SNR is reasonably (as a rule of thumb, e.g., 10 dB) larger than the threshold SNR γ_{th}. For example, with the values $\bar{\gamma}_{\text{SR}} = 20$ dB in the DL direction ($\bar{\gamma}_{\text{RD}} = 20$ dB in the UL direction) and $\gamma_{\text{th}} = 10$ dB used in the plots of the previous subsection, the SNR loss is only about 0.5 dB. On the other hand in fixed-gain UL relaying, the backhaul link SNR needs to be reasonably (again, e.g., 10 dB) larger than the average link SNR between the scheduled UE (cf. any UE in the other cases) and the distributed antenna to guarantee insignificant SNR loss. Furthermore, the VG protocol is favorable in UL relaying also because the SNR loss of the FG protocol increases with more UEs.

By taking limits $\bar{\gamma}_{\text{SR}} \to \infty$ and $\bar{\gamma}_{\text{RD}} \to \infty$ of (7.27), (7.28), and (7.41), the downlink and uplink outage capacity of the DAS become

$$\mathcal{C}_{\text{out}}(\delta) = \log_2\left(1 - \bar{\gamma}_{\text{RD}} \log_e\left(1 - \delta^{1/N_{\text{D}}}\right)\right), \tag{7.59a}$$

$$\mathcal{C}_{\text{out}}(\delta) = \log_2\left(1 - \bar{\gamma}_{\text{SR}} \log_e\left(1 - \delta^{1/N_{\text{D}}}\right)\right), \tag{7.59b}$$

respectively. With balanced service links, similar asymptotic substitutions into (7.33), (7.34), and (7.45) yield the ergodic capacity as

$$\bar{\mathcal{C}} = \frac{1}{\log_e(2)} \sum_{m=1}^{N_{\text{D}}} (-1)^{m-1} \binom{N_{\text{D}}}{m} \exp\left(\frac{m}{\bar{\gamma}_{\text{RD}}}\right) E_1\left(\frac{m}{\bar{\gamma}_{\text{RD}}}\right), \tag{7.60a}$$

$$\bar{\mathcal{C}} = \frac{1}{\log_e(2)} \sum_{m=1}^{N_{\text{D}}} (-1)^{m-1} \binom{N_{\text{D}}}{m} \exp\left(\frac{m}{\bar{\gamma}_{\text{SR}}}\right) E_1\left(\frac{m}{\bar{\gamma}_{\text{SR}}}\right), \tag{7.60b}$$

in the downlink and uplink DAS, respectively.

Finally, Fig. 7.10 shows the relative outage capacity of the relay link versus a DAS to illustrate the capacity loss due to the non-ideal backhaul link in multihop relaying. Similarly, the relative ergodic capacity of different relaying protocols is plotted in Fig. 7.11. It can be especially noted that, by selecting properly the SNR operation area of the backhaul link, the performance of relaying can be guaranteed to be very close to that of the DAS. For example, non-ideal relaying achieves 93.2–99.8% of the 1%-outage capacity and 95.6–97.7% of the ergodic capacity of the ideal DAS when the backhaul link SNR is 30 dB, i.e., 10 dB above the service link SNRs. The loss is typically lower in DF relaying than in AF relaying.

A rather unexpected observation can be also made from these numerical results: Relative system capacity decreases with more UEs (except in the case of the UL outage capacity when using the FG protocol), i.e.,

opportunistic multiuser scheduling may actually make a relay link relatively worse w.r.t. basic round-robin scheduling. This is because the backhaul link becomes relatively more significant bottleneck when multiuser scheduling improves the service link in both the DAS and the relay link.

7.5 Conclusions

This chapter derived closed-form expressions for outage probability, outage capacity, average end-to-end signal-to-noise ratio (SNR), the amount of fading, and ergodic capacity in a single-cell multihop infrastructure relay link. The system consists of a base station, a backhaul link with multiple relay nodes, and multiple users sharing a service link. The analysis covered single-user communication, round-robin scheduling, and multiuser diversity by maximum-SNR scheduling as well as both amplify-and-forward (AF) and decode-and-forward (DF) processing.

In the case of non-regenerative resource block-wise processing, the results compared variable- and fixed-gain amplification that yield different normalization for relay transmit power. These AF protocols are equivalent in the downlink direction, while the fixed-gain protocol was shown to be better in terms of the average end-to-end SNR in the uplink direction although the variable-gain protocol is much better in terms of all other performance measures. Yet, the DF protocol is in general better than either AF protocol. Thus, variable-gain amplification is recommended for uplink transmission at the cost of slightly more complex implementation if (even more complex) regenerative processing is not possible instead.

The presented performance measures show that opportunistic multiuser scheduling in the relay link yields significant diversity, capacity and SNR improvement over single-user transmission and round-robin scheduling. For example in terms of outage capacity, the SNR gain is remarkable 10–20 dB depending on the number of active users. Finally, the multihop relay link was compared to a single-hop distributed antenna system which showed that AF and, especially, DF relaying can achieve performance comparable to the distributed antenna system when reasonably high average backhaul link SNR between the base station and the serving relay node is guaranteed. Relaying is thereby a potential technique for avoiding expensive cable connections. However, it was also noticed that opportunistic scheduling may increase the relative capacity loss of relaying compared to the distributed antenna system.

8. Capacity Analysis of OFDM(A) Relaying Protocols

Relaying protocols are essentially signal transformers between a relay input and output. Since source–relay and relay–destination links can be of totally different nature, the design of such interfaces becomes a key factor for the performance and complexity of relaying systems. Further, multicarrier modulation adds a new dimension to protocol design which, in the following, yields various imaginable ways to connect an OFDM point-to-point backhaul link to an OFDMA point-to-multipoint service link; this combination of OFDM and OFDMA is herein referred to as OFDM(A).

This chapter studies a comprehensive set of OFDM(A) relaying protocols which are based on the following design choices (cf. Section 2.2.5 for more details): Whether to perform time-domain, frequency-domain, resource block-wise, or symbol-wise processing; Whether to apply regenerative forwarding or not; Whether to implement random, fixed, or adaptive pairing of subchannels; Whether to buffer data over fading states or not; And how to allocate half-duplex time slots. The joint effect of these design choices is analyzed by means of closed-form performance expressions in a unified framework, where a fixed infrastructure-based relay node (RN) is deployed for serving multiple users beyond base station (BS) coverage area. In particular, the main contribution of this chapter is to calculate the average system capacity over fast-fading channels when adopting each of the proposed relaying protocols and to apply the new expressions for thorough numerical performance comparison in an example system.

The remainder of this chapter[1] is organized as follows. Sections 8.1 and 8.2 present a brief introduction to the scope of the study and to the considered system setup, respectively. The main analysis is presented in Section 8.3 followed by its application for numerical performance evaluation in Section 8.4. Finally, Section 8.5 summarizes the discussion.

[1]This chapter is partially based on the material presented in **[233, 235, 236]**.

8.1 Introduction

The common denominator of many modern wireless systems is the adoption of orthogonal frequency-division multiplexing (OFDM) and its multi-user variation, orthogonal frequency-division multiple access (OFDMA). In cellular downlink communication, RN deployment usually leads to a hybrid OFDM(A) system, i.e., cascading a point-to-point (BS–RN) OFDM backhaul link with a point-to-multipoint (RN–users) OFDMA service link. Consequently, such a hybrid cascade admits a wide diversity of options to design *relaying protocols*, i.e., interfaces providing signal transformation between two links of different types. This is mainly due to the multicarrier nature of wideband OFDM(A) transmission over frequency-selective fading multipath channels. For reasoned system design, it is important to assess the performance of different potential protocols using a unified analytical framework which is the target of this chapter.

The literature survey of Chapter 2 shows that protocol design choices are typically studied separately (with little comparison to other possible protocols) and by means of simulations. The state-of-the-art does not explain how to combine all design choices together and what their joint performance is: these questions are addressed herein. Especially, analysis is now conducted by means of closed-form expressions to make the contribution less specific to any particular simulation setup. The performance metric adopted in this chapter is average system capacity which is analyzed previously under the assumption of single-carrier transmission over frequency-flat narrowband channels. Although one may interpret that the earlier results correspond to a single subcarrier in OFDM(A), such trivial extrapolation covers only a limited set of feasible relaying protocols, e.g., the conventional classification to amplify-and-forward (AF) and decode-and-forward (DF) protocols is far from being comprehensive enough.

The scope of the current study is on infrastructure-based RNs while other literature is often directed toward systems in which mobile terminals cooperatively act as relays for others. For example, many existing studies assume intense, e.g., “Rayleigh”, fading at all hops, which is reasonable for user cooperation but highly impractical for modeling cellular relay links where both ends of the first hop (BS and RN) are stationary in the downlink direction. In summary, the existing literature does not cover extensively enough the design and analysis of relaying protocols in the context of infrastructure relays and cellular systems.

As an initial minor contribution, Section 8.2 sets up a unified analytical framework for evaluating the performance of different OFDM(A) relaying protocols and conducting discerning comparison. In particular, the framework incorporates six main design choices which generate a set of 18 new protocols that have not been studied in a large scale before. As a by-product, the study thus reflects also the interconnections between the choices that need to be taken into account in reasoned protocol design.

The framework and its underlying models are formulated for the focal cellular application where a fixed infrastructure-based RN is deployed for serving multiple user equipments (UEs) beyond BS coverage area. As its main advantage, the framework is tailored to allow focusing the analysis on the performance of relaying protocols after higher-level protocols, e.g., subchannel allocation and scheduling, have already taken place. Although the framework is specified under the assumption of half-duplex time-division duplexing (TDD) operation in the relay, it would be a rather straightforward task to translate the results to the case of half-duplex frequency-division duplexing (FDD) or even full-duplex (FD) relaying.

The main contribution of this chapter, presented in Section 8.3, is to evaluate the performance of the proposed protocols by deriving new closed-form expressions for the average system capacity over fading channels. A distributed antenna system (DAS) with an out-of-band backhaul link is also analyzed as a reference case. In Section 8.4, the analytical results then facilitate extensive numerical comparison between the different protocols assuming an example vehicular system, which is the secondary contribution of this chapter. Furthermore, the framework itself could be used also for the analysis of multiantenna scenarios and mobile relays by simply changing the channel fading models and then reworking the analysis following the steps provided herein.

Altogether, the following analytical and numerical results provide valuable information for choosing relaying protocols for the future OFDM(A) relaying systems. The results are universal, so to say, since they represent the ultimate performance bounds achieved by combining the abstract design choices while implementation-specific non-idealities do not obscure the conclusions. Especially, it can be seen that some design choices, which may admit high implementation complexity, do not yet offer substantially better system capacity than others resulting in simpler protocols. Finally, comparison with the distributed antenna system reveals the performance loss due to avoiding a dedicated out-of-band backhaul.

8.2 System Model

The analysis of this chapter considers a relay-enhanced downlink cellular system that comprises a base station (BS) and a fixed infrastructure relay node (RN) which serves N_{D} user equipments (UEs) as illustrated in Fig. 8.1. Having the scope on the downlink communication direction, the specific acronyms BS, RN, and UE are used interchangeably with generic terms source, relay, and destination, respectively, throughout the following discussions. Likewise, the respective source–relay and relay–destination channels are referred to as *backhaul* and *service* links.

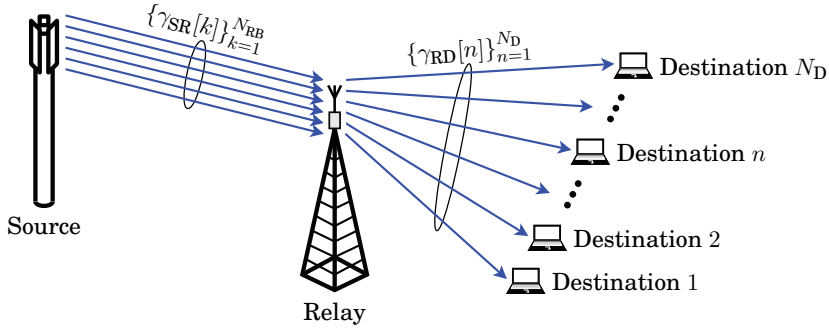

Figure 8.1. Two-hop infrastructure relay link in which $\gamma_{\mathrm{SR}}[k]$ and $\gamma_{\mathrm{RD}}[n]$ denote the instantaneous signal-to-noise ratios of the OFDM(A) resource blocks in the respective backhaul and service links.

The focus is on typical cellular scenarios in which the RN is deployed for BS coverage extension or gap-filling, i.e., to cover areas where direct BS–UE connections cannot be established. Consequently, the system setup and analysis consider only subchannels that are allocated for relaying and only active UEs that are connected to the RN while in reality there may be also inactive UEs and UEs that are connected directly to the BS over some other subchannels. Likewise, the handover of UEs between the BS and the RN as well as the assignment of subchannels for backhaul and service links is done by a higher-layer protocol which is transparent for link-layer relaying protocols. Thus, the design of relaying protocols does not affect the performance of UEs that are within the BS coverage area.

8.2.1 Two-Hop OFDM(A) Transmission

As a baseline, standard assumptions are invoked in order to regard OFDM and OFDMA transmission as a set of narrowband signals which propagate through perfectly orthogonal linear subchannels. In particular, mul-

tipath delay spread is shorter than the cyclic prefix, frequency and time synchronization is realized well enough, and channel coherence time is longer than several radio frames such that channel estimation, channel state information (CSI) feedback, coordination among transceivers and the actual data payload transmission can be completed while the channels remain approximately stationary. In essence, these assumptions imply that there is no significant inter-carrier interference (ICI) or inter-symbol interference (ISI), or that their effect can be modeled accurately by simply increasing the receiver noise figure. Additive receiver noise is assumed to be white and Gaussian and to include all possible nonlinear distortion and ambient interference in addition to usual thermal noise.

At both links, data designated for the UEs is multiplexed into OFDM(A) symbols comprising N_{RB} orthogonal resource blocks (RBs), each of which consists of several subcarriers. This implementation detail is adopted from practical systems where signaling on a per-subcarrier basis would be unfeasible due to excessive channel estimation and feedback overhead. Hence, adjacent subcarriers on highly-correlated subchannels are usually grouped into chunks, i.e., resource blocks in the context of LTE and LTE-Advanced [1, 2], which can be handled more economically. For brevity, the proposed framework models the signal-to-noise ratios (SNRs) of the frequency-domain RBs without presenting explicit time-domain signals.

The RN is assumed to operate in a TDD mode, i.e., it alternately receives and transmits: In each cycle of $T_{\mathrm{SR}} + T_{\mathrm{RD}}$ symbols, the first T_{SR} symbols are reserved for the backhaul link and the rest T_{RD} symbols are reserved for the service link. In particular, the BS transmits OFDM symbols in a unicast mode to the RN which processes them according to one of the relaying protocols. The obtained data is then multiplexed into OFDMA symbols which the RN (re-)transmits in a broadcast mode to the UEs while the BS is silent. For simplicity, it is assumed that a higher-layer protocol allocates exactly one RB for each active UE and all of them can be served, i.e., the system is never overloaded due to constraint $N_{\mathrm{D}} \leq N_{\mathrm{RB}}$.

Variables $t_{\mathrm{SR}} \triangleq T_{\mathrm{SR}}/(T_{\mathrm{SR}}+T_{\mathrm{RD}})$ and $t_{\mathrm{RD}} = 1-t_{\mathrm{SR}}$ represent relative TDD time shares given for the respective backhaul and service links. When translating the framework to FDD relaying, they could be understood as the frequency shares of the links; however, adjustment during operation may be difficult in practice. Similar translation to FD relaying is also rather straightforward by setting $t_{\mathrm{SR}} = t_{\mathrm{RD}} = 1$ due to frequency reuse, if residual self-interference is included in the receiver noise figure.

Table 8.1. Summary of the considered relaying protocols and their underlying design choices indicating the type of processing performed in the relay node.

Design choices	OFDM(A) relaying protocols																	
time-domain	✓																	
frequency-domain	∀	✓	✓	✓	✓	✓	✓	✓	✓	✓	✓	✓	✓	✓	✓	✓	✓	✓
amplify-and-forward (AF)	✓	✓	✓	✓														
decode-and-forward (DF)					✓	✓	✓	✓	✓	✓	✓	✓	✓	✓	✓	✓	✓	✓
symbol-wise (SW)	✓				✓	✓	✓	✓										
resource block-wise (RW)		✓	✓	✓					✓	✓	✓	✓	✓	✓	✓	✓	✓	✓
random pairing (RP)	✓	✓							✓			✓		✓			✓	
fixed pairing (FP)			✓							✓			✓		✓			✓
adaptive pairing (AP)				✓							✓					✓		
no buffering (NB)	✓	✓	✓	✓	✓		✓		✓	✓	✓			✓	✓	✓		
with buffering (WB)						✓		✓				✓	✓				✓	✓
uniform resources (UR)	✓	✓	✓	✓	✓	✓			✓	✓	✓	✓	✓					
optimized resources (OR)							✓	✓						✓	✓	✓	✓	✓

8.2.2 Design Choices and Relaying Protocols

As explained earlier, the term "relaying protocol" refers to the signal transformation interface between OFDM backhaul and OFDMA service links. The set of 18 relaying protocols analyzed in this chapter arise from six key design choices as enumerated in Table 8.1 where the rows represent the choices and the columns on the right-hand side show their feasible combinations, i.e., the protocols. This table serves also as a handy glossary for the abbreviations used throughout result figures in Section 8.4.

In an early stage of protocol design, baseline choices are first made between time-domain and frequency-domain processing, and between RB-wise (RW) and symbol-wise (SW) processing. Obviously, almost all feasible OFDM(A) protocols adopt frequency-domain processing since options for time-domain processing become rather limited due to the fundamental fact that data samples are transmitted on frequency-domain subcarriers. In the case of RW processing, an additional design choice is made between three different ways to perform subchannel pairing from the backhaul link to the service link. The conventional design choice between amplify-and-forward (AF) and decode-and-forward (DF) retransmission is the least restricted by other design choices. With DF processing, protocol design can additionally choose to include buffering over fading states and

to allow the change of modulation and coding scheme which facilitates the adjustment of time or frequency resources given for the backhaul and service links. These design choices and the interconnections of the protocols are specified in more detail in Section 2.2.5 (e.g., cf. Fig. 2.5 at Page 29).

An interconnection worth to single out is the fact that symbol-wise (SW) amplification could be implemented also in the frequency domain although it is not advised due to unnecessarily increased complexity as indicated by the crossbar on a marker in Table 8.1. However, this streamlines the analysis which can be thus formulated completely in terms of frequency-domain RBs without modeling actual time-domain operations.

8.2.3 Channel Fading Models

The radio channels at the backhaul and service links are modeled as described next. At this point, the analytical framework becomes specific to a *downlink* cellular system with an *infrastructure-based* RN. Since the BS is obviously also a part of infrastructure, the fading models are selected based on the presumption that the backhaul and service links are fixed-to-fixed and fixed-to-mobile channels, respectively.

In spite of limiting the scope to downlink direction, most of the obtained analytical results are still directly applicable also in the counterpart *uplink* cellular system with an infrastructure-based RN. This is because the downlink–uplink duality manifests itself in such a way that reversing the communication direction usually induces only a parameter swap in the expressions. However, as observed in Sections 5.4 and 7.3, there are few specific cases where some relaying protocols perform differently in downlink and uplink directions because intense fading has different impact depending on whether it takes place after or before the relay.

OFDM Backhaul Link (BS–RN)

The instantaneous SNR of the kth backhaul RB is denoted by $\gamma_{\mathrm{SR}}[k]$. As both the BS and the RN are fixed nodes in the considered system, the fluctuation of the backhaul channel is negligible. However, it is not necessarily a line-of-sight link and may be subject to multipath propagation due to obstacles in between the chosen BS and RN sites. It is reasonable to model the backhaul channel as frequency-selective and static, i.e.,

$$\gamma_{\mathrm{SR}}[k] = \bar{\gamma}_{\mathrm{SR}}[k] \triangleq \mathcal{E}\{\gamma_{\mathrm{SR}}[k]\} \tag{8.1}$$

which does not necessarily yield the same value for all k.

The SNRs are sorted in descending order for notational convenience, i.e.,

$$\bar{\gamma}_{\mathrm{SR}}[1] \geq \bar{\gamma}_{\mathrm{SR}}[2] \geq \ldots \geq \bar{\gamma}_{\mathrm{SR}}[N_{\mathrm{RB}}], \tag{8.2}$$

and for the same purpose, the mean SNR of backhaul RBs is denoted by

$$\bar{\gamma}_{\mathrm{SR}} \triangleq \frac{1}{N_{\mathrm{RB}}} \sum_{k=1}^{N_{\mathrm{RB}}} \bar{\gamma}_{\mathrm{SR}}[k]. \tag{8.3}$$

Finally, the instantaneous and average per-link capacities [bit/s/Hz] of the kth backhaul RB, equal to each other, are expressed as

$$\mathcal{C}_{\mathrm{SR}}[k] = \bar{\mathcal{C}}_{\mathrm{SR}}[k] \triangleq \mathcal{E}\{\mathcal{C}_{\mathrm{SR}}[k]\} = t_{\mathrm{SR}} \log_2\left(1 + \bar{\gamma}_{\mathrm{SR}}[k]\right), \tag{8.4}$$

where one should note scaling by the resource share of the backhaul link.

It is easy to extend the framework and translate obtained analytical results to multihop scenarios, where the infrastructure-based backhaul link consists of M hops between the BS and the last RN which is connected to the UEs (cf. Fig. 2.3(g) at Page 19). The SNR of the kth backhaul RB in the mth hop can be denoted by $\bar{\gamma}_{\mathrm{SR}[m]}[k]$. With all protocols that adopt RB-wise processing, the M-hop backhaul link is compressed into a virtual single-hop link as already shown in Section 7.2.2. With protocols that adopt symbol-wise DF processing, the same is achieved by defining

$$\sum_{k=1}^{N_{\mathrm{RB}}} \log_2(1 + \bar{\gamma}_{\mathrm{SR}}[k]) \triangleq \min_{m=1,2,\ldots,M} \left\{ \sum_{k=1}^{N_{\mathrm{RB}}} \log_2(1 + \bar{\gamma}_{\mathrm{SR}[m]}[k]) \right\}. \tag{8.5}$$

OFDMA Service Link (RN–UEs)

The instantaneous SNR of the nth UE is denoted by $\gamma_{\mathrm{RD}}[n]$. The UEs are mobile in the considered system, and thus all RN–UE channels are modeled by multipath Rayleigh fading that is typical for non-line-of-sight conditions. The probability density function (PDF) of $\gamma_{\mathrm{RD}}[n]$ becomes that of an exponential random variable:

$$f_{\gamma_{\mathrm{RD}}[n]}(x) = \frac{1}{\bar{\gamma}_{\mathrm{RD}}[n]} \exp\left(-\frac{x}{\bar{\gamma}_{\mathrm{RD}}[n]}\right) \quad \text{for } x \geq 0, \tag{8.6}$$

where $\bar{\gamma}_{\mathrm{RD}}[n] \triangleq \mathcal{E}\{\gamma_{\mathrm{RD}}[n]\}$ is the average SNR of the RB. One should note that the distance and path loss to the RN are in practice different from every UE which renders unequal values for $\bar{\gamma}_{\mathrm{RD}}[n]$, $n = 1, 2, \ldots, N_{\mathrm{D}}$.

Random variables $\{\gamma_{\mathrm{RD}}[n]\}_{n=1}^{N_{\mathrm{D}}}$ can be regarded as mutually independent because the correlation of fast fading is generally low among spatially distributed nodes. Actually, this property is the main reason for invoking the assumption that each UE is given exactly one service RB. Otherwise the

analysis would become tedious, or even impossible, because correlation within $\{\gamma_{\mathrm{RD}}[n]\}_{n=1}^{N_{\mathrm{D}}}$ cannot be easily neglected if two or more variables correspond to different RBs propagated from the RN to a particular UE over the same physical multipath channel. If not invoking the assumption, the following analysis is, however, still applicable as a good approximation for two extreme cases: when multiple RBs given for one UE are located on adjacent frequencies (within coherence bandwidth) such that they can be considered to propagate through roughly the same narrowband channel; and when the RBs are spread far away from each other over the OFDMA bandwidth such that they are subject to almost uncorrelated channels.

The instantaneous per-link capacity [bit/s/Hz] of the nth UE is

$$\mathcal{C}_{\mathrm{RD}}[n] = t_{\mathrm{RD}} \log_2\left(1+\gamma_{\mathrm{RD}}[n]\right), \tag{8.7}$$

reflecting the resource share $t_{\mathrm{RD}} = 1 - t_{\mathrm{SR}}$ allocated for the service link. Thereby, the average per-link capacity [bit/s/Hz] of the nth UE becomes

$$\bar{\mathcal{C}}_{\mathrm{RD}}[n] \triangleq \mathcal{E}\{\mathcal{C}_{\mathrm{RD}}[n]\} = \frac{t_{\mathrm{RD}}}{\log_e(2)} \exp\left(\frac{1}{\bar{\gamma}_{\mathrm{RD}}[n]}\right) E_1\left(\frac{1}{\bar{\gamma}_{\mathrm{RD}}[n]}\right), \tag{8.8}$$

where $E_1(\cdot)$ denotes the exponential integral function [3, Eq. 5.1.1], as it is well known for narrowband Rayleigh-fading channels [87, 155].

8.3 Analysis of Average System Capacity

Building upon the analytical framework, this section evaluates average system capacity [bit/s/Hz] over fading channels for the relaying protocols. The analysis is organized such that amplify-and-forward (AF) and decode-and-forward (DF) protocols are discussed separately, and the complexity of protocols increases gradually toward the end of the section. Finally, the reference distributed antenna system (DAS) is also evaluated.

8.3.1 Amplify-and-Forward Protocols

In the cases of AF, i.e., non-regenerative, protocols, the RN simply scales the signal on the kth backhaul RB by a factor $\beta[k]$ before retransmission. Thus, modulation and coding cannot be changed in the relay and the allocation of uniform resources (UR) with $t_{\mathrm{SR}} = t_{\mathrm{RD}} = 1/2$ is inherently built into all AF protocols. Gain $\beta^2[k]$ corresponding to the amplification factor is chosen such that the total transmit power is normalized to the same value for all AF protocols. In particular, the value of $\beta[k]$ differentiates

time-domain processing from frequency-domain processing, i.e., symbol-wise (SW) amplification from resource block-wise (RW) amplification.

With all AF protocols, the instantaneous capacity of a "virtual one-hop connection", which is first carried by the kth backhaul RB and then routed to the nth UE at the service link, can be expressed [142] as

$$\mathcal{C}[k,n] = \frac{1}{2}\log_2\left(1 + \frac{\bar{\gamma}_{\mathrm{SR}}[k]\,\gamma_{\mathrm{RD}}[n]}{\gamma_{\mathrm{RD}}[n] + \frac{1}{\sigma_{\mathrm{R}}^2\beta^2[k]}}\right), \tag{8.9}$$

where σ_{R}^2 denotes the noise power per RB at the relay input.

The notion "virtual one-hop connection" emphasizes above the fact that all RBs transmitted by the BS are designated directly for the UEs and not for the RN which becomes a transparent router. Thus, all combinations of k and n are not feasible for the above expression but they are defined by the routing scheme; the AF protocols may result in random, fixed, or adaptive pairing of RBs. In particular, it is denoted that the $\bar{v}[n]$th service RB is assigned for the nth UE, and $w[n]$ defines the potential permutation of RBs in the RN. These index functions $\bar{v}[n]$ and $w[n]$ are an integral part of the analysis and should be kept in mind.

Time-Domain Amplification

In symbol-wise (SW) processing, the time-domain signal waveform is simply amplified with a frequency-flat scalar gain. To normalize the sum transmit power, all backhaul RBs are subject to the same factor

$$\beta[k] = \frac{1}{\sigma_{\mathrm{R}}} \cdot \frac{1}{\sqrt{\bar{\gamma}_{\mathrm{SR}} + 1}}, \tag{8.10}$$

in which $\bar{\gamma}_{\mathrm{SR}}$ is the mean SNR of backhaul RBs from (8.3).

The time-domain AF protocol results inherently in random pairing (RP) because RBs could be reordered only in the frequency domain and, thus, the RN will inevitably forward the RBs in the same order as they are received from the BS, i.e., $w[n] = n$. By substituting (8.10) in (8.9) and using (8.6), the average system capacity is then calculated as

$$\begin{aligned}\bar{\mathcal{C}} &= \sum_{n=1}^{N_{\mathrm{D}}} \mathcal{E}\left\{\mathcal{C}[\bar{v}[n], n]\right\} \\ &= \sum_{n=1}^{N_{\mathrm{D}}} \frac{1}{2}\int_0^\infty \log_2\left(1 + \frac{\bar{\gamma}_{\mathrm{SR}}[\bar{v}[n]]\,x}{\bar{\gamma}_{\mathrm{SR}} + 1 + x}\right) f_{\gamma_{\mathrm{RD}}[n]}(x)\,\mathrm{d}x \\ &= \sum_{n=1}^{N_{\mathrm{D}}} \mathcal{I}_{\text{AF-SW}}(\bar{\gamma}_{\mathrm{SR}}[\bar{v}[n]], \bar{\gamma}_{\mathrm{SR}}, \bar{\gamma}_{\mathrm{RD}}[n]),\end{aligned} \tag{8.11}$$

where the integral $\mathcal{I}_{\text{AF-SW}}$ admits a closed-form expression involving the exponential integral function, $E_1(z) \triangleq \int_z^\infty \frac{e^{-t}}{t}\,\mathrm{d}t$ [3, Eq. 5.1.1], after sepa-

rating the logarithm of a product into a sum of logarithms and applying integration by parts:

$$\begin{aligned}&\mathcal{I}_{\text{AF-SW}}(a_1, a_2, b) \\ &= \frac{1}{2}\int_0^\infty \log_2\left(1+\frac{a_1\,x}{a_2+1+x}\right)\frac{1}{b}\exp\left(-\frac{x}{b}\right)\,\mathrm{d}x \\ &= \frac{1/2}{\log_e(2)}\left[\exp\left(\frac{a_2+1}{(a_1+1)b}\right)E_1\left(\frac{a_2+1}{(a_1+1)b}\right)-\exp\left(\frac{a_2+1}{b}\right)E_1\left(\frac{a_2+1}{b}\right)\right].\end{aligned} \tag{8.12}$$

Frequency-Domain Amplification

In resource block-wise (RW) processing, the per-RB transmit powers are equalized by amplifying the kth backhaul RB with factor

$$\beta[k] = \frac{1}{\sigma_{\text{R}}}\cdot\frac{1}{\sqrt{\bar{\gamma}_{\text{SR}}[k]+1}}. \tag{8.13}$$

Consequently, the total sum transmit power becomes the same as for time-domain amplification with (8.10).

The following analysis covers first the two protocols that do not adapt the reordering of RBs based on instantaneous SNRs. With RP or fixed pairing (FP), the average system capacity, calculated by substituting (8.13) in (8.9) and then using (8.6), is given by

$$\begin{aligned}\bar{\mathcal{C}} &= \sum_{n=1}^{N_{\text{D}}}\mathcal{E}\left\{\mathcal{C}[\bar{v}[n],\bar{w}[n]]\right\} \\ &= \sum_{n=1}^{N_{\text{D}}}\frac{1}{2}\int_0^\infty \log_2\left(1+\frac{\bar{\gamma}_{\text{SR}}[\bar{v}[n]]\,x}{\bar{\gamma}_{\text{SR}}[\bar{v}[n]]+1+x}\right)f_{\gamma_{\text{RD}}[\bar{w}[n]]}(x)\,\mathrm{d}x \\ &= \sum_{n=1}^{N_{\text{D}}}\mathcal{I}_{\text{AF-RW}}(\bar{\gamma}_{\text{SR}}[\bar{v}[n]],\bar{\gamma}_{\text{RD}}[\bar{w}[n]]),\end{aligned} \tag{8.14}$$

where the integral $\mathcal{I}_{\text{AF-RW}}$ admits the following closed-form expression:

$$\begin{aligned}\mathcal{I}_{\text{AF-RW}}(a,b) &= \mathcal{I}_{\text{AF-SW}}(a,a,b) \\ &= \frac{1/2}{\log_e(2)}\exp\left(\frac{1}{b}\right)\left[E_1\left(\frac{1}{b}\right)-\exp\left(\frac{a}{b}\right)E_1\left(\frac{a+1}{b}\right)\right].\end{aligned} \tag{8.15}$$

Actually, this is simply a reduced form of the integral used in (8.11) obtained from (8.12) by setting $a = a_1 = a_2$.

Forwarding the RBs in the same order as they are received results in RP for which the average system capacity is given by (8.14) with $\bar{w}[n] = n$ and $\bar{v}[n]$ represents the random order of RBs in the backhaul link. On the other hand, optimized fixed pairing (FP) should route the nth backhaul RB (which has the nth largest average backhaul SNR) for the $\bar{w}^*[n]$th UE (which has the nth largest average service SNR). Thus, the average system capacity for FP is given by (8.14) with $\bar{v}[n] = n$ and $\bar{w}[n] = \bar{w}^*[n]$.

Optimized adaptive pairing (AP) is implemented by reordering the RBs based on instantaneous SNRs such that the nth backhaul RB is routed to the $w^*[n]$th UE (which has the nth largest instantaneous service SNR). Thus, the analysis requires the PDF of the nth largest random variable among $\{\gamma_{\text{RD}}[n]\}_{n=1}^{N_\text{D}}$, i.e., $f_{\gamma_{\text{RD}}[w^*[n]]}(x)$, which can be derived based on order statistics as shown in Appendix A.3.

Finally, the average system capacity is calculated for optimized AP by substituting (8.13) in (8.9) and using (A.17) from Appendix A.3 as follows:

$$\begin{aligned}\bar{\mathcal{C}} &= \sum_{n=1}^{N_\text{D}} \mathcal{E}\left\{\mathcal{C}[n, w^*[n]]\right\} \\ &= \sum_{n=1}^{N_\text{D}} \frac{1}{2} \int_0^\infty \log_2\left(1 + \frac{\bar{\gamma}_{\text{SR}}[n]\, x}{\bar{\gamma}_{\text{SR}}[n] + 1 + x}\right) f_{\gamma_{\text{RD}}[w^*[n]]}(x)\, \mathrm{d}x \\ &= \sum_{n=1}^{N_\text{D}} \sum_{m=1}^{M[n,N_\text{D}]} a[m, n, N_\text{D}] \cdot \mathcal{I}_{\text{AF-RW}}(\bar{\gamma}_{\text{SR}}[n], b[m, n, N_\text{D}]), \end{aligned} \tag{8.16}$$

for which the integral $\mathcal{I}_{\text{AF-RW}}$ is the same as what is already expressed in (8.15), and the computation of $M[n, N_\text{D}]$, $a[m, n, N_\text{D}]$ and $b[m, n, N_\text{D}]$ is explained in Appendix A.3.

8.3.2 Decode-and-Forward Protocols

In the cases of DF, i.e., regenerative, protocols, the RN decodes and re-encodes (in one form or another) signals over the interface between the backhaul and service links. The following analysis is divided according to the two main categories considering first protocols that adopt resource block-wise (RW) processing and later those that adopt symbol-wise (SW) processing. Finally, the allocation of optimal resources (OR) is analyzed as a supplement for all the DF protocols.

Resource Block-wise Processing

With all DF protocols that perform RW processing, the instantaneous capacity of a "virtual one-hop connection", which is first carried by the kth backhaul RB and then routed to the nth UE at the service link, can be expressed **[235, 296]** by employing (8.4) and (8.7) as

$$\begin{aligned}\mathcal{C}[k, n] &= \min\left\{\mathcal{B}[k, n] + \mathcal{C}_{\text{SR}}[k], \mathcal{C}_{\text{RD}}[n]\right\} \\ &= \min\left\{\mathcal{B}[k, n] + t_{\text{SR}} \log_2\left(1 + \bar{\gamma}_{\text{SR}}[k]\right), t_{\text{RD}} \log_2\left(1 + \gamma_{\text{RD}}[n]\right)\right\}, \end{aligned} \tag{8.17}$$

in which $\mathcal{B}[k, n]$ denotes instantaneous buffer status, i.e., the amount of data remaining in a buffer (if used) before BS transmission. Buffering over fading states allows the RN to avoid data loss or idle time due to

instantaneous mismatch between backhaul and service links while otherwise the "virtual one-hop connection" is always limited by the weaker link. In particular, even if $\mathcal{C}_{\text{SR}}[k] < \mathcal{C}_{\text{RD}}[n]$ instantaneously, the RN can continue transmitting with rate $\mathcal{C}_{\text{RD}}[n]$ by taking additional data from the buffer and, if $\mathcal{C}_{\text{SR}}[k] > \mathcal{C}_{\text{RD}}[n]$, the surplus data from the backhaul link is stored in the buffer for future transmission. After completing one cycle of BS and RN transmissions, new buffer status becomes $\mathcal{B}[k,n] + \mathcal{C}_{\text{SR}}[k] - \mathcal{C}_{\text{RD}}[n]$.

It shall be again presumed that the $\bar{v}[n]$th service RB is assigned for the nth UE, and $w[n]$ defines the potential permutation of RBs in the RN. As with AF protocols that adopt RW processing, the feasible combinations of k and n for the above expression are defined by the routing scheme which can be based on random, fixed or adaptive pairing of RBs.

The following analysis considers first the case of no buffering (NB) which is modeled with (8.17) by setting $\mathcal{B}[k,n] = 0$. It can be observed that the analysis of RB-wise DF protocols without buffering becomes similar to that of AF protocols with frequency-domain processing. The main difference in the expressions is the replacement of (8.9) by (8.17), where $\mathcal{B}[k,n] = 0$, but otherwise the derivations follow the same steps.

In the cases of random pairing (RP) and fixed pairing (FP), the average system capacity is calculated by using (8.6) and (8.17). Thus, the DF counterpart of (8.14), derived for corresponding AF protocols, becomes

$$\begin{aligned}\bar{\mathcal{C}} &= \sum_{n=1}^{N_{\text{D}}} \mathcal{E}\left\{\mathcal{C}[\bar{v}[n], \bar{w}[n]]\right\} \\ &= \sum_{n=1}^{N_{\text{D}}} \int_0^{\infty} \min\left\{t_{\text{SR}} \log_2\left(1 + \bar{\gamma}_{\text{SR}}[\bar{v}[n]]\right), t_{\text{RD}} \log_2\left(1+x\right)\right\} f_{\gamma_{\text{RD}}[\bar{w}[n]]}(x)\,\mathrm{d}x \\ &= \sum_{n=1}^{N_{\text{D}}} \mathcal{I}_{\text{DF-RW}}(t_{\text{RD}}, \bar{\gamma}_{\text{SR}}[\bar{v}[n]], \bar{\gamma}_{\text{RD}}[\bar{w}[n]]). \end{aligned} \tag{8.18}$$

The integral $\mathcal{I}_{\text{DF-RW}}$ admits, after partitioning it into a sum of two integrals over respective intervals $[0, (a+1)^{\frac{1-t}{t}} - 1]$ and $[(a+1)^{\frac{1-t}{t}} - 1, \infty)$ and applying integration by parts, the following compact closed-form expression in terms of the exponential integral function:

$$\begin{aligned}&\mathcal{I}_{\text{DF-RW}}(t,a,b) \\ &= \int_0^{\infty} \min\left\{(1-t)\log_2(1+a), t\log_2(1+x)\right\} \frac{\exp\left(-\frac{x}{b}\right)}{b}\,\mathrm{d}x \\ &= \frac{t}{\log_e(2)} \exp\left(\frac{1}{b}\right)\left[E_1\left(\frac{1}{b}\right) - E_1\left(\frac{(a+1)^{\frac{1-t}{t}}}{b}\right)\right].\end{aligned} \tag{8.19}$$

As with AF protocols, $\bar{w}[n] = n$ for RP while $\bar{v}[n] = n$ and $\bar{w}[n] = \bar{w}^*[n]$, which denotes the index of the nth largest average service SNR, for FP.

In the case of adaptive pairing (AP), the average system capacity is calculated by using (8.17) and (A.17) as follows (cf. (8.16) for AF protocols):

$$\begin{aligned}\bar{\mathcal{C}} &= \sum_{n=1}^{N_{\mathrm{D}}} \mathcal{E}\left\{\mathcal{C}[n, w^*[n]]\right\} \\ &= \sum_{n=1}^{N_{\mathrm{D}}} \int_0^{\infty} \min\left\{t_{\mathrm{SR}} \log_2\left(1+\bar{\gamma}_{\mathrm{SR}}[n]\right), t_{\mathrm{RD}} \log_2\left(1+x\right)\right\} f_{\gamma_{\mathrm{RD}}[w^*[n]]}(x)\, \mathrm{d}x \\ &= \sum_{n=1}^{N_{\mathrm{D}}} \sum_{m=1}^{M[n,N_{\mathrm{D}}]} a[m,n,N_{\mathrm{D}}] \cdot \mathcal{I}_{\text{DF-RW}}(t_{\mathrm{RD}}, \bar{\gamma}_{\mathrm{SR}}[n], b[m,n,N_{\mathrm{D}}]), \end{aligned} \tag{8.20}$$

for which the integral $\mathcal{I}_{\text{DF-RW}}$ is already solved in (8.19) and the derivation of $M[n, N_{\mathrm{D}}]$, $a[m, n, N_{\mathrm{D}}]$ and $b[m, n, N_{\mathrm{D}}]$, which are based on the order statistics of $\{\gamma_{\mathrm{RD}}[n]\}_{n=1}^{N_{\mathrm{D}}}$, is explained in Appendix A.3.

The analysis proceeds now to DF relaying with buffering (WB) where the fast fading of the service link is compensated such that the average capacity of each UE becomes the minimum of the average per-hop per-RB capacities (cf. the average of the minimum instantaneous capacity without buffering). When letting the maximum buffer size grow asymptotically, which means the buffer never overflows or underflows, one can show that

$$\mathcal{E}\{\min\left\{\mathcal{B}[k,n] + \mathcal{C}_{\mathrm{SR}}[k], \mathcal{C}_{\mathrm{RD}}[n]\right\}\} \longrightarrow \min\left\{\mathcal{E}\{\mathcal{C}_{\mathrm{SR}}[k]\}, \mathcal{E}\{\mathcal{C}_{\mathrm{RD}}[n]\}\right\} \tag{8.21}$$

by following the rigorous proofs provided in [303]. In addition, the simulations in **[296]** and [303] indicate that already rather small finite buffers operate in practice similarly to an infinite buffer and the above limit can be reasonably replaced by an equality without causing much error.

By adopting property (8.21) as an accurate approximation, the average system capacity for RW protocols with buffering is directly calculated with the substitution of readily available expressions (8.4) and (8.8) as

$$\begin{aligned}\bar{\mathcal{C}} &= \sum_{n=1}^{N_{\mathrm{D}}} \mathcal{E}\left\{\mathcal{C}[\bar{v}[n], \bar{w}[n]]\right\} \\ &= \sum_{n=1}^{N_{\mathrm{D}}} \min\left\{\mathcal{E}\{\mathcal{C}_{\mathrm{SR}}[\bar{v}[n]]\}, \mathcal{E}\{\mathcal{C}_{\mathrm{RD}}[\bar{w}[n]]\}\right\} \\ &= \sum_{n=1}^{N_{\mathrm{D}}} \min\left\{ t_{\mathrm{SR}} \log_2\left(1+\bar{\gamma}_{\mathrm{SR}}[\bar{v}[n]]\right), \right. \\ &\qquad \left. \frac{t_{\mathrm{RD}}}{\log_e(2)} \exp\left(\frac{1}{\bar{\gamma}_{\mathrm{RD}}[\bar{w}[n]]}\right) E_1\left(\frac{1}{\bar{\gamma}_{\mathrm{RD}}[\bar{w}[n]]}\right) \right\}. \end{aligned} \tag{8.22}$$

Again, RP yields $\bar{w}[n] = n$ and FP yields $\bar{v}[n] = n$ with $\bar{w}[n] = \bar{w}^*[n]$, which denotes the index of the nth largest average service SNR. Adaptive pairing (AP) is not analyzed herein, since it is not relevant or useful with buffering as the effect of fading is already averaged out.

Symbol-wise Processing

When DF protocols are implemented with SW processing, the RN jointly decodes data from all backhaul RBs and redistributes it for the service RBs. In particular, there is no "virtual one-hop connection" from the BS to each UE, but the RN acts more like a stand-alone BS from the UEs' perspective. Consequently, the overall performance is limited by the minimum per-link sum capacity which is an upper bound for the case achieved with RW processing (the sum of minimum per-RB capacities).

The instantaneous system capacity can be expressed **[235, 296]** as

$$\mathcal{C} = \min\left\{\mathcal{B} + \mathcal{C}_{\mathrm{SR}}, \mathcal{C}_{\mathrm{RD}}\right\} \tag{8.23}$$

in which $\mathcal{B}$ denotes the buffer status before BS transmission and, after substituting (8.4) and (8.7), the instantaneous backhaul and service link capacities are given by

$$\mathcal{C}_{\mathrm{SR}} \triangleq \sum_{k=1}^{N_{\mathrm{RB}}} \mathcal{C}_{\mathrm{SR}}[k] = t_{\mathrm{SR}} \sum_{k=1}^{N_{\mathrm{RB}}} \log_2(1 + \bar{\gamma}_{\mathrm{SR}}[k]), \tag{8.24}$$

$$\mathcal{C}_{\mathrm{RD}} \triangleq \sum_{n=1}^{N_{\mathrm{D}}} \mathcal{C}_{\mathrm{RD}}[n] = t_{\mathrm{RD}} \sum_{n=1}^{N_{\mathrm{D}}} \log_2(1 + \gamma_{\mathrm{RD}}[n]), \tag{8.25}$$

respectively.

The buffering mechanism is essentially the same as with RW processing except that there is a single common buffer for all UEs' data. Next, the cases of no buffering (NB) and with buffering (WB) are considered separately when evaluating the average system capacity.

Without buffering, the average system capacity could be directly determined by calculating the expectation of (8.23) where $\mathcal{B} = 0$. The substitution of (8.6) and (8.25) yields

$$\begin{aligned} \bar{\mathcal{C}} &= \mathcal{E}\{\min\left\{\mathcal{C}_{\mathrm{SR}}, \mathcal{C}_{\mathrm{RD}}\right\}\} \\ &= \int_0^\infty \cdots \int_0^\infty \min\left\{\bar{\mathcal{C}}_{\mathrm{SR}}, t_{\mathrm{RD}} \sum_{n=1}^{N_{\mathrm{D}}} \log_2(1 + x_n)\right\} \prod_{n=1}^{N_{\mathrm{D}}} f_{\gamma_{\mathrm{RD}}[n]}(x_n) \prod_{n=1}^{N_{\mathrm{D}}} \mathrm{d}x_n, \end{aligned} \tag{8.26}$$

for which $\bar{\mathcal{C}}_{\mathrm{SR}} = \mathcal{C}_{\mathrm{SR}}$ is given in (8.24). This N_{D}-fold integral is cumbersome to calculate and admits closed-form solutions only in special cases. For example, it is reduced to $\mathcal{I}_{\text{DF-RW}}$ already solved in (8.19) when $N_{\mathrm{D}} = 1$. Approximations may be also devised by converting it into the form of a single tractable integral: The approach of **[235]** exploits the *central limit theorem* in order to replace $\mathcal{C}_{\mathrm{RD}}$ by a Gaussian random variable when $\gamma_{\mathrm{RD}}[n]$ are identically distributed for all n, $N_{\mathrm{D}} = N_{\mathrm{RB}}$, and N_{RB} is large. However, it is not necessary or meaningful to restrict the analysis herein to the cases of identical RN–UE path losses and full system load.

The maximum system capacity, as expressed above, is achieved when the shares of backhaul capacity allotted for each UE are adapted based on instantaneous SNRs. Yet, the benefits of symbol-wise processing can be realized well also by using a simpler suboptimal protocol where the nth UE is assigned fixed frequency share $\bar{\phi}[n]$, $0 \leq \bar{\phi}[n] \leq 1$, of the total backhaul capacity. The average system capacity with this implementation is calculated with the substitution of (8.6) as

$$\begin{aligned}\bar{\mathcal{C}} &= \sum_{n=1}^{N_{\mathrm{D}}} \mathcal{E}\left\{\min\left\{\bar{\phi}[n]\cdot\mathcal{C}_{\mathrm{SR}}, \mathcal{C}_{\mathrm{RD}}[n]\right\}\right\} \\ &= \sum_{n=1}^{N_{\mathrm{D}}} \int_0^{\infty} \min\left\{\bar{\phi}[n]\cdot\bar{\mathcal{C}}_{\mathrm{SR}}, t_{\mathrm{RD}}\log_2(1+x)\right\} f_{\gamma_{\mathrm{RD}}[n]}(x)\,\mathrm{d}x \\ &= \sum_{n=1}^{N_{\mathrm{D}}} \mathcal{I}_{\text{DF-SW}}(t_{\mathrm{RD}}, \bar{\phi}[n]\cdot\bar{\mathcal{C}}_{\mathrm{SR}}, \bar{\gamma}_{\mathrm{RD}}[n]), \end{aligned} \tag{8.27}$$

where the integral $\mathcal{I}_{\text{DF-SW}}$ admits a closed-form expression which can be transformed into the form of $\mathcal{I}_{\text{DF-RW}}(t, 2^{\frac{a}{1-t}}-1, b)$ expressed in (8.19) as

$$\begin{aligned}&\mathcal{I}_{\text{DF-SW}}(t,a,b) \\ &= \int_0^{\infty} \min\left\{a, t\log_2(1+x)\right\} \frac{\exp\left(-\frac{x}{b}\right)}{b}\,\mathrm{d}x \\ &= \int_0^{\infty} \min\left\{(1-t)\log_2(1+(2^{\frac{a}{1-t}}-1)), t\log_2(1+x)\right\} \frac{\exp\left(-\frac{x}{b}\right)}{b}\,\mathrm{d}x \\ &= \frac{t}{\log_e(2)}\exp\left(\frac{1}{b}\right)\left[E_1\left(\frac{1}{b}\right) - E_1\left(\frac{2^{\frac{a}{t}}}{b}\right)\right]. \end{aligned} \tag{8.28}$$

In general, the shares $\{\bar{\phi}[n]\}_{n=1}^{N_{\mathrm{D}}}$ can be optimized in various ways subject to the constraint $\sum_{n=1}^{N_{\mathrm{D}}}\bar{\phi}[n] = 1$. As demonstrated later in numerical results, good performance is achieved when they are set relatively to the average service link capacities, i.e.,

$$\bar{\phi}[n] = \frac{\bar{\mathcal{C}}_{\mathrm{RD}}[n]}{\bar{\mathcal{C}}_{\mathrm{RD}}}, \tag{8.29}$$

for which $\bar{\mathcal{C}}_{\mathrm{RD}}[n]$ is given in (8.8) and

$$\bar{\mathcal{C}}_{\mathrm{RD}} \triangleq \sum_{n=1}^{N_{\mathrm{D}}}\bar{\mathcal{C}}_{\mathrm{RD}}[n] = \frac{t_{\mathrm{RD}}}{\log_e(2)}\sum_{n=1}^{N_{\mathrm{D}}}\exp\left(\frac{1}{\bar{\gamma}_{\mathrm{RD}}[n]}\right)E_1\left(\frac{1}{\bar{\gamma}_{\mathrm{RD}}[n]}\right). \tag{8.30}$$

Finally, it should be recalled that the usage of a buffer essentially compensates for the effect of fading on the service link as emphasized earlier. With buffering (WB), the average system capacity thus becomes simply the minimum of average per-link sum capacities (cf. the average of minimum per-link sum capacity for NB) which can be expressed as

$$\bar{\mathcal{C}} = \min\left\{\mathcal{E}\{\mathcal{C}_{\mathrm{SR}}\}, \mathcal{E}\{\mathcal{C}_{\mathrm{RD}}\}\right\} = \min\left\{\bar{\mathcal{C}}_{\mathrm{SR}}, \bar{\mathcal{C}}_{\mathrm{RD}}\right\}. \tag{8.31}$$

Above $\bar{\mathcal{C}}_{\mathrm{SR}} = \mathcal{C}_{\mathrm{SR}}$ which is given in (8.24), and $\bar{\mathcal{C}}_{\mathrm{RD}}$ is expressed in (8.30).

Optimized Resource Allocation

All AF protocols and the baseline DF protocols result in the allocation of uniform resources (UR) for the backhaul and service links, i.e., $t_{\mathrm{SR}} = t_{\mathrm{RD}} = 1/2$. However, the capacity analysis suggests that system performance is, in principle, defined by the weaker one of the two links. Whenever the links are unbalanced in terms of system load or mean SNRs, the performance of DF protocols can be thus improved by allocating optimal resources (OR) such that larger time share is given for the weaker link.

The reasoning to optimize the service time share is formalized as

$$t_{\mathrm{RD}}^{*} = \arg \max_{0 \leq t_{\mathrm{RD}} \leq 1} \bar{\mathcal{C}} \tag{8.32}$$

in which $\bar{\mathcal{C}}$ is the average system capacity derived for one of the protocols. Consequently, the optimal backhaul time share becomes $t_{\mathrm{SR}}^{*} = 1 - t_{\mathrm{RD}}^{*}$.

With resource block-wise (RW) processing, optimization problem (8.32) can be solved only numerically. Fortunately, the system capacity expressions to be maximized are well-behaved: They all are continuous and contain a single global maximum in the interval $0 \leq t_{\mathrm{RD}} \leq 1$. Thus, it is straightforward and justified to apply any numerical (iterative) off-the-shelf algorithm which can maximize scalar functions.

Similarly, symbol-wise (SW) processing without buffering requires numerical optimization to solve (8.32). On the contrary, a closed-form solution is available for the counterpart with buffering (WB): The two links are balanced (which maximizes $\bar{\mathcal{C}}$) by choosing $t_{\mathrm{RD}} = 1 - t_{\mathrm{SR}}$ such that $\bar{\mathcal{C}}_{\mathrm{SR}} = \bar{\mathcal{C}}_{\mathrm{RD}}$ in (8.31). Thus,

$$t_{\mathrm{RD}}^{*} = \frac{\sum_{k=1}^{N_{\mathrm{RB}}} \log_e(1 + \bar{\gamma}_{\mathrm{SR}}[k])}{\sum_{k=1}^{N_{\mathrm{RB}}} \log_e(1 + \bar{\gamma}_{\mathrm{SR}}[k]) + \sum_{n=1}^{N_{\mathrm{D}}} \exp(\frac{1}{\bar{\gamma}_{\mathrm{RD}}[n]}) E_1(\frac{1}{\bar{\gamma}_{\mathrm{RD}}[n]})}. \tag{8.33}$$

By substituting (8.24), (8.30), (8.33) and $t_{\mathrm{SR}}^{*} = 1 - t_{\mathrm{RD}}^{*}$ into (8.31), the average system capacity with OR becomes

$$\bar{\mathcal{C}} = \left[\frac{1}{\sum_{k=1}^{N_{\mathrm{RB}}} \log_2(1 + \bar{\gamma}_{\mathrm{SR}}[k])} + \frac{\log_e(2)}{\sum_{n=1}^{N_{\mathrm{D}}} \exp(\frac{1}{\bar{\gamma}_{\mathrm{RD}}[n]}) E_1(\frac{1}{\bar{\gamma}_{\mathrm{RD}}[n]})} \right]^{-1}. \tag{8.34}$$

Furthermore, approximate solutions of (8.32) can be reasoned, as follows, for all DF protocols whenever

$$\frac{1}{N_{\mathrm{RB}}} \sum_{k=1}^{N_{\mathrm{RB}}} \log_2(1 + \gamma_{\mathrm{SR}}[k]) \approx \frac{1}{N_{\mathrm{D}}} \sum_{n=1}^{N_{\mathrm{D}}} \log_2(1 + \gamma_{\mathrm{RD}}[n]), \tag{8.35}$$

i.e., the instantaneous per-RB capacities are approximately in balance. In RW processing, this condition guarantees that the allocation of UR is

approximately optimal, i.e.,

$$t_{\mathrm{RD}}^{*} \approx \frac{1}{2}. \tag{8.36}$$

In SW processing, the link imbalance is essentially defined by system load $\lambda = N_{\mathrm{D}}/N_{\mathrm{RB}}$. In particular, when $N_{\mathrm{D}} \ll N_{\mathrm{RB}}$, SW processing with UR allocation leads to significant overcapacity in the backhaul link compared to the service link. This is avoided by setting $t_{\mathrm{SR}}N_{\mathrm{RB}} \approx t_{\mathrm{RD}}N_{\mathrm{D}}$, i.e.,

$$t_{\mathrm{RD}}^{*} \approx \frac{N_{\mathrm{RB}}}{N_{\mathrm{RB}} + N_{\mathrm{D}}} = \frac{1}{1+\lambda} \tag{8.37}$$

which can be seen as a simplified form of (8.33). When $\lambda = 1$, $t_{\mathrm{RD}}^{*} \approx 1/2$, i.e., the allocation of uniform resources is approximately optimal with full system load in SW processing (cf. with any load level in RW processing).

8.3.3 Reference Case: Out-of-Band Backhaul Link

The key reference case for relaying is a system with an out-of-band backhaul link preserving all in-band resources for the service link, i.e., $t_{\mathrm{SR}} = 0$ and $t_{\mathrm{RD}} = 1$. Such reference systems can be realized in various ways, e.g., the relay link may be seen as a *distributed antenna system* (DAS) with a wired (e.g., optical fiber) or a dedicated microwave connection between the BS and the RN which becomes effectively a remote BS antenna [40]. Alternatively, the reference case corresponds to the deployment of an extra stand-alone BS which replaces the RN at the same location.

By substituting (8.8), the average reference system capacity becomes

$$\bar{\mathcal{C}} = \sum_{n=1}^{N_{\mathrm{D}}} \bar{\mathcal{C}}_{\mathrm{RD}}[n] = \frac{1}{\log_e(2)} \sum_{n=1}^{N_{\mathrm{D}}} \exp\left(\frac{1}{\bar{\gamma}_{\mathrm{RD}}[n]}\right) E_1\left(\frac{1}{\bar{\gamma}_{\mathrm{RD}}[n]}\right). \tag{8.38}$$

This expression represents an upper bound for the average system capacity of all the in-band relaying protocols considered in earlier sections (with both uniform and optimal resource allocation).

It should be noted that it is rather unfair to compare an in-band relay link to an out-of-band DAS in terms of mere system capacity because their installation and operation costs differ substantially. Moreover, RNs may be installed at sites which cannot support an out-of-band backhaul at all, and, on the other hand, it is pointless to discard a wired backhaul that is already available when reusing an old site. However, the comparison is relevant for system design when considering the overall trade-off between performance and expenses: It yields the capacity degradation which needs to be tolerated with different relaying protocols in order to avoid establishing an out-of-band backhaul connection or deploying extra BSs; indeed, capacity is usually more than halved in the case of half-duplex relaying.

8.4 Performance Evaluation

This section exploits the unified analytical framework for the numerical analysis of relay-enhanced downlink cellular systems. Illustrative results are generated in the scope of an example vehicular communication system setup which is specified in the next subsection. In particular, all the 18 considered OFDM(A) relaying protocols are compared thoroughly in terms of average system capacity. Therefore, the analytical expressions provided in the previous section are implemented and numerical values are computed for them which facilitates discussions on the characteristics of the protocols in the latter subsection.

8.4.1 Example System Setup

Numerical illustrations inevitably require to specify an example setup although every derived analytical expression itself is applicable for all kind of scenarios. Herein, the performance evaluation considers the suburban vehicular system of Fig. 8.2 adopting OFDM(A) parameters from Long-Term Evolution (LTE) [1, 2] and channel models from the Wireless World Initiative New Radio (WINNER) project [120]. For additional reference results, the setup is similar to those assumed in **[233, 235]** except that UEs are now spatially distributed. Consequently, SNR parameters to be substituted in the analytical expressions are summarized in Table 8.2.

OFDM(A) Parameters

The number of resource blocks (RBs) is chosen as $N_{\mathrm{RB}} = 15$ which corresponds to an LTE system [1] that reserves 3 MHz sub-band for serving UEs in the RN coverage area. The physical resource blocks (PRBs) of LTE span 12 adjacent subcarriers over 0.5 ms slots while the subcarrier spacing is 15 kHz [2], i.e., 180 kHz is allocated for each PRB. All subcarriers within one RB are assumed to be subject to approximately the same channel coefficient, i.e., each RB goes through a frequency-flat channel. Thus, there are 180 occupied subcarriers (the size of the fast Fourier transform (FFT) is $N_{\mathrm{FFT}} = 256$ samples) which allocate 2.7 MHz plus guard bands.

Backhaul Link (BS–RN)

In principle, cellular relay nodes are deployed at the edge of BS transmission range to minimize the unnecessary overlapping of coverage areas. Thus, it is reasonable to assume that a RN observes a single snapshot channel generated from the WINNER B5f non-line-of-sight (NLOS)

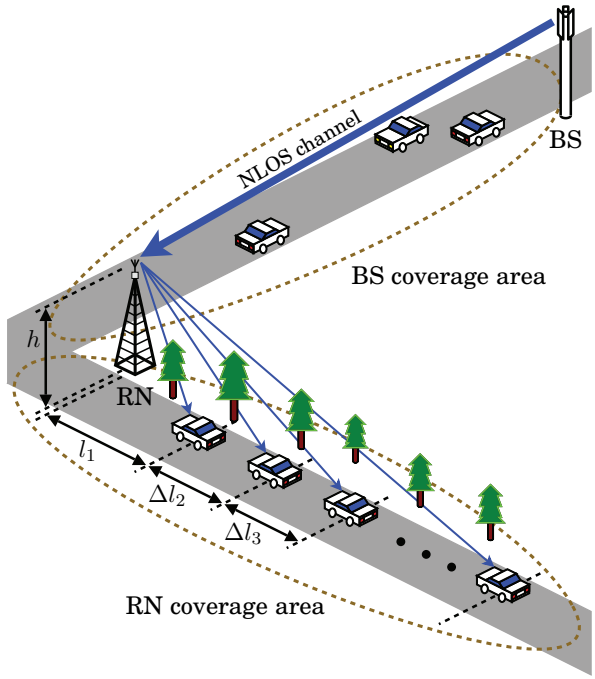

Figure 8.2. Example system setup for a rural vehicular communication scenario. The elevation of the RN antenna is set to $h = 23.5$ m and the kth car is located horizontally at distance $l_k = l_{k-1} + \Delta l_k$ [m] from the RN ($l_0 = 50$ m).

model [120] that is developed specifically for rooftop-to-below rooftop channels between a BS and a stationary RN. The SNR value $\bar{\gamma}_{\mathrm{SR}}[k]$ is measured at the center of the kth RB and these samples are sorted in descending order to comply with the notation used for mathematical analysis.

In the numerical results, this model is first applied repeatedly for evaluating the average system capacity with a set of randomized snapshot BS–RN channels. This illustrates the effect of RN deployment at different locations, although each RN actually observes a static backhaul link.

Service Link (RN–UEs)

The primary coverage area of the RN is an around 200-meter straight stretch of road. The system is assumed to have in total N_{RB} cars, out of which N_{D} random ones carry an active UE. Furthermore, scheduling may assign any permutation of service RBs for the active UEs. Therefore, the following numerical results are also averaged over the $N_{\mathrm{RB}}!/(N_{\mathrm{RB}} - N_{\mathrm{D}})!$ possible UE permutations using the Monte Carlo method.

As illustrated in Fig. 8.2, the horizontal coordinate of the kth car is $l_k = l_{k-1} + \Delta l_k$ [m], where $\Delta l_k \geq 0$ denotes the distance between the

cars, and the RN antenna is placed $h = 23.5$ m higher than the UE antennas. Thus, the length of the propagation path from the RN to the UE at the kth car is $d_k = \sqrt{h^2 + l_k^2}$ [m]. With WINNER C1 suburban NLOS channel model [120], the path loss to the UE at the kth car becomes $30.46 + 35.74 \log_{10} d_k$ [dB] for 2 GHz carrier frequency, and it is necessary to set an offset $l_0 = 50$ m (such that $l_k \geq l_0$ for all k) since the model is not valid for shorter distances. The SNR value $\bar{\gamma}_{\mathrm{RD}}[k]$ is calculated based on path loss and transmit power, while the mean SNR of UEs is defined as

$$\bar{\gamma}_{\mathrm{RD}} \triangleq \frac{1}{N_{\mathrm{RB}}} \sum_{k=1}^{N_{\mathrm{RB}}} \bar{\gamma}_{\mathrm{RD}}[k] \tag{8.39}$$

which normalizes the per-UE transmit power with any system load.

In the numerical results, the system performance is first evaluated over different randomized UE geometries which are generated by modeling the arrivals of cars at the beginning of the road as homogeneous Poisson process. Thus, by assuming that all cars have the same velocity, Δl_k, $k = 1, 2, \ldots, N_{\mathrm{RB}}$, become independent and identically distributed exponential random variables for which one may reasonably choose parameter value $\mathcal{E}\{\Delta l_k\} = 10$ m corresponding to a traffic jam situation.

Representative Average SNRs

The later numerical results illustrate the performance of the protocols also in a representative snapshot scenario without averaging over different RN locations and UE geometries. However, choosing just a random snapshot might lead to optimistic or pessimistic channels and biased observations. Instead, the numerical analysis adopts a reasonably typical snapshot which is obtained by averaging the sorted backhaul SNRs over 10^6 random instances and setting the distance between the cars to $\Delta l_k = 10$ m for all k (cf. $\mathcal{E}\{\Delta l_k\} = 10$ m) in the service link. The explicit SNR parameters substituted in the expressions are summarized in Table 8.2 in order to allow the numerical results to be reproduced.

Table 8.2. The average signal-to-noise ratios of resource blocks in a typical representative scenario with full system load ($N_{\mathrm{D}} = N_{\mathrm{RB}} = 15$).

(a) Backhaul link RBs

$\{\bar{\gamma}_{\mathrm{SR}}[k]/\bar{\gamma}_{\mathrm{SR}}\}_{k=1}^{N_{\mathrm{RB}}}$ [dB]				
4.57	3.44	2.56	1.82	1.10
0.41	-0.29	-1.00	-1.77	-2.61
-3.55	-4.66	-6.04	-7.92	-11.01

(b) Service link RBs

$\{\bar{\gamma}_{\mathrm{RD}}[k]/\bar{\gamma}_{\mathrm{RD}}\}_{k=1}^{N_{\mathrm{RB}}}$ [dB]				
7.39	5.01	2.89	1.01	-0.69
-2.23	-3.64	-4.94	-6.14	-7.25
-8.30	-9.28	-10.20	-11.07	-11.90

8.4.2 Numerical Results and Discussion

In the following, the analytical results are used for the comparison of the OFDM(A) relaying protocols in the example vehicular system. The expressions are implemented carefully because they involve a specific product of functions, $\exp(x)\,E_1(x)$, which may be subject to computational problems as explained in Appendix A.4. The study is divided into two steps such that all protocols listed in Table 8.1 are evaluated; after first considering protocols with uniform resource allocation, it is feasible to illustrate the benefit of optimized resource allocation by the remaining protocols.

The Effects of BS–RN Channel Condition and UE Geometry
The first numerical results, shown in Fig. 8.3, illustrate the cumulative distribution functions (CDFs) of the average system capacity $\bar{\mathcal{C}}$, i.e.,

$$F_{\bar{\mathcal{C}}}(x) \triangleq \text{Prob}(\bar{\mathcal{C}} \leq x) = \frac{1}{K}\sum_{k=1}^{K} \mathrm{U}(x - \bar{\mathcal{C}}[k]), \tag{8.40}$$

where $\mathrm{U}(\cdot)$ is the unit step function. These empirical distributions are generated by evaluating a large ($K = 10^6$) set of values $\{\bar{\mathcal{C}}[k]\}_{k=1}^{K}$ for the analytical expressions over randomized RN locations and UE geometries, i.e., different scenarios, as specified in the previous subsection.

In general *for all scenarios*, it can be observed that amplify-and-forward (AF) protocols are inferior to decode-and-forward (DF) protocols; fixed pairing (FP) and adaptive pairing (AP) perform similarly but offer improvement over random pairing (RP); symbol-wise (SW) processing is better for DF protocols but performs similarly to resource block-wise (RW) processing with AF protocols; and the combination of buffering and optimized resource (OR) allocation brings significant gains with SW processing. A closer look shall be shortly taken at these characteristics by varying system parameters such as $\bar{\gamma}_{\mathrm{SR}}$, $\lambda = N_{\mathrm{D}}/N_{\mathrm{RB}}$, and $t_{\mathrm{RD}} = 1 - t_{\mathrm{SR}}$.

As shown by Fig. 8.3, there is roughly 0.6 Mbit/s capacity difference, or spread, between the worst and the best scenario with any protocol. In particular, the shape of the distribution is approximately the same with all protocols, i.e., the choice of a particular relaying protocol manifests itself as a mere shift in the cumulative distribution function. Thus, the *relative* characteristics and the superiority order of the relaying protocols can be reasonably inferred from any snapshot scenario (as they are the same for all scenarios) although the RN location and UE geometry affect the *absolute* performance. This justifies the usage of the representative average SNR parameters (Table 8.2) in the following discussions.

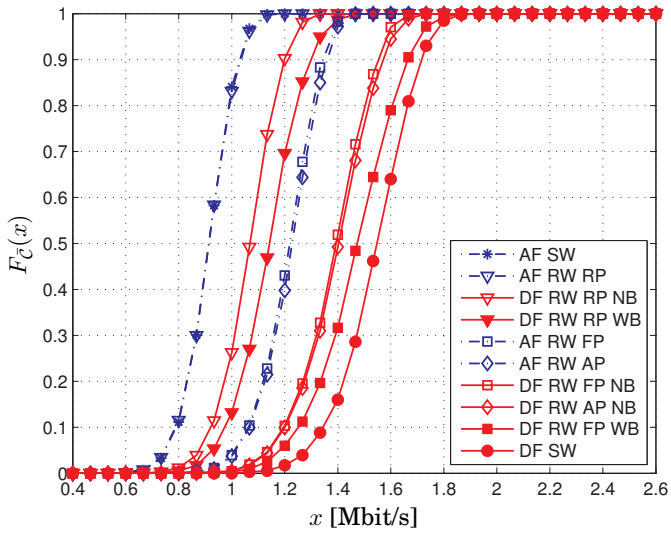

(a) all protocols with uniform resource (UR) allocation

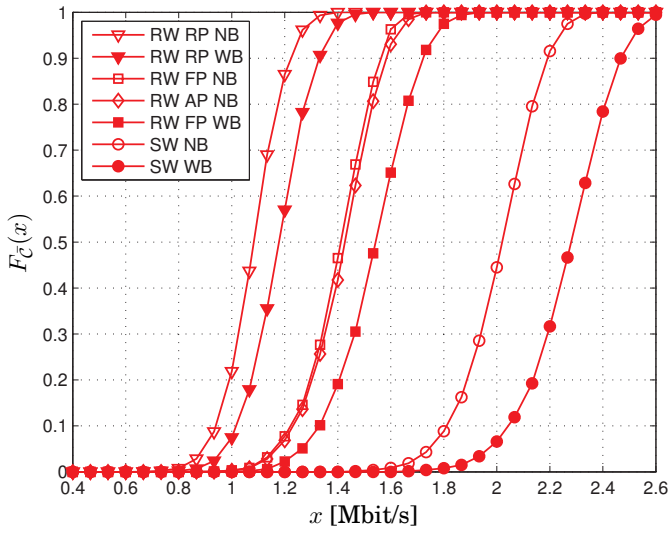

(b) DF protocols with optimized resource (OR) allocation

Figure 8.3. Variation of the average system capacity over different RN locations and UE geometries when $\bar{\gamma}_{\mathrm{SR}} = 11$ dB, $\bar{\gamma}_{\mathrm{RD}} = 15$ dB, and $\lambda = N_{\mathrm{D}}/N_{\mathrm{RB}} = 1/3$ (moderate system load). The abbreviations are defined in Table 8.1.

AF and DF Protocols with Uniform Resource Allocation

Figure 8.4 shows the average capacity of the relaying protocols when utilizing uniform resource (UR) allocation ($t_{\mathrm{SR}} = t_{\mathrm{RD}} = 1/2$). Firstly, these results highlight the importance of proper protocol design: At maximum (when $\bar{\gamma}_{\mathrm{SR}} = 10$–$12$ dB), the best protocol achieves 63% higher capacity than the worst one. Correspondingly, different design choices may improve capacity up to 38% (resp. up to 18%) within the set of DF protocols (resp. AF protocols). Furthermore, DF protocols are clearly superior to their AF counterparts. In fact, the best AF protocol (requiring rather complex signaling) achieves approximately the same capacity as the worst but simplest DF protocol for all $\bar{\gamma}_{\mathrm{SR}}$. This is in line with what can be expected based on the analytical expressions since (8.17) used with DF protocols represents an upper bound for (8.9) used with AF protocols. The difference is conceptually explained by the fact that AF protocols forward also relay input noise while DF protocols (re-)generate clean signals.

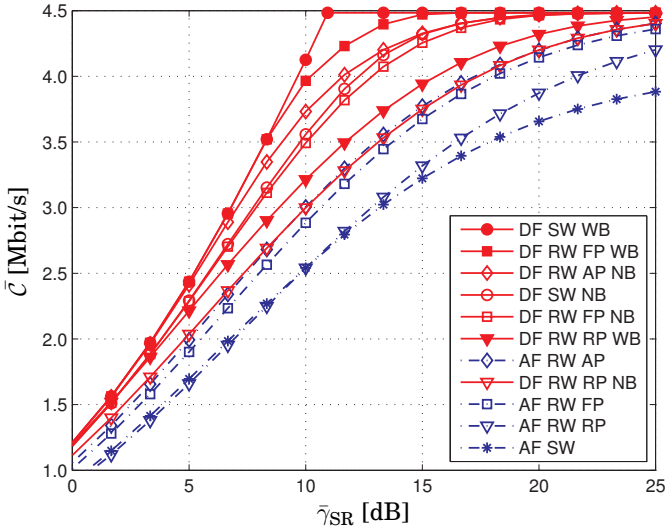

Figure 8.4. Average system capacity in terms of the mean SNR of the backhaul resource blocks with uniform resource (UR) allocation when $\bar{\gamma}_{\mathrm{RD}} = 15$ dB and $\lambda = N_{\mathrm{D}}/N_{\mathrm{RB}} = 1$ (full system load). For reference, a distributed antenna system offers 8.97 Mbit/s capacity. The abbreviations are defined in Table 8.1.

Secondly, the results of Fig. 8.4 explain how to position the RN at the edge of the BS coverage area since the variable $\bar{\gamma}_{\mathrm{SR}}$ is essentially determined by the BS–RN distance when the BS transmit power is fixed. The differences of the protocols become minimal at both extremes: When the RN is deployed far away (low $\bar{\gamma}_{\mathrm{SR}}$), the backhaul link becomes the bottleneck of the system and all protocols achieve low capacity; but even if the

RN is deployed close to the BS (high $\bar{\gamma}_{\mathrm{SR}}$), the backhaul link still consumes significant amount of in-band channel resources due to which the relay link achieves at best 50% of the capacity of a distributed antenna system. The simplest protocol (with time-domain amplification) is an exception as it converges at high $\bar{\gamma}_{\mathrm{SR}}$ to around 10% lower capacity than all the other protocols. The conceptual idea that contributes to the differences of time-domain and frequency-domain amplification can be inferred by comparing (8.10) to (8.13): In contrast to frequency-selective frequency-domain amplification, time-domain amplification is restricted to use frequency-flat scalar gain and deep fades at the backhaul link cannot be compensated. In conclusion, the RN should be positioned such that the backhaul and service links are approximately in balance according to (8.35), which can be achieved by assigning 3–5 dB fading margin for the service link, e.g., $\bar{\gamma}_{\mathrm{SR}} = 10$–$12$ dB is a good target when $\bar{\gamma}_{\mathrm{RD}} = 15$ dB.

Figure 8.5 illustrates the effect of system load on the average capacity (cf. Fig. 8.4 with full system load). As shown by Fig. 8.5(a), time-domain symbol-wise (SW) and frequency-domain resource block-wise (RW) amplification result in approximately the same capacity with any system load if the pairing of RBs is random; yet the former is considerably simpler to implement than the latter. For AF protocols, the optimization of the pairing of RBs brings 18–36% relative and up to 0.5 Mbit/s absolute capacity improvement. Fixed pairing (FP) based on average SNRs and adaptive pairing (AP) based on instantaneous SNRs perform quite similarly. The maximum capacity loss due to choosing the considerably simpler FP implementation is merely 4%, observed at full system load.

As shown by Fig. 8.5(b), the optimization of the pairing of RBs brings 23–29% (resp. 22–26%) relative and up to 0.7 Mbit/s (resp. up to 0.8 Mbit/s) absolute capacity improvement for DF protocols without buffering (resp. with buffering). Choosing the considerably simpler FP implementation is again favorable, as it results in only 6% capacity loss at full system load and performs otherwise similarly to the AP implementation. In general, DF protocols with SW processing are clearly superior to their counterparts with RW processing, except at the full system load. This is also coherent with the expectations given by the analytical expressions. In particular, the capacity of RW processing is evaluated as a sum of minima in (8.18), (8.20), and (8.22) while SW processing leads to a minimum of sums in (8.27) and (8.31); the latter is obviously larger than the former. Furthermore, they realize the benefits of buffering quite differently. With

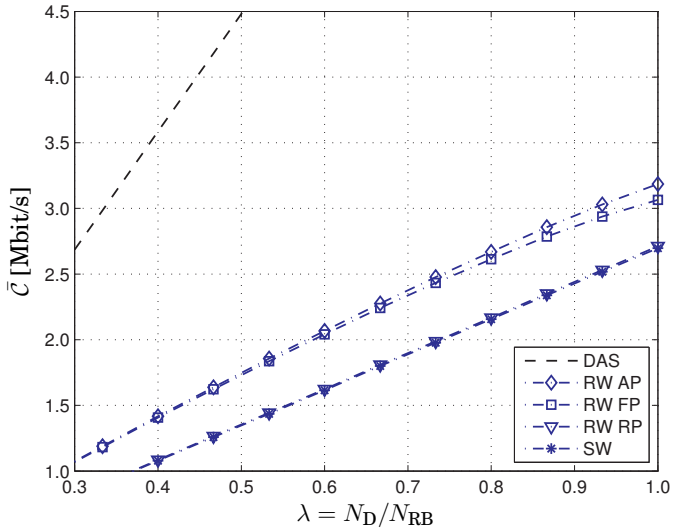

(a) amplify-and-forward (AF) protocols

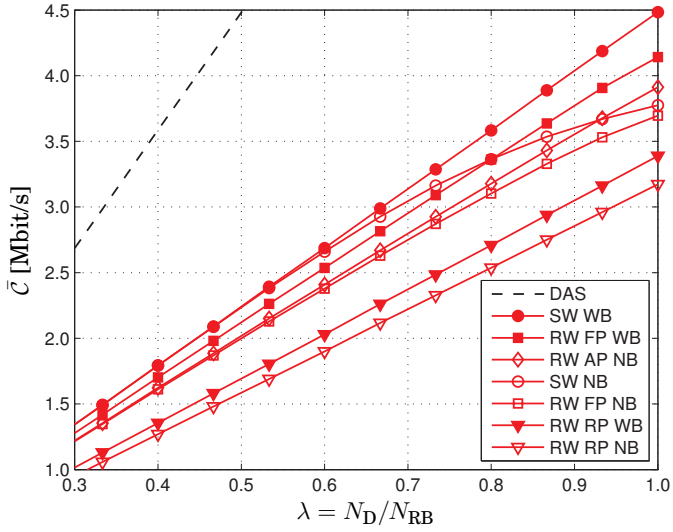

(b) decode-and-forward (DF) protocols

Figure 8.5. Average system capacity in terms of the relative system load with uniform resource (UR) allocation when $\bar{\gamma}_{\mathrm{SR}} = 11$ dB and $\bar{\gamma}_{\mathrm{RD}} = 15$ dB. The abbreviations are defined in Table 8.1.

RW processing, buffering brings moderate 4–12% capacity improvement over the whole range of system load levels. On the other hand, buffering does not offer any benefit with SW processing at low system load but the capacity improvement grows up to 19% at high load. The benefit of buffering can be inferred from the analytical expressions as well since it transforms expectations of minima shown in (8.18), (8.20), and (8.27) into minima of expectations shown in (8.22) and (8.31), where the latter is in general larger than the former.

DF Protocols with Optimized Resource Allocation

Figure 8.6 illustrates how to reach optimized resource (OR) allocation (cf. previous figures with UR allocation) with different DF protocols when solving (8.32). It should be recalled that AF protocols may be implemented only with UR allocation and, thus, they are not discussed herein. Figure 8.6(a) represents low system load, when SW processing without buffering (resp. with buffering) can achieve 31% (resp. 49%) higher capacity by using the optimal time sharing factor t_{RD}^{*} instead of uniform allocation $t_{\mathrm{RD}} = 1/2$. In the same case, all DF protocols applying RW processing gain less than 2% higher capacity with OR allocation. In the case of full load, considered in Fig. 8.6(b), all DF protocols (with both RW and SW processing) achieve only at maximum 1% higher capacity by implementing OR allocation, which becomes a design choice that only adds unnecessary complexity to the protocol. The potential of OR allocation can be justified also with the analytical expressions. In particular, (8.18), (8.20), (8.22), (8.27), and (8.31) conceptually include a minimum of two factors such that one decreases and the other increases in terms of t_{RD}. Thus, the system capacity can be improved by balancing the two factors.

Figure 8.7 illustrates how the exact optimal time sharing factor t_{RD}^{*} formulated in (8.33) varies w.r.t. the approximation (8.37) at different system load levels. The approximation is seen to follow closely the median value of t_{RD}^{*} over all UE permutations. In particular, the approximation is always within ± 0.1 from the exact value such that the largest deviations are observed around $\lambda = 1/3$. The approximation is the most accurate at very low and reasonably high system load levels. In general, these deviations translate to quite small capacity loss as seen next.

Figure 8.8 illustrates the average capacity of DF protocols with symbol-wise processing when they apply UR allocation using $t_{\mathrm{RD}} = 1/2$ or OR allocation using the values of t_{RD}^{*} illustrated in Fig. 8.7. The results show

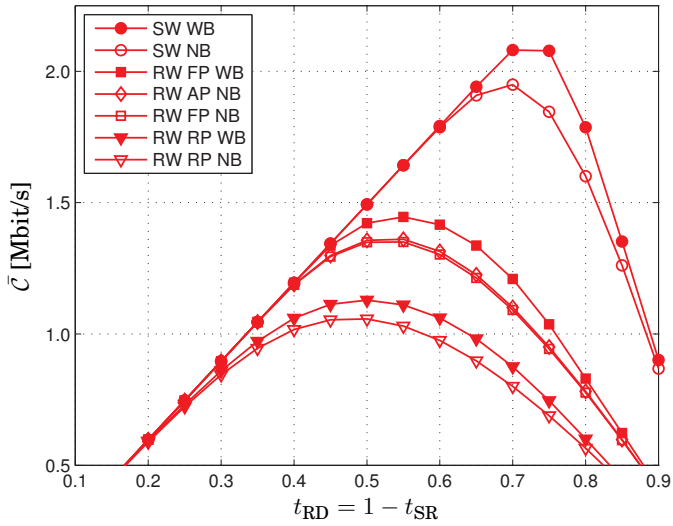

(a) $\lambda = N_{\mathrm{D}}/N_{\mathrm{RB}} = 1/3$

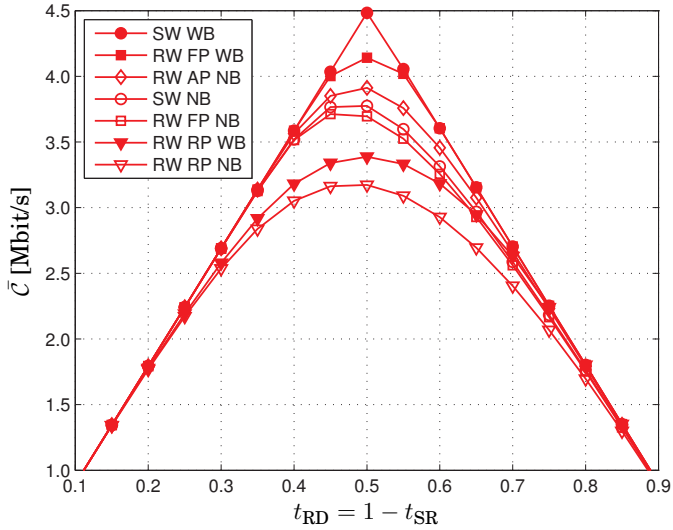

(b) $\lambda = N_{\mathrm{D}}/N_{\mathrm{RB}} = 1$

Figure 8.6. Average system capacity in terms of the service link time share when $\bar{\gamma}_{\mathrm{SR}} = 11$ dB and $\bar{\gamma}_{\mathrm{RD}} = 15$ dB. For reference, a distributed antenna system (DAS) offers (a) 2.99 Mbit/s and (b) 8.97 Mbit/s capacity. The abbreviations are defined in Table 8.1.

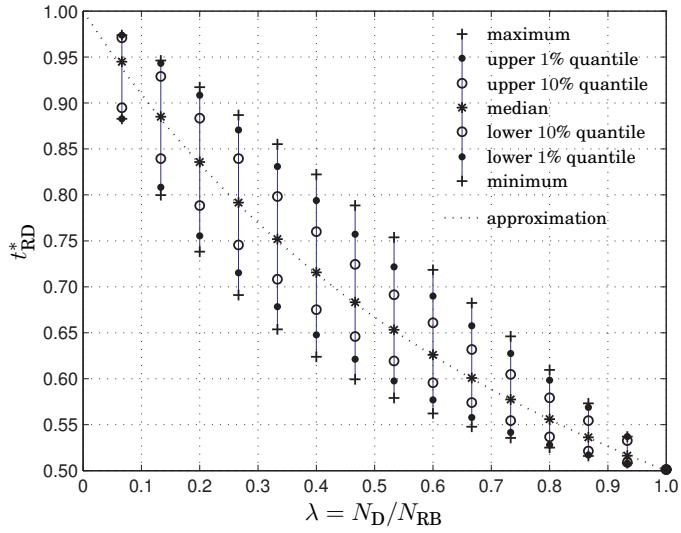

Figure 8.7. Fluctuation of the optimal service link time share expressed by (8.33) in terms of the relative system load when $\bar{\gamma}_{\mathrm{SR}} = 11$ dB and $\bar{\gamma}_{\mathrm{RD}} = 15$ dB.

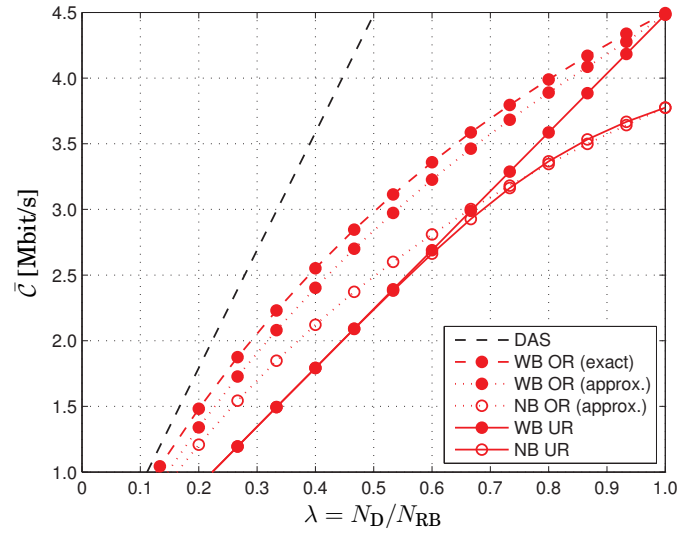

Figure 8.8. Average system capacity of DF protocols in terms of the relative system load with symbol-wise (SW) processing when $\bar{\gamma}_{\mathrm{SR}} = 11$ dB and $\bar{\gamma}_{\mathrm{RD}} = 15$ dB. The abbreviations are defined in Table 8.1.

that OR allocation offers up to 0.4 Mbit/s (resp. up to 0.8 Mbit/s) absolute capacity improvement without buffering (resp. with buffering) w.r.t. UR allocation. When the system is not fully loaded, the usage of the approximation (8.37) instead of the exact solution (8.33) results in a constant 0.1 Mbit/s loss of capacity, which translates to 7% (resp. to 3%) relative loss at $\lambda = 1/3$ (resp. at $\lambda = 2/3$) assumed in Fig. 8.6(a). Furthermore, Fig. 8.8 shows that OR allocation decreases the advantage of a distributed antenna system (DAS): The decode-and-forward (DF) protocol that applies SW processing with buffering achieves 83% (resp. 75%) of the capacity of a DAS at $\lambda = 1/5$ (resp. at $\lambda = 1/3$). In contrast, relaying protocols that use UR allocation achieve at maximum 50% of the capacity of a DAS as shown by Fig. 8.4. However, OR allocation converges to UR allocation in the case full system load as also seen in Fig. 8.6(b).

8.5 Conclusions

This chapter presented a unified framework for evaluating the ergodic capacity of infrastructure-based OFDM(A) relay links by means of closed-form expressions. The analysis covered a comprehensive set of relaying protocols developed by combining the most essential design choices. In particular, the design of relaying protocols should not only consider the conventional division between amplify-and-forward and decode-and-forward processing but, with wideband transmission, it also needs to take into account various other choices such as processing in different domains, the pairing of subcarriers, and the possibilities for buffering or adjusting time sharing between backhaul and service links to name but a few.

Consequently, the analysis was applied to assess and compare the performance of the OFDM(A) relaying protocols in an example suburban vehicular system. The numerical results revealed the importance of proper protocol design: Some design choices bring substantial capacity improvement (both relatively and absolutely) without adding much extra complexity, while one can also identify cases where the extra complexity is not worthwhile. The presented analysis provides useful information for specifying new systems, because it allows one to evaluate and compare the performance gains due to the design choices that are the key factors determining the complexity and cost of the system architecture.

9. Conclusions

This dissertation reported a study on multihop relaying in radio networks. It should be situated in the research field of signal processing in wireless communications which is concerned with the physical- and link-layer aspects of radio transceiver devices and transmission systems. To that end, the study contributed by developing and analyzing communication strategies for rationalizing resource usage in multihop links and signal processing techniques for improving the design of relaying protocols.

The motivation for this thesis arose from the advent of relaying as technology to realize dense networks which can economically provide high-rate ubiquitous services. This opened up new research challenges to find out how to operate relay links optimally under spectrum and transmit power limits and how to improve signal processing in relays. Some thrust was also given by the lack of earlier rigorous analytical works on the topic.

The scope of this thesis was inherently limited to concepts covered by the research field. Additionally, the study remained strictly within the framework of orthogonal frequency-division multiplexing (OFDM), albeit allowing interpretations in the context of other modulation techniques. Likewise, relays were explicitly regarded, whenever necessary, as fixed infrastructure-based nodes although a major part of the results would also apply to mobile relaying in the context of cooperative communications.

The remainder of the last chapter is organized into three parts to sum up and extend beyond the storyline of this thesis while recalling the main observations thereof. First, Section 9.1 recapitulates contributions on countermeasures for self-interference in full-duplex relays and trade-offs between relaying modes. Second, Section 9.2 highlights key results from the analysis of old and new relaying protocols. At last, this dissertation comes to an end in Section 9.3 where, as an ultimate conclusion, prospective lines of follow-up research are outlined to envision topics which could be interpolated in and extrapolated from the foregoing material.

9.1 Design and Analysis of Duplexing Modes

The first part of this dissertation concerned the design and analysis of relaying *modes* which was the major theme in the contributions of Chapters 3–5 and Section 6.4.1. The main results are summarized also in **[207]**. The operation mode of a relay node defines how an end-to-end multihop link (re)uses available frequency resources in each hop. In this study, the status quo views to relaying modes were reformed which rendered potential for significantly improved link-level spectral efficiency.

The full-duplex relaying mode was promoted as a feasible, advantageous alternative to conventional half-duplex operation while inherent loopback self-interference was recognized and dealt with at multiple phases. At first, the mitigation of self-interference was investigated by covering passive physical isolation, subtractive cancellation, and suppression by spatial filtering. Especially, significant novelty lied in the multiantenna concepts. The proposed mitigation schemes were evaluated extensively based on Monte Carlo simulations, statistical analysis with closed-form expressions, and experimental results using channel measurement data. The results revealed the effect of channel estimation error, distortion induced at the transmit side, and loopback channel rank as well as their relations to antenna and stream configurations.

The study indicated that significant level of residual interference will remain even with advanced mitigation schemes which gave motivation for developing transmit power control to still alleviate the effect at the second phase. Finally, system design was facilitated by developing criteria for choosing rationally between full-duplex and half-duplex relaying when the former is subject to residual distortion and the latter needs more spectrum resources. This was formulated as a fundamental rate–interference trade-off leading to opportunistic mode switching during operation for which conditions to prefer one mode over the other were characterized.

9.2 Design and Analysis of Forwarding Protocols

The second part of this dissertation concerned the design and analysis of relaying *protocols* which was the major theme in the contributions of Chapters 6–8. The forwarding protocol of a relay node specifies signal processing between reception and retransmission. In this study, all cardinal protocols were evaluated in the case of infrastructure-based relaying.

One half of the analysis adopted narrowband single-subcarrier system models in an implicit OFDM context. Different variations of amplify-and-forward and decode-and-forward protocols were analyzed in the case of multiuser multihop relaying by deriving closed-form expressions for a large set of performance metrics. The results characterized the benefit of multiuser scheduling and the cost of having a wireless backhaul. In principle, they are valid under any duplexing scheme but more specific analysis was conducted for directly evaluating the relaying modes.

The other half of the analysis adopted explicit wideband multicarrier system models. A new framework was developed for studying the delay spread properties of non-regenerative multihop OFDM links in conjunction with inter-carrier and inter-symbol interference. The results characterized the interplay between the number of hops, time synchronization and OFDM symbol parameters. A comprehensive set of OFDM(A) relaying protocols was also identified and evaluated in terms of system capacity. In all chapters, the results covered both downlink and uplink transmission reflecting their differences in infrastructure-based relaying.

9.3 Directions for Future Work

The presented study is rather comprehensive within the scope specified for it in Chapter 1 while it consistently prefers addressing central problems and general techniques to seizing upon marginal issues; there are no obvious wide gaps to be filled later on. Hence, prospective follow-up research will need either to limit its scope by specializing in technicalities which are dismissed herein or to advance beyond the present scope.

On the one hand, future work adopting a narrower scope than this study may address implementation details that could not be covered herein and consider more specific system scenarios at the cost of losing generality. Especially, the mitigation of self-interference in full-duplex relaying was formulated herein in a transparent way to allow for generic solutions that are applicable together with any conventional relaying protocol while the joint design of interference mitigation and specific protocols may certainly bring synergy benefit. Furthermore, since joint design can be repeated separately for each family of relaying protocols, or even for each protocol variation, options for further research are plenty, albeit fragmented.

Representative implementation aspects worth to mention are related to channel state information and how it is acquired. In particular, this study

aimed at revealing the general, ultimate performance limits of advanced relaying modes and protocols when they are not further hindered by all implementation-specific non-idealities. The presented concepts can be implemented in practical systems using only limited, or otherwise imperfect, channel state information which will obviously incur losses; evaluating and characterizing their effects were left as open research problems.

On the other hand, future work may adopt a scope that is wider than, or different from, the present one. The analysis of link-level OFDM(A) relaying protocols could be extended to include also different variations of user scheduling which was herein regarded as an independent task from the forwarding protocols and studied separately. Related works have previously formulated this aspect as specific resource-allocation problems which are solved using general optimization tools. Instead, it would be interesting to enumerate all essential design choices for scheduling and identify their interconnections with the present forwarding protocols.

When moving outside of the scope of this study, the design and analysis of mobile relays still allow discovering some open research topics in spite of the large body of literature already available in that area. Especially, the self-interference situation of small portable full-duplex devices is more difficult than that of infrastructure-based nodes which gives motivation for further research on mitigation schemes. Moreover, full-scale OFDM(A) relay links are still understudied in a rigorous analytical sense as opposed to typical simulations and narrowband single-subcarrier analyses. When omitting completely the context of relaying, it is worth to recognize that other communication scenarios could also achieve significantly improved spectral efficiency by exploiting full-duplex concepts analogous to those developed herein, e.g., transmit power adaptation and opportunistic switching between operation modes. Actually, the presented self-interference mitigation techniques are not restricted to full-duplex relays and they could be used as a baseline for more advanced schemes.

Finally, it is also worth to acknowledge that one could reproduce all the contents of this dissertation in the context of some other transmission technique than OFDM adopted herein; only time will tell whether this emerges as a relevant research idea. Yet the scope limitation is well justified for the present thesis because OFDM with its variations (which include even single-carrier frequency-division multiple access in a broad sense) has become *the* standard modulation for modern wideband transmission and its status seems unshakable at least in the near future.

A. Appendix

Some detailed mathematical derivations and discussions on technicalities are relegated herein since they are not so important for following the general storyline of the thesis and grasping its contributions. Yet these points may be vital for verifying baseline analytical expressions and distinctive implementation details. Furthermore, a part of them emerge in several locations throughout the manuscript and, thus, these appendices clarify cross-referencing between the self-contained technical chapters.

Appendix A.1 characterizes the statistics of rational expressions involving a gamma-distributed random variable and two constants. Especially, closed-form expressions are presented for the associated cumulative distribution function using the transform of random variables and for the expectation of the fraction in terms of the exponential integral function.

Appendix A.2 derives compact closed-form expressions for the multi-fold convolutions of exponential power–delay profiles. In particular, the derivations are presented in the form of propositions with proofs by mathematical induction and organized into two parts covering separately the respective cases of non-identical and identical channel profiles.

Appendix A.3 presents the order statistics of non-identical exponential random variables. The associated probability distributions are expressed as weighted sums of those known for the case of unordered exponential variables. This contributes a new versatile tool which is useful in many other applications also outside of the scope of this thesis since earlier literature typically resorts to the assumption of identical distributions or features intractable expressions due to explicit coefficient substitutions.

Appendix A.4 reports a numerical instability problem in the evaluation of a product of the exponential function and the exponential integral function, which appears frequently in the capacity analysis of various wireless systems. Thereby, appropriate alternative implementations are employed for circumventing the problem in the numerical results of this thesis.

A.1 Statistics of Transformed Gamma Random Variables

In Section 3.5.2, the analysis of cancellation and suppression for the mitigation of self-interference in full-duplex relays leads to a specific family of transformed gamma random variables. Their statistics are derived herein for completeness while preserving the flow of the main text.

Let X be a random variable that follows the gamma distribution with parameters k ("shape") and θ ("scale"), i.e., $X \sim \mathcal{G}(k, \theta)$. Any textbook in statistics gives its cumulative distribution function (CDF) for $x \geq 0$ as

$$F_X(x) = 1 - \frac{\Gamma\left(k, \frac{x}{\theta}\right)}{\Gamma(k)}, \tag{A.1}$$

where $\Gamma(k, z) = \int_z^\infty s^{k-1} \exp(-s)\, \mathrm{d}s$ and $\Gamma(k) = \Gamma(k, 0)$ are the upper incomplete and (complete) gamma functions, respectively. In the present applications, k is an integer and related with the number of antennas and spatial streams. Thus, $\Gamma\left(k, z\right) = (k-1)! \sum_{l=0}^{k-1} \frac{z^l}{l!} \exp(-z)$ [80, Eq. 8.352.4].

The analysis exploits transformed gamma variables of the form

$$Y \triangleq \frac{a}{X + b} \leq \frac{a}{b}, \tag{A.2}$$

in which a and b are real non-negative constants and the inequality represents the maximum of additional isolation in the presence of noisy side information. The inverse function of (A.2) is given by $X = \frac{a - bY}{Y}$ which is monotonically decreasing in terms of Y.

The standard transform of random variables yields the CDF of Y used in the analysis for $y \geq 0$ as

$$F_Y(y) = \begin{cases} 1 - F_X\left(\frac{a - by}{y}\right), & \text{if } 0 \leq y \leq \frac{a}{b}, \\ 1, & \text{if } y > \frac{a}{b}. \end{cases} \tag{A.3}$$

The end result (3.52) used in the analysis is obtained by substituting the CDF of gamma distribution into the above expression.

The analysis needs also the average of Y which is solved as follows:

$$\begin{aligned} \mathcal{E}\{Y\} &\triangleq \int_0^\infty \frac{a}{x + b} \frac{\mathrm{d}F_X(x)}{\mathrm{d}x}\, \mathrm{d}x \\ &= \int_0^\infty \frac{a}{x + b} \frac{x^{k-1}}{\theta^k \Gamma(k)} \exp\left(-\frac{x}{\theta}\right)\, \mathrm{d}x \\ &= \frac{a}{\theta} \exp\left(\frac{b}{\theta}\right) E_k\left(\frac{b}{\theta}\right). \end{aligned} \tag{A.4}$$

The second form corresponds to an alternative integral representation for the upper incomplete gamma function $\Gamma(k, z) = \frac{\exp(-z)\, z^k}{\Gamma(1-k)} \int_0^\infty \frac{\exp(-s) s^{-k}}{s+z}\, \mathrm{d}s$ [80, Eq. 8.353.3], and the last form uses the generalized exponential integral $E_k(z) = z^{k-1}\, \Gamma(1 - k, z)$ [3, Eq. 5.1.45]. The end result used in the analysis is restated in (3.53).

A.2 Convolution of Exponential Power–Delay Profiles

In Chapter 6, the study of non-regenerative multihop OFDM relaying involves the characterization of cascaded multipath channels. Especially, the new analytical framework is based on an M-fold convolution of power–delay profiles (PDPs), which is defined in its general form as

$$P_M(t) \triangleq P_1\left(t, g[1], \tau[1], s[1]\right) * \ldots * P_1\left(t, g[M], \tau[M], s[M]\right), \tag{A.5}$$

and wherein the convolution operation $(*)$ is given for two PDPs by

$$\hat{P}(t) * P(t) = \int_{-\infty}^{\infty} \hat{P}(x) P(t-x)\,\mathrm{d}x. \tag{A.6}$$

The respective parameters $\{g[m]\}_{m=1}^{M}$, $\{\tau[m]\}_{m=1}^{M}$, and $\{s[m]\}_{m=1}^{M}$ specify the gain, lag, and delay spread of each channel in the cascade. The resulting $P_M(t)$ can be referred to as the hypoexponential PDP when each subchannel is modeled by the classic (single-)exponential PDP, i.e.,

$$P_1(t) = P_1(t, g_1, \tau_1, s_1) = \frac{g_1}{s_1} \exp\left(-\frac{t-\tau_1}{s_1}\right) \mathrm{U}(t-\tau_1), \tag{A.7}$$

where $\mathrm{U}(\cdot)$ represents the unit step function for which $\mathrm{U}(t) = 0$ when $t < 0$ and $\mathrm{U}(t) = 1$ when $t \geq 0$.

In the following, the multiple convolutions appearing in the definition of the hypoexponential power–delay profile, given by (A.5) with (A.7), are calculated analytically in order to obtain more tractable representation without convolution operations as $P_M(t) \triangleq P_M(t, g_M, \tau_M, \{s[m]\}_{m=1}^{M})$. The derivations are formulated by exploiting the induction principle. In particular, the alternative forms of (A.5), when delay spread parameters in $\{s[m]\}_{m=1}^{M}$ are unequal or equal, are first postulated in two respective propositions which are then proved.

A.2.1 Asymmetric Delay Spread

Proposition

When $s[m_1] \neq s[m_2]$ for all $m_1 \neq m_2$, (A.5) with (A.7) becomes

$$P_M(t) = \sum_{l=1}^{M} \left(\prod_{\substack{m=1 \\ m \neq l}}^{M} \frac{s[l]}{s[l] - s[m]} \right) P_1(t, g_M, \tau_M, s[l]), \tag{A.8}$$

where $g_M = \prod_{m=1}^{M} g[m]$ and $\tau_M = \sum_{m=1}^{M} \tau[m]$.

Proof

First, it can be directly seen that the equation is true for the base case where $M = 1$ since (A.8) is reduced to (A.7). As an induction hypothesis,

the equation is assumed to be true in the case where $M = \hat{M} - 1$. In the succeeding case where $M = \hat{M}$, the hypoexponential PDP then becomes

$$\begin{aligned} P_{\hat{M}}(t) &= P_{\hat{M}-1}(t, g_{\hat{M}-1}, \tau_{\hat{M}-1}, \{s[1], \ldots, s[\hat{M}-1]\}) * P_1(t, g[\hat{M}], \tau[\hat{M}], s[\hat{M}]) \\ &= \sum_{l=1}^{\hat{M}-1} \left(\prod_{\substack{m=1 \\ m \neq l}}^{\hat{M}-1} \frac{s[l]}{s[l] - s[m]} \right) \int_{-\infty}^{\infty} P_1(x, g_{\hat{M}-1}, \tau_{\hat{M}-1}, s[l]) \\ &\qquad \times P_1(t - x, g[\hat{M}], \tau[\hat{M}], s[\hat{M}])\, \mathrm{d}x \\ &= \sum_{l=1}^{\hat{M}-1} \left(\prod_{\substack{m=1 \\ m \neq l}}^{\hat{M}} \frac{s[l]}{s[l] - s[m]} \right) P_1(t, g_{\hat{M}}, \tau_{\hat{M}}, s[l]) \\ &\quad + \sum_{l=1}^{\hat{M}-1} \left(\prod_{\substack{m=1 \\ m \neq l}}^{\hat{M}-1} \frac{s[l]}{s[l] - s[m]} \right) \frac{s[\hat{M}]}{s[\hat{M}] - s[l]} P_1(t, g_{\hat{M}}, \tau_{\hat{M}}, s[\hat{M}]) \end{aligned} \tag{A.9}$$

by exploiting (A.6) with (A.7) and (A.8). Especially, $g_{\hat{M}} = g_{\hat{M}-1} g[\hat{M}]$ and $\tau_{\hat{M}} = \tau_{\hat{M}-1} + \tau[\hat{M}]$. The final form conforms to (A.8) due to the identity

$$\sum_{l=1}^{\hat{M}-1} \left(\prod_{\substack{m=1 \\ m \neq l}}^{\hat{M}-1} \frac{s[l]}{s[l] - s[m]} \right) \frac{s[\hat{M}]}{s[\hat{M}] - s[l]} = \prod_{m=1}^{\hat{M}-1} \frac{s[\hat{M}]}{s[\hat{M}] - s[m]}. \tag{A.10}$$

Hence, the equation is true by mathematical induction for any $M \geq 1$ which completes the proof. ■

A.2.2 Symmetric Delay Spread

Proposition

When $s[m_1] = s[m_2] = s_1$ for all m_1 and m_2, (A.5) with (A.7) becomes

$$P_M(t) = \frac{(t - \tau_M)^{M-1}}{s_1^{M-1}(M-1)!} P_1(t, g_M, \tau_M, s_1), \tag{A.11}$$

where $g_M = \prod_{m=1}^{M} g[m]$ and $\tau_M = \sum_{m=1}^{M} \tau[m]$.

Proof

The deduction follows the same steps as in the asymmetric case. The equation clearly holds true for $M = 1$ and, assuming it is also true for $M = \hat{M} - 1$, the hypoexponential PDP becomes

$$\begin{aligned} P_{\hat{M}}(t) &= \int_{-\infty}^{\infty} \frac{(t - \tau_{\hat{M}-1})^{\hat{M}-2}}{s_1^{\hat{M}-2}(\hat{M}-2)!} P_1(x, g_{\hat{M}-1}, \tau_{\hat{M}-1}, s_1) P_1(t - x, g[\hat{M}], \tau[\hat{M}], s_1) \mathrm{d}x \\ &= \int_{\tau_{\hat{M}-1}}^{t-\tau[\hat{M}]} \frac{(x - \tau_{\hat{M}-1})^{\hat{M}-2}}{s_1^{\hat{M}-1}(\hat{M}-2)!} \mathrm{d}x \, \frac{g_{\hat{M}}}{s_1} \exp\left(-\frac{t - \tau_{\hat{M}}}{s_1} \right) \mathrm{U}(t - \tau_{\hat{M}}). \end{aligned} \tag{A.12}$$

The last expression is reduced to a form which is equivalent to (A.11) after calculating the integral of a polynomial. Hence, the equation is true by mathematical induction for any $M \geq 1$. ■

A.3 Order Statistics for Exponential Distribution

The order statistics of non-identical exponential random variables are exploited in Chapters 7 and 8. Although their derivation is already outlined in many textbooks, e.g., [9,47], the specific weighted sum form of the probability density function (PDF) and the notation adopted in the analysis deserve a brief summary for the reader's convenience. Similar, but more condensed, descriptions are available also in the appendix of **[236]**.

The exponential random variables at hand represent the instantaneous signal-to-noise ratios of Rayleigh-fading channels; Chapter 7 analyzes opportunistic scheduling using the distribution of the largest variable while Chapter 8 analyzes adaptive subchannel pairing using the marginal distributions of the complete variable set after ordering.

A.3.1 Derivation of Probability Distributions

Let $\{\gamma_{\mathrm{RD}}[n]\}_{n=1}^{N}$ be a set of N independent but not (necessarily) identically distributed exponential random variables and denote the average of the nth variable by $\bar{\gamma}_{\mathrm{RD}}[n] = \mathcal{E}\{\gamma_{\mathrm{RD}}[n]\}$. The respective cumulative distribution functions (CDFs) are given by

$$F_{\gamma_{\mathrm{RD}}[n]}(x) = 1 - \exp\left(-\frac{x}{\bar{\gamma}_{\mathrm{RD}}[n]}\right) \quad \text{for } x \geq 0. \tag{A.13}$$

The performance analysis of the aforementioned chapters needs the PDF of $\gamma_{\mathrm{RD}}[w^*[n]]$, i.e., $f_{\gamma_{\mathrm{RD}}[w^*[n]]}(\cdot)$, where $w^*[n]$ is the index of the nth largest random variable.[1] However, any trivial form is not suitable for the calculations since it should facilitate further manipulation, e.g., integration.

The derivation is based on the generic formula of order statistics readily available in [47, Eq. 5.2.1]: The CDF of the nth largest variable is

$$F_{\gamma_{\mathrm{RD}}[w^*[n]]}(x) = \sum_{m=N-n+1}^{N} \sum_{\mathfrak{P}_m} \prod_{l=1}^{m} F_{\gamma_{\mathrm{RD}}[i_l]}(x) \prod_{l=m+1}^{N} \left(1 - F_{\gamma_{\mathrm{RD}}[i_l]}(x)\right), \tag{A.14}$$

in which the summation over $\mathfrak{P}_m$ extends for all $\binom{N}{m}$ index permutations $(i_1, \ldots, i_N)$ of the set $\{1, 2, \ldots, N\}$ for which $i_1 < \cdots < i_m$ and $i_{m+1} < \cdots < i_N$. In other words, the sum extends over all possible partitions of the variables $\{\gamma_{\mathrm{RD}}[n]\}_{n=1}^{N}$ into two disjoint sets that contain m and $N - m$ elements for which $\gamma_{\mathrm{RD}}[n_1] \leq x$ and $\gamma_{\mathrm{RD}}[n_2] > x$, respectively.

[1] One may notice that the adopted indexing scheme deviates slightly from that of classical order statistics [9,47], which are usually formulated for the rth smallest, i.e., the $(N - r + 1)$th largest, variable. This notational choice is made due to the fact that the upper extremes are typically more significant for the analysis of wireless systems than the lower extremes.

In the specific case of exponential distribution considered herein, the substitution of CDFs from (A.13) into (A.14) yields, after expanding the products and recollecting all the common terms,

$$F_{\gamma_{\mathrm{RD}}[w^*[n]]}(x) = 1 - \sum_{m=n}^{N} (-1)^{m-n} \binom{m-1}{n-1} \sum_{\mathfrak{C}_m} \exp\left(- \sum_{l=1}^{m} \frac{x}{\bar{\gamma}_{\mathrm{RD}}[i_l]} \right), \quad \text{(A.15)}$$

in which the summation over $\mathfrak{C}_m$ extends for all $\binom{N}{m}$ index combinations $(i_1, \ldots, i_m)$ of the set $\{1, 2, \ldots, N\}$. In order to compress the notation and to obtain a tractable expression that hides the unnecessary complexity, the above double summation is then rewritten in an equivalent form of single summation given by

$$F_{\gamma_{\mathrm{RD}}[w^*[n]]}(x) = 1 - \sum_{m=1}^{M[n,N]} a[m,n,N] \cdot \exp\left(- \frac{x}{b[m,n,N]} \right), \quad \text{(A.16)}$$

for which constants $\{a[m,n,N]\}_{m=1}^{M[n,N]}$ and $\{b[m,n,N]\}_{m=1}^{M[n,N]}$ are straightforwardly collected from (A.15).

Finally, the derivative of the CDF yields the PDF of $\gamma_{\mathrm{RD}}[w^*[n]]$ as

$$\begin{aligned} f_{\gamma_{\mathrm{RD}}[w^*[n]]}(x) &= \frac{\mathrm{d}}{\mathrm{d}x} F_{\gamma_{\mathrm{RD}}[w^*[n]]}(x) \\ &= \sum_{m=1}^{M[n,N]} a[m,n,N] \cdot \frac{1}{b[m,n,N]} \exp\left(- \frac{x}{b[m,n,N]} \right). \end{aligned} \quad \text{(A.17)}$$

This specific form is convenient in the performance analysis because it is a sum of $M[n,N]$ elementary probability densities. In particular, the mth PDF, associated with an exponential random variable having average $b[m,n,N] > 0$, is weighted by $a[m,n,N]$.[2] In general, many statistical performance metrics thus become, in the case of order statistics, weighted summations of those obtained in the case of an exponential distribution.

A.3.2 Discussion on Special Cases

In the general case of any m, n and N, the coefficients $a[m,n,N]$ and $b[m,n,N]$ cannot be tractably expressed in a closed form, mainly due to evident indexing difficulties. Thus, the analysis needs to be carried out without explicitly substituting the coefficients into the expressions. However, this does not reduce the usefulness of (A.17), since $\{a[m,n,N]\}_{m=1}^{M[n,N]}$ and $\{b[m,n,N]\}_{m=1}^{M[n,N]}$ can be always precalculated and tabulated for any given $\{\bar{\gamma}_{\mathrm{RD}}[n]\}_{n=1}^{N}$ before implementing the performance expressions in a

[2] Although $\sum_{m=1}^{M[n,N]} a[m,n,N] = 1$, (A.16) and (A.17) do not represent a "mixture distribution" because $a[m,n,N]$ is negative for some m.

computer program and determining numerical values from them. Actually, a simple algorithm with two nested loops corresponding to the two summations of (A.15) is sufficient for this purpose.

As also shown by (A.15), the above PDF and CDF expressions comprise

$$M[n,N] = \sum_{m=n}^{N} \binom{N}{m} = 2^N - \sum_{m=1}^{n} \binom{N}{m-1} \tag{A.18}$$

sum terms. In particular, the largest variable $\gamma_{\mathrm{RD}}[w^*[1]]$ generates the most computationally demanding expressions for which $M[1,N] = 2^N - 1 \approx 10^{0.3N}$. Consequently, the usage of (A.15)–(A.17) is feasible only up to, say, $N = 20$ (with at maximum around one million terms) but beyond that the exponential growth quickly prohibits the implementation of the exact expressions. For example, the numerical results of Section 8.4 for systems in which $N \leq 15$ are still well within the practical range. On the contrary, the statistics of the smallest variable $\gamma_{\mathrm{RD}}[w^*[N]]$ need always only a single term which can be stated in a closed form, i.e.,

$$a[1,N,N] = 1, \tag{A.19a}$$

$$b[1,N,N] = \left(\sum_{n=1}^{N} \frac{1}{\bar{\gamma}_{\mathrm{RD}}[n]} \right)^{-1}, \tag{A.19b}$$

and $M[N,N] = 1$ with any N.

The number of terms can be reduced from (A.18) by combining common factors if $\sum_{l=1}^{m} \frac{1}{\bar{\gamma}_{\mathrm{RD}}[i_l]} = \sum_{l=1}^{m} \frac{1}{\bar{\gamma}_{\mathrm{RD}}[j_l]}$ for some disjoint m-combinations $(i_1, \ldots, i_m)$ and $(j_1, \ldots, j_m)$ of the set $\{1, 2, \ldots, N\}$. In the extreme special case of identical distributions, i.e., when $\bar{\gamma}_{\mathrm{RD}}[n] = \bar{\gamma}_{\mathrm{RD}}$ for all n, the coefficients of (A.17) become

$$a[m,n,N] = (-1)^{m-1} \binom{m+n-2}{n-1} \binom{N}{m+n-1}, \tag{A.20a}$$

$$b[m,n,N] = \frac{\bar{\gamma}_{\mathrm{RD}}}{m+n-1}, \tag{A.20b}$$

and the number of terms is reduced to $M[n,N] = N - n + 1$. The preliminary capacity analysis presented in the related conference papers **[233, 235]** resorts to this simplified case. Furthermore, these coefficients become even more compact for the largest variable $\gamma_{\mathrm{RD}}[w^*[1]]$:

$$a[m,1,N] = (-1)^{m-1} \binom{N}{m}, \tag{A.21a}$$

$$b[m,1,N] = \frac{\bar{\gamma}_{\mathrm{RD}}}{m}, \tag{A.21b}$$

and $M[1,N] = N$. This simplified case is considered throughout the analysis of **[232]** and, consequently, in the numerical performance results presented in Chapter 7 although the analysis itself is generalized herein to allow for non-identical distributions.

A.4 Remark on Numerical Evaluation of $\exp(x)\,E_1(x)$

The implementation of many ergodic capacity expressions presented in this thesis leads to the numerical evaluation of $\exp(x)\,E_1(x)$ for which both $\exp(x)$ and $E_1(x)$ are implemented accurately in all common mathematical software packages. However, it should be noted that this specific product is subject to computational problems in some cases when calculating $\exp(x)$ and $E_1(x)$ separately for large x as originally reported in **[223]**.

This issue is briefly elaborated next since it appears frequently in applications that are in the scope of this thesis. Furthermore, it has also more general influence on the implementation of ergodic capacity expressions for other kind of systems, e.g., the product $\exp(x)\,E_1(x)$ can be found within the expressions of many landmark papers on the analysis of multi-antenna diversity combining techniques [6, 170, 171]. The integral form of this very product dates back to early 1990s [87, 155].

In essence, the computational problem arises from the multiplication of a very large positive number by a very small positive number. For example, according to IEEE Standard 754 [115], double-precision floating-point arithmetic can handle positive numbers that are within the range

$$\left[2^{-1074},\,(2-2^{-52})\cdot 2^{1023}\right] \approx \left[5\cdot 10^{-324},\,2\cdot 10^{308}\right] \approx \left[E_1(737.8),\,\exp(709.8)\right].$$

Thus, the increasing term $\exp(x)$ overflows and the decreasing term $E_1(x)$ underflows whenever $x > 740$ and their product is bound to become indeterminate although the true value is of the same magnitude as $1/x$ and could be represented well with double precision. Moreover, numerical accuracy may be degraded with large x even if the overflow of $\exp(x)$ does not yet happen. It turns out that assuming $x \ll 740$ is rather strict limitation with the applications at hand and, thus, the stability issue manifests itself especially at the high signal-to-noise ratio regime.

Consequently, direct numerical integration according to [155, Eqs. 4,5],

$$\exp(x)\,E_1(x) = \int_0^\infty \log_e\left(1+\frac{t}{x}\right)\exp(-t)\,\mathrm{d}t, \tag{A.22}$$

may be preferred in some applications, instead of using standard "off-the-shelf" implementations of $\exp(x)$ and $E_1(x)$ separately, because the above integrand does not suffer from similar stability issues. Alternatively, the usage of bounds or approximations may be considered, e.g.,

$$\frac{1}{1+x} < \exp(x)\,E_1(x) < \frac{1}{x} \tag{A.23}$$

holds for all $x > 0$ [3, Eq. 5.1.19] and is tight at both sides for large x.

The numerical results of this thesis apply the converging asymptotic expansion [3, Eq. 5.1.51],

$$\exp(x)\,E_1(x) \approx \frac{1}{x} - \frac{1}{x^2} + \frac{1\cdot 2}{x^3} - \frac{1\cdot 2\cdot 3}{x^4} + \ldots, \tag{A.24}$$

whenever either of the product terms becomes indeterminate at large x. For the above expression, it was found empirically that using eight terms is more than sufficient to regard the residual error as infinitesimal in the present applications such that there is no visible bias in any of the numerical performance plots.

Bibliography

[1] *3rd Generation Partnership Project; Technical Specification Group Radio Access Network; Evolved Universal Terrestrial Radio Access (E-UTRA); Base Station (BS) Radio Transmission and Reception (Release 8)*, 3GPP TS 36.104 V8.10.0, June 2010.

[2] *3rd Generation Partnership Project; Technical Specification Group Radio Access Network; Evolved Universal Terrestrial Radio Access (E-UTRA); Physical Channels and Modulation (Release 8)*, 3GPP TS 36.211 V8.9.0, December 2009.

[3] M. Abramowitz and I. A. Stegun, Eds., *Handbook of Mathematical Functions with Formulas, Graphs, and Mathematical Tables*. Dover Publications, 1972.

[4] A. Adinoyi and H. Yanikomeroglu, "Cooperative relaying in multi-antenna fixed relay networks," *IEEE Transactions on Wireless Communications*, vol. 6, no. 2, pp. 533–544, February 2007.

[5] A. Agustin and J. Vidal, "Amplify-and-forward cooperation under interference-limited spatial reuse of the relay slot," *IEEE Transactions on Wireless Communications*, vol. 7, no. 5, pp. 1952–1962, May 2008.

[6] M.-S. Alouini and A. J. Goldsmith, "Capacity of Rayleigh fading channels under different adaptive transmission and diversity-combining techniques," *IEEE Transactions on Vehicular Technology*, vol. 48, no. 4, pp. 1165–1181, July 1999.

[7] G. Amarasuriya, C. Tellambura, and M. Ardakani, "Asymptotically-exact performance bounds of AF multi-hop relaying over Nakagami fading," *IEEE Transactions on Communications*, vol. 59, no. 4, pp. 962–967, April 2011.

[8] P. A. Anghel and M. Kaveh, "Exact symbol error probability of a cooperative network in a Rayleigh-fading environment," *IEEE Transactions on Wireless Communications*, vol. 3, no. 5, pp. 1416–1421, September 2004.

[9] B. C. Arnold, N. Balakrishnan, and H. N. Nagaraja, *A First Course in Order Statistics*. Wiley-Interscience, 1992.

[10] K. Azarian, H. El Gamal, and P. Schniter, "On the achievable diversity–multiplexing tradeoff in half-duplex cooperative channels," *IEEE Transactions on Information Theory*, vol. 51, no. 12, pp. 4152–4172, December 2005.

[11] N. C. Beaulieu, G. Farhadi, and Y. Chen, "A precise approximation for performance evaluation of amplify-and-forward multihop relaying systems," *IEEE Transactions on Wireless Communications*, vol. 10, no. 12, pp. 3985–3989, December 2011.

[12] N. C. Beaulieu and J. Hu, "A closed-form expression for the outage probability of decode-and-forward relaying in dissimilar Rayleigh fading channels," *IEEE Communications Letters*, vol. 10, no. 12, pp. 813–815, December 2006.

[13] A. S. Behbahani, R. Merched, and A. M. Eltawil, "Optimizations of a MIMO relay network," *IEEE Transactions on Signal Processing*, vol. 56, no. 10, pp. 5062–5073, October 2008.

[14] P. A. Bello, "Characterization of randomly time-variant linear channels," *IEEE Transactions on Communications Systems*, vol. 11, no. 4, pp. 360–393, December 1963.

[15] D. Benevides da Costa and S. Aïssa, "Capacity analysis of cooperative systems with relay selection in Nakagami-m fading," *IEEE Communications Letters*, vol. 13, no. 9, pp. 637–639, September 2009.

[16] D. Benevides da Costa and S. Aïssa, "Dual-hop decode-and-forward relaying systems with relay selection and maximal-ratio schemes," *Electronics Letters*, vol. 45, no. 9, pp. 460–461, April 2009.

[17] D. Benevides da Costa and S. Aïssa, "Amplify-and-forward relaying in channel-noise-assisted cooperative networks with relay selection," *IEEE Communications Letters*, vol. 14, no. 7, pp. 608–610, July 2010.

[18] D. Benevides da Costa and M. D. Yacoub, "Dual-hop transmissions with semi-blind relays over Nakagami-m fading channels," *Electronics Letters*, vol. 44, no. 3, pp. 214–216, January 2008.

[19] E. Björnson, P. Zetterberg, M. Bengtsson, and B. Ottersten, "Capacity limits and multiplexing gains of MIMO channels with transceiver impairments," *IEEE Communications Letters*, vol. 17, no. 1, pp. 91–94, January 2013.

[20] A. Bletsas, H. Shin, and M. Z. Win, "Cooperative communications with outage-optimal opportunistic relaying," *IEEE Transactions on Wireless Communications*, vol. 6, no. 9, pp. 3450–3460, September 2007.

[21] A. Bletsas, H. Shin, and M. Z. Win, "Outage analysis for co-operative communication with multiple amplify-and-forward relays," *Electronics Letters*, vol. 43, no. 6, pp. 51–52, March 2007.

[22] A. Bletsas, H. Shin, and M. Z. Win, "Outage optimality of opportunistic amplify-and-forward relaying," *IEEE Communications Letters*, vol. 11, no. 3, pp. 261–263, March 2007.

[23] D. W. Bliss, P. A. Parker, and A. R. Margetts, "Simultaneous transmission and reception for improved wireless network performance," in *Proc. 14th IEEE Workshop on Statistical Signal Processing*, August 2007.

[24] F. Boccardi, K. Yu, and A. Alexiou, "High data rate relay transmissions with multiple antennas," *IEEE Transactions on Communications*, vol. 57, no. 12, pp. 3547–3551, December 2009.

[25] H. Bölcskei, R. U. Nabar, Ö. Oyman, and A. J. Paulraj, "Capacity scaling laws in MIMO relay networks," *IEEE Transactions on Wireless Communications*, vol. 5, no. 6, pp. 1433–1444, June 2006.

[26] A. Bou Saleh, S. Redana, B. Raaf, T. Riihonen, J. Hämäläinen, and R. Wichman, "Performance of amplify-and-forward and decode-and-forward relays in LTE-Advanced," in *Proc. IEEE 70th Vehicular Technology Conference*, September 2009.

[27] J. Boyer, D. D. Falconer, and H. Yanikomeroglu, "Multihop diversity in wireless relaying channels," *IEEE Transactions on Communications*, vol. 52, no. 10, pp. 1820–1830, October 2004.

[28] J. Boyer, D. D. Falconer, and H. Yanikomeroglu, "Cooperative connectivity models for wireless relay networks," *IEEE Transactions on Wireless Communications*, vol. 6, no. 6, pp. 1992–2000, June 2007.

[29] D. G. Brennan, "Linear diversity combining techniques," *Proceedings of the IRE*, vol. 47, no. 6, pp. 1075–1102, June 1959.

[30] R. Brugger and D. Hemingway, "OFDM receivers — impact on coverage of inter-symbol interference and FFT window positioning," *EBU Technical Review*, no. 295, July 2003.

[31] V. R. Cadambe and S. A. Jafar, "Degrees of freedom of wireless networks with relays, feedback, cooperation, and full duplex operation," *IEEE Transactions on Information Theory*, vol. 55, no. 5, pp. 2334–2344, May 2009.

[32] C.-B. Chae, T. Tang, R. W. Heath, Jr., and S. Cho, "MIMO relaying with linear processing for multiuser transmission in fixed relay networks," *IEEE Transactions on Signal Processing*, vol. 56, no. 2, pp. 727–738, February 2008.

[33] B. K. Chalise and L. Vandendorpe, "Outage probability analysis of a MIMO relay channel with orthogonal space-time block codes," *IEEE Communications Letters*, vol. 12, no. 4, pp. 280–282, April 2008.

[34] B. K. Chalise and L. Vandendorpe, "MIMO relay design for multipoint-to-multipoint communications with imperfect channel state information," *IEEE Transactions on Signal Processing*, vol. 57, no. 7, pp. 2785–2796, July 2009.

[35] B. K. Chalise and L. Vandendorpe, "Performance analysis of linear receivers in a MIMO relaying system," *IEEE Communications Letters*, vol. 13, no. 5, pp. 330–332, May 2009.

[36] U. Charash, "Reception through Nakagami fading multipath channels with random delays," *IEEE Transactions on Communications*, vol. 27, no. 4, pp. 657–670, April 1979.

[37] S. Chen, M. A. Beach, and J. P. McGeehan, "Division-free duplex for wireless applications," *Electronics Letters*, vol. 34, no. 2, pp. 147–148, January 1998.

[38] S. Chen, F. Liu, X. Zhang, C. Xiong, and D. Yang, "Symbol error performance analysis of OFDM relaying system with subcarrier mapping scheme," *IEEE Communications Letters*, vol. 14, no. 7, pp. 638–640, July 2010.

[39] D. Choi and D. Park, "Effective self interference cancellation in full duplex relay systems," *Electronics Letters*, vol. 48, no. 2, pp. 129–130, January 2012.

[40] W. Choi and J. G. Andrews, "Downlink performance and capacity of distributed antenna systems in a multicell environment," *IEEE Transactions on Wireless Communications*, vol. 6, no. 1, pp. 69–73, January 2007.

[41] B. Chun, E.-R. Jeong, J. Joung, Y. Oh, and Y. H. Lee, "Pre-nulling for self-interference suppression in full-duplex relays," in *Proc. APSIPA Annual Summit and Conference*, October 2009.

[42] B. Chun and Y. H. Lee, "A spatial self-interference nullification method for full duplex amplify-and-forward MIMO relays," in *Proc. IEEE Wireless Communications and Networking Conference*, April 2010.

[43] B. Chun and H. Park, "A spatial-domain joint-nulling method of self-interference in full-duplex relays," *IEEE Communications Letters*, vol. 16, no. 4, pp. 436–438, April 2012.

[44] L. J. Cimini, Jr., "Analysis and simulation of a digital mobile channel using orthogonal frequency division multiplexing," *IEEE Transactions on Communications*, vol. 33, no. 7, pp. 665–675, July 1985.

[45] T. M. Cover and A. A. El Gamal, "Capacity theorems for the relay channel," *IEEE Transactions on Information Theory*, vol. 25, no. 5, pp. 572–584, September 1979.

[46] D. Dardari, V. Tralli, and A. Vaccari, "A theoretical characterization of nonlinear distortion effects in OFDM systems," *IEEE Transactions on Communications*, vol. 48, no. 10, pp. 1755–1764, October 2000.

[47] H. A. David and H. N. Nagaraja, *Order Statistics*, 3rd ed. Wiley-Interscience, 2003.

[48] B. P. Day, A. R. Margetts, D. W. Bliss, and P. Schniter, "Full-duplex bidirectional MIMO: Achievable rates under limited dynamic range," *IEEE Transactions on Signal Processing*, vol. 60, no. 7, pp. 3702–3713, July 2012.

[49] B. P. Day, A. R. Margetts, D. W. Bliss, and P. Schniter, "Full-duplex MIMO relaying: Achievable rates under limited dynamic range," *IEEE Journal on Selected Areas in Communications*, vol. 30, no. 8, pp. 1541–1553, September 2012.

[50] X. Deng and A. M. Haimovich, "Power allocation for cooperative relaying in wireless networks," *IEEE Communications Letters*, vol. 9, no. 11, pp. 994–996, November 2005.

[51] M. Ding, S. Liu, H. Luo, and W. Chen, "MMSE based greedy antenna selection scheme for AF MIMO relay systems," *IEEE Signal Processing Letters*, vol. 17, no. 5, pp. 433–436, May 2010.

[52] Z. Ding, I. Krikidis, B. Rong, J. S. Thompson, C. Wang, and S. Yang, "On combating the half-duplex constraint in modern cooperative networks: Protocols and techniques," *IEEE Wireless Communications*, vol. 19, no. 6, pp. 20–27, December 2012.

[53] K. Doppler, A. Hottinen, and T. Riihonen, "Apparatus, method and computer program product providing relay division multiple access," United States Patent Application Publication, no. US 2007/0217433 A1, September 2007.

[54] K. Doppler, T. Riihonen, and A. Hottinen, "Relay," United States Patent Application Publication, no. US 2009/0227202 A1, September 2009.

[55] M. Duarte, C. Dick, and A. Sabharwal, "Experiment-driven characterization of full-duplex wireless systems," *IEEE Transactions on Wireless Communications*, vol. 11, no. 12, pp. 4296–4307, December 2012.

[56] E. Everett, M. Duarte, C. Dick, and A. Sabharwal, "Empowering full-duplex wireless communication by exploiting directional diversity," in *Proc. 45th Annual Asilomar Conference on Signals, Systems, and Computers*, November 2011.

[57] M. Failly, Ed., *COST 207: Digital land mobile radio communications (final report)*. Commission of the European Communities, 1989, no. EUR 12160.

[58] L. Fan, X. Lei, and W. Li, "Exact closed-form expression for ergodic capacity of amplify-and-forward relaying in channel-noise-assisted cooperative networks with relay selection," *IEEE Communications Letters*, vol. 15, no. 3, pp. 332–333, March 2011.

[59] Y. Fan and J. S. Thompson, "MIMO configurations for relay channels: Theory and practice," *IEEE Transactions on Wireless Communications*, vol. 6, no. 5, pp. 1774–1786, May 2007.

[60] Y. Fan, C. Wang, H. V. Poor, and J. S. Thompson, "Cooperative multiplexing: Toward higher spectral efficiency in multiple-antenna relay networks," *IEEE Transactions on Information Theory*, vol. 55, no. 9, pp. 3909–3926, September 2009.

[61] Y. Fan, C. Wang, J. S. Thompson, and H. V. Poor, "Recovering multiplexing loss through successive relaying using repetition coding," *IEEE Transactions on Wireless Communications*, vol. 6, no. 12, pp. 4484–4493, December 2007.

[62] G. Farhadi and N. C. Beaulieu, "On the ergodic capacity of wireless relaying systems over Rayleigh fading channels," *IEEE Transactions on Wireless Communications*, vol. 7, no. 11, pp. 4462–4467, November 2008.

[63] G. Farhadi and N. C. Beaulieu, "On the performance of amplify-and-forward cooperative systems with fixed gain relays," *IEEE Transactions on Wireless Communications*, vol. 7, no. 5, pp. 1851–1856, May 2008.

[64] G. Farhadi and N. C. Beaulieu, "On the ergodic capacity of multi-hop wireless relaying systems," *IEEE Transactions on Wireless Communications*, vol. 8, no. 5, pp. 2286–2291, May 2009.

[65] G. Farhadi and N. C. Beaulieu, "Power-optimized amplify-and-forward multi-hop relaying systems," *IEEE Transactions on Wireless Communications*, vol. 8, no. 9, pp. 4634–4643, September 2009.

[66] G. Farhadi and N. C. Beaulieu, "Capacity of amplify-and-forward multihop relaying systems under adaptive transmission," *IEEE Transactions on Communications*, vol. 58, no. 3, pp. 758–763, March 2010.

[67] G. Farhadi and N. C. Beaulieu, "Fixed relaying versus selective relaying in multi-hop diversity transmission systems," *IEEE Transactions on Communications*, vol. 58, no. 3, pp. 956–965, March 2010.

[68] G. Farhadi and N. C. Beaulieu, "A general framework for symbol error probability analysis of wireless systems and its application in amplify-and-forward multihop relaying," *IEEE Transactions on Vehicular Technology*, vol. 59, no. 3, pp. 1505–1511, March 2010.

[69] G. Farhadi and N. C. Beaulieu, "A low complexity receiver for noncoherent amplify-and-forward cooperative systems," *IEEE Transactions on Communications*, vol. 58, no. 9, pp. 2499–2504, September 2010.

[70] G. Farhadi and N. C. Beaulieu, "Low complexity receivers for coherent amplify-and-forward cooperative systems," *IEEE Transactions on Communications*, vol. 58, no. 10, pp. 3001–3010, October 2010.

[71] G. Farhadi and J. M. Cioffi, "Spectral efficient multihop relaying based on alternate transmission," *IEEE Transactions on Wireless Communications*, vol. 10, no. 11, pp. 3601–3606, November 2011.

[72] G. Faria, J. A. Henriksson, E. Stare, and P. Talmola, "DVB-H: Digital broadcast services to handheld devices," *Proceedings of the IEEE*, vol. 94, no. 1, pp. 194–209, January 2006.

[73] G. Fettweis, M. Löhning, D. Petrovic, M. Windisch, P. Zillmann, and W. Rave, "Dirty RF: A new paradigm," *International Journal of Wireless Information Networks*, vol. 14, no. 2, pp. 133–148, June 2007.

[74] A. Firag, H. A. Suraweera, P. J. Smith, and C. Yuen, "Dual-hop MIMO amplify-and-forward relay channel capacity with keyhole effect," *IEEE Communications Letters*, vol. 15, no. 10, pp. 1050–1052, October 2011.

[75] M. A. Gatzianas, L. G. Georgiadis, and G. K. Karagiannidis, "Gain adaptation policies for dual-hop nonregenerative relayed systems," *IEEE Transactions on Communications*, vol. 55, no. 8, pp. 1472–1477, August 2007.

[76] Y. Ge, S. Wen, Y.-H. Ang, and Y.-C. Liang, "Optimal relay selection in IEEE 802.16j multihop relay vehicular networks," *IEEE Transactions on Vehicular Technology*, vol. 59, no. 5, pp. 2198–2206, June 2010.

[77] A. J. Goldsmith and P. P. Varaiya, "Capacity of fading channels with channel side information," *IEEE Transactions on Information Theory*, vol. 43, no. 6, pp. 1986–1992, November 1997.

[78] K. S. Gomadam and S. A. Jafar, "Optimal relay functionality for SNR maximization in memoryless relay networks," *IEEE Journal on Selected Areas in Communications*, vol. 25, no. 2, pp. 390–401, February 2007.

[79] K. S. Gomadam and S. A. Jafar, "Duality of MIMO multiple access channel and broadcast channel with amplify-and-forward relays," *IEEE Transactions on Communications*, vol. 58, no. 1, pp. 211–217, January 2010.

[80] I. S. Gradshteyn and I. M. Ryzhik, *Table of Integrals, Series, and Products*, 7th ed. Academic Press, 2007.

[81] F. Gregorio, J. Cousseau, S. Werner, T. Riihonen, and R. Wichman, "Compensation of IQ imbalance and transmitter nonlinearities in broadband MIMO-OFDM," in *Proc. IEEE International Symposium on Circuits and Systems*, May 2011.

[82] F. Gregorio, J. Cousseau, S. Werner, T. Riihonen, and R. Wichman, "Power amplifier linearization technique with IQ imbalance and crosstalk compensation for broadband MIMO-OFDM transmitters," *EURASIP Journal on Advances in Signal Processing*, vol. 2011, no. 19, pp. 1–15, July 2011.

[83] F. Gregorio, J. Cousseau, S. Werner, R. Wichman, and T. Riihonen, "Sequential compensation of RF impairments in OFDM systems," in *Proc. IEEE Wireless Communications and Networking Conference*, April 2010.

[84] W. Guan and H. Luo, "Joint MMSE transceiver design in non-regenerative MIMO relay systems," *IEEE Communications Letters*, vol. 12, no. 7, pp. 517–519, July 2008.

[85] W. Guan, H. Luo, and W. Chen, "Linear relaying scheme for MIMO relay system with QoS requirements," *IEEE Signal Processing Letters*, vol. 15, pp. 697–700, 2008.

[86] B. Gui and L. J. Cimini, Jr., "Bit loading algorithms for cooperative OFDM systems," *EURASIP Journal on Wireless Communications and Networking*, vol. 2008, Article ID 476797, 9 pages, 2008.

[87] C. G. Günther, "Comment on "Estimate of channel capacity in Rayleigh fading environment"," *IEEE Transactions on Vehicular Technology*, vol. 45, no. 2, pp. 401–403, May 1996.

[88] Z. Hadzi-Velkov, N. Zlatanov, and G. K. Karagiannidis, "On the second order statistics of the multihop Rayleigh fading channel," *IEEE Transactions on Communications*, vol. 57, no. 6, pp. 1815–1823, June 2009.

[89] H. Hamazumi, K. Imamura, N. Iai, K. Shibuya, and M. Sasaki, "A study of a loop interference canceller for the relay stations in an SFN for digital terrestrial broadcasting," in *Proc. IEEE Global Telecommunications Conference*, November–December 2000.

[90] I. Hammerström and A. Wittneben, "Joint power allocation for nonregenerative MIMO-OFDM relay links," in *Proc. IEEE International Conference on Acoustics, Speech and Signal Processing*, May 2006.

[91] I. Hammerström and A. Wittneben, "On the optimal power allocation for nonregenerative OFDM relay links," in *Proc. IEEE International Conference on Communications*, June 2006.

[92] I. Hammerström and A. Wittneben, "Power allocation schemes for amplify-and-forward MIMO-OFDM relay links," *IEEE Transactions on Wireless Communications*, vol. 6, no. 8, pp. 2798–2802, August 2007.

[93] S. Han, S. Ahn, E. Oh, and D. Hong, "Effect of channel-estimation error on BER performance in cooperative transmission," *IEEE Transactions on Vehicular Technology*, vol. 58, no. 4, pp. 2083–2088, May 2009.

[94] Y. Han, S. H. Ting, C. K. Ho, and W. H. Chin, "Performance bounds for two-way amplify-and-forward relaying," *IEEE Transactions on Wireless Communications*, vol. 8, no. 1, pp. 432–439, January 2009.

[95] Z. Han, T. Himsoon, W. P. Siriwongpairat, and K. J. R. Liu, "Resource allocation for multiuser cooperative OFDM networks: Who helps whom and how to cooperate," *IEEE Transactions on Vehicular Technology*, vol. 58, no. 5, pp. 2378–2391, June 2009.

[96] K. Haneda, E. Kahra, S. Wyne, C. Icheln, and P. Vainikainen, "Measurement of loop-back interference channels for outdoor-to-indoor full-duplex radio relays," in *Proc. 4th European Conference on Antennas and Propagation*, April 2010.

[97] K. Haneda, V.-M. Kolmonen, T. Riihonen, R. Wichman, P. Vainikainen, and J. Takada, "Evaluation of relay transmission in outdoor-to-indoor propagation channels," in *Proc. 1st COST-2100 Workshop on MIMO and Cooperative Communications*, June 2008.

[98] K. Haneda, T. Riihonen, V.-M. Kolmonen, R. Wichman, P. Vainikainen, and J. Takada, "Measurement based analysis of gain-diversity tradeoff in relay transmission," in *Proc. 5th COST-2100 Management Committee Meeting*, June 2008.

[99] M. O. Hasna and M.-S. Alouini, "End-to-end performance of transmission systems with relays over Rayleigh-fading channels," *IEEE Transactions on Wireless Communications*, vol. 2, no. 6, pp. 1126–1131, November 2003.

[100] M. O. Hasna and M.-S. Alouini, "Outage probability of multihop transmission over Nakagami fading channels," *IEEE Communications Letters*, vol. 7, no. 5, pp. 216–218, May 2003.

[101] M. O. Hasna and M.-S. Alouini, "Harmonic mean and end-to-end performance of transmission systems with relays," *IEEE Transactions on Communications*, vol. 52, no. 1, pp. 130–135, January 2004.

[102] M. O. Hasna and M.-S. Alouini, "Optimal power allocation for relayed transmissions over Rayleigh-fading channels," *IEEE Transactions on Wireless Communications*, vol. 3, no. 6, pp. 1999–2004, November 2004.

[103] M. O. Hasna and M.-S. Alouini, "A performance study of dual-hop transmissions with fixed gain relays," *IEEE Transactions on Wireless Communications*, vol. 3, no. 6, pp. 1963–1968, November 2004.

[104] A. Hazmi, J. Rinne, and M. Renfors, "Diversity based DVB-T in-door repeater in slowly mobile loop interference environment," in *Proc. 10th International OFDM-Workshop*, August–September 2005.

[105] M. Herdin, "A chunk based OFDM amplify-and-forward relaying scheme for 4G mobile radio systems," in *Proc. IEEE International Conference on Communications*, June 2006.

[106] M. Herdin and G. Auer, "Pilot design for OFDM amplify-and-forward with chunk reordering," in *Proc. IEEE Wireless Communications and Networking Conference*, March 2007.

[107] A. Høst-Madsen and J. Zhang, "Capacity bounds and power allocation for wireless relay channels," *IEEE Transactions on Information Theory*, vol. 51, no. 6, pp. 2020–2040, June 2005.

[108] A. Hottinen and T. Heikkinen, "Subchannel assignment in OFDM relay nodes," in *Proc. 40th Annual Conference on Information Sciences and Systems*, March 2006.

[109] A. Hottinen and T. Heikkinen, "Optimal subchannel assignment in a two-hop OFDM relay," in *Proc. 8th IEEE Workshop on Signal Processing Advances in Wireless Communications*, June 2007.

[110] Y. Hua, "An overview of beamforming and power allocation for MIMO relays," in *Proc. Military Communications Conference*, October–November 2010.

[111] Y. Huang, L. Yang, M. Bengtsson, and B. Ottersten, "A limited feedback joint precoding for amplify-and-forward relaying," *IEEE Transactions on Signal Processing*, vol. 58, no. 3, pp. 1347–1357, March 2010.

[112] T. E. Hunter, S. Sanayei, and A. Nosratinia, "Outage analysis of coded cooperation," *IEEE Transactions on Information Theory*, vol. 52, no. 2, pp. 375–391, February 2006.

[113] M. Husso, J. Hämäläinen, R. Jäntti, J. Nieminen, T. Riihonen, and R. Wichman, "Performance of on-off scheduling strategy in the presence of transmit beamforming," *Physical Communication*, vol. 4, no. 1, pp. 3–12, March 2011.

[114] K.-S. Hwang, Y.-C. Ko, and M.-S. Alouini, "Performance analysis of incremental opportunistic relaying over identically and non-identically distributed cooperative paths," *IEEE Transactions on Wireless Communications*, vol. 8, no. 4, pp. 1953–1961, April 2009.

[115] *IEEE Standard for Floating-Point Arithmetic*, IEEE Std 754-2008, June 2008.

[116] A. Ikhlef, J. Kim, and R. Schober, "Mimicking full-duplex relaying using half-duplex relays with buffers," *IEEE Transactions on Vehicular Technology*, vol. 61, no. 7, pp. 3025–3037, September 2012.

[117] S. Ikki and M. H. Ahmed, "Performance analysis of cooperative diversity wireless networks over Nakagami-m fading channel," *IEEE Communications Letters*, vol. 11, no. 4, pp. 334–336, April 2007.

[118] S. S. Ikki and M. H. Ahmed, "Exact error probability and channel capacity of the best-relay cooperative-diversity networks," *IEEE Signal Processing Letters*, vol. 16, no. 12, pp. 1051–1054, December 2009.

[119] T. Isotalo, P. Lähdekorpi, and J. Lempiäinen, "Improving HSDPA indoor coverage and throughput by repeater and dedicated indoor system," *EURASIP Journal on Wireless Communications and Networking*, vol. 2008, Article ID 951481, 11 pages, 2008.

[120] *IST-4-027756 WINNER II D1.1.2 V1.1: WINNER II Channel Models*, November 2007.

[121] M. Janani, A. Hedayat, T. E. Hunter, and A. Nosratinia, "Coded cooperation in wireless communications: Space-time transmission and iterative decoding," *IEEE Transactions on Signal Processing*, vol. 52, no. 2, pp. 362–371, February 2004.

[122] J. L. W. V. Jensen, "Sur les fonctions convexes et les inégalités entre les valeurs moyennes," *Acta Mathematica*, vol. 30, no. 1, pp. 175–193, December 1906.

[123] C. Jeong and H.-M. Kim, "Precoder design of non-regenerative relays with covariance feedback," *IEEE Communications Letters*, vol. 13, no. 12, pp. 920–922, December 2009.

[124] S. Jin, M. R. McKay, C. Zhong, and K.-K. Wong, "Ergodic capacity analysis of amplify-and-forward MIMO dual-hop systems," *IEEE Transactions on Information Theory*, vol. 56, no. 5, pp. 2204–2224, May 2010.

[125] H. Ju, E. Oh, and D. Hong, "Improving efficiency of resource usage in two-hop full duplex relay systems based on resource sharing and interference cancellation," *IEEE Transactions on Wireless Communications*, vol. 8, no. 8, pp. 3933–3938, August 2009.

[126] M. Kaneko, K. Hayashi, P. Popovski, K. Ikeda, H. Sakai, and R. Prasad, "Amplify-and-forward cooperative diversity schemes for multi-carrier systems," *IEEE Transactions on Wireless Communications*, vol. 7, no. 5, pp. 1845–1850, May 2008.

[127] T. Kang and V. Rodoplu, "Algorithms for the MIMO single relay channel," *IEEE Transactions on Wireless Communications*, vol. 6, no. 5, pp. 1596–1600, May 2007.

[128] Y. Y. Kang and J. H. Cho, "Capacity of MIMO wireless channel with full-duplex amplify-and-forward relay," in *Proc. 20th IEEE International Symposium on Personal, Indoor and Mobile Radio Communications*, September 2009.

[129] G. K. Karagiannidis, "Performance bounds of multihop wireless communications with blind relays over generalized fading channels," *IEEE Transactions on Wireless Communications*, vol. 5, no. 3, pp. 498–503, March 2006.

[130] G. K. Karagiannidis, T. A. Tsiftsis, and R. K. Mallik, "Bounds for multihop relayed communications in Nakagami-m fading," *IEEE Transactions on Communications*, vol. 54, no. 1, pp. 18–22, January 2006.

[131] J. Karedal, S. Wyne, P. Almers, F. Tufvesson, and A. F. Molisch, "A measurement-based statistical model for industrial ultra-wideband channels," *IEEE Transactions on Wireless Communications*, vol. 6, no. 8, pp. 3028–3037, August 2007.

[132] B. Khoshnevis, W. Yu, and R. Adve, "Grassmannian beamforming for MIMO amplify-and-forward relaying," *IEEE Journal on Selected Areas in Communications*, vol. 26, no. 8, pp. 1397–1407, October 2008.

[133] J.-B. Kim and D. Kim, "Comparison of two SNR-based feedback schemes in multiuser dual-hop amplify-and-forward relaying networks," *IEEE Communications Letters*, vol. 12, no. 8, pp. 557–559, August 2008.

[134] Y. Kim and H. Liu, "Infrastructure relay transmission with cooperative MIMO," *IEEE Transactions on Vehicular Technology*, vol. 57, no. 4, pp. 2180–2188, July 2008.

[135] G. M. Kraidy, J. J. Boutros, and A. Guillen i Fabregas, "Approaching the outage probability of the amplify-and-forward relay fading channel," *IEEE Communications Letters*, vol. 11, no. 10, pp. 808–810, October 2007.

[136] G. Kramer, M. Gastpar, and P. Gupta, "Cooperative strategies and capacity theorems for relay networks," *IEEE Transactions on Information Theory*, vol. 51, no. 9, pp. 3037–3063, September 2005.

[137] I. Krikidis and J.-C. Belfiore, "Scheduling for amplify-and-forward cooperative networks," *IEEE Transactions on Vehicular Technology*, vol. 56, no. 6, pp. 3780–3790, November 2007.

[138] I. Krikidis and J.-C. Belfiore, "Three scheduling schemes for amplify-and-forward relay environments," *IEEE Communications Letters*, vol. 11, no. 5, pp. 414–416, May 2007.

[139] I. Krikidis, J. S. Thompson, S. McLaughlin, and N. Goertz, "Max-min relay selection for legacy amplify-and-forward systems with interference," *IEEE Transactions on Wireless Communications*, vol. 8, no. 6, pp. 3016–3027, June 2009.

[140] H. W. Kuhn, "The Hungarian method for the assignment problem," *Naval Research Logistics Quarterly*, vol. 2, no. 1–2, pp. 83–97, March 1955.

[141] T. Kwon, S. Lim, S. Choi, and D. Hong, "Optimal duplex mode for DF relay in terms of the outage probability," *IEEE Transactions on Vehicular Technology*, vol. 59, no. 7, pp. 3628–3634, September 2010.

[142] J. N. Laneman, D. N. C. Tse, and G. W. Wornell, "Cooperative diversity in wireless networks: Efficient protocols and outage behavior," *IEEE Transactions on Information Theory*, vol. 50, no. 12, pp. 3062–3080, December 2004.

[143] J. N. Laneman and G. W. Wornell, "Distributed space–time-coded protocols for exploiting cooperative diversity in wireless networks," *IEEE Transactions on Information Theory*, vol. 49, no. 10, pp. 2415–2425, October 2003.

[144] P. Larsson and M. Prytz, "MIMO on-frequency repeater with self-interference cancellation and mitigation," in *Proc. 69th IEEE Vehicular Technology Conference*, April 2009.

[145] V.-A. Le, R.-A. Pitaval, S. Blostein, T. Riihonen, and R. Wichman, "Green cooperative communication using threshold-based relay selection protocols," in *Proc. International Conference on Green Circuits and Systems*, June 2010.

[146] V.-A. Le, R.-A. Pitaval, S. Blostein, T. Riihonen, and R. Wichman, "One-bit CSI feedback selection schemes for energy-efficient multiuser and multirelay systems," *IEEE Transactions on Wireless Communications*, vol. 12, no. 3, pp. 1149–1161, March 2013.

[147] V.-A. Le, T. Riihonen, R. Wichman, and S. Blostein, "One-bit feedback selection schemes for power-efficient multiuser and multirelay systems," in *Proc. IEEE Wireless Communications and Networking Conference*, April 2010.

[148] V.-A. Le, T. Riihonen, R. Wichman, and S. Blostein, "Outage performance of an energy-efficient relaying protocol over Nakagami fading channels," in *Proc. 25th Biennial Symposium on Communications*, May 2010.

[149] I.-H. Lee and D. Kim, "Coverage extension and power allocation in dual-hop space–time transmission with multiple antennas in each node," *IEEE Transactions on Vehicular Technology*, vol. 56, no. 6, pp. 3524–3532, November 2007.

[150] I.-H. Lee and D. Kim, "Decouple-and-forward relaying for dual-hop Alamouti transmissions," *IEEE Communications Letters*, vol. 12, no. 2, pp. 97–99, February 2008.

[151] I.-H. Lee and D. Kim, "Probability of SNR gain by dual-hop relaying over single-hop transmission in SISO Rayleigh fading channels," *IEEE Communications Letters*, vol. 12, no. 10, pp. 734–736, October 2008.

[152] I.-H. Lee and D. Kim, "Outage probability of multi-hop MIMO relaying with transmit antenna selection and ideal relay gain over Rayleigh fading channels," *IEEE Transactions on Communications*, vol. 57, no. 2, pp. 357–360, February 2009.

[153] K.-J. Lee, J.-S. Kim, G. Caire, and I. Lee, "Asymptotic ergodic capacity analysis for MIMO amplify-and-forward relay networks," *IEEE Transactions on Wireless Communications*, vol. 9, no. 9, pp. 2712–2717, September 2010.

[154] S. Lee, M. Han, and D. Hong, "Average SNR and ergodic capacity analysis for opportunistic DF relaying with outage over Rayleigh fading channels," *IEEE Transactions on Wireless Communications*, vol. 8, no. 6, pp. 2807–2812, June 2009.

[155] W. C. Y. Lee, "Estimate of channel capacity in Rayleigh fading environment," *IEEE Transactions on Vehicular Technology*, vol. 39, no. 3, pp. 187–189, August 1990.

[156] Y. Lee, M.-H. Tsai, and S.-I. Sou, "Performance of decode-and-forward cooperative communications with multiple dual-hop relays over Nakagami-m fading channels," *IEEE Transactions on Wireless Communications*, vol. 8, no. 6, pp. 2853–2859, June 2009.

[157] Y.-N. Lee, J.-C. Chen, Y.-C. Wang, and J.-T. Chen, "A novel distributed scheduling algorithm for downlink relay networks," *IEEE Transactions on Wireless Communications*, vol. 6, no. 6, pp. 1985–1991, June 2007.

[158] J. Leinonen, T. Riihonen, J. Hämäläinen, and M. Juntti, "Subchannel allocation in relay-enhanced OFDMA downlink with imperfect feedback," in *Proc. IEEE Global Communications Conference*, December 2009.

[159] C. Li, X. Wang, L. Yang, and W.-P. Zhu, "A joint source and relay power allocation scheme for a class of MIMO relay systems," *IEEE Transactions on Signal Processing*, vol. 57, no. 12, pp. 4852–4860, December 2009.

[160] Q. Li, K. H. Li, and K. C. Teh, "Achieving optimal diversity-multiplexing tradeoff for full-duplex MIMO multihop relay networks," *IEEE Transactions on Information Theory*, vol. 57, no. 1, pp. 303–316, January 2011.

[161] Q. Li, S. H. Ting, A. Pandharipande, and Y. Han, "Adaptive two-way relaying and outage analysis," *IEEE Transactions on Wireless Communications*, vol. 8, no. 6, pp. 3288–3299, June 2009.

[162] Y. Li, W. Wang, J. Kong, and M. Peng, "Subcarrier pairing for amplify-and-forward and decode-and-forward OFDM relay links," *IEEE Communications Letters*, vol. 13, no. 4, pp. 209–211, April 2009.

[163] Y. Liang, V. V. Veeravalli, and H. V. Poor, "Resource allocation for wireless fading relay channels: Max-min solution," *IEEE Transactions on Information Theory*, vol. 53, no. 10, pp. 3432–3453, October 2007.

[164] P. Lioliou, M. Viberg, M. Coldrey, and F. Athley, "Self-interference suppression in full-duplex MIMO relays," in *Proc. 44th Annual Asilomar Conference on Signals, Systems, and Computers*, November 2010.

[165] Y. Liu, R. Hoshyar, X. Yang, and R. Tafazolli, "Integrated radio resource allocation for multihop cellular networks with fixed relay stations," *IEEE Journal on Selected Areas in Communications*, vol. 24, no. 11, pp. 2137–2146, November 2006.

[166] H. Long, J. Kuang, S. Shen, K. Zheng, and W. Wang, "Adaptive spatial channel mapping in MIMO relay systems: A unified framework," *IEEE Signal Processing Letters*, vol. 17, no. 3, pp. 257–260, March 2010.

[167] R. H. Y. Louie, Y. Li, H. A. Suraweera, and B. Vucetic, "Performance analysis of beamforming in two hop amplify and forward relay networks with antenna correlation," *IEEE Transactions on Wireless Communications*, vol. 8, no. 6, pp. 3132–3141, June 2009.

[168] R. H. Y. Louie, Y. Li, and B. Vucetic, "Zero forcing in general two-hop relay networks," *IEEE Transactions on Vehicular Technology*, vol. 59, no. 1, pp. 191–202, January 2010.

[169] J. Ma, G. Y. Li, J. Zhang, T. Kuze, and H. Iura, "A new coupling channel estimator for cross-talk cancellation at wireless relay stations," in *Proc. IEEE Global Communications Conference*, December 2009.

[170] A. Maaref and S. Aïssa, "Shannon capacity of STBC in Rayleigh fading channels," *Electronics Letters*, vol. 40, no. 13, pp. 817–819, June 2004.

[171] R. K. Mallik, M. Z. Win, J. W. Shao, M.-S. Alouini, and A. J. Goldsmith, "Channel capacity of adaptive transmission with maximal ratio combining in correlated Rayleigh fading," *IEEE Transactions on Wireless Communications*, vol. 3, no. 4, pp. 1124–1133, July 2004.

[172] P. Mathecken, T. Riihonen, N. N. Tchamov, S. Werner, M. Valkama, and R. Wichman, "Characterization of OFDM radio link under PLL-based oscillator phase noise and multipath fading channel," *IEEE Transactions on Communications*, vol. 60, no. 6, pp. 1479–1485, June 2012.

[173] P. Mathecken, T. Riihonen, S. Werner, and R. Wichman, "Accurate characterization and compensation of phase noise in OFDM receiver," in *Proc. 45th Annual Asilomar Conference on Signals, Systems, and Computers*, November 2011.

[174] P. Mathecken, T. Riihonen, S. Werner, and R. Wichman, "Performance analysis of OFDM with Wiener phase noise and frequency selective fading channel," *IEEE Transactions on Communications*, vol. 59, no. 5, pp. 1321–1331, May 2011.

[175] H. Mheidat and M. Uysal, "Impact of receive diversity on the performance of amplify-and-forward relaying under APS and IPS power constraints," *IEEE Communications Letters*, vol. 10, no. 6, pp. 468–470, June 2006.

[176] D. S. Michalopoulos and G. K. Karagiannidis, "Distributed switch and stay combining (DSSC) with a single decode and forward relay," *IEEE Communications Letters*, vol. 11, no. 5, pp. 408–410, May 2007.

[177] D. S. Michalopoulos and G. K. Karagiannidis, "Performance analysis of single relay selection in Rayleigh fading," *IEEE Transactions on Wireless Communications*, vol. 7, no. 10, pp. 3718–3724, October 2008.

[178] D. S. Michalopoulos and G. K. Karagiannidis, "PHY-layer fairness in amplify and forward cooperative diversity systems," *IEEE Transactions on Wireless Communications*, vol. 7, no. 3, pp. 1073–1083, March 2008.

[179] D. S. Michalopoulos and G. K. Karagiannidis, "Two-relay distributed switch and stay combining," *IEEE Transactions on Communications*, vol. 56, no. 11, pp. 1790–1794, November 2008.

[180] D. S. Michalopoulos and G. K. Karagiannidis, "Bypassing orthogonal relaying transmissions via spatial signal separation," *IEEE Transactions on Communications*, vol. 58, no. 10, pp. 3028–3038, October 2010.

[181] D. S. Michalopoulos, G. K. Karagiannidis, T. A. Tsiftsis, and R. K. Mallik, "Distributed transmit antenna selection (DTAS) under performance or energy consumption constraints," *IEEE Transactions on Wireless Communications*, vol. 7, no. 4, pp. 1168–1173, April 2008.

[182] H. Min, S. Lee, K. Kwak, and D. Hong, "Effect of multiple antennas at the source on outage probability for amplify-and-forward relaying systems," *IEEE Transactions on Wireless Communications*, vol. 8, no. 2, pp. 633–637, February 2009.

[183] R. Mo and Y. H. Chew, "MMSE-based joint source and relay precoding design for amplify-and-forward MIMO relay networks," *IEEE Transactions on Wireless Communications*, vol. 8, no. 9, pp. 4668–4676, September 2009.

[184] R. Mo and Y. H. Chew, "Precoder design for non-regenerative MIMO relay systems," *IEEE Transactions on Wireless Communications*, vol. 8, no. 10, pp. 5041–5049, October 2009.

[185] A. F. Molisch et al., "A comprehensive standardized model for ultrawideband propagation channels," *IEEE Transactions on Antennas and Propagation*, vol. 54, no. 11, pp. 3151–3166, November 2006.

[186] M. Morelli, C.-C. J. Kuo, and M.-O. Pun, "Synchronization techniques for orthogonal frequency division multiple access (OFDMA): A tutorial review," *Proceedings of the IEEE*, vol. 95, no. 7, pp. 1394–1427, July 2007.

[187] O. Muñoz-Medina, J. Vidal, and A. Agustin, "Linear transceiver design in nonregenerative relays with channel state information," *IEEE Transactions on Signal Processing*, vol. 55, no. 6, pp. 2593–2604, June 2007.

[188] R. U. Nabar, H. Bölcskei, and F. W. Kneubühler, "Fading relay channels: performance limits and space-time signal design," *IEEE Journal on Selected Areas in Communications*, vol. 22, no. 6, pp. 1099–1109, August 2004.

[189] M. Nakagami, "The m-distribution — a general formula of intensity distribution of rapid fading," in *Statistical Methods in Radio Wave Propagation: Proceedings of a Symposium held at the University of California, Los Angeles, June 18–20, 1958*. Pergamon Press, 1960, pp. 3–36.

[190] K. M. Nasr, J. P. Cosmas, M. Bard, and J. Gledhill, "Performance of an echo canceller and channel estimator for on-channel repeaters in DVB-T/H networks," *IEEE Transactions on Broadcasting*, vol. 53, no. 3, pp. 609–618, September 2007.

[191] T. Nechiporenko, K. T. Phan, C. Tellambura, and H. H. Nguyen, "On the capacity of Rayleigh fading cooperative systems under adaptive transmission," *IEEE Transactions on Wireless Communications*, vol. 8, no. 4, pp. 1626–1631, April 2009.

[192] D. W. K. Ng, E. S. Lo, and R. Schober, "Dynamic resource allocation in MIMO-OFDMA systems with full-duplex and hybrid relaying," *IEEE Transactions on Communications*, vol. 60, no. 5, pp. 1291–1304, May 2012.

[193] T. J. Oechtering, R. F. Wyrembelski, and H. Boche, "Multiantenna bidirectional broadcast channels — optimal transmit strategies," *IEEE Transactions on Signal Processing*, vol. 57, no. 5, pp. 1948–1958, May 2009.

[194] A. Osseiran and A. Logothesis, "A new full rate relaying method for 4G OFDM systems," *IEEE Transactions on Wireless Communications*, vol. 8, no. 8, pp. 3996–4003, August 2009.

[195] Ö. Oyman and A. J. Paulraj, "Design and analysis of linear distributed MIMO relaying algorithms," *IEE Proceedings-Communications*, vol. 153, no. 4, pp. 565–572, August 2006.

[196] C. S. Patel, G. L. Stüber, and T. G. Pratt, "Statistical properties of amplify and forward relay fading channels," *IEEE Transactions on Vehicular Technology*, vol. 55, no. 1, pp. 1–9, January 2006.

[197] R. Penrose, "A generalized inverse for matrices," *Mathematical Proceedings of the Cambridge Philosophical Society*, vol. 51, no. 3, pp. 406–413, July 1955.

[198] P. Persson, M. Coldrey, A. Wolfgang, and P. Bohlin, "Design and evaluation of a 2 x 2 MIMO repeater," in *Proc. 3rd European Conference on Antennas and Propagation*, March 2009.

[199] S. W. Peters and R. W. Heath, Jr., "Nonregenerative MIMO relaying with optimal transmit antenna selection," *IEEE Signal Processing Letters*, vol. 15, pp. 421–424, 2008.

[200] J. Ping and S. H. Ting, "Rate performance of AF two-way relaying in low SNR region," *IEEE Communications Letters*, vol. 13, no. 4, pp. 233–235, April 2009.

[201] R.-A. Pitaval, T. Riihonen, R. Wichman, and S. Blostein, "Performance evaluation of relay deployment strategies in multi-cell single frequency networks," in *Proc. IEEE Wireless Communications and Networking Conference*, April 2010.

[202] P. Popovski and H. Yomo, "Wireless network coding by amplify-and-forward for bi-directional traffic flows," *IEEE Communications Letters*, vol. 11, no. 1, pp. 16–18, January 2007.

[203] P. Rabiei, W. Namgoong, and N. Al-Dhahir, "On the performance of OFDM-based amplify-and-forward relay networks in the presence of phase noise," *IEEE Transactions on Communications*, vol. 59, no. 5, pp. 1458–1466, May 2011.

[204] B. Rankov and A. Wittneben, "Spectral efficient protocols for half-duplex fading relay channels," *IEEE Journal on Selected Areas in Communications*, vol. 25, no. 2, pp. 379–389, February 2007.

[205] V. del Razo, T. Riihonen, F. Gregorio, S. Werner, and R. Wichman, "Nonlinear amplifier distortion in cooperative amplify-and-forward OFDM systems," in *Proc. IEEE Wireless Communications and Networking Conference*, April 2009.

[206] A. Ribeiro, X. Cai, and G. B. Giannakis, "Symbol error probabilities for general cooperative links," *IEEE Transactions on Wireless Communications*, vol. 4, no. 3, pp. 1264–1273, May 2005.

[207] T. Riihonen, "Recent advances in full-duplex relaying," in *Proc. XXXIII Finnish URSI Convention on Radio Science*, April 2013.

[208] T. Riihonen, A. Balakrishnan, K. Haneda, S. Wyne, S. Werner, and R. Wichman, "Optimal eigenbeamforming for suppressing self-interference in full-duplex MIMO relays," in *Proc. 45th Annual Conference on Information Sciences and Systems*, March 2011.

[209] T. Riihonen, K. Doppler, and A. Hottinen, "Performance of spatially distributed large interference relay networks," in *Proc. International Zurich Seminar on Communications*, February 2006.

[210] T. Riihonen, K. Haneda, S. Werner, and R. Wichman, "SINR analysis of full-duplex OFDM repeaters," in *Proc. 20th IEEE International Symposium on Personal, Indoor and Mobile Radio Communications*, September 2009.

[211] T. Riihonen, S. Werner, J. Cousseau, and R. Wichman, "Design of co-phasing allpass filters for full-duplex OFDM relays," in *Proc. 42nd Annual Asilomar Conference on Signals, Systems, and Computers*, October 2008.

[212] T. Riihonen, S. Werner, F. Gregorio, R. Wichman, and J. Hämäläinen, "BEP analysis of OFDM relay links with nonlinear power amplifiers," in *Proc. IEEE Wireless Communications and Networking Conference*, April 2010.

[213] T. Riihonen, S. Werner, and R. Wichman, "Comparison of full-duplex and half-duplex modes with a fixed amplify-and-forward relay," in *Proc. IEEE Wireless Communications and Networking Conference*, April 2009.

[214] T. Riihonen, S. Werner, and R. Wichman, "Optimized gain control for single-frequency relaying with loop interference," *IEEE Transactions on Wireless Communications*, vol. 8, no. 6, pp. 2801–2806, June 2009.

[215] T. Riihonen, S. Werner, and R. Wichman, "Spatial loop interference suppression in full-duplex MIMO relays," in *Proc. 43rd Annual Asilomar Conference on Signals, Systems, and Computers*, November 2009.

[216] T. Riihonen, S. Werner, and R. Wichman, "Generalized exponential decay model for power-delay profiles of multipath channels," in *Proc. XXXII Finnish URSI Convention on Radio Science*, August 2010.

[217] T. Riihonen, S. Werner, and R. Wichman, "Hypoexponential power–delay profile and performance of multihop OFDM relay links," *IEEE Transactions on Wireless Communications*, vol. 9, no. 12, pp. 3878–3888, December 2010.

[218] T. Riihonen, S. Werner, and R. Wichman, "Rate–interference trade-off between duplex modes in decode-and-forward relaying," in *Proc. 21st IEEE International Symposium on Personal, Indoor and Mobile Radio Communications*, September 2010.

[219] T. Riihonen, S. Werner, and R. Wichman, "Residual self-interference in full-duplex MIMO relays after null-space projection and cancellation," in *Proc. 44th Annual Asilomar Conference on Signals, Systems, and Computers*, November 2010.

[220] T. Riihonen, S. Werner, and R. Wichman, "Hybrid full-duplex/half-duplex relaying with transmit power adaptation," *IEEE Transactions on Wireless Communications*, vol. 10, no. 9, pp. 3074–3085, September 2011.

[221] T. Riihonen, S. Werner, and R. Wichman, "Mitigation of loopback self-interference in full-duplex MIMO relays," *IEEE Transactions on Signal Processing*, vol. 59, no. 12, pp. 5983–5993, December 2011.

[222] T. Riihonen, S. Werner, and R. Wichman, "Transmit power optimization for multiantenna decode-and-forward relays with loopback self-interference from full-duplex operation," in *Proc. 45th Annual Asilomar Conference on Signals, Systems, and Computers*, November 2011.

[223] T. Riihonen, S. Werner, and R. Wichman, "Comments on 'Simple formulas for SIMO and MISO ergodic capacities'," *Electronics Letters*, vol. 48, no. 2, p. 127, January 2012.

[224] T. Riihonen, S. Werner, R. Wichman, and J. Hämäläinen, "Outage probabilities in infrastructure-based single-frequency relay links," in *Proc. IEEE Wireless Communications and Networking Conference*, April 2009.

[225] T. Riihonen, S. Werner, R. Wichman, and E. Zacarías B., "On the feasibility of full-duplex relaying in the presence of loop interference," in *Proc. 10th IEEE Workshop on Signal Processing Advances in Wireless Communications*, June 2009.

[226] T. Riihonen and R. Wichman, "On signal bandwidths in cooperative communications," in *Proc. Nokia-TKK Research Seminar*, May 2006.

[227] T. Riihonen and R. Wichman, "Power allocation for a single-frequency fixed-gain relay network," in *Proc. 18th IEEE International Symposium on Personal, Indoor and Mobile Radio Communications*, September 2007.

[228] T. Riihonen and R. Wichman, "Delay diversity methods for parallel OFDM relays," in *Proc. XXXI Finnish URSI Convention on Radio Science*, October 2008.

[229] T. Riihonen, R. Wichman, and J. Hämäläinen, "Delay spread and its effect on bandwidth in Gaussian parallel relay networks," in *Proc. 17th IEEE International Symposium on Personal, Indoor and Mobile Radio Communications*, September 2006.

[230] T. Riihonen, R. Wichman, and J. Hämäläinen, "Diversity analysis of a parallel amplify and forward relay network," in *Proc. 8th IEEE Workshop on Signal Processing Advances in Wireless Communications*, June 2007.

[231] T. Riihonen, R. Wichman, and J. Hämäläinen, "Co-phasing full-duplex relay link with non-ideal feedback information," in *Proc. IEEE International Symposium on Wireless Communication Systems*, October 2008.

[232] T. Riihonen, R. Wichman, and J. Hämäläinen, "Performance analysis of maximum SNR scheduling with an infrastructure relay link," *Wireless Personal Communications*, vol. 56, no. 2, pp. 277–299, January 2011.

[233] T. Riihonen, R. Wichman, J. Hämäläinen, and A. Hottinen, "Analysis of subcarrier pairing in a cellular OFDMA relay link," in *Proc. International ITG Workshop on Smart Antennas*, February 2008.

[234] T. Riihonen, R. Wichman, and T. Roman, "Rate optimization for 2D OFDM relaying," *IEEE Communications Letters*, vol. 11, no. 7, pp. 586–588, July 2007.

[235] T. Riihonen, R. Wichman, and S. Werner, "Capacity evaluation of DF protocols for OFDMA infrastructure relay links," in *Proc. IEEE Global Communications Conference*, December 2009.

[236] T. Riihonen, R. Wichman, and S. Werner, "Evaluation of OFDM(A) relaying protocols: Capacity analysis in infrastructure framework," *IEEE Transactions on Vehicular Technology*, vol. 61, no. 1, pp. 360–374, January 2012.

[237] Y. Rong and F. Gao, "Optimal beamforming for non-regenerative MIMO relays with direct link," *IEEE Communications Letters*, vol. 13, no. 12, pp. 926–928, December 2009.

[238] Y. Rong and Y. Hua, "Optimality of diagonalization of multi-hop MIMO relays," *IEEE Transactions on Wireless Communications*, vol. 8, no. 12, pp. 6068–6077, December 2009.

[239] Y. Rong, X. Tang, and Y. Hua, "A unified framework for optimizing linear nonregenerative multicarrier MIMO relay communication systems," *IEEE Transactions on Signal Processing*, vol. 57, no. 12, pp. 4837–4851, December 2009.

[240] S. M. Ross, *Introduction to Probability Models*. Academic Press, 2000.

[241] B. Sainath and N. B. Mehta, "Generalizing the amplify-and-forward relay gain model: An optimal SEP perspective," *IEEE Transactions on Wireless Communications*, vol. 11, no. 11, pp. 4118–4127, November 2012.

[242] A. A. M. Saleh, A. J. Rustako, Jr., and R. S. Roman, "Distributed antennas for indoor radio communications," *IEEE Transactions on Communications*, vol. 35, no. 12, pp. 1245–1251, December 1987.

[243] A. A. M. Saleh and R. A. Valenzuela, "A statistical model for indoor multipath propagation," *IEEE Journal on Selected Areas in Communications*, vol. 5, no. 2, pp. 128–137, February 1987.

[244] K. Salehian, M. Guillet, B. Caron, and A. Kennedy, "On-channel repeater for digital television broadcasting service," *IEEE Transactions on Broadcasting*, vol. 48, no. 2, pp. 97–102, June 2002.

[245] M. Salem, A. Adinoyi, M. Rahman, H. Yanikomeroglu, D. Falconer, Y.-D. Kim, E. Kim, and Y.-C. Cheong, "An overview of radio resource management in relay-enhanced OFDMA-based networks," *IEEE Communications Surveys & Tutorials*, vol. 12, no. 3, pp. 422–438, July-September 2010.

[246] J. Sangiamwong, T. Asai, J. Hagiwara, Y. Okumura, and T. Ohya, "Joint multi-filter design for full-duplex MU-MIMO relaying," in *Proc. 69th IEEE Vehicular Technology Conference*, April 2009.

[247] K. G. Seddik, A. K. Sadek, W. Su, and K. J. R. Liu, "Outage analysis and optimal power allocation for multinode relay networks," *IEEE Signal Processing Letters*, vol. 14, no. 6, pp. 377–380, June 2007.

[248] D. Senaratne and C. Tellambura, "Unified exact performance analysis of two-hop amplify-and-forward relaying in Nakagami fading," *IEEE Transactions on Vehicular Technology*, vol. 59, no. 3, pp. 1529–1534, March 2010.

[249] A. Sendonaris, E. Erkip, and B. Aazhang, "User cooperation diversity — part I: System description," *IEEE Transactions on Communications*, vol. 51, no. 11, pp. 1927–1938, November 2003.

[250] A. Sendonaris, E. Erkip, and B. Aazhang, "User cooperation diversity — part II: Implementation aspects and performance analysis," *IEEE Transactions on Communications*, vol. 51, no. 11, pp. 1939–1948, November 2003.

[251] J. Shapira and S. Miller, *CDMA Radio with Repeaters*. Springer, 2007.

[252] H. Shi, T. Abe, T. Asai, and H. Yoshino, "Relaying schemes using matrix triangularization for MIMO wireless networks," *IEEE Transactions on Communications*, vol. 55, no. 9, pp. 1683–1688, September 2007.

[253] K. Shibuya, "Broadcast-wave relay technology for digital terrestrial television broadcasting," *Proceedings of the IEEE*, vol. 94, no. 1, pp. 269–273, January 2006.

[254] H. Shin and J. B. Song, "MRC analysis of cooperative diversity with fixed-gain relays in Nakagami-m fading channels," *IEEE Transactions on Wireless Communications*, vol. 7, no. 6, pp. 2069–2074, June 2008.

[255] S. Simoens, O. Muñoz-Medina, J. Vidal, and A. del Coso, "On the Gaussian MIMO relay channel with full channel state information," *IEEE Transactions on Signal Processing*, vol. 57, no. 9, pp. 3588–3599, September 2009.

[256] S. Simoens, O. Muñoz-Medina, J. Vidal, and A. Del Coso, "Compress-and-forward cooperative MIMO relaying with full channel state information," *IEEE Transactions on Signal Processing*, vol. 58, no. 2, pp. 781–791, February 2010.

[257] B. Sklar, "Rayleigh fading channels in mobile digital communication systems — part I: Characterization," *IEEE Communications Magazine*, vol. 35, no. 9, pp. 136–146, September 1997.

[258] B. Sklar, "Rayleigh fading channels in mobile digital communication systems — part II: Mitigation," *IEEE Communications Magazine*, vol. 35, no. 9, pp. 148–155, September 1997.

[259] S. Sohaib and D. K. C. So, "Asynchronous polarized cooperative MIMO communication," in *Proc. 69th IEEE Vehicular Technology Conference*, April 2009.

[260] S. Sohaib and D. K. C. So, "Energy analysis of asynchronous polarized cooperative MIMO protocol," in *Proc. 21st IEEE International Symposium on Personal, Indoor and Mobile Radio Communications*, September 2010.

[261] Y. Song, H. Shin, and E.-K. Hong, "MIMO cooperative diversity with scalar-gain amplify-and-forward relaying," *IEEE Transactions on Communications*, vol. 57, no. 7, pp. 1932–1938, July 2009.

[262] M. Soysa, H. A. Suraweera, C. Tellambura, and H. K. Garg, "Partial and opportunistic relay selection with outdated channel estimates," *IEEE Transactions on Communications*, vol. 60, no. 3, pp. 840–850, March 2012.

[263] H. Steendam and M. Moeneclaey, "Analysis and optimization of the performance of OFDM on frequency-selective time-selective fading channels," *IEEE Transactions on Communications*, vol. 47, no. 12, pp. 1811–1819, December 1999.

[264] A. Stefanov and E. Erkip, "Cooperative coding for wireless networks," *IEEE Transactions on Communications*, vol. 52, no. 9, pp. 1470–1476, September 2004.

[265] A. I. Sulyman, G. Takahara, H. S. Hassanein, and M. Kousa, "Multi-hop capacity of MIMO-multiplexing relaying systems," *IEEE Transactions on Wireless Communications*, vol. 8, no. 6, pp. 3095–3103, June 2009.

[266] Q. Sun, D. C. Cox, H. C. Huang, and A. Lozano, "Estimation of continuous flat fading MIMO channels," *IEEE Transactions on Wireless Communications*, vol. 1, no. 4, pp. 549–553, October 2002.

[267] C. K. Sung and I. B. Collings, "Multiuser cooperative multiplexing with interference suppression in wireless relay networks," *IEEE Transactions on Wireless Communications*, vol. 9, no. 8, pp. 2528–2538, August 2010.

[268] H. A. Suraweera and J. Armstrong, "Performance of OFDM-based dual-hop amplify-and-forward relaying," *IEEE Communications Letters*, vol. 11, no. 9, pp. 726–728, September 2007.

[269] H. A. Suraweera, H. K. Garg, and A. Nallanathan, "Performance analysis of two hop amplify-and-forward systems with interference at the relay," *IEEE Communications Letters*, vol. 14, no. 8, pp. 692–694, August 2010.

[270] H. A. Suraweera and G. K. Karagiannidis, "Closed-form error analysis of the non-identical Nakagami-m relay fading channel," *IEEE Communications Letters*, vol. 12, no. 4, pp. 259–261, April 2008.

[271] H. A. Suraweera, G. K. Karagiannidis, and P. J. Smith, "Performance analysis of the dual-hop asymmetric fading channel," *IEEE Transactions on Wireless Communications*, vol. 8, no. 6, pp. 2783–2788, June 2009.

[272] H. A. Suraweera, R. H. Y. Louie, Y. Li, G. K. Karagiannidis, and B. Vucetic, "Two hop amplify-and-forward transmission in mixed Rayleigh and Rician fading channels," *IEEE Communications Letters*, vol. 13, no. 4, pp. 227–229, April 2009.

[273] H. A. Suraweera, D. S. Michalopoulos, and G. K. Karagiannidis, "Performance of distributed diversity systems with a single amplify-and-forward relay," *IEEE Transactions on Vehicular Technology*, vol. 58, no. 5, pp. 2603–2608, June 2009.

[274] H. A. Suraweera, D. S. Michalopoulos, and G. K. Karagiannidis, "Semi-blind amplify-and-forward with partial relay selection," *Electronics Letters*, vol. 45, no. 6, pp. 317–319, March 2009.

[275] H. A. Suraweera, D. S. Michalopoulos, and C. Yuen, "Performance analysis of fixed gain relay systems with a single interferer in Nakagami-m fading channels," *IEEE Transactions on Vehicular Technology*, vol. 61, no. 3, pp. 1457–1463, March 2012.

[276] H. A. Suraweera, P. J. Smith, and J. Armstrong, "Outage probability of cooperative relay networks in Nakagami-m fading channels," *IEEE Communications Letters*, vol. 10, no. 12, pp. 834–836, December 2006.

[277] H. A. Suraweera, P. J. Smith, A. Nallanathan, and J. S. Thompson, "Amplify-and-forward relaying with optimal and suboptimal transmit antenna selection," *IEEE Transactions on Wireless Communications*, vol. 10, no. 6, pp. 1874–1885, June 2011.

[278] H. A. Suraweera, M. Soysa, C. Tellambura, and H. K. Garg, "Performance analysis of partial relay selection with feedback delay," *IEEE Signal Processing Letters*, vol. 17, no. 6, pp. 531–534, June 2010.

[279] H. A. Suraweera, T. A. Tsiftsis, G. K. Karagiannidis, and A. Nallanathan, "Effect of feedback delay on amplify-and-forward relay networks with beamforming," *IEEE Transactions on Vehicular Technology*, vol. 60, no. 3, pp. 1265–1271, March 2011.

[280] H. Suzuki, T. V. Anh Tran, I. B. Collings, G. Daniels, and M. Hedley, "Transmitter noise effect on the performance of a MIMO-OFDM hardware implementation achieving improved coverage," *IEEE Journal on Selected Areas in Communications*, vol. 26, no. 6, pp. 867–876, August 2008.

[281] X. Tang and Y. Hua, "Optimal design of non-regenerative MIMO wireless relays," *IEEE Transactions on Wireless Communications*, vol. 6, no. 4, pp. 1398–1407, April 2007.

[282] R. Tannious and A. Nosratinia, "Spectrally-efficient relay selection with limited feedback," *IEEE Journal on Selected Areas in Communications*, vol. 26, no. 8, pp. 1419–1428, October 2008.

[283] S. Thoen, L. Van der Perre, and M. Engels, "Modeling the channel time-variance for fixed wireless communications," *IEEE Communications Letters*, vol. 6, no. 8, pp. 331–333, August 2002.

[284] M. Torabi and D. Haccoun, "Capacity of amplify-and-forward selective relaying with adaptive transmission under outdated channel information," *IEEE Transactions on Vehicular Technology*, vol. 60, no. 5, pp. 2416–2422, June 2011.

[285] M. Torabi, D. Haccoun, and J.-F. Frigon, "Impact of outdated relay selection on the capacity of AF opportunistic relaying systems with adaptive transmission over non-identically distributed links," *IEEE Transactions on Wireless Communications*, vol. 10, no. 11, pp. 3626–3631, November 2011.

[286] L.-S. Tsai and D.-S. Shiu, "Capacity scaling and coverage for repeater-aided MIMO systems in line-of-sight environments," *IEEE Transactions on Wireless Communications*, vol. 9, no. 5, pp. 1617–1627, May 2010.

[287] F.-S. Tseng and W.-R. Wu, "Linear MMSE transceiver design in amplify-and-forward MIMO relay systems," *IEEE Transactions on Vehicular Technology*, vol. 59, no. 2, pp. 754–765, February 2010.

[288] F.-S. Tseng, W.-R. Wu, and J.-Y. Wu, "Joint source/relay precoder design in nonregenerative cooperative systems using an MMSE criterion," *IEEE Transactions on Wireless Communications*, vol. 8, no. 10, pp. 4928–4933, October 2009.

[289] T. A. Tsiftsis, G. K. Karagiannidis, and S. A. Kotsopoulos, "Dual-hop wireless communications with combined gain relays," *IEE Proceedings-Communications*, vol. 152, no. 5, pp. 528–532, October 2005.

[290] T. A. Tsiftsis, G. K. Karagiannidis, S. A. Kotsopoulos, and F.-N. Pavlidou, "BER analysis of collaborative dual-hop wireless transmissions," *Electronics Letters*, vol. 40, no. 11, pp. 679–681, May 2004.

[291] T. A. Tsiftsis, G. K. Karagiannidis, P. T. Mathiopoulos, and S. A. Kotsopoulos, "Nonregenerative dual-hop cooperative links with selection diversity," *EURASIP Journal on Wireless Communications and Networking*, vol. 2006, Article ID 17862, 8 pages, 2006.

[292] T. Unger and A. Klein, "Duplex schemes in multiple antenna two-hop relaying," *EURASIP Journal on Advances in Signal Processing*, vol. 2008, Article ID 128592, 14 pages, 2008.

[293] E. C. Van Der Meulen, "Three-terminal communication channels," *Advances in Applied Probability*, vol. 3, pp. 120–154, 1971.

[294] J. L. Vicario, A. Bel, J. A. Lopez-Salcedo, and G. Seco, "Opportunistic relay selection with outdated CSI: Outage probability and diversity analysis," *IEEE Transactions on Wireless Communications*, vol. 8, no. 6, pp. 2872–2876, June 2009.

[295] H. Viswanathan and S. Mukherjee, "Performance of cellular networks with relays and centralized scheduling," *IEEE Transactions on Wireless Communications*, vol. 4, no. 5, pp. 2318–2328, September 2005.

[296] F. Vitiello, T. Riihonen, J. Hämäläinen, and S. Redana, "On buffering at the relay node in LTE-Advanced," in *Proc. IEEE 74th Vehicular Technology Conference*, September 2011.

[297] J. Wagner, B. Rankov, and A. Wittneben, "Large n analysis of amplify-and-forward MIMO relay channels with correlated Rayleigh fading," *IEEE Transactions on Information Theory*, vol. 54, no. 12, pp. 5735–5746, December 2008.

[298] B. Wang, J. Zhang, and A. Høst-Madsen, "On the capacity of MIMO relay channels," *IEEE Transactions on Information Theory*, vol. 51, no. 1, pp. 29–43, January 2005.

[299] O. Waqar, M. Ghogho, and D. McLernon, "Tight bounds for ergodic capacity of dual-hop fixed-gain relay networks under Rayleigh fading," *IEEE Communications Letters*, vol. 15, no. 4, pp. 413–415, April 2011.

[300] S. Wei, D. L. Goeckel, and P. A. Kelly, "Convergence of the complex envelope of bandlimited OFDM signals," *IEEE Transactions on Information Theory*, vol. 56, no. 10, pp. 4893–4904, October 2010.

[301] S. B. Weinstein, "The history of orthogonal frequency-division multiplexing," *IEEE Communications Magazine*, vol. 47, no. 11, pp. 26–35, November 2009.

[302] L. Wu, K. Niu, Z. He, W. Xu, and J. Lin, "Ergodic capacity of dual-hop transmissions over composite multipath/shadowing channels," *Electronics Letters*, vol. 45, no. 19, pp. 975–976, September 2009.

[303] B. Xia, Y. Fan, J. S. Thompson, and H. V. Poor, "Buffering in a three-node relay network," *IEEE Transactions on Wireless Communications*, vol. 7, no. 11, pp. 4492–4496, November 2008.

[304] L. Yang, M. O. Hasna, and M.-S. Alouini, "Average outage duration of multihop communication systems with regenerative relays," *IEEE Transactions on Wireless Communications*, vol. 4, no. 4, pp. 1366–1371, July 2005.

[305] L. Yang and Q. T. Zhang, "Outage performance of MIMO relay channels with maximal ratio transmission," *Electronics Letters*, vol. 45, no. 5, pp. 273–274, February 2009.

[306] S. Yang and J.-C. Belfiore, "Optimal space–time codes for the MIMO amplify-and-forward cooperative channel," *IEEE Transactions on Information Theory*, vol. 53, no. 2, pp. 647–663, February 2007.

[307] S. Yao and M. Skoglund, "Hybrid digital-analog relaying for cooperative transmission over slow fading channels," *IEEE Transactions on Information Theory*, vol. 55, no. 3, pp. 944–951, March 2009.

[308] M. Yuksel and E. Erkip, "Multiple-antenna cooperative wireless systems: A diversity–multiplexing tradeoff perspective," *IEEE Transactions on Information Theory*, vol. 53, no. 10, pp. 3371–3393, October 2007.

[309] E. Zacarías B., S. Werner, R. Wichman, and T. Riihonen, "Single-bit closed-loop quasi-orthogonal space-time codes for MIMO systems," in *Proc. 10th IEEE Workshop on Signal Processing Advances in Wireless Communications*, June 2009.

[310] B. Zhang, Z. He, K. Niu, and L. Zhang, "Robust linear beamforming for MIMO relay broadcast channel with limited feedback," *IEEE Signal Processing Letters*, vol. 17, no. 2, pp. 209–212, February 2010.

[311] R. Zhang, C. C. Chai, and Y.-C. Liang, "Joint beamforming and power control for multiantenna relay broadcast channel with QoS constraints," *IEEE Transactions on Signal Processing*, vol. 57, no. 2, pp. 726–737, February 2009.

[312] W. Zhang, U. Mitra, and M. Chiang, "Optimization of amplify-and-forward multicarrier two-hop transmission," *IEEE Transactions on Communications*, vol. 59, no. 5, pp. 1434–1445, May 2011.

[313] X. Zhang, M. Tao, W. Jiao, and C. S. Ng, "End-to-end outage minimization in OFDM based linear relay networks," *IEEE Transactions on Communications*, vol. 57, no. 10, pp. 3034–3044, October 2009.

[314] X. J. Zhang and Y. Gong, "Adaptive power allocation for multihop regenerative relaying with limited feedback," *IEEE Transactions on Vehicular Technology*, vol. 58, no. 7, pp. 3862–3867, September 2009.

[315] Z. Zhang and T. M. Duman, "Capacity-approaching turbo coding and iterative decoding for relay channels," *IEEE Transactions on Communications*, vol. 53, no. 11, pp. 1895–1905, November 2005.

[316] B. Zhao and M. C. Valenti, "Distributed turbo coded diversity for relay channel," *Electronics Letters*, vol. 39, no. 10, pp. 786–787, May 2003.

[317] Y. Zhao, R. Adve, and T. J. Lim, "Symbol error rate of selection amplify-and-forward relay systems," *IEEE Communications Letters*, vol. 10, no. 11, pp. 757–759, November 2006.

[318] C. Zhong, M. Matthaiou, G. K. Karagiannidis, and T. Ratnarajah, "Generic ergodic capacity bounds for fixed-gain AF dual-hop relaying systems," *IEEE Transactions on Vehicular Technology*, vol. 60, no. 8, pp. 3814–3824, October 2011.

[319] Y. Zhu, Y. Xin, and P.-Y. Kam, "Outage probability of Rician fading relay channels," *IEEE Transactions on Vehicular Technology*, vol. 57, no. 4, pp. 2648–2652, July 2008.

[320] Y. Zou, J. Zhu, B. Zheng, and Y.-D. Yao, "An adaptive cooperation diversity scheme with best-relay selection in cognitive radio networks," *IEEE Transactions on Signal Processing*, vol. 58, no. 10, pp. 5438–5445, October 2010.

"The work in this thesis, for example aspects on full-duplex transmission, is seminal and pioneering. The candidate's contribution to the dissertation is excellent and very much beyond of what is typically expected."
-- Dr. Himal A. Suraweera

"This is one of the most comprehensive theses that I have seen in this area. It has made significant contributions which were presented very well, too."
-- Dr. Golnaz Farhadi

"He [Taneli] and his thesis are exceptional cases."
-- Dr. Stefan Werner

"You [Taneli] would already have enough material for two or three dissertations."
-- Prof. Risto Wichman

Aalto-DD 81/2014

ISBN 978-952-60-5714-9
ISBN 978-952-60-5715-6 (pdf)
ISSN-L 1799-4934
ISSN 1799-4934
ISSN 1799-4942 (pdf)

Aalto University
School of Electrical Engineering
Department of Signal Processing and Acoustics
www.aalto.fi

BUSINESS + ECONOMY

ART + DESIGN + ARCHITECTURE

SCIENCE + TECHNOLOGY

CROSSOVER

DOCTORAL DISSERTATIONS